Cardiff School of Engineering
Cardiff University

# An investigation of the strength of brickwork walls when subject to flood loading

**Daniel M Herbert**

BEng, MSc

Thesis submitted to Cardiff University in candidature for the degree of Doctor of Philosophy

August 2013

## Declaration

This work has not previously been accepted in substance for any degree and is not concurrently submitted in candidature for any other higher degree.

Signed:……..(Candidate) Date:…….

**Statement 1**

This thesis is being submitted in partial fulfilment of the requirements for the degree of ……..(insert as appropriate PhD, MPhil, EngD)

Signed:……..(Candidate) Date:…….

**Statement 2**

This thesis is the result of my own independent work/investigation, except where otherwise stated. Other sources are acknowledged by explicit references.

Signed:……..(Candidate) Date:…….

**Statement 3**

I hereby give consent for my thesis, if accepted, to be available for photocopying, inter-library loan and for the title and summary to be made available to outside organisations.

Signed:……..(Candidate) Date:…….

## Acknowledgements

I would like to acknowledge the support and assistance given by my supervisors Prof. Emeritus Tim Hughes, Dr Diane Gardner and Dr Michael Harbottle throughout the duration of the research project. I would also like to thank Tim for his help in gaining funding for the project, which was in part funded by the EPSRC.

I would like to acknowledge Jeremy Thomas from INSA Toulouse for collaborating on part of the research programme, which considered the uniform loading capacity of blockwork wall panels.

I would like to thank the technical staff at the School of Engineering, in particular Harry for driving the centrifuge and manufacturing test equipment, Carl, Ian and Steph for their help with cutting the bricks and making the models, Brian, Len and Des for their help and advice on testing.

Thanks are also due to Dr Mark Eaton and Dr Rhys Pullin for their help with the digital image correlation system.

Finally I would like to thank my wife, Amy for her encouragement and support during the project, and my daughter Lucia for brightening up my day.

## Summary

The main purpose of this programme of research was to establish characteristic water levels to which new and existing properties of masonry construction can be protected against flooding. Typical flood protection systems often rely on the structural strength of the building and in doing so generate significant lateral loadings. Current guidance appears to be based on the results of a single experimental study and no calculation technique is currently available to determine suitable characteristic levels. The research aim was addressed by conducting a series of experimental tests at model scale and by developing a theoretical analysis.

Model scale masonry wall panels were successfully tested in a geotechnical centrifuge and were subject to hydraulic loading or uniform wind loading. Wind loading was considered to allow validation of the experimental procedure to results in the literature. Wall panels were constructed from both brick and block units and the effect of different mortar strengths, openings, vertical loadings and cavity construction were assessed. The experimental procedure showed very good repeatability in terms of ultimate load and generally a yield line type failure mode was observed.

A theoretical analysis based on yield line analysis was developed using spreadsheet software and verified using the results from the experimental programme. The analysis gave a good approximation of the experimental ultimate loads, but the optimised failure mode was not always consistent with that observed in the tests. A parametric study was completed to assess the effect of varying parameters not considered in the experimental study and in addition a typical domestic property was modelled to assess its resistance against flood loading. The characteristic water level for the weakest wall of the property was found to exceed the value given in the guidance, of 0.6 m, by 38 % and signified the importance of completing the correct modelling procedure.

## Contents

## Index of Figures

## Index of Tables

# Nomenclature

| Symbol | Description | Units |
|---|---|---|
| $\alpha$ | Dimensional parameter for yield line pattern | - |
| $\beta$ | Dimensional parameter for yield line pattern | - |
| $\delta$ | Deflection | - |
| $\gamma$ | Dimensional parameter for yield line pattern | - |
| $\gamma_f$ | Factor of safety for loads | - |
| $\gamma_M$ | Factor of safety for materials (control of execution) | - |
| $\lambda$ | Factor for support conditions for vertical loading | - |
| $\theta_i$ | Rotation of plastic hinge or slab i | ° |
| $\rho_{brick}$ | Density of masonry | $kg/m^3$ |
| $\rho_w$ | Density of water | $kg/m^3$ |
| $\sigma$ | Stress | $N/mm^2$ |
| $\omega$ | Coefficient of friction | - |
| A | Plan area of property | $m^2$ |
| $A_i$ | Gradient of element side i | - |
| $a_p$ | Constant for pressure equation | - |
| b | Width of masonry wallette specimen | mm |
| $B_i$ | Constant for equation of element side i | m |
| $b_p$ | Constant for pressure equation | - |
| $C_d$ | Shape factor for hydrodynamic pressure | - |
| $C_f$ | Compression depth factor for vertical load | - |
| $c_j$ | Constant for equation of yield line j (for opening yield lines) | m |
| $c_p$ | Constant for pressure equation | - |
| D | Depth of water | m |
| $D_{Eq}$ | Equivalent depth of water for cavity wall assembly | m |
| $D_{Inner}$ | Depth of water for inner leaf of cavity wall assembly | m |
| $D_{Outer}$ | Depth of water for outer leaf of cavity wall assembly | m |
| d1 | Direction 1 – test direction parallel to the bed joints | - |
| d2 | Direction 2 – test direction perpendicular to the bed joints | - |
| dx | Length of yield line cut in x direction (for opening yield lines) | m |
| dy | Length of yield line cut in y direction (for opening yield lines) | m |
| E | Young's Modulus | $N/mm^2$ |
| ExtWD | External work done | kJ |
| F | Friction force | kNm/m |

| | | |
|---|---|---|
| $F_{d1}$ | Fixity direction 1 | - |
| $F_{d2}$ | Fixity direction 2 | - |
| $f_{ix}$ | Flexural strength for wallette specimen i | $N/mm^2$ |
| $F_{i,max}$ | Maximum load for wallette specimen i | N |
| $F_{LHS}$ | Force acting on left hand side of element | kN |
| FoS | Factor of safety | - |
| $F_{RHS}$ | Force acting on right hand side of element | kN |
| $F_{Total}$ | Total force acting on element | kN |
| $f_{x1}$ | Flexural strength of masonry in direction 1 | $N/mm^2$ |
| $f_{x2}$ | Flexural strength of masonry in direction 2 | $N/mm^2$ |
| $f_{xk}$ | Characteristic flexural strength | $N/mm^2$ |
| g | Earth's gravity | $m/s^2$ |
| H | Height of wall panel | m |
| $H_{bl}$ | Height of masonry unit | m |
| $h_F$ | Height of floor | m |
| i | Node, element side, specimen number or compressive strength class | - |
| IntWD | Internal work done | kJ |
| j | Slab or yield line number or number of storeys | - |
| L | Length of wall panel | m |
| $l_{arm}$ | Lever arm for frictional resistance method | m |
| $L_{bl}$ | Length of masonry unit | m |
| $l_s$ | Length of masonry wallette specimen | mm |
| $l_1$ | Spacing of outer bearings – wallette specimen | mm |
| $l_2$ | Spacing of inner bearings – wallette specimen | mm |
| $m_j$ | Gradient of yield line j (for opening yield lines) | - |
| Mi | Mortar strength class, where i represents designated compressive strength | $N/mm^2$ |
| $MR_{d1}$ | Moment resistance direction 1 | kNm |
| $MR_{d2}$ | Moment resistance direction 2 | kNm |
| $MR_p$ | Plastic moment resistance | kNm |
| $Mx_{LHS}$ | Moment of force on LHS of element in x direction | kNm |
| $Mx_{RHS}$ | Moment of force on RHS of element in x direction | kNm |
| $Mx_{Total}$ | Total moment of force on element in x direction | kNm |
| $My_{LHS}$ | Moment of force on LHS of element in y direction | kNm |

| | | |
|---|---|---|
| $My_{RHS}$ | Moment of force on RHS of element in y direction | kNm |
| $My_{Total}$ | Moment of force on element in y direction | kNm |
| $N_i$ | Node i | - |
| OH | Opening height | m |
| OL | Opening length | m |
| OsH | Vertical position of opening | m |
| OsL | Horizontal position of opening | m |
| P | Distributed load | $kN/m^2$ |
| $P_i$ | Pressure at node i | $kN/m^2$ |
| $P_{ihd}$ | Hydrodynamic pressure at node i | $kN/m^2$ |
| $P_{ihs}$ | Hydrostatic pressure at node i | $kN/m^2$ |
| $P_{int}$ | Intersection points on opening edge | m |
| $P_{ties}$ | Wall tie pressure | $kN/m^2$ |
| $P_{UDL}$ | Uniformly distributed load | $kN/m^2$ |
| ReFoS | Required factor of safety | - |
| SA1 | Spreadsheet analysis one | - |
| SA2 | Spreadsheet analysis two (corner lever) | - |
| $S_i$ | Slab i | - |
| t | Thickness of units – wallette specimen test | mm |
| $T_{bl}$ | Thickness of masonry unit | m |
| Type | Yield line type for opening | - |
| v | Velocity for hydrodynamic pressure | m/s |
| $V_{av}$ | Average vertical load | kN/m |
| $V_i$ | Vertical load at node i | kN/m |
| $V_{udl}$ | Uniformly distributed vertical load at top of wall panel | kN/m |
| $V_{udlF}$ | Uniformly distributed vertical load on floor | $kN/m^2$ |
| $V_{udlR}$ | Uniformly distributed vertical load on roof | $kN/m^2$ |
| $w_F$ | Width of floor | m |
| $w_R$ | Width of roof | m |
| xa | x coordinate of intersection point on opening edge | m |
| xb | x coordinate of intersection point on opening edge | m |
| xc | Lever arm in x direction or<br>x coordinate of intersection point on opening edge | m |
| $x_i$ | Coordinate of node in x direction | m |
| ya | y coordinate of intersection point on opening edge | m |

| | | |
|---|---|---|
| yb | y coordinate of intersection point on opening edge | m |
| yc | Lever arm in y direction or<br>y coordinate of intersection point on opening edge | m |
| $y_i$ | Coordinate of node in y direction | m |
| Z | Section modulus | $mm^3$ |

# Chapter 1 Introduction

## 1.1 Background

Flooding is becoming a widespread issue and can cause extensive damage to properties and their owner's contents when it strikes. A national flood risk assessment has recently identified that there are approximately 2.75 million properties at risk of flooding in England, Scotland and Wales (Environment Agency, 2009, Environment Agency Wales, 2009, SEPA, 2011). Reasons for a higher number of flood events may be due to changes in climatic conditions, rising sea levels, change in land use and development in flood catchment areas (Jenkins et al., 2009, Pitt, 2008, Stern, 2007, Wheater, 2006). Construction within a river basin can often result in reduced ground permeability leading to greater surface water volumes being directed into streams and rivers. Many communities have historically been established alongside rivers or on flood plain areas and the effects of further development have not been considered until recently (Communities & Local Government, 2010, Pitt, 2008). New developments are likely to be prevented from being placed in flood prone areas, but this still leaves a significant number of existing properties that are at risk.

Flood defence schemes, such as barriers and dykes, can help in many cases, but the current economic downturn is leading to reduced capital being available for such projects (Leake, 2007). In addition to this, two thirds of the government's expenditure in the UK has been required simply to maintain and improve existing flood protection schemes (Environment Agency, 2009). Installing large protection schemes will not always be the best option to protect properties and allowing land to flood in some cases can reduce the damage downstream. Property owners will therefore need to turn to products that will provide resilience or resistance to flood waters. Properties can quickly be put back into service with limited cost following a flood when suitable measures have been taken (Pitt, 2008). The employment of such schemes has been limited, due to low awareness, required initial capital outlay and limited pressure from government and insurance companies to install such products. The situation is likely to change in the near future due to recommended changes in building regulations and government policy (Pitt, 2008). Properties subject to multiple flooding events may become difficult or impossible to insure, so such measures may be the only option in such situations.

Property owners have the option of utilising resilient materials and design, allowing the property to be quickly returned to a habitable state after flooding. Alternatively, a flood resistant system can be installed to the exterior of the building that will prevent floodwater entry. Flood resistant products frequently rely on the structure of the building to retain the water, but very limited work has been conducted to assess the implications of this scenario. A review of the literature has identified a single experimental study on full-scale (prototype) masonry walls that suggested sealing to no greater than 0.9 m (Pace, 1988). Moreover the tests conducted were more relevant to construction techniques used in North America and only considered wall panels of one size. The effect of different edge support conditions and vertical imposed loads, due to multiple storey construction, were also not considered in the study. The suggested characteristic sealing height therefore may not be suitable as a blanket value for all types of masonry construction. Later to this, a purely theoretical approach has been presented that concluded that properties could be sealed to a height of between 0.9 and 1 m (Kelman and Spence, 2003a).

Building codes do not offer any specific guidance to allow the calculation of a characteristic sealing height, yet government advice often suggests not to exceed 0.9 m (BSI, 2005c, FEMA, 2009, ODPM, 2003). Interim guidance given by the UK government suggested that structural damage would likely occur if a depth of water over 1 m was applied to the walls, but without justification (ODPM, 2003). It was however advised that external walls should be examined by a suitably qualified person for expected flood depths of between 0.6 and 0.9 m. Later guidance in the UK (Communities & Local Government, 2007) reduced the characteristic height to 0.6 m and direct reference was given to the work conducted by Pace (1988), however the guidance seems contradictory to the maximum sealing height of 0.9m that was found by Pace. Government policy was heavily criticised in the wake of extensive flooding in 2007, focussing on the lack of clear rules in planning and building regulations (Pitt, 2008).

There is clearly a need to develop a suitable method to establish the characteristic height to which waterproofing products should be applied when protecting against floodwaters. One approach would be to consider the walls of a property as individual panels with the appropriate edge support conditions and applied vertical loading. A theoretical analysis could then be developed to establish the ultimate water level that could be retained by the wall panel. Incorporation of suitable factors of safety would then allow a characteristic sealing height to be found for a particular wall panel. The

problem with a purely theoretical approach is that the very limited data available in the literature would not allow a thorough validation process to be completed. Another approach would be to conduct a series of experimental tests, similarly on wall panels, to establish the water level retained at ultimate limit state. Again with the application of suitable factors of safety the characteristic sealing height could be established for a particular wall panel. The drawback of establishing the characteristic sealing height by experimentation alone would be that a large number of tests would need to be completed to consider every possible scenario. A more suitable approach would be to develop a theoretical analysis alongside a series of experimental tests, which would allow validation to be completed. To allow a thorough validation process it would be necessary to consider a number of different parameters in the experimental study, including masonry materials type, mortar strength, vertical loads, openings, support conditions and cavity type arrangements. The validated analysis could then be used to evaluate any masonry structure and, with the incorporation of the correct factors of safety, determine the appropriate characteristic height to which waterproofing should be applied.

The experimental study could be completed at full (prototype) scale, however this would likely be time consuming, expensive and could involve significant health and safety considerations. An alternative approach would be to conduct the tests at reduced (model) scale, employing a centrifuge to correctly model self weight. Masonry arch structures have previously been successfully modelled using a centrifuge and the results were shown to compare well to those of the prototype (Davies et al., 1998). The results of a number of experimental studies, where uniform (wind) lateral loading was applied to masonry wall panels, have been published in the literature (Anderson, 1976, de Vekey et al., 1986, Duarte, 1998, Edgell and Kjaer, 2000, Gairns and Scrivener, 1988, Haseltine et al., 1977, Hendry, 1973, Sinha et al., 1979, West et al., 1977, West et al., 1986). This existing data could prove beneficial in the validation of the model scale experimental procedure if a series of uniform lateral loading tests were additionally conducted.

### 1.2 Aims and objectives of research

The main aim of the research programme was to determine the experimental ultimate loads and modes of masonry subject to hydraulic loads, and the objectives were:

- To develop a suitable method to manufacture and test, using the centrifuge, model scale masonry wall panels.

- Apply uniform (wind) lateral loads to the wall panels in order to validate the experimental procedure using previous results in the literature and current design procedures.
- Apply non-uniform (hydraulic) lateral loads to the wall panels to establish their performance.
- Develop a suitable analysis to determine the ultimate and characteristic loads
- Verify the analysis using the experimental results, and with results from the literature where possible.
- Complete a parametric study using the analysis to assess the influence of various factors on the failure load.
- Apply the analysis to the structure of a typical domestic property to asses its performance when subject to hydraulic loads.

### 1.3 Layout of thesis

Chapter 1 presents the background to the project, justifies the need for the research, and describes the aims and objectives of the programme.

Chapter 2 reviews the literature and focuses on the behaviour of masonry assemblages subject to uniform and non-uniform lateral (out of plane) loading. This includes a review of both theoretical analysis and the findings of previous experimental research programmes. Previous works where masonry testing was completed at small scale are also evaluated, in order to establish the accuracy of such models when compared to the prototype.

Chapter 3 presents the development of the analyses, firstly detailing the theory utilised, followed by the application of the theory to uniformly and non-uniformly loaded masonry wall panels, and finally illustrates how this is incorporated into the spreadsheet analyses.

Chapter 4 details the development of the experimental programme completed at reduced scale. Consideration is initially given to a suitable scale and size for the masonry specimens as well as appropriate boundary conditions. Following this the methods for the manufacture of the model scale masonry units, small assemblages and wall panels are presented. Details of the centrifuge testing procedure, including the selection of suitable instrumentation and loading techniques, are given. Finally, the testing procedure for wallettes and wall ties specimens is presented.

Chapter 5 provides the results found from the small assemblage tests completed alongside the wall panel tests. The results of flexural tests completed for both brick and block wallette specimens are detailed, discussed and compared to values given by Eurocode 6 (BSI, 2005c). Results are also detailed and discussed of tests of wall ties at both model and prototype scale. Finally a brief comparison is made of the compressive strength of model and prototype scale mortars manufactured during the wall tie tests.

Chapter 6 presents and discusses the results found from the tests of model scale masonry wall panels subject to uniformly distributed lateral loads. The effect of masonry material type, mortar strength, vertical axial load, openings in the wall panel and cavity construction are investigated. The response of the wall panels both in and out of plane is also discussed. Comparison to results completed at prototype scale from the literature is made where possible. Finally consideration is given to the effects of the increased gravitational force on the wall panels.

Chapter 7 provides the results of the tests of model scale masonry wall panels that were subject to non-uniform hydraulic lateral loads. The effect of masonry material type, mortar strength, vertical axial load, openings in the wall panel and cavity construction are similarly investigated. The response of the wall panels to the hydraulic lateral load is discussed and comparison is made to the very limited experimental data in the literature.

Chapter 8 presents a verification of the analyses developed in Chapter 3 using the experimental results given in Chapters 6 and 7. A parametric study is completed, to assess the effect of failure mode, panel size, vertical load, boundary conditions, and opening size and position on the failure load. In addition to this the results from the analyses are compared to experimental and theoretical data from the literature. Finally the analysis is used to assess the performance of a typical domestic property when subject to hydraulic lateral loads.

Chapter 9 presents the conclusions drawn from the research programme, discusses the importance and implications of the findings, and finally details some possible areas where further work could be carried out.

# Chapter 2 Literature review

## 2.1 Overview

This Chapter presents a review of the literature focussed on the behaviour of masonry assemblages subject to uniform and non-uniform lateral (out of plane) loading. Due to the nature of this research programme, attention has particularly been given to such studies that consider both experimentation and analysis combined or a purely theoretical approach. Further to this, a review of works completed at model scale is presented and the effects of reducing the scale of the model are examined.

## 2.2 A brief history of masonry

Masonry has been used as a building material for thousands of years. Early masonry used a variety of materials, such as natural stone, formed dried mud and fired mud (Hamilton, 1939). The units were sometimes laid dry, but mortars of tar, lime mud and sand were also widely used. The Egyptians, Greeks and later the Romans are probably best known for their vast use of masonry to build many different types of structure. The Romans were particularly proficient in the construction of arches, developing impressive aqueducts for the delivery of water. At around the 12$^{th}$ century gothic master builders in Europe started to construct imposing masonry structures in the form of churches and cathedrals (Heyman, 1966). Advances in design were suggested due to competition between different masons and a quest to drive more natural light inside (Fitchen, 1981, Herbert, 2009, Mark, 1984). During these eras the masons had a limited knowledge of structural analysis techniques therefore relied on rules of proportion, the success of others, and experimentation (Herbert, 2009, Heyman, 1992, Huerta, 2006).

Brickwork masonry suffered a decline after the collapse of the Roman Empire and only started to regain popularity in the 15$^{th}$ century (Lynch, 2007). Masonry and in particular the use of brick really came to prominence in the 18th century with the onset of industrialisation in the UK. Masonry was used for many structures at this time, including bridges, tunnels, canals, factories and their chimneys. The discovery of structural analysis, as we know it now, was only made just prior to this era, whilst some of the fundamental principles were forged during this and later centuries (Fordham, 1938).

Modern day uses of masonry are somewhat limited compared to its diverse past. In the UK the majority of masonry construction is focussed on low-rise housing and the use of steel and concrete has surpassed it for other structures. Emerging countries are however utilising masonry for a wider range of projects, including high-rise housing, and commercial and industrial developments (Correa, 2012).

### 2.3 Masonry materials and construction

Masonry typically comprises of units and mortar that are laid in a specific manner or bond to form a strong composite material. The materials used for the units varies widely and includes natural stone, manufactured stone, clay, concrete, aerated cement, mud, and blast furnace slag. Early mortars were lime based and provided advantages over dry laying in that discrepancies in the units and movement in the structure could be accommodated (McDonald, 2000). Cement based mortars, introduced in the 19$^{th}$ century, offered higher strength compared to their lime counterparts, but are less accommodating to structural movement (Gutteridge, 1931, McDonald, 2000). Typical UK masonry construction comprises single or multiple leafs of masonry units, where the latter are interconnected using metal ties, as shown by Figure 2.1. Damp proof courses, of plastic, bitumen or special brick, are installed at the base of the walls to stop water in the ground travelling upwards into the structure. The general form of construction provides a self-buttressing effect along with additional strengthening effects of floors and roofs. Walls are however quite slender so correct consideration of dead and imposed loadings need to be made in their design.

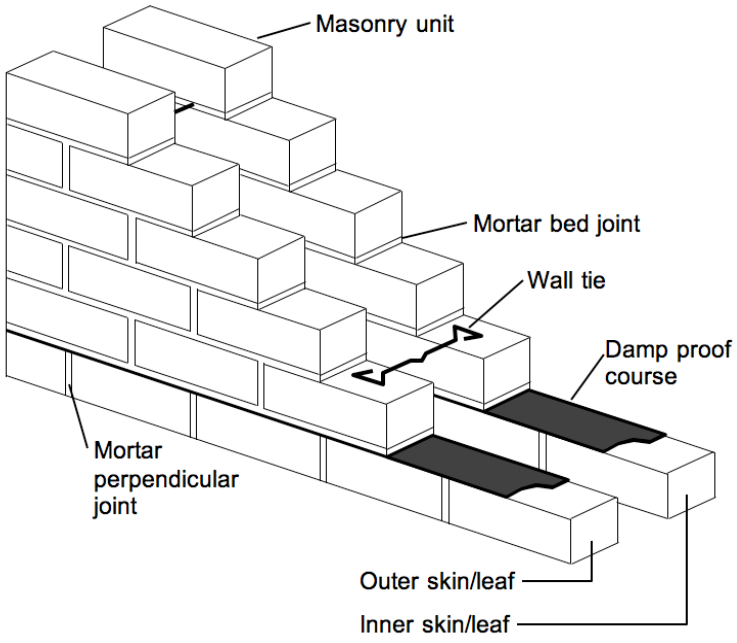


**Figure 2.1.** Typical masonry construction

## 2.4 Experimental investigations of the strength of masonry walls subject to uniform lateral loads

### 2.4.1 Wall panels without openings

Early uniform lateral loading tests were carried out with brick specimens, where all edges of the specimens were either simply supported or constrained (Davey and Thomas, 1950). Load was applied initially by means of hydraulic jacks and later by airbags, as depicted in Figure 2.2. The specimens constrained at the edges were found to fail at higher loads than those that were simply supported. The simply supported specimens tended to fail at the same load as when cracking was initially observed, but the constrained panels sustained further loading following initial cracking due to the occurrence of arching in both directions. The ultimate load of the simply supported specimens was more than doubled when a considerable vertical surcharge of 500 kN was added. The failure pattern shown for one of the specimens was typical of a yield line type failure, as shown in Figure 2.3, although no reference to the exact support conditions used for the test was made. It should be noted that the specimens were of significant thickness, at 225 or 343 mm, and no dimensions were given for the panels' overall size.

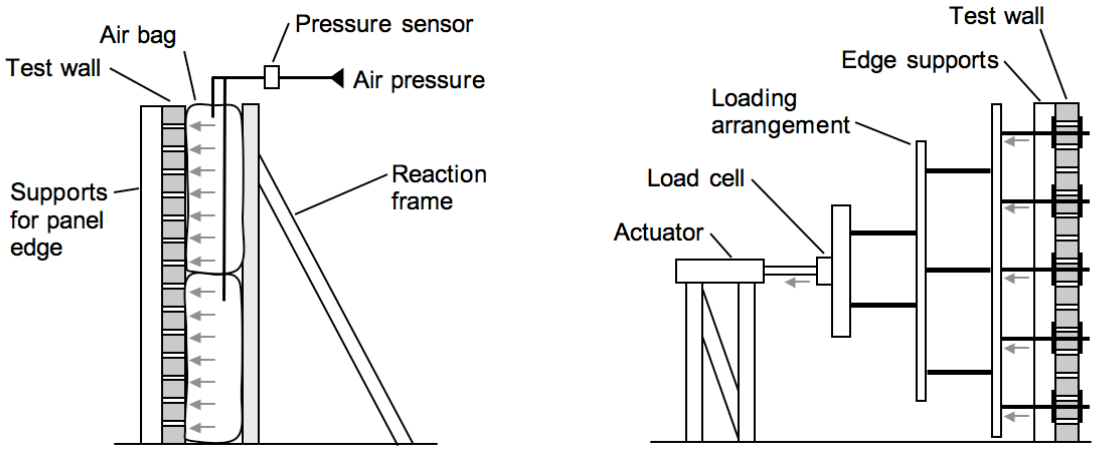


**Figure 2.2.** Typical testing arrangements for laterally loaded wall panels: (a) air bag loading and (b) hydraulic jack loading

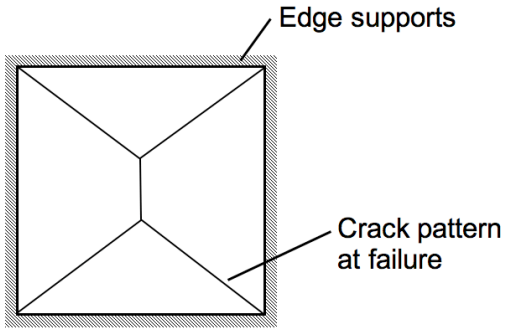


**Figure 2.3.** Failure mode found for a laterally loaded wall panel supported on all edges (Davey and Thomas,1950)

It was recognised (Hendry, 1973) that even though the code of practice (BSI, 1970) in place at the time provided a requirement for wind loading there was a deficiency in the understanding of the strength of masonry wall panels when subject to lateral loads. A series of tests were therefore carried out on masonry wall panels to establish the failure modes and ultimate loads, and provided vital data to enable the assessment of design methods to be completed (Hendry, 1973). Tests were conducted at model (1:6) scale and the uniform lateral loading was applied by means of an airbag. Specimens of different aspect ratios, thicknesses and edge support conditions were assessed in the study, and in addition small specimens were tested to assess tensile strengths. It was found that the shorter wall panels tended to fail at higher loads and also showed a stiffer response when compared to the longer walls. Panels simply supported on all edges failed at higher loads than those with the top free and the modes recorded were similar to classical yield line patterns established for reinforced concrete (Johansen, 1972), as presented in Figure 2.4.

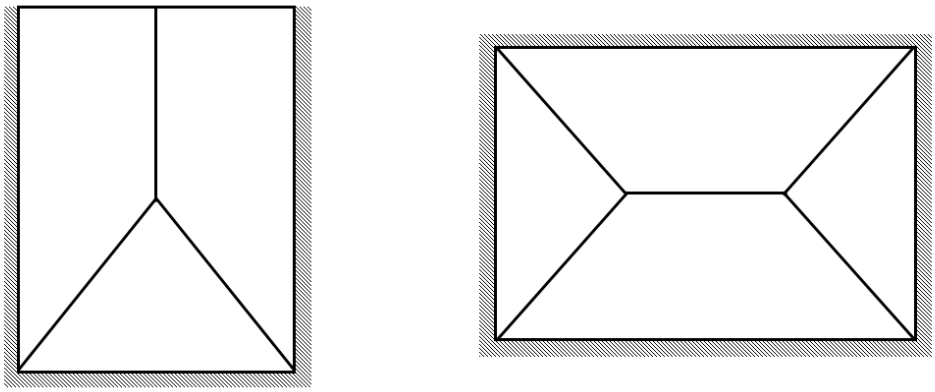

(a) (b)

**Figure 2.4.** Failure modes found for panels simply supported on (a) 3 edges (top free) and (b) 4 edges (Hendry, 1973)

At this time a number of other researchers began to experimentally investigate the strength of masonry wall panels subject to lateral loads as is discussed in the following section. The aim of the programme of work was to provide experimental results for the verification of theoretical methods (Edgell, 2005, West et al.,1977), such that design provisions could be incorporated into the draft standard that would later become the Code of Practice for the use of masonry (BSI, 1978).

Lateral loading tests of concrete block specimens were completed (Anderson, 1976) using a hydraulic actuator and framework to evenly distribute the load over the specimen, as shown by Figure 2.2b. All panels were tested with the top free and either simple supports or fixed supports, in the form of returns, at the vertical edges. The ultimate load was found to increase when the vertical edges were restrained compared to those that were simply supported for panels of the same loaded length. Increasing the material thickness from 90 to 190 mm resulted in almost a quadrupling of the ultimate loads. As was observed in the study completed with 1:6 scale brick specimens, as was discussed above (Hendry, 1973), longer walls tended to fail at lower loads and were of lower stiffness. Similar yield line type crack patterns were observed in the specimens and were in line with those recorded in previous studies, as shown in Figure 2.4a.

The findings of an extensive study were reported (West et al., 1977) where a number of different parameters were considered to evaluate their effect on the performance of the wall panels, including: aspect ratio, support conditions, masonry type and mortar type. Different lengths (1.5 to 5.5 m) of single storey wall panels were tested with the vertical edges partially restrained and the top edge free. The ultimate load was found to reduce with both increased length and lower mortar strength. The majority of the specimens failed in a yield line pattern in line with that observed in previous studies, as shown in Figure 2.4, although slip at the damp proof course occurred in some tests leading to a horizontal spanning type failure. As was established in previous research, adding restraint at the top edge of the wall panels increased the ultimate loads. Further tests completed with specimens of varying height (1.3 to 3.6 m) found that the ultimate load increased as specimen height decreased. Brick and block cavity walls were tested with butterfly and vertical strip type wall ties, where the latter were found to be better at transferring load between the two leafs. The ultimate loads of the cavity walls were generally found to be equivalent to the sum of the values for the individual leaves and it was possible to improve the performance by incorporating additional ties.

A series of tests were reported (Sinha, 1978) of 1:3 scale wall panel specimens that were manufactured with M12 compressive strength mortar containing a rapid setting cement. Wall panels equivalent to a single storey height were simply supported at the horizontal edges and fully restrained at the vertical edges. The vertical edge supports comprised a masonry return, which was pre-stressed to ensure failure occurred in the wall rather than the in return. A number of aspect ratios were considered and the height was generally maintained constant during the study. As was found in previous studies, the ultimate load decreased with increasing panel length, although this relationship diminished at larger aspect ratios. It was not clear why a mortar of such high compressive strength was utilised and why rapid setting cement was incorporated in the manufacture of the mortar. Further tests were completed (Sinha et al., 1979) of wall panel specimens of different aspect ratios, where one vertical edge was left unrestrained. The wall panels were again manufactured at 1:3 scale and utilised a M12 compressive strength mortar. Similarly to the results for the panels with both vertical edges restrained, the ultimate load decreased with panel length. The wall panels that were previously tested (Sinha, 1978) with both vertical edges fixed were not identical in size, but the most comparable specimens attained loads in excess of double of those found for wall panels with one vertical edge free (Sinha et al., 1979). Failure modes were not given for any of the specimens in either study.

As part of a wider investigation of the flexural strength characteristics of concrete and autoclaved aerated cement (AAC) blocks (de Vekey and West,1980), the findings of uniform loading tests on wall panel specimens were also reported. The wall panels were all of single storey height and were constructed using an M4 compressive strength mixture mortar. Panel lengths of between 2.6 and 5.5 m were tested and the ultimate load was observed to decrease with length, which was in line with the results discussed above for brick specimens. Very little additional information was given, particularly with regards to support conditions or failure modes, although it was likely that the panels were tested with the top free and all other edges supported as per the previous study conducted with brick specimens (West et al, 1977) as discussed above.

A series of tests were carried out (Anderson, 1984) to evaluate if wall panels subject to uniform lateral loads could act as arches when positioned horizontally between rigid abutments. The test jig was designed such that no horizontal support was offered at the base of the specimen and a jack was utilised at one vertical support to

enable the level of thrust to be maintained during the test. Relatively small specimens were tested in the programme of three blocks in height and up to eight blocks in length. It was initially found difficult to sustain the thrust at the vertical supports, however after strengthening the test jig it was observed that the wall panels did form three pinned arches that spanned horizontally. Significant thrusts were recorded at the vertical supports of up to 247 kN/m and the ultimate loads attained were between 3 to 9 times that of initial cracking.

Previous testing programmes had only generally evaluated the performance of individual wall panels and in actual buildings there are likely to be more complex interactions occurring at the junctions between different elements. To examine the robustness of a complete building, a full-scale two-storey prototype house was constructed in a laboratory complete with roof and floor structures (Templeton et al., 1986). In one of a series of tests on the house the gable wall of the building was subject to uniform lateral loading using a series of air bags. Cracking was found to occur at a load equal to approximately a third of the total load applied to the gable wall. Loading was continued until significant cracking was observed, but was halted prior to collapse to allow investigation of the damage to the structure. Limited cracking was observed in the ground floor wall and was generally along the DPC. The first floor and roof joist junction appeared to provide support to the first floor wall, leading to a yield line crack pattern. The apex panel, to the ridge, was adequately supported at the junction with the rafters, but horizontal cracks suggested it was spanning vertically. Cracks also developed in the perpendicular walls and were stated as being due to tension developing as the gable wall deflected. Little mention was made of the wall ties, with only one section detailed as failing along the edge of the apex panel, suggesting they performed their load transfer function adequately. It was concluded from the study that the recommended support and tying methods detailed in the building regulations resulted in a conservative design for withstanding such loads (Edgell and de Vekey, 1986).

The results were presented (West et al., 1986) from the continuation of the experimental programme that was first reported in 1977 (West et al., 1977). Further tests of brick wall panels were conducted of different heights, lengths and thicknesses. The lateral strength of the brick wall panels were found to increase significantly with thickness, for example the strength of a storey height wall panel of length 2.7 m was more than tripled when the thickness was increased from 102.5 mm to 215 mm. As previously found the lateral strength was found to reduce as the

length or height of the panel increased and was valid for the different thicknesses investigated. Results were also provided for a series of tests on single storey height blockwork walls of both concrete and AAC of different lengths and thicknesses. Various support conditions were examined, including: all edges supported, top free, vertical edge free, vertical and horizontal spanning. The ultimate loads were found to more than double for the concrete blocks and triple for the AAC blocks when the thickness was increased from 100 to 200 mm. Again the ultimate load was found to decrease with panel length and incorporating a simple support to the top of the AAC block panels improved the performance. The ultimate loads of the vertically spanning panels, tested with both vertical edges free, reduced by a significant 74 % when compared to the panel supported on all edges. Little discussion was given to the results from the one way horizontally spanning wall panels that failed in an arching mechanism and the ultimate loads were found to vary between repeat tests, suggesting some difficulties may have been encountered in the procedure. The results from cavity wall panels were not presented, however as a general conclusion to the extensive work programme it was stated that the ultimate loads of cavity wall panels were always found to be at least equivalent to the sum of the strength of the individual leaves.

A comprehensive study of single storey high (2.6m) AAC blockwork walls was completed and the effect of length, unit thickness, support conditions and cavity construction were investigated (de Vekey et al., 1986). As was found with brick specimens previously tested, the strength of the single leaf walls increased with greater support at the edges. A number of one way horizontal spanning walls were also tested and although it was found that arching action occurred in some cases, the behaviour was affected by the quality of construction. Failure patterns were also in line with the yield line types observed in the tests with brick units. The ultimate loads sustained by the cavity walls (AAC or brick and AAC) tested were at least equivalent to the sum of the individual leaves when sufficiently stiff ties were incorporated and was in agreement with the findings of previous studies. It was observed that the unloaded leaf or both leaves cracked during the tests, but this did not appear to be dependant on the material type (brick or AAC block) used for the leaves.

Single storey brick and block wall panels were tested to assess the effect of unit geometry on the ultimate load (Gairns and Scrivener, 1988). The panels were of various lengths, but were all simply supported on four edges. It was reported that

uplift had occurred at the corners of wall panels tested prior to the commencement of this programme of work. To avoid uplift the panels were clamped to the supports at the top and bottom corners, although no comment was made to the deviation from true simple support conditions. Block specimens were shown to be weaker, failing at lower loads than the brick walls. The two materials showed different behaviour in lateral loading and was suggested that allowances needed to be made in calculation methods for this. Variations were attributed to difference in the dimensional format of the material and unit self-weight. The effect of imposed vertical loading was also stated as having a significant effect on both the vertical and horizontal moment resistance, although was not considered in the experimental study.

A series of tests of masonry wall panels were conducted (Ng, 1996) at 1:2 scale and the effect of aspect ratio, where both the height and length were varied, was considered. Support conditions of simple supports at all edges, vertical edge free and top edge free were examined in the programme. Wall panels were constructed using M12 compressive strength mortar and a rapid hardening cement. Support reactions, strains on the surface of the wall panel and deflections were measured during the tests. The ultimate loads obtained for the panels with all edges simply supported and the top free were quite similar and may have been influenced by the short panel lengths, of up to 2.4 m at prototype scale, examined in the study. The panels with the vertical edge free however attained an ultimate load of about half of the panel with the top edge free, which was attributed to the anisotropy in the flexural strengths. Failure modes were generally in line with yield line patterns as discussed above. For panels where some initial cracking occurred prior to failure it was observed that the magnitude of the strains in the direction of cracking reduced, whilst those in a direction perpendicular increased.

The use of thin joints between masonry units has been gaining popularity due to speed of construction and improved thermal performance, however little data regarding the performance under lateral load is available. The results of a study carried out to assess the strength of thin joint masonry wall panels was reported (Fried et al., 2005). The specimen were constructed from two different strength grades of dense concrete blocks of the same thickness. Wall panels of relatively small dimensions were simply supported on all edges and subjected to uniform lateral load by means on an airbag. The specimen constructed from the stronger block failed at a higher lateral load, but both were observed to have similar failure patterns. The failure modes were dissimilar to the yield line pattern as shown in

Figure 2.4b and were more akin to patterns observed in one way spanning panels. The high bond strength between the block and mortar and small panel dimensions may have influenced the failure modes observed.

### 2.4.2 Wall panels with openings

The ultimate loads for a number of single storey high brick wall panels with openings were reported (West et al., 1986) and were of lengths between 2.7 and 5.5 m. However, no details were given on the size of the opening and the method employed to cover the opening during test. In light of this it was difficult to make any further assessment of any possible effects of the openings on the ultimate loads of the wall panels.

A series of storey high wall panels with central openings, constructed at a reduced 1:2 scale, were tested and the effect of aspect ratio and support conditions were investigated (Duarte, 1998, Duarte and Sinha, 1992). M12 compressive strength mortar with rapid hardening cement was used to manufacture the wall panels. The wall panels were equivalent to a single storey high panel (2.4 m) at prototype scale and lengths of between 2.4 and 3.6 m were considered. In all cases the window was of identical dimensions and positioned centrally, offset to the right or to the top of the panel. The support conditions considered were simple supports on all edges, top edge unsupported or vertical edge unsupported. A wooden board was used to cover the opening in all tests, however blocks were placed at the corners of the board, which resulted in point loads being induced at the corners of the opening. The authors seem to suggest that there may have been some issues with placing a wooden board over the opening without the wooden blocks, although they did not provide any detail with respect to the problems or reasoning for the approach taken. The assumption of point loads may not have been truly representative of the actual conditions in a wall panel with an opening, where line loads may be more likely around the perimeter of the opening. It was difficult to make a judgement on the effect of the opening on the ultimate load since control panels without openings were not tested. The ultimate load was however found to decrease with panel length and also decreased with the reduction of edge supports as was found by others as discussed above. Positioning the opening to the right of the centre increased the ultimate load by 17 % for fully simply supported panels, whilst positioning the opening at the top of the panel with the top edge free increased the ultimate load by 6 %.

A study investigated the lateral strength of a number of single storey wall panels with and without openings manufactured from both brick and block (Chong, 1993, Chong et al., 1991, Chong et al., 1992). Two cavity wall panels were also constructed in the programme. The panels were all single storey in height, were of lengths of either 2.9 or 5.6 m and manufactured using M4 compressive strength class mortar. Window frames were built into the openings in the panels and filled with wooden board in lieu of glass, although no fixings were inserted into the masonry. Three different sized window openings and a door sized opening were positioned in panels. The strength of the single leaf brick wall panels with openings was found to reduce by between 17 and 36 % compared to the corresponding wall panel without an opening, whilst for the block specimens a greater reduction of 51 % was reported. The strength of the cavity wall panel without an opening was similar to the sum of the strength of the individual leaves. The cavity wall with an opening attained a strength equal to 80 % of the sum of the strength of the individual leaves and the deviation was suggested due to absence of the board in the frame of one of the leaves. Failure modes observed in the cavity specimens were in line with those found in the corresponding single leaf specimens.

The findings of a series of tests of wall panels with and without openings were reported (Edgell and Kjaer, 2000) that were part of a study that was initiated to investigate the suitability of yield line analysis and commercially available software packages for computing the ultimate loads of such panels. A number of variables were considered in the study, including panel length and height, opening position, and edge support conditions. The opening was positioned centrally, to the top or the side of the wall panel and was generally large in proportion to the area of the wall. A window frame was not fitted to the opening, but instead was covered with a wooden board during testing. It was observed that the opening caused a reduction in the ultimate load of between approximately 7 and 68 % when compared to the results from control specimens without openings. The highest reduction in the ultimate load (68 %) was recorded when the opening was positioned to correspond with the vertical free edge of the specimen.

### 2.4.3 Wall panels subject to combined lateral and vertical loads

Lateral loading tests, using air bags, were completed of single storey brickwork walls subject to axial pre-compression (West et al., 1971). Single leaf and cavity walls were examined in the study and the effect of different materials and support conditions were considered. The testing arrangement permitted the single leaf and

cavity walls without vertical supports (returns) to be tested with pre-compressive loads of up to 600kN/m. The walls without returns were short, at 1.37 m in length, in comparison to their height and so were found to fail as a three-pinned arches. The compressive strengths of the unit and mortar combinations tested were found to have little effect on the ultimate load. It was established that the ultimate load of the cavity walls was equivalent to two thirds of the strength of the sum of the individual leaves. Increasing the tie density had no effect on the ultimate load of the cavity wall however a significant strengthening effect was observed when the cavity was filled with polyurethane foam and this suggested that the wall ties did not permit full composite action to occur. The behaviour was different to that reported for the two-way spanning panels discussed above, where the strength was generally equivalent to the sum of the strength of the individual leaves, and may have been influenced by the different support conditions. Slightly longer single leaf walls, of 2.1 m length, built with returns at their ends were found to fail at loads that were approximately double those recorded for the wall panels without returns. Walls with returns acted as two-way spanning panels and were recorded as failing in a yield line pattern, likely as shown in Figure 2.4b, rather than as a three-pinned arch. The testing arrangement only allowed the wall panels with returns to be vertically loaded up to a maximum of 73 kN/m. It was also noted that the walls tended to extend in height during test and pressure applied to the top of the wall had to be relieved to maintain a constant axial load.

Further tests of single storey cavity wall specimens of lengths between 1.22 to 4.72 m were reported (Hendry et al., 1971). To more realistically simulate axial loading conditions the test walls were built into the ground floor of an experimental five storey structure and all vertical loading was applied to the inner leaf only. Hydraulic jacks or air bags were used to laterally load the walls and it was found that with increased length of the test wall the ultimate loads tended to decrease. The walls without returns failed as three pinned arches and the inclusion of returns increased the ultimate loads, and this behaviour was in line with that established in the previous study (West et al., 1971) as discussed above. The short walls with returns tended to fail at the returns and then act as three pinned arches, whilst the longer walls showed a yield line type failure, in line with that presented in Figure 2.4b. Similar levels of uplift, at the top of the wall panels, were observed (Hendry et al., 1971) to those found in the previous study (West et al., 1971).

Slender wall specimens, unsupported at their vertical edges, were subjected to combined vertical axial and lateral load to assess the interaction between the two forms of loading (Bean Popehn et al., 2008). The wall panels were constructed from both brick and block masonry units and subject to vertical axial loads up to 462 kN/m. A reasonably linear load-deflection relationship was observed before cracking, after which the walls tended to fail as a three pinned arches, which was in line with the findings of the studies discussed above (Hendry et al., 1971, West et al., 1971. The concrete block specimens sustained higher lateral loads than the clay brick walls and was due to the difference in unit thickness.

### 2.4.4 Tests to determine mechanical properties of masonry

#### 2.4.4.1 Flexural strength

Researchers have generally conducted tests of small masonry assemblages alongside tests of masonry wall panels in order to establish parameters for theoretical analysis. Masonry prisms were tested (Hendry, 1973) to determine the flexural strength parallel to the bed joints, whilst wallette specimens were used to establish the flexural strength perpendicular to the bed joints (direction 2), as shown in Figures 2.5a and 2.5b respectively. The flexural strength was found to increase as the mortar strength was increased from M4 to M12 compressive strength class and exceeded code requirements (BSI, 1970) relevant to the period of the investigation. It was reported (Hendry, 1973) that no account was made in the code (BSI, 1970) for the variation of flexural strength with mortar strength.

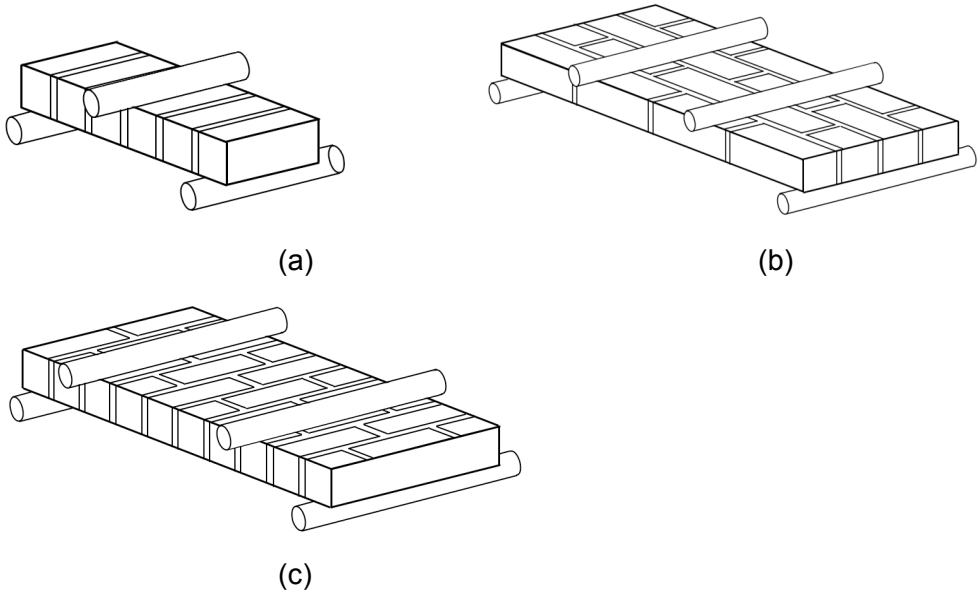


**Figure 2.5.** Masonry specimens to determine flexural strength: (a) prism specimen for strength in direction 1, (b) wallette for strength in direction 2 and (c) wallette for strength in direction 1

Masonry prisms constructed from concrete block were tested (Anderson, 1976) and the size and support configurations utilised were found to have little effect on the flexural strength values obtained. The effect of size, support conditions and preload during testing were also investigated for concrete block wallettes that were tested to determine the flexural strength in direction 2. It was found that the wallette size and support conditions did not significantly influence the magnitude of the flexural strengths. There appeared to be some effect of preload on the flexural strength that was more evident in the thinner 90 mm specimens, however control wallettes with zero applied load of the same format were not tested. The failure mode was influenced by the preload, where failure generally occurred through the mortar joints and units when zero preload was applied and was restricted to the mortar joints near the edge of the specimen when preload was applied. The failure mode was likely influenced by the method used to apply the preload, which imposed a load at a localised point rather than distributing the load uniformly along the wallette.

An extensive study of wallette specimens was conducted (West et al., 1977) in order to evaluate the flexural strength of masonry. A number of different types of brick masonry units and mortar types were considered in the study. Two separate wallette specimens were tested in order to determine the flexural strength in direction 2 and direction 1, as shown by Figures 2.5b and 2.4c respectively. The masonry's flexural capacity was found to increase slightly with higher mortar strength, but more so as the water absorption rate of the brick diminished. The strength of the wallettes tested in the perpendicular direction was typically three times that of those tested in the parallel direction. Tables of characteristic flexural strengths were determined from the wallette test results for use with the proposed yield line design method (Haseltine et al., 1977), and these incorporated the variation in both mortar strength and water absorbency.

A series of wallettes were constructed with the perpendicular joints left unfilled to assess the effect of this on flexural strength (Sinha et al., 1979). It was often commonplace to leave these joints unfilled, generally on walls that were hidden on the inside of structures to save time and materials. The effect of leaving these joints unfilled resulted in a 44% reduction of flexural strength in both test directions. It was perhaps interesting that leaving these joints unfilled provided such a significant effect on the strength in the direction 1 (Figure 2.5b). It should be noted that the format of the wallettes differed to those shown in Figure 2.5 and may have been attributed to them being carried out before the introduction of the masonry standard (BSI, 1978).

The results from a comprehensive set of tests on blockwork wallettes were reported (de Vekey and West, 1980) that were carried out in order to establish characteristic strengths to be incorporated into the standard (BSI, 1978). Blocks of lightweight and dense aggregate as well as AAC were tested and the effect of mortar compressive strength, water absorption, unit compressive strength, unit thickness, suction and density on the flexural strength were examined. The flexural strength of all the block specimens in direction 1 was found to be only dependant on the compressive strength class of the mortar, regardless of the block type. In direction 2 relationships were derived for several of the factors examined, but the most suitable parameters were established as the mortar compressive strength class and unit compressive strength. Increased unit thickness, from 100 to 215 mm, had the effect of reducing the flexural strength in both directions.

A comparative study was completed to examine the effect of specimen format on flexural strength (Fried et al., 1986) and it was found that the flexural strength in direction 1 obtained from tests on prisms exceeded that of tests completed on wallettes. It was suggested that the difference in strength was attributed to the interaction of the perpendicular mortar joint in the wallette specimens. Conversion factors were proposed such that the equivalent wallette flexural strength in direction 1 could be obtained from experimental tests on either prisms or individual joints, such as the couplet or bond wrench test. Further conversion factors were given to establish the flexural strength in direction 2 from identical experimental tests. The wallette tests given in the standard (BSI, 1978) were more suited to laboratory environments and simplifying the test procedures to either a pier or bond wrench test would be more appropriate for on site quality control.

A theoretical approach was developed that derived the flexural strength in direction 2 from a combination of the strength of the mortar joints in the perpendicular direction and a torsional shear resistance (Curtin, 1986). Considering this it was proposed (Curtin, 1986) that the flexural strength in direction 2 could be calculated from the flexural strength in direction 1 and a multiple of the shear strength of the masonry. The derivation of the method implied that failure in direction 2 was due to tensile failure in the perpendicular mortar joints and shear failure in the bed joints, so may not be applicable if failure occurred through the units themselves. Experimental procedures were not completed to confirm the relationship, but some correlation was shown to the results of previous researchers. It was found that the theoretical results displayed a reduction in the orthogonal ratio of flexural strengths as mortar strength

was reduced, which was also observed in the experimental results used for comparative purposes. The standard (BSI, 1978), however provided a reasonably consistent orthogonal ratio for brick masonry regardless of mortar strength and was suggested (Curtin, 1986) to be due to the conservative design approach employed in the standard. It was noted (Curtin, 1986) that the theoretical approach was simplified mathematically and a number of assumptions were made regarding the shear effect.

The effect of varying a number of parameters on the flexural strength of brick and block wallette specimens was examined (De Vekey et al., 1986, West et al., 1986). A number of the parameters investigated were concerned with on-site variables and included: moisture content (condition), mortar joint thickness, grading of aggregate, quality and curing conditions. Both brick and block specimens were sensitive to the moisture condition and the highest flexural strengths were generally obtained when the units were conditioned prior to laying. Reducing the mortar joint thickness was reported to significantly increase the flexural strength in direction 2 of brick specimens, but did not affect the strength in direction 1. The flexural strength was influenced by the grading of the sand and was reduced when the grading became either increasingly finer or coarser compared to building sand (0 to 2.36 mm grading) utilised in the study. The quality of the brick laying resulted in a reduced flexural strength and the greatest effect was observed for the weaker M4 compressive strength mortar compared to M12 strength. The requirements of the standard (BSI, 1978) were not attained when the workmanship was very poor when M4 mortar was used. Maintaining a polyethylene covering over the wallettes for a curing period of 28 days was not always reported to have resulted in higher flexural strengths, but was suggested to be more important for attaining consistency between similar specimens. The findings illustrated the importance of appropriate on-site control measures for designs that utilised the flexural strength of the masonry.

To examine the effect of unit size a series of wallettes were built from block materials, but utilising a brick sized unit (de Vekey et al., 1986). It was found that the strength of the specimens in direction 1 were comparable regardless of unit size, however a significant increase in the flexural strength in direction 2 was given for the brick sized units. It was suggested that the increased strength in direction 2 may have been due to the increased number of mortar joints in the specimen, which permitted a higher strain capacity, and the difference in the specimen test format. In further tests the format of the specimen was found to influence the flexural strength of the block specimens, where a reduction in size resulted in a slightly lower strength

and also a higher coefficient of variation. It was also found that values for block wallettes originally included in the standard (BSI, 1978) were lower than those achievable in tests (de Vekey et al., 1986). Differences were attributed to the specimen size, position of the supports in relation to the mortar joints and the moisture content of the units. An improved manufacturing procedure and specimen format was proposed for the block specimens and was included in the revision of the standard

Small cross beam specimens were tested in flexure (Ng, 1996) to establish the bi-axial failure criterion necessary for the proposed theoretical finite element analysis (FEA). The advantage of the cross beam test over wallette tests was data could be provided in both test directions simultaneously. Load was applied to the centre of the cross beam assembly and the reaction forces were measured at the supports, which enabled the bi-axial load behaviour to be established. Load shedding was observed in the test specimens when cracking in one direction preceded the other. Upon cracking a residual load capacity was observed in the cracked direction, but the majority of the load was transferred to the un-cracked direction.

A series of wallette tests of thin joint masonry were complete, where the specimens were constructed using blocks of two different compressive strengths (Fried et al., 2005). The flexural strength of the wallettes was found to increase with the compressive strength of the block, although a different failure mode was observed in the direction 1 specimens. Failure occurred through the blocks or along the mortar joint, in the stronger and weaker blocks respectively, and was suggested as being due to different properties at the block interface. Characteristic flexural strengths were compared to the British standard (BSI, 2005a) for specimens of ordinary mortar and found to be significantly higher. No comparison was made to the Eurocode standard (BSI, 2005c) that included specific values for thin joint mortars, but when checked the experimental values still exceeded the code.

#### 2.4.4.2 Cavity wall ties

Cavity wall ties are thought to have been in use since the 19$^{th}$ century in the UK, but guidance on their use was not introduced until more recently (de Vekey, 1986). Early tests of wall ties were completed for butterfly and strip type ties that were built into brick couplets and it was found that the latter type was significantly stronger in both tension and shear (Thomas, 1968). The behaviour in compression and shear was also observed to vary with mortar strength, with higher values attained with M4

compressive strength mixes or stronger. Higher tensile strengths for the butterfly ties were given when one end was built into a storey high wall panel, suggesting some effects due to pre-compression. Recommended working loads for the ties in compression and shear were determined from the findings. Compressive, tensile and shear strength characteristics along with minimum spacing requirements and embedment lengths were later provided in the code of practice for the structural use of masonry (BSI, 1978).

Characteristic design strengths provided in the British Standard were for standard types of wall ties and precluded the use of others, due to lack of design data. In addition the durability of wall ties was in question due to an increasing amount of failures in service (de Vekey, 1986). To enable strength and durability to be assessed, standardised test methods were developed that were similar to those used in previous research (BSI, 1986, BSI, 2000a, BSI, 2000b). Detailed information for the design of wall ties, including assessment of loading due to the action of wind to calculate the required density, was provided in a draft standard (BSI, 1987). Ties were now grouped into a 'type' rather than being classified by their shape according to their typical use. Similarly the masonry code of practice was updated to include the same terminology and additional guidance was provided for the treatment at edges, such as openings (BSI, 2001a, BSI, 2005a, BSI, 2005b). The guidance in the Eurocode regarding wall ties is fairly limited, compared to previous standards, requiring either a minimum installed density or design according to the assumed wind loading (BSI, 2005c).

A study was completed (Tutt, 1988) to establish the strength and requirements for replacement ties that would be used in situations where excessive corrosion had rendered the existing ties incapable of transferring loads from one leaf to the other. Two types of ties were examined in the study: resin anchored and expansion type, whilst tests were carried out of both couplets and ties installed in wall panels. It was established that the strength of both types of replacement ties exceeded the strength of butterfly type ties in compression and tension. Using replacement ties may also present an opportunity to improve the performance of existing cavity walls when subject to lateral loadings, in addition to replacing defective ties.

## 2.5 Theoretical analysis of the strength of masonry walls subject to uniform lateral loads

### 2.5.1 Yield line analysis

Yield line analysis was developed for the assessment of the ultimate strength of reinforced concrete wall panels subject to lateral loads (Johansen, 1972). Although concrete is generally a brittle material on its own, the use of steel reinforcement enables elastic-plastic behaviour to occur. When reinforced concrete is subject to lateral loads beyond the elastic limit cracks propagate from the point of highest moment towards the supports (Jones, 1962). The cracked section can still sustain tensile forces in section due to the presence of the reinforcing steel. The concern raised by many workers in the field of masonry (Hendry, 1973, Haseltine et al., 1977, Sinha, 1978) was that since un-reinforced masonry was considered brittle, once a crack developed no tensile strength would be sustainable. It has, however, been reported that masonry can retain some strength beyond the elastic limit (Brincker, 1984, Haseltine and Tutt, 1986), which has been suggested to be associated with arching and friction between the masonry units (Lourenco, 2000). As will be discussed in the following section, masonry wall panels subject to uniform lateral loads have generally been modelled with acceptable correlation to the experimental failure patterns and ultimate loads using the yield line theory. The composition and manufacturing process of masonry panels results in a degree of natural inherent variability, which must also be considered when applying the yield line method. Two approaches have been considered to establish the moment of resistance: flexural strength obtained from wallette tests or a friction/overturning resistance and are considered separately in the following section.

#### 2.5.1.1 Yield line analysis utilising flexural strength

Values calculated by yield line analysis were reported (Hendry, 1973) to significantly underestimate the experimental strength of the wall panels, however no details of the actual values calculated were provided. The flexural strengths used in the analysis were determined from experimental tests on prisms and wallettes as discussed in Section 2.4.5. The analytical strength correlated well to the experimental strength when a single value of flexural strength was utilised in the analysis, although no details were given on which strength was used in the procedure. It is questioned why such an approach of using only one value of flexural strength was taken, particularly since it was established (Hendry, 1973) that the strength was significantly different in directions 1 and 2. It was concluded (Hendry, 1973) that the methods available for the calculation of ultimate loads of panels supported on all edges or with the top free

may not be completely suitable and that further experimental tests were required to make an improved evaluation.

The ultimate loads calculated (Anderson, 1976) for concrete block wall panels using the yield line method from the draft masonry standard (BSI, 1978) were found to be approximately half the experimental values. A series of tests were completed (Anderson, 1976) to determine the flexural strength from concrete block wallettes as discussed in Section 2.4.5, however the values adopted in the analysis were from the masonry code and were significantly lower. It was not clear why a comparison was not performed using the experimentally derived flexural strengths, but it would be likely that an improved representation of the experimental wall panel strengths would have been given if this approach were taken. No comment was given on the values given by the analysis and no investigation was completed to assess if the experimental failure modes were similar to the theoretical yield line patterns (Anderson, 1976).

The ultimate loads computed by yield line analysis (Haseltine et al., 1977) were compared to the results from an extensive experimental study (West et al., (1977), which was previously discussed in Section 2.4.1. The theoretical results generally followed the experimentally established values reasonably well and were on average within 19 %. The method overestimated the strength of shorter walls, but these walls had been observed to have a tendency to fail as one way horizontally spanning slabs rather than as two way spanning that was assumed in the analysis. The yield line method was also advantageous since the correct edge restraint conditions could easily be modelled and different strengths in the horizontal and vertical directions could be included. The method was shown to be applicable to cavity walls when the ties were sufficiently stiff to transfer loads. For cavity walls the ultimate loads were then simply determined from the sum of the strengths of the individual leafs.

Based on the findings discussed above (Haseltine et al., 1977) the yield line method was adopted into the draft masonry standard BS5628 Part 1 Code of practice for use of masonry that was published in 1978 (BSI, 1978). The design method employed in the standard was simplified by incorporating tables for bending moment coefficients for different edge restraint conditions and therefore avoided the need to complete the analysis from first principles. The yield line method incorporated in the standard was a limit state analysis approach and characteristic loads were calculated by inclusion of suitable safety factors. Although the method did not directly allow for openings in

the panels, it was proposed that in such cases the wall could be subdivided into sections to allow calculations to be completed.

A fracture line method was proposed (Sinha, 1978) for the calculation of the lateral strength of masonry walls and was essentially a modified yield line method that included elastic parameters. The facture line method was an attempt to account for the variation in stiffness with direction in addition to flexural strength. Values computed using the yield line method were on average 19 % higher than the experimental ultimate loads determined in the same study (Sinha, 1978). The fracture line method provided an improved prediction of the experimental ultimate loads compared to the yield line analysis and were within 1 %. Inclusion of the elastic parameters effectively reduced the flexural strength in direction 2 in the analysis and therefore explained why an improved correlation was observed. Additional tests were however required to establish the elastic modulus in directions 1 and 2 and difficulties were reported in obtaining values from bending tests so values were instead derived from compression tests (Sinha, 1978). The main concern with this method was the need for the additional elastic parameters, which were likely to be complex to determine for the masonry being evaluated (Lovegrove, 1988). Further experimental and analytical results for similar wall panels were reported (Sinha et al., 1979) with where one vertical edge was unsupported. The yield line method was generally found to overestimate the ultimate loads of the wall panels by an average 53 %, however in this case no comparison to the fracture line method was presented. It was not clear why the fracture line method was not considered, particularly since the author had earlier proposed solutions for wall panels with one free vertical edge (Sinha, 1978).

The results from experimental tests of both concrete and AAC block were compared (de vekey and West, 1980) to values computed using the yield line method given in the standard (BSI, 1978). Although little discussion was provided of the results it was found that the strength of the AAC block walls were overestimated by an average 29 %, whilst the concrete block specimens were underestimated by 22 %. The flexural strengths used in the calculations were based on values tabulated according to the compressive strength of the block. The AAC and concrete block compressive strengths were equal so no disparity was given in the analytical results. In addition the results were likely affected by the assumption of fully fixed vertical edge support conditions in lieu of the partial support conditions utilised in the tests.

A design guide was developed to enable engineers to understand and implement the yield line methods presented in the standard and a number of example calculations were included (Morton, 1986). Later to this, a method was presented to allow easier calculation of design loads that was based on the approach in the standard (Golding, 1991). Rather than adopting tabulated coefficients, a graphical approach was utilised to allow calculation of design parameters. Various edge support conditions were represented by different curves in an attempt to avoid the previously required iteration between tabulated values. It was also suggested (Golding, 1991) that non-uniformly loaded panels could be designed by considering the total load applied as an equivalent uniform distribution.

Theoretical values were computed for wall panels using yield line analysis (Haseltine and Tutt, 1986) and compared to the results from a previous experimental study (West et al., 1986, de Vekey et al., 1986) that was discussed in Section 2.4.1. For all wall panel combinations it was found that the yield line method provided an acceptable correlation to the experimental findings when the flexural strength values were based on those obtained form the corresponding wallettes. The effect of self-weight at the base of the panel was correctly considered in the analysis. Values for short walls tended to be over estimated, but this was not anticipated to be problematic as the dimensions of the walls were below those typically used in design. Cavity walls were dealt with as previously discussed, by summating the calculated loads for individual leafs, and compared well to the experimental values. A summary of a number of results for walls with small or large openings positioned at the centre and the top unsupported were also presented. It was established that the presence of glazing or simple supports to the opening had little effect on the experimental loads. A reasonable correlation to the results from yield line analysis was observed for the panels with openings. The method given in the Standard (BSI, 1978) was also applied (Haseltine and Tutt, 1986) using the tabulated characteristic values of flexural strength. It was found a factor of safety of 3 was attained by all specimens, except those of thickness over 215 mm where a safety factor of 2.5 was reached, on application of the method in the standard. It was suggested (Haseltine and Tutt, 1986) that despite masonry being a brittle material that the non-linear behaviour observed in the experimental tests and the capacity to sustain loading following initial cracking partly justified the application of the yield line method. Variability in the results was also partly though to be due to the complex failure modes particularly in direction 2 where a combination of tensile failure, crushing and torsional shear failure occurred. It was concluded that despite the lack of full theoretical justification for the

use of the yield line theory with masonry it allowed characteristic loads, if a little conservative in some cases, to be determined.

A proposal was made (Lovegrove, 1988) that the yield line method could be correctly applied to masonry if the energy to produce a crack was considered in place of the moment resistance. The method still required wallette tests to be completed, but the level of energy was determined rather than the moment. Using this approach resulted in essentially the same end equations and ultimate loads, so the real difference is questioned. It was also suggested that differences in actual and theoretical results could in some cases be due to a combination of shear and bending failure occurring, which the yield line analysis did not account for.

Theoretical values were calculated using yield line analysis for a series of wall panels that were constructed from either brick or concrete block (Gairns and Scrivener, 1988). Yield line analysis provided the best correlation to the experimental values when compared to the elastic or strip methods, but was found to overestimate the strength of the bricks specimens. The yield line patterns utilised in the analysis were not given, so it was difficult to make a judgement on how accurately the experimental failure mode was modelled.

The results from a series of experimental tests of wall panels with openings were compared to analytical values calculated by the yield line method (Duarte, 1998, Duarte and Sinha, 1992). The crack pattern for the yield line analysis was postulated for each wall panel and the ultimate load was determined from first principles using the virtual work method. Mean experimental wallette flexural strengths were used to determine the ultimate loads using yield line analysis. An acceptable correlation was found between the experimental results and those found in the yield line analysis, although the method tended to underestimate the experimental loads by an average 8 %. Comparison was also made (Duarte, 1998) to the previously described fracture line method (Sinha, 1978). The fracture line method did not model the experimental ultimate loads as well as the yield line method and generally underestimated the experimental loads by an average 24 %. The differences between the ultimate loads calculated by the yield line method and fracture line method were due to the reasons discussed above.

A yield line analysis of wall panels with and without openings was completed and was compared to the results from experimental tests (Chong, 1993). It was reported

that the ultimate loads computed generally overestimated the experimental values by an average 29 %, whilst the failure modes were modelled well. Very little information was however given on the actual failure modes used in the yield line analysis or indeed the analysis itself. It was not clear how the openings were considered in the analysis and in particular how the loads applied to the opening were dealt with.

Although wall panels with openings had been tested previously and compared reasonably well to results from yield line analysis and other methods, guidance in the standards was limited (Edgell and Kjaer, 2000). In an attempt to address this issue the results from an experimental programme of brick and block panels, with and without openings, were compared to theoretical values calculated using a yield line based design guide and two commercially available software packages. Theoretical results were generally found to be conservative for both the walls with and without openings, but were similar for the different methods. It was suggested that the results might have been affected by basing them on a single set of wallette flexural strengths, rather than on specimens constructed with each wall panel.

The strength of wall panels constructed with thin joints was calculated (Fried at al., 2005) using the yield line method from the standard (BSI, 2005a). It was found that the analytical strength of the walls panels significantly exceeded the experimental values when both the mean experimental and characteristic wallette strengths were utilised. The higher experimental ultimate loads were attributed to the strength of the bond between the block and mortar. The failure modes of the wall panels were different to those assumed in the analysis, although no discussion of this was made. The small dimensions chosen for the wall panels (L 2.65 m x H 1.75 m) may have also affected the results and were perhaps not particularly representative of panel sizes used in practice. It was concluded that the calculation method in the standard should be approached with caution for walls constructed with thin mortar joints.

The calculation methods incorporated into the harmonised Eurocode revision of the masonry standard (BSI, 2005c) were identical to those developed for the British Standard (BSI, 1978), as discussed above. Allowances have been made for different material types by means of a National Annex (BSI, 2005d). The guidance for dealing with openings has remained limited and it is stated that design should be made using a suitable method such as yield line or by FEA. Simplified methods for the design of walls subject to lateral loads are given in Part 3 of the standard (BSI, 2006). A

graphical approach provides limitations to the panel dimensions based on the design load for a limited number of edge support conditions.

#### 2.5.1.2 Yield line analysis utilising friction / overturning resistance

A method was developed to establish the moment resistance for cracked masonry wall panels that was based solely on the self-weight of the material (Martini, 1998). Vertical moments were determined from the overturning resistance by consideration of the static equilibrium of the vertical loads at the point of collapse, as illustrated by Figure 2.6a. Material crushing at the hinge point formed between the two sections was not considered in the method, which effectively implied infinite stress capacity at the interface. The horizontal moment of resistance was determined from the frictional force couple acting at the interface between the units due to the dead load of the masonry above, as shown by Figure 2.6b. Bending about the horizontal axis was suggested to cause a reduction in the contact area between the units and would affect the frictional resistance, but the result of varying this was not considered. A two-way spanning masonry wall panel was examined that was unsupported at the top edge and subject to a uniform lateral load (Martini, 1998). The masonry units were dry laid and therefore the panel had no tensile strength in bending. A yield line method was applied to determine the ultimate load and compared well to the ultimate loads obtained from finite element analysis. The assumed crack pattern for the yield line analysis was in line with that observed in the finite element models, but was dissimilar to the failure mode typically found for masonry specimens tested with the top edge unsupported, as shown by Figure 2.7. A value was assumed for the coefficient of friction in the model, but was not verified by experimentation. It was concluded that further consideration should be given to how the horizontal moments were developed and determining suitable values for the coefficient of friction.

A method was utilised (Kelman and Spence, 2003a) that was similar to described above (Martini, 1998) to determine the moment resistance due to self-weight in cracked sections. The calculation method for the vertical moment resistance was modified (Kelman and Spence, 2003a) to incorporate a compression depth factor that limited the proximity of the hinge point formed to the edge of the section. The use of the compression depth factor avoided the assumption of infinite stress at the interface, which was ignored in the previous method (Martini, 1998). Friction due to self-weight at the unit interface was similarly considered to provide horizontal moment resistance, but was determined using a different lever arm between the applied moment and point of rotation to that previously adopted (Martini, 1998). No

reasoning or theoretical justification was provided with regards to the selection of the particular lever arm used in the method (Kelman and Spence, 2003a). The method proposed was incorporated into a yield line analysis (Kelman and Spence, 2003a) to establish the maximum depth of water that could be retained by masonry wall panels and is discussed in more detail in Section 2.6.

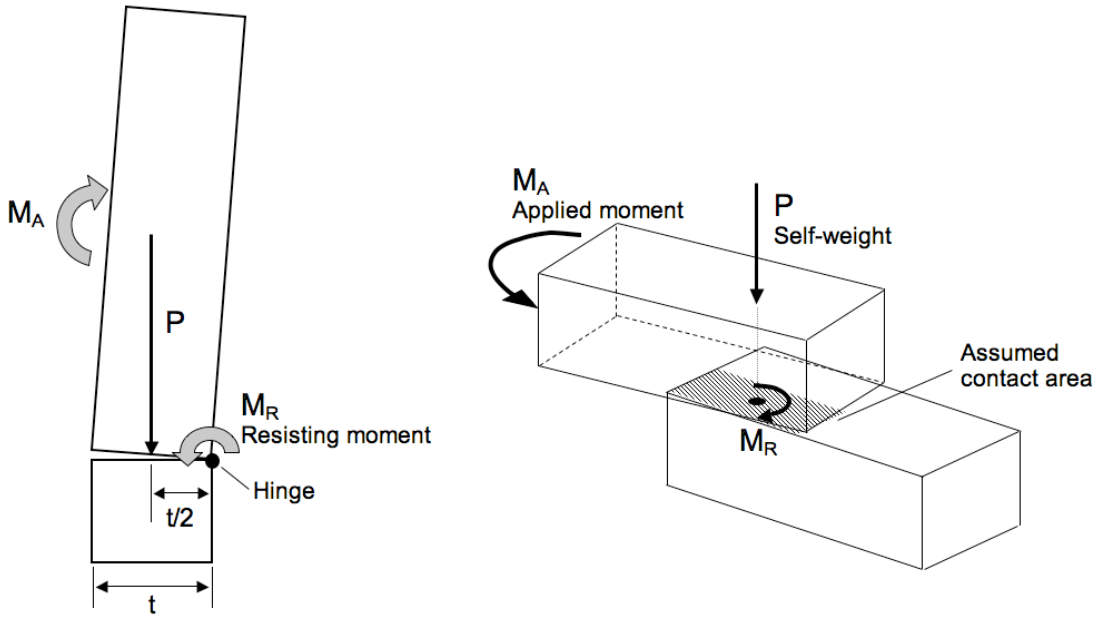


(a) (b)

**Figure 2.6.** Lateral capacity due to: (a) overturning resistance and (b) frictional behaviour at interface between blocks (Martini, 1998)

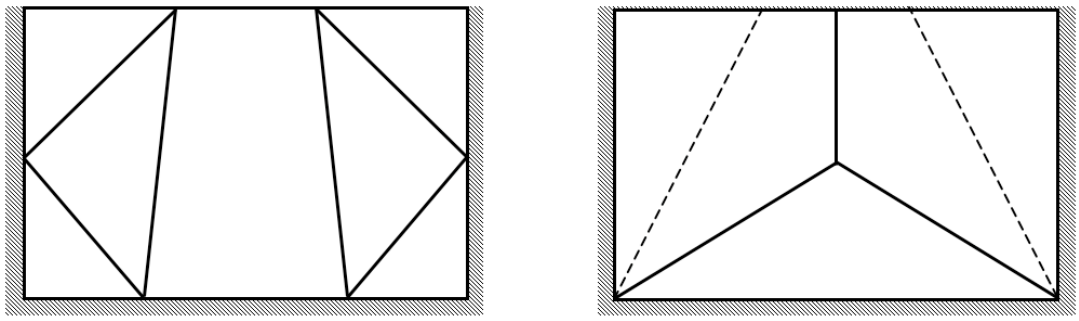

(a) (b)

**Figure 2.7.** (a) Failure mode adopted by Martini (1998) and (b) typical failure modes observed for masonry specimens with the top edge free (dotted lines show alternative mode)

### 2.5.2. Elastic plate and finite element analysis

The following section examines the previous application of both elastic and non-linear models to laterally loaded masonry wall panels to establish the theoretical loads at first cracking or ultimate limit state. Elastic analysis has been applied using plate analysis techniques (Timoshenko and Woinowsky-Krieger, 1959) or by utilising an elastic failure criterion in a Finite Element analysis (FEA). Non-linear failure criterions have also been developed, as discussed below, that have been applied using FEA methods.

Experimental tests (Hendry, 1973), as discussed in Section 2.4.1, were compared to the results from an elastic FEA, where the failure criterion was specified as the flexural strength of the masonry. It was found (Hendry, 1973) that the FEA model was unable to predict the ultimate loads of the experimental specimens with acceptable precision. The inaccuracy of the FEA model was suggested to be a combination of the non-linear stress-strain behaviour of masonry, the elastic parameters used in the analysis and the failure criterion being complicated by the anisotropic behaviour of the masonry.

The results from an elastic plate analysis (Haseltine et al., 1977) were compared to the experimental results of a previous study (West et al., 1977). The results determined by elastic analysis compared well to those of the experimental values and generally underestimated the ultimate loads by an average 22 %. However, it was reported (Haseltine et al., 1977) that the partial vertical edge restraints used in the experimental study could not be readily modelled using the method and were therefore not considered. It was also found that the solutions used provided limited flexibility to deal with wall panels with orthogonal ratios of flexural strengths that differed to those established in the experimental study.

Ultimate loads were computed using an elastic plate analysis (Hasletine and Tutt, 1986) and were generally found to significantly underestimated the experimental ultimate loads of the brick and block wall panels tested in a previous study (de Vekey et al., 1986). The poor correlation observed was due to the elastic method being unable to correctly model the partial restraints at the vertical edges of the experimental specimens and anisotropic stiffness. It was suggested (Hasletine and Tutt, 1986) that the overly conservative elastic approach would not be a suitable design method, as it would have implications in terms of economic cost. The use of FEA was discussed (Hasletine and Tutt, 1986), although no attempt was made to

apply the method to assess its suitability. It was commented that further tests would be required to establish material parameters (stiffness) for a wide variety of masonry types to allow successful application of FEA.

A non-linear FEA program was developed (May and Tellett, 1986) for the analysis of masonry walls subject to uniform lateral loads. The program ensured that the non-linear behaviour of masonry was correctly modelled such that the ultimate loads were predicted with improved accuracy compared to those determined via a linear model. Panels with different support conditions and openings could be analysed in the program. The FEA program previously developed (May and Tellett, 1986) was utilised with a biaxial failure criterion that enabled the orthotropic properties of masonry to be correctly modelled (May and Ma, 1986). Some assumptions were made in the failure criterion due to lack of experimental data, and in particular the values of Young's moduli were assumed as multiples of the unit compressive strength, rather than adopting values determined from experimental tests. Ultimate loads and load-displacement curves generated from the program were found to correlate well to experimental values obtained from wall panels with and without openings tested in a previous programme (Haseltine et al., 1977). The accuracy of the results are however questioned in light of the fact that the stiffness was not derived experimentally. Values calculated by the yield line method given in the standard (BSI, 1978) were found to overestimate the ultimate loads by 25 % and it was suggested that this was due to the elastic-brittle response of the material.

The findings of an experimental programme that considered brick and block wall panels were compared to the results of an elastic analysis (Gairns and Scrivener, 1988). The analysis was used to calculate the load at first cracking and its application was warranted due to the initial linear load-deflection response observed. It was established that there was significant scatter in the theoretical results and the load at first cracking was generally underestimated by the method.

The results of an elastic analysis were compared to findings from an experimental programme (Duarte, 1993, Duarte and Sinha, 1992). The wall panels modelled contained an opening of identical dimensions, but were of different lengths and utilised a number of edge support configurations. Parameters for the elastic analysis were determined from material tests rather than adopting assumed values. The elastic approach was found to significantly underestimate the ultimate load that was found in the experimental tests by an average 31 %. It was suggested (Duarte and

Sinha, 1992) that the method underestimated the experimental findings as failure was assumed to occur when the lowest value of flexural strength was attained. The elastic analysis therefore did not allow for the continued strength post initial cracking that was observed in the experimental tests.

The non-linear FEA programme (May and Tellett, 1986) incorporating the bi-axial failure criterion (May and Ma, 1986) that was discussed above was further developed to establish the theoretical strength of wall panels with and without openings (Chong, 1993). The FEA tended to underestimate the actual wall strengths when the corresponding wallette strengths were used. It was suggested that the wallette flexural strengths were related to the weakest joint in the specimens. When mean flexural strength values, determine by statistical simulation, were utilised in the analysis an improved correlation was observed. The stiffness of the opening frame could also be taken into account in the analysis and it was found to have a significant stiffening effect. A number of assumptions were made regarding the material behaviour and properties in the FEA. It was accepted that further work should be conducted to verify, or otherwise, these assumptions.

The results from experimental tests of 1:2 scale wall panels of differing aspect ratios were found to compare well to a FEA method that incorporated the effects of bi-axial bending, load shedding and post cracking behaviour (Ng, 1996). As discussed above tests on small cross beam specimens were used to derive the bi-axial failure criterion and establish the load shedding behaviour for the model. The FEA programme utilised was previously developed by Rotter at the University of Edinburgh. FEA provided the most accurate theoretical loads in this study, whilst yield and fracture line methods tended to over estimate the values. The load-deflection response of the experimental specimens was modelled well using the FEA approach developed in the study. The FEA method was applied to the results from others and gave a reasonable correlation. Discrepancies were suggested due to the particular test set up or material parameters not being available.

A yield line method was presented (Martini, 1998) where the moment resistance was based solely on the self-weight of the masonry, as discussed in Section 2.5.1.2. To validate the results from the yield line analysis a FEA was developed where the interactions of the units were based on a discrete cracking model (Martini, 1998). The wall panel considered in the analysis was supported along three edges and free at the top edge, and comprised dry laid blocks. The FEA process adopted enabled

the interactions of the units to be modelled in addition to considering the deformation of the units themselves. It was found that at low loads the forces in the wall panel were dominated by bending and shear about the base, whilst at higher loads torsional forces about the vertical edges were more significant. Results from the FEA compared well to those obtained from the yield line analysis in terms of both the ultimate load and failure mode. No validation was however completed of the FEA model by experimentation. It was also found that the FEA model was very computationally demanding, due to the consideration of both the interactions of the units and the unit deformation, and might not be the optimum approach to determine ultimate loads in such cases (Martini, 1998).

A method was proposed that utilised correction factors to allow for the effect of material properties varying with position in a wall panel (Rafiq et al., 2003). An existing non-linear FEA program (May and Tellett, 1986) was adopted in the study. The correction factors were determined by completing a “back comparison” of the displacements from a reference panel, previously tested in an experimental study, to the values from the FEA. It was possible to apply the correction factors to different panel configurations by establishing similar elements in the wall in question when compared to the reference. Improved results in terms of both ultimate load and crack pattern were determined when the correction factors were applied. The method was later further developed and employed a complex cellular automata technique that could establish similar elements in the wall under investigation (Zhou et al., 2006). Based on the data from the reference panel it was possible to determine the ultimate load and crack pattern directly without the use of FEA.

A recent review of numerical methods to determine ultimate loads of laterally loaded masonry panels was completed (Sui and Rafiq, 2009). It was suggested that the results of FEA were not as promising as expected, although this seems contradictory to some of the studies previously discussed above. Generally the problems were said to be associated with obtaining suitable models that accurately define relationships between the materials that form the wall panel. It was proposed that the cellular automata technique (Zhou et al., 2006), as discussed above, might prove more successful in terms of establishing more accurate ultimate loads.

### 2.5.3 Numerical limit state analysis approaches

A limit state analysis was developed for block assemblages where zero tensile strength capacity was assumed (Orduna and Lourenco, 2005a, Orduna and

Lourenco, 2005b). The model considered the interactions between torsion, sliding (shear) and bending, in a state of vertical stress, when subject to in or out of plane loads. Simplifications were made to the initial model to ensure computation of the problem could be achieved and included the effects of limiting the compressive strength at the interface. A previous attempt at solving such a mathematical problem was made by minimisation of the load factor on the variable loads and was found to underestimate the results. The solution presented considered the behaviour during loading (and unloading) by varying the compressive stress capacity at the interface in each iteration until convergence or the required level was obtained. The process of determining the load factor for the variable loads, as a proportion of the normal loads, was then completed at the computed stress level. There was limited experimental data available to validate the model so comparison was made to results of FEA. Two walls made from dry assembled blocks were examined, where the first was simply supported at one vertical edge and the second at both edges. The failure modes determined from the proposed model and FEA were similar, while the mode obtained by minimisation differed greatly. Load factors calculated from the model were within 3 and 10 % of the values obtained from FEA for the first and second walls respectively. The minimisation approach significantly underestimated the ultimate load factor in both cases. It was concluded that experimental data would aid the validation process, but care would be required in assembly of the model, particularly with regards to contact between the blocks, so that the assumptions made were valid. A statement in the work suggested that the computational model may have been limited to a maximum size, though no actual values were given.

A method has been presented for the determination of upper and lower bounds for the out-of-plane strength of a dry assembled masonry wall (Casapulla, 2008). In the model it was assumed that lateral forces were resisted by a combination of frictional forces and overturning behaviour. Rotational resistances at the block interface were as a result of the interaction of the shear stress due to self-weight and the torsion moment. A similar failure mechanism was chosen for the theoretical model as observed in an experimental study and the ultimate load, as a factor of the normal load, was determined using the virtual work method. Minimisation of the resulting virtual work equation provided the upper bound solution to the problem and the lower bound was given by reducing the coefficient of friction to zero. Geometric parameters for the wall and unit were varied and it was found that the collapse load was most sensitive to panel width, but thickness also influenced stability. The value used for the coefficient of friction was found to have minimal effect compared to panel width.

The upper and lower bound results were generally shown to enclose the experimental values obtained in a previous study.

### 2.5.4 Arching and buckling analysis

Arching theory has been applied to wall panels that span vertically and horizontally to determine ultimate loads. The results of a series of experimental tests of vertically spanning wall panels subject to vertical and lateral loads were compared to values calculated using arch theory (Hendry et al., 1971). Good correlation was found between the experimental and theoretical results when the wall panels were unsupported at the vertical edges. In a further study it was found that the theoretical values of the ultimate loads calculated using arch theory were reasonably consistent with the experimental values from vertically spanning panels when the vertical pre-compression was of low magnitude (West et al., 1971). Crushing of the material occurred at higher levels of vertical pre-compression so the arch theory tended to over estimate the lateral strength.

A modified arch theory was also developed that allowed the ultimate loads of wall panels with returns (supports at the vertical edges) to be established (Hendry et al., 1971). The method assumed that failure occurred by hinging at the top, bottom and centre of the panel and that the returns provided a stiffening effect. Part of the applied lateral loading was effectively considered to be sustained by the return, as a tensile force only, and a triangular loading distribution was assumed. The results provided by the method showed a reasonable correlation to the experimental findings, however the validity of the method is questioned since the bending moments along the return were neglected and the failure mode in the experimental tests differed to that assumed in the analysis.

A method was presented that included the elastic effects, material self-weight and deformation (crushing) of vertically spanning wall panel specimens in order to provide an improved correlation to experimental results (Morton and Hendry, 1971). The arch theory previously used assumed no tensile strength existed between the units such that at zero pre-compression no lateral load capacity existed. The modified theory, based on a virtual work method, provided good correlation to previous experimental results, showing a positive lateral capacity at zero pre-compression and a corresponding reduction at higher levels. The method was only applicable to cases where the masonry was not vertically confined, as no effect was considered of variable pre-compression during failure.

It was proposed that the strength of a horizontally spanning wall could be determined either by consideration of its pre-cracking elastic or post-cracking response (Anderson, 1984). The pre-cracking theory developed included elastic properties of the wall and abutments, however values determined by the method were significantly lower than experimental values recorded. Post-cracking theory was based upon a modified arch theory that allowed for yielding at the abutments and hinges. The modified theory showed an improved correlation to the experimental results (Anderson, 1984) in comparison to the arch theory presented in the Standard (BSI, 1978).

The results from a series of experimental tests on slender brick and block specimens were compared to those determined using a linear elastic buckling method (Bean Popehn et al., 2008). The walls were tall in comparison to their width and the application of the linear elastic buckling method was considered valid. The theoretical results that were calculated were found to compare reasonably well to the experimental values, but were sensitive to both eccentricities in the axial load and imperfection in the construction of the masonry wall.

### 2.5.5 Empirical methods

#### 2.5.5.1 Length/height empirical relationship

An empirical relationship was developed between the ultimate load and the effective length of the panel, although this was only applicable to panels supported on three sides with the top edge being free (Haseltine et al., 1977, West et al., 1977). The effective length was stated as being equal to the actual length of the panel multiplied by the ratio of the actual panel height and storey height. Empirical curves were developed for different combinations of bricks, varying by compressive strength, and mortar compressive strength class. It would be possible to determine the lateral strength of a wall panel of specific length and height by simply calculating the effective length and consulting the empirical curve for the correct brick/mortar combination. Further tests were suggested to be necessary to verify the relationship for different material thicknesses and masonry types. The results of further tests of both brick and block (concrete and AAC) walls of different heights, lengths and thicknesses were shown to follow the empirical effective length relationship (West et al., 1986). Results were again only compared for wall panels with the top edge free, so it is questioned how useful such a relationship is since it could not be applied to other support conditions.

#### 2.5.5.2 Strip method

The strip method was a method developed empirically for brick specimens, which essentially considered the wall panel as two separate unit width strips that spanned perpendicular to each other (Baker, 1981). The results from a series of tests on brick and block wall panels of various lengths were compared to those computed using the strip method (Gairns and Scrivener, 1988). Values calculated using the strip method tended to underestimate the ultimate loads of the experimental panels, where the brick and block specimens were up to 24 and 50 % lower respectively. Results of tests by others for three and four sided support conditions were also compared to the strip method. The strip method tended to underestimate the strength of the block panels, but provided a reasonable correlation to the brick. The strip method was applied to brick wall panels with openings, where all edges were simply supported or the top or vertical edges were free (Duarte, 1998). The strip method was found to both over and underestimate the experimental ultimate loads of the wall panels by up to 27 and 92 % respectively. The validity of the design process was questioned (Duarte, 1998) since when the design strength was attained in one direction no further load could be sustained by the panel.

## 2.6 Experimental investigations of the strength of masonry walls subject to non-uniform (hydraulic) lateral load

Very limited research is available in the literature that considers the experimental evaluation of the load capacity of masonry when subject to non-uniform hydraulic lateral loads. A single study was identified that examined the effect of non-uniform lateral loads on both walls constructed of brick and block at prototype scale (Pace and Campbell, 1978, Pace, 1988). The tests were part of a larger programme to determine what steps could be taken to ensure buildings were protected during flood events. Initial tests were completed of single storey brick and block veneer wall panels that were tied to a timber inner structure by wall ties, as illustrated by Figure 2.7. Brick and block walls with the top unsupported failed at water levels of 0.73 and 1.07 m respectively. Inclusion of an opening within the brick wall was found to have no significant effect on the ultimate load. A further test conducted of a brick wall with restraint at the top sustained a higher water level of 1.45 m, but was found to fail suddenly. Later a test was completed of a complete building of which the exterior was waterproofed using reinforced plastic sheeting. The water level was raised to a maximum height of 1.22 m during the test. It was found that at a level of 0.91 m the structure could safely support the load, however at a level of 1.22 m permanent deformations and cracking were observed. It was recommended by the report that

masonry buildings should be waterproofed to a maximum height of 0.91 m, however limited evidence of numerical simulation of the experimental arrangement was provided by the authors in support of the experimental data. This clearly demonstrates the need for further programme of experimental tests accompanied by the development of a suitable analytical model.

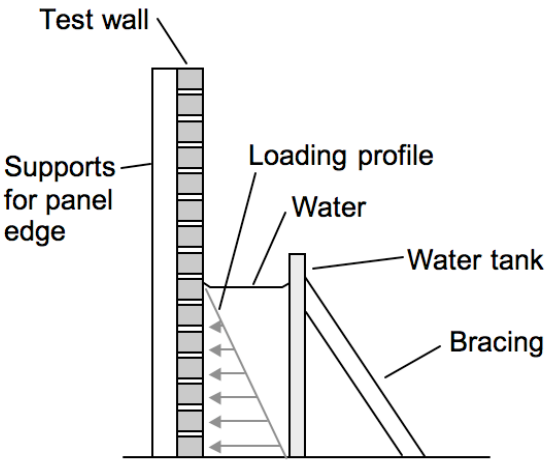


**Figure 2.8.** Simplified typical set-up for hydraulic loading tests (Pace, 1988)

### 2.7 Theoretical investigations of the strength of masonry walls subject to non-uniform (hydraulic) lateral load

More recently a yield line method has been presented to determine the flood load capacity of masonry wall panels (Kelman and Spence, 2003a). The moment resistance of the masonry to lateral loads was based on self-weight only, as discussed above, and the wall panels were essentially treated as cracked sections with no tensile strength capacity. The values adopted in the analysis for the compression depth factor and the coefficient of friction did not appear to be based on actual material properties, but a sensitivity analysis was completed to examine the influence of each coefficient/factor on the ultimate water level. Yield line analysis was completed for a number of different sized wall panels typical of properties and solutions were determined numerically. It was concluded that structural failure would occur at water levels of between 1.0 and 1.5 m when no hydrodynamic effects were considered. Incorporating velocity into the calculations reduced the ultimate water level to below 0.5m. The main concern with the analysis was with the adoption of parameters that were not derived from actual material tests. It was acknowledged that the value for the coefficient of friction utilised within the study should be further investigated. As was discussed in Chapter 1 by application of a suitable waterproofing system the walls of a property effectively become a flood defence and

knowledge of hydrodynamic effects would be important to consider in the future, as well as the hydrostatic effects that are considered in this programme of work.

Very little guidance is provided in the Standards regarding the calculation of characteristic water levels that can be retained by masonry subjected to flood loads (BSI, 2005c). The standard simply refers to using the calculation methods for arching or two-way spanning wall panels as given for uniform wind loads. As discussed previously, these methods were developed alongside experimental testing programmes carried out with uniform loading only. Although it has been suggested previously that the non-uniform loading may be replaced by a uniform load of equal magnitude, no such experimental tests appear to have been completed to verify this (Golding, 1991). Caution should be given to characteristic water levels calculated by this method due to the lack of experimental verification.

## 2.8 Modelling masonry at a reduced scale

### 2.8.1 Masonry unit materials

Researchers have generally adopted masonry units made from prototype materials for models at reduced scale. A number have used units that have been extruded and fired directly at the required scale. The advantage of this process was that identical base materials could be used for the prototype and model. Difficulties have been found in obtaining similar mechanical properties in the model scale units and variations in density, compressive strength and stiffness have been reported (Egermann et al., 1991, Murthy and Hendry, 1966). Some researchers have adopted conversion factors for unit compressive strengths to allow comparison to prototype tests (Hendry and Murthy, 1965, Murthy and Hendry, 1966). The firing process has also been reported to cause issues with dimensional stability and result in a rough surface finish (Hughes et al., 2002, Taunton, 1997). Discrepancies in the dimensions of the model units also increasingly become an issue with reduced scale, particularly when trying to achieve consistent mortar joints (Taunton, 1997).

The issues associated with masonry manufactured and fired at small scale has resulted in a number of researchers opting to cut the model units from brick and block prototype materials (Davies et al., 1998, Hughes et al., 2002, Mohammed, 2006, Sweeney et al., 2005, Taunton, 1997, Tomazevic and Velechovsky, 1992). Cutting, carried out using a diamond saw, results in model scale units with comparable material properties to the prototype and improved surface finish. Previous researchers identified two possible areas of concern that might affect the

mechanical performance when utilising cut units, namely the position and orientation in the prototype brick. To evaluate the effect of the former, a series of tests were conducted on model units cut at different depths in prototype bricks and no significant difference was observed in the mechanical properties (Taunton, 1997). The cutting process for smaller scale bricks resulted in the bed joints of the model and prototype being perpendicular to each other, as shown by Figure 2.9.

Compressive strength tests on brick units showed that there was an increase in compressive strength in the model bricks that were orientated in this manner (Mohammed, 2006, Mohammed et al., 2011). Further tests completed on brick cubes, of identical dimensions, that were loaded on different faces showed similar results and compressive strength increased by an average of 26%. The variation observed was suggested as being due to a combination of anisotropy in the prototype masonry unit due to the manufacturing process and size effect found in brittle materials. The tensile strength tests of units showed a gradual increase as scale was reduced, rather than a step change as observed in the compressive tests. No clear trend was found when the different scale units were subjected to flexure.

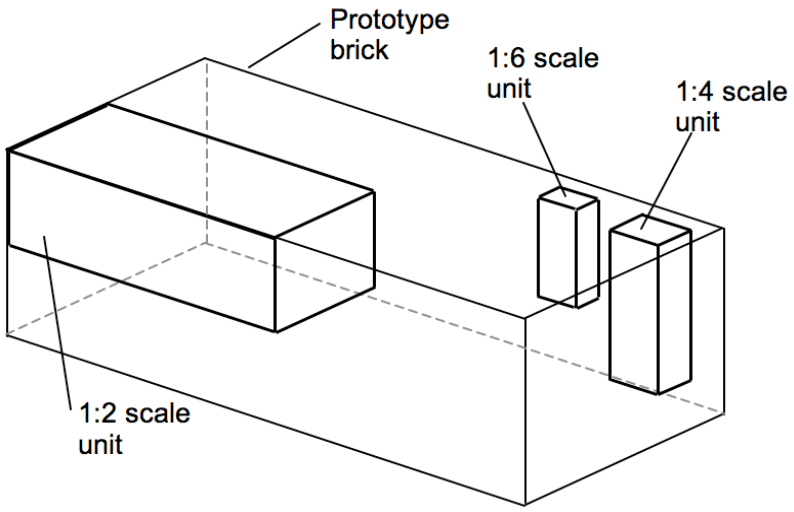


**Figure 2.9.** Orientation of model scale bricks in the cutting process (Mohammed et al., 2011)

Another approach taken by other researchers was to manufacture special, termed “complete”, masonry units that correctly scaled the material’s stress-strain response (Tomazevic and Klemenc, 1997, Tomazevic et al., 1996, Tomazevic and Velechovsky, 1992). This approach requires either the manufacture of special materials or the selection of an alternative that possesses the required mechanical

properties. Developing complete materials was found to be quite time consuming and involved a reasonable amount of trial and error. Complete units have been manufactured by both casting and firing and a good correlation has been shown to the response required.

### 2.8.2 Model scale mortar

The aggregate used in the model scale mortar requires consideration, particularly at the smaller scales. Prototype mortar typically utilise normal building sand of 0 to 2 mm grading and the maximum grain size would exceed the joint height at a scale of 1:5 (assuming a 10 mm prototype mortar joint height). Researchers constructing models at scales of 1:2 and 1:3 have provided little information on the composition of the mortar used and it was likely that normal building sand was utilised (Duarte and Sinha, 1992, Ng, 1996, Sinha, 1978, Sinha et al., 1979, Sweeney et al., 2005). At smaller scales a finer grading or correctly scaled aggregates have generally been used (Davies et al., 1998, Egermann et al., 1991, Hendry and Murthy, 1965, Hughes and Kitching, 2000, Mohammed et al., 2011, Murthy and Hendry, 1966, Sinha and Hendry, 1968, Taunton, 1997). Comparative tests on prototype and correctly scaled model scale mortars of the same strength class have revealed that they have similar mechanical properties (Mohammed, 2006). Average compressive strength and stiffness showed good correlation between prototype and model scale mortars, and was within 6 and 3 % respectively, although the flexural strength of the mortar was 27 % higher in the model scale mortar.

### 2.8.3 Modelling of masonry assemblies and structures at reduced scale

The use of small-scale masonry models has been adopted by a number of researchers to examine different structural problems. The effect of scale has been assessed in a number of studies when direct comparison to prototype behaviour has been made. The results from such studies have tended to be somewhat contradictory and this is therefore explored in more depth in this section.

A study was completed of 1:3 and 1:6 scale masonry loaded in compression, in which the columns (piers) and wall specimens that were tested showed comparable ultimate loads and behaviour to that of the prototype (Hendry and Murthy, 1965, Murthy and Hendry, 1966). Similar results were observed when columns were tested to evaluate the effect of load eccentricity and slenderness. The mean stiffness of the model scale wall specimens was lower than for the prototype, but no explanation was offered for the effect observed. A series of additional tests were conducted at 1:6

scale to assess the response of shear loading on cross wall type masonry structures (Murthy and Hendry, 1966). The shear capacity of wall specimens improved with increased compressive stress and exceeded the relationship provided in the standards. A test conducted of a three storey bay type structure found that increasing the number of shear walls had a significant stiffening effect. Weights were added to the structure to ensure that the stress levels were modelled correctly. Comparisons to prototype results were not made, likely due to absence of data. The study was later expanded to consider the effect of slenderness on the compressive strength of 1:6 scale wall specimens (Sinha and Hendry, 1968). The test results suggested that the reduction in strength with increasing slenderness was not as significant as prescribed by the standards.

Tests on prototype and 1:3.8 model scale adobe brick specimens showed an increase in both compressive strength and flexural strength with a reduction in scale (Krawinkler, 1988). The results were suggested to be due to the weakest link theory and increased mortar bond strength with reduction in scale. The latter was explained by an increase in surface area to volume ratio with scale allowing a greater amount of water to enter the masonry resulting in a stronger bond. It was concluded that material tests at prototype and model scale should be completed alongside structural tests to allow comparisons to be established during analysis.

Compression tests of wall brick wall panels were completed at 1:2,1:4 and prototype scale and the results were in line with those of previous studies (Egermann et al., 1991). A reasonable correlation was found between the compressive strength at the three different scales and similar failure modes were observed, but stiffness significantly reduced with scale. It was concluded that the reduction in stiffness was likely due to a reduced compaction of the mortar with scale due to a diminishing self-weight effect, and differing gradings of mortar constituents between scales.

Tests were completed of 1:2 scale masonry cross beams to determine their bi-axial bending behaviour when subjected to out of plane loading (Ng, 1996). Failure of the cross beams were either simultaneously in both directions, or in one direction proceeded by the other. In the later type a large proportion of the load was transferred to the un-cracked direction, with a small residual capacity remaining in the cracked direction. The cross beams behaved similarly to the 1:2 scale wall panel specimens that were tested, as previously discussed above. The results from the cross beam tests were used to further develop an existing FEA program for the

analysis of wall panel specimens. The effect of self-weight did not appear to be considered in the cross beam tests and conducting further tests at prototype scale would be beneficial to verify the relationships observed.

Comparative compressive strength tests of masonry specimens at prototype, 1:2, 1:4 and 1:6 scale have shown a very slight increase in strength with a reduction in scale (Hughes et al., 2002, Hughes and Kitching, 2000). In the study, all the bricks used were from the same batch and the model scale units were cut from the prototype. Previous researchers had shown a reasonable correlation in strength with scale. Variation from this was suggested to be due to the scatter normally associated with masonry testing and by the inherent selection caused by weaker bricks failing during cutting.

Research has recently been published that compares the behaviour of masonry specimens at model scales of 1:2, 1:4 and 1:6 to the prototype scale (Mohammed, 2006, Mohammed and Hughes, 2011, Mohammed et al., 2011). The model scale masonry specimens used in the study were all cut from the same prototype units. Contrary to the results of previous studies, compressive strengths obtained from the masonry (triplet) specimens increased with a reduction in scale, although similar failure mechanisms were observed. The increase in compressive strength was attributed to a combination of three factors: a brittle materials type size effect in the units, anisotropy in unit strength due to the manufacturing process and strengthening effect occurring as the mortar joint thickness decreased. The stiffness of the triplet specimens was found to be similar across the scales, differing to the reduction in stiffness with scale found by previous researchers. The difference in stiffness was attributed to the construction technique used in the study, which involved the specimens being constructed flat rather than vertically therefore eliminating any potential compacting effects due to self-weight. Consideration was not given to the difference in test specimen type between studies, where generally wall specimens had been tested previously rather than triplets.

The results of shear tests on triplet specimens showed similar failure modes, but no significant trend with a reduction in scale (Mohammed and Hughes, 2011). Similar behaviour was observed in the diagonal tensile strength tests, where the mean shear strength showed no significant variation with scale. The stress-strain response for the 1:6 scale specimens in diagonal tension was much more ductile after the initial linear stage than for the other scales. Flexural strength tests of wallettes for a plane of

failure parallel to the bed joints showed no real variation with scale and similar failure modes were recorded. The bond wrench tests however revealed a reduction in strength with scale and it was suggested that the results were influenced by the variation in mortar compressive strengths between the scales. A slight reduction in strength with scale was found for the flexural strength tests conducted perpendicular to the bed joints. The 1:6 specimens failed in the mortar joints only rather than through the units and mortar joints and is suggested to have resulted in the lower strength observed for these. It was concluded that in general scale models provided a good representation of prototype behaviour and that small assemblages should be tested alongside structural assemblies to provide parameters for theoretical analysis.

Uniform lateral loading tests of storey height masonry panels have been conducted at scales of 1:2, 1:3 and 1:6 as discussed in Section 2.4 (Duarte, 1993, Hendry, 1973, Ng, 1996, Sinha, 1978, Sinha et al., 1979). In all cases the panels were loaded using air bags and pressure was increased incrementally. The failure modes of the wall panels were found to be similar to those observed in prototype scale specimens and acceptable repeatability was shown. Differences in self-weight between the model and prototype do not appear to have been considered in any of the studies. Comparing the results to prototype tests would allow an assessment of this effect to be made, but would not be straightforward due to differences in materials, dimensions and support conditions. Masonry wall panels of 1:12 scale have also been subjected to blast loading (Hughes et al., 2002). Tests have been completed using a centrifuge to correctly model the effect of scaling on the explosive.

A number of researchers have modelled masonry arch bridges and scales as low as 1:55 have been successfully adopted (Davies et al., 1998, Hughes et al., 2002, Pippard and Ashby, 1939, Pippard and Chitty, 1941, Royles and Hendry, 1991, Taunton, 1997). Masonry arches generally fail as a mechanism, so the self-weight of the arch and fill material can have a significant effect on the ultimate load. Although researchers attempted to model the effect of the self-weight of the fill material by adding superimposed loads to the arch, gravity scale effects appear to have been neglected and the accuracy of these results are therefore drawn into doubt (Pippard and Ashby, 1939, Pippard and Chitty, 1941, Royles and Hendry, 1991). Royles and Hendry (1991) suggested that a scale factor could be applied to the model scale findings to allow comparison to results from prototype scale tests, but with little theoretical underpinning. A satisfactory correlation was however reported by Royles and Hendry (1991) to the prototype scale tests results after the application of the

scaling factor. Correct modelling of the self-weight effects and interactions of the fill within the arch structure were later ensured by conducting tests using a centrifuge (Davies et al., 1998, Hughes et al., 2002, Taunton, 1997). The correlation between the prototype failure modes and ultimate loads was found to be very good for the centrifuge tests. Comparison of the load-deflection response was only made in the centrifuge test and the stiffness was found to be lower in the model (Davies et al., 1998). The reduction in stiffness in the model arch was attributed to the grading of the constituents of the model scale mortar (Davies et al., 1998).

Scale models have been employed by a number of researchers to assess the effect of seismic action on masonry built structures. Shaking table tests of 1:2, 1:4, 1:5 and 1:7 model scale masonry structures have been successfully performed (Sweeney et al., 2005, Tomazevic and Klemenc, 1997, Tomazevic and Velechovsky, 1992). The dynamic responses were found to compare well to theoretical values determined for the prototypes. The failure modes identified in the tests were also shown to simulate those seen in real structures that have been subjected to natural earthquakes (Tomazevic and Velechovsky, 1992). To ensure that the model correctly represents the dynamic response of the prototype, consideration must be given to the effect of scaling on material density. When prototype materials have been employed in the studies the effect of self-weight has been considered by adding additional dead load to the structure or by pre-stressing using cables (Sweeney et al., 2005, Tomazevic and Velechovsky, 1992). “Complete” materials (Section 2.8.1) have also been utilised in tests, which were specially manufactured to provide, as far as possible, the correct scaling of density and material properties (Tomazevic and Klemenc, 1997). Material tests were completed alongside the structural tests in all studies to provide parameters for theoretical analysis.

### 2.9 Summary

The literature review has revealed that there is a wealth of information regarding the experimental strength of masonry when subject to uniform loads. A number of researchers have modelled the experimental results of uniform loading tests using the yield line method, elastic plate analysis, FEA and numerical limit state approaches. The failure modes used in the yield line method were generally comparable to those observed in experimental studies, although the ultimate loads were both over and underestimated. Considering the inherent natural variability in masonry and the fact that the flexural strengths were determined form tests with their own associated variability then the ultimate loads may be considered to be a good

representation of the experimental values. The main advantages of the yield line method are that: (i) it can be readily applied to panels of different shapes and edge support conditions, (ii) openings and vertical loads can be readily incorporated, and (iii) its application requires no specialist computer software. The concern raised by many researchers was that due to the brittle nature of masonry that moments of resistance would not be maintained at the point of cracking. Others have shown that some resistance was maintained after cracking and that frictional and self-weight effects may account for such behaviour (Brincker, 1984, Haseltine and Tutt, 1986, Lourenco, 2000).

Elastic plate analysis has been found to be difficult to apply, since the existing solutions do not readily lend themselves for application to masonry panels with different support conditions and orthotropic material properties. FEA was found to be disadvantageous in terms of the requirements for computing power, a suitable and accurate material model and the necessity for a bespoke/commercial software package. The accuracy of the material model is likely the most important consideration to obtaining suitable results, especially as the material parameters and interactions required for the model are not always straightforward to establish. However, advantages offered by FEA include its ready application to panels of different sizes and edge support conditions, and the ability to consider openings. Perhaps the most significant advantage of FEA over yield line analysis is that displacements can be obtained from the model, such that the load deflection response can be compared to experimental findings. Comparing the load deflection response can aid in the verification of the model and particularly establish whether the failure criterion utilised is a true representation of the actual material. A number of researchers have developed numerical limit state methods to determine the ultimate loads of masonry wall panels subject to lateral load. At the moment the numerical methods still appear to be in their infancy and there is a limitation on the size of panel that can be considered in the analysis. It is also not clear whether openings could be readily catered for in the numerical approaches described. Similarly to the FEA approach, the accuracy of the numerical methods depend on the material model selected.

In comparison to the substantial amount of research completed for uniformly loaded masonry, only one experimental study was identified that had been conducted to establish the ultimate loads of masonry wall panels subject to hydraulic loading. A yield line approach has been proposed (Kelman and Spence, 2003a) to allow the

determination of ultimate water levels of hydraulically loaded wall panels, however this was not verified by experimentation. Cleary there is a need of further experimental data for hydraulic loading conditions to facilitate the development of an appropriate model to address the concerns raised in Chapter 1 Section 1.1.

A number of researchers have successfully modelled masonry at reduced scales as low as 1:55. Structures such as walls, buildings and arch bridges have been tested with static or dynamic loadings. Prototype behaviour, in terms of ultimate load and mode, has generally been well modelled in the previous research programmes. The stiffness of such structures has been found to reduce with scale and was thought to be associated with the gradings of the constituents of the mortar or a reduced compaction effect of the mortar during construction.

The importance of considering the required increase in density of the masonry with scale (self-weight) appears to have been neglected by some researchers in the field, but has been correctly considered by others by employing superimposed loadings, pre-stressing, special (complete) materials or by conducting testing within a centrifuge. For the problem of hydraulic loading of masonry wall panels it would be necessary to conduct testing within a centrifuge to ensure the self-weight of the water used to laterally load the wall panel is correctly considered.

# Chapter 3 Development of the spreadsheet analyses

This Chapter details the process that was followed to develop the analyses using standard spreadsheet software. The first section of this Chapter details the theory that was utilised in the analyses, whilst the second section discusses the application of the method to uniformly and non-uniformly loaded masonry wall panels, and the final section illustrates how this was incorporated into the spreadsheets. Two analyses were developed, the first allowed for the condition where the yield lines formed from the corners of the specimen, whilst the second allowed for the situation where the yield lines formed at a position away from the corner such that corner levers were developed. The analyses are a development of an unpublished analysis method that was devised by TG Hughes (2009, pers. comm., 22 Sept) at Cardiff University.

## 3.1 Theory of the problem

### 3.1.1 Background to the problem

The problem was to determine the characteristic load of a masonry structure that was subject to either wind or hydraulic lateral loads. The structure would typically be that of a brick or block built domestic or commercial property. Rather than consider the structure in its entirety, it was proposed to consider each wall as a separate element, termed a wall panel, with the appropriate boundary conditions and vertical loadings applied. This would simplify the requirements for the analysis process. There were two possible approaches that could have been utilised to determine the characteristic load, the first was an elastic approach e.g. using plate analysis or finite element analysis, and the second was to utilise an ultimate limit state method such as the yield line method. The advantages and disadvantages of each approach have been discussed in Chapter 2. The key requirements for the analysis method were that it would be straightforward to apply to the particular wall panel under consideration and that no specialist software would be required. The analysis would also have to be flexible such that it could deal with wall panels of different dimensions and vertical loading conditions, different masonry unit sizes and strengths, calculate the impact of openings in the wall panel, and the strength of cavity wall assemblies.

A finite element analysis method was not adopted here, as it would have required the development of bespoke software or the use of expensive commercial software. The ultimate load would also depend on the particular material model utilised in the

analysis, for example a tensile-compressive type failure criterion or a block interface model. The method might also not meet the flexibility requirements outlined above and require considerable computational resources.

The yield line method was deemed most suitable for the solution of the problem in this situation despite the drawbacks outlined in Chapter 2. The stepwise approach of the yield line method would readily lend itself to the use of standard spreadsheet software to develop the analytical solution. The method would also meet the flexibility requirements outlined above. The ultimate limit state approach would provide the ultimate load for the wall panel in question and applying the appropriate safety factors during or post analysis would establish the characteristic load.

### 3.1.2 Theory of the yield line method

To apply the yield line method a failure mechanism is firstly postulated for the particular wall panel under consideration. For a two way spanning wall panel that is simply supported on all edges then the failure mechanism shown by Figure 3.1 (Jones, 1962) is valid. It is assumed that the wall panel is subject to a uniformly distributed load and is able to sustain both tensile and compressive stress in the section. The wall panel initially behaves elastically in the section A B of the load deflection curve, as shown by Figure 3.2 (Horne, 1979). Beyond the elastic limit yielding initially occurs at the position of the largest bending moment, which is at the centre of the slab, as shown by Figure 3.1a. Yielding corresponds to region C of the load deflection curve. The yielding process will result in the uncracked sections of the wall panel being required to sustain a higher moment. A further increase in load results in further yielding in the sections adjacent to the initial cracks, which are now subject to the highest bending moments. This process then continues with further application of the load, such that the cracks eventually meet the corners of the wall panel, as shown by Figure 3.1b. In this state the wall panel is in equilibrium, just prior to point D on the load deflection curve, and the application of any further load will result in fully plastic behaviour.

The actual process of establishing the ultimate load first assumes unit deflection, $\delta$, occurs at the centre of the failure mechanism postulated (at point e), as shown by Figure 3.1b (Jones, 1962). The failure mechanism is assumed to be symmetric and the moment resistance is equal in both directions, so it is only necessary to consider one element of the wall panel. For slab element 1 the unit deflection results in a

rotation, $\theta_{Slab1}$, about the axes of rotation in the y direction, as shown by Figure 3.3a and given by equation 3.1.

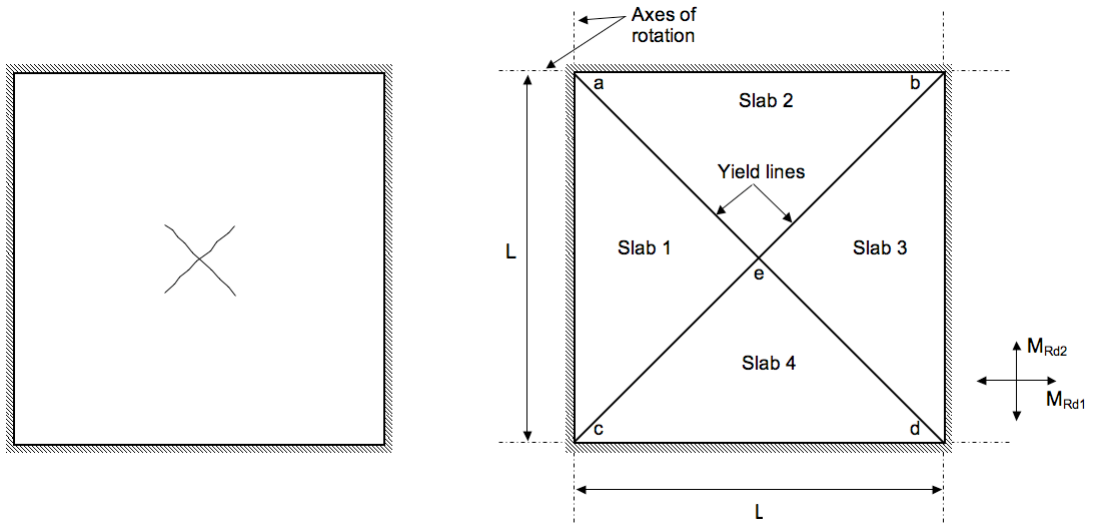


(a) (b)

**Figure 3.1.** Two way spanning wall panel (a) initial yielding and (b) final failure mechanism postulated (Jones, 1962)

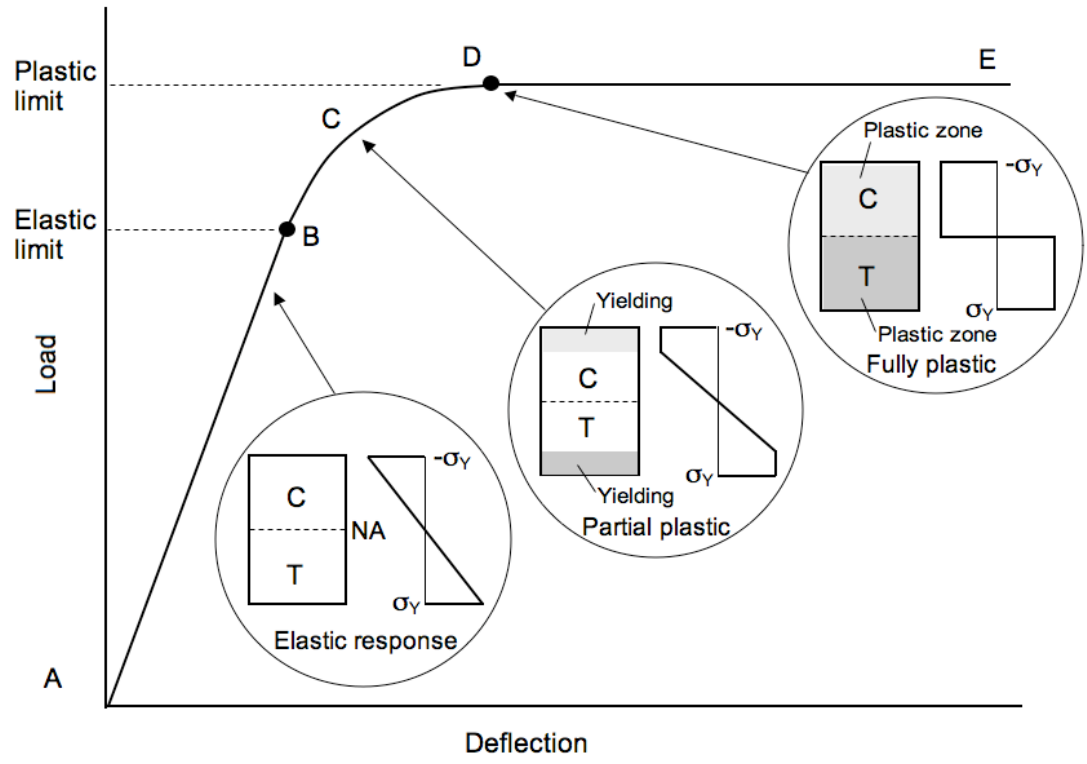


**Figure 3.2.** Idealised load deflection response for two way spanning wall panel (Horne, 1979)

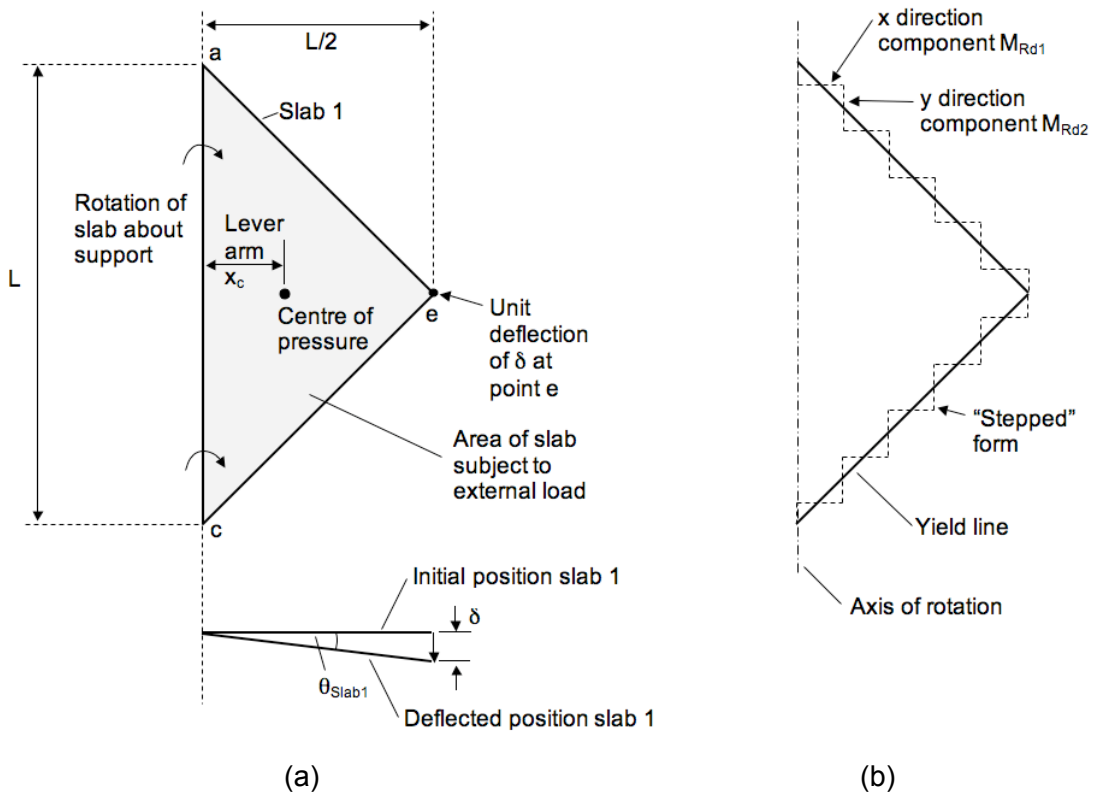


**Figure 3.3.** (a) Centre of pressure and deflection of slab 1, and (b) "stepped" form of diagonal yield line (Jones, 1962)

The diagonal yield lines of slab 1 can be thought of as following a "stepped" form, as shown by Figure 3.3b (Jones, 1962). The moment resistance along the stepped line comprises a component in the x direction, $M_{Rd1}$, and a component in the y direction, $M_{Rd2}$. For slab 1, rotation at failure occurs about the y axis and the moment resistance component about this axis, $M_{Rd2}$, is used to determine the internal work done, $IntWD_{Slab1}$, as given by equation 3.2. The total length of the yield line is equivalent to all the y direction components of the yield line, which is the total length of slab 1 in the y direction. Likewise for slab 2, rotation occurs about the x axis so only the moment resistance in the x direction, $M_{Rd1}$, contributes to the internal work done. The expression for the internal work done for slab 2 is identical to that given by equation 3.2, except $M_{Rd1}$ is substituted for $M_{Rd2}$. Due to symmetry the expressions for internal work done are identical for slabs 1 and 3 and likewise for slabs 2 and 4.

The total external work done on the slab 1, $ExtWD_{Slab1}$, by the external load is equal to the load acting on the slab area multiplied by the lever arm to the centroid and the rotation, as given by equation 3.3. In this case the centroid, or centre of pressure, is at a one third of the length of the triangular element in the x direction. The external

work done for slabs 2, 3 and 4 is identical to that given for slab 1 due to symmetry. Equating the total internal and external work done, for all slab elements, provides the expression given by equation 3.4. The ultimate load can therefore be established for a given value of moment resistance. A similar process can be followed to apply the yield line method to wall panels of different shapes or edge support conditions. For full restraint at the panel edges the moment resistance must also be included in the computation of the total internal work done.

$$\theta_{Slab1} = Tan^{-1}\frac{2\delta}{L} \approx \frac{2\delta}{L} \qquad 3.1$$

$$IntWD_{Slab1} = LM_{Rd2}\theta_{Slab1} = 2\delta M_{Rd2} \qquad 3.2$$

$$ExtWD_{Slab1} = PArea_{Slab1}x_{c\,Slab1}\theta_{Slab1}$$
$$ExtWD_{Slab1} = \frac{1}{6}\delta PL^2 \qquad 3.3$$

$$IntWD_{Total} = ExtWD_{Total}$$
$$8\delta\left(M_{Rd1} + M_{Rd2}\right) = \frac{2}{3}\delta PL^2 \therefore P = \frac{12\left(M_{Rd1} + M_{Rd2}\right)}{L^2} \qquad 3.4$$

### 3.2 Application of the yield line method to masonry subject to uniform and non-uniform lateral loads

The following section describes how the yield line method is applied to masonry wall panels of different shapes and with different edge support conditions. The consideration of hydraulic loads, that would result in a non-uniform loading profile being applied to the slab elements, required a new method to be developed to allow the correct computation of the external work done. The calculation of the internal work done is described in terms of a plastic moment as detailed in Section 3.1.2. This is considered to be due to flexural (bending) strength, but consideration is also given to methods proposed in the literature that are based on a frictional and overturning resistance.

#### 3.2.1 Boundary conditions and failure modes

A typical masonry building can be subdivided into elements termed wall panels with the appropriate boundary conditions applied at their edges. Depending on the particular case the boundary conditions for the edges of the wall panel can be free,

simply supported, clamped or partially supported. A discussion of suitable boundary conditions is given in Chapter 4 Section 4.1.3. Possible arrangements for a wall panel include supports at all edges, top edge free and a vertical edge free, as shown by Figures 3.4a, 3.4b and 3.4c respectively.

(a) (b) (c)

**Figure 3.4.** Wall panel support conditions: (a) supported on all edges, (b) top free, and (c) vertical edge free

To apply the yield line method to the wall panel a suitable crack pattern must be postulated for the problem. For the case of a wall panel supported on all edges an envelope type failure pattern is assumed, as shown by Figure 3.5a. The patterns assumed for a panel with the top edge free and vertical edge free are shown by Figures 3.5b and 3.5c respectively. Such patterns have been classically adopted for the analysis of reinforced concrete slabs (Jones, 1962) and have been shown to be valid failure modes for masonry wall panels (West et al., 1977). A case where the bottom edge is truly classed as free would be unlikely due to the friction between the masonry and the structure below, which would be enhanced by the self weight of the masonry and any imposed loading applied to it. In each case the position of the yield lines separating the slabs is specified by the dimensional parameters $\alpha$ and $\beta$, where the subscripts L and R refer the left and right of the panel respectively.

A special case is also possible when the yield lines do not coincide with the corners of the specimen, as shown by Figure 3.6. When the edges are simply supported the corners can pivot about supports resulting in the section of the panel in the corner moving backwards. For clamped edges the corner of the wall panel will be restrained from pivoting and will instead yield along the pivot line. An additional parameter, $\gamma$, is required to define the position of the yield lines separating the slabs in the corner lever analysis.

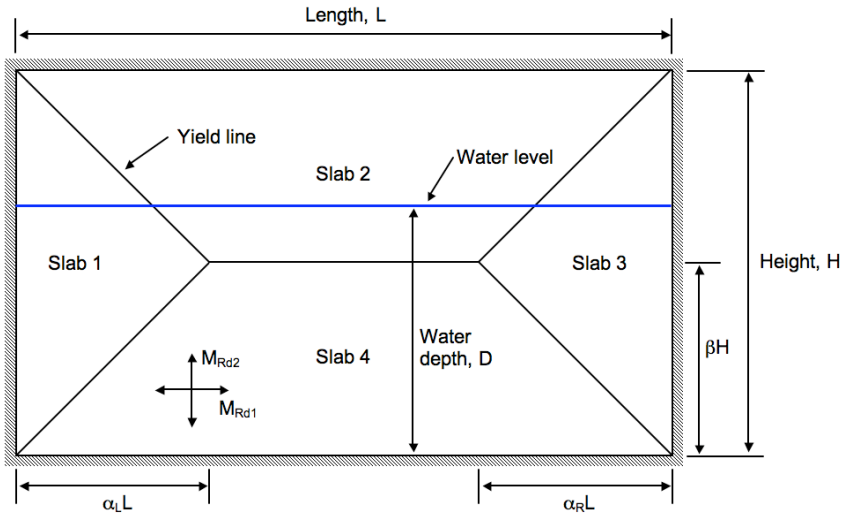


(a)

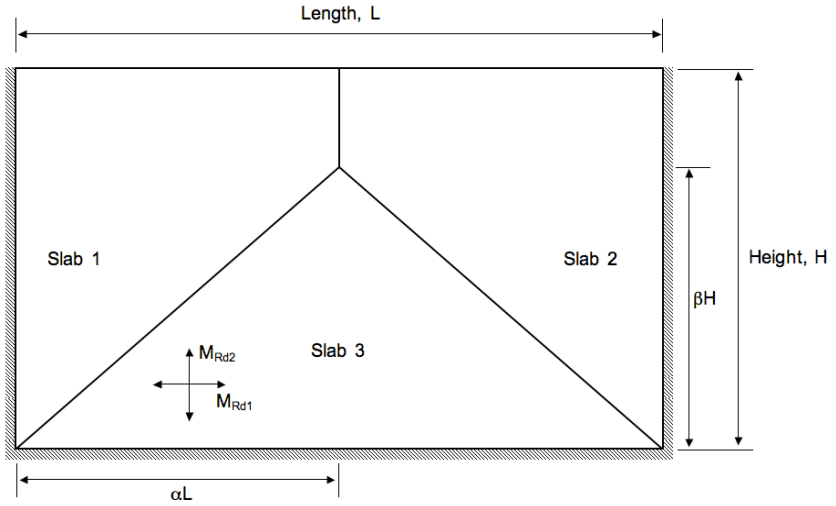


(b)

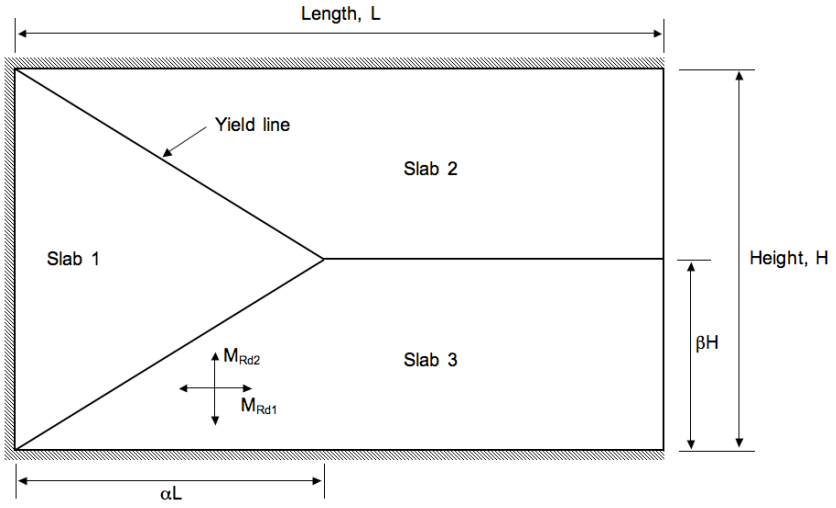


(c)

**Figure 3.5.** Yield line patterns postulated for wall panels supported on: (a) 4 sides, (b) 3 sides with top free and (c) 3 sides with vertical edge free

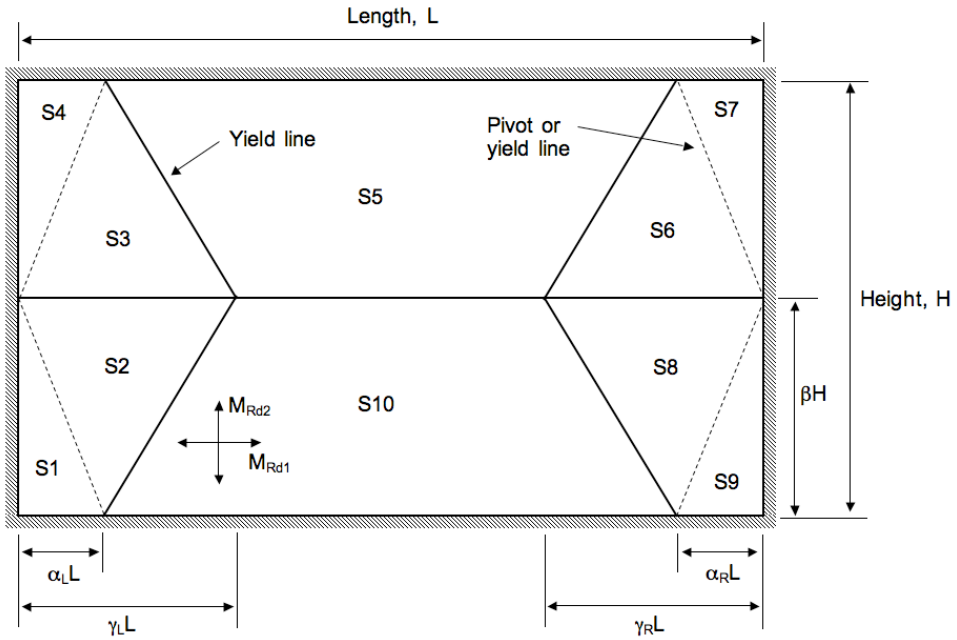


**Figure 3.6.** Corner lever pattern for wall panel supported on 4 sides

### 3.2.2 Calculation of the external work done by the lateral load

As described in Section 3.1.3 it is necessary to determine the external work done on the wall panel at limit state. Unit deflection of the mechanism is assumed to occur at limit state and a suitable reference position is selected for this. For example, for the wall panel supported on four sides the yield line separating slabs 2 and 4 is selected to move by unit displacement. The external work done could be readily computed for slabs that were already triangular in form, by following the method detailed in Section 3.1.2. Irregular shaped slabs are split into smaller elements to enable the centres of pressure and the external work done to be determined. The most appropriate method is to split the slabs into triangular elements, for example slab 4 of the wall panel supported on four sides can be split into two elements as shown by Figure 3.7.

For the case of a uniformly distributed lateral load, UDL, the centres of pressure can be readily found for each triangular element and the external work done can be calculated following the process detailed in Section 3.1.2. However, when a non-uniform hydraulic lateral load is applied to the slab, the centres of pressures will be dependent on the loading profiles over each element. To determine the total load on a hydraulically loaded element it is necessary to integrate the loading profile over the area of the triangular element. The moment due to the load is similarly determined for each element, which enables the centres of pressure to be established. The method employed is presented in detail below.

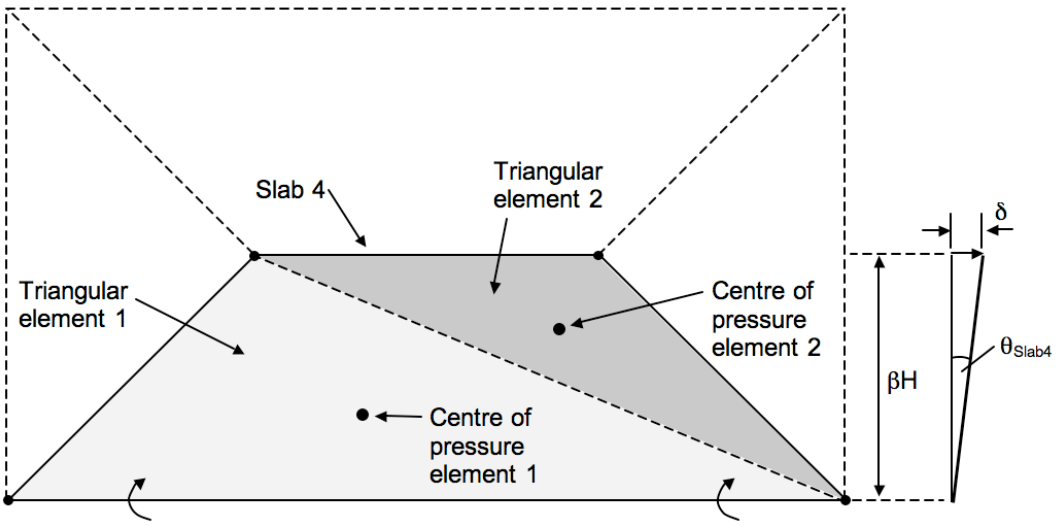


**Figure 3.7.** Splitting slab 4 into triangular elements to determine centre of pressures and external work done

To determine the total load and the centre of pressure for a generalised triangular element subject to lateral load a local nodal coordinate system is firstly established, as shown by Figure 3.8. The hydrostatic pressure, $P_{ihs}$, at each node, $N_i$, is then determined from the depth of the water, D, applied to the element, as given by equation 3.5, where $\rho_w$ is the density of water and g is the Earth's gravity. An existing method (Kelman and Spence, 2003a) was followed to establish the hydrodynamic pressure per unit area, $P_{ihd}$, at each node, where the drag equation was adopted, as given by equation 3.6, where v is the velocity of the water. A shape factor, $C_d$, is also included to account for the length and height of the wall panel as well as the direction of flow, which was omitted in the existing method (Kelman and Spence, 2003a). The approach employed does not allow for variation in velocity with depth, but completing the analysis with the peak velocity enables the worst case conditions to be assessed. The total load at each node comprises the hydrostatic, hydrodynamic and uniformly distributed ($P_{udl}$) loads as given by equation 3.7. For the case of hydrostatic loading only then the velocity and UDL components are set to zero. Likewise for the case of a UDL only then the density of water is set equal to zero. The pressure at any position within the triangular element can be described by a general two-dimensional linear pressure equation, as given by equation 3.8. The pressure equations at each node are given by equations 3.9 to 3.11. The constants $a_p$, $b_p$ and $c_p$ can be determined by substitution of the pressure equations at each node of the element, as given by equations 3.12 to 3.14.

$$P_{ihs} = \rho_w g\left(D - y_i\right) \qquad 3.5$$

$$P_{ihd} = \frac{C_d \rho_w v^2}{2} \qquad 3.6$$

$$P_i = \rho_w g\left(D - y_i\right) + \frac{C_d \rho_w v^2}{2} + P_{udl} \qquad 3.7$$

$$P_i = a_p + b_p x_i + c_p y_i \qquad 3.8$$

$$P_1 = a_p + b_p x_1 + c_p y_1 \qquad 3.9$$

$$P_2 = a_p + b_p x_2 + c_p y_2 \qquad 3.10$$

$$P_3 = a_p + b_p x_3 + c_p y_3 \qquad 3.11$$

$$a_p = P_3 - b_p x_3 - c_p y_3 \qquad 3.12$$

$$b_p = \frac{P_2 - P_3 - c_p\left(y_2 - y_3\right)}{\left(x_2 - x_3\right)} \qquad 3.13$$

$$c_p = \frac{\left(P_1 - P_2\right)\left(x_2 - x_3\right) - \left(P_2 - P_3\right)\left(x_1 - x_2\right)}{\left(y_1 - y_2\right)\left(x_2 - x_3\right) - \left(y_2 - y_3\right)\left(x_1 - x_2\right)} \qquad 3.14$$

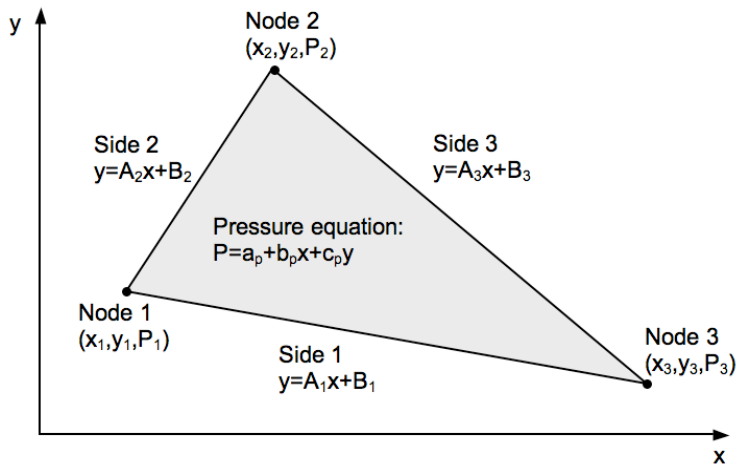


**Figure 3.8.** Generalised triangular element of slab

To allow integration over the area of the generalised triangle the equations for the sides of the element are defined, for example for side 1 the gradient, $A_1$, and constant, $B_1$, are determined from the nodal coordinates as given by equations 3.15 and 3.16. Similar equations are established for sides 2 and 3.

$$A_1 = \frac{(y_1 - y_3)}{(x_1 - x_3)} \qquad 3.15$$

$$B_1 = y_1 - A_1 x_1 \qquad 3.16$$

Integration of the pressure function is subsequently completed over the area of the triangle in both the x and y directions. To allow integration to proceed the triangular elements are split further into left and right sub elements as shown by Figure 3.9. The forces acting on the left, $F_{LHS}$, and right, $F_{RHS}$, sub elements are given by equations 3.17 and 3.18 respectively. Integration of the pressure equation is then completed in the y direction between limits corresponding to the equations of the lines between the nodes and secondly in the x direction between the limits of the x coordinates of the nodes. At limit state the centre of pressure of the triangular sub elements deflects and results in moments Mx and My in the x and y directions respectively as shown by Figure 3.10. The moments were determined by integrating the pressure function multiplied by the distance to the centre of pressure over the triangular sub elements, as given by equations 3.19 to 3.22. The expansion of the integrals is given in appendix 1.

$$F_{LHS} = \int_{x_1}^{x_2} \int_{y=A_1x+B_1}^{y=A_2x+B_2} \left(a_p + b_p x + c_p y\right) dy dx \qquad 3.17$$

$$F_{RHS} = \int_{x_2}^{x_3} \int_{y=A_1x+B_1}^{y=A_3x+B_3} \left(a_p + b_p x + c_p y\right) dy dx \qquad 3.18$$

$$Mx_{LHS} = \int_{x_1}^{x_2} \int_{y=A_1x+B_1}^{y=A_2x+B_2} \left(a_p + b_p x + c_p y\right) x dy dx \qquad 3.19$$

$$My_{LHS} = \int_{x_1}^{x_2} \int_{y=A_1x+B_1}^{y=A_2x+B_2} \left(a_p + b_p x + c_p y\right) y dy dx \qquad 3.20$$

$$Mx_{RHS} = \int_{x_2}^{x_3} \int_{y=A_1x+B_1}^{y=A_3x+B_3} \left(a_p + b_p x + c_p y\right) x dy dx \qquad 3.21$$

$$My_{RHS} = \int_{x_2}^{x_3} \int_{y=A_1x+B_1}^{y=A_3x+B_3} \left(a_p + b_p x + c_p y\right) y dy dx \qquad 3.22$$

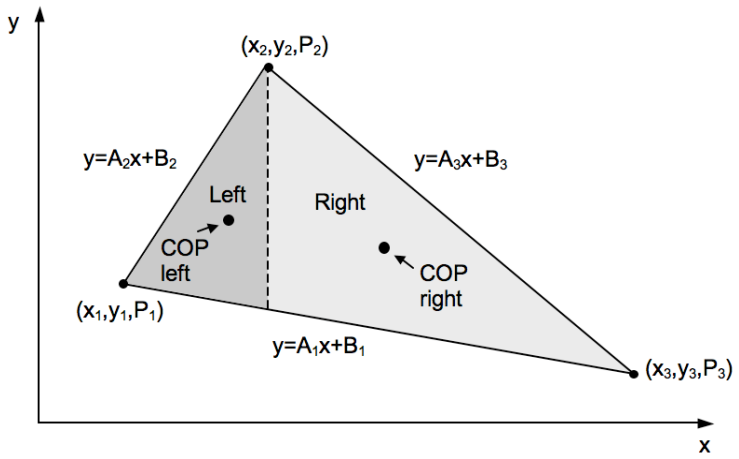


**Figure 3.9.** Splitting triangular element into left and right sub elements

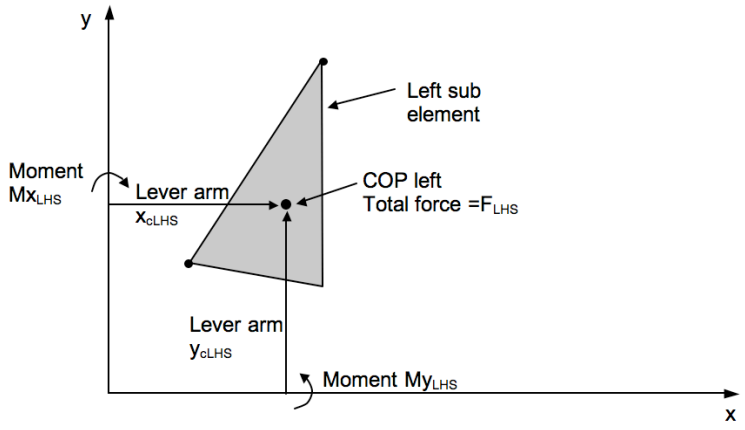


(a)

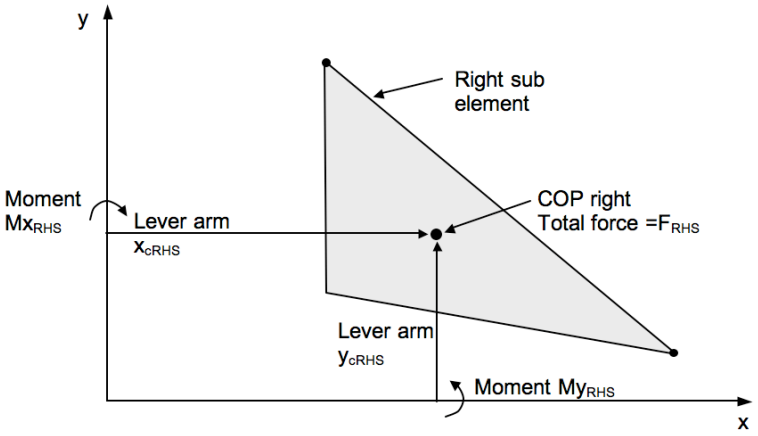


(b)

**Figure 3.10.** Moments and lever arms for the forces acting on the (a) left and (b) right sub elements

The total force, $F_{Total}$, acting on the generalised triangular element is the sum of the forces acting on each sub element, as given by equation 3.23. Likewise the corresponding total moments in the x and y directions are the summation of the moments acting on each sub element, as given by equations 3.24 and 3.25 respectively. The x and y lever arms to the equivalent centre of pressure for the triangular element, denoted by $x_c$ and $y_c$ respectively, are then determined by dividing the total moment by the total force, as given by equations 3.26 and 3.27.

$$F_{Total} = F_{LHS} + F_{RHS} \quad 3.23$$

$$Mx_{Total} = Mx_{LHS} + Mx_{RHS} \quad 3.24$$

$$My_{Total} = My_{LHS} + My_{RHS} \quad 3.25$$

$$x_c = \frac{Mx_{Total}}{F_{Total}} \quad 3.26$$

$$y_c = \frac{My_{Total}}{F_{Total}} \quad 3.27$$

Slab 4, as shown by Figure 3.7, comprises two triangular elements, and therefore this process is repeated for each element. The rotation of slab 4 is limited to the x axis as a result of the restraint offered by the supports in the y direction, therefore the total moment comprises the sum of the forces acting on each element multiplied by the lever arm in the y direction, as given by equation 3.28. Assuming unit deflection then the rotation of the slab is given by equation 3.29. Likewise for slab 1 rotation only occurs about the y axis, leading to the total moment as given by equation 3.30. Slab 1 is of triangular shape already, as shown by Figure 3.5a, so does not require splitting into additional elements. The corresponding rotation for slab 1 is given by equation 3.31.

$$M_{Slab4} = F_{TotalA1} y_{cA1} + F_{TotalA2} y_{cA2} \quad 3.28$$

$$\theta_{Slab4} = \frac{1}{\beta H} \quad 3.29$$

$$M_{Slab1} = F_{TotalA1} x_{cA1} \quad 3.30$$

$$\theta_{Slab1} = \frac{1}{\alpha_L L} \quad 3.31$$

The lever arms $x_c$ and $y_c$ are calculated for the sub elements with reference to the global coordinate system without taking into account the actual axis of rotation of the slab. Slab 2 does not rotate about the global x axis, but about the top of the wall panel, as shown by Figure 3.11a. Likewise slab 3 rotates about the right edge of the wall panel rather than the global y axis, as shown by Figure 3.11b. The actual lever arms between the axis of rotation are determined by subtracting the calculated values of $y_c$ from the panel height for slab 2, and $x_c$ from the panel length for slab 3. The moments for slab 2 and 3 are given by equations 3.32 and 3.34. The corresponding rotations of slabs 2 and 3 due to unit deflection are given by equations 3.33 and 3.35 respectively. Following this the external work done by any slab can be computed by multiplying the moment by the rotation as given by equation 3.36. The total external work done by the wall panel comprises the external work done for each slab, as given by equation 3.37.

$$M_{Slab2} = F_{TotalA1}\left(H - y_{cA1}\right) + F_{TotalA2}\left(H - y_{cA2}\right) \qquad 3.32$$

$$\theta_{Slab2} = \frac{1}{\left(H - \beta H\right)} \qquad 3.33$$

$$M_{Slab3} = F_{TotalA1}\left(L - x_{cA1}\right) \qquad 3.34$$

$$\theta_{Slab3} = \frac{1}{\left(L - \alpha_R L\right)} \qquad 3.35$$

$$ExtWD_{Slabj} = \theta_{Slabj} M_{Slabj} \qquad 3.36$$

$$ExtWD_{Total} = \sum_{j=1}^{n} ExtWD_{Slabj} \qquad 3.37$$

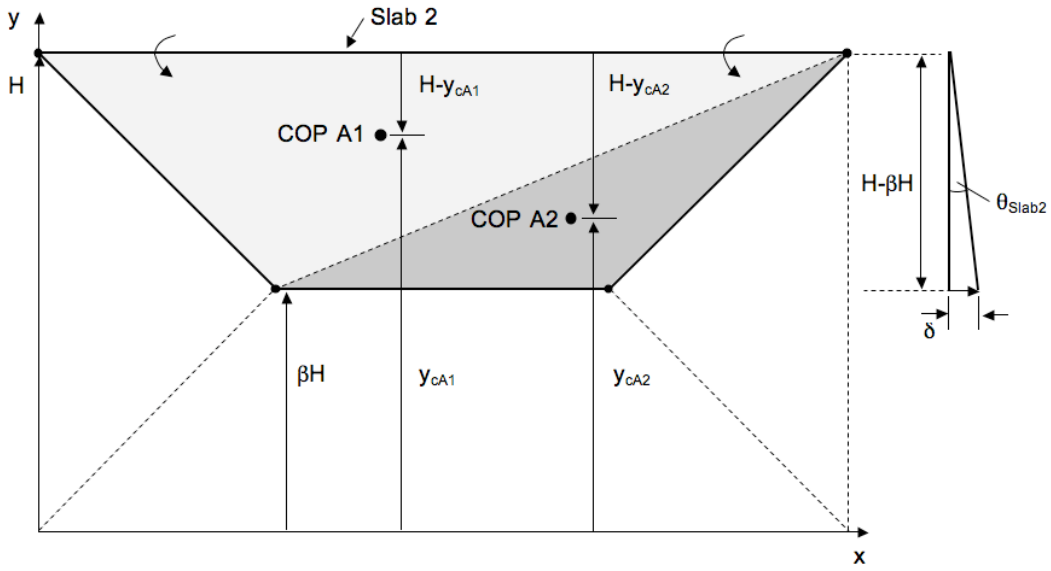


(a)

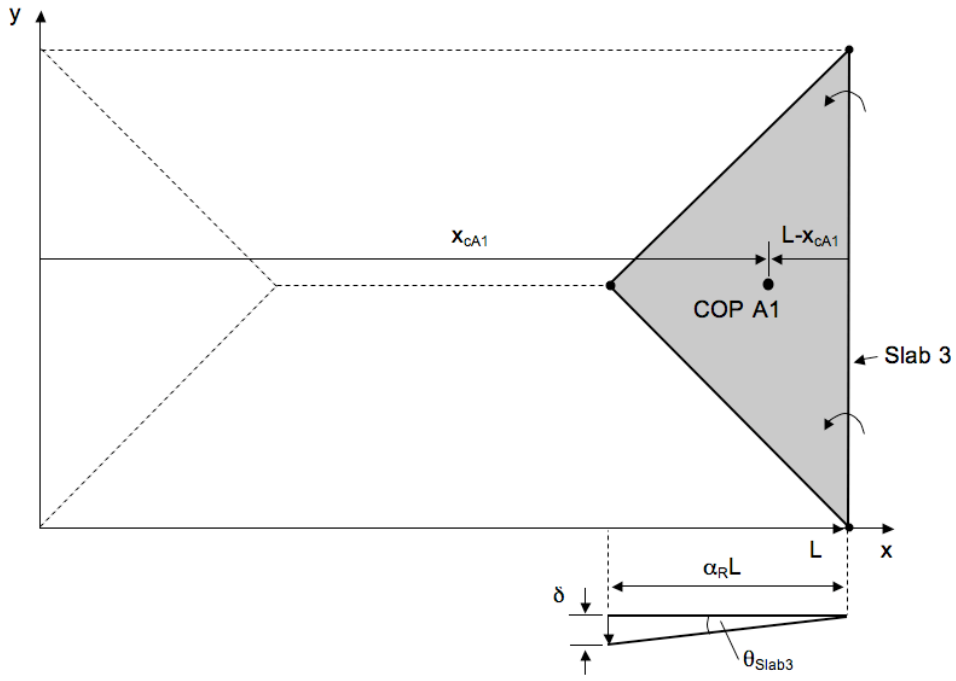


(b)

**Figure 3.11.** Lever arms for slabs (a) 2 and (b) 3

#### 3.2.2.1 Establishing the correct hydraulic loading profile over the wall panel

The depth of water is a variable for the hydraulic loading conditions, and partial coverage of the slabs may occur, as shown by Figure 3.12. In the method described in the preceding section some nodes of the triangular elements will lie above the water level and the loading applied to these will be zero (for hydraulic loads only). Clearly the loading profile over the element would be incorrect, since this would infer

that the load at the water level would be a positive value rather than zero. To account for this it is necessary to further split some slabs into additional elements and impose constraints on the position of a number of the yield lines. Slabs 1 and 3 of the wall panel supported on 4 sides, are each split into two elements and additional nodes are introduced at the water level, as shown by Figure 3.13. The nodes for the two elements in slab 2 are also repositioned such that they move in relation to the water level, as shown by Figure 3.13. The x coordinates of the nodes along the upper diagonal yield lines are determined by a similar triangles relationship. Clearly slabs 1 to 3 will now be subject to the correct loading profile if it is assumed that the height of the central yield line, determined by $\beta$, is at or below the water level. To ensure that this condition is maintained a constraint is imposed such that $\beta H$ is always less than or equal to D. It is likely that the central yield line will be at or below D for the case of a wall panel supported on four edges due to the load being concentrated towards the base of the panel. For wall panels with the top edge free, where the failure mode assumed is as shown by Figure 3.5b, then it is possible that the water level can be either above or below the node specified by $\beta$ and the constraint on $\beta H$ is therefore relaxed for this case. To impose a uniformly distributed load on the wall panel the depth of the water is set equal to the height of the wall panel in addition to setting the density of water to zero as detailed above. This ensures that the loading profile over the slabs is correct. When D=H the two upper nodes of the second element of slabs 2 and 3 converge and result in a zero error in the calculations of the applied force and centre of pressure. To avoid this a finite quantity is added to the actual position of the nodes, of value between 0.00001 and 0.00012, such that they do not coincide with each other, as shown by Figure 3.14. Offsetting the nodes by such a small value results in a negligible error in the results.

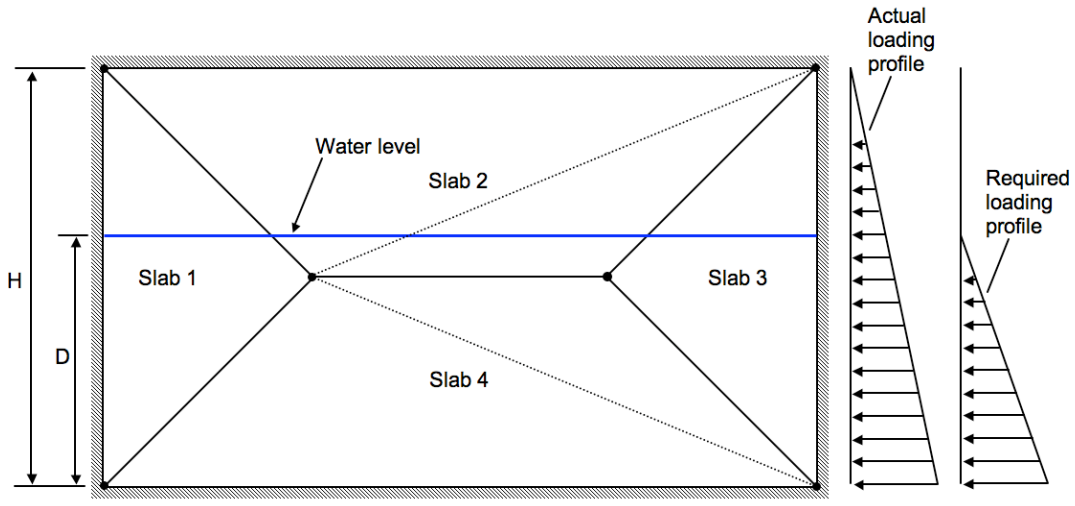


**Figure 3.12.** Loading profile for wall panel subject to hydraulic load

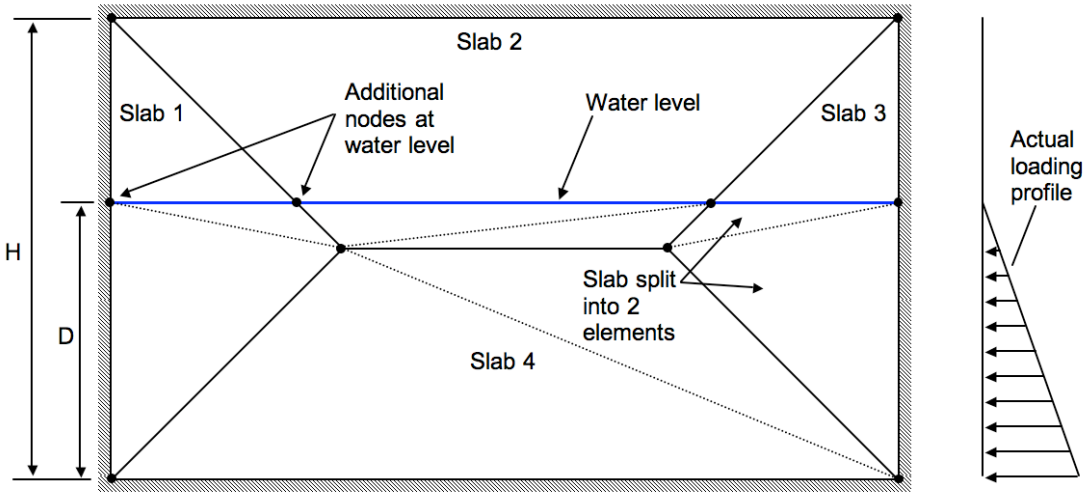


**Figure 3.13.** Splitting slabs into additional elements to obtain correct loading profile

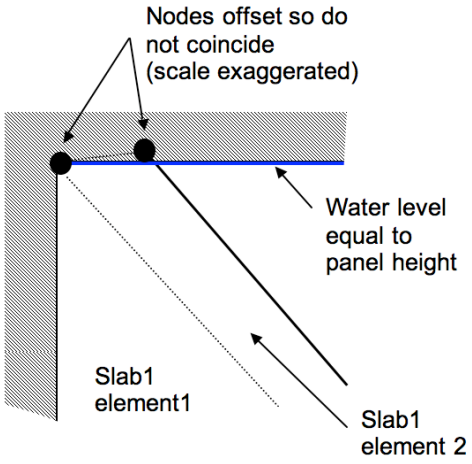


**Figure 3.14.** Offsetting the nodes to avoid zero error in calculations when D=H (scale exaggerated)

### 3.2.2.2 Cavity walls and consideration of wall tie loads

Cavity wall panels employ wall ties that join the two leaves together and when subject to the lateral load, part of the loading is transferred from one leaf to the other. This assumes that the wall ties are able to transfer such loading without failure. A cavity wall may be considered as two separate wall panels taking into account the action of the wall ties. The wall ties are accounted for by subtracting their contribution to load resistance from the load applied at each node of the triangular elements. Equation 3.7 was modified to include the contribution of the tie load at each node, as given by equation 3.38, where $P_{ties}$ is the uniformly distributed load due to the ties.

$$P_i = \rho_w g\left(D - y_i\right) + \frac{C_d \rho_w v^2}{2} + P_{udl} - P_{ties} \qquad 3.38$$

The areas of the slab above the water level, for the case of hydraulic loading, are subject to the tie loads and would additionally be subject to the uniformly distributed load for combined loading conditions. To ensure that the wall tie loads, or combined loads, are correctly applied above the water level, additional elements are created, as shown by Figure 3.15. The loading at each node of the additional elements is set equal to $P_{udl}$ less the tie loads.

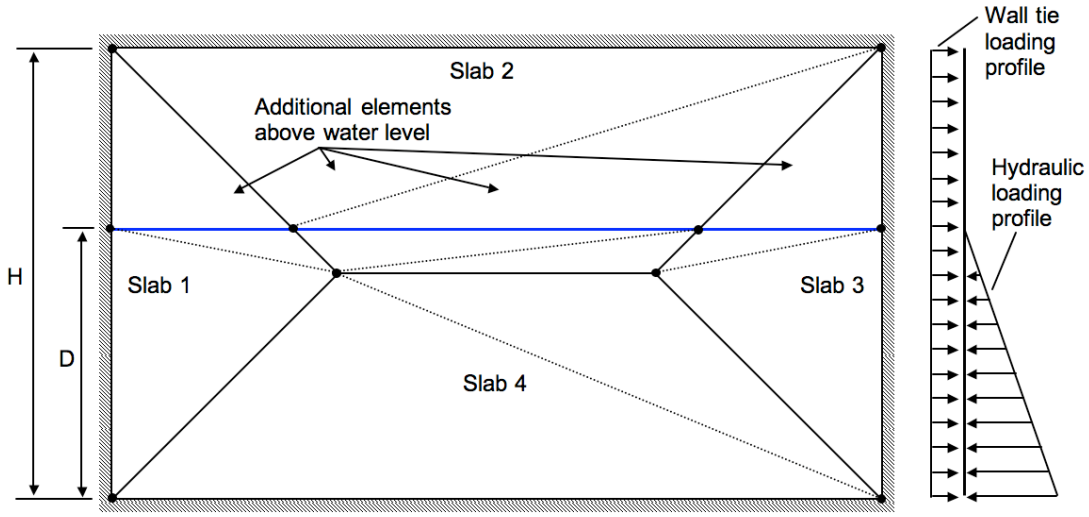


**Figure 3.15.** Additional elements for wall tie loads required above water level

### 3.2.3 Calculation of internal work done

The internal work done is calculated along each yield line in turn and comprises the moment resistance in the corresponding direction multiplied by both the length of the yield line and the rotation. This is completed for directions both parallel and perpendicular to the bed joints, taking into account the fixity of the particular yield line. The nodal coordinates established for the calculation of the external work done are used here to define the start and end points of each yield line. The moment resistance per unit length, $M_{Rdl}$, is then calculated from the flexural strength, $f_{xl}$, of the masonry, as given by equation 3.39, where subscript l can refer to direction 1 or 2 and Z is the section modulus.

$$M_{Rdl} = f_{xl} Z \qquad 3.39$$

Any surcharge applied vertically to the top of the wall panel, as discussed in Chapter 4 Section 4.1.4, and the vertical load due to self-weight would have a positive benefit

on the moment resistance in direction 1. To ensure that this is correctly considered the total vertical load, $V_i$, per unit length at the height of each node is determined, following equation 3.40. The total load comprises the uniformly distributed component applied to the top of the wall, $V_{udl}$, and self-weight imposed by the section of the wall panel above the node. The vertical load varies along a yield line that starts and ends at different y coordinates and to allow for this the average load is computed, as given by equation 3.41.

$$V_i = V_{udl} + \rho_{Brick} T_{bl} g\left(h - y_i\right) \qquad 3.40$$

$$V_{av} = \frac{V_1 + V_2}{2} \qquad 3.41$$

The positive benefit from the vertical loading to the moment resistance in direction 1 is taken into account by considering a resistance to overturning as shown by Figure 3.16a. If the hinge point is positioned at the edge of the masonry section then an infinite stress capacity is assumed. The actual position of the hinge point is therefore considered to be at the centre of a stress block, as shown by Figure 3.16b, such that a limiting compressive stress level is imposed. A compression depth factor, $C_f$, is utilised to allow for the hinge to be positioned away from the edge of the specimen (Kelman and Spence, 2003a). The magnitude of $C_f$ can be varied to account for the strength of the particular masonry material in question. The value of $C_f$ is selected manually in the analysis. To avoid material crushing the reaction force may be assumed to be in the middle third of the masonry section, resulting in a value of 1/3 for $C_f$. The moment resistance in direction 1, $M_{RPd1}$, per unit length due to the vertical loading is given by equation 3.42, where $T_{bl}$ is the thickness of the masonry units. The total moment resistance in direction 1, per unit length, is therefore a combination of the flexural strength and the overturning resistance as given by equation 3.43.

$$M_{RPd1} = V_{av} C_f \frac{T_{bl}}{2} \qquad 3.42$$

$$M_{Rd1}^{total} = V_{av} C_f \frac{T_{bl}}{2} + M_{Rd1} \qquad 3.43$$

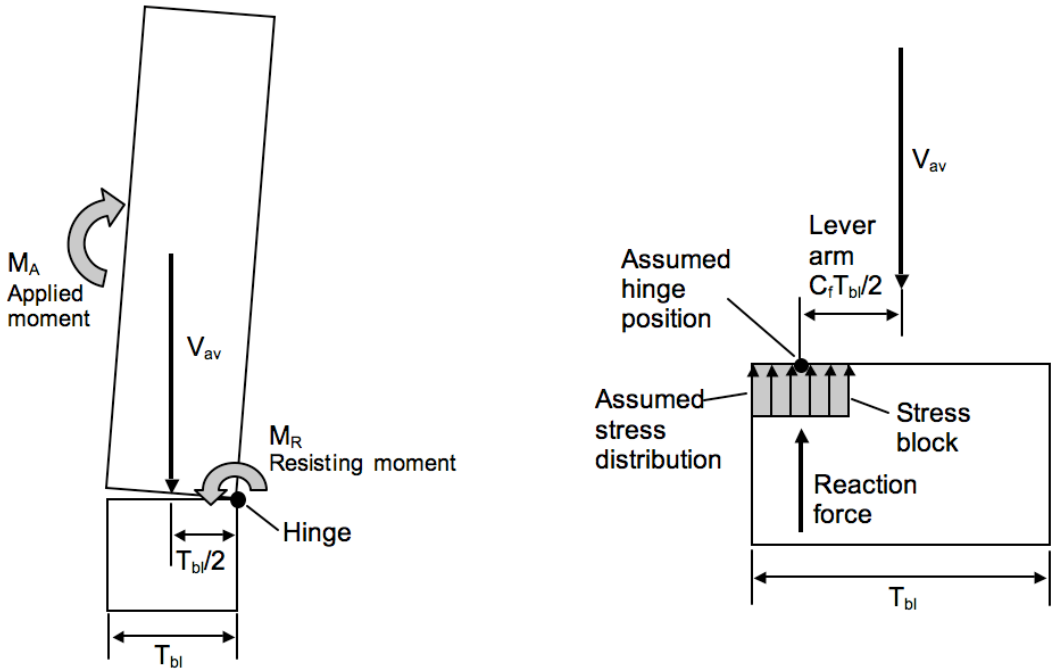


(a) (b)

**Figure 3.16.** (a) Overturning resistance due to vertical loading and (b) assumed position of hinge point at centre of stress block

Using the nodal coordinates, the length of the yield line, in the x or y direction, can be calculated, whilst the rotation is determined from the slab rotations, as shown by Figure 3.17. Following this, the internal work done is computed along each yield line in directions 1 and 2, as given by equations 3.44 and 3.45 respectively. The total internal work done is equal to the internal work done at each yield line, as given by equation 3.46.

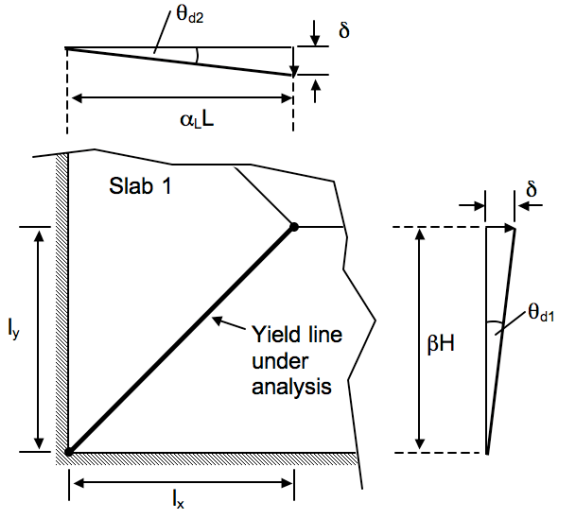


**Figure 3.17.** Calculation of yield line length and rotation

$$IntWDd1_{YLj} = \left[\left(V_{av} C_f \frac{Tbl}{2} + M_{Rd1}\right) l_x \theta_{d1}\right]_{YLj} \quad 3.44$$

$$IntWDd2_{YLj} = \left[M_{Rd2} l_y \theta_{d2}\right]_{YLj} \quad 3.45$$

$$IntWD_{Total} = \sum_{j=1}^{n} IntWD_{YLj} \quad 3.46$$

#### 3.2.3.1 Moment resistance due to friction and vertical load (overturning)

A method has been presented (Martini, 1998) in which post cracking moments of resistance were developed due to the vertical load. It was assumed (Martini, 1998) that the masonry had no tensile strength in directions 1 or 2. In direction 1 the moment of resistance was purely due to the vertical load and self-weight, and would be equivalent to that given by equation 3.44 when $M_{Rd1}$ was zero (by setting $f_{xd1}$=0). It was assumed (Martini, 1998) that the hinge point was at the edge of the section and therefore the compression factor, $C_f$, was equal to 1.

In direction 2 it was proposed (Martini, 1998) that the moment of resistance was due to the frictional force couple acting at the interface between adjacent units of the wall panel as they rotated during failure, as shown by Figure 3.18a. The frictional force, F, was assumed to be due to the self-weight of the masonry above and any additional surcharge applied at the top of the wall. It was proposed that bending about direction 1 would reduce the width of the contact area and affect the frictional resistance, as shown by Figure 3.18b. The frictional force due to the vertical load was given by equation 3.47, where $\omega$ was the coefficient of friction and $L_{bl}$ was the length of the masonry unit. The moment of resistance then followed by multiplying the force due to friction by the lever arm to centre of rotation, as given by equation 3.48. The frictional forces only occurred at the unit interfaces and to determine the equivalent moment it was necessary to divide by the unit height, $H_{bl}$. To simplify the calculation an equivalent lever arm was used, as given by equation 3.49, and the moment of resistance was then given by equation 3.50.

$$F = \omega V_{av} \frac{L_{bl}}{4} \quad 3.47$$

$$MR_{Pd2} = F \frac{L_{bl}}{4} \frac{1}{H_{bl}} \quad 3.48$$

$$l_{arm} = \frac{L_{bl}}{16 H_{bl}} \qquad 3.49$$

$$MR_{Pd2} = V_{av} l_{arm} \omega \qquad 3.50$$

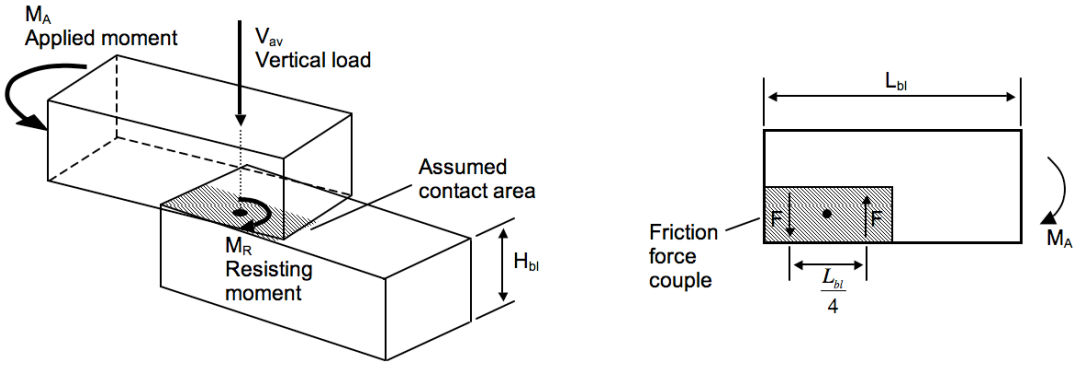


(a) (b)

**Figure 3.18.** (a) Development of a moment of resistance in direction 2 due to vertical load and (b) frictional force couple at interface (Martini, 1998)

A similar approach was proposed (Kelman and Spence, 2003a) to that detailed above (Martini, 1998) to determine the moment resistance in direction 1, but correctly included a compression depth factor to limit the stress level at the hinge point. Calculation of the moment resistance in direction 1 would follow by utilising equation 3.44 when $MR_{d1}$ was zero (by setting $f_{xd1}$=0).

The moment resistance in direction 2 was determined following a similar method to that given above (Martini, 1998), but a different equivalent lever arm was proposed, as given by equation 3.51 (Kelman and Spence, 2003a). Little explanation was given with regards to the exact derivation of the lever arm in this case (Kelman and Spence, 2003a). It should be noted that the lever arm was identical to that used in calculation of the moment resistance in direction 1, as given by equation 3.42.

$$l_{arm} = \frac{C_f T_{bl}}{2} \qquad 3.51$$

To allow both the frictional and flexural strength methods to be considered in one analysis the expression giving the total internal work done along a yield line in direction 2, as given by equation 3.45, is modified to include the frictional component given by equation 3.50. The resulting equation for the total internal work done along a yield line in direction 2 is given by equation 3.52. By setting $M_{Rd2}$ to zero (by setting

$f_{xd2}$=0) then only frictional resistance at the interface is considered, whilst to utilise only flexural strength in the analysis then the coefficient of friction is set to zero. Although the analysis allows for both flexural strength and frictional methods it is not intended to utilise both methods at the same time.

$$IntWDd2_{YLj} = \left[\left(V_{av} l_{arm} \omega + MR_{d2}\right) y \theta_{d2}\right]_{YLj} \qquad 3.52$$

### 3.2.4 Determining the ultimate load

The lowest value of the ultimate load is obtained when the internal work done is equal to the external work done, as given by equation 3.53. The equation can be solved for the particular case in question by simultaneously optimising the parameters $\alpha$ and $\beta$ that determine the position of the yield lines, and the magnitude of the lateral loading applied to the wall. For the case of hydraulic loading only this involves optimising the depth of water, D, against the wall, whilst for uniform loading the magnitude of $P_{udl}$ is optimised. Combined loading can also be considered, by setting either D or $P_{udl}$ to a predefined value and optimising the other parameter that is not held constant. The stepwise approach to the calculation of both the external and internal energy makes the process suitable for solution using a computer program or spreadsheet with optimisation capabilities.

$$\frac{IntWD_{Total}}{ExtWD_{Total}} = 1 \qquad 3.53$$

## 3.3 Development of the spreadsheet analysis tool

The method outlined in Section 3.2 was suitable for solution using a bespoke computer program or via a spreadsheet with an optimisation tool. The solution could have been completed using a number of different programming languages, but the end result could be difficult for others without programming knowledge to interpret or understand. To avoid this it was decided to develop the solution using readily available Microsoft Excel spreadsheet software that included a built in Solver optimisation tool. The Solver tool allows for the optimisation of the value of a cell within the spreadsheet, termed the target cell, by varying other cells, called adjustable cells. Constraints can also be employed in the solver to limit the values of the adjustable cells. The following section details the development of the spreadsheet analysis according to the yield line approach outlined in Section 3.2 and the application of the Solver tool. Two analyses were developed, Spreadsheet

Analysis 1 (SA1) allowed for the condition where the yield lines formed to the corners of the slab, as shown by Figure 3.5, and Spreadsheet Analysis 2 (SA2) allowed for corners levers, as shown by Figure 3.6. The following section focuses on the development of SA1 and the differences in the approach required for SA2 are detailed in Section 3.3.7. The spreadsheet is split into a number of sections, termed boxes, and within each box a specific data entry or calculation task was completed.

### 3.3.1 Establishing yield line pattern, nodal coordinates and nodal forces

The yield line pattern for SA1 was selected such that it was possible to consider a range of cases where all edges were supported or when specific edges were unconstrained, as shown by Figure 3.19. This allowed the cases previously shown by Figure 3.5 to be considered in one analysis, for example the position of the nodes for the top edge free and vertical edge free are shown by Figures 3.20 and 3.21 respectively. The layout of the panel is specified in terms of nodes, N1 to N18. The nodes at the corners of the wall panel were determined from the length and height for the specific case under analysis, which were entered into Box A, as shown by Figure 3.22. Nodes at the junctions of the yield lines are specified in terms of the variable parameters $\alpha$L, $\alpha$R, $\beta$ and $\gamma$. Additional nodes are specified, as discussed in Section 3.2, for the depth of water and to enable the forces within each slab formed to be readily determined. The position of each node is calculated in Box J, as shown by Figure 3.23, from the parameters in Box A. Multiples of the finite quantity, called roundoff and specified in Box K, are added to the actual nodal positions in a systematic manner to avoid zero errors when nodes could coincide, as described in Section 3.2. Additional parameters such as the thickness and unit length and height are also specified in Box A for use elsewhere in the analysis.

At failure the wall panel is split into a maximum of 5 slab elements, denoted S1 to S5, by the yield lines. Each yield line is specified by the letter J followed by a number, for example J1 refers to the yield line between nodes N1 and N17. Slab elements are sub divided into triangular areas, denoted by the letter A followed by a number, to allow the determination of the external work done as detailed in Section 3.2.2. The triangular areas A1 to A14 are located below the water level, whilst areas A15 to A30 are positioned above the water level to allow for wall tie loads or combined hydraulic and uniformly distributed loading conditions. A number of triangular areas are required above the water level to account for the different yield line patterns possible with the top edge free or supported, and whether yield line J8 (between nodes N3

and N5) is above or below the water level when the top edge of the panel is free, as shown by Figure 3.20 a and b respectively.

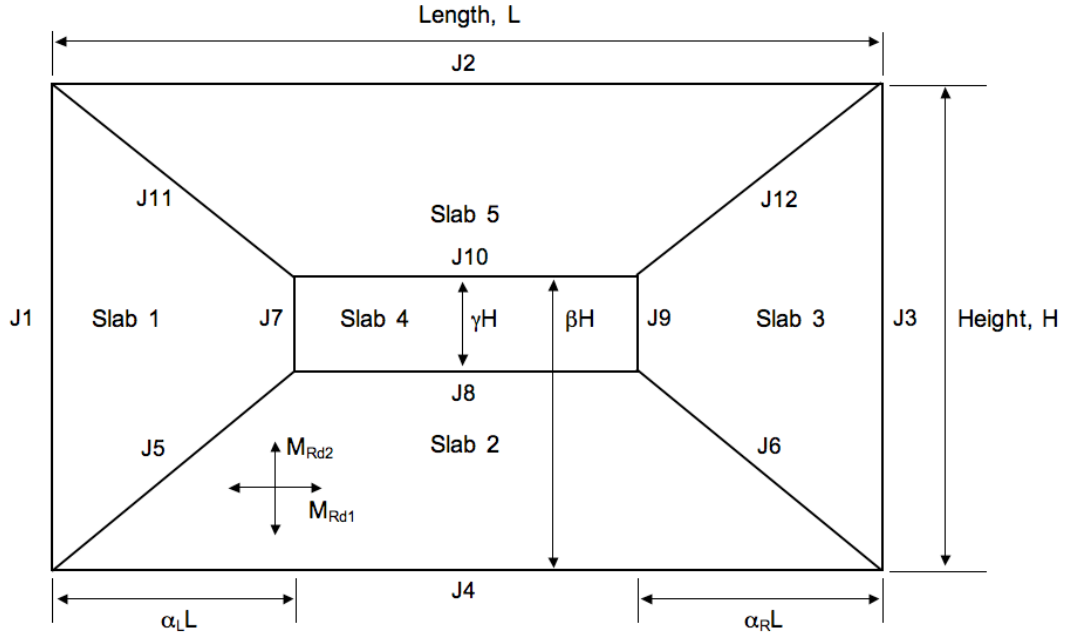


(a)

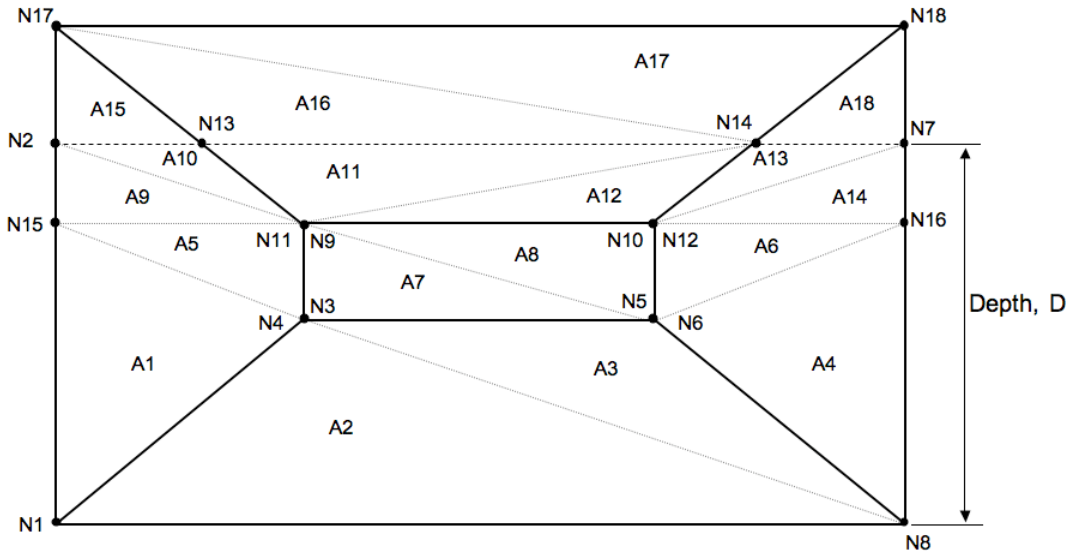


(b)

**Figure 3.19.** Yield line pattern selected for SA1: (a) layout of slab elements and yield lines, and (b) position of nodes and division into triangular elements

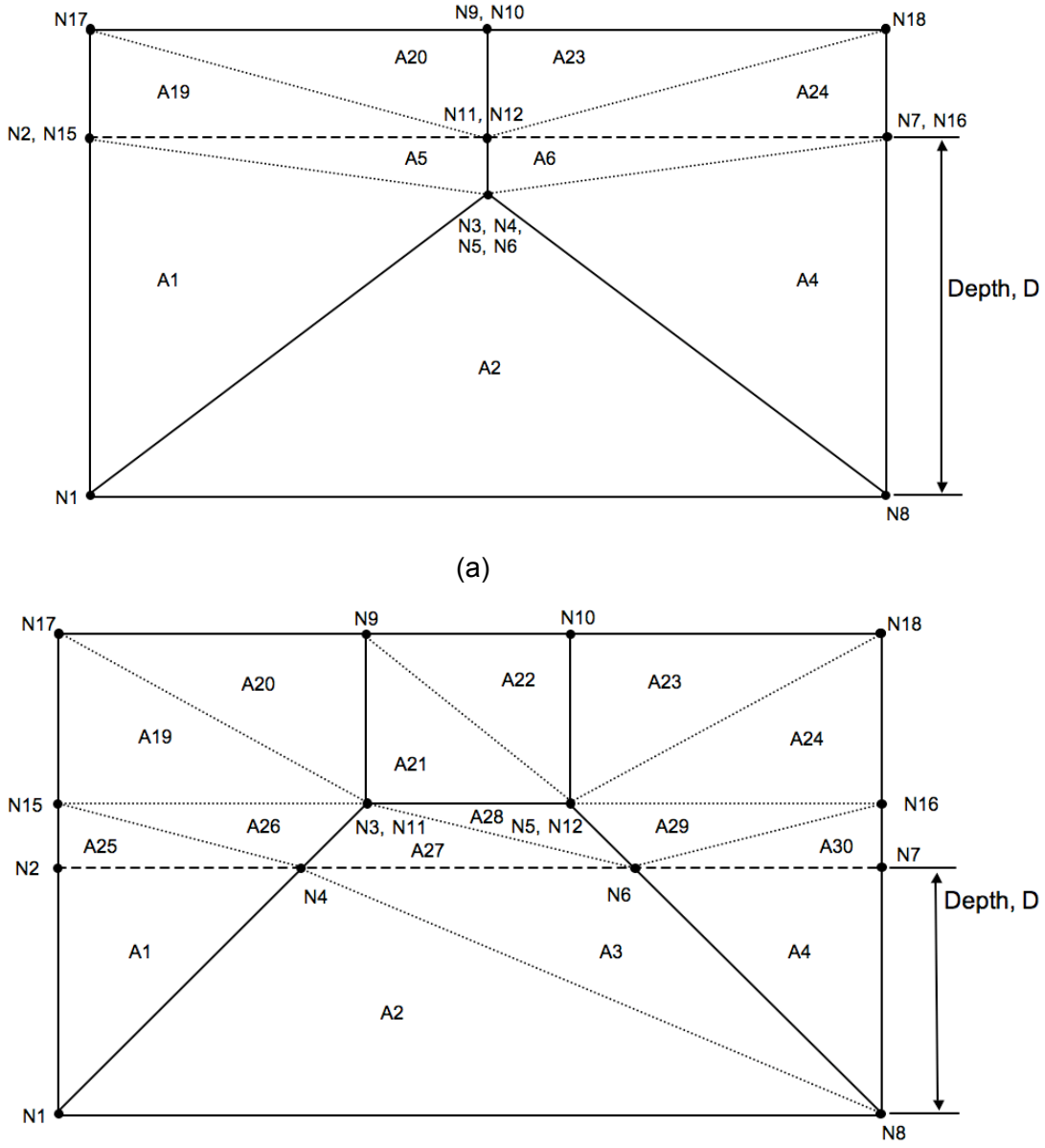


**Figure 3.20.** Possible yield line patterns in SA1 for top edge free when (a) D is above J8 and (b) D is below J8

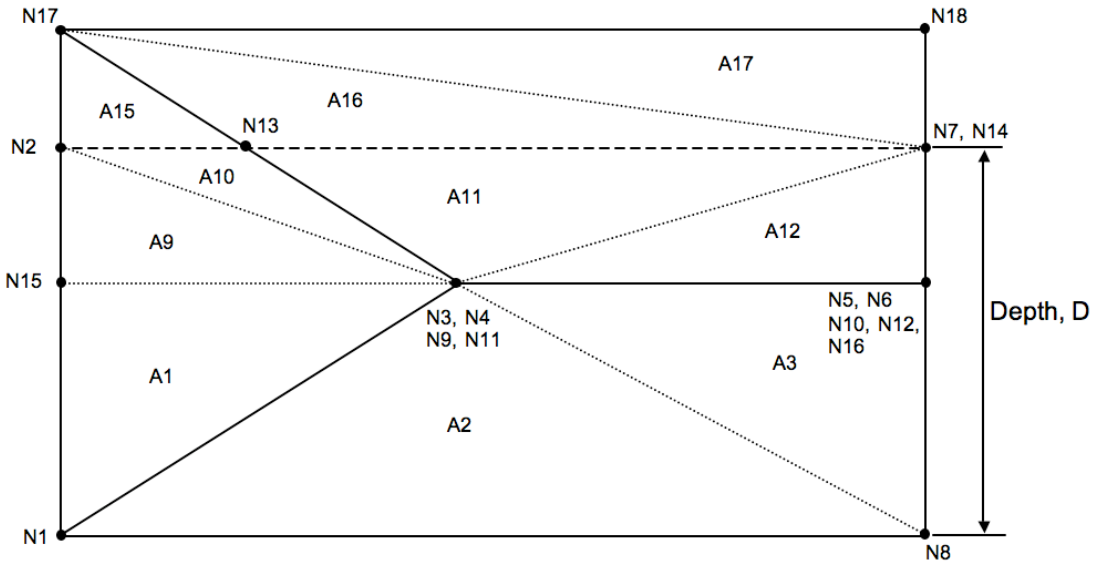


**Figure 3.21.** Position of nodes in the SA1 for right vertical edge free

**Box A: Wall dimensions**

| | | | |
|---|---|---|---|
| Length | 4.755 | m | h/l ratio μ |
| Height | 2.452 | m | 0.516 |
| Depth of water | 2.452 | m | |
| Thickness wall | 0.103 | m | |
| Unit height | 0.065 | m | |
| Unit length | 0.215 | m | |
| αL | 0.500 | no units | |
| αR | 0.500 | no units | |
| β (top SS or C) | 0.500 | no units | |
| γ | 0.000 | no units | |
| αL*L | 2.377 | m | |
| αR*L | 2.377 | m | |
| β*H | 1.226 | m | |
| γ*H | 0.000 | m | |
| αL+αR | 1.000 | no units | |
| beta-small | 0.500 | no units | |

**Figure 3.22.** Data entry for the dimensions of the wall panel in Box A

**Box J: Nodal coordinates and forces**

| Node | Coordinate (m) | | Horizontal pressure | Vertical load |
|---|---|---|---|---|
| | x | y | kN/m2 | kN/m |
| N1 | 0.000 | 0.000 | 2.869 | 9.014 |
| N2 | 0.000 | 2.452 | 2.869 | 4.507 |
| N3 | 2.377 | 1.226 | 2.869 | 6.761 |
| N4 | 2.377 | 1.226 | 2.869 | 6.761 |
| N5 | 2.378 | 1.226 | 2.869 | 6.761 |
| N6 | 2.378 | 1.226 | 2.869 | 6.761 |
| N7 | 4.755 | 2.452 | 2.869 | 4.507 |
| N8 | 4.755 | 0.000 | 2.869 | 9.014 |
| N9 | 2.377 | 1.226 | 2.869 | 6.760 |
| N10 | 2.378 | 1.226 | 2.869 | 6.760 |
| N11 | 2.377 | 1.226 | 2.869 | 6.760 |
| N12 | 2.378 | 1.226 | 2.869 | 6.760 |
| N13 | 0.000 | 2.452 | 2.869 | 4.507 |
| N14 | 4.755 | 2.452 | 2.869 | 4.507 |
| N15 | 0.000 | 1.226 | 2.869 | 6.761 |
| N16 | 4.755 | 1.226 | 2.869 | 6.760 |
| T1 | 0.000 | 2.452 | 2.869 | 4.507 |
| T2 | 4.755 | 2.452 | 2.869 | 4.507 |

**Figure 3.23.** Nodal coordinates and forces in Box J

The edge support conditions for the wall panel are selected in Box B, as shown by Figure 3.24, which also provides a graphical display of the yield line and opening positions. The buttons alongside each support allow the support conditions to be varied between free, simply supported and clamped, which are denoted by F, S and C respectively. A further button is utilised to include the moment resistance, due to self-weight and vertical imposed loads, along yield line J4 when the base was simply supported. For fully clamped conditions at the base the moment resistance is automatically included and the cell was greyed out using conditional formatting in the spreadsheet to prevent confusion. The proportion of the fully clamped conditions can be varied at the side supports to allow for partial support conditions, such as the use of ties to connect the panel to another structure or second wall panel. Here 0 % represents conditions equal to a simple support, 100 % is fully clamped and a value in between is considered as a partial support. Conditional formatting is similarly used to grey out the content of the fixity cells for free or simply supported edge conditions.

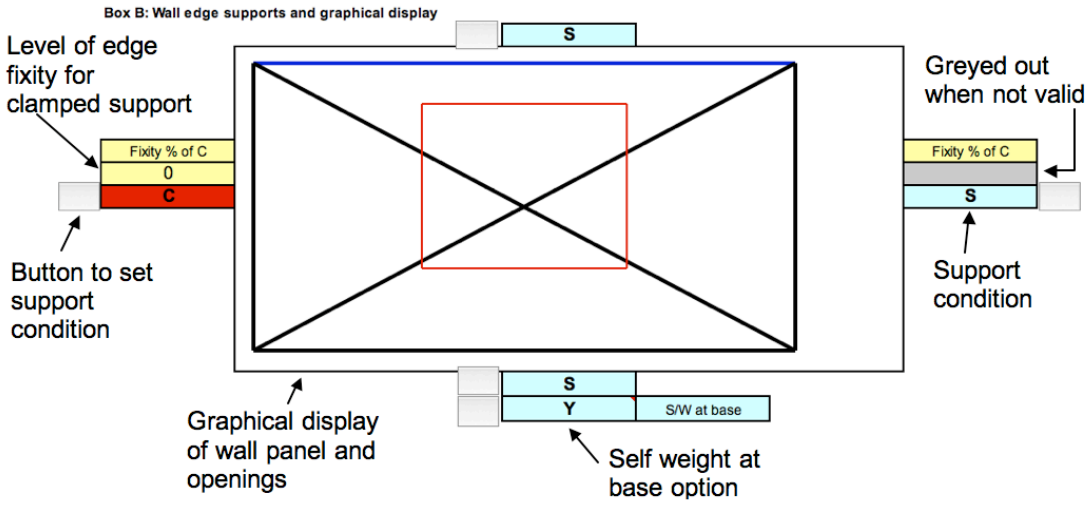


**Figure 3.24.** Selection of edge support conditions and graphical display of yield line positions in Box B

The spreadsheet allows for either hydraulic (hydrostatic and hydrodynamic) or uniform loading conditions or a combination of the two types of loading. The parameters used to determine the lateral pressure are entered in Box D, as shown by Figure 3.25, whilst the depth of water is inputted in Box A. For the case of pure uniform loading the depth of water is set to the height of the wall, whilst the density and velocity are set to zero. The horizontal pressure per unit area at each node is determined from the hydrostatic, hydrodynamic and uniform lateral load and computed in Box J using equation 3.38. A node would not experience any hydraulic lateral pressure when the water level was below the height of the node and to account for this an "IF" statement is employed such that negative values are not computed. Switching between the required parameters for hydraulic and uniform loading conditions is completed using a macro and is discussed in further detail in Section 3.3.6.

**Box D: Lateral load parameters**

| | | |
|---|---|---|
| Density of water $\rho_w$ | 0.0 | $kg/m^3$ |
| Velocity of water v | 0.000 | m/s |
| Shape factor $C_d$ | 0.000 | no units |
| Uniform distributed load $P_{udl}$ | 2.869 | $kN/m^2$ |
| Cavity tie load $P_{ties}$ | 0.000 | $kN/m^2$ |
| bm coefficient | 0.0391 | no units |

**Figure 3.25.** Lateral load parameters for hydraulic and uniform loading conditions in Box D

### 3.3.2 Calculation of vertical axial load

The vertical loading applied to the top of the wall panel can be calculated using two methods (Option 1 or 2) or specified by the user (Option 3) in Box E, as shown by Figure 3.26. Option 1 allows for the load to be calculated from the contribution from the walls, floor and roof above the wall panel in question, as shown by Figure 3.27. The total load for option 1 is given by equation 3.54, where $V_{udlR}$ and $V_{udlF}$ are the uniformly distributed loads on the roof and floor respectively. The floor and roof widths, $w_F$ and $w_R$ respectively, for option 1 correspond to the half the distance between the supports, which are the outer wall and intermediate wall for the case shown by Figure 3.27. For the case of a single storey property, where j=1, then the vertical loading at the top of the wall comprises of only the roof loads. Option 2 allows for the vertical load to be calculated using a previously proposed method (Kelman and Spence, 2003a) that is based on the plan area of the property, A, and a factor (lambda) that accounts for the support conditions of the floor and roof, as given by equation 3.55. A lambda value of 0.25 implies the same conditions as shown for option 1 in Figure 3.27, whilst a value of 0.5 represents a structure without an intermediate wall. Alternatively the user can calculate the vertical load using an alternative method and input this into the spreadsheet via option 3. The vertical loading condition to be used in the analysis is specified by selecting the appropriate radio button alongside Box E, as shown by Figure 3.26. The total vertical load at each node is the summation of the applied and self-weight components and is computed using equation 3.40 in Box J.

**Box E: Vertical axial loading to top of wall**

| | | | | |
|---|---|---|---|---|
| Number of floors, j | 2 | minimum of 1 | | Common parameters |
| Floor height | 2.400 | m | | |
| Floor load | 0.491 | kN/m$^2$ | | |
| Floor width | 2.750 | m | | Option 1 |
| Roof load | 0.687 | kN/m$^2$ | | |
| Roof width | 2.750 | m | | |
| Load | 7.649 | kN/m | ○ | |
| Area | 55.000 | m$^2$ | | Option 2 |
| Lambda | 0.250 | | | |
| Load | 7.816 | kN/m | ○ | |
| User defined load | 4.507 | kN/m | ◉ | Option 3 |
| Vertical loading in analysis | 4.507 | kN/m | | |

**Figure 3.26.** Options for vertical axial loading to top of wall in Box E

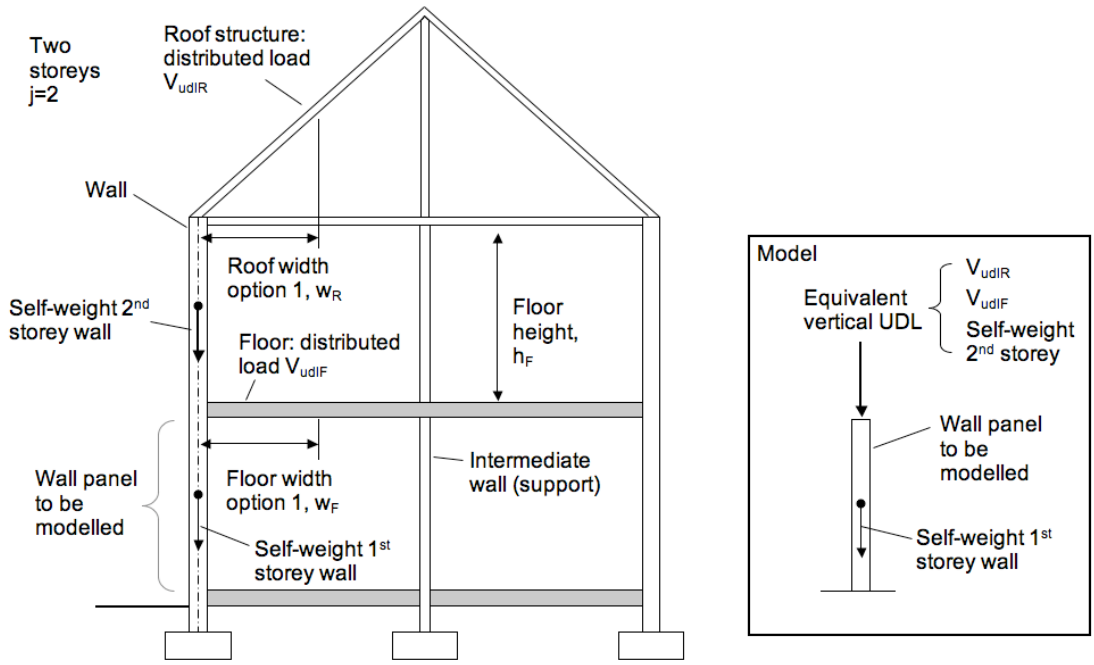


**Figure 3.27.** Vertical loading for option 1 (a) actual structure and (b) equivalent model

$$V_{udl} = V_{udlR} w_R + (j-1)(V_{udlF} w_F + \rho_{Brick} T_{bl} h_F g) \qquad 3.54$$

$$V_{udl} = (j-1)(\rho_{Brick} T_{bl} h_F g) + (j-1)(V_{udlR} + V_{udlF}) \frac{A}{L} \lambda \qquad 3.55$$

### 3.3.3 Calculation of external work done

The total forces and corresponding lever arms are calculated for each triangular element following the method detailed in Section 3.2.2. This process is completed in Box L, as shown by Figure 3.28. The external work done on each slab is then calculated from the moments from each triangular area contained in the slab and the rotation according to equation 3.36 in Box M, as shown by Figure 3.29. It is assumed that at failure unit deflection occurred simultaneously at nodes N3, N5, N9 and N10 and that the deflection is small. The rotations of each slab are calculated as previously described in Section 3.2.2. The total external work done is then found by summing the values calculated for each slab, using equation 3.37.

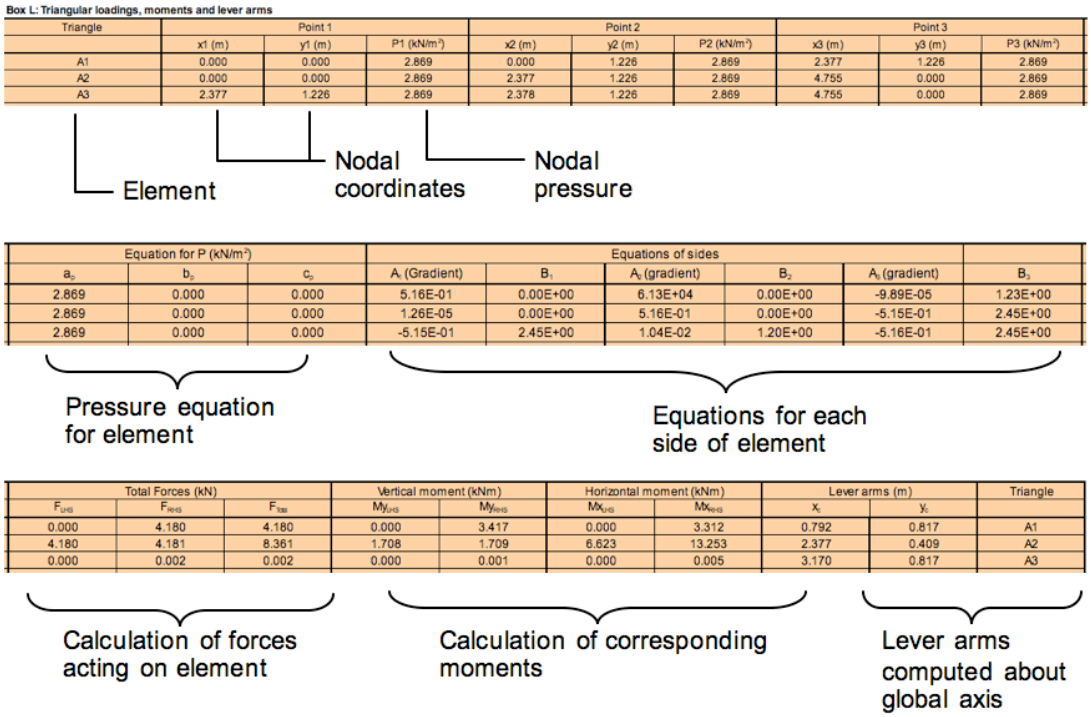


**Figure 3.28.** Calculation of total forces and corresponding levers arms for triangular elements in Box L (shown for elements A1 to A3)

**Box M: External work done on slabs**

| Slab | Moments M (kNm) | Angle θ | Energy E (kJ) |
|---|---|---|---|
| S1 | 6.627 | 0.421 | 2.788 |
| S2 | 3.418 | 0.816 | 2.789 |
| S3 | 6.626 | 0.421 | 2.788 |
| S4 | 0.000 | 1 | 0.000 |
| S5 | 3.419 | 0.816 | 2.789 |
| | | Total | 11.153 |

**Figure 3.29.** External work done on each slab and the total for the panel in Box M

### 3.3.4 Calculation of internal work done

The spreadsheet allows for the internal work done along the yield lines to be calculated using the flexural strength of the masonry or either of the frictional/overturning resistance methods outlined in Section 3.2.3.1. For the flexural strength method the bending strengths of the masonry are either prescribed values given by the national annex to EC6 (BSI, 2005d) or from experimental wallette tests according to BS EN 1052-2 (BSI, 1999). The flexural strengths for direction 1 ($f_{x1}$) and direction 2 ($f_{x2}$) are inserted into Box Q on a second sheet titled “Parameters”, as shown by Figure 3.30. Direction 1 corresponds to a test direction parallel to the bed joints and likewise direction 2 corresponds to a test direction perpendicular to the bed joints. The density of the masonry is also specified in box Q alongside the particular

masonry type. The selection of the required masonry type and mortar compressive strength class is made in Box C by use of the scroll buttons alongside the box, as shown by Figure 3.31. The Lookup function in the spreadsheet is utilised to select the appropriate values from Box Q according to the masonry type and mortar strength class selected by the user and are displayed in Box C. The moment resistance per unit length in directions 1 and 2 are calculated using equation 3.39 in Box K, as shown by Figure 3.32.

**Box Q: Flexural strength and density parameters for wall**

Flexural strengths from Table NA.6 in NA to BS EN 1996-1-1:2005

Custom 1- 3 can be changed by user

| | $f_{x1}$ parallel test to bed joints (N/mm$^2$) | | | $f_{x2}$ perpendicular to test direction (N/mm$^2$) | | | Density (kg/m$^3$) |
|---|---|---|---|---|---|---|---|
| Masonry type↓ Mortar strength class→ | M12 | M6 & M4 | M2 | M12 | M6 & M4 | M2 | |
| Clay brick water abs<7% | 0.70 | 0.50 | 0.40 | 2.00 | 1.50 | 1.20 | 2000.00 |
| Clay brick water abs 7-12% | 0.50 | 0.40 | 0.35 | 1.50 | 1.10 | 1.00 | 1828.00 |
| Clay brick water abs >12% | 0.40 | 0.30 | 0.25 | 1.10 | 0.90 | 0.80 | 2000.00 |
| CaSi bricks | 0.30 | 0.30 | 0.20 | 0.90 | 0.90 | 0.60 | 2000.00 |
| Concrete bricks | 0.30 | 0.30 | 0.20 | 0.90 | 0.90 | 0.60 | 2000.00 |
| 2.9N Concrete blocks | 0.25 | 0.25 | 0.20 | 0.40 | 0.40 | 0.40 | 2000.00 |
| 3.6N Concrete blocks | 0.25 | 0.25 | 0.20 | 0.45 | 0.45 | 0.40 | 772.00 |
| 7.3N Concrete blocks | 0.25 | 0.25 | 0.20 | 0.60 | 0.60 | 0.50 | 2000.00 |
| 10.4N Concrete blocks | 0.25 | 0.25 | 0.20 | 0.75 | 0.75 | 0.60 | 2000.00 |
| ≥17.5N Concrete blocks | 0.25 | 0.25 | 0.20 | 0.90 | 0.90 | 0.70 | 1828.00 |
| Custom 1 (brick test) | 0.36 | 0.66 | 0.44 | 0.99 | 1.45 | 1.02 | 1828.00 |
| Custom 2 (brick block test) | 0.00 | 0.33 | 0.50 | 0.00 | 0.96 | 1.28 | 1828.00 |
| Custom 3 (AAC block test) | 0.00 | 0.27 | 0.41 | 0.00 | 0.55 | 0.67 | 772.00 |

**Figure 3.30.** Flexural strength and density parameters for wall panel in Box Q

**Box C: Material properties**

| | | |
|---|---|---|
| Masonry type | Custom 1 (brick test) | |
| Mortar strength class | M6 & M4 | |
| Density of masonry | 1828.0 | kg/m3 |
| $f_{x1}$ | 0.660 | N/mm$^2$ |
| $f_{x2}$ | 1.450 | N/mm$^2$ |
| Cf for vertical load | 0.333 | no units |

Selection of masonry type

Selection of mortar strength class

Values from Box Q

**Figure 3.31.** Material properties selection in Box C

**Box K: Modelling parameters**

| | | |
|---|---|---|
| Gravity constant, g | 9.81 | m/s$^2$ |
| Section modulus, Z | 1.751 | mm$^3$ |
| Moment $M_{Rd2}$ | 2.539 | kNm |
| Moment $M_{Rd1}$ | 1.156 | kNm |
| small | 0.0001 | no units |
| large | 0.9999 | no units |
| roundoff | 0.00001 | no units |

**Figure 3.32.** Modelling parameters in Box K

For the friction/overturning method the frictional parameters are set in Box H, as shown by Figure 3.33, where the lever arm (Kelman and Spence, 2003a, Martini, 1998) can be utilised by selecting the appropriate radio button alongside. The lever arm used in the analysis is calculated according to equation 3.49. When utilising

either friction/overturning method it is necessary to set the flexural strength to zero, this can be achieved by entering a value of zero in the custom section of Box Q.

**Box H: Friction plastic moments**

| | | |
|---|---|---|
| Coeffcient of friction | 0.000 | no units |
| Martini lever arm | 0.044 | m |
| Kelman lever arm | 0.017 | m |
| L_arm in analysis | 0.044 | |

**Figure 3.33.** Parameters for friction/overturning method in Box H

The internal energy along each yield line is computed in Box N, as shown by Figure 3.34, following the method outlined in Section 3.2.3. Fixity of the yield lines due to the edge support conditions that can be selected in Box B were dealt with in the fixity section of Box N. A value of 1 corresponded to fixity, whilst 0 corresponded to no fixity. For example if yield line J1 is simply supported then the fixity in direction 2 ($F_{d2}$) would be 0, as it would be free to rotate about direction 2 at failure and would not contribute to the internal energy, whilst in direction 1 ($F_{d1}$), J1 is constrained against rotation due to the support conditions. The edge support conditions selected in Box B are utilised within an IF statement, as given by equation 3.56, to select the corresponding level of fixity for the yield lines at the perimeter of the panel. For completeness a fixity of 1 is entered into the cells that corresponded to the constrained directions as discussed above.

Additional logical statements are required to ensure that the correct level of fixity is selected when particular yield lines could be positioned at the edge of the panel. For the case when a vertical edge is free, as shown by Figure 3.35a, then the yield lines J6, J7, J9 and J12 can also be at the free edge and their fixity about the direction 2 is zero. A logical statement, as given by equation 3.57, ensured the correct fixity of these yield lines under this support condition. An additional check of the geometry is necessary in the logical statement for yield line J7, as given by equation 3.58, since other failure modes are possible where J7 is not at the free edge, as shown by Figure 3.35b. Yield lines J6 and J12 can also be of zero fixity in direction 1 when they are at the vertical free edge, however it is not necessary to include a logical statement for this condition. Here the length of the yield lines J6 and J12 in direction 1 are small due to the geometry of the problem, such that the corresponding energy calculated is negligible. Similar statements are used to ensure the correct fixity when

the top or bottom of the wall panel is free, as given by equations 3.59 and 3.60 respectively.

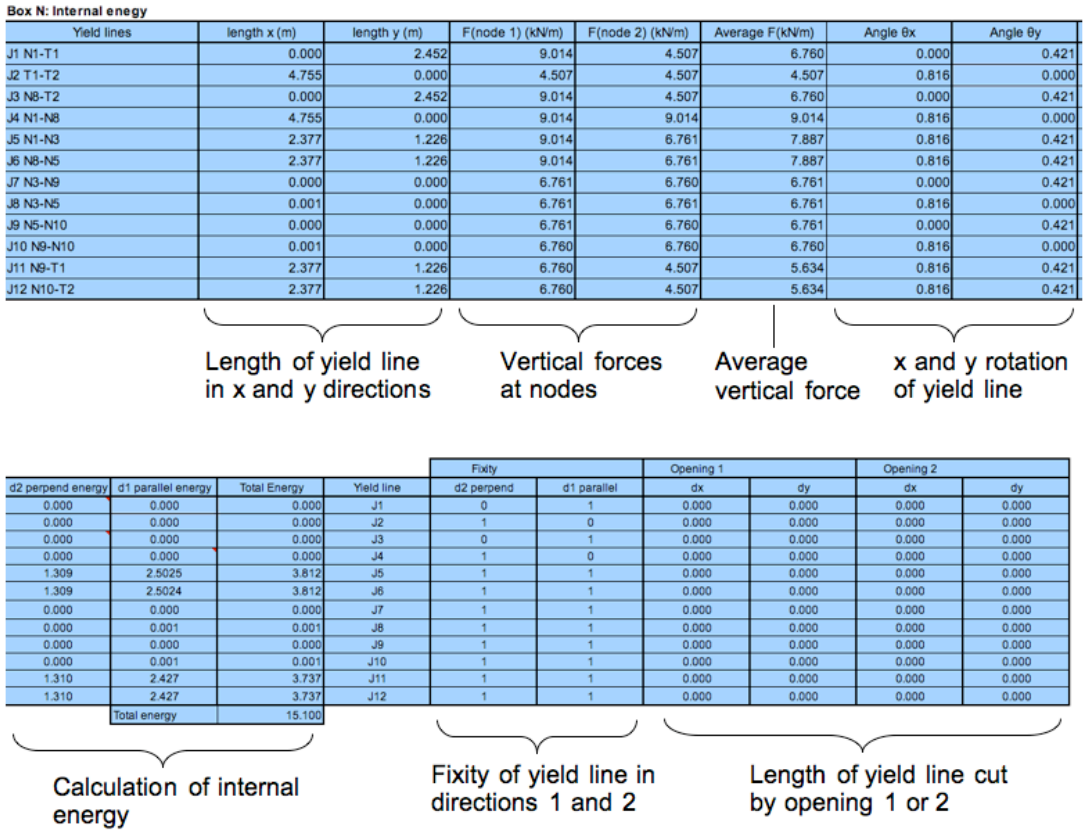

**Box N: Internal enegy**

| Yield lines | length x (m) | length y (m) | F(node 1) (kN/m) | F(node 2) (kN/m) | Average F(kN/m) | Angle θx | Angle θy |
|---|---|---|---|---|---|---|---|
| J1 N1-T1 | 0.000 | 2.452 | 9.014 | 4.507 | 6.760 | 0.000 | 0.421 |
| J2 T1-T2 | 4.755 | 0.000 | 4.507 | 4.507 | 4.507 | 0.816 | 0.000 |
| J3 N8-T2 | 0.000 | 2.452 | 9.014 | 4.507 | 6.760 | 0.000 | 0.421 |
| J4 N1-N8 | 4.755 | 0.000 | 9.014 | 9.014 | 9.014 | 0.816 | 0.000 |
| J5 N1-N3 | 2.377 | 1.226 | 9.014 | 6.761 | 7.887 | 0.816 | 0.421 |
| J6 N8-N5 | 2.377 | 1.226 | 9.014 | 6.761 | 7.887 | 0.816 | 0.421 |
| J7 N3-N9 | 0.000 | 0.000 | 6.761 | 6.760 | 6.761 | 0.000 | 0.421 |
| J8 N3-N5 | 0.001 | 0.000 | 6.761 | 6.761 | 6.761 | 0.816 | 0.000 |
| J9 N5-N10 | 0.000 | 0.000 | 6.761 | 6.760 | 6.761 | 0.000 | 0.421 |
| J10 N9-N10 | 0.001 | 0.000 | 6.760 | 6.760 | 6.760 | 0.816 | 0.000 |
| J11 N9-T1 | 2.377 | 1.226 | 6.760 | 4.507 | 5.634 | 0.816 | 0.421 |
| J12 N10-T2 | 2.377 | 1.226 | 6.760 | 4.507 | 5.634 | 0.816 | 0.421 |

Length of yield line in x and y directions

Vertical forces at nodes

Average vertical force

x and y rotation of yield line

| | | | | Fixity | | Opening 1 | | Opening 2 | |
|---|---|---|---|---|---|---|---|---|---|
| d2 perpend energy | d1 parallel energy | Total Energy | Yield line | d2 perpend | d1 parallel | dx | dy | dx | dy |
| 0.000 | 0.000 | 0.000 | J1 | 0 | 1 | 0.000 | 0.000 | 0.000 | 0.000 |
| 0.000 | 0.000 | 0.000 | J2 | 1 | 0 | 0.000 | 0.000 | 0.000 | 0.000 |
| 0.000 | 0.000 | 0.000 | J3 | 0 | 1 | 0.000 | 0.000 | 0.000 | 0.000 |
| 0.000 | 0.000 | 0.000 | J4 | 1 | 0 | 0.000 | 0.000 | 0.000 | 0.000 |
| 1.309 | 2.5025 | 3.812 | J5 | 1 | 1 | 0.000 | 0.000 | 0.000 | 0.000 |
| 1.309 | 2.5024 | 3.812 | J6 | 1 | 1 | 0.000 | 0.000 | 0.000 | 0.000 |
| 0.000 | 0.000 | 0.000 | J7 | 1 | 1 | 0.000 | 0.000 | 0.000 | 0.000 |
| 0.000 | 0.001 | 0.001 | J8 | 1 | 1 | 0.000 | 0.000 | 0.000 | 0.000 |
| 0.000 | 0.000 | 0.000 | J9 | 1 | 1 | 0.000 | 0.000 | 0.000 | 0.000 |
| 0.000 | 0.001 | 0.001 | J10 | 1 | 1 | 0.000 | 0.000 | 0.000 | 0.000 |
| 1.310 | 2.427 | 3.737 | J11 | 1 | 1 | 0.000 | 0.000 | 0.000 | 0.000 |
| 1.310 | 2.427 | 3.737 | J12 | 1 | 1 | 0.000 | 0.000 | 0.000 | 0.000 |
| | Total energy | 15.100 | | | | | | | |

Calculation of internal energy

Fixity of yield line in directions 1 and 2

Length of yield line cut by opening 1 or 2

**Figure 3.34.** Calculation of internal energy in Box N

$$IF\left(Edge = clamped,1,0\right) \qquad 3.56$$

$$IF\left(Edge_{RHS} = free,0,1\right) \qquad 3.57$$

$$IF\left(AND\left(Edge_{RHS} = free,1-\alpha L-\alpha R<0.001\right),0,1\right) \qquad 3.58$$

$$IF\left(AND\left(Edge_{TOP} = free,\beta>0.999\right),0,1\right) \qquad 3.59$$

$$IF\left(\beta-\gamma<0.001,0,IF\left(Edge_{BOTTOM} = free,0,1\right)\right) \qquad 3.60$$

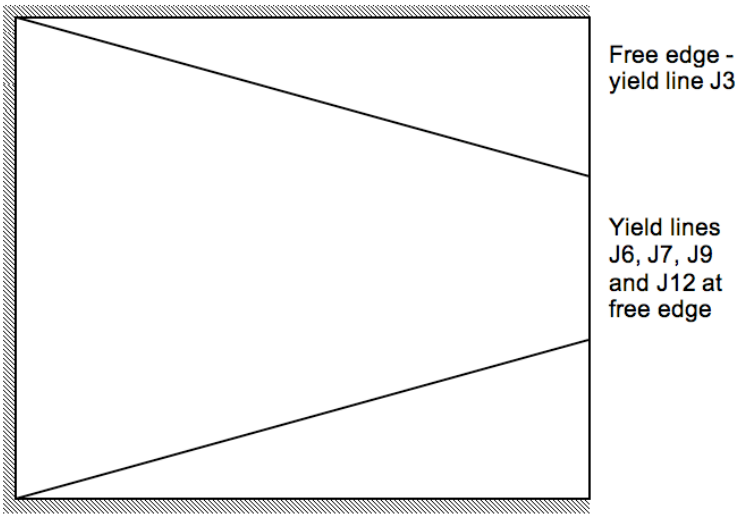


(a)

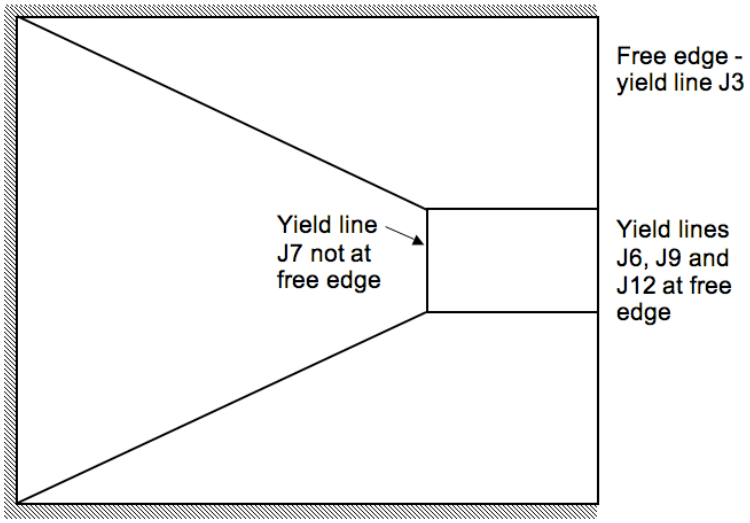


(b)

**Figure 3.35.** Fixity for the case of a vertical free edge: (a) yield lines J6, J7, J9 and J12 at free edge and (b) yield line J7 not at free edge

The sections of the yield lines, defined as dx and dy, that are within any openings in the wall panel are automatically entered in the opening section of Box N. These are computed in Box O and further discussion of how this is completed is given in Section 3.3.4.1 below. Equations 3.44 and 3.52, that determined the internal energy expended along a yield line in directions 1 and 2 respectively, are modified such that the section of any yield line within an opening and the fixity were taken into account. The modified equations for directions 1 and 2 are given by equations 3.61 and 3.62 respectively. A logical statement is incorporated into equation 3.61 for yield line J4 only to allow for self-weight at the base of the wall panel when simple support conditions and self-weight are selected in Box B. Partial support conditions at the left

and right vertical edges of wall panel, which corresponded to yield lines J1 and J3 respectively, can also be specified in Box B. For this case the internal energy in direction 2 for yield lines J1 and J3 is multiplied by the proportion specified in Box B. The total internal energy expended along each yield line comprises the sum of the energy calculated in directions 1 and 2. The total internal work done is then the summation of the energy expended along all yield lines.

$$IntWDd1_{YLj} = \left[\left(V_{av}C_f\frac{Tbl}{2} + MR_{d1}\right)\left(l_x - dx_1 - dx_2\right)\theta_{d1}F_{d1}\right]_{YLj} \qquad 3.61$$

$$IntWDd2_{YLj} = \left[\left(V_{av}l_{arm}\omega + MR_{d2}\right)\left(l_y - dy_1 - dy_2\right)\theta_{d2}F_{d2}\right]_{YLj} \qquad 3.62$$

### 3.3.4.1 Treatment of openings

The analysis allows for two openings to be positioned in the wall panel and the positions and dimensions of the openings are entered into Box G, as shown by Figure 3.36. It is assumed in the analysis that the opening is covered such that the work done by the external force is proportioned over the entire area of the panel including the opening. For the case of uniform wind loading this assumption requires that any window or door assembly would be able to sustain such loading. For flood loadings a protection system would likely be required to protect the windows or doors from the ingress of water and would have be designed to sustain such loadings.

Introducing an opening into the wall panel affects the internal energy when it coincides with the yield line pattern. When the opening is positioned such that the edges bisected the postulated yield line pattern, as shown by Figure 3.37, then no internal energy is expended along the sections inside the opening. The nodes where unit deflection is assumed (N3, N5, N9 and N10) are within the opening in this case. It is therefore assumed that the yield lines continue into the opening and are effectively cut by the opening edge. The amount of yield line cut depends on the size and position of the opening. It is therefore necessary to determine how much of each yield line is cut, if at all, by the particular opening configuration. The amount cut is taken into account in the computation of the internal energy in Box N. A similar approach has been taken by others to determine the internal energy of slabs with openings, but the yield line positions for particular opening configurations were postulated prior to determining the work done (Islam and Park, 1971, Wagner, 1994).

**Box G: Opening positions and dimensions**

| | Opening 1 | Opening 2 | |
|---|---|---|---|
| OsL | 1.478 | 0.000 | m |
| OsH | 0.700 | 0.000 | m |
| OL | 1.800 | 0.000 | m |
| OH | 1.400 | 0.000 | m |

**Figure 3.36.** Input of opening positions and dimensions in Box G

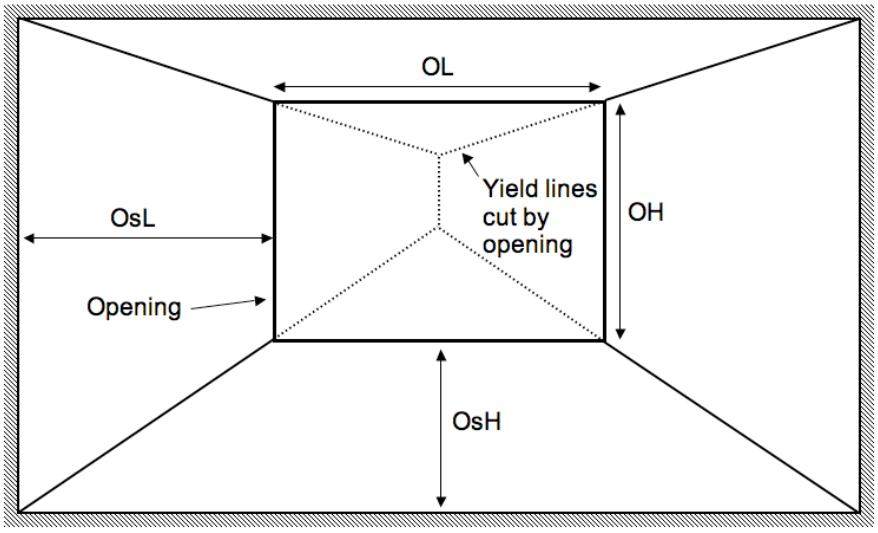


**Figure 3.37.** Opening cutting through yield line

To determine the amount of a yield line cut, if any, by a particular opening it is firstly necessary to establish if the yield line cuts through any edge of the opening. From the nodal coordinates of the yield line the gradient, $m_j$, and constant, $c_j$, are established in Box O, as shown by Figure 3.38. A hypothetical x or y point coordinate is then determined on the edge of each side of the opening using the m and c values and the opening dimensions. For a cut of the left edge, as shown by Figure 3.39a, the y coordinate of the point is given by equation 3.63. Whilst for a cut of the bottom edge, as shown by Figure 3.39b, the x coordinate of the point is given using equation 3.64. Similar equations are used to determine any points on the right and top edges. At this stage the start and end nodal locations of the actual yield line are not considered, such that a further hypothetical cut point could occur on the second edge as shown by Figure 3.39. The x or y cut point coordinate is then evaluated using a logical statement to see if it is between the upper and lower bounds of the particular edge of the opening, as shown by Figure 3.40a. For example for the left hand edge the upper and lower bounds are the opening y position (OsH) and the overall height of the opening (OsH+OH) and the resulting logical expression is given by equation 3.65. Where the logical statement is true the x and y coordinates of the point are inserted into the corresponding cells of “intersection points 1” in Box O, as shown by

Figure 3.40b. Any yield line could only cut through a maximum of two edges of the opening so the four (x,y) intersection coordinates in “intersection points 1” are reduced to two (x,y) coordinates in the “intersection points 2” part of Box O, as shown by Figure 3.41.

**Box O: Opening yield lines**

| Opening 1 | Node 1 | | Node 2 | | Line equation | |
|---|---|---|---|---|---|---|
| Joint Line | x1 | y1 | x2 | y2 | m | c |
| J1 N1-T1 | 0.000 | 0.000 | 0.000 | 2.452 | 6.13E+04 | 0.00E+00 |
| J2 T1-T2 | 0.000 | 2.452 | 4.755 | 2.452 | 2.10E-06 | 2.45E+00 |
| J3 N8-T2 | 4.755 | 0.000 | 4.755 | 2.452 | 2.23E+04 | -1.06E+05 |
| J4 N1-N8 | 0.000 | 0.000 | 4.755 | 0.000 | 1.26E-05 | 0.00E+00 |
| J5 N1-N3 | 0.000 | 0.000 | 2.378 | 1.128 | 4.74E-01 | 0.00E+00 |
| J6 N8-N5 | 4.755 | 0.000 | 2.378 | 1.128 | -4.75E-01 | 2.26E+00 |
| J7 N3-N9 | 2.378 | 1.128 | 2.378 | 1.888 | 3.80E+04 | -9.04E+04 |
| J8 N3-N5 | 2.378 | 1.128 | 2.378 | 1.128 | 2.06E-02 | 1.08E+00 |
| J9 N5-N10 | 2.378 | 1.128 | 2.378 | 1.888 | 3.80E+04 | -9.04E+04 |
| J10 N9-N10 | 2.378 | 1.888 | 2.378 | 1.888 | 2.06E-02 | 1.84E+00 |
| J11 N9-T1 | 2.378 | 1.888 | 0.000 | 2.452 | -2.37E-01 | 2.45E+00 |
| J12 N10-T2 | 2.378 | 1.888 | 4.755 | 2.452 | 2.37E-01 | 1.32E+00 |

Node 1 coordinates

Node 2 coordinates

Equation of yield line

(a)

| LHS | TOP | RHS | BTM |
|---|---|---|---|
| y | x | y | x |
| 9.06E+04 | 3.43E-05 | 2.01E+05 | 1.14E-05 |
| 2.45E+00 | -1.67E+05 | 2.45E+00 | -8.33E+05 |
| -7.31E+04 | 4.76E+00 | -3.29E+04 | 4.76E+00 |
| 1.86E-05 | 1.66E+05 | 4.14E-05 | 5.55E+04 |
| 7.01E-01 | 4.43E+00 | 1.55E+00 | 1.48E+00 |
| 1.56E+00 | 3.29E-01 | 7.01E-01 | 3.28E+00 |
| -3.42E+04 | 2.38E+00 | 3.42E+04 | 2.38E+00 |
| 1.11E+00 | 4.96E+01 | 1.15E+00 | -1.84E+01 |
| -3.42E+04 | 2.38E+00 | 3.42E+04 | 2.38E+00 |
| 1.87E+00 | 1.27E+01 | 1.91E+00 | -5.53E+01 |
| 2.10E+00 | 1.48E+00 | 1.67E+00 | 7.39E+00 |
| 1.67E+00 | 3.27E+00 | 2.10E+00 | -2.63E+00 |

Point on bottom edge of opening

Point on right edge of opening

Point on top edge of opening

Point on left edge of opening

(b)

**Figure 3.38.** (a) Calculation of the equation for each yield line and (b) the hypothetical point on the edge of opening in Box O

$$y_i = m_j OsL + c_j \qquad 3.63$$

$$x_i = \frac{\left(OsH - c_j\right)}{m_j} \qquad 3.64$$

$$AND\left(y_i > OsH, y_i < \left(OsH + OH\right)\right) \qquad 3.65$$

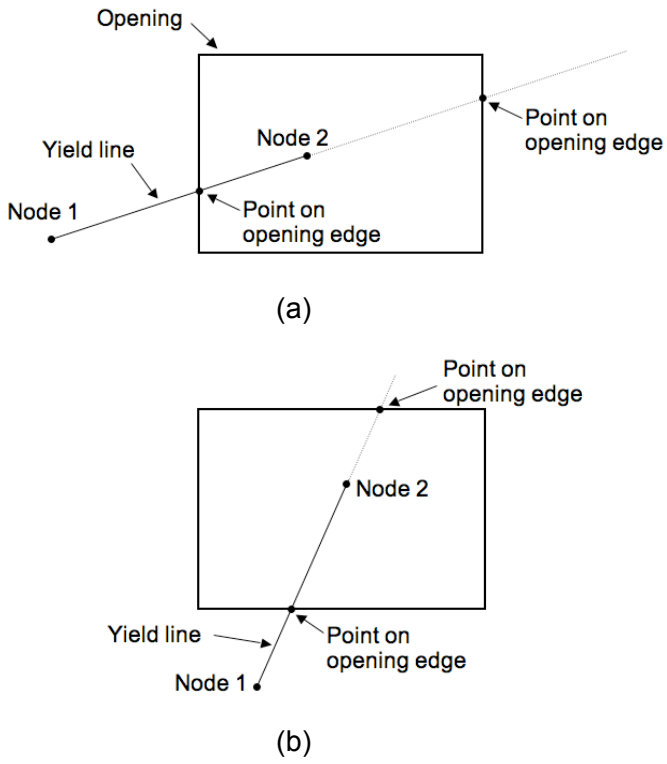


**Figure 3.39.** Determining point on edge of opening: (a) yield line cutting left edge and (b) yield line cutting bottom edge

The next stage is to determine how much of the yield line was within the opening. Firstly a logical statement, as given by equation 3.66, is used to determine whether the start and end nodes, $N_1$ and $N_2$, of the yield line are inside (true) or outside (false) the opening, as shown by Figure 3.41. The yield line is then classified into one of 6 types, as shown by Figure 3.42, using a nested logical statement as given by equation 3.67. Here $N_1$ and $N_2$ are the true or false answers returned by equation 3.66, $P_{int}$ are the intersection points, $x_a$ is the first intersection point x coordinate, and $x_1$ and $x_2$ are the x coordinates of nodes 1 and 2 respectively. For yield line types 3 and 4 it is further necessary to establish which of the two intersection points on the opening edges are between the nodes. For yield line type 3, logical statements for the x and y directions, as given by equations 3.68 and 3.69, are used to check the distance between the node outside the opening and the two possible points on the edges of the opening, as shown by Figure 3.43. The ABS function is employed to account for the situation where N2 is to the left or below the points on the edge of the opening. A similar process is completed for yield line type 4 where the subscripts 2 are replaced by 1 in equations 3.68 and 3.69, since N1 is now outside the opening.

| LHS | TOP | RHS | BTM |
|---|---|---|---|
| cut | cut | cut | cut |
| FALSE | FALSE | FALSE | FALSE |
| FALSE | FALSE | FALSE | FALSE |
| FALSE | FALSE | FALSE | FALSE |
| FALSE | FALSE | FALSE | FALSE |
| TRUE | FALSE | TRUE | FALSE |
| TRUE | FALSE | TRUE | FALSE |
| FALSE | TRUE | FALSE | TRUE |
| TRUE | FALSE | TRUE | FALSE |
| FALSE | TRUE | FALSE | TRUE |
| TRUE | FALSE | TRUE | FALSE |
| FALSE | TRUE | TRUE | FALSE |
| TRUE | TRUE | FALSE | FALSE |

Check if points are within upper and lower bounds of edge

(a)

| Intersection points 1 | | | | | | | |
|---|---|---|---|---|---|---|---|
| xLHS | yLHS | xTOP | yTOP | xRHS | yRHS | xBTM | yBTM |
| | | | | | | | |
| | | | | | | | |
| | | | | | | | |
| | | | | | | | |
| 1.478 | 0.701 | | | 3.278 | 1.555 | | |
| 1.478 | 1.555 | | | 3.278 | 0.701 | | |
| | | 2.378 | 2.100 | | | 2.378 | 0.700 |
| 1.478 | 1.109 | | | 3.278 | 1.146 | | |
| | | 2.378 | 2.100 | | | 2.378 | 0.700 |
| 1.478 | 1.870 | | | 3.278 | 1.907 | | |
| | | 1.484 | 2.100 | 3.278 | 1.675 | | |
| 1.478 | 1.674 | 3.271 | 2.100 | | | | |

If point on LHS within bounds of edge paste coordinates of intersection point

(b)

**Figure 3.40.** (a) Checking if point within lower and upper bounds of opening edge and (b) if true pasting coordinates into intersection points 1 in Box O

$$N_i = AND\left(x_i > OsL, x_i < OsL + OL, y_i > OsH, y_i < OsH + OH\right) \tag{3.66}$$

$$Type = IF\left(\begin{array}{l} AND\left(N_1 = T, N_2 = T\right), 2, \\ IF\left(\begin{array}{l} AND\left(N_1 = T, N_2 = F\right), 3, \\ IF\left(\begin{array}{l} AND\left(N_1 = F, N_2 = T\right), 4, \\ IF\left(\begin{array}{l} AND\left(N_1 = F, N_2 = F, SUM\left(P_{\text{int}}\right) = 0\right), 1, \\ IF\left(SIGN\left(x_a - x_1\right) = SIGN\left(x_a - x_2\right), 6, 5\right) \end{array}\right) \end{array}\right) \end{array}\right) \end{array}\right) \tag{3.67}$$

$$x_c = IF\left(ABS\left(x_2 - x_a\right) < ABS\left(x_2 - x_b\right), x_a, x_b\right) \tag{3.68}$$

$$y_c = IF\left(ABS\left(y_2 - y_a\right) < ABS\left(y_2 - y_b\right), y_a, y_b\right) \tag{3.69}$$

| Node in or out | | Type | Intersection points 2 | | | | Type=3 or 4 | |
|---|---|---|---|---|---|---|---|---|
| node 1 | node 2 | Number | xa | ya | xb | yb | xc | yc |
| FALSE | FALSE | 1 | | | | | | |
| FALSE | FALSE | 1 | | | | | | |
| FALSE | FALSE | 1 | | | | | | |
| FALSE | FALSE | 1 | | | | | | |
| FALSE | TRUE | 4 | 1.478 | 0.701 | 3.278 | 1.555 | 1.478 | 0.701 |
| FALSE | TRUE | 4 | 1.478 | 1.555 | 3.278 | 0.701 | 3.278 | 0.701 |
| TRUE | TRUE | 2 | 2.378 | 2.100 | 2.378 | 0.700 | | |
| TRUE | TRUE | 2 | 1.478 | 1.109 | 3.278 | 1.146 | | |
| TRUE | TRUE | 2 | 2.378 | 2.100 | 2.378 | 0.700 | | |
| TRUE | TRUE | 2 | 1.478 | 1.870 | 3.278 | 1.907 | | |
| TRUE | FALSE | 3 | 1.484 | 2.100 | 3.278 | 1.675 | 1.484 | 2.100 |
| TRUE | FALSE | 3 | 1.478 | 1.674 | 3.271 | 2.100 | 3.271 | 2.100 |

Check if yield line node inside or outside opening

Determine yield line type

Reduced intersection points

For type 3 or 4 determine correct point on opening edge

**Figure 3.41.** Box O determination of nodal location in openings, yield line type and yield line intersection points

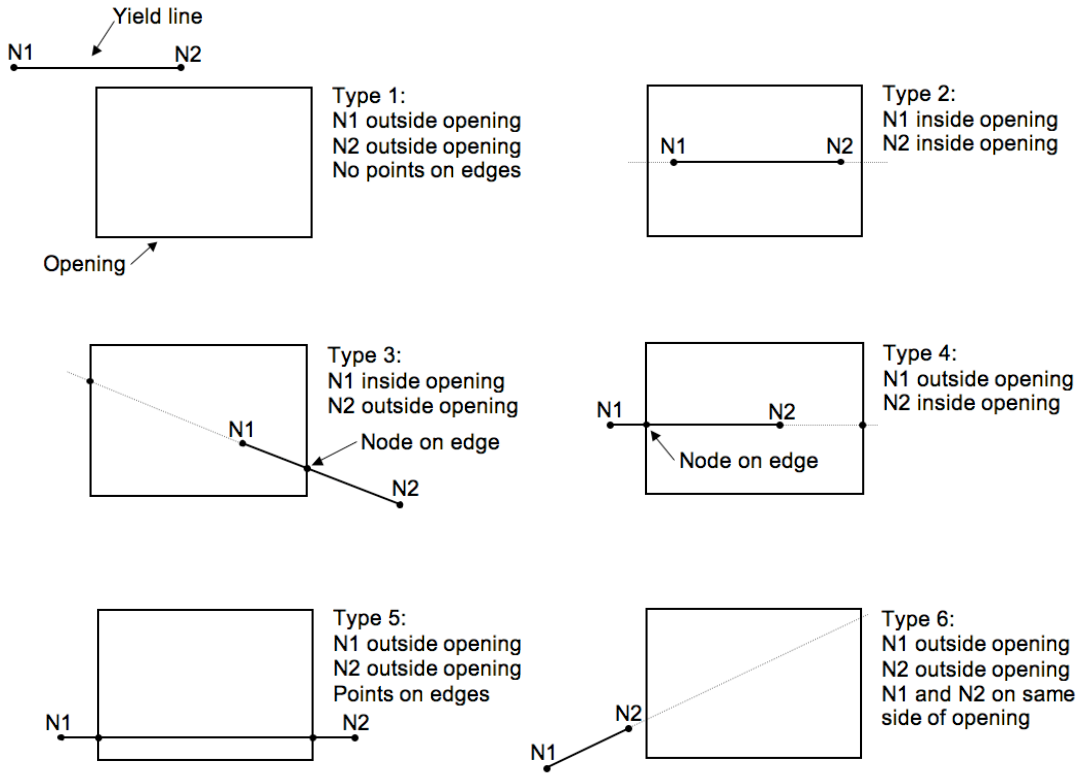


**Figure 3.42.** Classification of yield line opening types

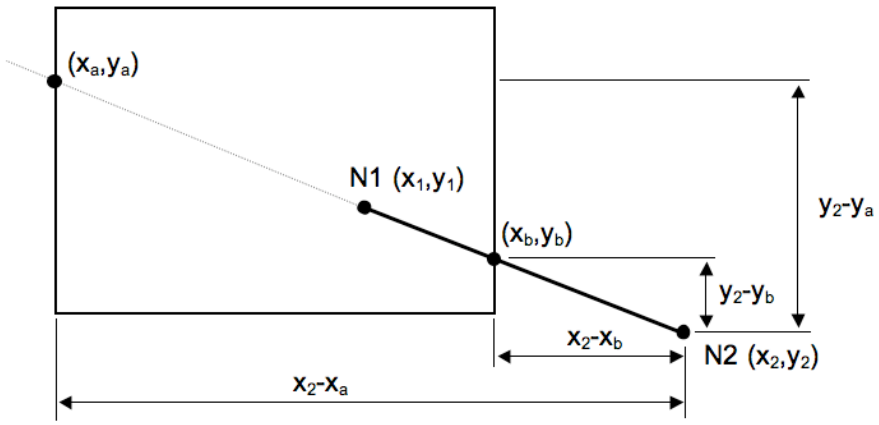


**Figure 3.43.** Determining the correct point on edge of opening for yield line type 3

Following this, the start and end points of the cut yield line for types 2 to 5 are finalised and the length and height of the section cut is calculated in Box O, as shown by Figure 3.44. A further logical statement is utilised to determine the correct start and end points according to the yield line type, as given by equations 3.70 and 3.71 for the x direction. Similar expressions are used for the y direction. The length and height of the cut section is simply determined by subtracting the finalised start and end points in the x and y directions respectively. The length or height of the cut section is subtracted from the overall length or height of the yield line in the internal energy calculations, previously given by equations 3.61 and 3.62 respectively.

$$x_{start} = IF\begin{pmatrix} OR(TYPE = 2, TYPE = 3)x_1, \\ IF\begin{pmatrix} TYPE = 4, x_c, \\ IF(TYPE = 5, x_a) \end{pmatrix} \end{pmatrix} \qquad 3.70$$

$$x_{end} = IF\begin{pmatrix} OR(TYPE = 2, TYPE = 4)x_2, \\ IF\begin{pmatrix} TYPE = 3, x_c, \\ IF(TYPE = 5, x_b) \end{pmatrix} \end{pmatrix} \qquad 3.71$$

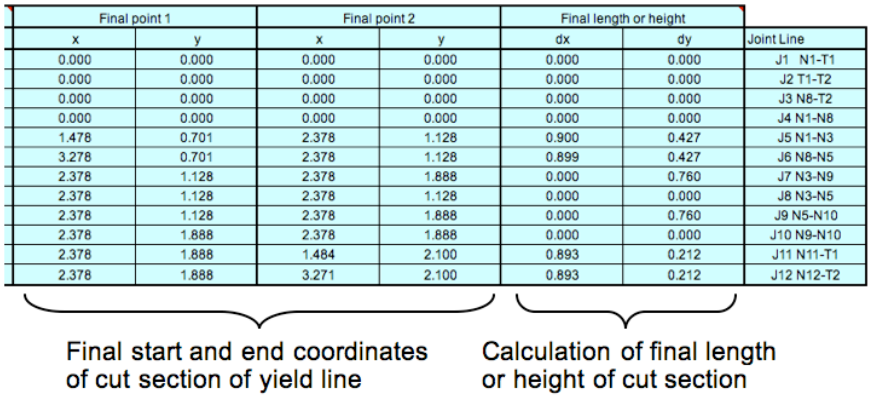

| Final point 1 | | Final point 2 | | Final length or height | | |
|---|---|---|---|---|---|---|
| x | y | x | y | dx | dy | Joint Line |
| 0.000 | 0.000 | 0.000 | 0.000 | 0.000 | 0.000 | J1 N1-T1 |
| 0.000 | 0.000 | 0.000 | 0.000 | 0.000 | 0.000 | J2 T1-T2 |
| 0.000 | 0.000 | 0.000 | 0.000 | 0.000 | 0.000 | J3 N8-T2 |
| 0.000 | 0.000 | 0.000 | 0.000 | 0.000 | 0.000 | J4 N1-N8 |
| 1.478 | 0.701 | 2.378 | 1.128 | 0.900 | 0.427 | J5 N1-N3 |
| 3.278 | 0.701 | 2.378 | 1.128 | 0.899 | 0.427 | J6 N8-N5 |
| 2.378 | 1.128 | 2.378 | 1.888 | 0.000 | 0.760 | J7 N3-N9 |
| 2.378 | 1.128 | 2.378 | 1.128 | 0.000 | 0.000 | J8 N3-N5 |
| 2.378 | 1.128 | 2.378 | 1.888 | 0.000 | 0.760 | J9 N5-N10 |
| 2.378 | 1.888 | 2.378 | 1.888 | 0.000 | 0.000 | J10 N9-N10 |
| 2.378 | 1.888 | 1.484 | 2.100 | 0.893 | 0.212 | J11 N11-T1 |
| 2.378 | 1.888 | 3.271 | 2.100 | 0.893 | 0.212 | J12 N12-T2 |



**Figure 3.44.** Finalising start and end coordinates of cut yield line and calculating length or height of cut section in Box O

### 3.3.5 Factors of safety and optimisation

The spreadsheet allows for factors of safety on the materials (control of execution) and applied loads by means of scroll buttons alongside the lower part of Box F, as shown by Figure 3.45. The Lookup function of the spreadsheet is utilised to select the value for the factor of safety from a predefined set contained in Box R in the "Parameters" sheet, as shown by Figure 3.46. The factors of safety on the materials (control of execution) and loads are summed into one value defined as the required factor of safety, ReFoS. The actual factor of safety between the total internal and external energy is also given in Box F. To determine the characteristic load of the wall panel the appropriate factors of safety are selected in the analysis. Guidance on the selection of appropriate factors of safety for the loads and materials is given in Chapter 8 Section 8.2.10.

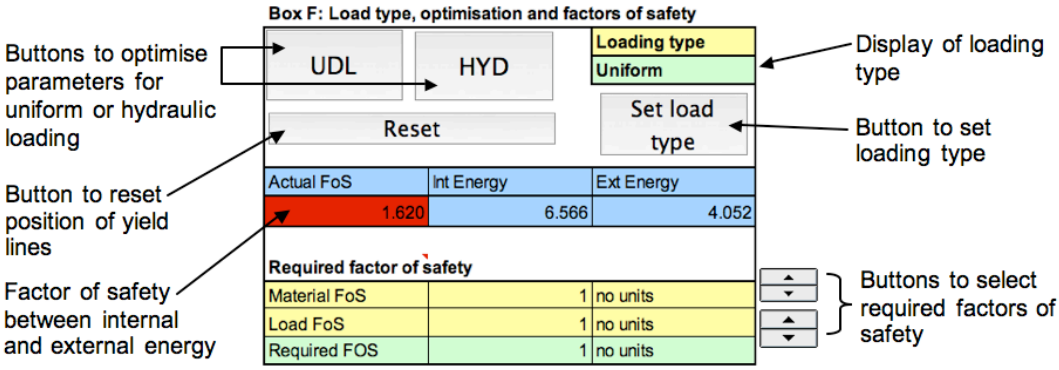



**Figure 3.45.** Load type and factors of safety selection, and buttons to initiate optimisation macros in Box F

**Box R: Factors of safety**

| | Material $\gamma_M$ | Load $\gamma_f$ |
|---|---|---|
| | 1.0 | 1.0 |
| | **2.3** | 1.5 |
| | 2.6 | 1.5 |
| | **2.7** | 1.5 |
| | 3.0 | 1.5 |

See Table NA.1 in NA to BS EN 1996-1-1:2005 for $\gamma_M$ values
See Table A2.a(A) in BS EN 1990:2005 for $\gamma_f$ values
Asummed that wind/hydraulic load is variable

**Figure 3.46.** Input for factors of safety in Box R

The Solver optimisation tool in the spreadsheet is used to establish the minimum ultimate load or water level for the case of a uniformly distributed or non-uniformly distributed lateral load respectively. This is completed by simultaneously varying the position of the yield lines, whilst adjusting the uniform load or water level subject to a series of constraints as given in Table 3.1. The positions of the yield lines are varied by adjusting the dimensional parameters $\alpha$L, $\alpha$R, $\gamma$ and $\beta$ using Solver. It is not possible to directly minimise the value of the target cell (corresponding to either D or $P_{udl}$) using Solver. To overcome this a second cell is set equal to D or $P_{udl}$, which is then set as the target cell to be minimised. The constraints are used to ensure that the dimensional parameters have finite values and to stop nodes overlapping or coinciding with each other, since such conditions can result in round off errors in the calculations. A constraint is also used to ensure that the factor of safety between the internal and external loads is equal to the total required factor of safety, ReFoS.

Two sets of Solver parameters are set up in the spreadsheet, the first is set to vary the uniform load for the case of wind loading and the second is set to vary the depth of water for the hydraulic loading conditions. The Solver tool is automatically invoked by using a macro in the spreadsheet. Two separate macros and associated buttons, as shown by Figure 3.45, are used to call either the parameters for the uniform or hydraulic loading cases. A further button is utilised in Box F to run a macro to set the initial parameters for the required load type. For the case of uniform loading the macro sets the depth equal to the height of the wall panel, the density of water to zero and an initial starting value of 1 kN/m$^2$ into the "$P_{udl}$" cell. Whilst for hydraulic loading $P_{udl}$ is set to zero, the density of water is set to 1000.0 kg/m$^3$ and the initial water level is set as 1 m. A reset button is incorporated to set the initial starting position of the yield lines, subject to the constraints, to those given in Figure 3.47.

**Table 3.1.** Constraints used in SA1

| Constraint | Purpose |
|---|---|
| β*H<=D | Ensure yield line J10 is below water level when top simply supported or fixed (water level can be above J10 when the top is free) |
| FoS=ReFoS | Ensure factor of safety between internal and external energy equal to required value |
| αL>=small | Limit minimum value of dimensional parameter alpha left to stop round off errors |
| αR>=small | Limit minimum value of dimensional parameter alpha right to stop round off errors |
| αL+αR<=large | Limit sum of alpha left and right to a maximum value to avoid yield lines being positioned outside area of wall panel and to stop alpha left and right overlapping |
| β<=large | Limit value of dimensional parameter beta to a maximum to stop yield lines being positioned outside area of wall panel |
| β>=small | Limit value of dimensional parameter beta to a minimum to stop round off errors |
| β-small>=γ | Ensure value of gamma is less than beta minus small such that they do not coincide and result in round off errors |
| γ>=small | Limit value of dimensional parameter gamma to a minimum to stop round off errors |

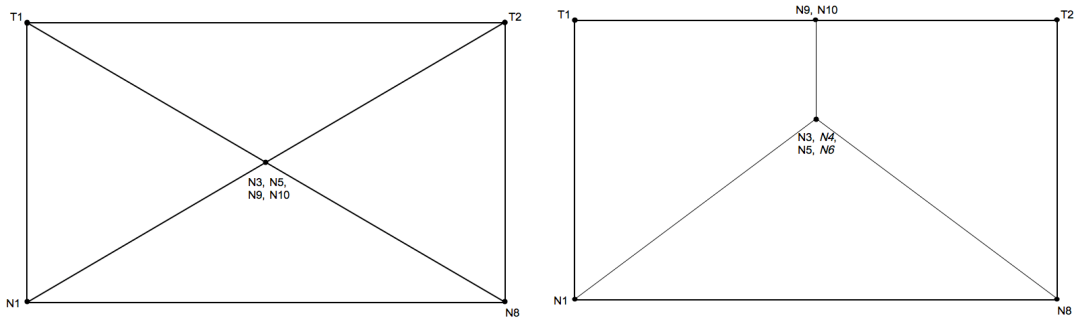


(a) (b)

**Figure 3.47.** Starting position for yield lines after reset: (a) top supported and (b) top free in SA1

### 3.3.6 Plotting figures

The parameters for the all the figures are collated and logically ordered in Box F, as shown by Figure 3.48, and comprise the nodal coordinates from Box J, the depth of water from Box A, the positions of the openings from Box G, the coordinates of the triangular subdivisions used in each slab and their corresponding centres of pressures from Box L, and the sections of the yield lines cut by the openings from Box O. Figures are generated using scatter type plot via the standard “insert chart” function in the spreadsheet. On the “calculation sheet” a figure is located in Box B, previously shown by Figure 3.24, to illustrate the layout of the problem and the

position of the yield lines and openings. A detailed figure of the wall panel that includes the position of the triangular subdivisions of the slabs along with their centres of pressures is located on a separate sheet titled “Main chart”, as shown by Figure 3.49. This chart aids in the visual verification of the position of the centres of pressure determined by the calculations in Box L. A further figure is located on another sheet titled “Opening chart” that includes the cut sections of the yield lines within the openings where present, as shown by Figure 3.50. The purpose of this sheet is to allow verification that the sections that are calculated as cut in Box O are correct.

**Box P: Figure plotting**

| Outer edge | x | y |
|---|---|---|
| N1 | 0.000 | 0.000 |
| T1 | 0.000 | 2.452 |
| T2 | 4.755 | 2.452 |
| N8 | 4.755 | 0.000 |
| N1 | 0.000 | 0.000 |
| Water level | | |
| N2 | 0.000 | 2.452 |
| N7 | 4.755 | 2.452 |
| Yield lines | | |
| N1 | 0.000 | 0.000 |
| N3 | 2.377 | 1.128 |
| N9 | 2.377 | 1.888 |
| N3 | 2.377 | 1.128 |
| N5 | 2.378 | 1.128 |
| N8 | 4.755 | 0.000 |
| N5 | 2.378 | 1.128 |
| N10 | 2.378 | 1.888 |
| T2 | 4.755 | 2.452 |
| N10 | 2.378 | 1.888 |
| N9 | 2.377 | 1.888 |
| T1 | 0.000 | 2.452 |

**Figure 3.48.** Section of Box P containing coordinates for figure plotting

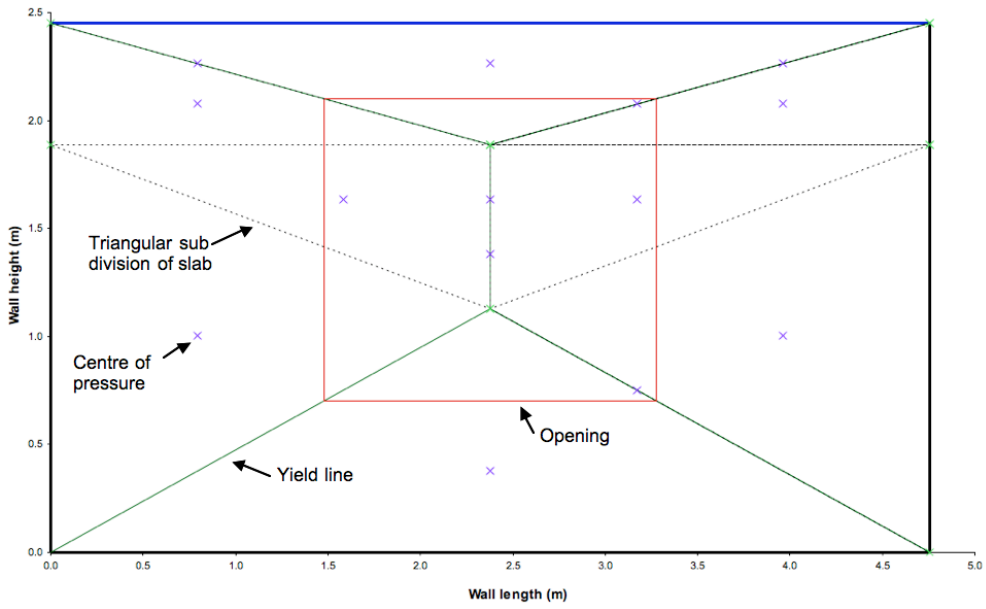


**Figure 3.49.** Main chart of wall panel in SA1 showing triangular subdivisions and centres of pressure

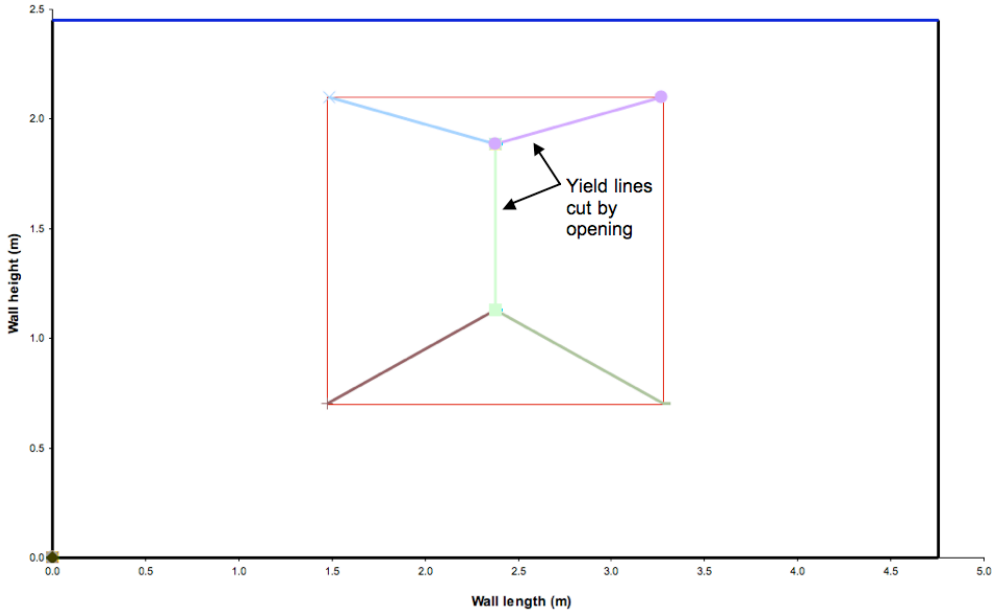


**Figure 3.50.** Opening chart in SA1 showing sections of yield lines cut by opening

### 3.3.7 Differences for corner lever spreadsheet analysis 2

Spreadsheet analysis 2 (SA2) is developed in an identical manner to SA1 and allows for the condition where instead of the yield lines forming into the corner of the wall panel, they formed a corner lever. The purpose of developing the analyses separately is to establish if there is a significant effect due to the formation of the corner levers on the ultimate load. The layout of the yield line pattern for SA2 is shown by Figure 3.51. The corner levers are only assumed to occur when the edges of the wall panel are either all simply supported or all clamped. SA2 allowed for one opening in the wall panel, but wall tie loads were not considered.

The main differences in the calculations for SA1 and SA2 are associated with the determination of the external and internal energy expended at the corner levers. This is due to the pivot or yield line formed at the corner lever being not being parallel to either the x or y axes. The line is considered to be either a pivot line when all edges are simply supported or a yield line when they are all clamped. The lever arms and deflections of the slab elements at the corners of the wall panel therefore need to be considered in relation to the pivot/yield line rather than the x or y axes. To determine the external work done the process outlined in Section 3.3.3 is followed to establish the total force at the centre of pressure and the lever arms, $x_c$ and $y_c$, for each triangular element. A further step is then required for triangular elements that are adjacent to the corner pivot/yield lines to determine the lever arm perpendicular to

the pivot/yield line. For triangular area A1, as shown by Figure 3.52, the required lever arm, $L_3$, is determined by trigonometry, as given by equation 3.72, where the lengths $L_1$ and $L_2$ and the angle $\theta_1$ are given by equations 3.73 to 3.75 respectively. The coordinates $x_1$ and $y_2$ are calculated using the equation of the line between nodes N3 and N14 (J6). A similar process is completed for the other triangular elements that are attributed to the corner levers. This excludes elements of slabs S5 and S10, which rotated about the upper and lower edges of the wall panel respectively as in SA1.

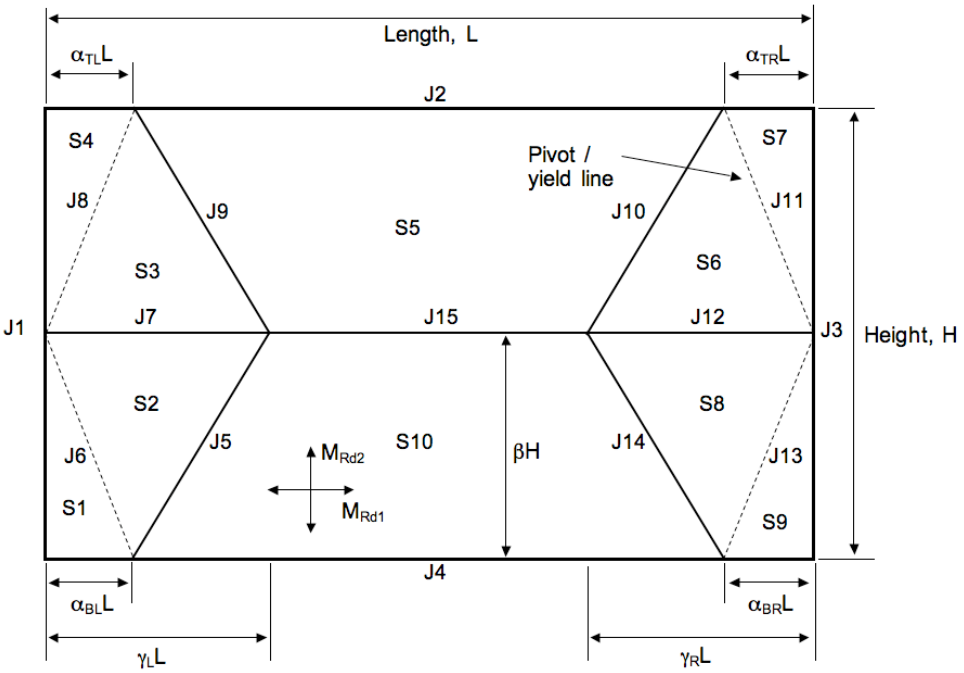


(a)

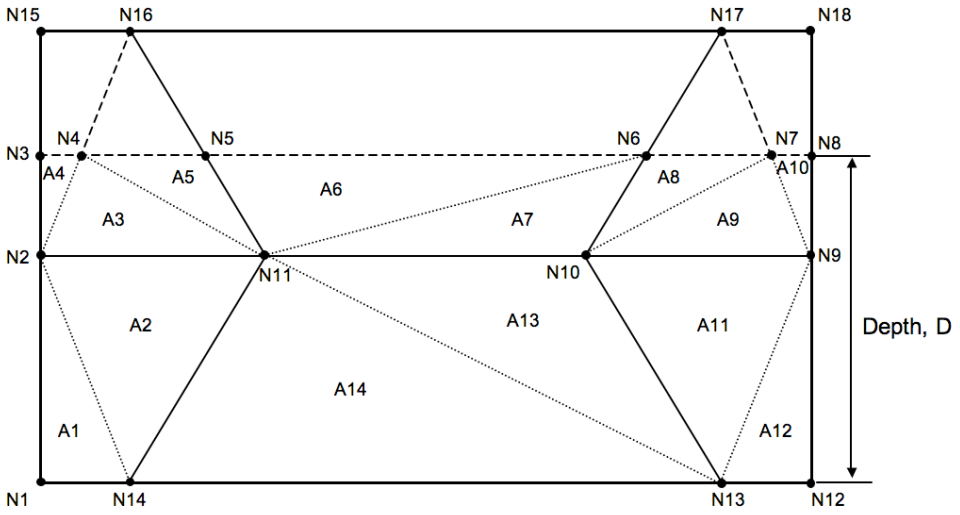


(b)

**Figure 3.51.** Layout of the yield line pattern for SA2: (a) layout of slab elements and yield lines, and (b) position of nodes and division into triangular elements

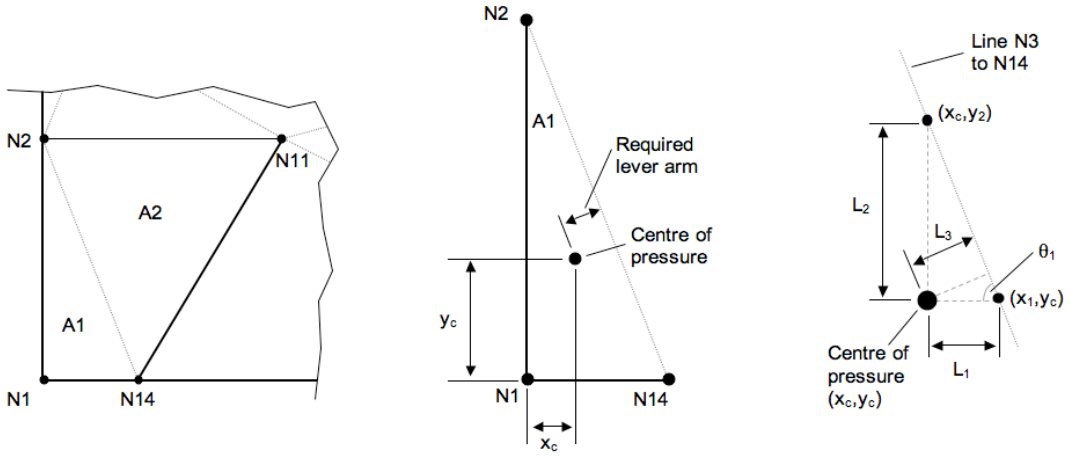


**Figure 3.52.** Calculation of perpendicular lever arm for triangular element A1 of slab S1 in SA2

$$L_3 = L_1 \sin\theta_1 \qquad 3.72$$

$$L_1 = x_1 - x_c \qquad 3.73$$

$$L_2 = y_2 - y_c \qquad 3.74$$

$$\theta_1 = \tan^{-1}\left(\frac{L_2}{L_1}\right) \qquad 3.75$$

To determine the work done for each corner lever slab it is necessary to calculate the rotation about their respective pivot/yield lines. Unit deflection is assumed along the yield line J15 at failure, so to establish the rotation for slabs S1 and S2 it is necessary to calculate the perpendicular length between node N11 and J6, as shown by Figure 3.53. The nodal coordinates are used to determine the perpendicular length, $L_4$, as given by equation 3.76, where the angle $\theta_2$ is given by equation 3.77. The rotation about line J6 is then given by equation 3.78. For the case of simple supports then line J6 is a pivot, such that S2 rotates in the direction of the load, whilst S1 rotates towards the load. The rotation is assumed negative for S1 for simple support conditions and the corresponding energy is therefore negative. For clamped edge support conditions no external energy contribution is assumed from S1. A similar process is completed for the remaining slabs attributed to the corner levers to determine the required rotation and external work done. The total external work done for the wall panel is calculated as described in Section 3.3.3.

$$L_4 = \left(x_{N11} - x_{N2}\right)\sin\theta_2 \qquad 3.76$$

$$\theta_2 = 90 - Tan^{-1}\frac{\left(x_{N14} - x_{N1}\right)}{\left(y_{N2} - y_{N1}\right)} \qquad 3.77$$

$$\theta_{Slab2} = \frac{1}{L_4} = -\theta_{Slab1} \qquad 3.78$$

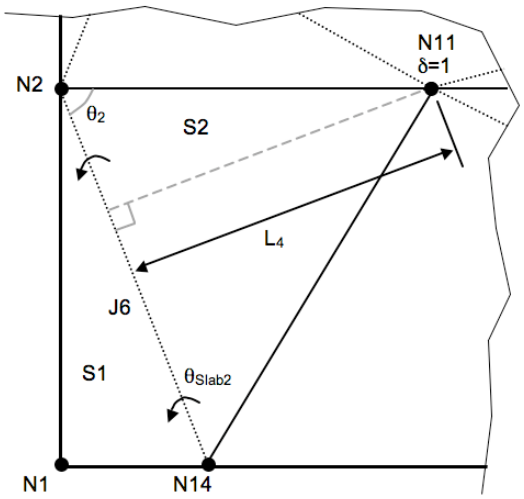


**Figure 3.53.** Calculation of rotation for slab S2 in SA2

The internal energy is calculated following the process outlined in Section 3.3.4, although the rotation for the yield lines at the corner levers are calculated using a different method. For yield line J6 it is assumed that rotation about the x axis occurred at a point that is coincident with a line that extended downwards from J6 and a vertical line originating from node N11, as shown by Figure 3.54. Here the length $L_5$ is calculated from the equation of the line between nodes N2 and N14 (J6), previously determined in the external work computations. Similarly, the rotation about the y direction for J6 is considered to be about a point coincident with a line extending horizontally from N11 and upwards parallel to J6, which for the pattern selected is equal to the length $\gamma_L L$, as shown by Figure 3.54. The resulting rotations for yield line J6 in the x and y directions are given by equations 3.79 and 3.80 respectively. This process allows the use of the moment resistances in directions 1 and 2, rather than having to determine or specify a moment resistance parallel to J6.

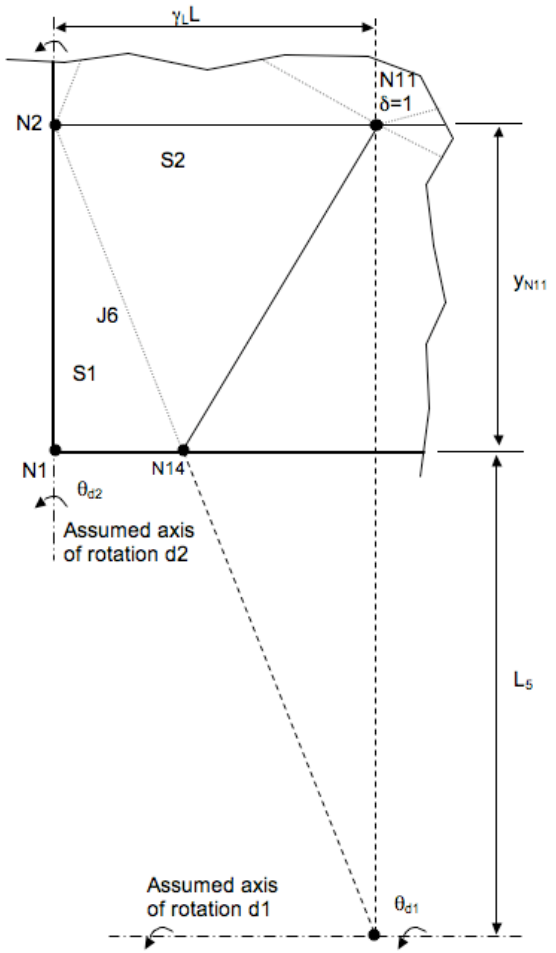


**Figure 3.54.** Rotation for yield line J6 in SA2

The rotation of J7 about the x axis comprises the components due to both S2 and S3 rotating. The rotation about J7 due to S2 is as given by equation 3.79 and a similar expression is developed for S3 following the process outlined above. As the nodes N14 and N16 tend to the corners of the wall panel, then the rotation of yield line J7 becomes very small. For this condition the internal energy along yield line J7 is also approximately zero. If nodes N13 and N17 also tend to the corners of the wall panel, then the failure mode is equivalent to that shown previously by Figure 3.5a. The rotations for yield lines J8, J11, J12 and J13 are determined in a similar manner. The optimisation process follows that described in Section 3.3.5. The constraints used in SA2 differ to those given for SA1, due to the additional dimensional parameters used to specify the position of the yield lines and are given by Table 3.2.

$$\theta_{d1} = \frac{1}{L_5 + y_{N11}} \qquad 3.79$$

$$\theta_{d2} = \frac{1}{\gamma_L L} \qquad 3.80$$

**Table 3.2.** Constraints used in SA2

| Constraint | Purpose |
|---|---|
| β*H<=D | Ensure yield line J15 is below water level when top simply supported or fixed |
| FoS=ReFoS | Ensure factor of safety between internal and external energy equal to required value |
| αBL>=small | Limit minimum value of dimensional parameters alpha left and right at top and bottom of wall panel to stop round off errors |
| αTL>=small | |
| αBR>=small | |
| αTR>=small | |
| αBL<=max | Limit maximum value of alpha on left side if required |
| αTL<=max | |
| αBR<=maxR | Limit maximum value of alpha on right side if required |
| αTR<=maxR | |
| γL>=αBL | Limit values of gamma left and right such that they are equal to or exceed the corresponding alpha values to stop nodes overlapping |
| γL>=αTL | |
| γR>=αBR | |
| γR>=αTR | |
| γL+γR<=large | Limit sum of gamma left and right to a maximum value to avoid yield lines being positioned outside area of wall panel and to stop alpha left and right overlapping |
| β<=large | Limit value of dimensional parameter beta to a maximum to stop yield lines being positioned outside area of wall panel |
| β>=small | Limit value of dimensional parameter beta to a minimum to stop round off errors |

### 3.4 Conclusions

Two spreadsheet analyses, SA1 and SA2, have been developed using the yield line method that allow the determination of the ultimate or characteristic loads of masonry wall panels due to the application of uniform and/or hydraulic lateral loading. The analyses have been developed using standard spreadsheet software and the Solver tool within the software has enabled the ultimate or characteristic load to be optimised. Characteristic loads are computed in the analysis by applying the appropriate factors of safety on materials and the applied loads. SA1 allows for the conditions where the yield lines form into the corners of the wall panel and SA2 allows for corner levers to be considered. A number of different edge support conditions can be considered in the analyses and the support given by wall ties can also be included in SA1. Moment resistance can be considered in terms of flexural strength or one of two previously proposed friction/overturning resistance methods in the analyses.

Two openings may be positioned within the wall panels and the analyses automatically determine the yield lines cut by the opening edges. A vertical surcharge may be applied to the top of the wall panel and may either be automatically determined according to the required parameters or manually inputted by the user. Output of the spreadsheet is by means of an ultimate or characteristic load, either as a water depth or uniformly distributed load, and graphical display of the failure mode. Validation of the analyses, as presented in Chapter 8, will be completed by means of an experimental program that is outlined in Chapter 4.

# Chapter 4 Experimental design

This Chapter presents the decision making and design process followed in order to achieve the aims of the experimental component of the research programme. Initial considerations are given to specimen scale, size and boundary conditions, after which the experimental design and procedure is discussed in further detail.

The main aim of the experimental programme was to determine the lateral load capacity of masonry walls when subjected to wind or hydrostatic forces. Constructing and testing the complete structure of a building would be too complex and time consuming, so instead panels representative of individual walls were considered. Traditionally, masonry specimens have been tested at full scale, but such studies can be expensive, protracted, have repeatability issues, require large laboratory space and there can be significant health and safety concerns. This study was completed at small scale to reduce the issues associated with full scale testing schemes. To correctly consider self-weight effects at this scale, wall panel testing was completed within a centrifuge. Testing the specimens remotely in the centrifuge required additional considerations in terms of how loading, measurement and monitoring would be completed. In addition a discussion is presented of the small assemblage tests that were carried out to determine the necessary parameters for the modelling process.

## 4.1 Initial considerations for the experimental design

### 4.1.1 Selection of a suitable scale for the masonry specimens

Prior to designing the experimental procedure, it was necessary to consider a suitable scale for the wall panel specimens. Mortar joint thickness and masonry unit size, in terms of handling, becomes more complicated as scale is reduced so it was important to select an appropriate value. The literature review discussed a number of studies that influenced the selection of a suitable scale (Davies et al., 1998, Hughes et al., 2002, Mohammed and Hughes, 2011, Mohammed et al., 2011). Firstly, researchers found that even though modelling at smaller scales was possible, a practical limit of 1:6 was established as the lower limit suitable for producing consistent specimens (Davies et al., 1998, Hughes et al., 2002). Secondly, the findings of a comprehensive study was reported (Mohammed and Hughes, 2011, Mohammed et al., 2011) that compared the mechanical properties of the prototype and 1:6 model scale specimens. In light of this, it was deemed beneficial to conduct the model scale programme at the same 1:6 scale as it would reduce or avoid the

need to complete prototype scale tests to compare mechanical properties. The same materials and, where possible, processes would need to be followed in order to make a valid comparison in this case.

### 4.1.2 Selection of appropriate dimensions for the wall panel specimens

The experimental research programme aims to determine the lateral capacity of the walls of a typical dwelling. Existing studies of masonry wall panels were discussed in the literature review and it was found that storey height panels were in the range of 2.1 to 2.7 m. In addition, a field study of properties previously conducted revealed that the mean storey height was 2.4 m (Kelman and Spence, 2003a). Modern properties are generally constructed with ceiling heights of 2.4 m to make use of standard material sizes and to comply with Regulations (ODPM, 2004). The floor and roof structures can be considered to support the walls, such that they may be subdivided into wall panels of 2.4 m in height, as shown by Figure 4.1. This information supports the selection of a wall panel height of 2.4 m for this programme.

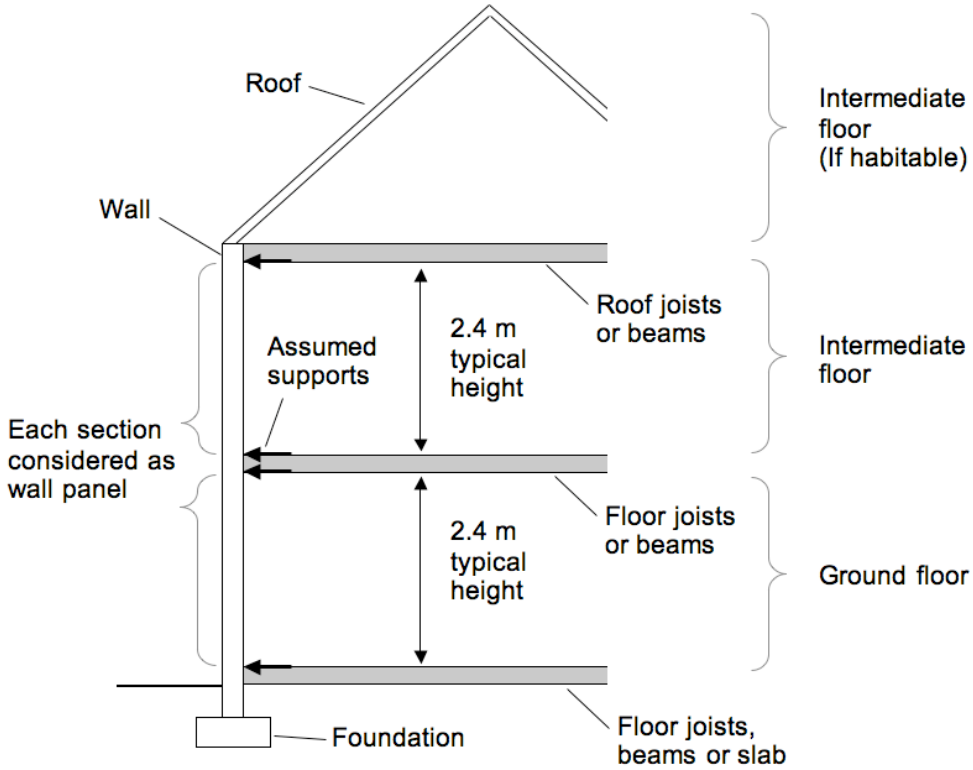


**Figure 4.1.** Cross-section of typical dwelling

The literature review established that panels previously tested were generally of between 1.5 to 5.5 m in length. A previous review of property plans revealed that their walls were typically in the range 1.0 to 6.0 m and considered lengths of 1 m increments within this range (Kelman and Spence, 2003a). It was found (Kelman and

Spence, 2003a) that wall lengths of 1.0 and 6.0 m were uncommon and concluded that a maximum upper limit of 5 m would be more appropriate. The capacity of the centrifuge was also a contributing factor to the length of panel selected. Allowing for a fixture to support the wall panels at the edges, a maximum length of 4.8 m at prototype scale could be catered for. The maximum wall panel length that could be accommodated by the centrifuge, of 4.8 m, was utilised in this study, since it was deemed to be more representative of the upper limit of length of a wall of a typical property. It was anticipated that the ultimate load would decrease with increasing panel length, so selecting the maximum length possible would allow the worst case scenario to be considered.

The exact panel height and length was influenced by masonry unit dimensions, as given by Table 4.1, mortar joint thickness and the tolerances employed. Standards require a mortar joint height of between 6 and 15mm, and bricklayers generally aim to achieve 10 to 12 mm (BSI, 2005c). A nominal mortar joint of 12 mm, equivalent to 2 mm at model scale, was selected for this programme, since it allowed for tolerances in the masonry specimens. Based on the height of a standard brick and the selected mortar joint thickness the exact panel height was 2.452 m comprising 32 courses. Likewise, for standard brick unit length and the same mortar joint the exact length was computed as 4.755 m and comprised 21 full units. For block sized units the dimensions selected for the wall panel required 10.5 and 10.66 units in length and height respectively. At 1:6 model scale the dimensions selected equated to a panel height and length of 408.6 and 792.5 mm respectively, as shown by Figure 4.2. The panel length and height remained fixed throughout the duration of this study as a number of other attributes were varied.

**Table 4.1.** Masonry unit nominal dimensions

| **Dimension (mm)** | **Brick** | | **Block** | |
|---|---|---|---|---|
| | **Prototype** | **Model** (1:6) | **Prototype** | **Model** (1:6) |
| Height | 65 | 10.8 | 215 | 35.8 |
| Length | 215 | 35.8 | 440 | 73.3 |
| Thickness | 102.5 | 17.1 | 100 | 16.7 |

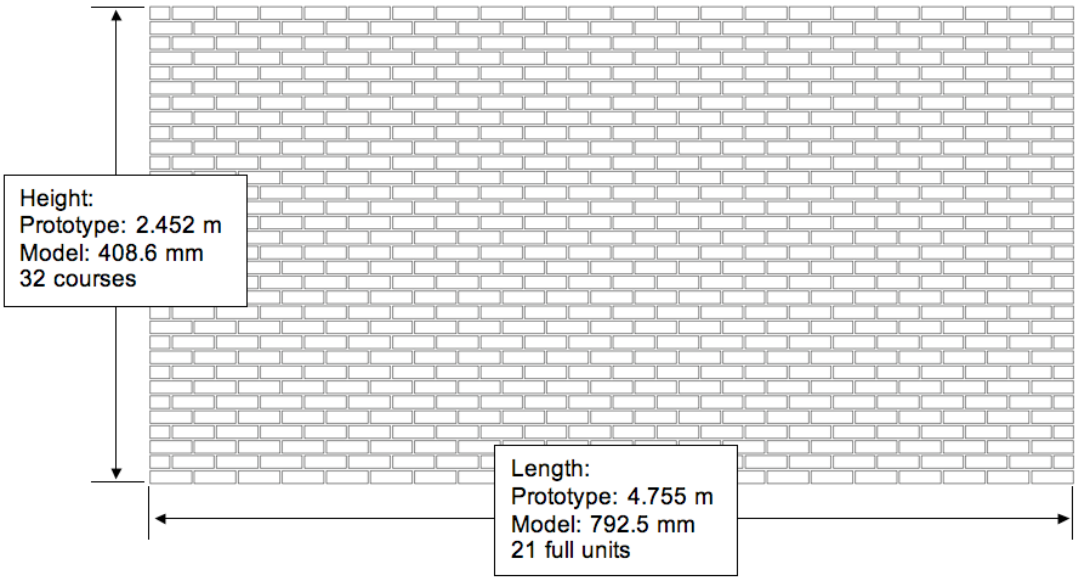


**Figure 4.2.** Wall panel dimensions

### 4.1.3 Boundary conditions for the edges of the wall panel

As previously discussed, the test wall panel was considered to be representative of a storey height section (2.4 m) of a property with the appropriate boundary conditions applied. For the ground floor section of panel, horizontal support is provided at the damp proof course (DPC) level and at the first floor junction, as shown by Figure 4.3. The DPC was assumed to be unable to provide tensile capacity. Shear or sliding resistance at the DPC was assumed due to the self-weight of the masonry, such that a simple support condition was most appropriate, as shown by Figure 4.3c. Ideally a DPC would have been built into the wall and the simple support at the base of the wall would have been positioned against the masonry course below the DPC. However, it was anticipated to be difficult to correctly model a DPC at reduced scale, so instead the DPC was omitted and the support was positioned against the first course of masonry in the wall panel. At first floor level there would be an interaction of the floor structure, wall and vertical loads imposed by masonry and roof structure above, as shown by Figures 4.1 and 4.3. It would be difficult to model the exact support conditions at the top of the wall panel at reduced scale, so the floor structure was assumed to provide a simple support to the wall panel, as shown by Figure 4.3d, in conjunction with a vertical axial load, as detailed in Section 4.1.4. For subsequent storey levels the top of the panel was similarly assumed to be simply supported by either the roof structure or further levels of floor. Walls parallel to the direction of the joists are required to be strapped to the floor or roof structure at regular intervals, such that the same support conditions were assumed (ODPM, 2004). For the case of

single storey properties where strapping was omitted, the upper edge was considered as free.

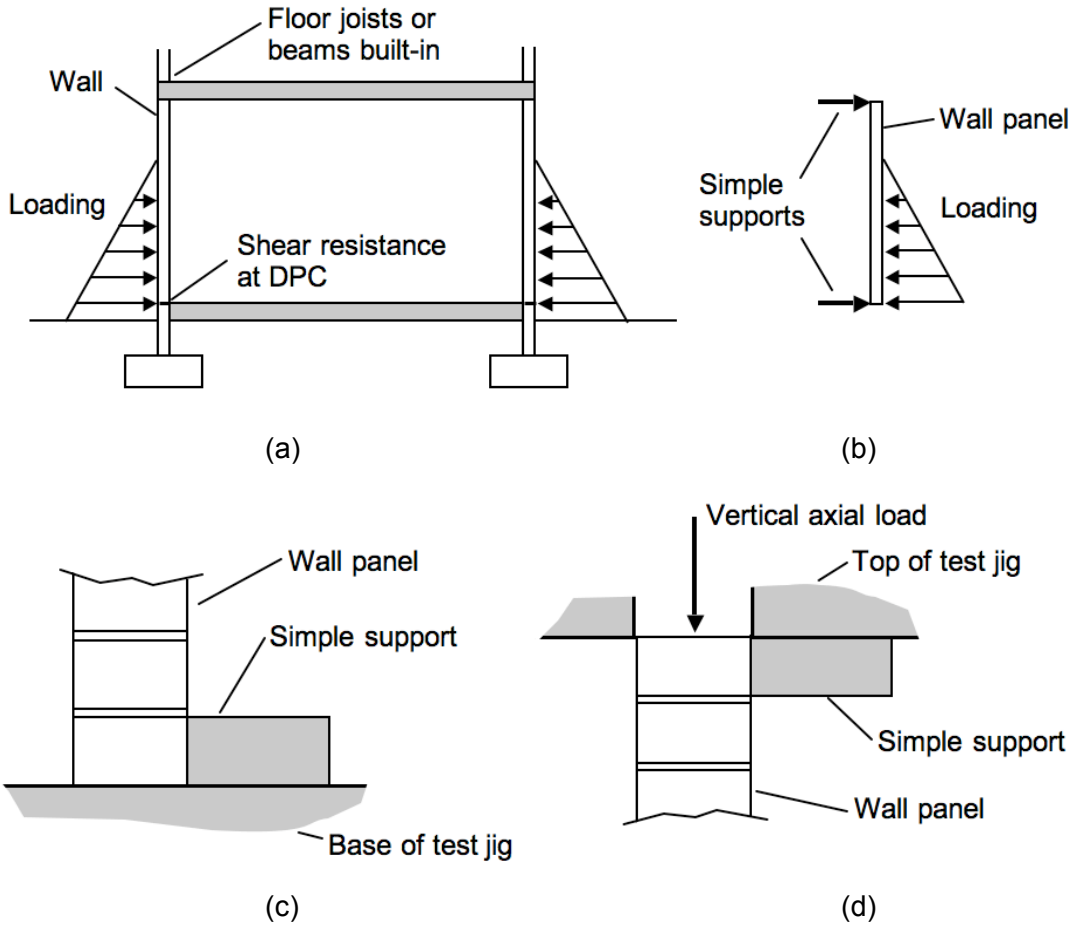


**Figure 4.3.** (a) Cross-section of property showing actual loading and horizontal support conditions, (b) consideration as individual wall panels with equivalent loading and supports, horizontal supports used at the (c) base and (d) top of wall panels during testing (Hydraulic loading conditions shown)

At the corners of a building the masonry units of one face are generally tied into those of the perpendicular faces, as shown by Figure 4.4a. Additional rotational restraint provided by tying-in offers partial support that would be greater than simple, but lower than fully clamped conditions. It was envisaged to be difficult to provide the correct level of partial support at model scale and exact values of restraint would be required for the theoretical modelling process. During testing, the masonry specimen would likely dilate and utilising a fixed or partially fixed boundary could have a significant influence on the failure modes and ultimate loads. Based on this reasoning, providing simple supports at the vertical edges was considered most appropriate for this programme, as shown by Figures 4.4b and c.

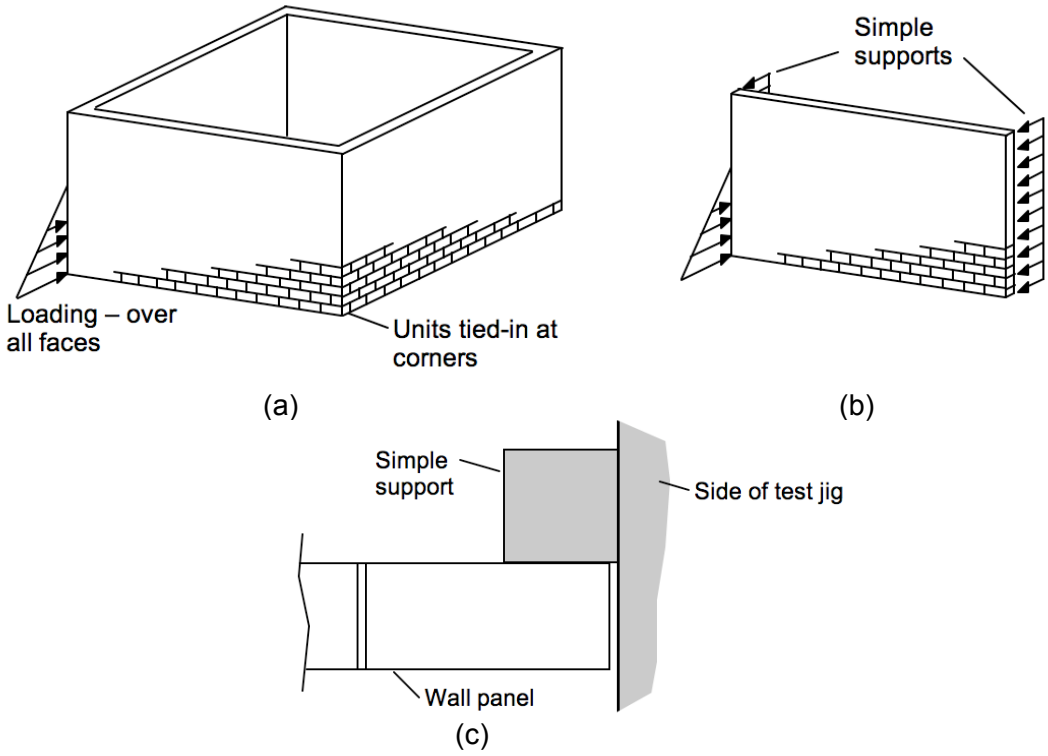


**Figure 4.4.** (a) Idealised property showing loading and vertical support conditions at wall corners, (b) consideration as individual wall panels with equivalent loading and supports, and (c) plan view of vertical supports used during testing (Hydraulic loading conditions shown)

Cavity wall arrangements are often employed in properties rather than solid walls to avoid water penetration into the interior and to improve thermal performance. Wall ties formed from metal strip or wire are utilised to hold the two leaves of masonry together and allow transfer of tensile and compressive forces. Current guidance allows the lateral load capacity of a cavity wall to be apportioned from the strengths of the individual leaves, where the wall ties are capable of transferring the appropriate loads (BSI, 2005c). In this study the inner and outer cavity leaves were initially tested as individual wall panels to assess their load capacities and failure modes. Tests of wall ties at model and prototype scale were conducted alongside to verify their capability to transfer compressive and tensile loads, details of which are presented in Section 4.4.5. Cavity wall assemblies were tested and compared to the results of the individual leaves to allow an assessment of the guidance to be made. For the case of the individual leaves, the same support conditions as previously described were assumed at the edges for both the inner and outer leaves. Similar horizontal supports for the outer leaf were justified due to the positioning of wall ties along the upper support and the filling of the cavity below DPC, as shown by Figure 4.5.

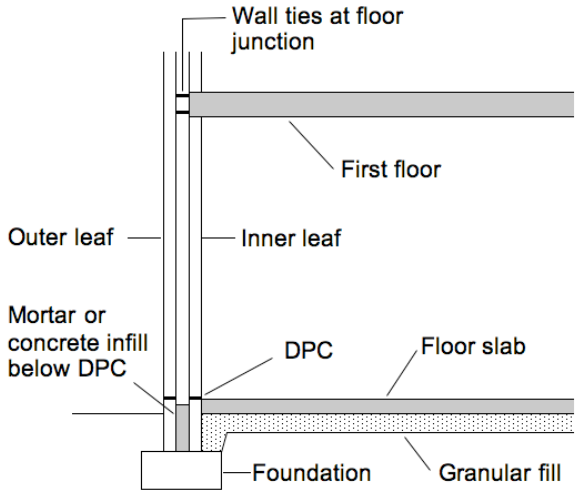


**Figure 4.5.** Typical cavity wall arrangement (ties between DPC and first floor omitted for clarity)

### 4.1.4 Consideration of vertical axial imposed loads

The walls of a property will be subject to vertical axial loading in certain cases. For the case of the ground floor storey inner wall, it will support the weight of the masonry above as well as the floor and roof structure, as shown by Figure 4.6. Often external sections of wall do not directly support the roof or floor structures and will only be subject to loads from the masonry above. When considering the walls of a property as discrete wall panels the required additional vertical loading must also be applied as required.

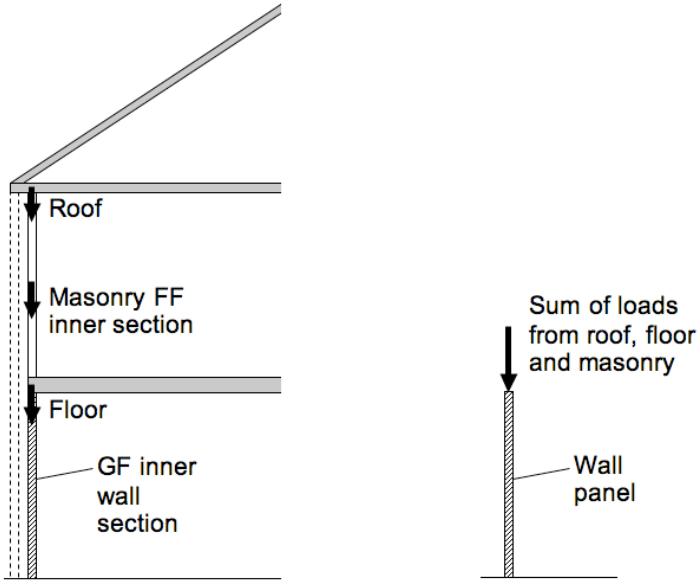


**Figure 4.6.** (a) Actual vertical loading of ground floor storey inner wall section, and (b) idealised case when considered as wall panel

## 4.2 Masonry unit manufacture

### 4.2.1 Brick sized masonry units - selection and cutting process

Model scale bricks can be manufactured using an identical extrusion and firing process as for the prototype. Previous researchers established that fired units tended to vary in dimensions, had a relatively rough surface finish and possessed dissimilar mechanical properties to the prototype (Hughes et al., 2002, Taunton, 1997). It was found that when the units were cut from the prototype that a good dimensional tolerance and surface finish could be achieved (Hughes et al., 2002, Taunton, 1997). Use of the prototype material for the model scale allowed direct comparisons of mechanical properties to be completed (Mohammed and Hughes, 2011, Mohammed et al., 2011).

The suitability of a masonry unit for cutting was based on a number of factors, including: presence of perforations or frogs, internal flaws, cracks or voids and the compressive strength (Mohammed, 2006). Perforations or frogs would reduce the material available for the cutting process, so solid bricks were deemed more suitable. Internal flaws, cracks or voids would likely result in the units breaking during the cutting process or premature failure during testing. Average strength bricks would be most suitable for the cutting process, since they would be less demanding to cut and comparable to those typically used in masonry structures (Mohammed, 2006). As discussed previously, a recently conducted programme of research had compared the effect of mechanical properties with scale (Mohammed and Hughes, 2011, Mohammed et al., 2011). Baggeridge Mellowed Red stock clay bricks were found to meet the criteria for the cutting process and had been used in the comparative study (Mohammed, 2006). For this reason the same brick was obtained and used throughout this study. The masonry was manufactured according to BS EN 771-1 (2003a) and the manufacturer's declared compressive strength was $\geq$21 N/mm$^2$ (Wienerberger, 2009). The water absorption of the brick was found to be between 7 and 12 % in a previous study (Mohammed, 2006).

A previously developed process (Taunton, 1997) was used to cut the model scale masonry units from the prototype. The procedure initially involved cutting the unit in half. Each half brick was then bonded, using epoxy paste, to a mounting plate that enables it to be secured onto an indexing brick saw, as shown by Figure 4.7a. A series of cuts were made through the brick parallel and then perpendicular to the cut end, as shown by Figures 4.7b and 4.8a. The sections were then removed from the base and cut to length. The cutting process yielded between 25 and 35 units per half

brick, depending on the presence of any internal flaws and finished units shown by Figure 4.8b. Undamaged model scale brick units were recycled after use where possible by removal of mortar mechanically or by using brick cleaning solution. It was not anticipated that utilising recycled bricks would significantly influence the flexural strength of the masonry and the proportion of recycled bricks used in each specimen was not monitored in the study.

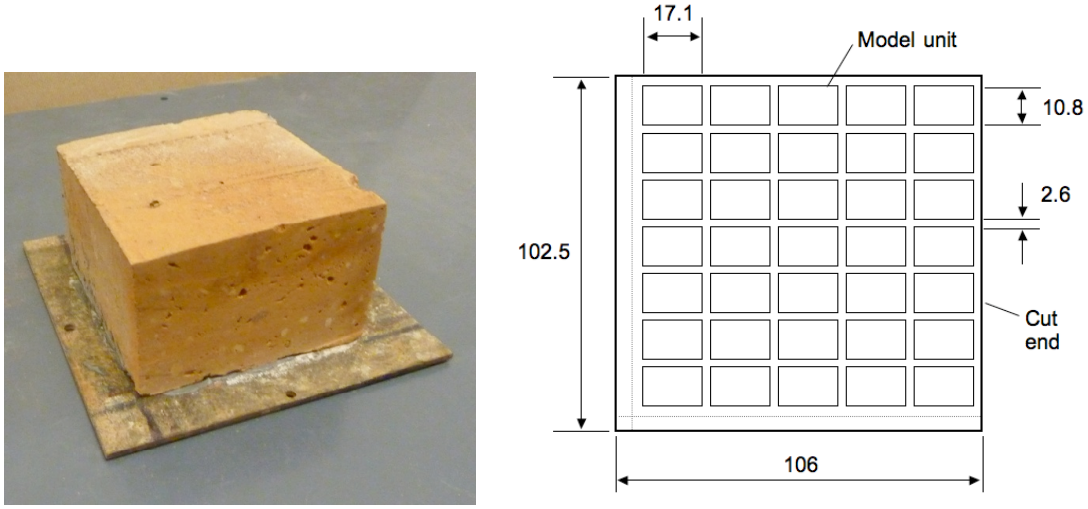


(a) (b)

**Figure 4.7.** (a) The half brick bonded to the steel plate, and (b) plan view of cutting dimensions in mm for model scale bricks

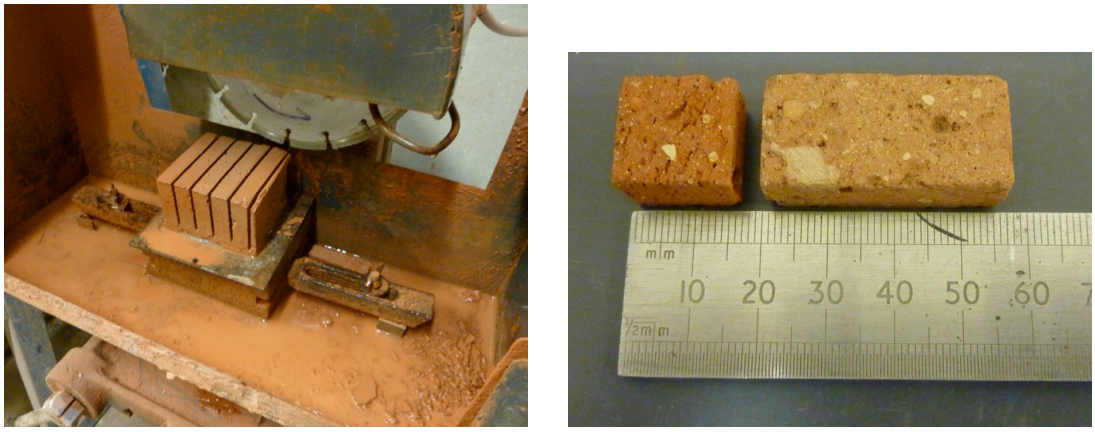


(a) (b)

**Figure 4.8.** (a) Cutting the half brick on an indexing saw, and (b) the finished full and half model scale (1:6) units

### 4.2.2 Block sized masonry units - cutting process

Block sized units were cut from prototype materials using a brick cutting saw fitted with an adjustable backstop. Slices were firstly cut off the prototype unit equal to the

model scale block thickness, as shown by Figure 4.9a. Each slice was then cut into one or more pieces equal to the model scale unit height, as shown by Figure 4.9b. Finally the units were cut to the required length and the completed units are shown in Figure 4.10. Two different prototype materials were cut successfully: clay bricks and aerated autoclaved cement (AAC) blocks. The bricks used were as previously described in Section 4.2.1. Standard grade Celcon AAC blocks of 3.6 N/mm$^2$ manufacturer's declared compressive strength were selected for the process and complied with BS EN 771-4 (2003b). In addition medium density concrete blocks were cut, however, the aggregate tended to chip at the edges during the process and resulted in a model unit of poor quality. The model scale blocks cut from brick (brick-blocks) were used in place of the medium density concrete material due to this issue with cutting. An alternative solution could have been to cast the model scale concrete blocks at small scale. Concrete blocks are quite porous and contain a significant number of voids due to the grading of the aggregates used. It was anticipated to be difficult to obtain a similar structure in the cast model units after correctly scaling the aggregate, so the casting process was not used in this study. Units cut from brick were recycled using the method described in Section 4.2.1. It was not possible to reuse the AAC units as the brick cleaning solution would break down the structure of the blocks, due to their main constituent comprising of cement. In addition mechanical cleaning was difficult due to the weak nature of the AAC material.

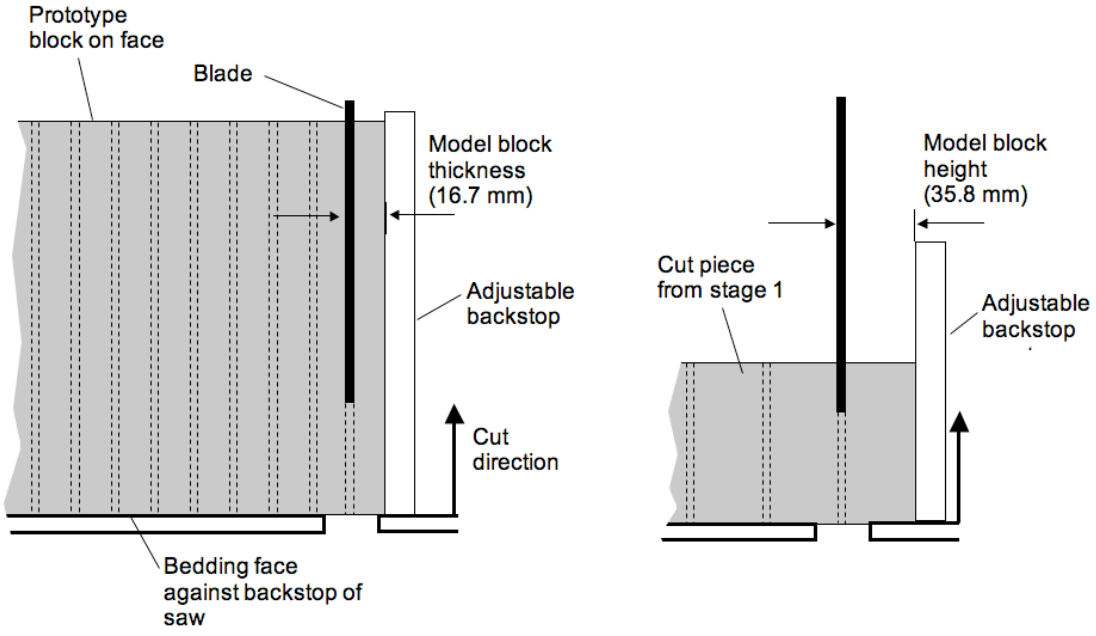


**Figure 4.9.** (a) Plan view of cutting block sized units to thickness, and (b) to height from prototype block (similar process completed to cut prototype brick units)

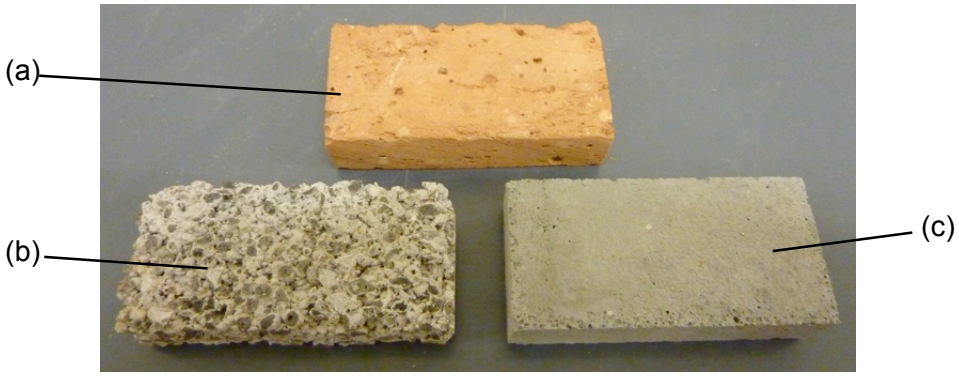


**Figure 4.10.** Model scale (1:6) block units of (a) brick, (b) medium density and (c) aerated block parent material

### 4.3 Specification of the mortar and its constituents

#### 4.3.1 Mortar specification

Cement based mortars were utilised in this program for three main reasons: (i) cement mortars are representative of both past and current building practices, (ii) previous studies have generally focused on cement mortars allowing direct comparisons to be made; and (iii) current design processes for laterally loaded wall panels were developed alongside experimental studies that primarily considered such mortars (Haseltine et al., 1977, West et al., 1977). To provide a workable mortar a chemical plasticiser was added to the mixture. Hydrated lime was used as the plasticiser in this study, since it was representative of traditional building practices, and was generally used in previous studies. Three different mortar compressive strength classes were considered in this study, as given by Table 4.2 (BSI, 2005d). The mortar is classified by a number that refers directly to the 28 day design compressive strength in $N/mm^2$ (BSI, 2005d). Trial mixes were completed to establish the required water to cement ratio to attain a suitable workability, as given by Table 4.2, and were maintained throughout the study.

#### 4.3.2 Cement specification

The cement type used in this study was ordinary Portland cement of classification CEMII and complied with BS EN 197-1 (2000c). Due to the length of the research programme it was necessary to use cement from different batches to ensure that it was fresh and freely flowing.

**Table 4.2.** Mixing ratios and water to cement ratios for prescribed masonry mortars (adapted from NA to BS 1996-1-1 (2005b))

| Mortar compressive strength class | Mixing ratio by mass Cement:Lime:Aggregate | Water to cement ratio |
|---|---|---|
| M6 | 1 : ¼ : 5 | 1.33 |
| M4 | 1 : ½ : 6½ | 1.8 |
| M2 | 1 : 1 : 10 | 2.7 |

### 4.3.3 Lime specification

The lime used in this programme was hydrated lime of designation CL90-S, which conformed to BS EN 459-1 (2001b). The same batch of lime was used throughout the study.

### 4.3.4 Aggregate specification

The aggregate used for prototype scale specimens was building sand of grading 0 to 2 mm according to BS EN 13139 (2002). The mortar joint height at model scale was typically 2 mm, and if building sand was utilised it was likely that the largest aggregates would prevent proper bedding of the masonry units (Hughes et al., 2002). Previous studies had proceeded by scaling the limits of aggregate size for the prototype and then selecting an aggregate that fitted within these limits, as shown by Figure 4.11 (Davies et al., 1998, Hughes et al., 2002, Mohammed et al., 2011). The aggregate that was the best fit between the upper and lower limits was identified as Congleton HST95 of grading 0.3 to 0.063 mm and was similarly used for this study. The grading curve for HST95 exceeded the scaled upper limit for sieve sizes of 0.125 mm and lower, but this was not anticipated to significantly affect the performance of the mortar. It should be noted that cement and lime are finely graded, such that they were directly used within the model scale mortars without further processing (Hughes et al., 2002).

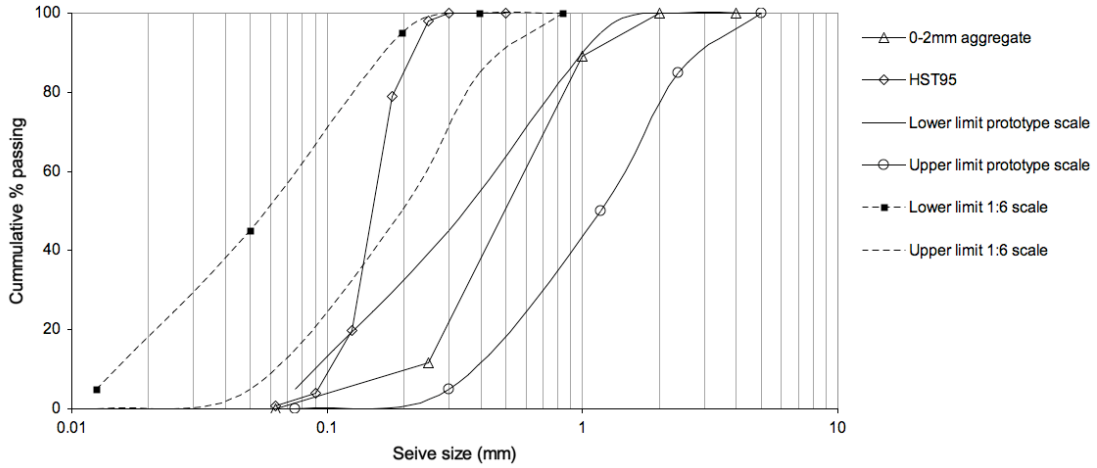


**Figure 4.11.** Particle size distribution for prototype and model scale aggregates

### 4.3.5 Mixing the mortar

The constituents of the mortar were measured by mass to the required ratio, given in Table 4.2, and dry mixed using a paddle mixer. Water was added by mass to achieve the required water to cement ratio, as given in Table 4.2. The mortar was used immediately after mixing.

### 4.3.6 Mortar cubes for compressive strength tests

Mortar cubes were cast at the end of the mixing process for every batch processed. The compressive strength of the cubes was used for two purposes; firstly as a quality control procedure between batches of mortar, and secondly to allow comparisons to be made between different masonry specimens that utilised the same mortar strength class.

Mortar cubes of 100, 70.7 or 50 mm are typically used to determine the compressive strength of mortar (RILEM, 1991a), whilst when flexural strength tests are additionally completed, prisms of 160 x 40 x 40 mm are specified (BSI, 1999a). Due to the small quantities of mortar used to manufacture the model scale specimens, it was more suitable to cast 25 mm mortar cubes than utilise the cubes or prisms of dimensions mentioned above. A previous study had established that there was a good correlation between the compressive strength of 25 and 70.6 mm mortar cubes, such that this choice was justified (Hendry and Murthy, 1965). When prototype scale specimens were manufactured both 100 and 25 mm mortar cubes were cast to assess the correlation.

Three mortar cubes were cast for each batch of mortar mixed and allowed to cure with the specimens for the same duration. Testing of 25mm mortar cubes was completed using a 20 kN universal testing machine, adopting a stroke controlled loading rate of 0.033 mm/s for 25mm mortar cubes, to allow direct comparison of the results presented here to a previous study (Mohammed, 2006). The larger 100 mm mortar cubes were tested at a loading rate of 5.33 kN/s using a Farnell manual compression test machine. All mortar cubes were tested until failure and the compressive strength was determined from the peak load.

## 4.4 Specimen manufacture

### 4.4.1 Specimen manufacture jig

Traditionally bricklayers construct masonry in a series of lifts, of maximum height 1.5 m, over consecutive days and work to the tolerances given by Table 4.3 (BSI, 2001a). Utilising lifts avoids overstressing the mortar in the courses below that have been laid already and reduces instability of the work as it rises. When considering this method for the model scale programme there were two areas of concern, firstly that it would take more than one day to complete the wall and therefore require multiple batches of mortar, and secondly that it would be difficult to achieve and maintain the required tolerances, as given by Table 4.3, when laying a course at a time.

**Table 4.3.** Permissible deviations in masonry for prototype and model scales (BSI, 2001a)

| **Dimension** | **Permissible deviation (mm)** | |
|---|---|---|
| | **Prototype scale** | **Model scale (1:6)** |
| Straightness - in any 5 m (prototype) or 0.83 m (model) length | ±5 | ±0.83 |
| Vertically in height - up to 3 m (prototype) or 0.5 m (model) length | ±10 | ±1.67 |
| Level of bed joints for brick masonry - up to 5 m (prototype) or 0.83 m (model) length | ±11 | ±1.83 |
| Level of bed joints for block masonry - up to 5 m (prototype) or 0.83 m (model) length | ±13 | ±2.16 |

An alternative approach taken by manufacturers of sectional or faced buildings systems is to construct the masonry panels horizontally in moulds (Mohammed, 2006, Thorp Precast, 2005). Mortar is added from above and is generally compacted

into the joints using vibration. The advantages of this method are that dimensions are consistent between panels and manufacturing time is considerably reduced. Previous researchers have taken a similar approach and have successfully manufactured masonry specimens at model scales of 1:3 and 1:6 (Baker, 1972, Mohammed, 2006). The mechanical properties of the 1:6 scale specimens were found to be of acceptable consistency (Mohammed, 2006). Constructing the specimens in this programme in a similar fashion would provide the advantages detailed above and was deemed the most suitable method.

The horizontal method of manufacture had only been employed to construct small specimens at 1:6 scale (Mohammed, 2006). Consistent joint widths were achieved by using plastic tile spacers in between the masonry units. The spacers were simply removed after sufficient mortar was added to secure the position of the units. For larger panel specimens, it would be very time consuming to position all the units using individual spacers. To reduce the time required to layout and construct the panels an assembly jig was designed and manufactured. The assembly jig comprised a base plate, aluminium frame and top plate. The base plate was drilled with a series of holes, within which pins were fitted to align the masonry units, as shown by Figure 4.12. As previously discussed, a 2 mm joint size at model scale was selected for this study. To allow for tolerances in the masonry units, pins of 1.6 mm diameter were utilised. The combination of a 2 mm joint and 1.6 mm pin allowed a 0.4 mm deviation in the height or length of any masonry unit. If no tolerance was allowed for it would likely be difficult to position the units and they could become jammed between the pins. The aluminium frame constrained the specimen at the edges as well as providing a means to attach the top and bottom plates.

The disadvantage of using pins to locate the masonry units was that voids would be present in the joints after removal of the base plate. A method was developed that allowed the base plate to be removed during manufacture as follows: after the joints were completely filled with mortar and sufficiently compacted the top plate was fixed to the frame, the entire jig was then rotated by 180° and the base plate was removed, as shown by Figure 4.13. With the base plate removed any voids were easily filled with mortar before curing commenced. For panels with openings a wooden former was positioned in the required location and the bricks that abutted were cut as necessary. The former was removed after the manufacturing process was complete.

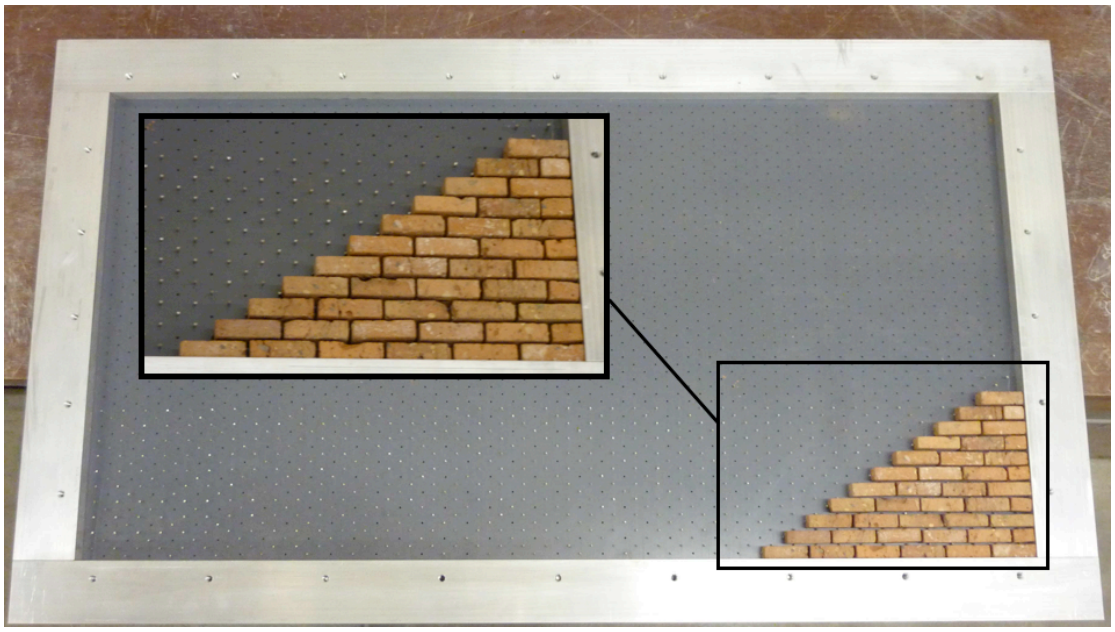

**Figure 4.12.** Specimen assembly jig (brick units shown)

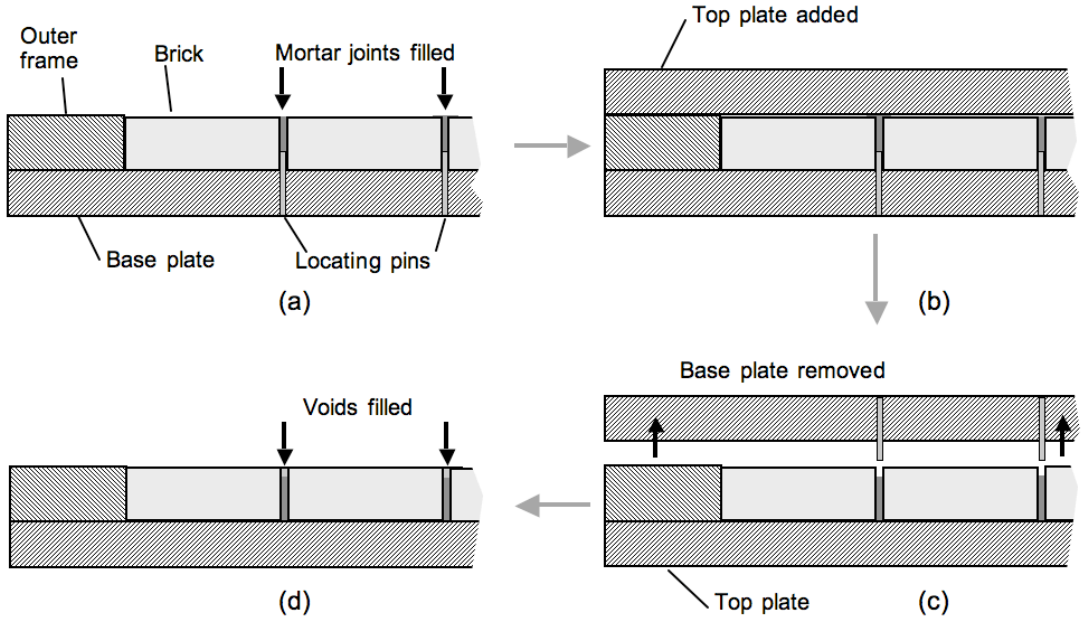


**Figure 4.13.** Manufacturing process route for specimen: (a) filling of mortar joints, (b) top plate fixed to frame, (c) jig rotated by 180° and base plate removed, and (d) filling of any voids left by pins

Small assemblages, termed wallettes, of two formats were required to be manufactured in order to assess the mechanical properties of the masonry, as detailed in Section 4.6. To enable these specimens to be manufactured using the same jig a series of spacers were designed, as shown by Figure 4.14. The main spacers constrained the edges of the specimens and additional spacers were used in

between adjacent specimens to stop any mortar entering the joints. This process enabled multiple wallette specimens to be manufactured in one process and ensured consistency.

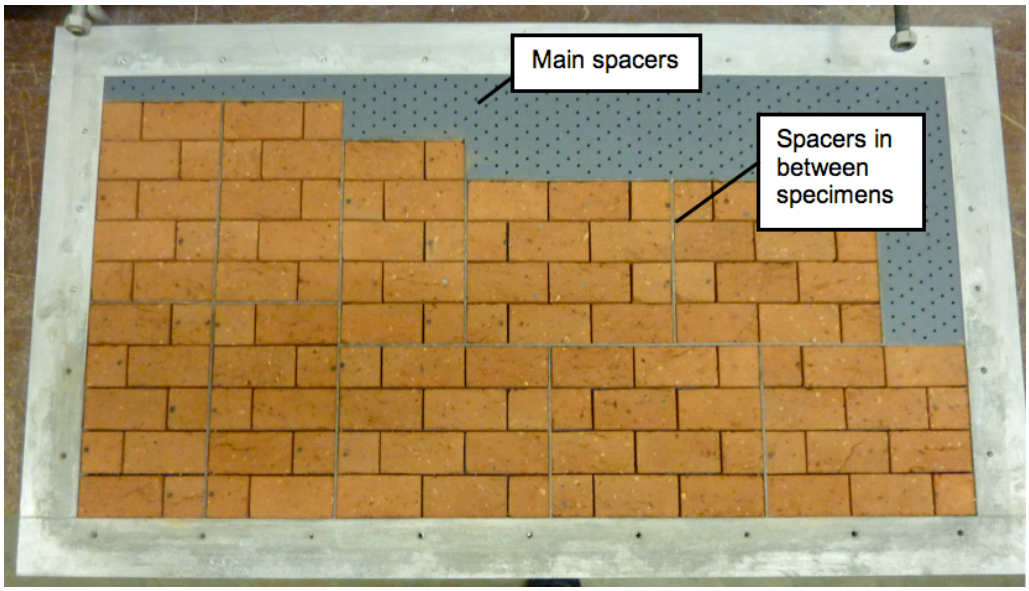


**Figure 4.14.** Perpendicular and parallel block wallette specimens laid out in assembly jig prior to mortar application

### 4.4.2 Soaking process

When insufficient moisture is present in the masonry units water is absorbed from the mortar, effectively reducing the amount available for the cement hydration process. It has been previously shown that the flexural strength of masonry assemblies was higher and more consistent when the moisture content of the units was adjusted prior to laying (de Vekey et al., 1986, West et al., 1986). In these studies brick and AAC blocks were conditioned by soaking prior to use, although no exact time duration was given. A previous study that utilised the same brick as selected for this programme determined that 20 minutes was a sufficient time to soak the units prior to use (Mohammed and Hughes, 2011). The same soaking time for the brick units was adopted for this study to allow comparisons to be made with the previous work. The water absorption rate of model scale AAC blocks was determined using the same method for the brick units (Mohammed, 2006) that was based on Standard BS EN 772-21 (2011). The method involved the regular weighing of 5 specimens soaked in a water bath over a 30 minute interval and then reweighing at 24 hours. It was found that at the same time interval of 20 minutes, the AAC units attained a moisture content of 85% of the value at 24 hours, as shown by Figure 4.15, compared to a

value of 95% given for brick (Mohammed, 2006). Initial trials with the AAC blocks indicated that the moisture content at a time of 20 minutes was suitable, since over-wetting of the mortar was not observed and it remained workable. In addition the specimen remained sufficiently moist during the curing process. For the reasons presented and to ensure consistency between specimens a soaking time of 20 minutes was deemed appropriate for the AAC block units.

Due to the time required to lay the masonry units out in the jig, it was likely that the moisture content would vary between those placed at the start and end of the process if all were soaked prior to positioning. To avoid this issue the masonry units were dry laid and then the entire jig was submersed in a water bath. The assembly was removed after the required soaking time of 20 minutes and excess water was allowed to drain for a further 20 minutes prior to applying any mortar. Additional holes were drilled in the base plate of the jig to aid excess water to drain. The masonry units were dried in the laboratory for 24 hours prior to the soaking process. Due to time constraints when manufacturing the wall panels it was not possible to determine the exact moisture content of the units after the soaking process.

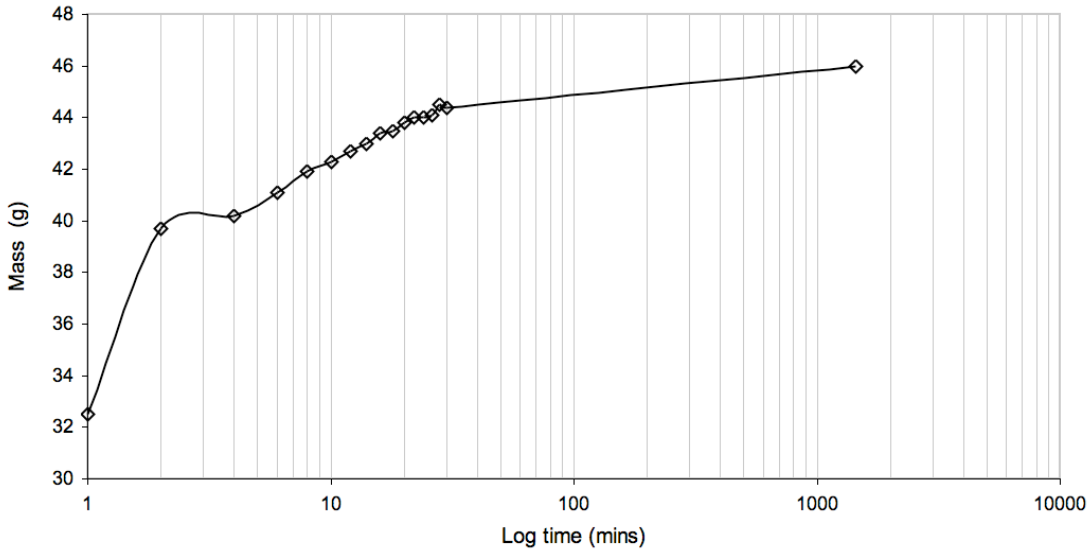


**Figure 4.15.** Average water absorbency of model scale AAC block units

### 4.4.3 Specimen curing conditions

Standards prescribe that masonry specimens should be stored at constant humidity conditions, at a temperature of between 10 and 30°C, and cured for 7 to 28 days prior to testing (BSI, 1999b, RILEM, 1991c, RILEM, 1991b). To ensure these conditions were satisfied specimens were wrapped in plastic film at the end of the

manufacturing process to ensure constant humidity levels and stored in the laboratory within the temperatures range specified. De-moulding was completed at an age of at least 2 days and mortar cubes manufactured for quality control purposes were stored with the specimens. All specimens were tested at 28±1 days, since this was consistent with previous studies (de Vekey et al., 1986, Mohammed, 2006, West et al., 1971). It was necessary to deviate from the constant humidity requirement to allow a paint finish to be applied to the specimens as required for the digital image correlation (DIC) measurement technique as described in Section 4.5.2. The plastic film was removed from the specimens 7 days prior to test to allow sufficient natural drying to take place such that the paint would adhere.

The mortar in prototype scale wall panels would be subject to higher stresses during curing than the mortar in the model scale wall panels, due to the self-weight of the masonry. To assess this effect, some model scale masonry specimens were subjected to a precompressive stress of 0.02N/mm$^2$, equal to that at the centre of the prototype wall panel. In addition to adhering to the curing process detailed above, these specimens were stored upright and weights were positioned along the tops of the assemblies to attain the required precompression.

### 4.4.4 Cavity wall specimens

Due to the complexity of manufacturing cavity wall specimens in a single stage, it was necessary to construct two individual wall panels and connect them together using wall ties prior to test, as shown by Figure 4.16a. Model scale wall ties, formed from steel fibres of 0.7 mm diameter, were first bonded to the inner wall panel, as shown by Figure 4.16b. The outer wall panel was then bonded to the ties. Initial tests utilised epoxy resin and epoxy cement to bond the ties to the inner and outer wall panels respectively. Later tests utilised a building adhesive to bond both ends of the ties as the longer curing time aided assembly. The assembly was allowed to cure for 24 hrs before testing. The required minimum wall tie density was 2.5 per m$^2$ at prototype scale (BSI, 2005c, BSI, 2005d). Additional wall ties were placed along the vertical and upper horizontal edges of the specimen, as shown by Figure 4.17, in accordance with guidance given by Building Regulations (ODPM, 2004) and Standards (BSI, 2001a) The depth of the cavity was 16.7 mm at model scale equivalent to 100 mm at prototype scale and conforms to current building practice.

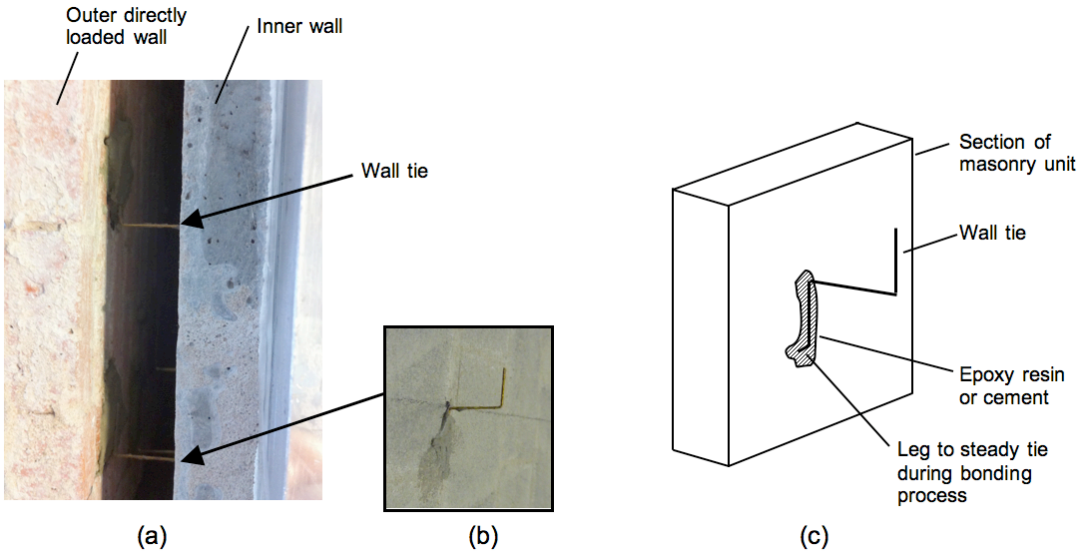


**Figure 4.16.** (a) Cavity wall tie shown bonded to inner and outer leaves after assembly in test jig, (b) cavity wall tie shown bonded to inner leaf before assembly and (c) schematic of wall tie

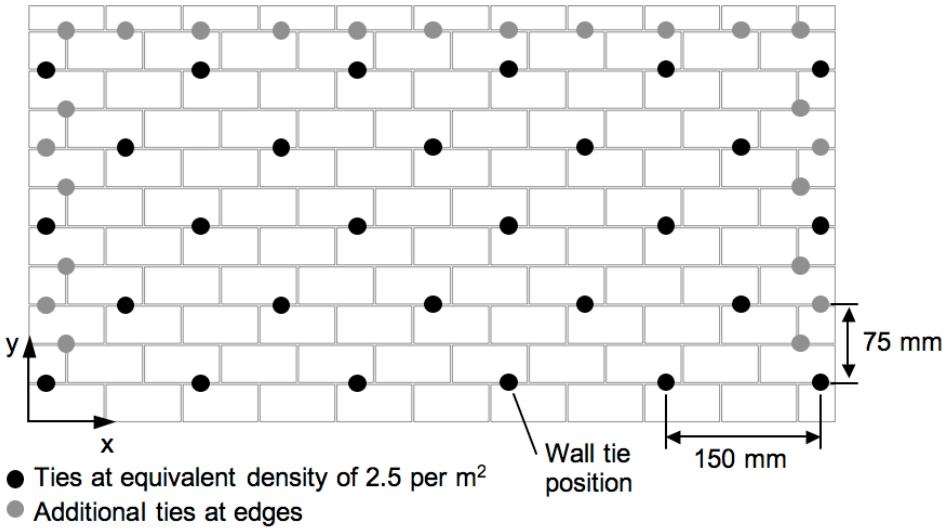


**Figure 4.17.** Position of wall ties on model scale wall panel

### 4.4.5 Wall tie couplet test specimens

To allow comparison of the behaviour of model wall ties and those typically used in the construction of properties it was necessary to manufacture and test specimens in both scales. Couplet specimens were manufactured according to standard BS EN 846-5:2000 to allow the tensile and compressive strength of wall ties to be determined (BSI, 2000d). The conditioning and curing procedures previously described were adhered to. Specimens manufactured at prototype scale utilised Staifix RT2 type 2 general purpose stainless steel ties of diameter 3.1 mm. Ties

formed from 0.7 mm steel fibres were either bedded in the model scale couplets or bonded onto the surface as described in Section 4.4.4.

## 4.5 Centrifuge testing arrangement

### 4.5.1 Measurement techniques for a laterally loaded wall panel

Previous research programmes at both prototype and model scales have utilised dial gauges and or displacement transducers to monitor out-of-plane displacements of the wall panel during test (Anderson, 1976, Anderson, 1984, Duarte and Sinha, 1992, Fried et al., 2005, Gairns and Scrivener, 1988, Hendry, 1973, Hendry et al., 1971, Pace, 1988, Templeton et al., 1986, West et al., 1977). In-plane displacements were only measured, by similar methods, when the effect of arching or preloading was considered (Anderson, 1984, Hendry et al., 1971). Vertical in-plane strains were measured on one occasion using DEMEC mechanical gauges (Hendry et al., 1971). In addition visual monitoring was generally used to document the position of any initial cracks and the crack pattern at failure.

In this programme testing would be completed in a centrifuge requiring consideration to be given to the robustness under enhanced gravity conditions and remote operation capabilities of any system utilised. In and out-of-plane deflections have successfully been measured in centrifuge tests of masonry structures using linear voltage displacement transducers (LVDT's) and laser sensors (Hughes et al., 2002). Clip gauges have been utilised to determine local strains during centrifuge tests (Hughes et al., 2002). Remote monitoring and recording of the output of these sensors is reasonably straightforward, and generally achieved by utilising a data logging system. The disadvantages of these types of sensors is that they are only able to provide localised data at one point, per sensor, and can obscure the surface for any visual monitoring.

Image processing techniques have been utilised to determine in-plane displacements and strains in soil and masonry specimens within the centrifuge, but values were only determined after post test processing (Hughes et al., 2002). Images from both video and still cameras have successfully been used in the processing techniques. Digital image correlation (DIC) presented advantages over previous image processing techniques, since real time processing could be completed. In-plane deflections and strains could be measured using a two-dimensional DIC system. Out-of-plane deflections could additionally be determined if a three-dimensional system was employed. No evidence was found in the literature of DIC systems being used in a

centrifuge so it was necessary to conduct a proving test before completing any specimen tests.

### 4.5.2 Overview, installation and proving tests of the DIC system

The DIC system comprised two digital still cameras that were linked to a computer via Firewire. The cameras denoted 0 and 1 were positioned in front of the specimen, as shown by Figure 4.18. Vic Snap capture software (2006, Correlated Solutions Inc., Columbia, SC, USA) allowed synchronised stereo images to be obtained of the specimen. Pre-test calibration of the system was completed by capturing images of a panel with markers positioned in a known grid layout in front of the cameras in different orientations (Featherston et al., 2011). The calibration process was completed in Vic3D analysis software (2006, Correlated Solutions Inc., Columbia, SC, USA), which determines the spatial (x,y and z) position of the grid from the stereo images. Analysis of the test specimen followed by essentially comparing the x-y position of the speckle pattern throughout the test to that of a reference image, taken pre loading, for each camera view, as shown by Figure 4.19. The data from each camera view and from the calibration process was then utilised by the software to determine the out-of-plane z deflections.

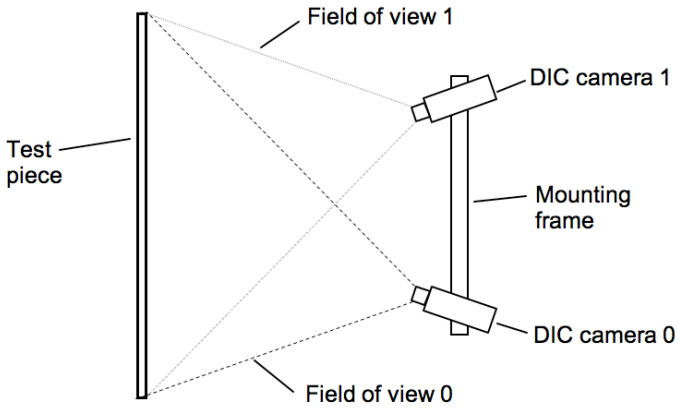


**Figure 4.18.** Plan view showing arrangement of DIC cameras and test piece

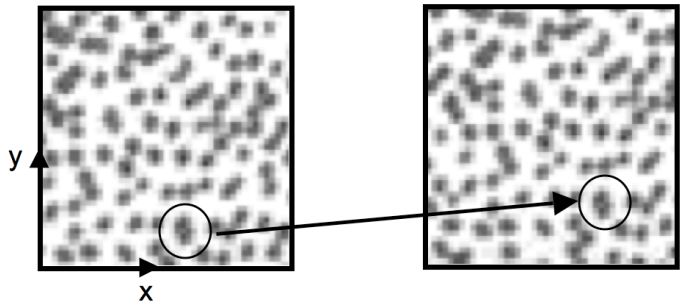


**Figure 4.19.** Tracking the position of the speckle pattern between (a) the reference image and (b) the image of the deformed specimen

Prior to conducting any proving tests with DIC it was necessary to design and install secure mountings for the system in the centrifuge. The cameras were required to be rigidly mounted, as any movements that occurred during test would affect the accuracy of the results. An aluminium extrusion system was utilised to provide a rigid yet fully adjustable mounting for the cameras and was positioned at the front of the gondola, as shown by Figure 4.20. The laptop was mounted in the centrifuge's equipment cabinet near to the centre of rotation to reduce the gravitational effects during operation, as shown by Figure 4.21. Backlighting for the specimen was provided by a series of low voltage halogen lamps. Since the PC was required to be local to the cameras it was necessary to install a wireless system to allow remote operation during test. A wireless access point (WAP) was mounted on the wall of the centrifuge pit and connected directly to a PC in the control room, as shown by Figure 4.21. RealVNC remote access software (RealVNC Ltd, Cambridge, UK) was utilised to enable the DIC system to be operated from the control room during test. The speckle pattern required for the DIC system was applied to the target prior to conducting the proving test. Thin tipped black marker pens were used to apply the speckles randomly over a base coat of matt white paint. A proving test, conducted at 125% of the required gravitational force, was successfully completed using a static target and verified that the system operated as required. Following this operation of the DIC system was verified by comparisons to values obtained via an LVDT and the results of this are presented in Section 4.5.5.

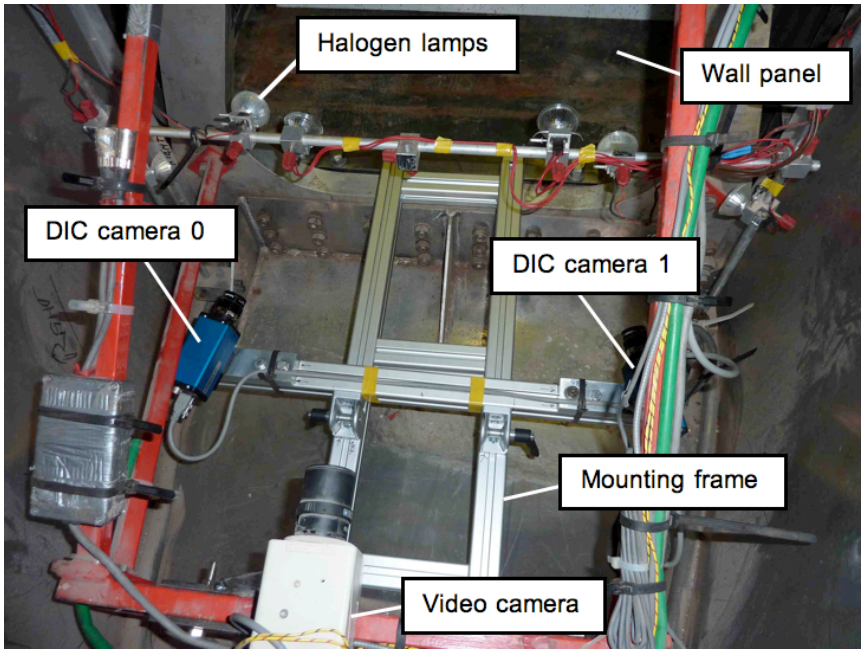


**Figure 4.20.** Mounting frame for DIC cameras on centrifuge gondola

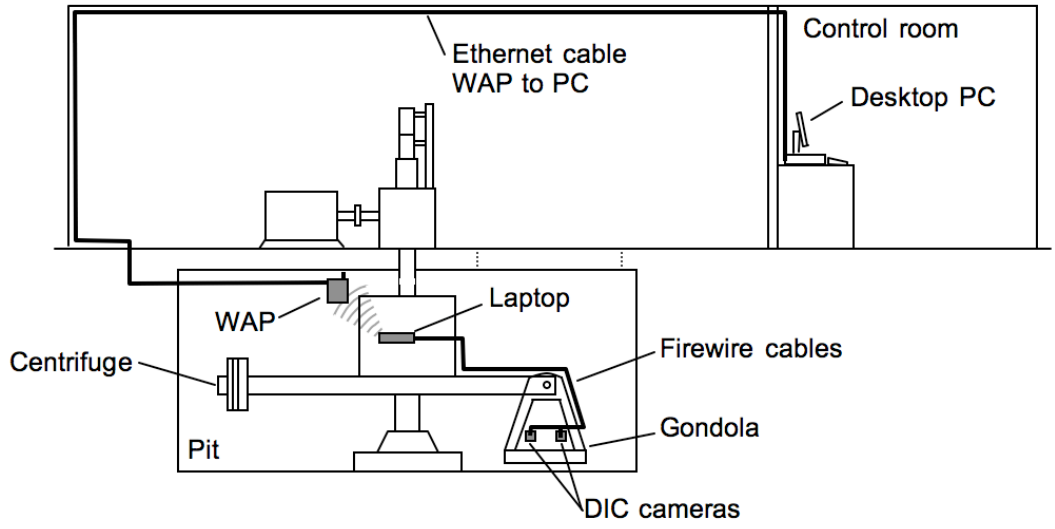


**Figure 4.21.** Schematic of the DIC and wireless system as installed in the centrifuge

### 4.5.3 Centrifuge test jig design

The centrifuge test jig was required to provide the following:

- Simple supports at the vertical and horizontal edges of the wall panel
- A means of applying axial vertical loading
- Reaction surfaces for both uniform and non-uniform lateral loadings
- Mountings for sensors and any other equipment
- Mountings to centrifuge gondola

A testing box of internal dimensions 800(l) x 500(w) x 460(h) mm was utilised for the study and fitted with mountings to allow it to be secured to the centrifuge gondola. A panel was bolted to the rear of the box to provide a reaction surface for the lateral load, whilst the front of the box was left open to allow viewing of the test, as shown by Figure 4.22. A top plate assembly was designed and manufactured to provide mountings for the upper horizontal support for the wall and the axial loading system, as well as provide the final reaction surface for the uniform loading tests. Supports for the remaining edges of the wall panel were also manufactured and secured to the test box as required. Horizontal supports were equivalent to the height of one course of bricks, whilst vertical supports were equal to the thickness of the brickwork. A mounting was manufactured to allow an LVDT to be positioned at the centre of the wall panel to allow initial verification of the results from the DIC system, as shown by Figure 4.23.

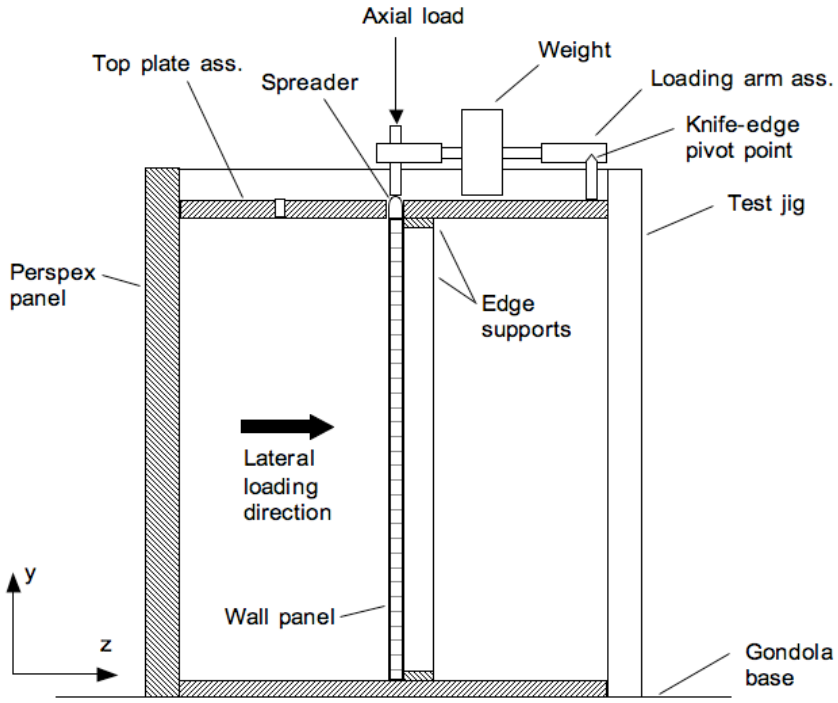


**Figure 4.22.** Cross section of test jig assembly

**Figure 4.23.** View of test jig showing position of LVDT

#### 4.5.3.1 Vertical axial loading arrangement

The axial loading mechanism comprised five lever arms that were each supported at one end on a knife-edge. Axial load was transferred to the top of the wall by the lever arms via a spreader plate and hardboard packer to allow for surface irregularities. Weights were added to the lever arm to provide the required axial loading for the wall panel under test, as shown by Figure 4.24. During test the centrifuge gondola does not attain a true horizontal position due to the action of the Earth's gravitational force. The applied centrifugal gravitational force varies through the specimen due to the small angle to the horizontal and causes a difference of between +3% and -10 % in the normal stress levels in comparison to the prototype. The difference in stress levels were reduced by adjusting the weights added to each arm. Where the g level was lower than required additional weight was added to the arm and likewise where the g level was higher than required weight was removed. The difference in normal stress was reduced to between +1% and – 2% by utilising this method. The design of the axial loading system would only suit simply or fully supported conditions at the top of the wall as it would be likely to provide some lateral restraint. The vertical axial displacement at the top of the wall was monitored using an LVDT mounted on the top plate assembly.

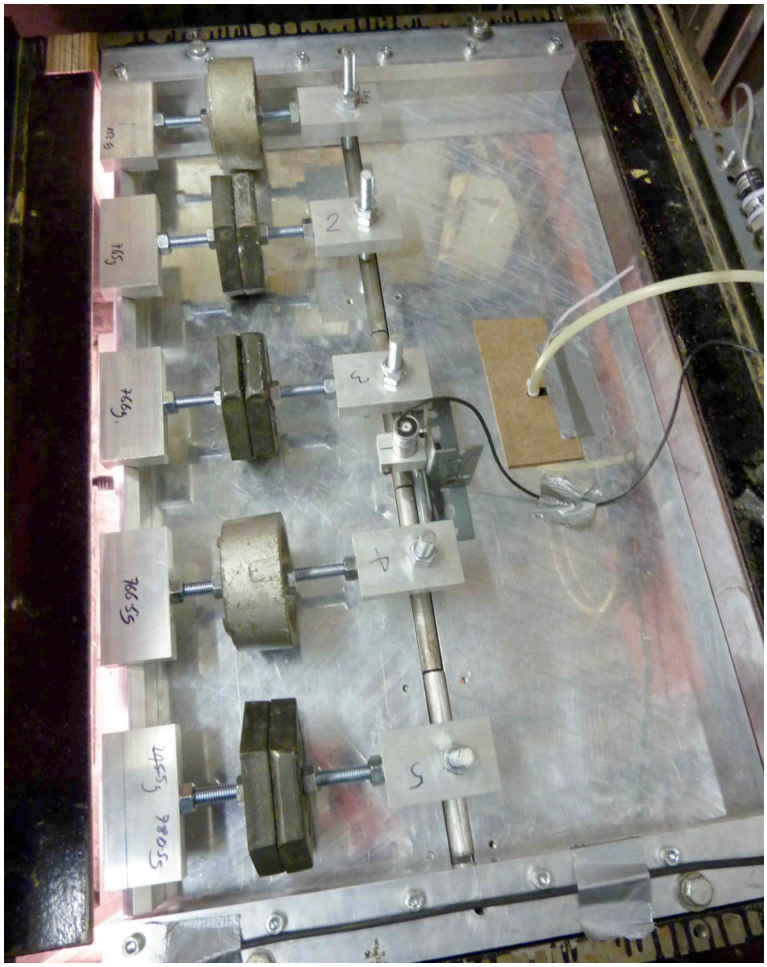

**Figure 4.24.** Axial loading mechanism assembled on test jig

#### 4.5.3.2 Uniform (wind) lateral loading arrangement

Uniform lateral loading tests to simulate imposed wind loadings on the wall panels were completed following the RILEM standard LUMC2 (1991c). Loading was applied using an inflatable air bag, constructed from thin polyethylene, positioned between the wall and the reaction surface, as shown by Figure 4.25. Air was supplied to the bag via the slip ring assembly on the centrifuge. Initially the bag air pressure was controlled through a manual pressure regulator situated in the control room. Later tests were controlled using a Proportion-Air (Proportion-Air Inc., McCordsville, IN, USA) electronic proportional pressure control valve mounted on the test jig. Control of the electronic valve was accomplished via a variable low voltage supply situated in the control room. Air pressure transducers were used to monitor the bag pressure in all tests. The output of the integral pressure transducer in the electronic valve was additionally monitored in later tests. A data logger was utilised to record the outputs from the sensors during the test process.

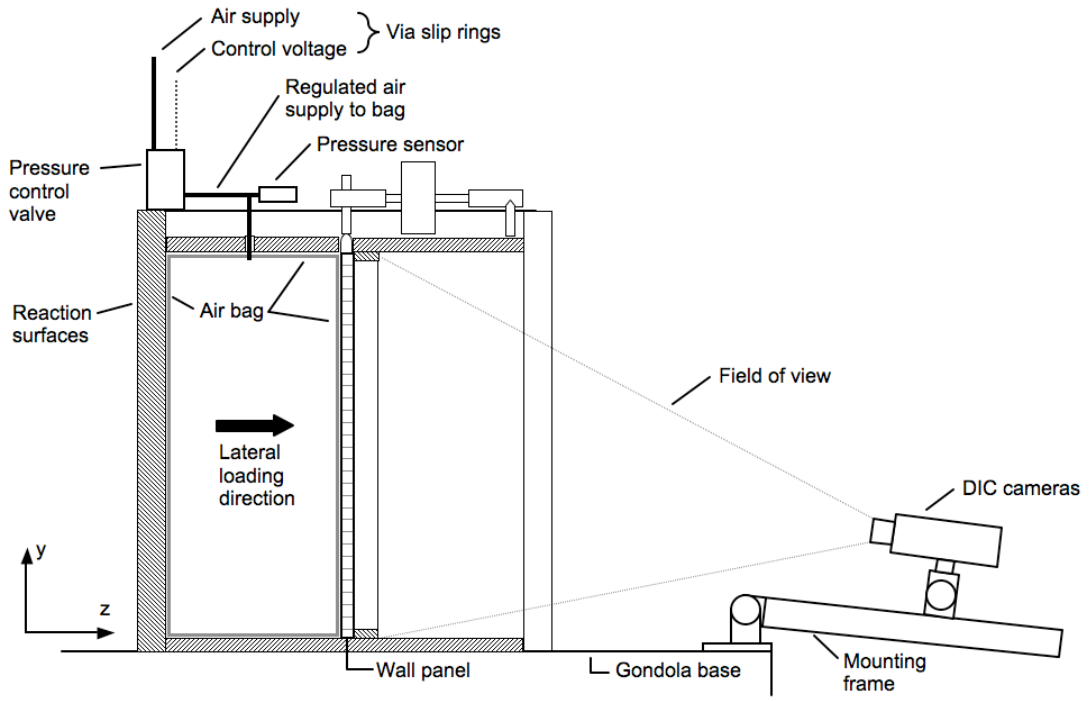


**Figure 4.25.** Uniform lateral loading test arrangement

#### 4.5.3.3 Non-uniform (hydraulic) lateral loading arrangement

There is no guidance in the standards for completing tests to evaluate the non-uniform hydraulic (water) lateral load capacity of masonry. The only previous study identified in the literature considered prototype scale wall panels where a framework was constructed against the specimen to form a tank to contain the water (Pace, 1988). In the tests the tank was filled with water and the deflection of the wall panel was monitored during the process. Leakage through the wall was apparent and due to this it was found difficult to maintain the water level in some cases. For this testing programme it was necessary to try and contain the water as much as possible to avoid it contacting the electronic equipment that was in close proximity. In addition the enhanced gravitational force imposed during centrifuge tests would likely force the water through the masonry more readily than experienced at normal gravity conditions, which the specimens would be subject to prior to testing. It would therefore be difficult to assess the effectiveness of any localised waterproofing system (sealing of the masonry only) without conducting the test. To reduce the possible issues mentioned a loose fitting thin polythene bag was used to contain the water during test, as shown by Figure 4.26. The reaction surface at the rear of the jig was brought forward to reduce the amount of water required for each level increment.

Water was delivered to the test jig via the slip rings and flow was remotely controlled via two solenoid valves. Flow was firstly directed to a measuring cylinder to enable precise control of the water level to be accomplished. A miniature video camera was used to monitor the water level in the measuring cylinder during the filling process. A second solenoid was used to release the water from the measuring into the water bag. This process ensured that the level increment at each fill was consistent. Measurement of the water level behind the specimen was made using a LVDT with a float attached. At the rear of the test jig a window was positioned upon which water level graduations were marked. A miniature video camera was positioned in front of the window to enable additional monitoring of the water level during test. As for the uniform loading tests a data logger was used to record the outputs of the sensors.

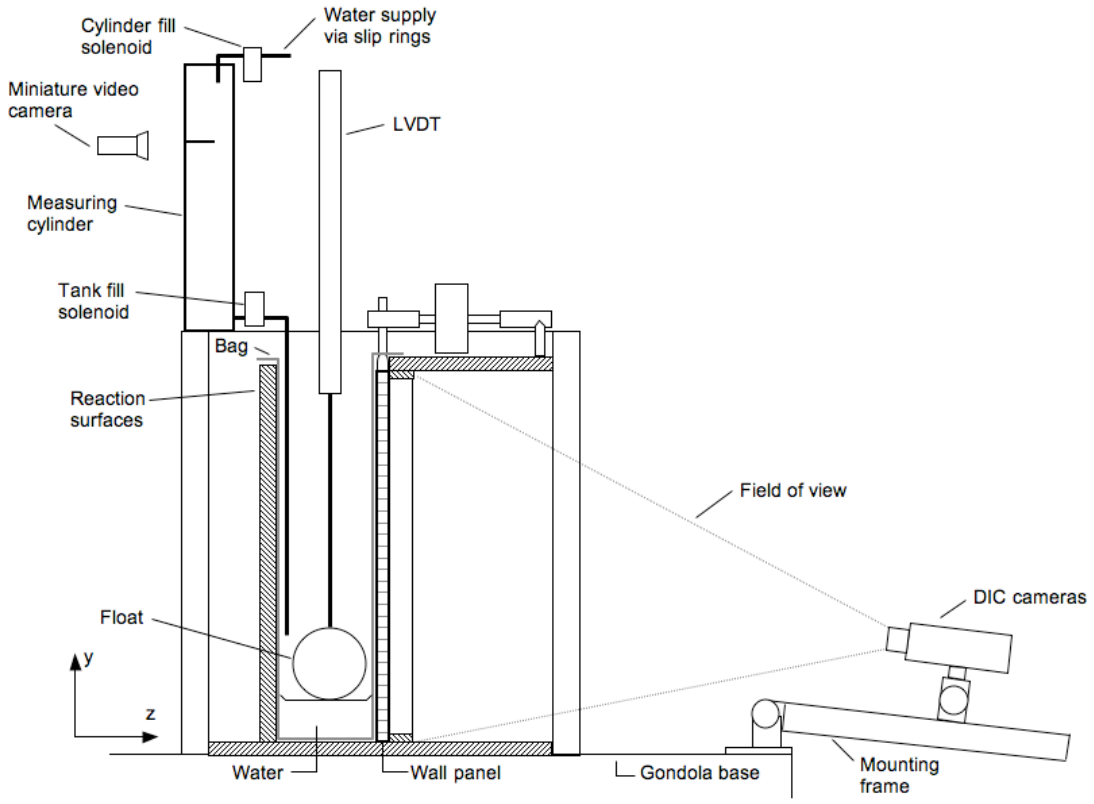


**Figure 4.26.** Non-uniform lateral loading test arrangement

### 4.5.4 Centrifuge testing procedure and initial analysis of data

The wall panel was loaded into the test jig and when a specimen with an opening was tested a plywood panel was placed over the opening prior to test to simulate the presence of a window. The test jig was then mounted on the gondola of the centrifuge and, if required, the correct axial loading was applied to the top of the wall. Following this the DIC system was calibrated and the sensors were checked for

correct operation. At start up of the centrifuge the DIC system was set to capture images every 10 s and the video system used to monitor the test was set to record. The image pair captured at the required operating speed was set as the reference in the DIC software. Deflections during the test were then determined from the reference image pair and this would avoid any potential effects of movement or settlement during the speed increment process. For the uniform loading tests the pressure was increased in approximately 0.2 kN/m$^2$ increments and for non-uniform tests the water level was increased in 10 mm increments. In both loading cases the out-of-plane deflections were allowed to stabilise before completing the next increment. Loading was continued until the ultimate limit state was attained. In the uniform loading tests the pressure in the air bag was reduced to zero at ultimate limit state, however it was not possible to remove the load in the non-uniform loading tests. The load, in terms of pressure or water level, at which initial cracking and the ultimate limit state occurred were recorded along with any other observations made during the test. After reaching the ultimate limit state the centrifuge was stopped and the specimen was recovered for photography and to record the crack pattern.

The data from each test comprised a data logger file, which contained readings from the pressure and displacement transducers, and a series of images taken by the DIC system. The loading increments were identified in the data logger file and the images at the steady state after increment were selected for analysis. These images were then loaded into the DIC software and the required data was extracted. In early tests the centrally mounted LVDT was used to verify the results from the DIC system, but was later removed as it was found to obscure the surface. The results of verification of the DIC system are presented in the following section. Video footage of the test procedure was also examined as required and still images were captured as necessary. Presentation and further analysis of the results was made using spreadsheet software. The schedule of wall panel specimens that were manufactured and tested is given in Tables 4.4 and 4.5, for uniform and non-uniform lateral loading tests respectively. Wall panels W1 to W3 and W5 to W7 were manufactured and tested as part of a joint research project with Jeremy Thomas from INSA Toulouse.

**Table 4.4.** Schedule of tests for wall panels – uniform (wind) lateral loading

| Specimen reference | Masonry type | Mortar compressive strength class | Axial loading | Additional description |
|---|---|---|---|---|
| W1 | AAC block | N/A | 1 storey | No mortar between units |
| W2 | AAC block | N/A | 1 storey | Sand between units |
| W3, 4 | AAC block | M2 | 1 storey | W4 repeat test |
| W5 | AAC block | M2 | 2 storeys | Additional axial load |
| W6-8 | Brick block | M2 | 1 storey | W7 and 8 repeat tests |
| W9-11 | Brick | M2 | 1 storey | W10 and 11 repeat tests |
| W12, 13 | Brick | M4 | 1 storey | W13 repeat test |
| W14 | Brick | M4 | 1 storey | Central opening |
| W15 | Brick outer AAC block inner | M2 | 1 storey (on inner leaf only) | Cavity wall assembly – outer leaf loaded directly |

**Table 4.5.** Schedule of tests for wall panels – non-uniform (hydraulic) lateral loading

| Specimen reference | Masonry type | Mortar compressive strength class | Axial loading | Additional description |
|---|---|---|---|---|
| H1, 2 | AAC block | M2 | 1 storey | H2 repeat test |
| H3, 4 | Brick block | M2 | 1 storey | H4 repeat test |
| H5, 6 | Brick | M2 | 1 storey | H6 repeat test |
| H7, 8 | Brick | M4 | 1 storey | H8 repeat test |
| H9 | Brick | M4 | Zero load | Top of wall unsupported |
| H10 | Brick | M4 | 1 storey, roof and floor | Self-weight and live load included for roof and floor |
| H11, 12 | Brick | M4 | 1 storey | Central opening, H12 repeat |
| H13, 14 | Brick outer AAC block inner | M2 | 1 storey (on inner leaf only) | Cavity wall assembly – outer leaf loaded directly, H14 repeat |
| H15 | Brick outer Brick block inner | M2 | 1 storey (on inner leaf only) | Cavity wall assembly – outer leaf loaded directly |

### 4.5.5 Verification of displacements from DIC using an LVDT

In initial tests an LVDT was additionally used to monitor the out-of-plane z deflections to verify the results from the DIC analysis. The point selected for DIC analysis was 40mm below the position of the LVDT, as presented in Figure 4.27. It was not possible to analyse a point directly adjacent to the LVDT as the support bracket

partially obscured the view of the wall and prevented any data being captured in this region, as shown in Figure 4.23. The z deflection obtained from DIC analysis showed good agreement to that measured by the LVDT for deflections up to 2.2mm, as evident in Figure 4.27. After initial cracking the values obtained from DIC analysis tended to underestimate the deflections when compared to those measured by the LVDT. This difference was considered to be due to the wall tending to act as two areas hinging about the initial crack and in doing so a small angle was formed between the two measuring points. The LVDT and mounting bracket was removed for subsequent tests to avoid any unnecessary loss of data.

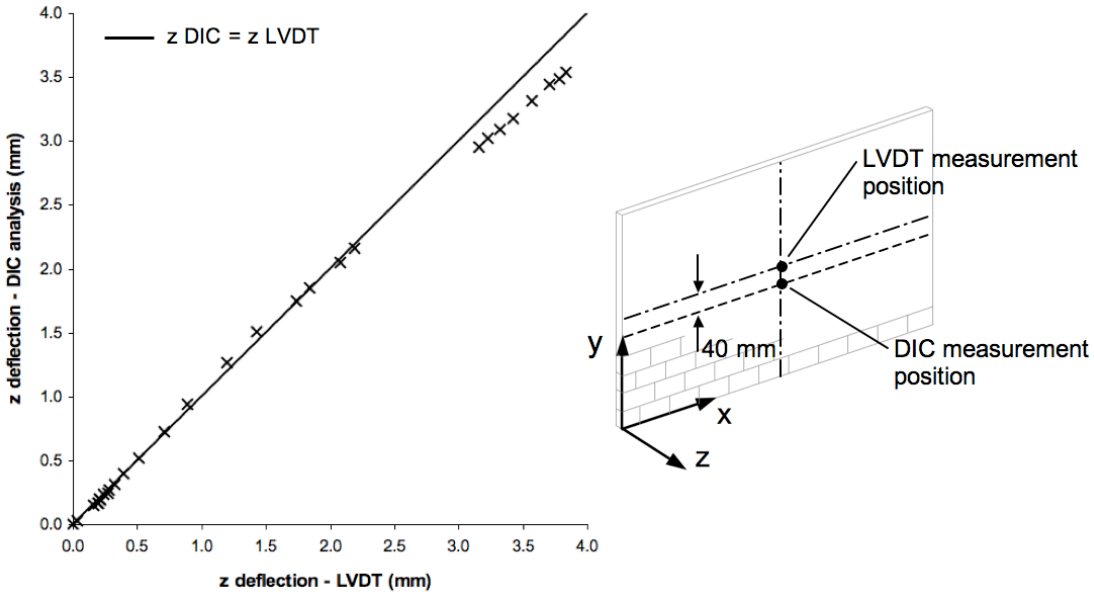


**Figure 4.27.** Comparison of z deflections measured using the LVDT and DIC system (completed for specimen W3 AAC block)

### 4.6 Testing arrangement and procedure for wallette specimens

Wallette specimens were tested according to standard BS EN 1052-2:1999 (1999b). Masonry is not isotropic so two different format specimens are required in order to assess the flexural strength in a plane of failure parallel to (direction 1) and perpendicular to (direction 2) the bed joints, as illustrated by Figures 4.28 and 4.29 respectively (BSI, 1999b). The dimensions of the specimens at model scale are given in Table 4.6. A minimum of 5 of each specimen were tested in line with the requirements of the standard. The specimens were tested horizontally in four point bending using a 20kN universal test machine, as shown by Figure 4.30. A stroke controlled loading rate of 0.005 mm/sec was used throughout the experimental programme, to permit direct comparison of the results presented here to a previous

study (Mohammed, 2006). The flexural strength, in N/mm$^2$, of the specimens was then determined from the peak load before failure using equation 4.1 (BSI, 1999b). For some specimens, the DIC system was used to measure the in and out-of-plane deflections during the test. In these cases, it was necessary to position a steel frame between the lower supports of the specimen and the base of the test machine to enable the DIC cameras to be positioned below, as shown by Figure 4.31. The schedule of wallette specimens that were manufactured and tested is given in Table 4.7. Wallette specimens F1, F2, F4 and F5 were manufactured and tested as part of a joint research project with Jeremy Thomas from INSA Toulouse.

$$f_{xi} = \frac{3F_{i,\max}\left(l_1 - l_2\right)}{2bt_u^{\,2}} \qquad 4.1$$

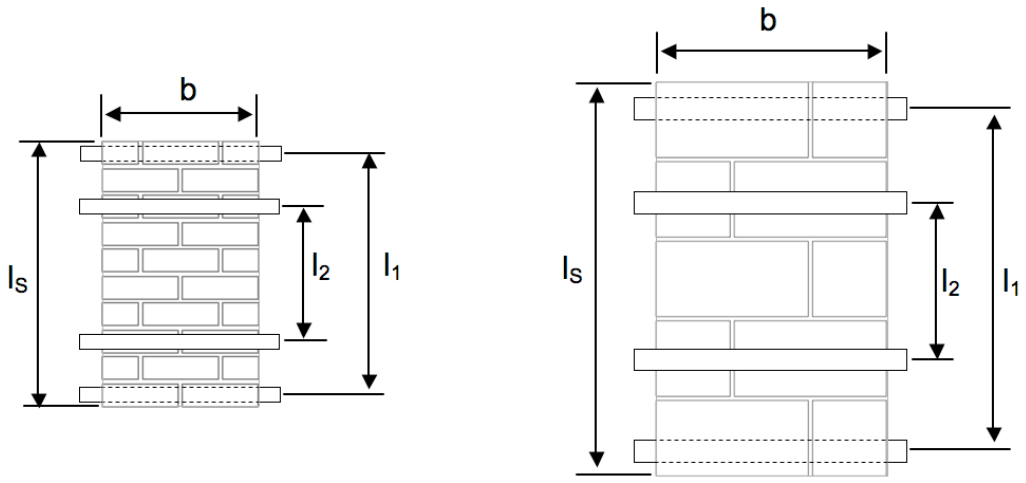


(a) (b)

**Figure 4.28.** Model scale flexural testing arrangement for a plane of failure parallel to bed joints (direction 1) for (a) brick and (b) block specimens

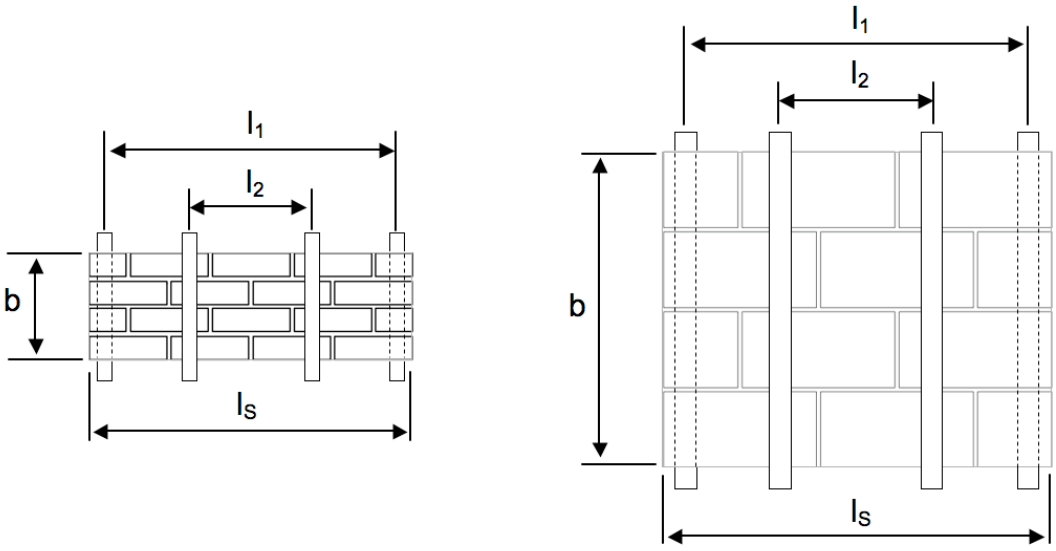


(a) (b)

**Figure 4.29.** Model scale flexural testing arrangement for a plane of failure perpendicular to bed joints (direction 2) for (a) brick and (b) block specimens

**Table 4.6.** Dimensions for the 1:6 scale flexural test wallette specimens

| Test specimen | Masonry format | Figure reference | b (mm) | $l_s$ (mm) | $l_1$ (mm) | $l_2$ (mm) |
|---|---|---|---|---|---|---|
| Plane of failure parallel to bed joints (direction 1) | Brick | 4.27a | 73 | 122 | 105 | 60 |
| | Block | 4.27b | 111 | 190 | 173 | 77 |
| Plane of failure perpendicular to bed joints (direction 2) | Brick | 4.28a | 47 | 148 | 131 | 58 |
| | Block | 4.28b | 152 | 187 | 170 | 76 |

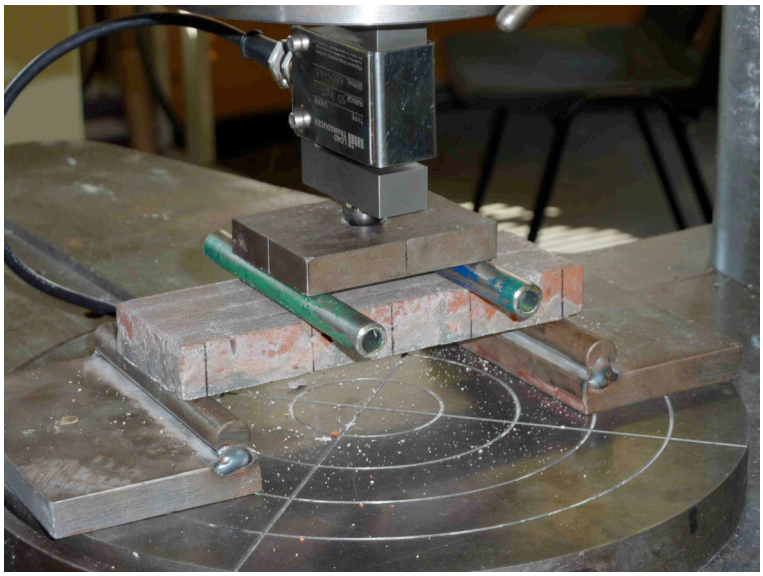

**Figure 4.30.** Testing arrangement for brick wallette specimens at model scale

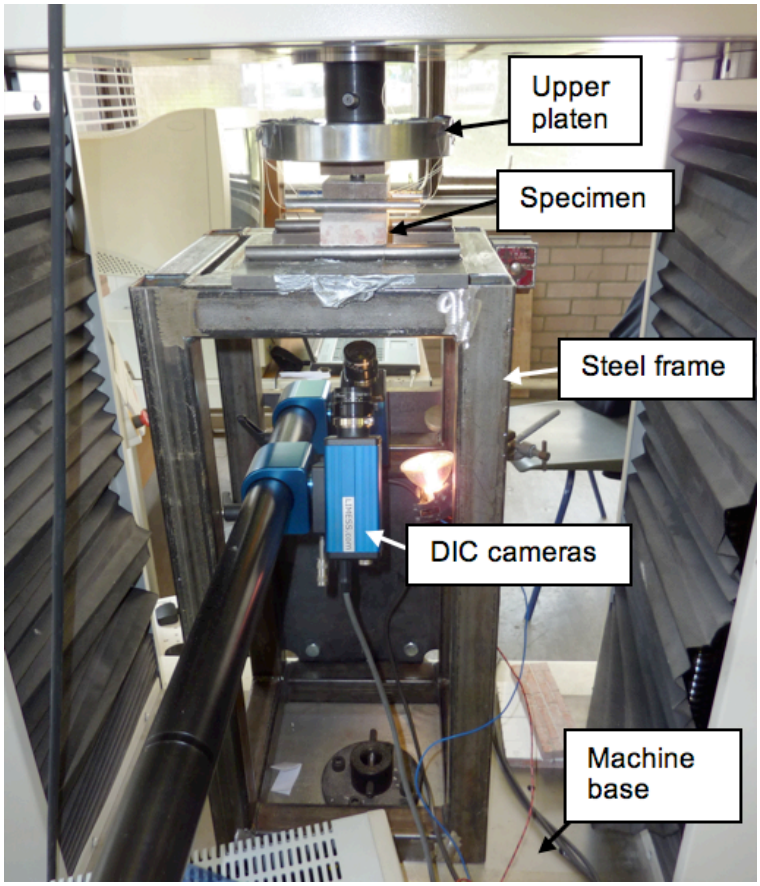


**Figure 4.31.** Testing arrangement for wallette specimens with the DIC system

**Table 4.7.** Schedule of tests for wallette specimens

| Test numbers | Masonry type | Mortar compressive strength class | Quantity of specimens per test | Additional details |
|---|---|---|---|---|
| F1 to 3 | AAC block | M2 | 5 | F2 and 3 repeat tests |
| F4 & 5 | Brick block | M2 | 5 | F5 repeat test |
| F6 & 7 | Brick | M2 | 6 | F7 repeat test |
| F8 & 9 | Brick | M4 | 6 | F10 repeat test |
| F10 | Brick | M4 | 6 | Pre-compression during curing |
| F11 | AAC block | M2 | 5 (y dir only) | No mortar in perpendicular joints |

### 4.7 Testing arrangement and procedure for wall ties

Wall ties were tested in tension and compression according to standard BS EN 846-5:2000 (2000d). The couplet specimens were manufactured as detailed in Section 4.4.5. Fixtures were manufactured to enable the couplet specimens to be pre-stressed during the test as described in the standard. The normal stress applied to the specimen was maintained at 0.1 ±0.001 N/mm$^2$ and was monitored using a

Gemini signal conditioning unit connected to a load cell. The displacement of the wall tie was measured using two LVDTs positioned on the upper surface of the couplet for the prototype specimens, as shown by Figure 4.32. The output of the LVDTs and test machine load were recorded using a data logger. Due to the small size of the model scale specimens, as apparent in Figure 4.33, it was not possible to utilise LVDTs to measure deflections and instead the machine displacement was monitored. Constant loading rates of 600 N/min and 20 N/min were used for the prototype and model scale specimens respectively. Loading was continued until failure or until a deflection of 5 mm (0.83 mm at model scale) was observed as dictated by the standard. The schedule for the wall tie test specimens that were manufactured and tested is given in Table 4.8.

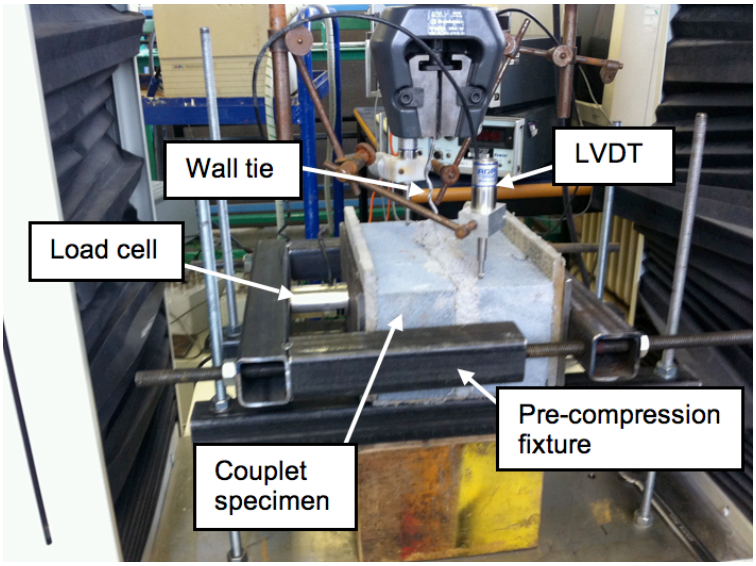


**Figure 4.32.** Testing arrangement for wall ties at prototype scale (compression test shown)

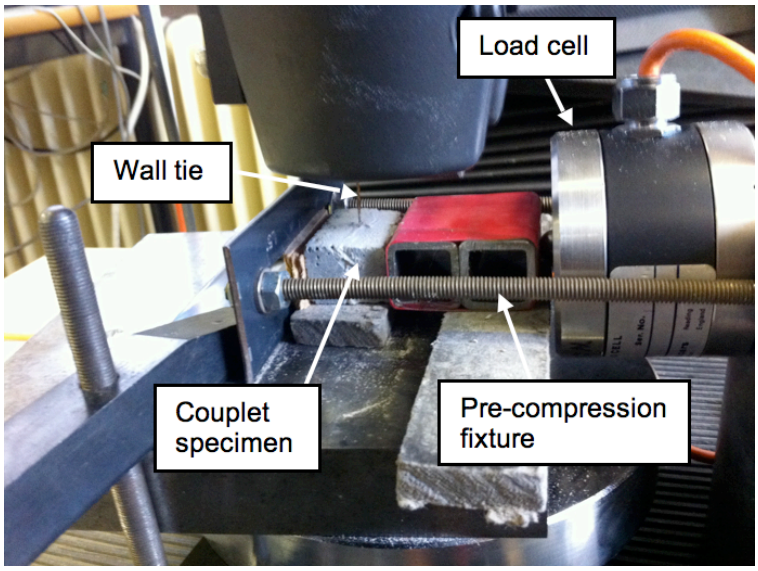


**Figure 4.33.** Testing arrangement for wall ties at model scale (compression test shown)

**Table 4.8.** Schedule of tests for wall tie specimens

| Test number | Scale | Material | Mortar compressive strength class | Tie type |
|---|---|---|---|---|
| WTPT1 | 1 (prototype) | AAC brick | M2 | Staifix RT2 tie |
| WTPT2 | 1 | AAC brick | M4 | " |
| WTPT3 | 1 | Brick | M2 | " |
| WTPT4 | 1 | Brick | M4 | " |
| WTM1 | 1:6 | AAC brick | M2 | Formed tie |
| WTM2 | 1:6 | AAC brick | M4 | " |
| WTM3 | 1:6 | Brick | M2 | " |
| WTM4 | 1:6 | Brick | M4 | " |
| WTM5 | 1:6 | Brick | N/A | Formed and bonded on |

### 4.8 Summary

The elements of a typical masonry property were considered as discrete wall panels with the appropriate boundary conditions and vertical loading applied. Masonry specimens were constructed at 1:6 scale using units cut from prototype scale materials and a correctly scaled mortar was utilised. A horizontal manufacturing method was successfully developed to allow the consistent construction of both wall panels and wallette specimens. Cavity wall specimens were formed by bonding wall ties between individual leaves and openings were easily formed in the panel during the manufacturing process. A method was developed to allow specimens to be

tested within the centrifuge and enabled self-weight effects to be correctly considered. Lateral loading was applied to the wall panels as either a uniformly distributed load to simulate wind loading or as a non-uniformly distributed load to model hydraulic loading conditions. Three dimensional DIC was successfully utilised to monitor and record the deflections both in and out-of-plane during the centrifuge tests. The out-of-plane displacements determined by DIC analysis showed a good correlation to those recorded by an LVDT. Additional monitoring and recording of the test procedure was completed using video equipment and a datalogger. Wallette specimens were tested at 1:6 scale to establish the flexural strength of the masonry according to standard BS EN 1052-2:1999 (1999b). Wall ties specimens, manufactured as couplets, were manufactured and tested successfully at both prototype and model scale to standard BS EN 846-5:2000 (2000d). Mortar cubes were manufactured alongside the masonry specimens and used for quality control and to allow comparison between different masonry specimens.

# Chapter 5 Small assemblage test results

This Chapter presents the results from the small assemblage tests completed alongside the wall panel tests. Flexural tests were completed of both brick and block specimens according to the method described in Chapter 4. The main purpose of these tests was to derive parameters for use in the theoretical analysis described in detail in Chapter 3. DIC was employed during some of the wallette tests to observe the process occurring during loading and failure of the specimens. In addition tests were conducted to evaluate the strength of wall ties at both prototype and model scale. Wall ties were manufactured by hand for the small-scale specimens and tests were performed to verify that they were a suitable representation of the prototype. Finally a brief comparison is made of the compressive strength of model and prototype scale mortars manufactured during the wall tie tests.

## 5.1 Wallette tests

A summary of the results of the wallette tests for direction 1 (test direction parallel to the bed joints) and direction 2 (test direction perpendicular to the bed joints) is given in Table 5.1. The coefficient of variation (COV) values for the average flexural strengths ($f_{xd1}$ and $f_{xd2}$) for all the specimens were generally in the range 10 to 25 %. Results reported in the literature have shown a higher degree of variation with COV values ranging from 3 to 44 % (de Vekey et al., 1986, Mohammed and Hughes, 2011, West et al., 1986). The use of a process that enabled sets of specimens to be manufactured together and consistently may have resulted in the COV values for the flexural strengths being towards the lower end of those reported in the literature. The COV values for the flexural strengths differed between the test directions, but there did not appear to be a trend in the results and it was likely that this difference was due to natural variability. The COV values for the mortar cubes were higher than expected for the AAC block, Brick M2 and M4 mortar strength where more than one batch of specimens was tested. This was attributed partly due to different batches of cement being used during the study and the differences in the moisture state of the cubes between tests.

**Table 5.1.** Flexural strengths for wallette specimens in direction 1 ($f_{xd1}$) and 2 ($f_{xd2}$)

| Test number | Masonry / mortar type | Flexural strength $f_{xd1}$ (N/mm$^2$) | COV $f_{xd1}$ (%) | Flexural strength $f_{xd2}$ (N/mm$^2$) | COV $f_{xd2}$ (%) | Mortar cube compressive strength (N/mm$^2$) | Mortar cube COV (%) |
|---|---|---|---|---|---|---|---|
| F1 to 3 | AAC block/M2 | 0.41 | 20.78 | 0.67 | 9.82 | 2.07 | 34.69 |
| F4 & 5 | Brick block/M2 | 0.50 | 22.02 | 1.28 | 13.56 | 1.52 | 7.62 |
| F6 & 7 | Brick/M2 | 0.44 | 15.58 | 1.02 | 22.27 | 2.47 | 48.45 |
| F8 & 9 | Brick/M4 | 0.66 | 24.74 | 1.45 | 20.76 | 4.54 | 46.63 |
| F10[1] | Brick/M4 | 0.94 | 11.25 | 1.37 | 23.31 | 4.20 | 5.23 |
| F11[2] | AAC block/M2 | NA | NA | 0.50 | 11.63 | 3.69 | 4.01 |

[1]Preloaded during curing stage

[2]No mortar in perpendicular joints

### 5.1.1 Brick specimens

The variation in flexural strength with mortar compressive strength for the brick specimens is shown in Figure 5.1. The compressive strength of the mortar was observed to affect the flexural strength of the brick specimens in both directions 1 and 2. The overall trend shown, in the absence of data in between the values tested, was of increased flexural strength in direction 2 with higher mortar strength. In direction 2 an increase of 50 % was found as the compressive strength of the mortar was increased from M2 to M4 designation. The failure modes for the brick specimens tested in direction 2 are presented in Figure 5.2. The dominant failure mode for the brick specimens tested in direction 2 was characterised by cracking in both the mortar and brick units, as shown in Figure 5.2a. In approximately 14% of the specimens tested, the crack traversed the central brick at the edge of the specimen instead of fracturing it, as shown in Figure 5.2b. This may have been due to the particular brick being less confined, slightly stronger than other units in the specimen or having a bond of lower strength to the surrounding mortar. Adding vertical preload to M4 mortar specimen F10 during curing marginally decreased the flexural strength in direction 2 when compared to corresponding test without preload, but this difference falls within the natural variability reported in the results and therefore additional investigation would be required to determine the significance of these observations. The failure mode for all the preloaded specimens was through both the perpendicular mortar joints and units, so any improvement in the strength in the bed joints would have little effect.

The general trend for the brick specimens tested in direction 1 was of increased average flexural strength ($f_{xd1}$) with mortar strength, as shown in Figure 5.1. The flexural strength in direction 1 was found to increase by 42 % as the compressive strength of the mortar was increased from M2 to M4 designation. The failure mode that was typically observed in the brick specimens tested in direction 1 is presented in Figure 5.3. The specimens tested in direction 1 always failed through a mortar bed joint positioned between the inner supports, however the exact location of the failed joint varied slightly between specimens. Failure tended to occur in the mortar rather than at the interface with the brick units suggesting that the mortar strength was the limiting factor. It would then be expected that a higher strength mortar would provide a greater flexural strength as was shown by the results. A significant improvement in the flexural strength in direction 1 was observed for the brick M4 specimen number F10 that was preloaded during the curing stage. The specimens in the set similarly failed in the mortar joint, such that the preloading more likely increased the internal bond strength of the mortar as opposed to the bond strength at the interface. Preloading effectively forced the constituents closer together, such that the size of internal voids in the mortar would be reduced leading to increased strength. Another explanation may be that excess water in the mortar mixture was forced out by the preloading and effectively reducing the water to cement ratio and therefore increasing the mortar strength.

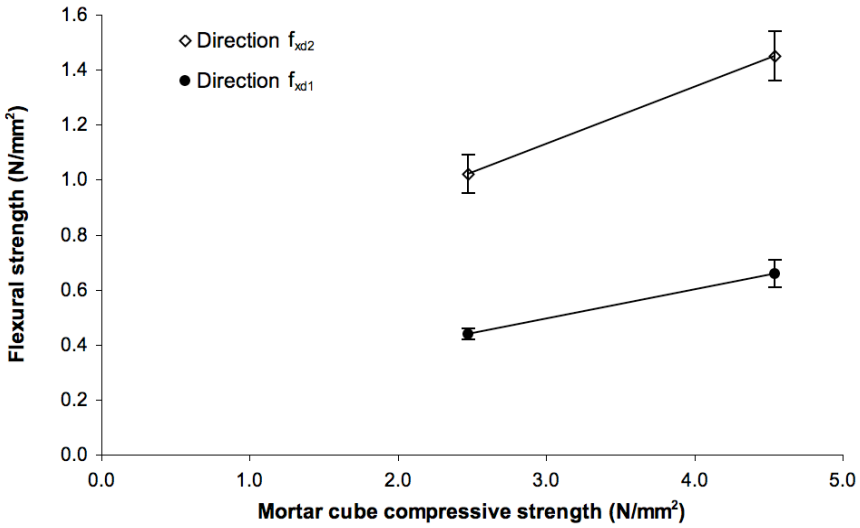


**Figure 5.1.** Variation in average flexural strength ($f_x$) with mortar strength for brick wallette specimens (error bars shown are standard error of the mean)

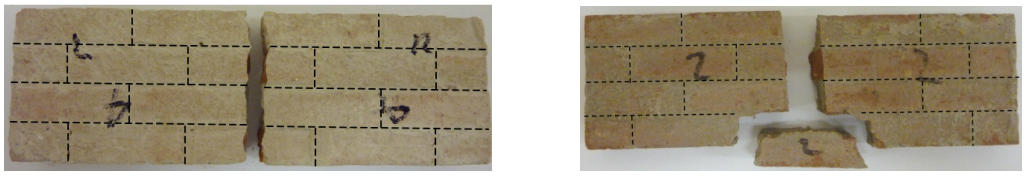

(a) (b)

**Figure 5.2.** Wallette specimen failure patterns for brick specimens tested in the direction 2, (a) dominant failure mode and (b) alternative failure mode (dashed lines show intact mortar joints)

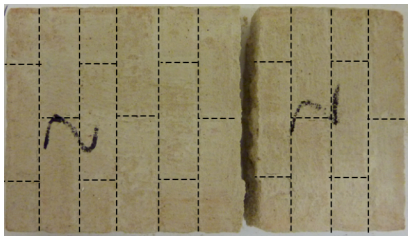

**Figure 5.3.** Typical wallette specimen failure pattern for brick specimens tested in the direction 1 (dashed lines show intact mortar joints)

Values of flexural strength prescribed by the National Annex to Eurocode 6 (EC6) (BSI, 2005d) are characteristic values ($f_{xk}$) that have been derived from experimental results (Haseltine et al., 1977). The characteristic values were derived for a 95 % confidence level, such that it would be expected that 95 % of all specimens tested would attain a strength at least equal to the characteristic value. The use of characteristic values in calculations would therefore provide safer results, as they would account for the variation expected in the flexural strengths of the wallettes. It was necessary to adjust the EC6 characteristic flexural strengths to obtain average values to allow comparison with the experimental results found in this study. Following this process would be more advantageous than deriving characteristic values for the experimental results and comparing them to the EC6 prescribed values, as it would permit use of the EC6 adjusted strengths in the analysis presented in Chapter 8. Ultimate loads or levels found in the analysis using the adjusted EC6 strengths would then be directly comparable to the experimental ultimate loads for the wall panels. The British Standard for the determination of flexural strength from masonry specimens (BSI, 1999b) states that the characteristic strength is equal to the average experimental strength divided by 1.5, where five specimens are tested. For larger sample groups a more complex method is given (BSI, 1999b) that requires knowledge of the strengths of the individual specimens. For the sample sizes used in this study it was found that the characteristic strengths

derived by either method were similar. It was therefore considered appropriate, in the absence of the underlying experimental data, to calculate the adjusted average EC6 values by multiplying the characteristic values by 1.5. The prescribed (characteristic) and adjusted EC6 flexural strengths are given in Table 5.2. The appropriate prescribed values were selected form the National Annex to EC6 (BSI, 2005d) with regards to the masonry units and mortar strengths used in this programme of research, as detailed in Chapter 4 Sections 4.2 and 4.3 respectively.

**Table 5.2.** Characteristic and adjusted EC6 flexural strengths (BSI, 2005d)

| **Masonry / mortar type** | **Flexural strength (N/mm$^2$)** | | | |
|---|---|---|---|---|
| | Characteristic as prescribed | | Adjusted average | |
| | $f_{xkd1}$ | $f_{xkd2}$ | $f_{xd1}$ | $f_{xd2}$ |
| AAC block / M2[1] | 0.20 | 0.40 | 0.30 | 0.60 |
| Brick / M2 and Brick block / M2[2] | 0.35 | 1.00 | 0.53 | 1.50 |
| Brick / M4[2] | 0.40 | 1.10 | 0.6 | 1.65 |

[1] For AAC block of 3.6 N/mm$^2$ unit compressive strength

[2] For brick with a water absorption of between 7 and 12 %

A comparison of the EC6 adjusted and average experimental flexural strength is presented in Figure 5.4 for the brick wallettes. It was found that the EC6 adjusted flexural strengths for direction 2 ($f_{xd2}$ EC6) were higher than those determined in the experimental tests regardless of mortar strength. The EC6 adjusted values exceed the experimental strengths by 47 and 14 % for M2 and M4 compressive strength class mortar respectively. Lower test values could be explained by variations in the observed failure modes and size effects in the aggregate or masonry assembly. The difference observed between the EC6 adjusted and test strength for the M4 strength mortar was also within the range associated with the inherent natural variability. In the tests that were completed to establish the published EC6 values only 5% of specimens were found to fail through the unit with the remainder failing only through the mortar joints (West et al., 1977). Failure in the mortar joints only would require the bond to be broken in both the perpendicular joints and the bed joints. It would be expected that a significant amount of torsional shearing would have to occur in the bed joints and this may result in a higher flexural strength when compared to a failure mode that occurred through the units and perpendicular joints. A previous study had established that there was a size effect between model (1:6) and prototype M4 mortar wallettes tested in direction 2 and strength was found to reduce with scale

(Mohammed and Hughes, 2011). Since the adjusted EC6 values were based on tests of prototype scale units only, this may account for the discrepancies observed between strengths. In addition it has been reported that the tensile bond strength of M4 mortar decreased as the grading of the aggregate became increasingly finer (Anderson and Held, 1986). However in a more recent study the effect of aggregate grading on the strength on M4 mortar was found to be less significant (Mohammed, 2006). It seems feasible to suggest that the test values were influenced by a combination of a size effect in the masonry assembly, differences in the failure mode and natural variability.

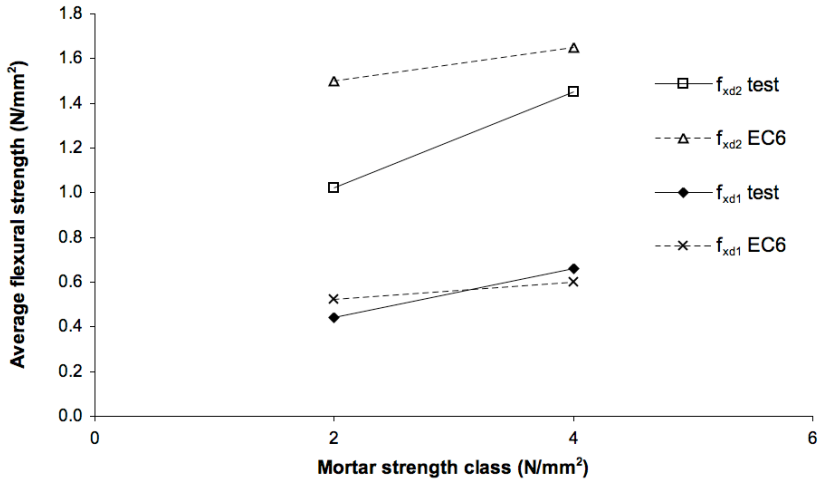


**Figure 5.4.** Comparison of average experimental ($f_x$ test) and adjusted EC6 ($f_x$ EC6) flexural strengths for M2 and M4 strength class mortar for brick wallettes

In direction 1 the experimental flexural strengths ($f_{xd1}$ Test) differed to the EC6 adjusted values ($f_{xd1}$ EC6), as shown in Figure 5.4. The EC6 adjusted strength exceeded the test value by 19 % for the M2 compressive strength mortar, whilst the EC6 adjusted strength for the M4 compressive strength mortar specimen was 9 % lower than the experimental value. It has been reported in a recent study (Mohammed and Hughes, 2006) that there was no clear effect of scale on the flexural strength of brick specimens constructed with M4 strength mortar tested in direction 1, which supports the findings of this programme. The differences in the EC6 adjusted and experimental strengths for the M4 compressive strength mortar were also within the expected natural variability associated with masonry testing.

The variations observed in the test and EC6 adjusted flexural strengths illustrate the importance of using the appropriate values, if available, in design processes.

Adopting code values may lead to design strengths of wall panels being overly conservative in some instances and overloaded in others. The variability in masonry typically means that onerous safety factors will be utilised in the calculations, such that safe designs should always be the result.

### 5.1.2 Block specimens

All block specimens were manufactured with M2 strength class mortar. The effect of material type was investigated and comparisons to the corresponding brick values were also made. The effect of leaving the perpendicular mortar joints unfilled during the flexural strength tests in direction 2 was additionally assessed for the AAC block material.

A comparison of the average flexural strengths for the brick and block specimens in test directions 1 and 2 is presented in Figure 5.5 and the typical failure modes observed in the block specimens are shown in Figures 5.6 and 5.7. It was apparent that the average flexural strength of the brick block specimens exceeded both the brick and AAC block specimens when tested in direction 2. It was expected that the strength of the brick specimens in direction 2 would exceed the block specimens due to the increased number of mortar joints in the specimen. Such behaviour had previously been shown in tests of AAC block and AAC brick sized units, with the latter achieving significantly higher strengths (de Vekey et al., 1986). It was suggested (de Vekey et al., 1986) that the results were due the increased number of mortar joints allowing strains to be redistributed, therefore allowing a higher flexural strength to be achieved. The opposite was, however, shown for the brick block and brick sized specimens here and this might have been due to the different failure modes observed. The brick specimens tended to fail through both the mortar joints and units, as shown in Figure 5.2a, whilst the brick block specimens failed only in the mortar joints, as shown in Figure 5.6a. The higher strength observed for the brick block specimens suggests that a sufficient bond was formed between the blocks and mortar. This behaviour also supports the statement made above that failure in the joints would result in a higher strength. The failure mode seemed to suggest that the strength of the brick block unit was higher than the brick unit as no rupture occurred in the former. It would be expected that a larger unit of the same material would fail at a lower load than a smaller unit due to a greater chance of there being a critically sized internal flaw, regardless of the size of the flaw in relation to the unit size. However, the behaviour observed here was contrary to this and some effect may have occurred due to the flaw size.

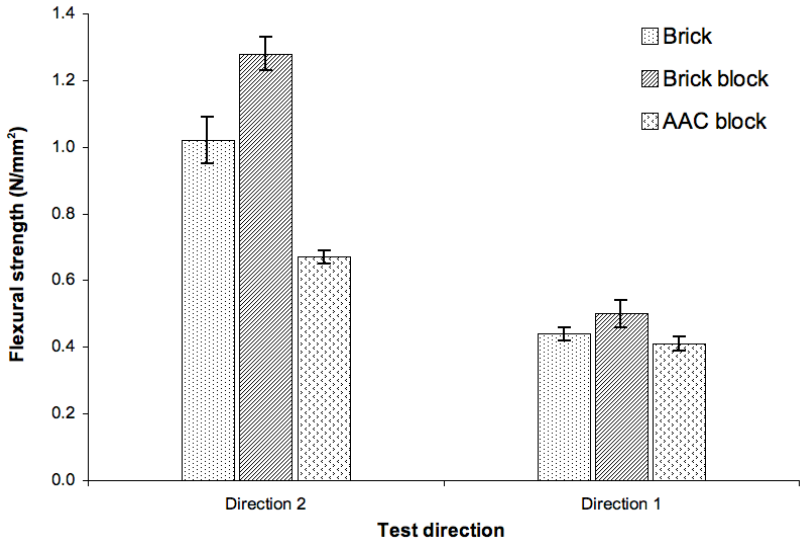


**Figure 5.5.** Comparison of average wallette flexural strength in test directions 1 and 2 for different masonry types manufactured with M2 strength class mortar (error bars shown are standard error of the mean)

The average strength of the AAC block specimens in direction 2 was lower than either the brick or brick block specimens due to the lower unit strength. The AAC block specimens tended to fail through the units, as shown in Figure 5.6b. This failure mode was expected due to unit and mortar strength reported as being of a similar value and hence there was no preferential failure route (de Vekey et al., 1986, Mohammed, 2006). When the perpendicular mortar joints were left unfilled it was found that the flexural strength in direction 2 decreased by 25%. A similar failure mode to the specimen with mortar in the perpendicular joints was observed, with the exception of additional failure occurring near the edge of the specimen, as shown in Figure 5.6c. The reduction in strength confirms the importance of the perpendicular mortar joints in the resistance of the masonry specimen to out-of-plane bending. Previous researchers had found that the flexural strength reduced by 44% for brick specimens constructed without mortar in the perpendicular joints (Sinha et al., 1979).

(a)

(b)

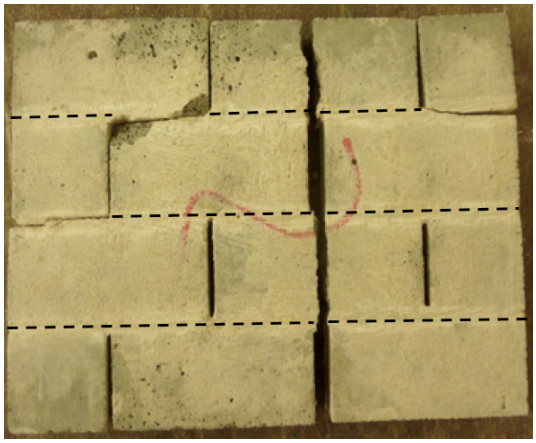

(c)

**Figure 5.6.** Typical wallette specimen failure patterns for specimens tested in direction 2: (a) brick block, (b) AAC block and (c) AAC block with no mortar in perpendicular joints (dashed lines show intact mortar joints)

The flexural strengths of the specimens manufactured with M2 strength mortar that were tested in direction 1 were comparable to each other, as shown in Figure 5.5. The failure modes observed were similar for both the brick and block specimens, as shown in Figures 5.3 and 5.7 respectively, being characterised by fracture in the mortar bed joint. The standard error of the means, shown by the error bars on Figure 5.5, suggest that there was no significant difference between the strength of the brick and brick block specimens. Likewise there was no significant difference between the brick and AAC block specimens. The higher strength found in the brick block specimen was likely due to the inherent variation in masonry test specimens rather than any other factor since similar failure modes were observed.

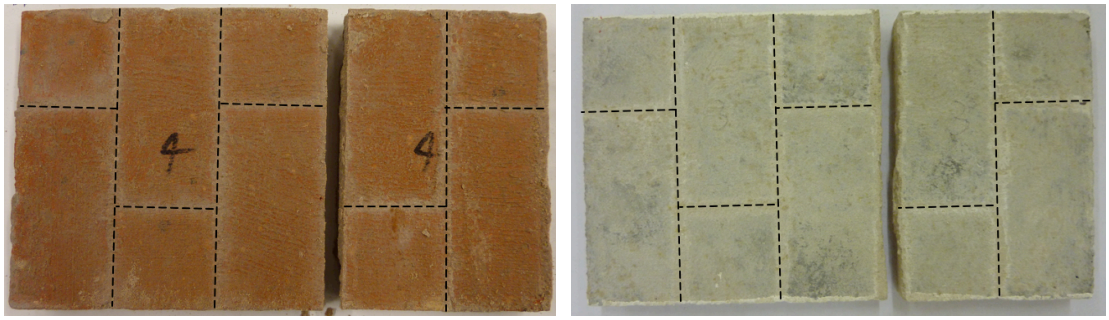

(a) (b)

**Figure 5.7.** Typical wallette specimen failure patterns for specimens tested in direction 1: (a) brick block and (b) AAC block (dashed lines show intact mortar joints)

Figure 5.8 presents a comparison of the average experimental and EC6 adjusted flexural strengths for the block specimens. The EC6 adjusted flexural strengths exceeded the experimental strengths of the brick block specimens by 5 and 17 % in directions 1 and 2 respectively. For the AAC block the experimental strengths exceeded the EC6 adjusted values by 37 % in direction 1 and 12 % in direction 2. Taking into account the natural variability likely in the flexural strength, then the EC6 adjusted values were considered to correlate well to the experimental values for the brick block in both test directions and the AAC block in direction 2. The experimental strength of the AAC block specimen in direction 1 may have significantly exceeded the EC6 adjusted value due to differences in the surface finish of the model and prototype scale blocks. The cutting process was found to expose the pores in the AAC units, which may have resulted in an improved bond between the mortar and the unit when compared to the prototype. Using the EC6 adjusted values in wall panel design calculations would therefore provide slightly conservative results for AAC block and would marginally overestimate the strength of the brick block.

The National Annex to EC6 (BSI, 2005d) does not provide flexural strengths for block sized clay masonry units, whilst the values specified for block are only valid for concrete, AAC or manufactured stone and are classified according to unit compressive strength. In the absence of this data, comparison was made to the EC6 adjusted flexural strengths for brick units with M2 compressive strength mortar, as given in Table 5.2. Generally solid clay blocks without voids or perforations would not be used in practice and this explains the omission of such data in EC6.

The reason for utilising the brick blocks was due to problems associated with cutting medium density concrete blocks. Although a casting approach could have been

followed, it may have taken a significant amount of time to develop a correctly scaled concrete block with properties comparable to the prototype. Variations in mechanical properties between each batch of blocks were also envisaged. The EC6 adjusted flexural strengths for concrete block units of the correct unit compressive strength (≥17.5 N/mm$^2$) were 0.30 and 1.05 N/mm$^2$ in directions 1 and 2 respectively. The experimental results suggest that brick block would be of comparable performance to concrete block in direction 2, but be stronger in direction 1. The results of tests of wall panels constructed from brick block would likely provide an upper bound for all blockwork and provide a different failure mode to the AAC block specimens.

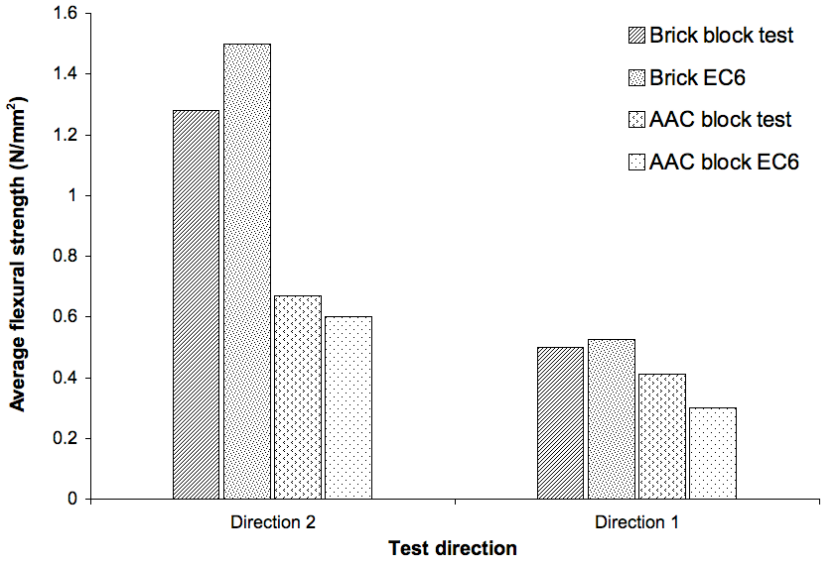


**Figure 5.8.** Comparison of average experimental ($f_x$ test) and adjusted EC6 ($f_x$ EC6) flexural strengths for test directions 1 and 2 for block wallettes with M2 strength class mortar

### 5.1.3 Orthogonal ratio

The orthogonal ratios of strengths for all the specimens tested are presented in Table 5.3. Lower values of orthogonal ratio result in a larger difference between the flexural strength of the specimens in the two directions. The ratios based on the experimental flexural strength for the AAC block exceeded the ratio of the EC6 adjusted flexural strengths and reflects the higher strength found in direction 1. The orthogonal ratio for brick block was however very similar to that of the EC6 adjusted value, which was based on the strengths for brick with M2 strength mortar. The ratios for the brick specimens manufactured with M2 and M4 strength mortar overestimate the ratio of the EC6 adjusted values, and the differences were due to the lower flexural strengths in direction 2. Applying preloading to specimen F10 provided an improvement in

flexural strength in direction 1 and resulted in a higher orthogonal ratio compared to the ratio of the EC6 adjusted strengths. Where the perpendicular mortar joints of the AAC block specimen F11 were left unfilled the orthogonal ratio was improved compared to that for specimens the AAC block specimens F1 to F3 due to the lower flexural strength in direction 2.

**Table 5.3.** Orthogonal ratio of flexural strengths

| Test number | Masonry / mortar type | Test average values $f_{xd1}/f_{xd2}$ | EC6 adjusted mean $f_{xd1}/f_{xd2}$ |
|---|---|---|---|
| F1 to 3 | AAC block/M2 | 0.61 | 0.5 |
| F4 & 5 | Brick block/M2 | 0.39 | 0.35[1] |
| F6 & 7 | Brick/M2 | 0.43 | 0.35 |
| F8 & 9 | Brick/M4 | 0.46 | 0.36 |
| F10[2] | Brick/M4 | 0.69 | 0.36 |
| F11[3] | AAC block/M2 | 0.83 | N/A[4] |

[1]Value given for brick with M2 strength class mortar

[2]Preloaded during curing stage

[3]Unfilled perpendicular mortar joints in direction 2 test specimen only and $f_{xd1}$ or $f_{xkd1}$ from test F1 to F3

[4]No EC6 value available for unfilled perpendicular joints

Figure 5.9 shows the variation in the inverse orthogonal ratio with the flexural strength in direction 1 for all brick specimens. It was generally found that the inverse of the orthogonal ratio increased as the flexural strength in direction 1 decreased and similar relationships have been reported by others (Hendry, 1990, Mohammed, 2006). As was discussed in the literature review, it has been proposed that the strength in direction 2 could be due to a combination of the mortar bond strength in the perpendicular joints and a shear resistance to torsion in the bed joints (Curtin, 1986). It was suggested (Curtin, 1986) that the flexural strength in direction 2 ($f_{xd1}$) may be equivalent to the strength in direction 1 ($f_{xd1}$) plus a multiple of characteristic shear strength ($f_{vko}$). The multipliers suggested for the shear strength were 3.5 and 4.5, which provided the lower and upper bounds respectively, as shown by the dashed lines in Figure 5.9. A characteristic shear strength ($f_{vko}$) of 0.35 was given in the method (Curtin, 1986) and was similarly adopted here. The line of best fit for the experimental results falls below the lower bound of the proposed relationship. This was perhaps to be expected, since a torsion type failure was not generally observed in the specimens tested. The failure mode expected for a torsion type failure would be characterised by a toothed type pattern restricted to the mortar joints. For the bricks used in this study it was apparent that the limiting factor of the flexural strength

in direction 2 was related to the units' modulus of rupture, rather than the shear resistance in the bed joints.

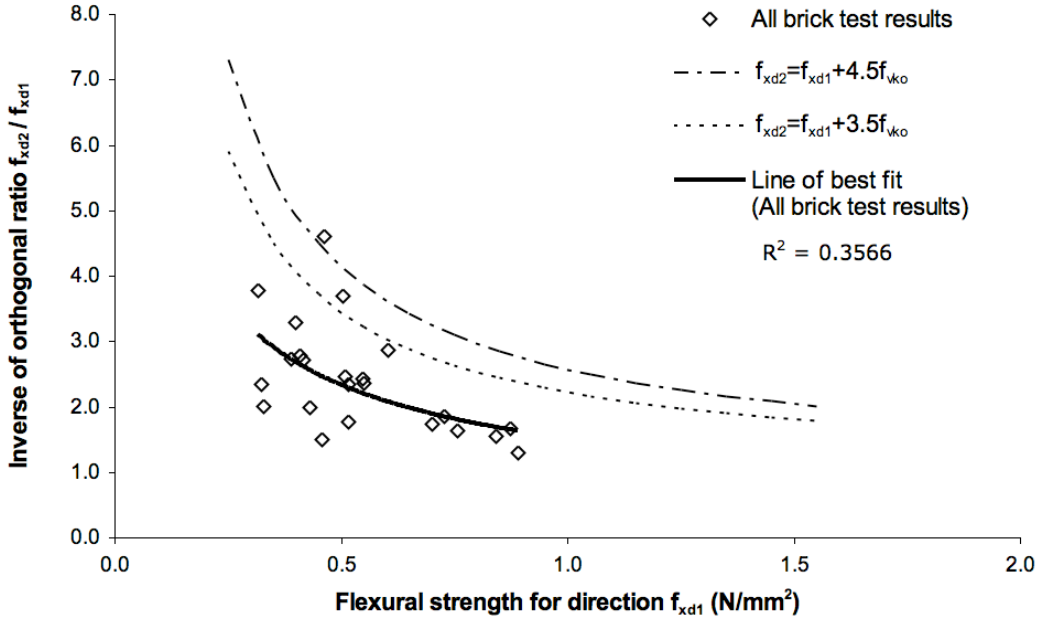


**Figure 5.9.** Variation in inverse of orthogonal ratio with direction 1 flexural strength for all brick specimens (Curtin, 1986)

### 5.1.4 Response of brick and block wallettes in flexure

The DIC system was employed during the test of specimen sets F3, 7, 9 and 12. Load-deflection curves were not directly comparable due to differences in size between direction 1 and 2 test specimens and the brick and block specimens, as previously given in Chapter 4 Section 4.6. The response was instead plotted as a stress-strain relationship, where the in-plane strain in the x or y direction, for test directions 2 and 1 respectively, were determined at the centre of the specimen over a 40 mm gauge length. The strains were computed using the Vic3D DIC software and the gauge length was selected such that it encompassed both part of the material and the mortar joint.

The typical stress x direction strain responses for brick specimens manufactured with M2 and M4 strength mortar, and AAC block specimens manufactured with M2 strength mortar are shown in Figure 5.10. The typical initial stress strain responses for the brick specimens were similar and approximately linear. The strains observed in the brick specimens were similar following the initial response, however the specimen manufactured with M4 mortar was able to sustain higher flexural stress than the specimen manufactured with M2 mortar before attaining an equivalent

strain. This suggests that there was limited difference between the strain capacity between the brick specimens, but the stiffness increased with mortar strength. The initial response of the AAC block specimen with filled perpendicular mortar joints was similar to that of the brick. The response that followed was of similar form to that of the brick specimen constructed with M2 strength mortar, but of lower stiffness and suggested that stiffness increased with the strength of the unit.

At higher stresses the response tended to become non-linear, as was also observed in previous tests of 1:3 scale brick specimens (Ng, 1996). Composite action of the material and mortar was likely occurring in the initial linear stage of the response, after which the difference in stiffness of the mortar and units resulted in non-linearity. The highest strains were found to be at the perpendicular joints prior to failure, as shown in Figure 5.11, suggesting that cracking initiated in these regions. Such cracking would reduce the strength of the assembly and impose higher stresses on the units leading to the failure mode observed.

The results do not seem to indicate that there was a torsion action occurring in the bed joint, particularly since failure was not apparent in the bed joints. The bricks and AAC blocks used in this study were of low compressive strength such that failure of this type would be dominant. Other researchers have completed tests of bricks of higher compressive strengths and found that failure tended to occur in the mortar joints only leading to a toothed type failure (Fried et al., 1986, West et al., 1977). This suggests that torsion-type behaviour will occur when the units can withstand the additional stresses imposed following the cracking of perpendicular joints. The initial response of AAC specimen F12 with no mortar in the perpendicular joints was of reduced stiffness to that of the specimen with filled joints, as shown in Figure 5.10. The response that followed was similar for both AAC block specimens and this suggests that cracking in the perpendicular joints may initiate at the end of the initial linear stage. The values of Young's Modulus, E, were calculated from the peak deflections and loads for the wallette specimens tested in direction 2 using a standard beam deflection formula for 4 point bending. The E values calculated for the AAC block, brick specimens manufactured with M2 strength mortar, and brick specimens manufactured with M4 strength mortar were 1036, 1237 and 1438 $N/mm^2$ respectively. The variation in the magnitude of the calculated E values between masonry material and mortar type supports the differences found in the flexural stress strain responses as observed in Figure 5.10.

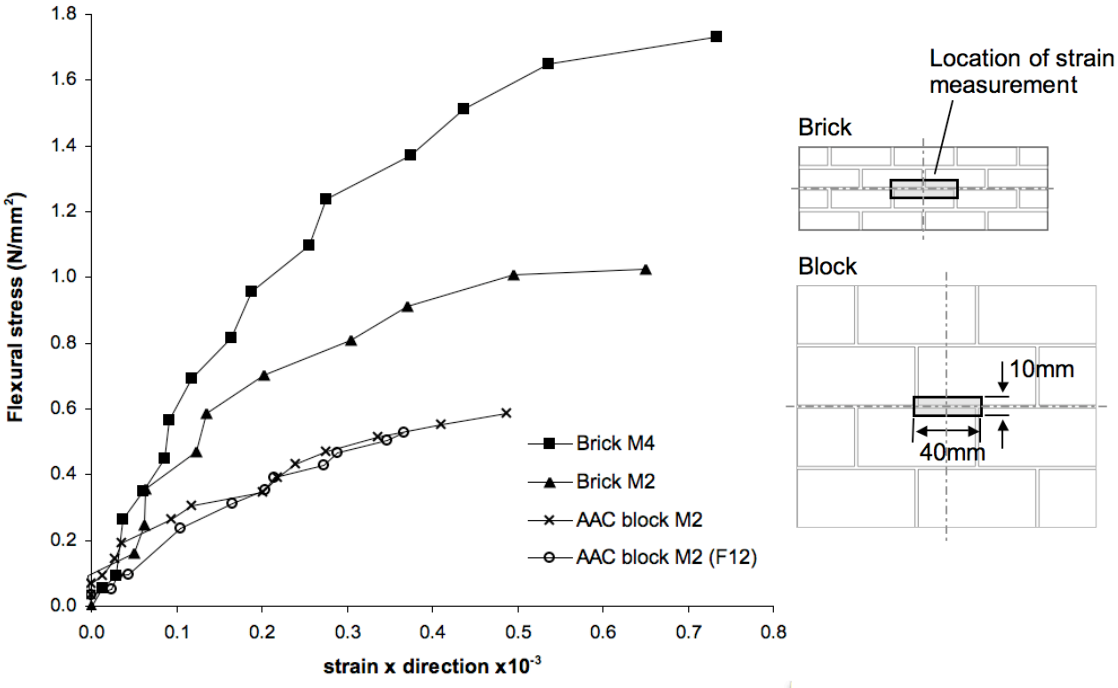


**Figure 5.10.** Stress x direction strain response for brick and block specimens tested in direction 2

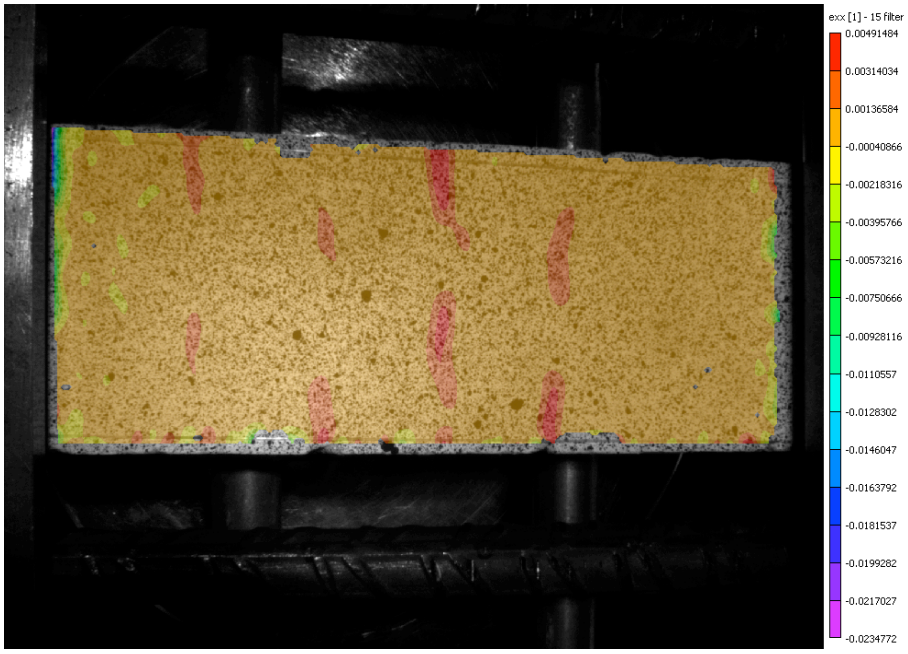


**Figure 5.11.** Contour plot of x direction strain for brick M4 mortar specimen tested in direction 2 at a stress of 1.72 N/mm$^2$ (just prior to failure)

Figure 5.12 provides the typical stress y direction strain responses for the brick wallettes with M2 and M4 strength class mortar and AAC block manufactured with M2 strength class mortar. The stress y direction strain response for all the specimens tested in direction 1 showed a higher degree of scatter and taking this into account

the stiffness was approximately the same regardless of material or mortar type. The form of the response was not clearly defined due to the scatter and it was difficult to ascertain if it was fully linear or if there was an initial linear stage followed by a reduction in stiffness. Higher strains were typically observed to be at the mortar joints prior to failure occurring, as shown in Figure 5.13, and it was likely that cracking initiated in the mortar, which was supported up by the similar failure modes recorded in all specimens. Softening type behaviour has been reported in the literature (Lourenco, 2000), although some have found a fully linear response followed by brittle failure (Ng, 1996). In the latter study a high strength M12 mortar was adopted that may have influenced the response observed. The E values calculated for the specimens tested in direction 1 were similar for the brick specimens constructed with M2 and M4 strength mortar, at 507 and 475 N/mm$^2$ respectively. The E value stiffness of the AAC block specimen was found to be higher, with an E value of 1036 N/mm$^2$. Stiffness orthotropy was found when comparing the E values calculated for the brick specimens in direction 1 and 2, whilst the AAC block was more isotropic in behaviour and was likely due to the similar strength of the units and mortar as discussed above. The magnitude of the E values calculated for both directions 1 and 2 were an order of 10 lower than those reported in the literature (Duarte, 1998, Ng, 1996), however these were determined for stronger M12 compressive strength mortar. The difference in the magnitude of the E values suggested that a more ductile response would be likely at 1:6 model scale.

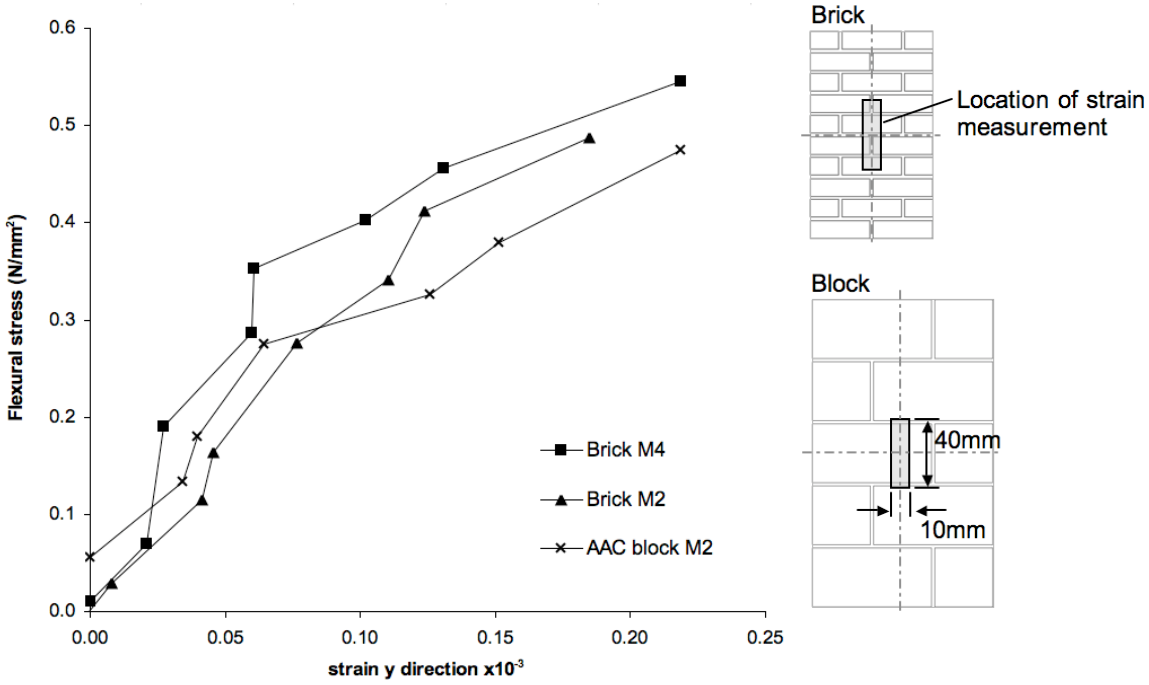


**Figure 5.12.** Stress y direction strain response for brick and block specimens tested in direction 1

Limitations were found when using the DIC system to monitor the out–of-plane behaviour of wallette specimens. Firstly the maximum sampling rate was limited to 0.5 sec, resulting in limited ability to capture post peak response. In some specimens post cracking strain softening was observed, although in no cases was a plastic type response seen. In many of the tests the specimens tended to fail very suddenly in a brittle type manner and even adopting a high speed DIC system may not provide any additional information. Secondly, scatter was found in the strain measurements at low values. Improved DIC software is emerging that would likely improve the results at low strains. Contact type measurement devices would not be ideal for such testing since they would likely be damaged at the point of specimen failure.

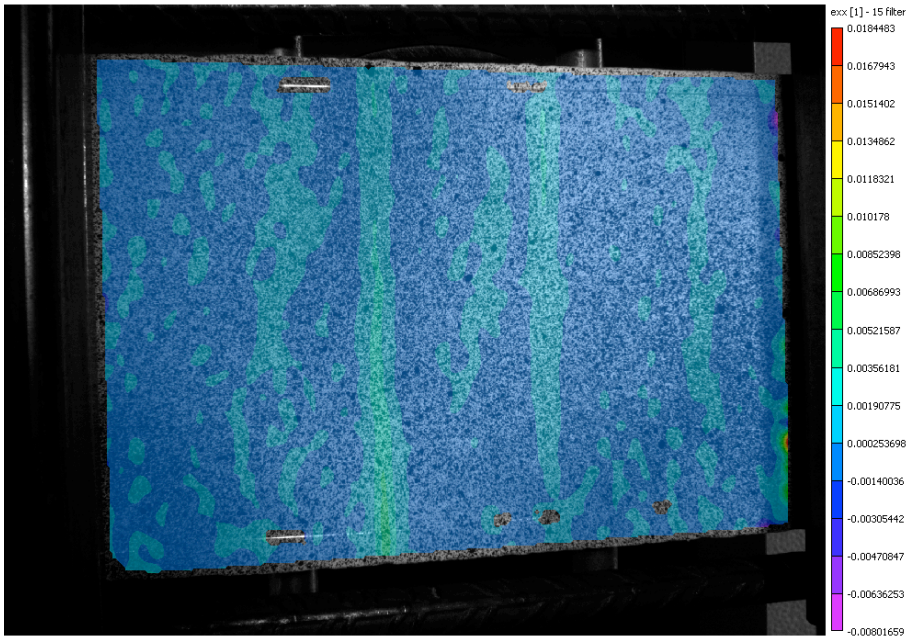


**Figure 5.13.** Contour plot of y direction strain for AAC block M2 mortar specimen tested in direction 1 at a stress of 0.47 N/mm$^2$ (just prior to failure)

### 5.2 Wall tie tests

#### 5.2.1 Compressive and tensile strength of wall ties

A summary of the average peak compressive and tensile loads for the prototype and model scale wall ties is presented in Table 5.4. Figure 5.14 shows the variation of the peak compressive and tensile loads with mortar compressive strength class and masonry material type for the wall tie couplet specimens manufactured at prototype scale. The failure modes observed for the prototype scale specimens tested in compression and tension are presented in Figures 5.15 to 5.17. Similar peak loads were observed for all prototype scale specimens tested in compression, regardless of mortar strength or masonry material type. This was due to similar failure modes

occurring in all prototype compressive specimens, characterised by buckling of the wall tie, as shown in Figure 5.15. The failure mode in compression was in agreement with those reported in the literature for similar wall ties (de Vekey and Reed, 1986). A slight increase in peak tensile load was observed for the AAC block specimens as the mortar strength increased from M2 to M4, as shown in Figure 5.14, although the standard error of the mean suggests that there was no significant difference between the results. The failure modes observed in the prototype scale AAC block specimens were identical and were a combination of splitting of the block and deformation of the end of the wall tie inside the mortar joint, as shown in Figures 5.16a and b respectively.

**Table 5.4.** Results of wall tie couplet tests at prototype and model scales

| Test number | Scale | Material / mortar type | Peak load compression test (N) | COV (%) | Peak load tensile test (N) | COV (%) |
|---|---|---|---|---|---|---|
| WTPT1 | 1 | AAC brick / M2 | 1242 | 9.92 | 1986 | 11.70 |
| WTPT2 | 1 | AAC brick / M4 | 1135 | 8.50 | 2106 | 5.15 |
| WTPT3 | 1 | Brick / M2 | 1159 | 5.16 | 2357 | 2.60 |
| WTPT4 | 1 | Brick / M4 | 1170 | 11.34 | 2778 | 4.48 |
| WTM1 | 1:6 | AAC brick / M2 | 71 (2545) | 21.80 | 71 (2543) | 11.79 |
| WTM2 | 1:6 | AAC brick / M4 | 94 (3380) | 15.66 | 87 (3117) | 14.18 |
| WTM3 | 1:6 | Brick / M2 | 133 (4787) | 12.67 | 131 (4729) | 20.30 |
| WTM4 | 1:6 | Brick / M4 | 150 (5388) | 10.93 | 182 (6564) | 22.68 |
| WTM5 | 1:6 | Brick bonded on | 108 (3876) | 10.01 | 6 (204) | 23.49 |

Note: the values in brackets are the equivalent prototype loads

Higher tensile strengths were recorded for the prototype scale brick specimens than the AAC block and they were found to increase with mortar strength, as shown in Figure 5.14. A slightly different failure mode was seen in the brick specimens, where a combination of deformation of the end of the tie occurred alongside stretching out of the drip section of the tie, as presented in Figure 5.17. As the tie deformed inside the mortar joint it also tended to result in cracking occurring along the mortar bed joint. The higher strength mortar likely provided greater resistance to deformation of the end of the tie and cracking along the mortar bed joint. In previous tests of similar wall ties in brick couplets, the tensile load capacity was also found to increase with mortar strength (de Vekey and Reed, 1986). A similar failure of the bond between the bricks was reported, but tie pull out also occurred. It was not noted if any stretching

out of the drip section occurred, however it only comprised of one drip rather than the multiple ones formed into the ties tested in this study.

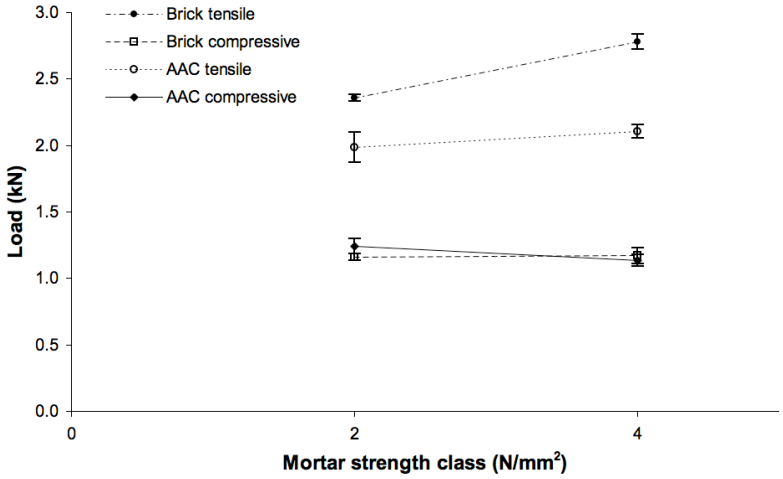


**Figure 5.14.** Variation of peak load with mortar strength class for prototype scale wall tie couplet specimens manufactured from different masonry materials (error bars shown are standard error of the mean)

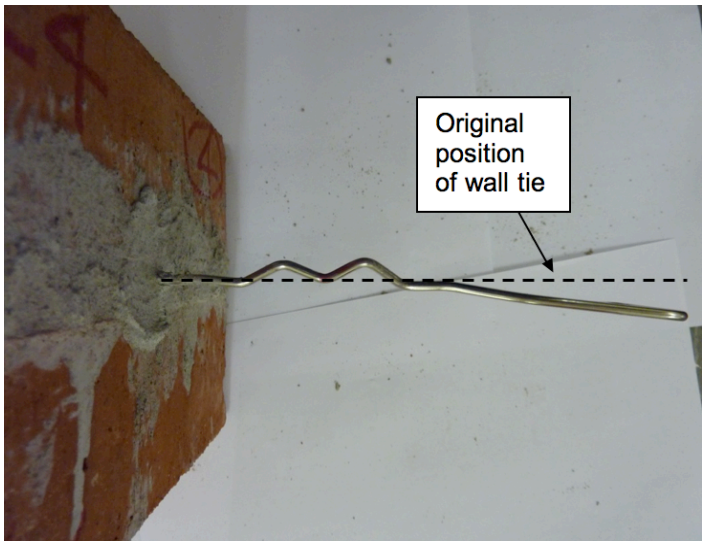


**Figure 5.15.** Failure mode in compression for prototype scale wall tie tests

For both types of material and mortar class, the tensile strength exceeded the compressive strength at prototype scale and was expected due to the differences in failure modes for the respective test directions. Characteristic strengths of 1300 and 1800 N in compression and tension respectively are given in the provisional British Standard for M2 class strength mortar (BSI, 1987). The characteristic strengths computed from the test values for both the brick and AAC block specimens constructed with M2 mortar were 1136 N in compression and 2032 N in tension. The

strength of the prototype scale wall ties exceeded the prescribed characteristic strength in tension, but did not meet the requirements in compression. However it should be noted that the ties were not directly specified as meeting the requirements of the provisional standard.

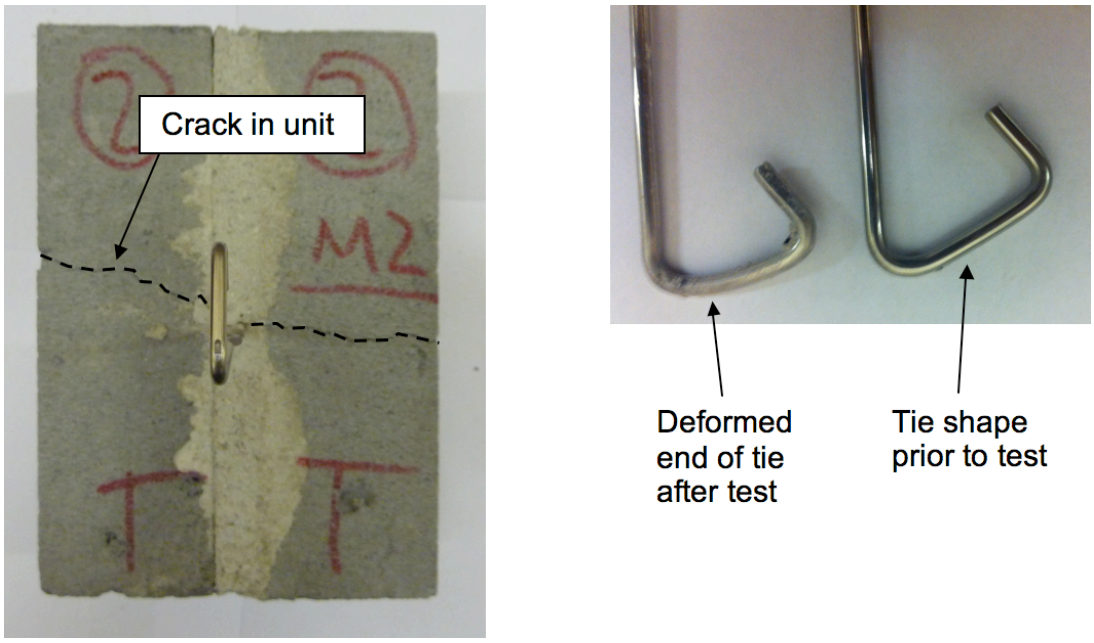


(a) (b)

**Figure 5.16.** Failure mode in tension for prototype scale AAC block showing (a) cracking in units and (b) deformation of tie end

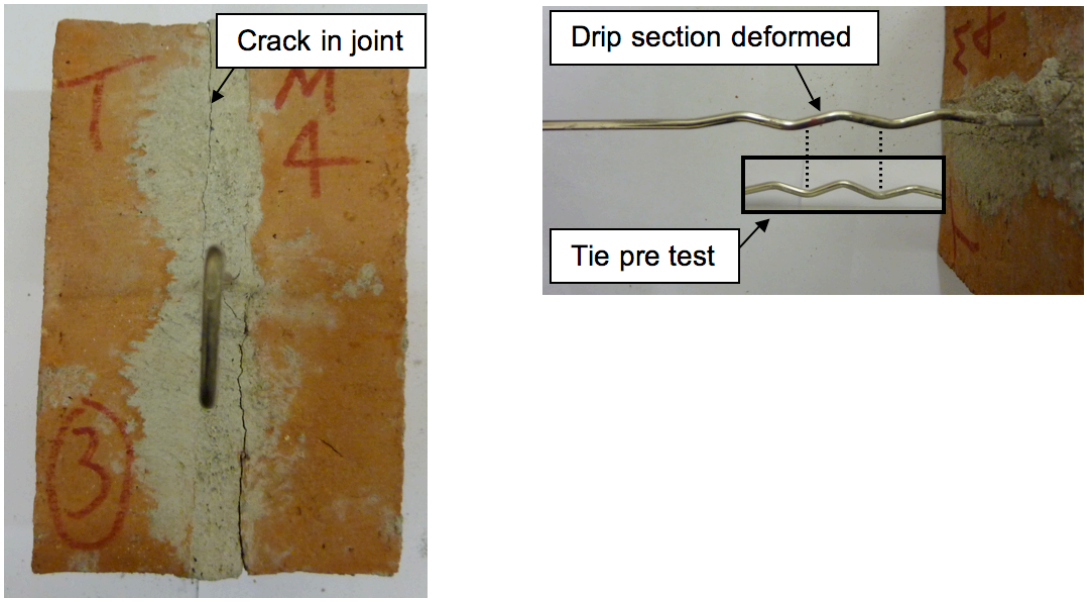


(a) (b)

**Figure 5.17.** Failure mode in tension for prototype scale brick showing (a) cracking in mortar bed joint and (b) deformation of drip section of tie

Figure 5.18 shows a comparison of the peak compressive load with different mortar strength classes for the model and prototype scale built-in wall tie couplet specimens. The failure modes found for the model scale wall ties tested in compression are presented in Figure 5.19. The compressive strength of the model scale wall ties exceeded that of the prototype when the scaling factor (of $6^2$) was applied to the results. Unlike at the prototype scale the peak load was affected by the compressive strength of the mortar. For the model AAC specimens this was likely due to the different failure mode observed compared to the prototype, where splitting of the couplet along the mortar joint tended to occur in the model scale specimen, as shown in Figure 5.19a, compared to buckling of the ties in the prototype, as presented in Figure 5.15. A higher bond strength would occur in the M4 mortar and therefore would be expected to increase the failure load for this particular mode, in the model scale specimens, as found.

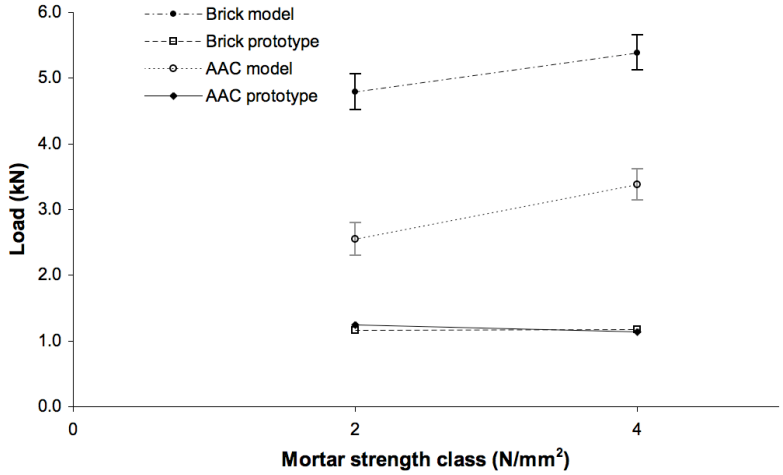


**Figure 5.18.** Variation of peak compressive load (scaled) with mortar strength class for model and prototype scale wall tie couplet specimens manufactured from different masonry materials (error bars shown are standard error of the mean)

The ties in the model scale brick specimens tended to buckle in compression, as shown in Figure 5.19b, in a similar manner to that observed in the prototype tests. The higher loads recorded in the model brick specimens compared to the prototype brick specimens could be explained by the absence of the drip section, and the nature of the wire used in the model ties, which would both contribute to a higher buckling load. It was not possible to replicate the drip section easily or accurately in the model scale ties so it was omitted. The wire used for the model scale wall ties was 35 % thicker than that of the theoretical 1:6 scale ties. The mortar strength effect shown in the model scale compressive specimens could be explained by the

stronger mortar resisting bending at the base of the tie. Any failure of the mortar near the base of the tie would allow the tie to rotate and likely initiate buckling at a lower load.

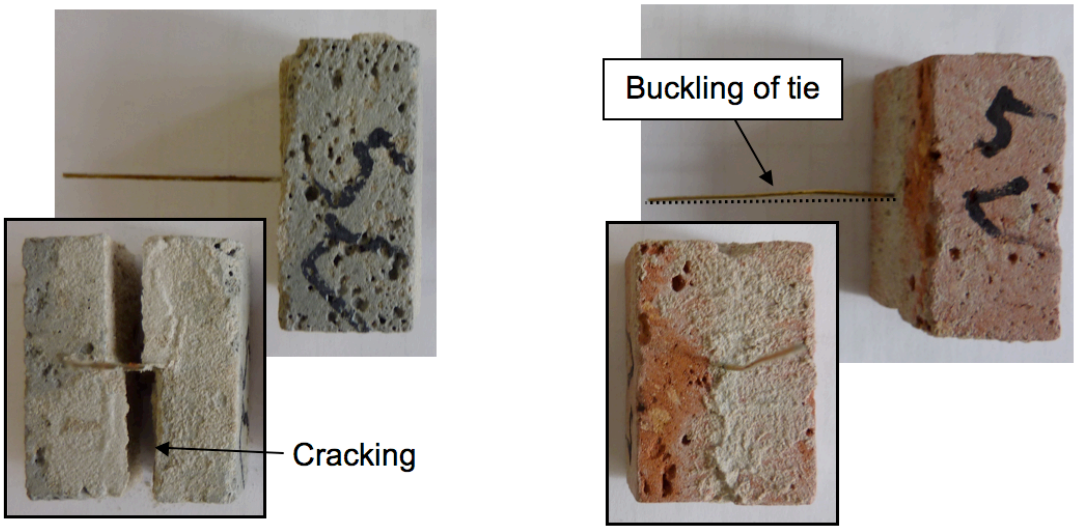


(a) (b)

**Figure 5.19.** Failure modes for model scale specimens in compression for (a) AAC block and (b) brick

A comparison of the peak tensile load sustained by the built-in model and prototype scale wall tie couplet specimens for mortars of different strengths is presented by Figure 5.20. The failure modes in tension observed for the model scale built-in ties are shown in Figure 5.21. It was observed that the tensile peak load for the model scale wall ties exceeded that found in the prototype tests, regardless of mortar strength. The peak tensile load of the model scale brick specimens was also affected by the mortar strength, where the stronger M4 strength mortar specimens sustained higher tensile loads. This could be explained by slightly different failure modes occurring in the model scale tests. The model scale AAC units similarly tended to split during test, but also failed along the mortar joint, as shown in Figure 5.21a. The model scale brick units tended to split completely along the mortar joint, rather than just crack, as presented in Figure 5.21b, which subsequently allowed the wall tie to pull out. No deformation of the model scale tie end was apparent when removed from the specimens after testing. The failure mode seemed to indicate that the model wall tie was stiffer and the response was governed more by the strength of the units and bond of the mortar.

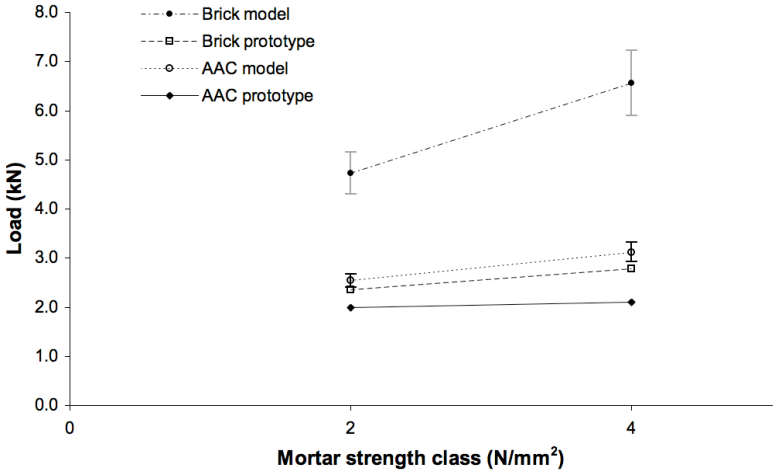


**Figure 5.20.** Variation of peak tensile load (scaled) with mortar strength class for model and prototype scale wall tie couplet specimens manufactured from different masonry materials (error bars shown are standard error of the mean)

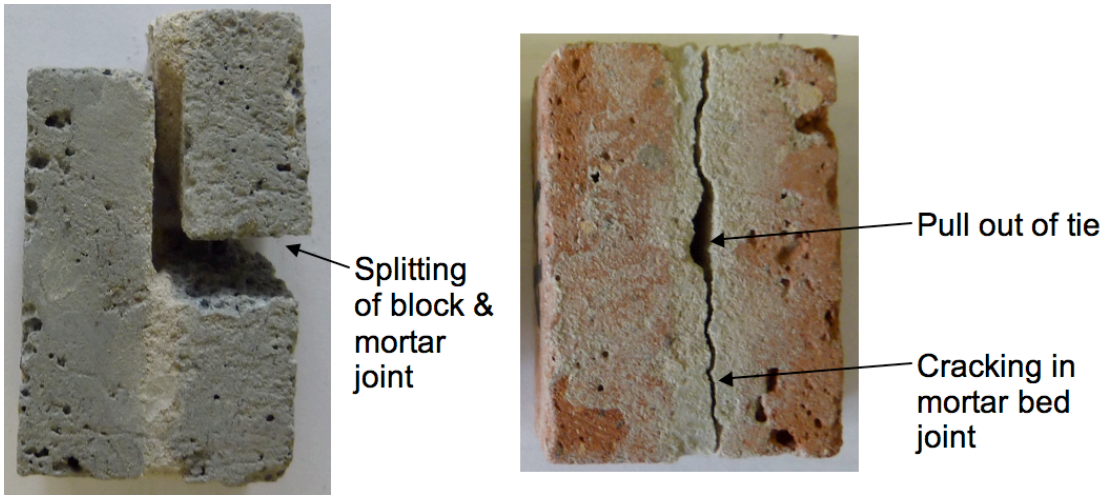


(a) (b)

**Figure 5.21.** Failure modes for model scale specimens in tension for (a) AAC block and (b) brick

The model scale wall tie that was bonded onto the brick, rather than embedded in the mortar joint, also exceeded the compressive strength of the prototype ties, as detailed in Table 5.4. The failure modes found for the bonded on wall tie when tested in compression and tension are shown in Figure 5.22. A similar failure mode of buckling in compression was observed for the wall ties bonded onto the brick to that of the model scale and prototype ties that were built into the mortar joint, but was followed by breaking away from the surface of the unit, as shown in Figure 5.22a. The failure load was lower than that found for the brick model scale built in ties and supports the statement made above that the mortar affected the load capacity for the

case of buckling. The bonded on ties did not perform in a very satisfactory manner in tension and failed at very low average load, as given in Table 5.4. It was difficult to achieve a good bond between the adhesive and the brick due to dust contamination, even after the application of a PVA primer to the surface prior to affixing the tie. Failure occurred between the primer and the surface of the brick, as shown in Figure 5.22b, rather than by failure of the adhesive used to affix the tie, suggesting a poor bond was formed.

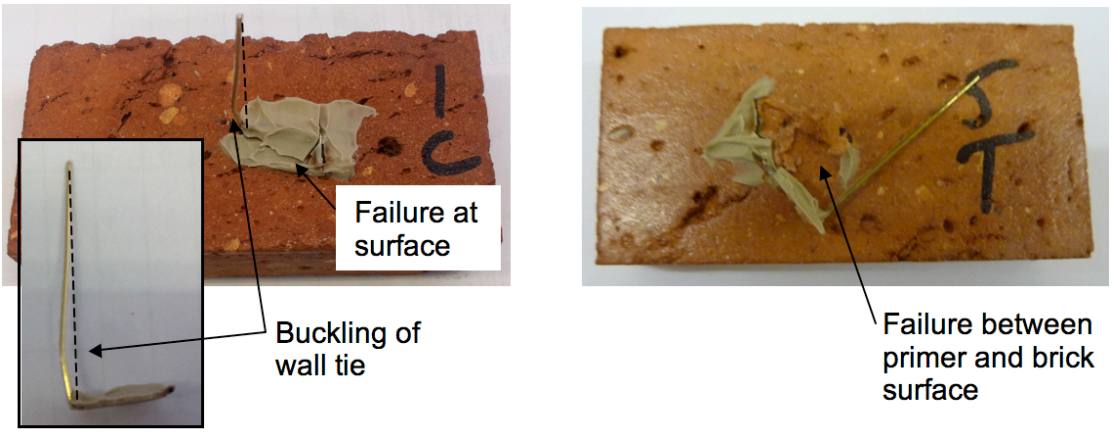


**Figure 5.22.** Failure modes of bonded on model scale wall ties in (a) compression and (b) tension

### 5.2.2 Load-deflection response of wall ties

Figure 5.23 shows the typical load z deflection responses for model and prototype scale wall ties tested in compression, where the couplets were manufactured with M2 compressive strength class mortar. The responses for the specimens manufactured with M4 mortar were similar and are therefore not presented here. The model scale wall ties were stiffer than the prototype tie in compression, and was likely due to the absence of the drip section and thicker wire used in the model ties as discussed previously. The bonded on wall ties were of a slightly lower stiffness than the built in model ties in compression and was likely due to a reduced restraint at the base of the tie due to the absence of mortar. The initial response of the bonded on ties was more comparable to that of the prototype scale built in ties. This suggests that the bonded on ties would perform in a comparable manner in compression when utilised in a model scale cavity wall assembly within the scaled range of working loads for the prototype ties. Guidance states that the load carried by each leaf in a cavity wall assembly may be a proportion of the total load when the wall ties are capable of transferring such loads (BSI, 2005c). To allow verification of this guidance it would be

beneficial if the wall ties did not buckle when incorporated in cavity wall assemblies and clearly the bonded on ties would satisfy this requirement.

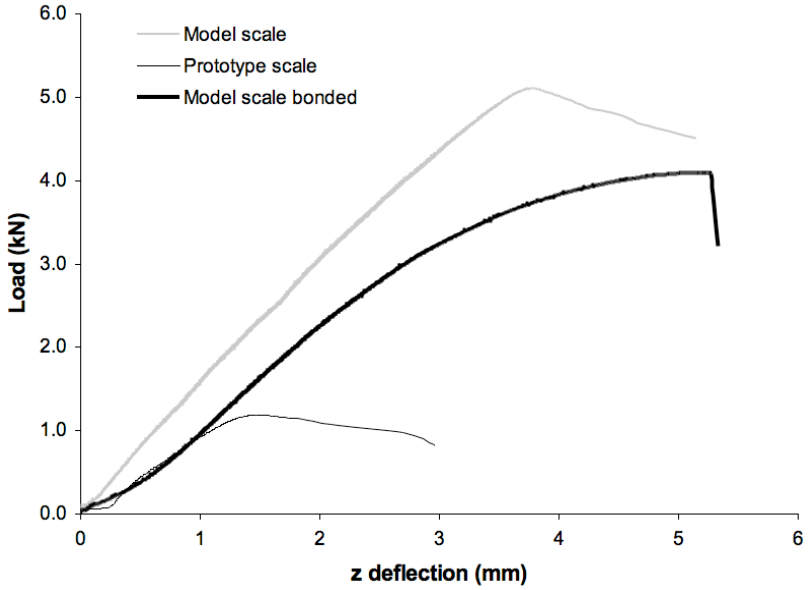


**Figure 5.23.** Load z deflection response for model and prototype scale wall ties tested in compression (M2 strength class mortar, model tie response scaled)

The typical load z deflection responses for the model and prototype scale wall ties tested in tension are presented in Figure 5.24. The responses shown are for couplets manufactured with M2 compressive strength class mortar and the responses for the M4 strength mortar were found to be similar. The built-in model scale wall ties were much stiffer in tension than either the prototype or bonded on model scale ties. The absence of the drip section and the thicker wire utilised in the model scale ties likely resulted in a difference in the response observed. The levels of deflection observed in the built-in model ties suggest that there was some deformation occurring either in the mortar or of the tie end prior to failure. The long non-linear section of the prototype scale tie response accounted for the deformation of the tie end and the extension of the drip section. The prototype tests were allowed to run past the maximum allowed deflection of 5 mm and were then manually stopped, which accounts for the drop in load at the end of the response. As was discussed above, the bonded on model scale tie did not perform well in tension and this was reflected in the response. Clearly the bonded on ties would perform a very limited function in tension, however since the wall panels were tested in compression this was not anticipated as being a concern. If a suction force were to be applied to the panel then

it would be necessary to build in the wall ties or investigate a more suitable primer or fixing solution.

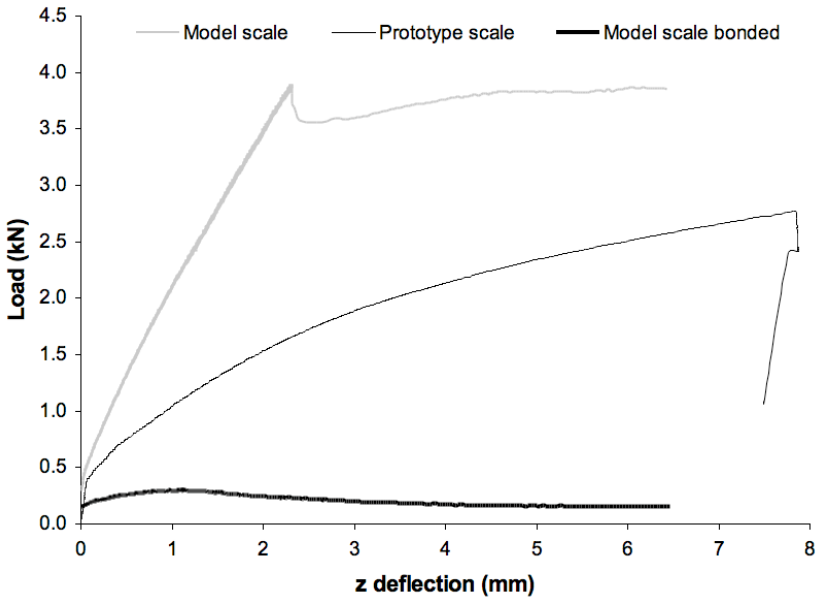


**Figure 5.24.** Load z deflection response for model and prototype scale wall ties tested in tension (M2 strength class mortar, model tie response scaled)

### 5.2.3 Comparison of model and prototype scale mortar strength

During the preparation of the wall tie couplet specimens both model and prototype mortars were mixed, which allowed comparison of their compressive strengths. In addition 100 mm cubes were cast alongside the 25 mm cubes for the prototype mortar in order to investigate any possible size effect in the mortar cube. The results of the compressive strength tests on the model and prototype mortars are given in Table 5.5.

The compressive strengths of the prototype scale mortars were found to be higher than the equivalent model scale mortars when 25 mm cubes were adopted. The model scale mortars however showed a much better relationship to the ideal prescribed compressive strength as given by the M number. The aggregate used for the model scale mortar was scaled, as discussed in Chapter 4, and was therefore significantly finer than that used in the prototype. In addition the aggregate for the prototype scale mortar was graded from 0-4mm sand, which resulted in a slightly higher proportion of coarse particles that were particularly evident when working the mortar during bricklaying. Variations in the compressive strength of the model and prototype scale mortars were therefore likely due to the differences in the gradings of

the aggregates. Similar results have been reported by others in the literature, where comparisons were made of mortars that utilised aggregates of different gradings (Anderson and Held, 1986). The results of 100 mm cube tests for the prototype scale mortars were lower than those recorded for the 25 mm cubes. It has been reported in the literature that the size of the cube adopted had no significant effect on the compressive strength for identical mortars (Hendry and Murthy, 1965). The variation in the strength of the 25 and 100 mm cubes was likely due to the latter being carried out in a manually operated test machine using a load, rather than displacement controlled rate.

**Table 5.5.** Mortar cube compressive strengths for wall tie tests

| **Mortar scale** | **Mortar strength class** | **Compressive strength (N/mm$^2$)** | |
|---|---|---|---|
| | | **25mm cube** | **100mm cube** |
| 1 | M2 | 4.99 (1.73) | 2.87 (1.92) |
| 1 | M4 | 8.14 (4.53) | 7.24 (0.10) |
| 1:6 | M2 | 2.11 (1.23) | - |
| 1:6 | M4 | 4.16 (3.15) | - |

Note values in brackets are COV (%)

### 5.3 Conclusions

The variation in the results of the wallette specimens was within the range previously reported in the literature. In addition similar failure modes were observed between specimens in each group. The manufacturing process employed therefore provided a good degree of repeatability in the results.

The general trend observed in the tests of brick wallette specimens tested in both directions 1 and 2 was of increased flexural strength as the compressive strength class of the mortar increased from M2 to M4. Similar failure modes, of cracking through the unit and mortar joints, were generally observed in the tests of brick specimens tested in direction 2. The failure mode of all brick specimens tested in direction 1 was characterised by cracking along a mortar bed joint near to the centre of the specimen. Pre-loading the brick wallettes during curing provided a 42% increase in the strength in direction 1 and the increase in strength could be due to the constituents of the mortar being forced closer together, resulting in a stronger bond, or excess water being forced out of the mortar mixture, effectively reducing the water to cement ratio. The average strengths of the brick specimens were not

always in line with the adjusted to average EC6 values and underlined the importance of using appropriate values where possible.

Brick block wallettes were stronger than the brick equivalents when tested in direction 2 and was possibly due to a size effect with respect to internal flaws since a different failure mode was observed. The flexural strength of AAC block wallettes tested in direction 2 were lower than either the brick or brick block specimens. Leaving the perpendicular mortar joints unfilled in the AAC block specimens had the effect of reducing the strength by 25% in direction 2 and revealed the contribution that the joints provided to the strength of the composite. Comparable flexural strengths were found for all blockwork specimens tested in direction 1 and was expected due to the similar failure modes observed. The average flexural strengths of the block wallettes were not always in agreement with the adjusted to average EC6 values. When brick blocks were utilised in wall panels they would likely be comparable to the response of concrete block in direction 2, but stronger in direction 1 and provide an upper bound for the results.

The stiffness of the brick wallettes tested in direction 2 was found to increase as mortar strength increased from M2 to M4 compressive strength class. The AAC block specimen initially behaved in a similar manner to the brick in direction 2, but was followed by a response of lower stiffness indicating that the stiffness increased as the unit strength became greater. The response in direction 2 comprised an initial linear behaviour followed by non-linearity and it was likely that the latter was due to cracking in the mortar joints. A greater degree of scatter was found in the response of the wallettes tested in direction 1 and the results suggested that the stiffness was similar regardless of unit or mortar type Post peak behaviour was difficult to capture, although strain softening was observed in some specimens.

The built-in model scale wall ties were stronger and stiffer in both compression and tension when compared to the prototype. Differences in peak loads were attributed to the comparatively thicker wire used and the absence of the formed in drip section in the centre of the tie. The characteristic strength of the prototype ties in compression fell short of the value prescribed in the provisional standard. Bonded on model scale wall ties performed well in compression tests and provided a similar load-deflection response to the prototype at lower values of load. Poor results were given in tests of the bonded on tie in tension due to failure of the bond between the primer and the brick surface. The bonded on wall ties would be representative of prototype ties

within their range of working loads, but would only be suitable for tests of cavity wall panels subject to compressive loadings only.

The strength of the model scale mortar was in line with the prescribed value as given by EC6. The compressive strength of the prototype scale mortar was higher than that of the model scale and was likely due to the different gradings of aggregates used in the mixtures.

The flexural strengths of the masonry specimens found by experimentation that were presented in this Chapter will be used within the analysis that was described in Chapter 3. The data will enable the analytical lateral strength of the wall panels, as described in Chapter 4, to be assessed and this is presented and discussed in Chapter 8.

# Chapter 6 Results of uniform (wind) lateral loading tests

This Chapter presents the results from the uniform (wind) loading tests completed on masonry wall panels in the centrifuge. A summary of the results of all the tests completed is presented in Table 6.1. Load at initial cracking was defined as the load at which any cracking was first evident as captured by the DIC analysis. The position and load at which any cracks developed could be identified earlier using DIC analysis than by visual means alone. It was expected that cracking in the horizontal direction would precede failure due to the orthogonal nature of the masonry, as was found in the tests of wallettes discussed in Chapter 5.

The average compressive strength of the M2 compressive strength mortar cubes for all wall panel tests was 2.99 N/mm$^2$ with a COV of 17.3 %, whilst for all the M4 compressive strength cubes was 7.61 N/mm$^2$ with a COV of 17.3 %. The COV values, based on the mortar cube compressive strengths for all tests, were similar and indicated that the variability was not influenced by mortar compressive strength. The average mortar cube compressive strengths from all tests exceed the prescribed strengths given by the national annex to BS EN 1996-1-1 (BSI, 2005d). The average compressive strengths of the mortar cubes for the corresponding wall panels, as given in Table 6.1, showed some variation between tests. It was not possible to use the same batch of cement throughout the study due to the length of the experimental programme. Variation in mortar cube strength was attributed to the different batches of cement used in the study, and considering this the COV values were deemed acceptable. It was not clear why the strength of the individual mortar cubes varied within each test, particularly since the same manufacturing process was utilised. Further analysis and discussion of the results for the wall panel tests is presented in the following sections in this Chapter. The discussion has been arranged according to whether the units were laid with or without cement mortar.

### 6.1 Block units laid dry or with sand mortar

To examine the load capacity of a wall panel with zero tensile strength two wall panels were constructed, the first comprising dry laid blocks (W1) and the second assembled from blocks laid with a sand mortar (W2). The load z deflection responses for specimens W1 and W2 are shown in Figure 6.1. The variation of z deflections with height, along a vertical centre line, and length, along a horizontal line 40 mm below the centre line, for specimens W1 and W2 at different loads are presented in Figures 6.2 and 6.3 respectively. Figures 6.4 and 6.5 present the contour plots of the

y deflections for specimens W1 and W2 respectively. From the load z deflection response it was evident that both the specimens initially responded linearly up to loads of 0.12 and 0.13 kN/m$^2$ for W1 and W2 respectively. During this linear stage the panels tended to deflect into the form of a smooth curve, as presented in Figure 6.2. The stiffness of the response then reduced and it was evident that hinges were forming in the vertical cross section of z deflections, as apparent in Figure 6.2. Specimen W1 appeared to form multiple hinges in the central section as well as hinging about the upper and lower supports. A single central hinge was formed in specimen W2 in addition to hinging occurring about the upper and lower horizontal supports.

**Table 6.1.** Summary of results from uniform loading tests

| Specimen reference | Masonry / mortar type | Additional description | Load (kN/m$^2$) | | Mortar cube | |
|---|---|---|---|---|---|---|
| | | | Initial cracking | Ultimate | Compressive strength (N/mm$^2$) | COV (%) |
| W1 | AAC block / N/A | Dry laid blocks | N/A | 0.47[1] | N/A | N/A |
| W2 | AAC block / N/A | Sand mortar | N/A | 0.24[1] | N/A | N/A |
| W3 | AAC block / M2 | | 1.57 | 2.09 | 2.39 | 10.4 |
| W4 | AAC block / M2 | | 1.45 | 1.59 | 2.57 | 13.1 |
| W5 | AAC block / M2 | 2 storey axial load | 2.07 | 2.37 | 2.86 | 9.1 |
| W6 | Brick block / M2 | | 2.78 | 4.87 | 2.43 | 15.0 |
| W7 | Brick block / M2 | | 2.40 | 5.12 | 2.86 | 12.1 |
| W8 | Brick block / M2 | | 1.61 | 4.48 | 2.71 | 15.2 |
| W9 | Brick / M2 | | 1.43 | 2.72 | 3.07 | 14.1 |
| W10 | Brick / M2 | | 2.23 | 2.86 | 3.52 | 10.3 |
| W11 | Brick / M2 | | 2.34 | 2.94 | 3.23 | 4.0 |
| W12 | Brick / M4 | | 3.84 | 4.59 | 6.31 | 8.8 |
| W13 | Brick / M4 | | 3.23 | 4.70 | 7.48 | 9.2 |
| W14 | Brick / M4 | Central opening | 3.09 | 4.62 | 9.04 | 8.8 |
| W15 | Brick outer & AAC block inner / M2 | Cavity wall – inner leaf axially loaded | 2.82 | 3.41 | 3.59 | 3.3 |

[1] Maximum load recorded before failure started to initiate

Note: all specimens axially loaded with the equivalent of 1 additional storey of masonry unless stated otherwise.

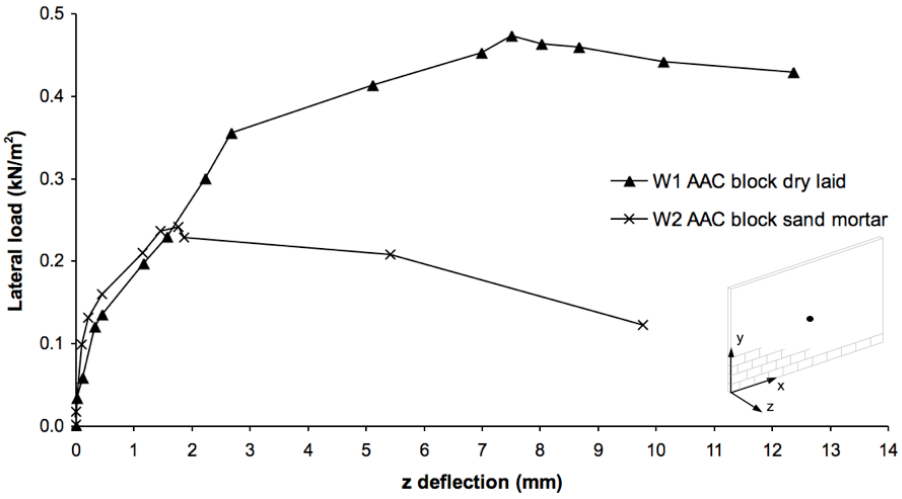


**Figure 6.1.** Load z deflection response for uniformly loaded AAC block specimens W1 and W2

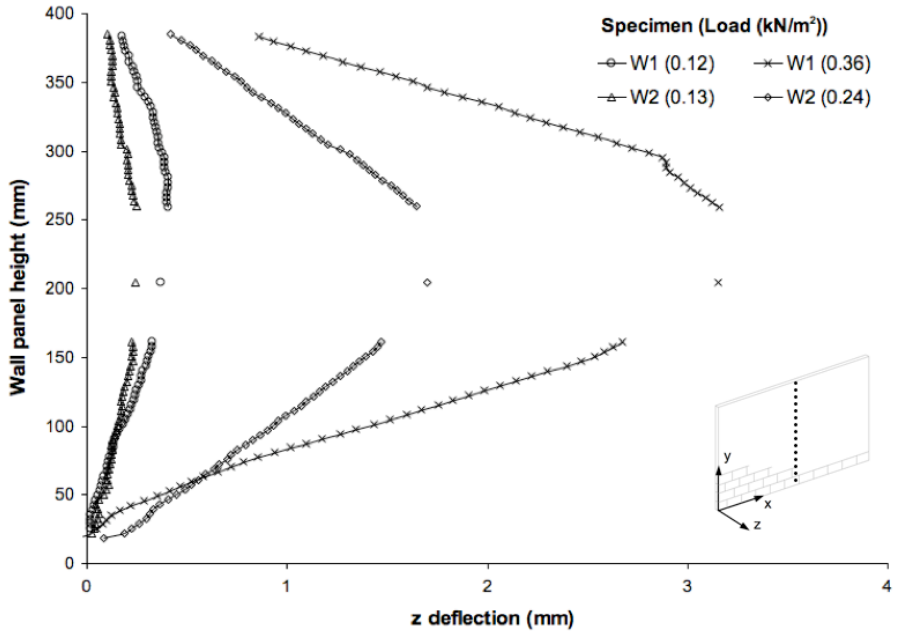


**Figure 6.2.** Wall panel height versus z deflection along vertical centre line for uniformly loaded AAC block specimens W1 (no mortar) and W2 (sand mortar) at different loads (Note: data near centre of specimen partially obscured by LVDT)

Specimen W1 showed a further reduction in stiffness and after reaching the ultimate load deflected at an approximately constant load. Panel W1 tended to form more of a curved shape in the horizontal section compared to W2, as shown in Figure 6.3, and a yield line mechanism was not apparent in the contour plot, as presented in Figure 6.4. The result suggested that the individual blocks were sliding, hinging and rotating, rather than forming distinct sub-sections in the panel as would be expected in a yield

line type failure. The deflections in the W1 panel were large prior to failure and it was anticipated that instability would have occurred before reaching such significant values. It was likely that the imposed loading and unit self-weight was therefore contributing to both frictional and overturning resistance.

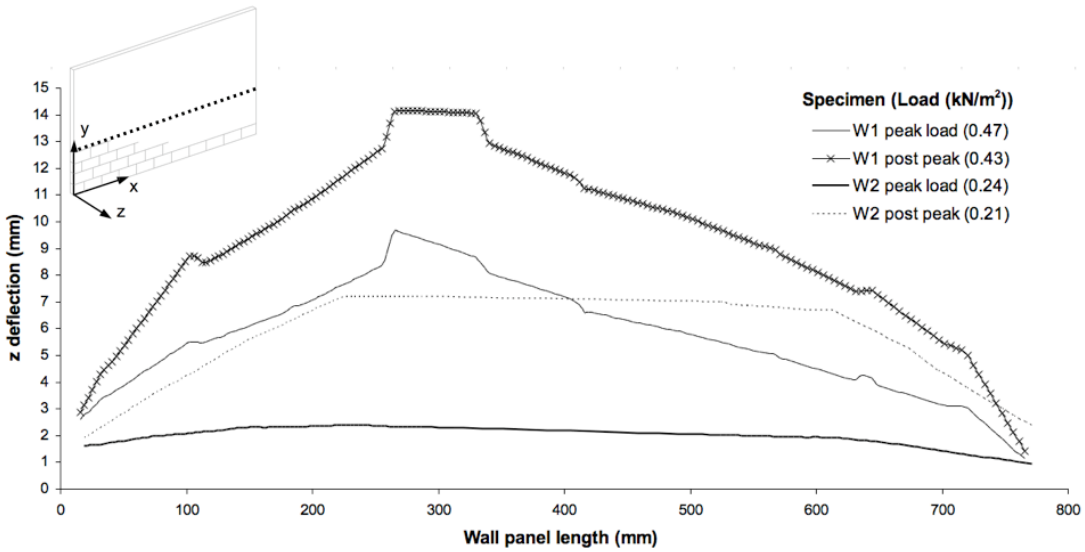


**Figure 6.3.** Z deflection versus wall panel length along horizontal line 40mm below the centre line for uniformly loaded AAC block specimens W1 (no mortar) and W2 (sand mortar) at different loads

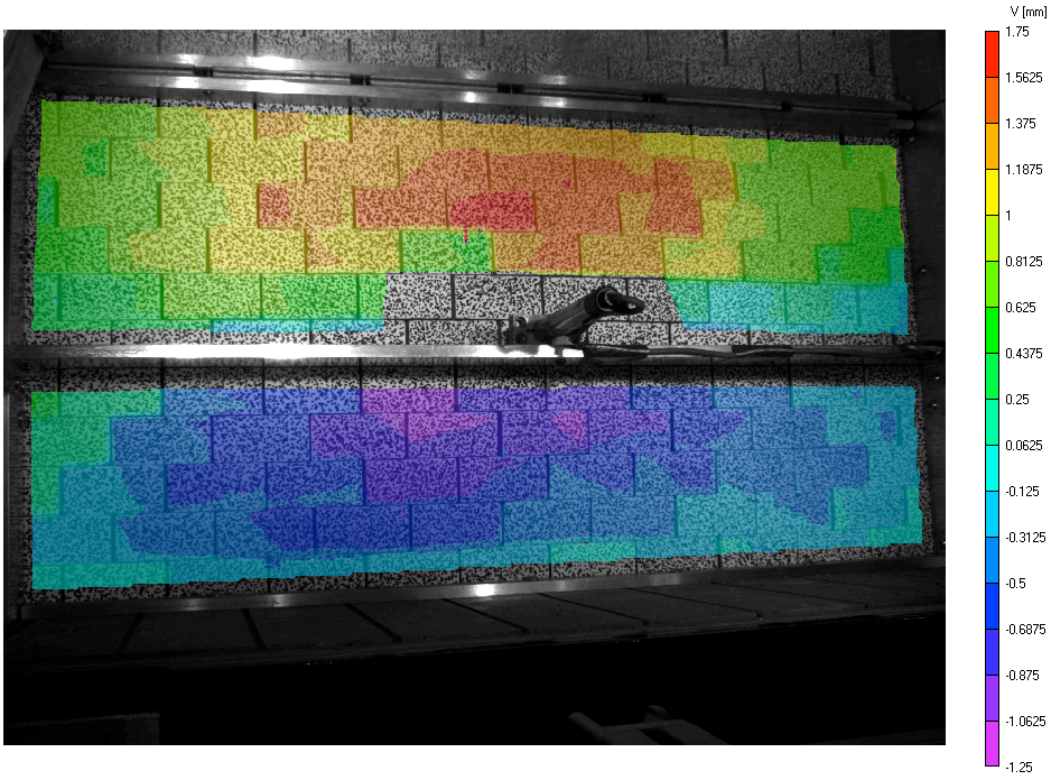


**Figure 6.4.** Contour plot of y deflections for AAC block specimen W1 (no mortar) at a load of 0.43 kN/m$^2$

After specimen W2 attained its ultimate load it continued to deflect, although the load tended to decrease rather than remain constant. At large deflections the volume of the air bag increased, as a result of the bag expanding to fill the void left by the moving wall, and it was found difficult to keep the load constant at such low values with the manual regulator initially used. On examination of the behaviour post peak it was apparent that a yield line mechanism developed, as shown in Figure 6.5. It was clear in the plot of displacements in the horizontal direction that the two side sections were rotating about the vertical supports, as apparent in Figure 6.3. The sand mortar, even with effectively zero tensile strength, tended to provide some resistance between the units such that they displaced as sub sections of the main panel. A small amount of water was applied to the sand after application to the masonry units to maintain its position, which may have resulted in suction between the units and sand resulting in the behaviour observed. Rotation, sliding and hinging only occurred along the yield lines rather than between individual units in specimen W2.

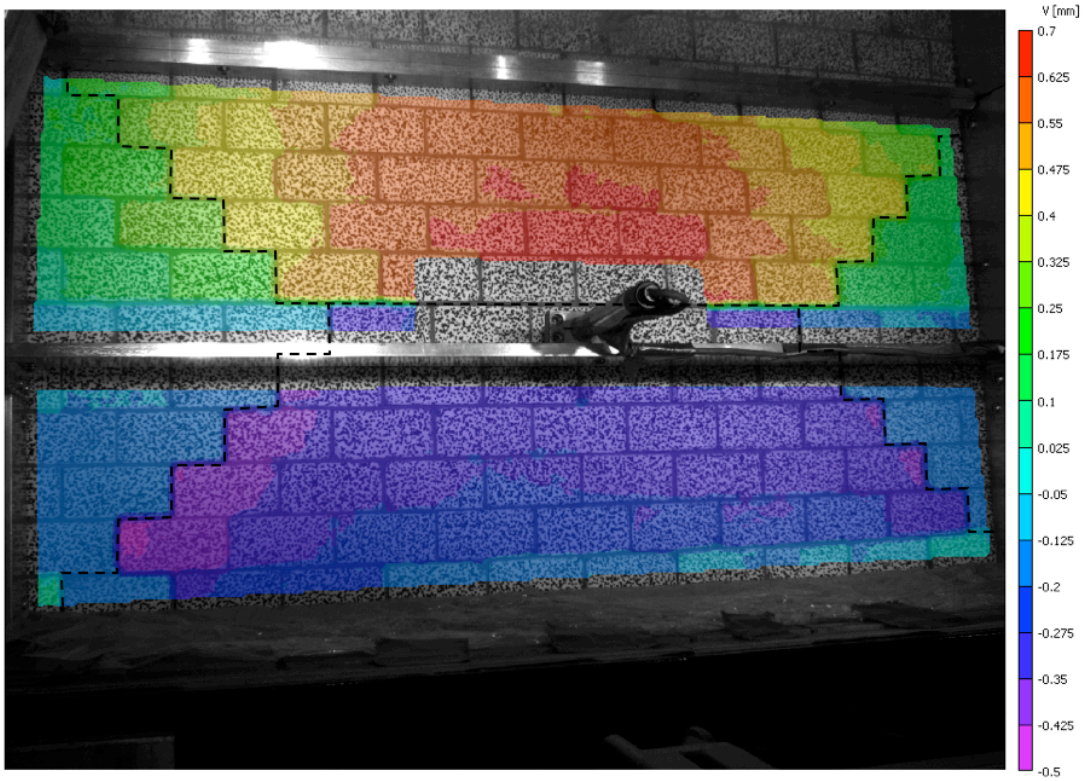


**Figure 6.5.** Contour plot of y deflections for AAC block specimen W2 (sand mortar) at a post peak load of 0.21 kN/m$^2$ (dashed line illustrates position of yield line pattern)

The differences in the ultimate load between specimens W1 and W2 was likely due to the different failure mechanisms occurring in each specimen. It was possible that the friction was lower between the units when sand was utilised, which subsequently

required a lower level of applied force to fail. Tolerances in the units from the cutting process resulted in some of the blocks not sitting perfectly square on their neighbours. This may have resulted in higher normal stresses being imposed on some units, or a section of the unit, than others and caused higher localised friction. The difference in localised friction at the block interfaces may have affected the failure mode observed. Other researchers have also reported that yield line patterns can be formed in dry assembled block walls when subject to uniform loading (Casapulla, 2008). Since it was found to be difficult to lay the units dry due to the tolerances achievable, further testing was not carried out with different materials.

## 6.2 Wall panels with cement mortar

### 6.2.1 Block specimens

#### 6.2.1.1 Failure mode and load deflection response

The failure modes observed for all the blocks specimens tested that were manufactured with cement mortar are shown in Figure 6.6. The typical variation of z deflections with height along a vertical centre line for the block specimens are presented in Figure 6.7, whilst Figure 6.8 shows a typical contour plot of z deflections at ultimate load. It was observed that the block specimens all tended to initially crack horizontally at or just above the centre of the panel. This behaviour was similar to that observed with the panel constructed with sand mortar and hinging was observed in a vertical section, as indicated in Figure 6.7. The cracking observed at ultimate load for the AAC block specimens differed to that for the brick block specimens. In the latter, cracks tended to be restricted to the mortar joints (specimens W6 to W8), although some cracking was evident in the units in specimen W7 possibly due to weaknesses in individual blocks. In the AAC block panels (specimens W3 to W5), cracks tended to pass straight through the units in a similar manner as was found in the tests of wallettes in direction 2 as discussed in Chapter 5 Section 5.1.2.

At the ultimate load the sections of the panels adjacent to the supports pivoted about the supports and negative deflection towards the load was observed at the corners, as evident in Figure 6.8. This behaviour occurred due to a number of reasons, firstly a lack of full restraint at the panel edges allowing the corners to pivot towards the direction of the load, secondly cracking at the edges occurring away from the corners, and finally the presence of the initial horizontal crack at mid-height that allowed rotation to occur between the upper and lower sections. For specimen W5, the imposed vertical axial loading was doubled, but did not appear to have any influence on the crack pattern at failure.

In previous tests of AAC blockwork reported in the literature (de Vekey et al., 1986) a panel of similar length to those in this study exhibited a different failure mode, where diagonal cracks formed into the corners of the specimen. A comparable failure mode to those observed in specimens W3 and W4 was however recorded (de Vekey et al., 1986) for a panel of nearly twice the length. Partial restraints were used in the previous study (de Vekey et al., 1986) at the vertical edges, which may have accounted for the differences in the crack patterns and explain why the longer panel failed in a similar mode to those observed here. No comparative results were found in the literature for stronger concrete block wall panels that were supported on all edges, however specimens that were tested with the top edge free tended to fail along the mortar joints rather than vertically through the units (Anderson, 1976).

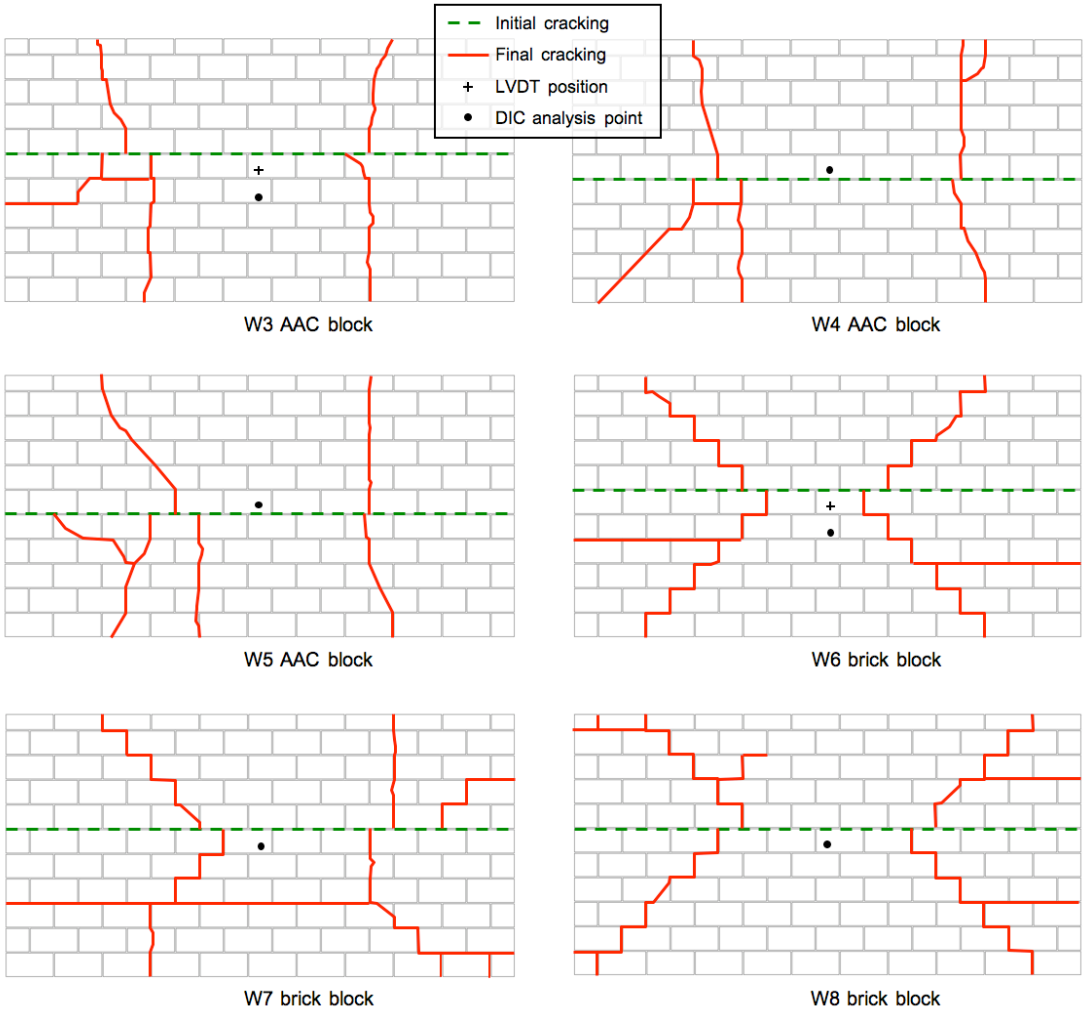


**Figure 6.6.** Failure modes observed for uniformly loaded block specimens (all constructed with M2 compressive strength class mortar)

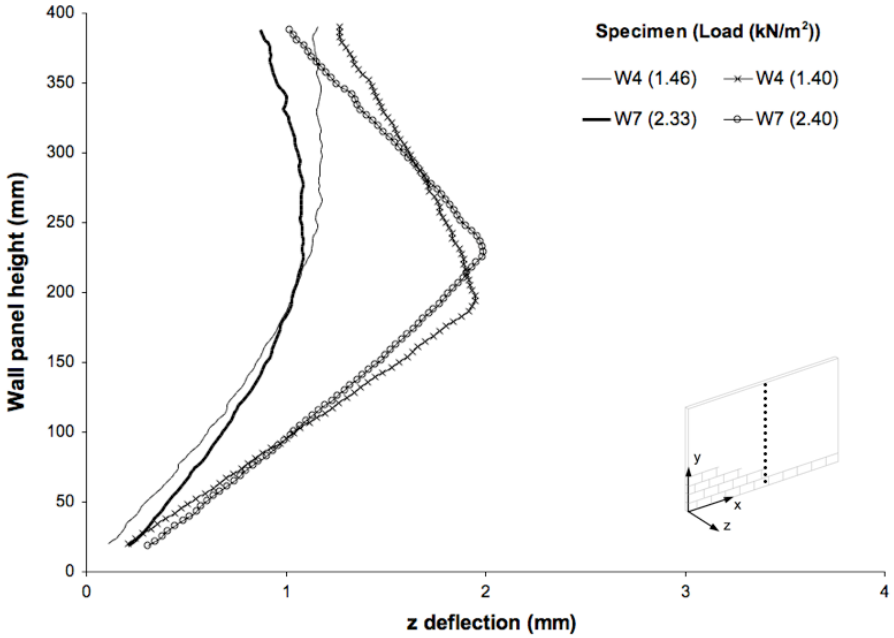


**Figure 6.7.** Wall panel height versus z deflection along vertical centre line for uniformly loaded AAC block (W4) and brick block (W7) specimens at different loads

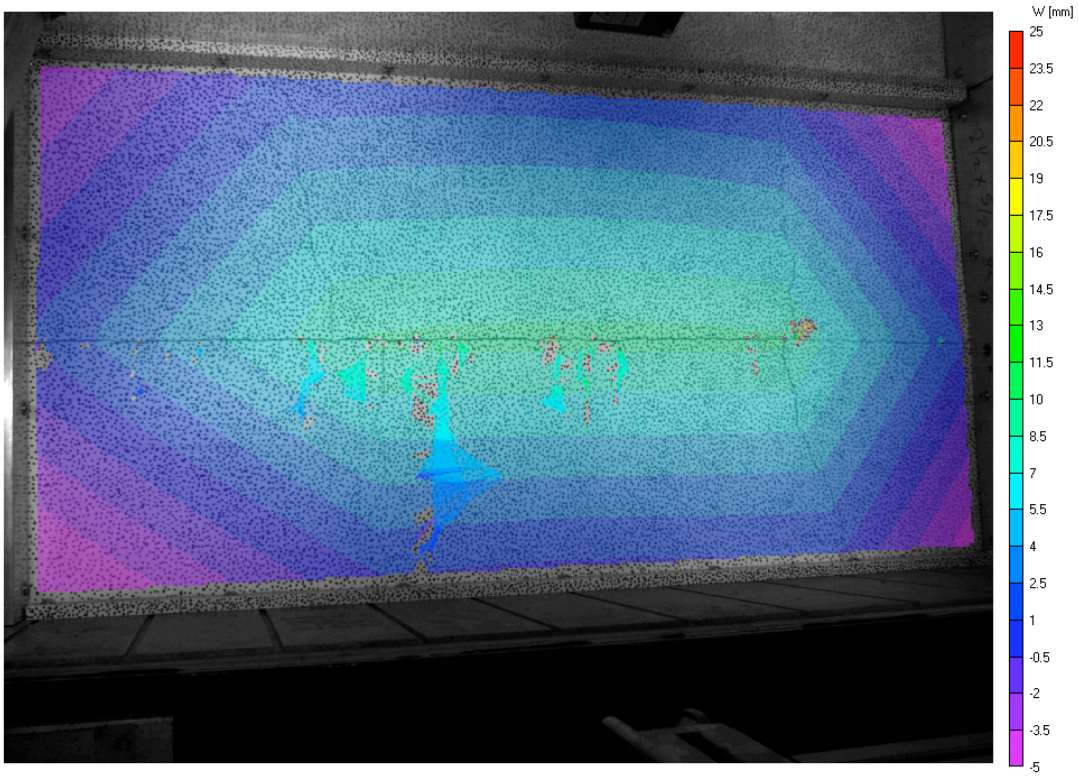


**Figure 6.8.** Contour plot of z deflections for AAC block specimen W4 at ultimate load showing negative deflection at panel corners

Some movement was found to occur at the supports in the initial tests and was particularly evident near the top support, as shown in Figure 6.7. The motion of the

centrifuge caused the panel to tilt back slightly during the start up procedure. In order to achieve the correct simple support arrangement the edges were not fixed into the jig, hence allowing movement to occur. In later tests the air bag was lightly inflated to maintain contact between the wall and the supports. In addition the wall panels were bedded onto a layer of silicone sealant that was applied to the supports to allow for tolerances in the masonry units, which may have prevented consistent contact along the supports. Wrapping film was placed over the layer of silicone to prevent adhesion between the wall panel and the supports. The layer applied was of minimal thickness and was wide in relation to its thickness, such that any effect due to the elasticity of the silicone would be negligible.

The load z deflection responses for the block specimens manufactured with cement mortar are presented in Figure 6.9. The general form of the load z deflection response for the block specimens comprised four stages: firstly an initial linear stage, secondly deflection at approximately constant load, thirdly an approximately linear response of reduced stiffness, and finally deflection at constant load. During the initial response the wall panels generally behaved linearly and no cracking was evident. The stiffness of the repeat specimens (AAC block: W3 and W4, Brick block: W6 to W8) correlated well in this region and the stiffness of the AAC block specimen W5 that was subject to additional vertical load was increased. Horizontal cracking followed the initial linear response and accounted for the deflection at constant load. In the flexural strength tests, as detailed in Chapter 5 Section 5.1.2, it was found that the brick block was marginally stronger than the AAC block in direction 1 and this explains why initial cracking occurred at higher loads in the brick block specimens. The load at which initial cracking occurred varied between repeat specimens and was likely due to the inherent natural variability in masonry. The formation of hinges in the vertical section following initial cracking, accounted for the reduction in stiffness compared to that observed prior to cracking. Following initial cracking, resistance to loading in direction 1 would still maintain a non-zero value, since a moment of resistance would be formed along the length of the crack due to the self-weight of the masonry and the vertical load applied at the top of the wall panel.

Some difference in the load-deflection response for repeat specimens following initial cracking could also be associated to the position where the deflections were measured using the DIC system, as presented in Figure 6.6. For specimens W3 and W6 an LVDT was additionally employed that partially obscured the area near the centre of the panel and prevented DIC measurements being made in this region.

Comparison of data from DIC analysis and from the LVDT is made in Section 6.2.1.3. The brick block specimens reached a higher load before failure compared to the AAC block specimens and this was expected due to the higher flexural strength found direction 2, as detailed in Chapter 5 Section 5.1.2. The ultimate loads of the repeat AAC block specimens (W3 and W4) were within 31 % of each other, whilst the brick block specimens (W6 to W8) were within 14 %. The mean ultimate load was 1.84 kN/m$^2$ and 4.82 kN/m$^2$ for the AAC and brick block specimens respectively. The variability of the ultimate loads was within the range of those reported in the literature for prototype scale tests (de Vekey et al., 1986). The exact mode at failure would influence the load attained and low variability would only be expected if very similar patterns were achieved. Some differences between cracking and ultimate loads could be attributed to the method of controlling the bag air pressure, since on tests W4 and W8 an electronic regulator was employed that improved the control precision.

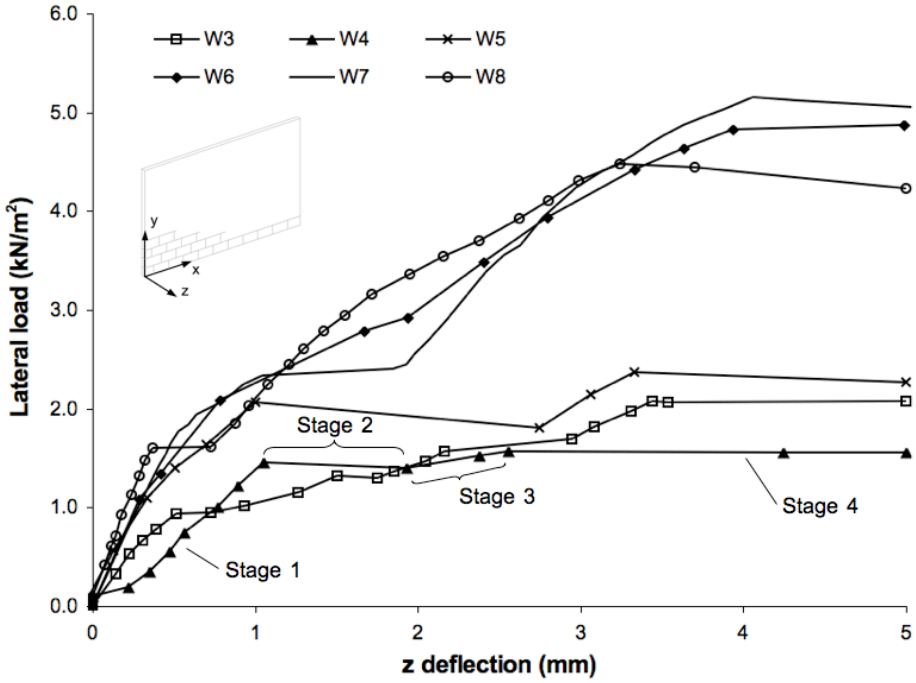


**Figure 6.9.** Load z deflection response for uniformly loaded block specimens with cement mortar (four stages of response annotated for specimen W4)

### 6.2.1.2 In-plane response of block specimens

Figure 6.10 presents the typical load in-plane y deflection response found for the AAC block and brick block specimens. Measurement of the y deflections were accomplished using two methods, an LVDT mounted on the top of the test jig, as shown by Figure 6.11, and via the DIC analysis. It was apparent that the in-plane

response of the block panels in the y direction differed depending on the method of measurement. This was perhaps expected since the point of measurement differed for the two techniques, as presented in Figure 6.11. The LVDT was positioned such that it measured the movement of the spreader, which was part of the axial loading system. When the wall panel displaced into a curved form it was likely that the top surface of the brick would form a small angle to the horizontal. Since the top surface of the spreader was curved, any tilting action would result in the LVDT experiencing an increasingly negative deflection (contraction). Conversely, the DIC measurement point was near the top of the wall panel (at a height of 390 mm) so measured the actual y deflection on the surface of the wall panel rather than deflection plus a rotational effect. The reading from the LVDT could therefore not be relied upon to show the actual response of the wall panels during test and discussion is only given for the results from DIC analysis.

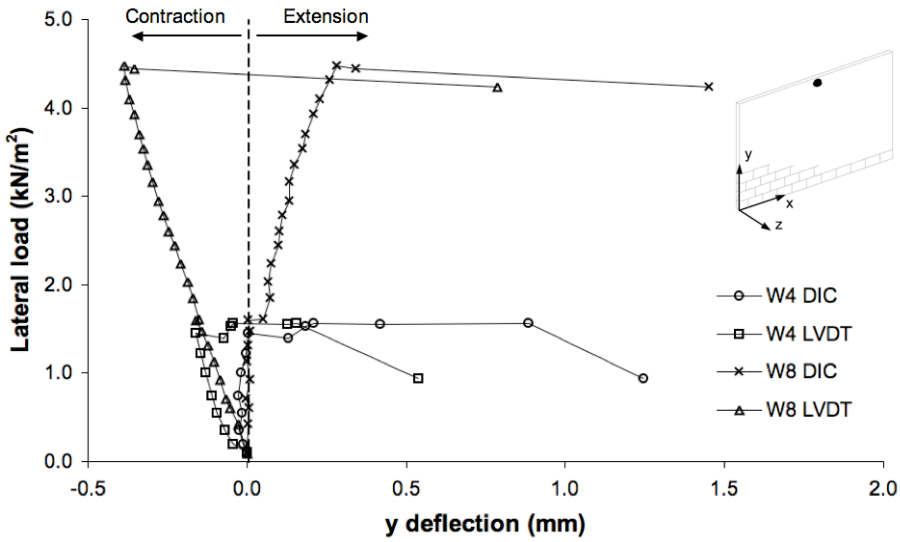


**Figure 6.10.** Load y deflection response measured at top of wall panels W4 (AAC block) and W8 (brick block) using LVDT and DIC analysis

Negligible y deflections were observed in the y direction prior to initial cracking occurring for both the AAC (W4) and brick block (W8) specimens, as shown in Figure 6.10. At initial cracking the wall panels showed a step change in height, likely as the arch mechanism formed. Further extension followed as rotations occurred about the horizontal supports and central crack, as indicated in Figure 6.7. The vertical supports at either end of the panel prevented the hinging mechanism from developing fully along the panel length and effectively limited the deflections in the y direction until the final collapse mechanism formed. Significant extensions, of 1.25

and 1.45 mm for specimens W4 and W8 respectively, however occurred when the final failure mechanism developed.

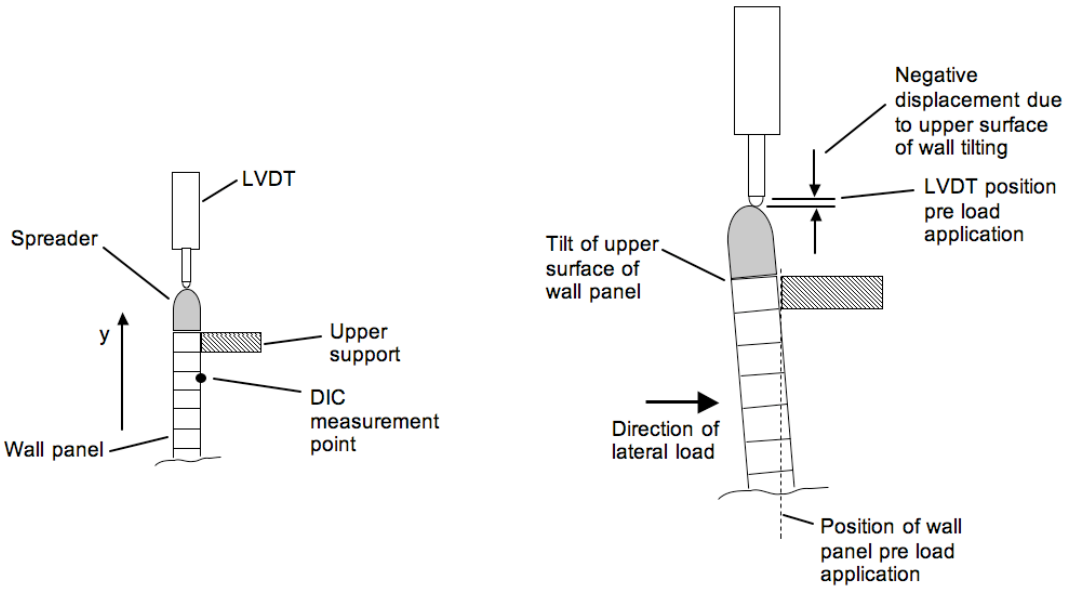


(a) (b)

**Figure 6.11.** (a) Point of measurement for LVDT and DIC for vertical y direction displacements and (b) illustration of wall panel tilting during load application (scale exaggerated)

In a previous study (Hendry et al., 1971) of wall panels that were subject to imposed vertical loads and restrained at the vertical edges it was found that the y deflections at the top of the wall were small until final failure occurred. At failure the wall panels were similarly found to dilate and failed in a yield line type pattern. The specimens previously tested (Hendry et al. (1971) that were unrestrained at the edges were found to dilate at an earlier stage during the lateral load application, which implied that the vertical supports had a significant effect on the failure process.

The typical load x deflection responses for the AAC and brick block specimens are presented in Figure 6.12. It should be noted that extension at the left end of the panel correlates to negative deflection values. The x deflections in the brick block specimen (W8) were negligible at loads below 2 kN/m$^2$, which corresponded closely to the point of initial cracking in the horizontal direction. The AAC block specimen (W4) similarly initially showed negligible x deflections, but the magnitude of the x deflections increased rapidly at the point of initial cracking. This may suggest that there was a transfer of load capacity from the y direction to the x direction following initial cracking as was observed in a previous study (Ng, 1996).

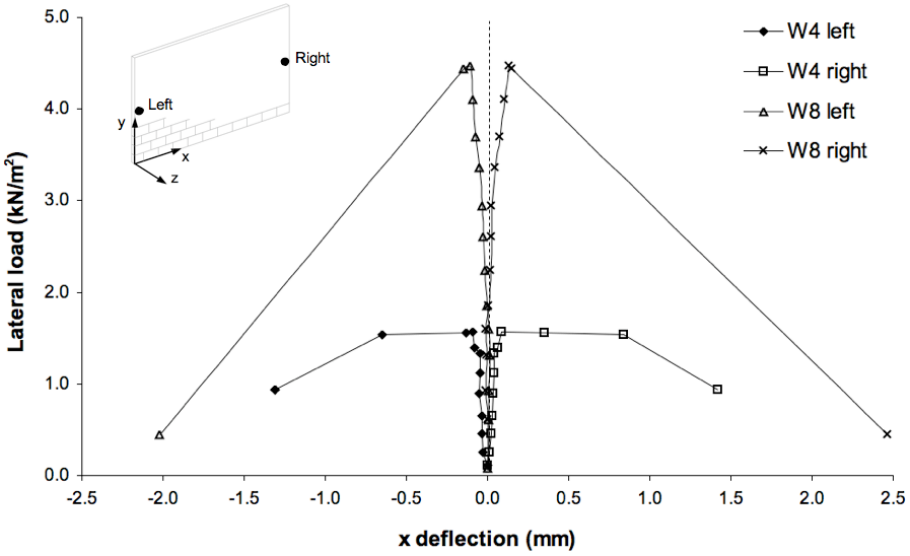


**Figure 6.12.** Load x deflection response measured at mid height at left and right edges of wall panels W4 (AAC block) and W8 (brick block)

Figure 6.13 shows the z deflections along a horizontal centre line for specimens W4 and W8. It was apparent that the block wall panels were of a curved form both pre and post initial cracking. For the wall panel to lengthen in the x direction as it displaced in the z direction suggests that there may have been some cracking occurring in the horizontal direction. The literature survey revealed no studies where the in-plane x displacements had been monitored during the testing of 2 way spanning panels. A study completed of 1 way horizontal spanning masonry specimens however revealed that significant thrusts were developed at the supports during the test, suggesting extension of the panel was occurring (Anderson, 1984).

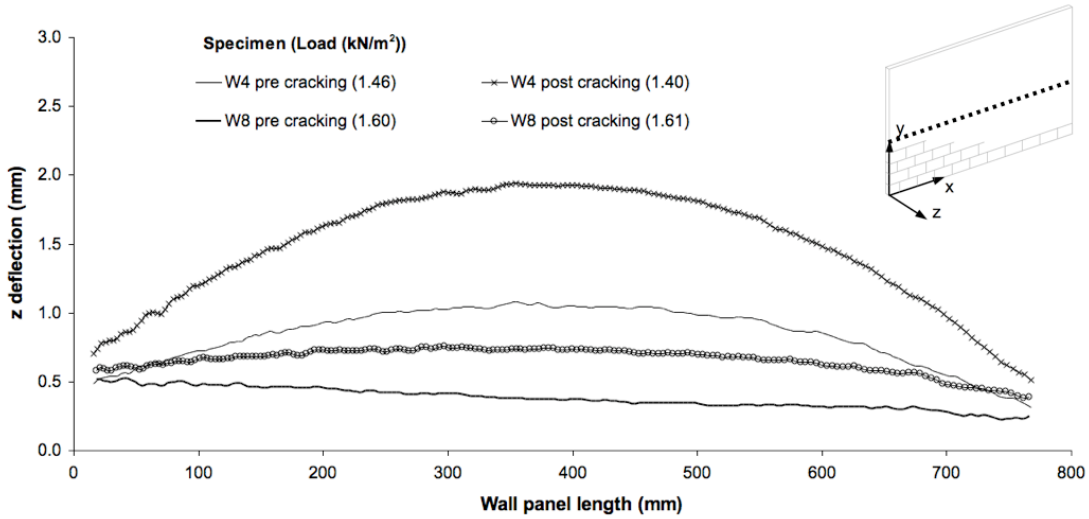


**Figure 6.13.** Z deflection versus wall panel length along horizontal centre line for uniformly loaded block specimens W4 (AAC) and W8 (brick block) at different loads

The extensions of specimens W4 and W8 at ultimate load were found to be approximately 17 % greater in the y direction compared to the x direction. Since the mechanism developed earlier in the y direction, due to strength orthotropy, it would explain the higher levels of extension found in this direction. In Chapter 4 Section 4.1.3 it was stated that the wall panel was expected to dilate during testing and that using fixed or partially fixed supports would influence the failure modes and ultimate loads. The in-plane behaviour observed in the x and y direction supports this statement and the selection of simple supports rather than fully clamped conditions. If the specimen was fully clamped at the edges, then friction forces would develop between the masonry and the support providing resistance to the extension and no rotation could occur. At the corner of an actual masonry building some resistance to extension would be likely, yet rotation would be able to occur following cracking. Fully clamped conditions would clearly not be appropriate in such conditions.

The typical load in-plane strain response in both the x and y directions is shown in Figure 6.14. The strains were similarly measured over a 40 mm gauge length as was used for the small assemblage tests presented in Chapter 5. It was observed that the strains measured in the y direction were initially very small and gradually increased with the application of higher lateral loads. The strains at both the centre of the panels and at the site of the initial horizontal crack were similar, due to the initial crack being situated near to the centre of the panel. It was not clear why there was a small drop in the strains in the y direction at the centre of the panel at a load of 0.75 kN/m$^2$, when the strains remained almost constant at the site of the initial horizontal crack. A significant increase in the y direction strains occurred at initial cracking after a load of 1.45 kN/m$^2$ was attained, although no reduction was observed at the centre of the panel due to the proximity of the two measurements. The strains in the x direction at the centre of the panel were negligible and did not increase until initial cracking occurred after a load of 1.45 kN/m$^2$ was reached, as shown in Figure 6.14. Following initial cracking the strains in the x direction reduced and did not show a significant rise until failure of the panel occurred.

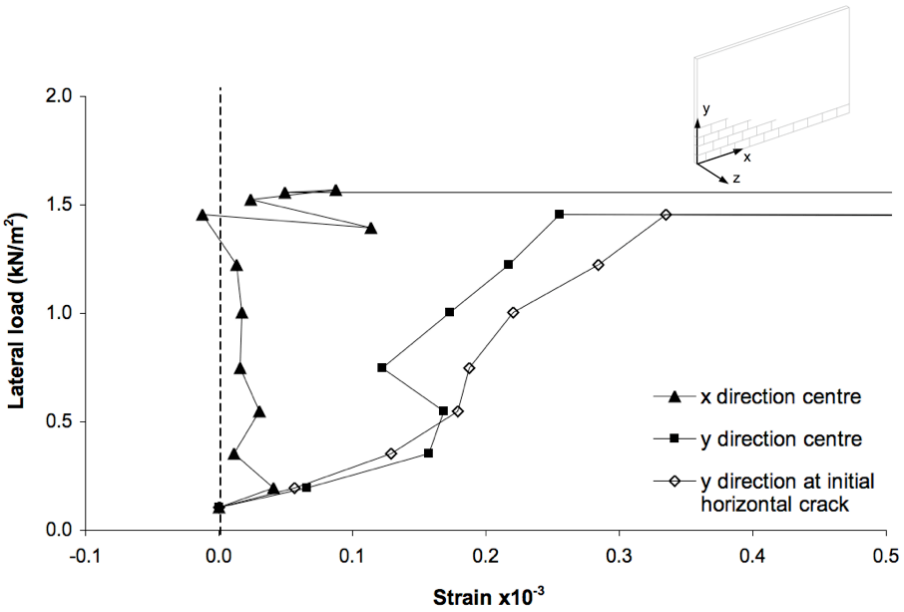


**Figure 6.14.** Load in-plane x and y direction strains measured during test for specimen W4 (AAC block)

### 6.2.2 Brick specimens

#### 6.2.2.1 Failure mode and load deflection response

The failure modes recorded for all the brick specimens tested that were subject to uniform loading are presented in Figure 6.15. Initial cracking was evident through the horizontal mortar bed joints for the brick wall panels similarly to that observed in the block specimens. The initial cracks were central or in the upper section of the panel, and likely positioned due to normal stress decreasing with elevation. The specimens sustained further loading until cracks, that were generally diagonal in direction, developed that allowed a failure mechanism to form. The patterns formed at failure were similar to those observed for the brick block specimens, although a higher proportion of the cracks passed through the units with increasing mortar strength. The effect of the opening was to force the cracks to develop from its corners rather than nearer to the vertical edges of the panels as observed in specimens W12 and W13 (Figure 6.15). This was expected since the highest bending stresses would be at the corners of the opening. Figure 6.16 shows a contour plot of z deflections recorded at ultimate load for specimen W13 and the response recorded for other specimens was similar. It was observed, from the contour plot of z deflections, that negative deflection occurred at the corners of the brick panel at failure, similarly to that found for the block specimens. The crack patterns were similar to those observed in previous studies completed at prototype and model (1:2) scale for similar support conditions (Duarte & Sinha, 1992, Edgell and Kjaer, 2000, West et al., 1977).

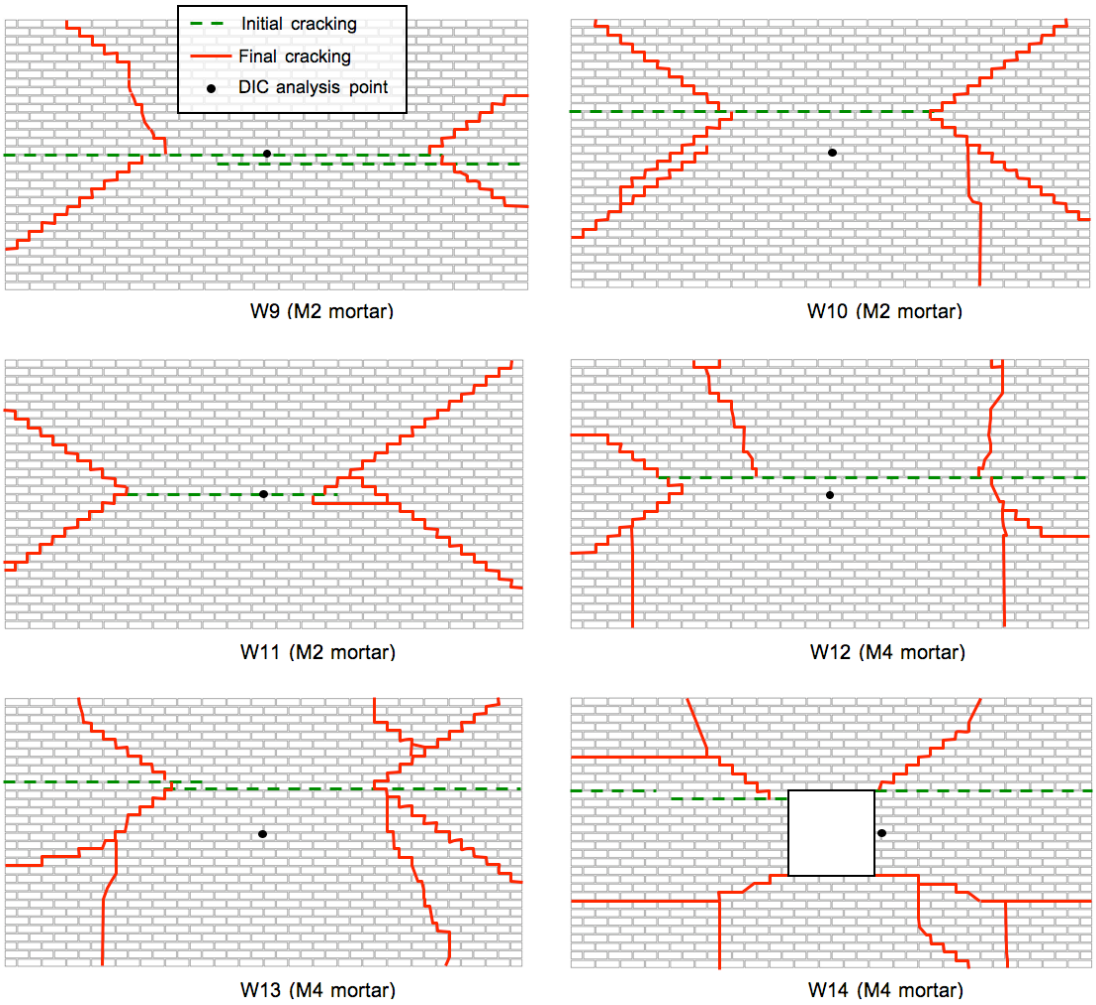


**Figure 6.15.** Failure modes observed for uniformly loaded brick specimens

The load z deflection responses for brick specimens W10 to W14 are shown in Figure 6.17. The initial load deflection response was found to be similar for all the specimens. Specimens W12 to W14 initially cracked at or near the peak of the linear response, whilst W10 and W11 appeared to reduce in stiffness before cracking was evident. W10 and W11 continued to exhibit a softening behaviour up until failure occurred. The response for W12 to W14 differed, as after initial cracking occurred the specimens deflected at constant load. Further loading was then sustained by W12 to W14, but at a reduced stiffness, up until failure. This behaviour was comparable to that observed for the block specimens and initial cracking likely resulted in the response of reduced stiffness. When the mechanism was fully developed at failure the specimens all tended to deflect at approximately constant load. It was evident that the increased mortar strength resulted in a higher ultimate load, which was also confirmed by the flexural tests of the wallettes as discussed in Chapter 5.

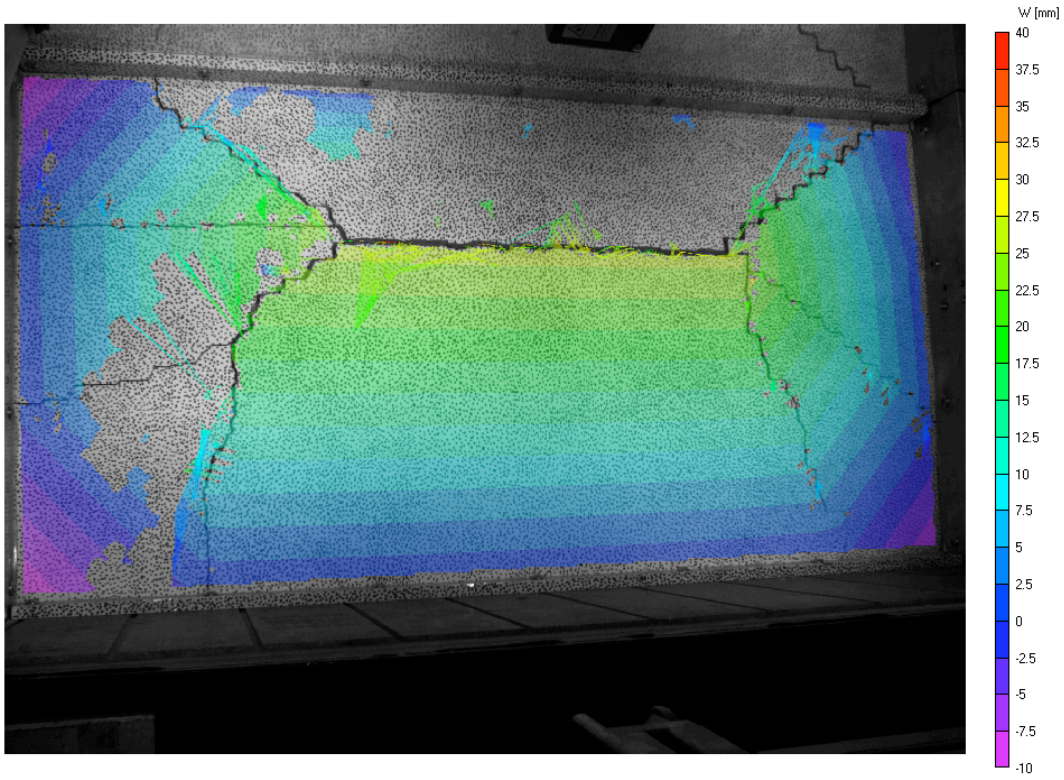


**Figure 6.16.** Contour plot of z deflections for brick specimen W13 (M4 compressive strength class mortar) at ultimate load showing negative deflection at panel corners

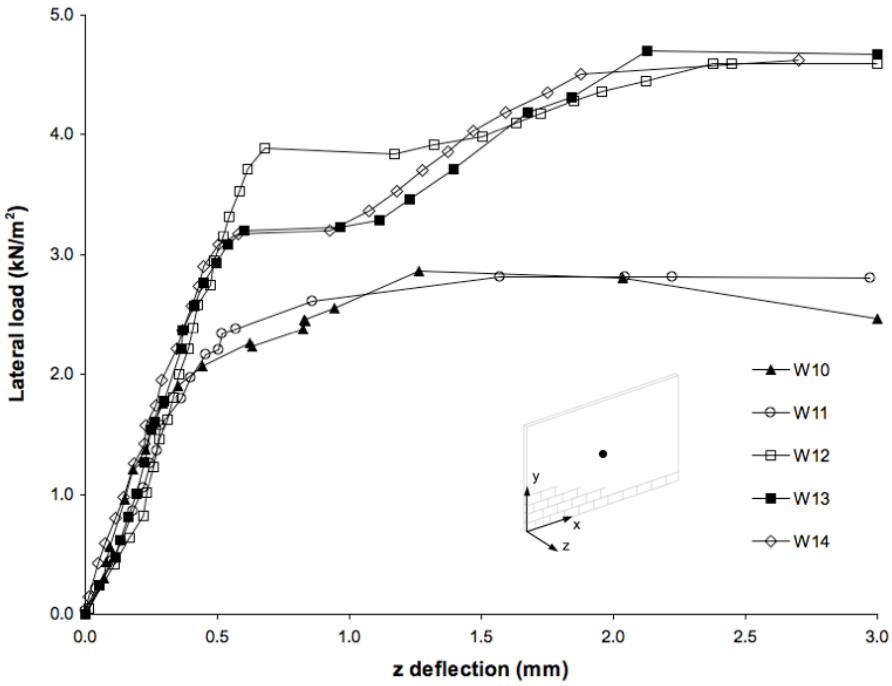


**Figure 6.17.** Load z deflection response for uniformly loaded brick specimens (specimen W9 omitted)

In the test of specimen W9 the supports were fitted with foam strips in an attempt to allow for tolerances in the masonry units. The foam strips however allowed significant displacements at the supports and affected the load-displacement response. Due to this specimen W9 has been omitted from figure 6.17. All later specimens were bedded on to a layer of silicone as described in Section 6.2.1.1.

Repeat specimens with the same masonry and mortar combinations showed similar ultimate loads, for specimens W9 to W11 constructed with M2 strength mortar the mean ultimate load was 2.84 kN/m$^2$ and were within 8 % of each other, whilst for specimens W12 and W13 manufactured with M4 strength mortar the mean ultimate load was 4.65 kN/m$^2$ and were within 2 %. The use of the improved electronically controlled regulator for all the brick specimens could account for the reduction in variation when compared to that recorded for the block specimens. Variability in repeat specimens was lower than that reported in the literature, where the average difference between results for prototype specimens was 39 % (West et al., 1977), whilst the values from a study completed at 1:2 scale were within 18 % (Duarte, 1988).

The average ultimate load for specimens constructed with M4 strength mortar (W12 and W13) was similar to the average for the brick block specimens (W6 to W8). This was perhaps not expected since a lower M2 strength mortar was used in the manufacture of the brick block panels and the flexural strengths of the brick block, in both directions 1 and 2, were lower than the brick with M4 strength mortar, as given in Chapter 5 Section 5.1. This suggests that there was some effect due to the size of the masonry unit and the number of mortar joints in the specimens that was only apparent in the wall panels and not the wallette tests. No studies were identified in the literature where wall panels were constructed from identical materials of different size formats. However, an effect of unit size for tests completed on AAC wallette specimens was reported in a previous study (de Vekey et al., 1986). In contrast to the behaviour observed in this research programme, it was previously found (de Vekey et al., 1986) that the strength increased as the unit size decreased and the number of mortar joints increased.

Inclusion of an opening in W14 did not appear to significantly affect the load-deflection response when compared to W12 or W13. The small size of the opening and the use of a board to cover it likely resulted in the similarities of the responses. A ultimate load of 5.9 kN/m$^2$ was given in a previous study conducted at 1:2 scale

(Duarte and Sinha, 1992), which exceeded the value found for W14 by 28 %. The load-deflection response reported in the previous study (Duarte and Sinha, 1992) was also of higher stiffness compared to that recorded for specimen W14. The difference between the ultimate load and the response may be attributed to the higher strength M12 mortar and the shorter panel length of 3.6 m previously utilised (Duarte and Sinha, 1992). The scaled deflection at the ultimate load previously given (Duarte and Sinha, 1992) of 0.7 mm was considerably lower than the value at failure for specimen W14, of 2.7 mm, and it was likely that there was some scale effect occurring in addition to the differences accredited to mortar strength and panel length. Other researchers have reported responses of lower stiffness when the scale of the test specimens were reduced (Davies et al., 1998, Egermann et al., 1991). The differences are suggested to be as a result of a reduction in mortar compaction and the grading of the mortar constituents through the scales (Davies et al., 1998, Egermann et al., 1991).

#### 6.2.2.2 In-plane response of brick specimens

The typical load y deflection responses for brick specimens constructed with M2 and M4 compressive strength class mortar are shown in Figure 6.18. The response of the other brick specimens were found to be similar, so are not reported here. The DIC analysis showed that there were negligible deflections in the y direction prior to initial cracking occurring and the initial response did not appear to be influenced by mortar strength. Both specimens W11 and W12 increased in height following initial cracking, although the response differed likely as a result of the dissimilar compressive strength of the mortar. The load z deflection responses along a vertical centre line for specimens W11 and W12 at pre and post initial cracking conditions are presented in Figure 6.19. It was observed that following initial cracking that three hinges developed in both specimens W11 and W12 in the vertical section. The increases in y deflections following initial cracking were therefore likely due to formation and displacement of the hinging mechanism. The behaviour shown in the y direction for the brick specimens was comparable to that found for the block specimens detailed in Section 6.2.1.2. The y deflection responses for the brick specimens also showed some similarities to those recorded in the z direction for the corresponding specimens, as shown in Figure 6.16.

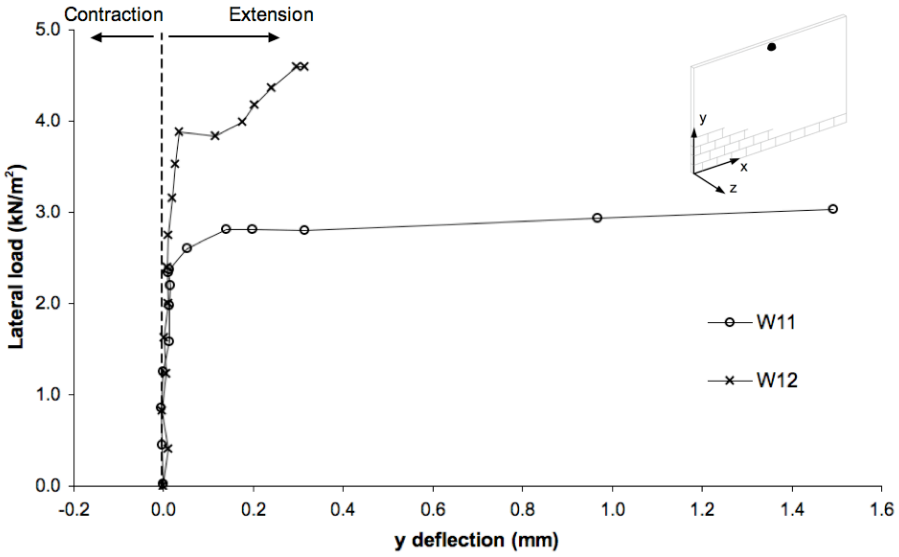


**Figure 6.18.** Load y deflection response measured at top of brick wall panels W11 (M2 strength mortar) and W12 (M4 strength mortar) using DIC analysis

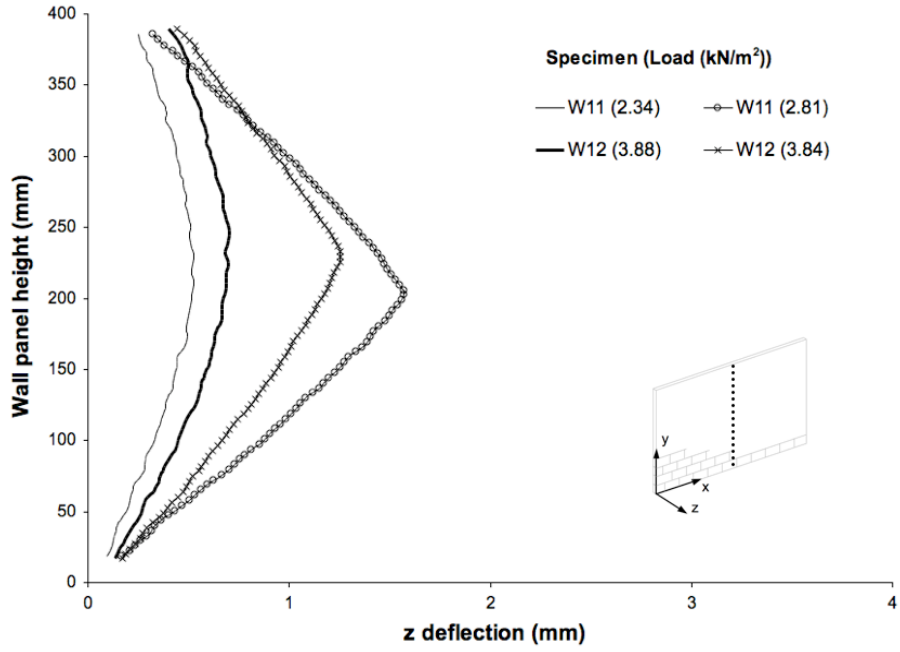


**Figure 6.19.** Wall panel height versus z deflection along vertical centre line for uniformly loaded brick specimens W11 (M2 strength mortar) and W12 (M4 strength mortar) at different loads

Figure 6.20 presents the load x deflection responses for brick specimens W11 and W12. The load-x deflection response was observed to be offset to the right and left of the origin for specimens W11 and W12 respectively and may be related to the lack of symmetry of the failure pattern about a vertical centre line. As observed in the block specimen wall tests, the deflections in the x direction were negligible before initial

cracking occurred in the wall panels. Following initial cracking, the x deflections increased in magnitude at a higher rate in specimen W11 than in W12. The difference in the response of specimens W11 and W12 was likely due to the higher post cracking load capacity found in specimen W12. A gradual transition from cracking to failure at near constant load was recorded in specimen W11, which permitted higher deflections to develop in the x direction. At the ultimate load the deflections in the x and y directions for specimen W11 were within 10 %, where the x deflection comprised the deflections at the left and right hand sides of the panel. Panel W12 continued to sustain significant further loading following initial cracking, though at a reduced stiffness, which resulted in deflections of lower magnitude in the x direction compared to those recorded in specimen W11. The deflections in the y direction were 90 % higher than those in the x direction for specimen W12 at the ultimate load. The results again illustrate that the use of fully clamped support conditions would not be appropriate, since they would have influenced the ability of the specimens to extend in both the x and y directions.

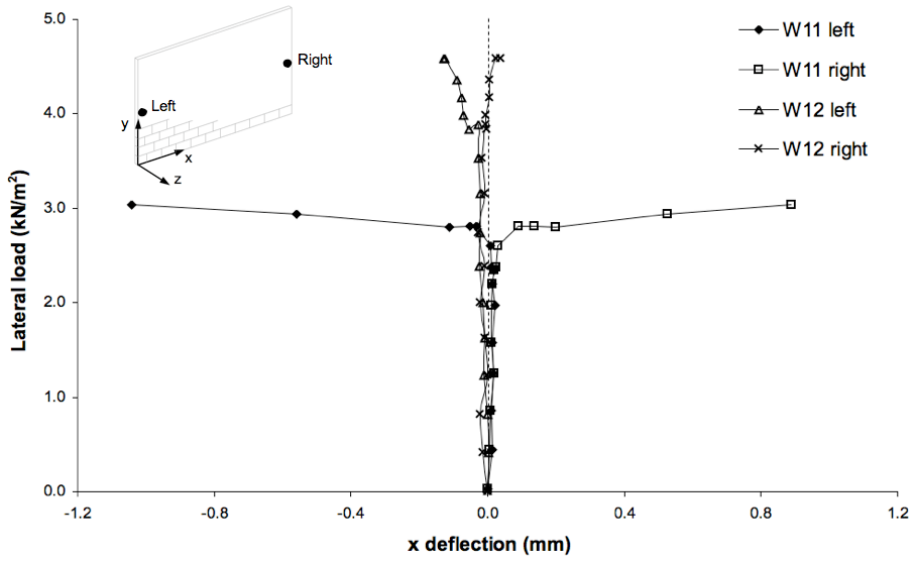


**Figure 6.20.** Load x deflection response measured at mid height at left and right edges of wall panels W11 (M2 strength mortar) and W12 (M4 strength mortar)

The load in-plane strain response in the x and y directions for brick wall panel W10 is shown in Figure 6.21. The responses of the other brick specimens were found to be similar and are not presented here. Contour plots of the strains in the y direction at initial cracking and in the x direction at ultimate load are shown by Figures 6.22 and 6.23 respectively. The in-plane strains in the y direction, measured over a 40 mm gauge length, were initially small and showed some scatter. The scatter apparent in

the results at very low values of strain was likely due to the limitations in resolution of the DIC system, as discussed in Chapter 5. The levels of strain in the y direction were marginally higher when measured over the crack and perhaps indicated the stiffness along the particular bed joint was lower than others in the panel. The strains in the y direction did not show any significant increase in magnitude until a load of 1.76 kN/m$^2$ was attained, which was lower than the load at initial cracking of 2.23 kN/m$^2$. Strains continued to rise at the centre of the panel as the crack formed, but were much more significant over the crack, as was evident in the corresponding contour plot of strains shown in Figure 6.22. This behaviour would be expected since the mouth of the crack would be opening up during its development. When the crack was visible, at a load of 2.46 kN/m$^2$, the strains in the y direction tended to decrease at the centre of the panel, but maintained a positive value rather than dropping to zero. Some curvature of the sections of the panel above and below the crack was evident after initial cracking occurred, as shown in Figure 6.19, so some residual strains would be expected. If the hinging mechanism was allowed to fully develop, for example by removing the vertical supports, then the strain would likely drop more significantly.

The strains in the x direction were typically of lower magnitude than in the y direction and showed a slightly higher degree of scatter, as apparent in Figure 6.21. It was difficult to ascertain if there was any effect on the magnitude of the strains in the x direction caused by initial cracking due to the scatter in the results. There did not appear to be sudden transfer of load from the y to x directions following initial cracking. An increase in the x direction strains was not really evident until just prior to failure at a load of 2.86 kN/m$^2$. The drop in strain in the x direction at the end of the response was likely associated with the development of further cracks at final failure, as was apparent in the corresponding contour plot of strains, as shown in Figure 6.23. As the diagonal cracks formed the strain was also found to drop marginally in the y direction at the centre of the panel, possibly due to the hinging mechanism being able to develop along the length of the panel.

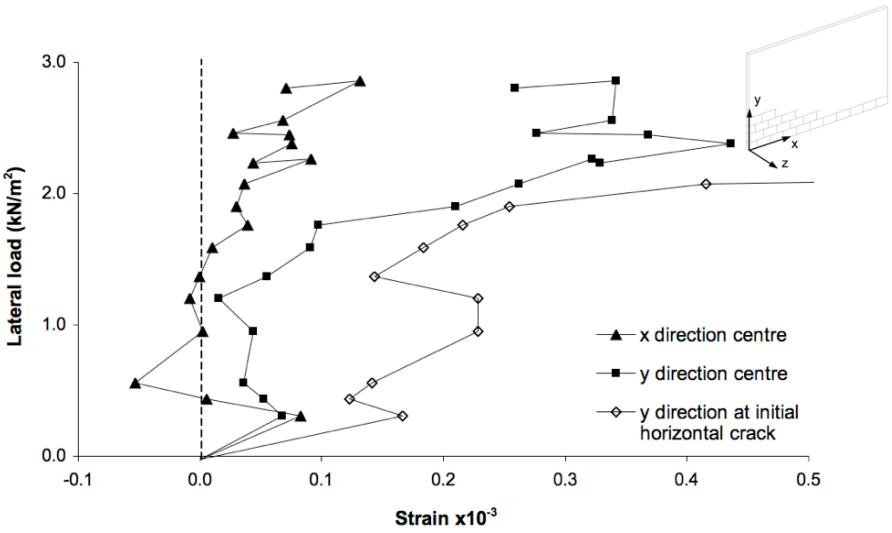


**Figure 6.21.** Load in-plane x and y direction strains measured during test for brick specimen W10 (M2 strength mortar)

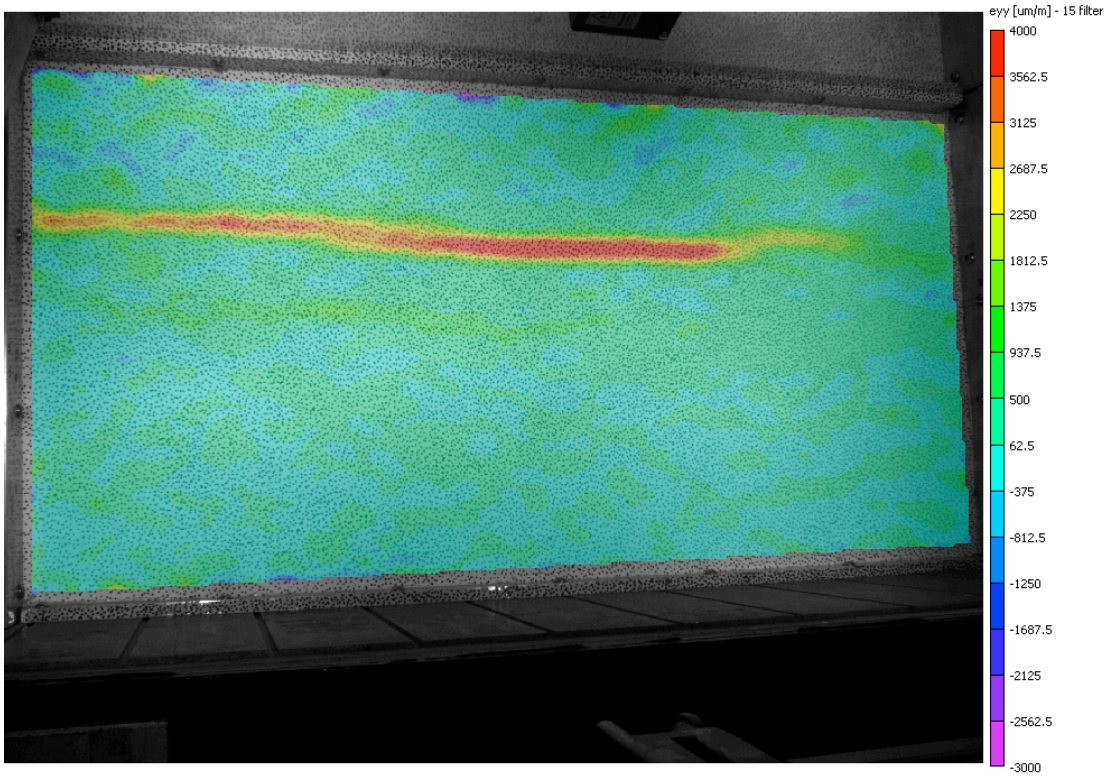


**Figure 6.22.** Contour plot of strain in the y direction for brick specimen W10 (M2 compressive strength class mortar) at a load of 2.23 kN/m$^2$ at initial cracking

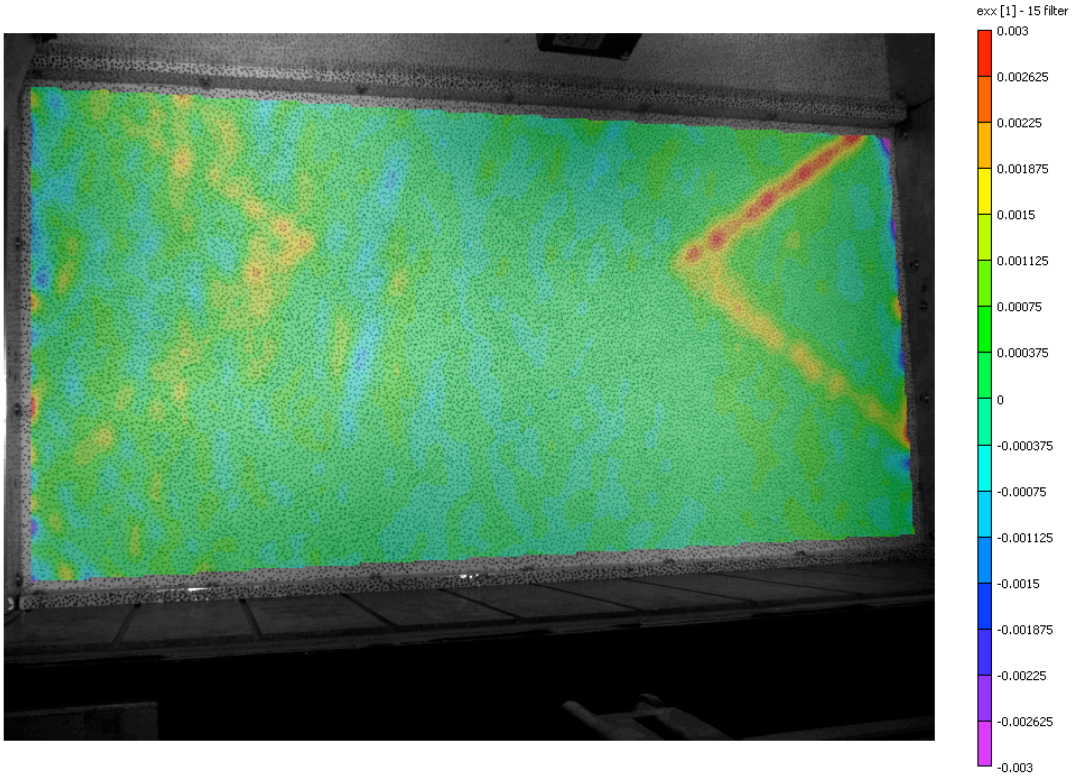


**Figure 6.23.** Contour plot of strain in the x direction for brick specimen W10 (M2 compressive strength class mortar) at a load of 2.86 kN/m$^2$ prior to failure

### 6.2.3 Cavity wall specimen

The failure modes for leaves of the AAC block / brick cavity wall specimen (W15) tested are presented in Figure 6.24. The inner AAC block leaf of specimen W15 initially cracked horizontally through the bed joints during the loading process, as shown in Figure 6.24a. The cavity wall panel (W15) sustained further loading before failure occurred at which point further cracks developed in the inner skin. The crack pattern was generally coincident with the position of the wall ties and showed some similarities to those observed for specimens W3 and W4. At the end of the test the outer brick wall panel was recovered and was found to have cracked horizontally at a position similar to the inner leaf, as presented in Figure 6.24b. The cracks at failure were in different positions to those of the inner leaf, but were similar to those observed in W9, W10 and W11. This confirmed that the higher density of wall ties at the vertical and upper horizontal edges of the panel were providing additional support to the edges of the outer leaf. It was not clear from the results in which order the wall panels failed, or if failure was simultaneous.

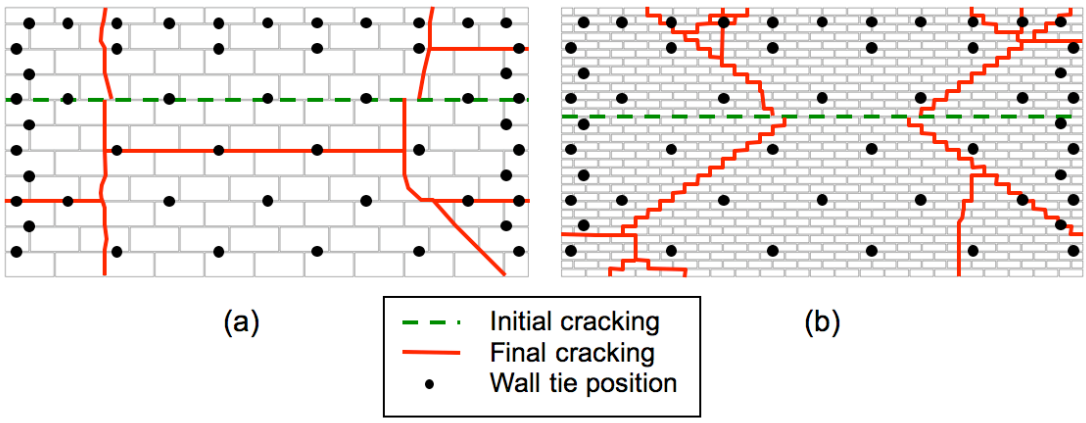


**Figure 6.24.** Failure modes observed for cavity wall specimen W15, (a) inner leaf and (b) outer leaf

The load z deflection response for the cavity wall specimen W15 measured on the inner AAC block leaf is shown in Figure 6.25. The initial load deflection response for the cavity wall assembly W15 was similar to that of the single leaf brick specimens. The post initial cracking response of W15 was more comparable to that shown in the brick specimen with M4 strength mortar (W12) and the AAC block specimen (W4), where deflection at constant load was followed by a response of reduced stiffness rather than the gradual softening recorded for the brick with M2 strength mortar specimen (W11). The response seemed to show that the brick leaf was controlling the initial behaviour, but the post cracking response was improved when compared to that of the individual brick leaf (W11). The post cracking response suggested that there was some effect due to the combination of the two materials, but it was not clear which was controlling the behaviour. The displacement at which the final failure mechanism developed was of equal magnitude to that of both W4 and W11 and so unfortunately did not provide any additional insight into the order in which the leaves failed.

Guidance in Eurocode 6 (EC6) (BSI, 2005c) states that the load carried by each leaf in a cavity wall assembly may be a proportion of the total load when the wall ties are capable of transferring such loads. In Chapter 5 it was demonstrated that the model scale wall ties could transfer compressive loads up to an average of 108 N before failure occurred. The ultimate load sustained by specimen W15 was equivalent to a total load on the wall panel of 1104 N. Assuming all the load was transferred to the inner skin and was uniformly distributed over all the ties, then each tie would be subject to a load of 22 N. The ties were subjected to one fifth of their maximum load

capacity and were therefore adequately sized to transfer such loads between the leaves. No buckling would be expected at this load and this was verified on examination of the ties after testing. It was considered that the wall ties satisfy the requirements in current guidance (BSI, 2005c) as detailed above.

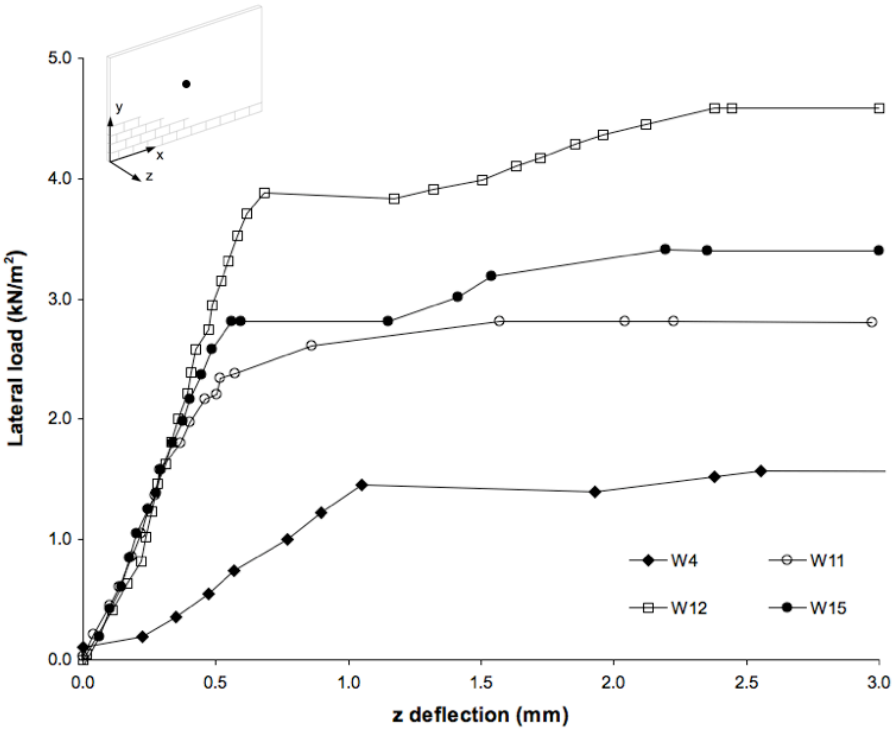


**Figure 6.25.** Load z deflection response for uniformly loaded cavity (W15), brick M2 mortar (W11), brick M4 mortar (W12) and AAC block (W4) specimens

The ultimate load for the AAC block work leaf alone could be assumed to be the average of specimens W3 and W4 at 1.84 kN/m$^2$. The average ultimate load for the brick specimens constructed with M2 mortar was 2.84 kN/m$^2$ based on the results from specimens W9 to W11. However, the outer brick leaf of the cavity wall was not subject to vertical axial load as was the case for specimens W9 to W11. To assess the possible impact of removing the vertical load on the ultimate load of the brick leaf the calculation method given in EC6 (BSI, 2005c) was utilised. Ultimate loads were calculated using the EC6 (BSI, 2005c) method for brick panels with and without vertical axial loading and it was found that a 5 % reduction was likely when the vertical load was omitted. The ultimate load for the outer brick leaf was therefore assumed to be 95 % of the average of specimens W9 to W11 at 2.70 kN/m$^2$. Based on guidance given in EC6 (BSI, 2005c) then the ultimate load may be based on the sum of the ultimate loads of the individual leaves. The ultimate load of W15, at 3.41 kN/m$^2$, was 33 % lower than the value from the sum of the individual leaves of 4.54

kN/m$^2$. The results suggest that some form of composite action was occurring, since the ultimate load of W15 exceeded those of either of the individual leaves. If no composite action took place then it may be likely that the ultimate load would be governed by that of the weaker inner AAC block leaf, however it was apparent that the ultimate load was almost double that of AAC block leaf alone.

In previous studies the ultimate loads of the cavity walls were reported to be similar to the sum of the ultimate loads of the individual leaves (de Vekey et al., 1986, West et al., 1977). The difference in the sum and actual ultimate loads for specimen W15 could be attributed to the edge support conditions of the outer leaf. The wall ties were responsible for supporting the edge of the outer leaf, since no additional supports were positioned at the perimeter. In the previous research programmes (de Vekey et al., 1986, West et al., 1977) identical edge support conditions were used for both the outer and inner leaves of the specimens. If additional simple supports were used at the edges of the outer leaf of W15, then the compressive load transferred to the inner leaf would be reduced and may result in a higher ultimate load. For the case of W15 it therefore may not be fully appropriate to sum the ultimate loads of the individual leaves without further investigation.

### 6.3 Effect of increased gravitational acceleration on wall panels

The effect of applying additional gravitational force was examined by analysing the variation in strain in the wall panel between the state of normal gravity (centrifuge at rest) and enhanced gravity (centrifuge at operating speed). The effect was evaluated for the AAC block specimens that were constructed with and without mortar (specimen numbers W1, W2 and W4). Strains were determined using the DIC system over a 40 mm gauge length at the top and bottom of the specimens, as shown in Figure 6.26. The gauge length was selected as it encompassed both units and joints. The strains at a state of normal gravity before starting the test were zero. The normal stress levels in the wall prior to starting the test were low at 0.004 and 0.005 N/mm$^2$ at the top and bottom locations respectively including the imposed vertical loadings. Figure 6.26 shows the strains in the y direction at a top and bottom locations when the centrifuge was at operating speed for AAC block specimens constructed with no mortar (W1), sand mortar (W2) and M2 compressive strength mortar (W4). Contour plots of the strains in the y direction when the centrifuge was at operating speed for specimens W1, W2 and W4 are shown by Figures 6.27, 6.28 and 6.29 respectively.

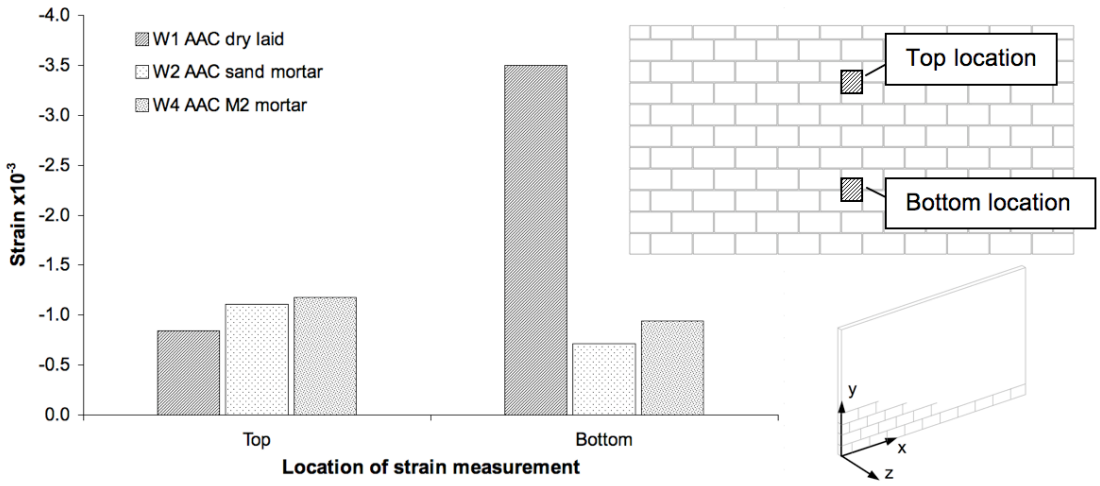


**Figure 6.26.** Vertical y direction strain in upper and lower sections of AAC block wall panels when centrifuge at operating speed

At the required operating speed the units in the wall panel were subject to additional normal stress due to the increased g level imposed by the centrifuge. Under these conditions the average normal stresses increased to 0.022 N/mm$^2$ at the top location and to 0.031 N/mm$^2$ at the bottom location. The general effect of the increased gravitational force, and the corresponding increased stress level, was seen to cause compressive strains in the wall panel, as presented in Figure 6.26. Since stress increased towards the bottom of the panel, due to the self-weight of the units, it was expected that higher levels of strain would also occur towards the base of the panel. However, marginally lower levels of strain were observed at the bottom of the wall panels compared to the top, with the exception of that at the bottom of the dry assembled specimen. The lower levels were due to the bottom of the wall panel being restrained by the base of the test fixture and may also be as a result of the concentrated imposed vertical axial load causing higher localised strains in the section of the wall panel directly below. The overall difference in strain between the top and bottom of the panels was generally low, which may suggest that the self-weight effect for the low-density AAC units was insignificant in comparison to that of the imposed loading. For example, by removing the imposed loading the average normal stress level at the top and bottom locations would reduce to 0.004 and 0.013 N/mm$^2$ respectively.

The higher strain recorded at the bottom of the dry assembled panel was due to the increased stress level closing up the small gaps between the blocks. This effect was observed in the y direction contour plot from DIC analysis, as shown in Figure 6.27.

Dilation occurred in some regions in the dry assembled wall panel and was likely due to a rocking action resulting from higher compressive strains at the opposite end of the unit. The small gaps between the dry laid units were as a result of the limited tolerances achievable in the cutting process. Higher strains were observed along some of the bed joints in the specimen constructed with sand mortar, suggesting some compaction of the sand between the units, as presented in Figure 6.28. These were more evident towards the top of the panel, which confirms the statement made above that the imposed loading caused some localised strain effect. No such action was apparent in the panel constructed with M2 mortar and the strains in the vertical direction were similar over the whole surface of the wall, as shown in Figure 6.29. In summary, the gravitational force imposed by the centrifuge increased the magnitude of the normal stress in the wall panels, which was demonstrated by the compressive strains observed at the required operating speed. The results shown certainly support the use of the centrifuge for the testing of model scale masonry wall panels.

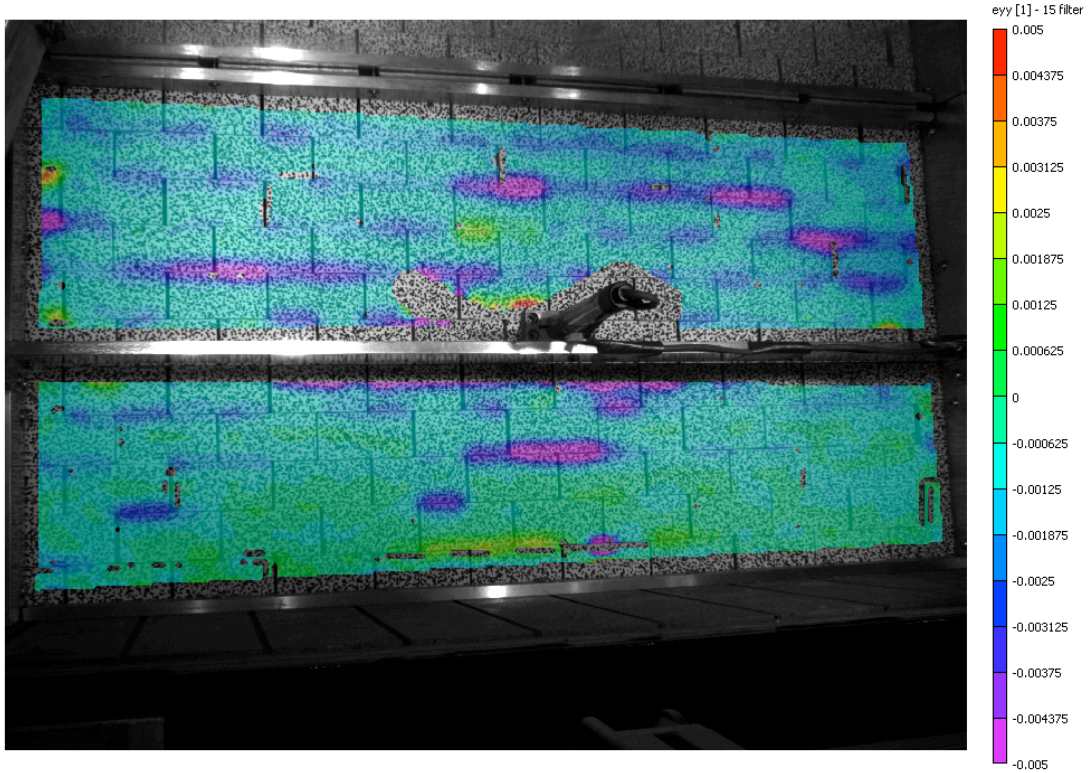


**Figure 6.27.** Contour plot of strain in the y direction for AAC block specimen W1 (no mortar) at centrifuge operating speed

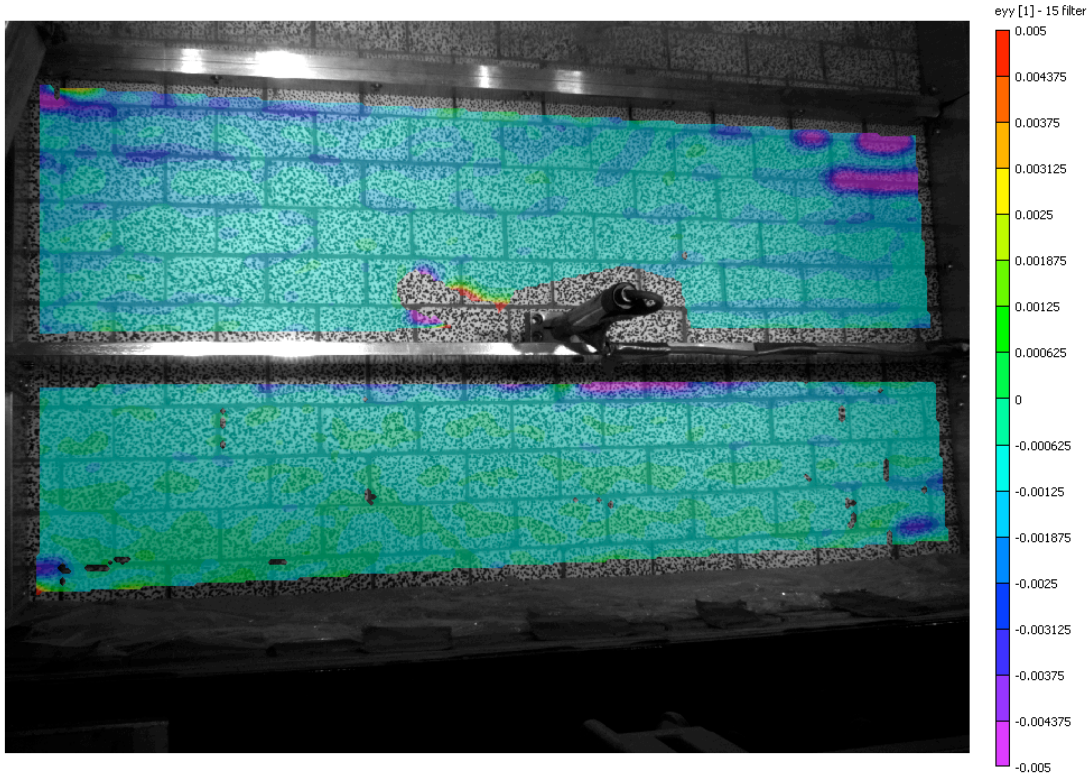


**Figure 6.28.** Contour plot of strain in the y direction for AAC block specimen W2 (sand mortar) at centrifuge operating speed

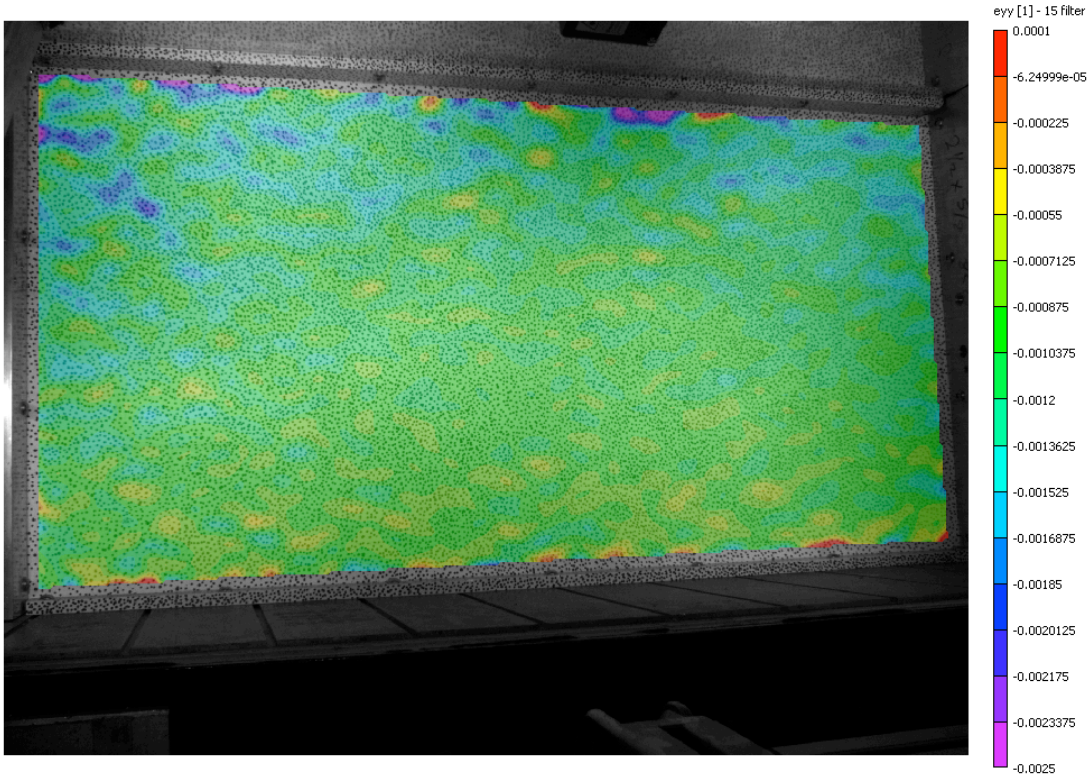


**Figure 6.29.** Contour plot of strain in the y direction for AAC block specimen W4 (M2 compressive strength mortar) at centrifuge operating speed

### 6.4 Conclusions

The dry assembled AAC block wall did not exhibit a yield line pattern, but deflected into a curved form in the x and y directions. The AAC block wall constructed with sand mortar however formed a yield line pattern at failure, but collapsed at a lower load. Higher levels of friction between the units and tolerances in the cutting process likely influenced the failure mode observed in the dry assembled panel. The lower collapse load found for the specimen constructed with sand mortar was attributed to the lower level of friction between the units along the lines of failure.

The mode of failure of the block specimens was dependant on the type of unit. The weaker AAC block permitted cracking to occur through the unit, whilst cracking was generally along the mortar joints for the brick block. Negative deflection was shown at the corners of the panel and was thought to be due to the support conditions, the cracks at failure not entering the corners and the initial crack traversing the entire panel. No effect on the failure mode was apparent when the vertical axial load was increased. The form of the response for the brick block and AAC block specimens was similar, however the AAC block panels were of a lower stiffness. Increasing the vertical axial load resulted in the initial stiffness of the AAC block panel being similar to the brick block. Variations between the ultimate loads for repeat specimens was in line with those reported in the literature.

Extension in the x and y directions only occurred in the block specimens following initial cracking and significant lengthening was observed at failure. The increase in length in the x direction that occurred at initial cracking and was thought to be due to the transfer of load to the un-cracked direction. Lengthening behaviour had previously been reported for 1 way spanning panels, but no existing data was apparent for 2 way spanning panels. A 17 % higher extension was found in the y direction when compared to the x direction at failure and was thought to be due to the development of the initial hinging mechanism. Rotation and some resistance to extension would likely be possible at the corners of a real building, so selecting fully clamped supports would not be appropriate. The extension and response in the vertical and horizontal sections observed supported the use of simple rather than fixed supports. Strains in the y direction were typically found to gradually increase during the load application process, but those in the x direction remained almost negligible.

The generalised failure mode for the brick specimens was characterised by initial cracking in the horizontal direction followed by diagonal cracking at failure. As mortar strength increased a higher proportion of the cracks at failure passed through the units rather than along the mortar joints. Negative deflection was observed at the corners of the specimens due to the diagonal cracks forming such that they did not enter the corners. The initial load deflection response was similar for all specimens. Specimens with weaker M2 mortar tended to soften following initial cracking, whilst those with M4 mortar were able to sustain further loading following deflection at constant load, albeit at a reduced stiffness. A low variability between the ultimate loads for repeat specimens was found. The effect of the opening on the ultimate load was shown to be minimal, likely due to its small size and the use of a board to cover it. The failure pattern differed to solid panels, since cracks initiated from the corners of the opening. Higher strength M4 mortar brick specimens failed at comparable loads to the brick block wall panels, suggesting that there was some influence due to the stiffness of the unit.

The brick specimens were observed to extend in both the x and y directions following initial cracking, further illustrating that fully clamped conditions would not be appropriate. The strains in the y direction continued to increase following initial cracking suggesting that there was not a sudden transfer of load from the y to the x direction.

The crack patterns observed in the cavity wall leaves were similar to those found for the individual wall tests. The load deflection response seemed to be initially similar to that of brick, but later showed a combined effect of the two materials. The ultimate load was lower than the sum of the individual leaves and more comparable to the twice the weaker leaf. It was likely that the support conditions for the outer loaded leaf influenced the failure mode. The wall ties were shown to be capable at transferring the compressive loads and typically only experienced a fifth of their ultimate load.

The strains in the AAC block wall panels were found to increase when the centrifuge was at the correct operating speed compared to prior to the test. Compressive strains were observed in all the wall panels at test speed and were due to the self-weight effects from the units and the additional imposed loadings. The results highlighted the importance of the using the centrifuge for reduced scale testing of masonry specimens.

# Chapter 7 Results of hydraulic lateral loading tests

This Chapter presents the results from the hydraulic (non-uniform) loading tests completed on masonry wall panels in the centrifuge. A summary of the results from all the tests that were completed is given in Table 7.1. A detailed discussion of the results from the tests completed is presented in the following sections in this Chapter.

The compressive strength of the mortar cubes and the corresponding COV for each wall panel test are given in Table 7.1. The average of all the M2 strength mortar cubes tested for all wall panel specimens in the hydraulic loading programme was 2.80 N/mm$^2$ with a COV of 12.9 %, whilst for the M4 strength cubes was 8.27 N/mm$^2$ with a COV of 10.6 %. The COV for all mortar cubes tested was of similar magnitude for the M2 and M4 strength specimens, suggesting variability was comparable for the two mortar strengths. The variation in compressive strength was attributed to different batches of cement being used through the study and was considered acceptable. A similar effect was found in the uniform loading tests as discussed in Chapter 6. The average strength of all the mortar cubes tested exceeded the prescribed strength given by the M number according to the national annex to BS EN 1996-1-1 (BSI, 2005d). In addition the variation in the strength of the individual mortar cubes differed between tests, as represented by the coefficient of variation values given in Table 7.1. Although the COV values were acceptable, it was not clear why such variation occurred between cubes manufactured from the same batch of mortar, which were prepared using the same method. The COV values were more consistent for the mortar cubes manufactured with the cavity wall specimens, where 6 instead of 3 cubes were tested. This suggests that increasing the sample size could provide a better understanding of the natural distribution of the data.

## 7.1 Block specimens

### 7.1.1 Failure mode and load deflection response

The failure modes observed for the AAC block (H1 and H2) and brick block (H3 and H4) wall panels, constructed with M2 compressive strength mortar, are shown in Figure 7.1. Initial horizontal cracking was observed to occur in the lower section of the wall panels and was at a height approximately equal to the mid point of the ultimate water level. The material used for the block appeared to influence the crack pattern at the ultimate water level. Cracks tended to form through the units and mortar joints for the AAC block panels (H1 and H2), whilst were generally restricted

to the mortar joints for the brick block specimens (H3 and H4) reflecting the relative strengths of the blocks and mortar. The failure modes were similar to those found for the uniform loading tests presented in Chapter 6 Section 6.2.1.1, but were offset towards the bottom of the panel. This was due to the hydraulic loading being concentrated towards the base of the panel and the upper section not experiencing any direct lateral loading.

**Table 7.1.** Summary of results from hydraulic loading tests

| Specimen reference | Masonry / mortar type | Additional description | Water level (mm) | | Mortar cube | |
|---|---|---|---|---|---|---|
| | | | Initial cracking | Ultimate | Compressive strength (N/mm$^2$) | COV (%) |
| H1 | AAC block / M2 | | 175 | 175 | 2.61 | 11.3 |
| H2 | AAC block / M2 | | 180 | 187 | 3.06 | 3.8 |
| H3 | Brick block / M2 | | 209 | 245 | 2.81 | 12.1 |
| H4 | Brick block / M2 | | 191 | 250 | 3.24 | 3.2 |
| H5 | Brick / M2 | | 208 | 208 | 3.19 | 3.8 |
| H6 | Brick / M2 | | 202 | 202 | 2.80 | 0.7 |
| H7 | Brick / M4 | | 210 | 247 | 9.00 | 3.7 |
| H8 | Brick / M4 | | 201 | 240 | 7.89 | 6.0 |
| H9 | Brick / M4 | Zero axial load & top free | 190 | 209 | 7.87 | 2.4 |
| H10 | Brick / M4 | 1 storey plus roof and floor loads | 220 | 247 | 7.74 | 13.5 |
| H11 | Brick / M4 | Central opening | 210 | 249 | 8.82 | 14.4 |
| H12 | Brick / M4 | Central opening | 230 | 250 | 8.27 | 4.1 |
| H13 | Brick outer & AAC block inner / M2 | Cavity wall – inner leaf axially loaded | 180 | 218 | 2.55 | 6.2 |
| H14 | Brick outer & AAC block inner / M2 | Cavity wall – inner leaf axially loaded | 190 | 229 | 3.08 | 6.6 |
| H15 | Brick outer & brick block inner / M2 | Cavity wall – inner leaf axially loaded | 219 | 289 | 2.33 | 6.1 |

Note: all specimens axially loaded with the equivalent of 1 additional storey of masonry unless stated otherwise.

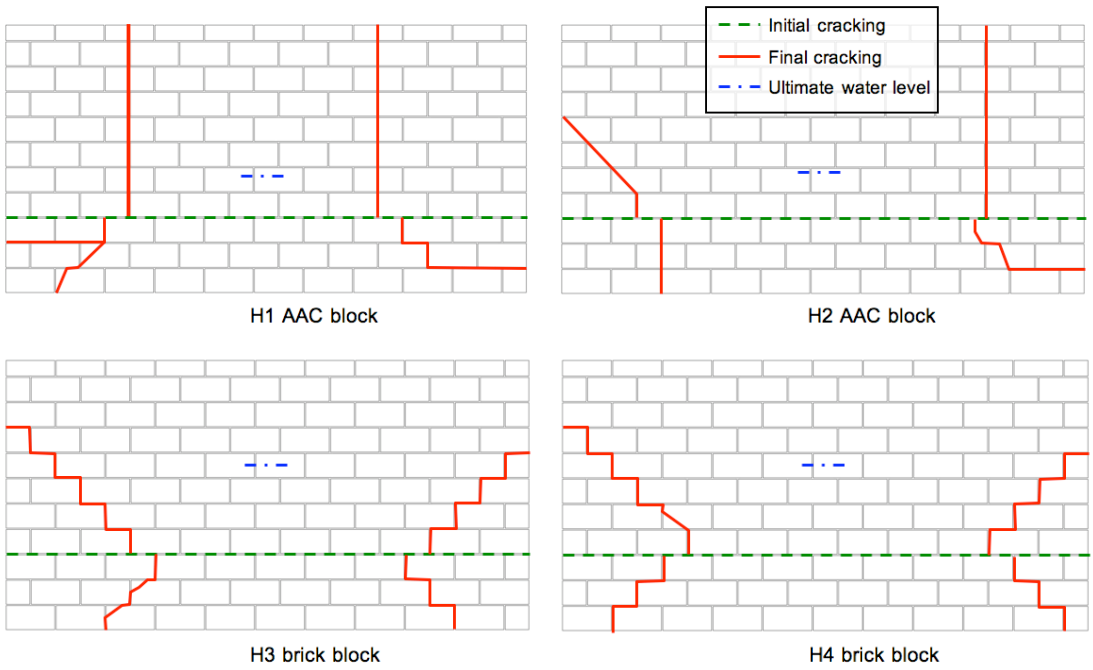


**Figure 7.1.** Failure modes observed for hydraulically loaded block specimens

Failure of the specimens was rapid and it was difficult to capture the process between formation of the final crack pattern and actual failure. This was in contrast to the behaviour shown in the uniform loading tests, where failure was more progressive. It was difficult to assess the magnitude of negative deflection at the panel corners as the mechanism displaced, due to this rapid behaviour. However negative deflection at the corners of the panels was observed immediately prior to failure when the final crack pattern was evident, as shown for specimen H4 in Figure 7.2. In the bottom section of the panel, negative deflection was likely due to the cracks not forming into the corners and a pivoting type action occurring about the supports. Similar behaviour only occurred in the upper sections of specimens H1 and H2 where the cracks formed in a direction towards the horizontal upper support. In specimens H2 (left edge), H3 and H4 the diagonal cracks tended towards the side supports in the upper section, such that negative deflection could only occur by curvature of this part of the panel and not by a pivoting effect.

The load z deflection responses for the hydraulically loaded block specimens are presented in Figure 7.3. The pre initial cracking load deflection behaviour comprised an initial linear stage, up until a water level of approximately 80 mm, followed by a curved response, where the stiffness gradually reduced as the water level increased. The response pre cracking was generally similar for all specimens, with the exception of specimen H4. The difference in the behaviour of specimen H4 was due

to the specimen moving back from the supports during the centrifuge start up procedure. It was not possible to apply any pre loading to the wall as in the uniform loading tests and it was difficult to maintain full contact prior to loading without affecting the actual support conditions. The pre cracking response was different to that found in the uniform loading tests, where the response was linear.

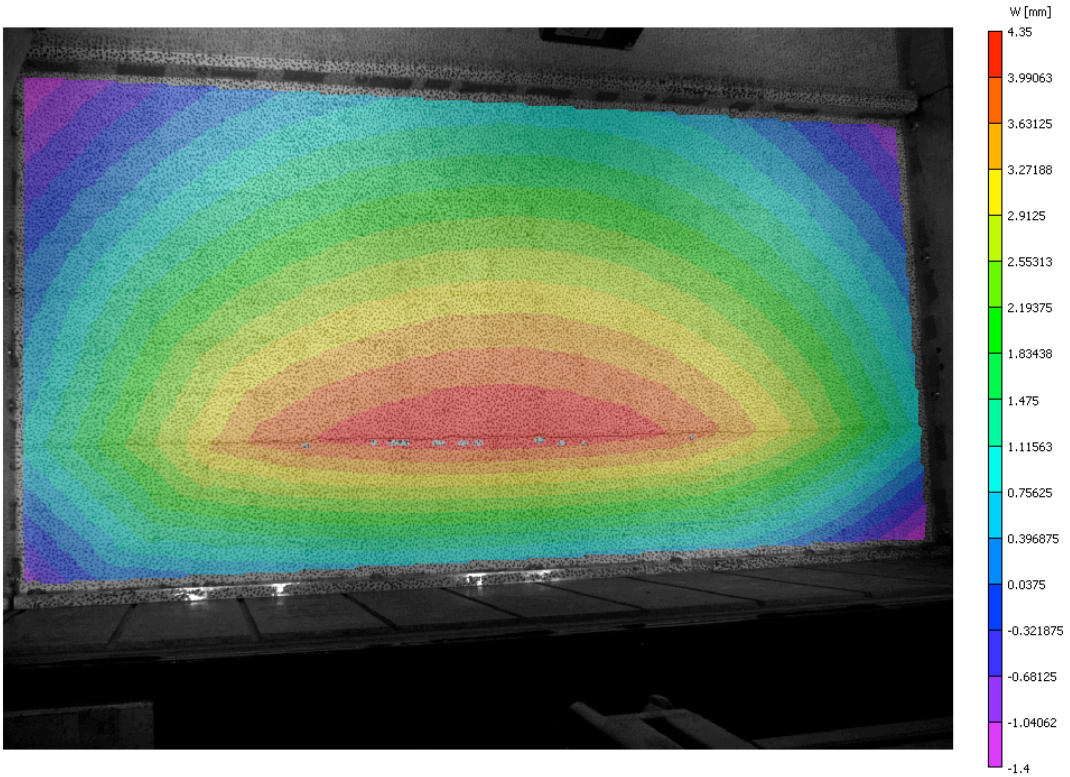


**Figure 7.2.** Contour plot of z deflections for brick block specimen H4 immediately prior to failure showing negative deflection at panel corners (water level of 250 mm)

At initial cracking the specimens deflected at constant load and the behaviour in the vertical section changed from a curved form to a mechanism where hinges formed, as shown in Figure 7.4. Post cracking the AAC block specimens H1 and H2 showed limited residual strength and only H2 was able to withstand further loading prior to failure. When subject to uniform loads, the AAC block panels showed a higher degree of residual strength than observed in these tests. The brick block specimens H3 and H4 provided a much greater capacity post cracking than the AAC block similar to that found in the uniform loading tests. The post cracking stiffness was however much lower than that found in the uniform loading tests and curved rather than linear in form. The higher residual strength in the brick block specimens was attributed to the higher flexural strength in direction 2, that was found in the tests of wallette specimens as given in Chapter 5. Peak deflections prior to failure were on average 40 % of those found in the uniform loading tests. It is likely that the position

of the initial crack influenced the peak deflection and the speed of the failure process. The section of the wall panel below the crack would be subject to higher in-plane rotations about the hinges at identical deflections as its height reduced. This would result in the lower section of the wall panel becoming unstable at lower levels of deflection, resulting in a more rapid progression to failure.

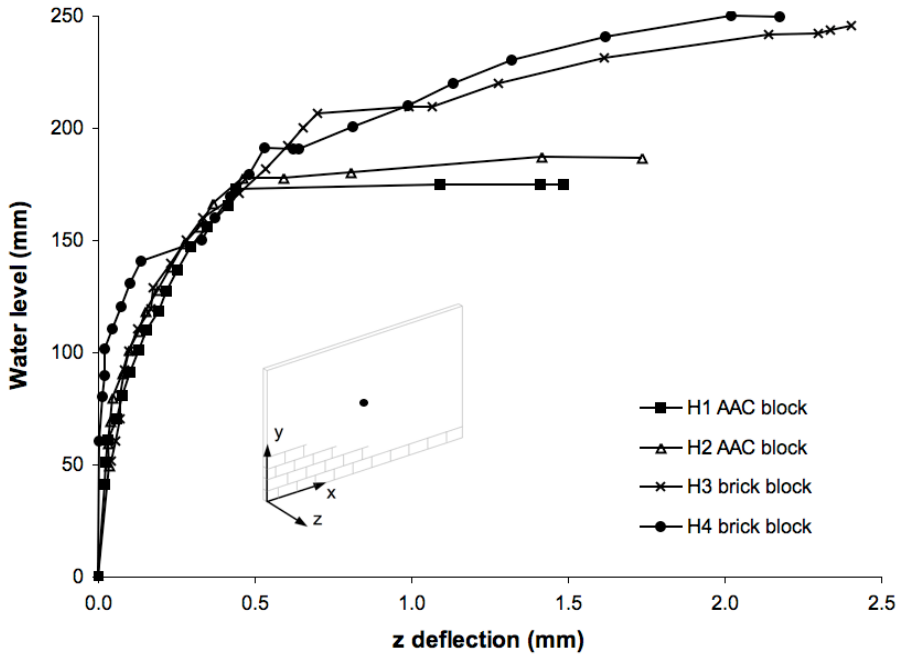


**Figure 7.3.** Load z deflection response for all hydraulically loaded block specimens

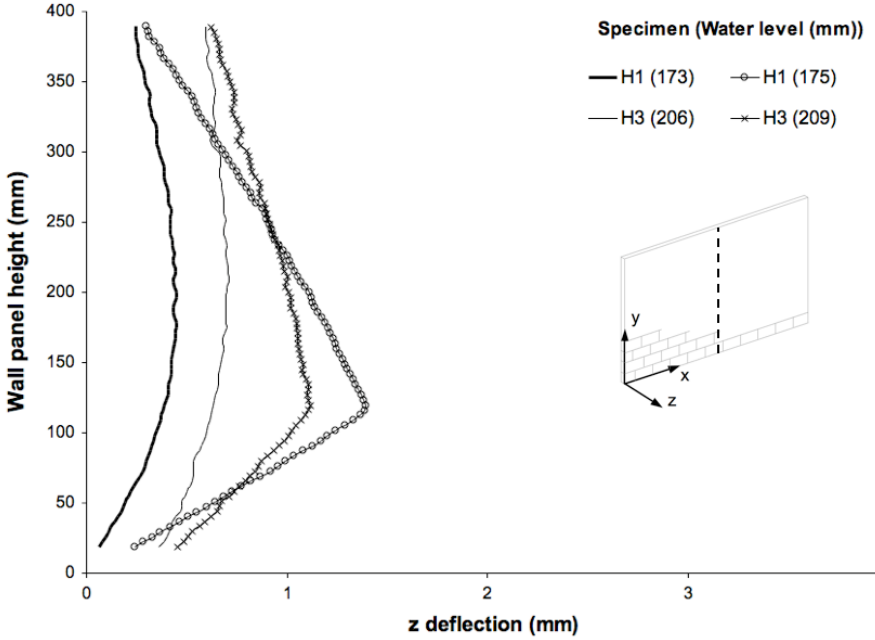


**Figure 7.4.** Wall panel height versus z deflection along vertical centre line for hydraulically loaded block specimens H1 (AAC block) and H3 (brick block) at different water levels

The repeat specimens failed at very similar water levels, where specimens H1 and H2 were within 7 % of each other, whilst specimens H3 and H4 were within 2 %. The mean ultimate water level was 181 mm for specimens H1 and H2 and 248 mm for specimens H3 and H4. In the only previous experimental study of blockwork walls subject to hydraulic loading (Pace, 1988) no repeats were conducted so it was difficult to establish the typical variation expected between specimens. In the absence of such data it was only possible to make a tentative comparison to the variation found in uniform loading tests, however such a comparison should be treated with caution due to the differing loading profiles. The variation between repeat hydraulically loaded specimens was much lower than determined for the uniform loading tests, as given in Chapter 6 Section 6.2.1.1, and was also much lower than those reported in the literature for uniform loading tests completed with AAC blockwork, where repeat specimens were within 14 % on average (de Vekey et al., 1986).

Very limited information was given for the only previously completed tests for hydraulic loading on concrete block conducted at prototype scale, with regards to the unit dimensions, type of mortar or block used (Pace, 1988). The results may also be questionable, since the tests were stopped before failure due to severe water leakage through the walls. The load-deflection response shown was however similar to that of specimens H1 and H2 with no residual capacity after an initially curved behaviour. The peak level of 1.10 m was of a similar magnitude to the scaled mean of specimens H1 and H2 at 1.09 m. It was suggested that 0.61 m was a characteristic water level for blockwork walls, but without any reasoning or justification. The results shown here illustrate that the block strength affected the ultimate water level and one characteristic level for all would clearly not be appropriate.

The deflection at the peak of the initial response in the previous study (Pace, 1988) was approximately 0.22 mm (at 1:6 scale) and was lower than those found for specimens H1 and H2 in this programme. Several reasons could account for the higher deflection found for H1 and H2, firstly small movements at the supports amplifying the central displacements, secondly a scaling effect resulting in a softer response as discussed in Chapter 6, and finally differences in the materials used for the block and mortar. When the movements at the supports were accounted for, by subtracting the initially observed movements from all other values of deflection, then

the central deflection reduced by approximately 17 %, but still exceeded the value given in the previous study (Pace, 1988).

A direct comparison of the utimate loads from the hydraulic and uniform loading tests was challenging due to the difference in loading distribution. It has been proposed that the pressure at half of the maximum water level, essentially the average hydraulic pressure, can be compared to the corresponding uniform values (Kelman and Spence, 2003a). Following this then the average ultimate water levels correspond to pressures of 5.33 and 7.28 kN/m$^2$ for the AAC and brick block specimens respectively. These values were significantly higher than the average ultimate loads from the corresponding uniform loading tests given in Chapter 6, which were 1.84 and 4.82 kN/m$^2$ for AAC and brick block respectively. It would be expected that the ultimate loads would be comparable between the two types of loading and clearly comparing the loads by such a method was not appropriate.

An improved method to allow comparison of the results between the uniform and hydraulic loading tests would be to consider the total loading applied to the wall panel in each case. For the uniformly loaded specimens the total load was simply the product of the uniform load and the area of the wall panel. In the case of the hydraulically loaded specimens it was necessary to determine the area of the loading profile from the depth and then multiply this by the panel length to obtain the total applied load. Using this method the total ultimate load for specimens H1 and H2 (AAC block) was 0.76 kN, which was 28 % higher than the corresponding ultimate load of 0.60 kN calculated from the results of the uniform loading tests (average for specimens W3 and W4). Similarly for the brick block specimens (H3 and H4) the total ultimate load was computed as 1.43 kN, which was 9 % lower than the total ultimate load of 1.56 kN for the uniformly loaded specimens (W6 to W8).

### 7.1.2 In-plane response of block specimens

The load y deflection responses for AAC block (H1) and brick block (H3) specimens are shown in Figure 7.5, where the y deflection was measured at the top of the wall panel. Similar responses were found for specimens H2 and H4, and these have been omitted from Figure 7.5 to improve the clarity. A negligible shortening effect in the y direction was typically observed in the block specimens prior to any cracking occurring. As discussed in Chapter 6 negligible deflections in the y direction were also found in the uniformly loaded block specimens prior to cracking. Following initial cracking extension occurred in the block specimens as a result of the formation of hinges. Significantly lower extensions were recorded compared to those found in the

uniform loading tests prior to failure. Lower y extensions were likely due to the rapid transition from a cracked to a failed state preventing significant displacement of the mechanism. The non-uniform loading distribution would result in the lower section of the wall panel being subject to a higher bending stress and may have caused the rapid failure observed. This was in contrast to the uniform tests the bending stress would be more consistent over the area of the wall panel, where a progressive failure was shown.

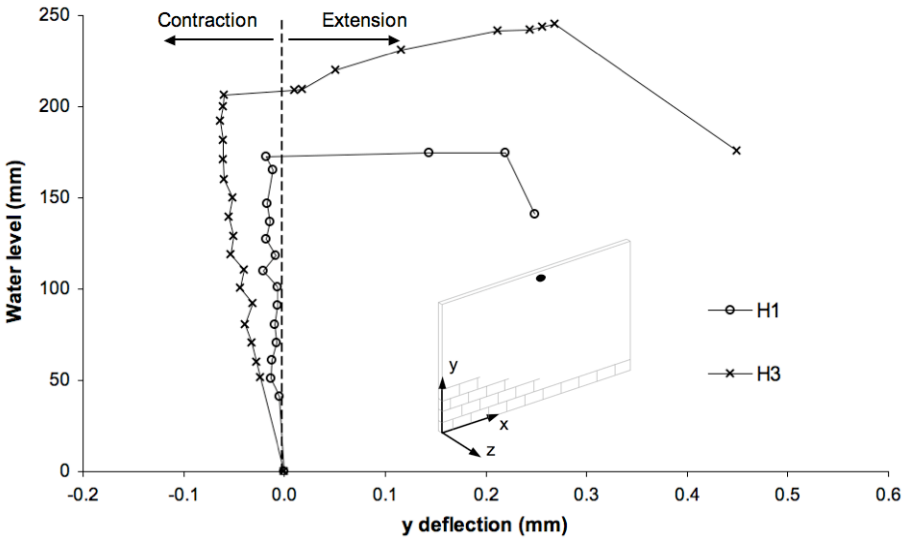


**Figure 7.5.** Load y deflection response measured at top of wall panels H1 (AAC block) and H3 (brick block) using DIC analysis

The load x deflection responses for specimens H1 and H3, measured at the left and right of the panel edges at mid height, are shown in Figure 7.6. The response of the both the AAC block and brick block panels in the x direction was negligible prior to initial cracking occurring. Post initial cracking, the AAC block and brick block specimens were both observed to extend in the x direction. In the uniform loading tests, discussed in Section 6.2.1.2, it was found that both the AAC and brick block specimens similarly extended following initial cracking and it was assumed that this was as a result in cracking in the specimen. It is suggested that similar cracking occurred in the hydraulically loaded block specimens, likely in the perpendicular mortar joints, which permitted the specimens to extend.

The extensions at ultimate water level were found to be 16 % lower in the y direction when compared to the x direction for the AAC block, whilst for the brick block the extensions in the y direction was almost double that in the x direction at 96 %. In the

uniform tests, as discussed in Section 6.2.1.2, it was found that the extension was 17 % higher in the y direction compared to the x direction for both the AAC and brick blocks and was suggested as being due to formation of hinges earlier in the y direction. The almost simultaneous and rapid development of the yield line type failure mechanism in both directions in specimen H1 could account for the difference to the uniform tests, since the initial vertical mechanism did not form independently. Initial cracking and failure were not coincident in the brick block specimen, which allowed y deflections of greater magnitude to occur prior to failure when compared to the AAC block specimen. The rapid failure process in the brick block specimen prevented significant deflections from occurring in the x direction and contributed to the different behaviour observed, when compared to the AAC block.

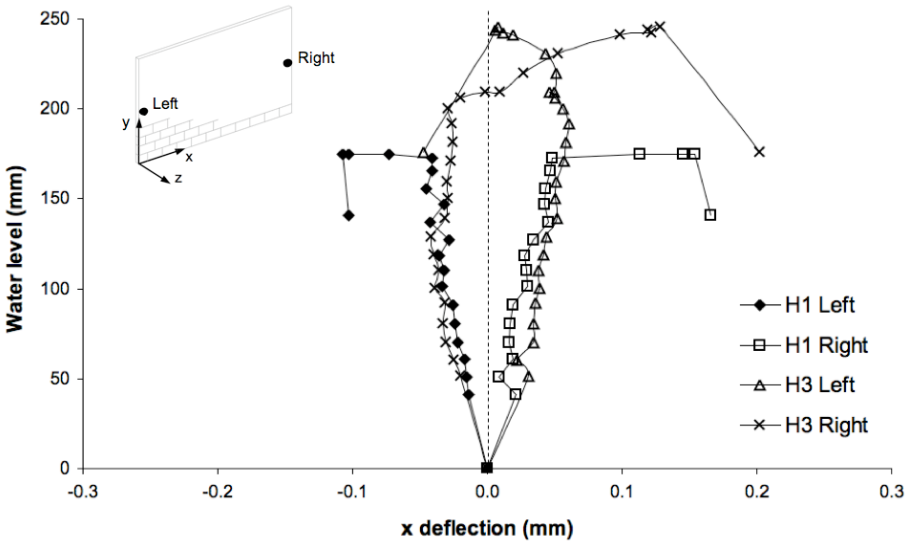


**Figure 7.6.** Load x deflection response measured at mid height at left and right edges of wall panels H1 (AAC block) and H3 (brick block)

Strains were measured over a 40 mm gauge length and computed using the Vic 3D software, similarly to that completed for the small assemblage tests, as presented in Chapter 5. The load in-plane strain response for specimens H1 and H3 are presented in Figure 7.7a and 7.7b respectively. The initial (pre cracking) load-strain response in the y direction was similar for the AAC block (H1) and brick block (H3) specimens, where negligible strains were recorded at the centre of the panel and the site of the initial crack. Following cracking the y direction strains at the centre of both panels remained small, however the strains at the site of the initial crack increased in magnitude. The behaviour observed suggested that the lateral loading was causing displacement of the mechanism formed following cracking, rather than any bending

of the sections above and below the crack. The strains measured in the x direction were also found to be of negligible magnitude at the centre of the AAC block (H1) and brick block (H3) specimens, as shown in Figures 7.7a and 7.7b respectively. The x direction strains were only observed to increase just prior to failure at the perpendicular mortar joints between the units, as shown in Figure 7.8. The largest x direction strains occurred in the bottom section of the wall panel, due to the non uniform loading distribution, and were in line with the position of the diagonal cracks at failure, presented in Figure 7.1

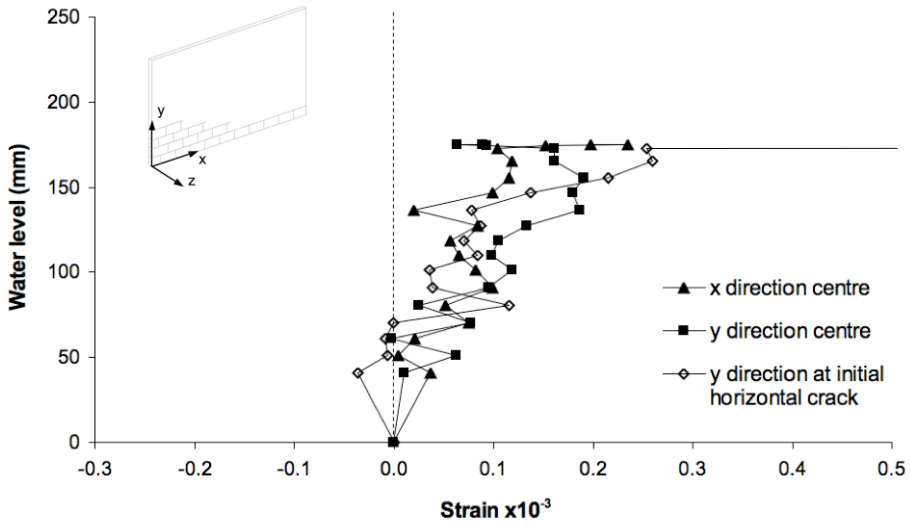


(a)

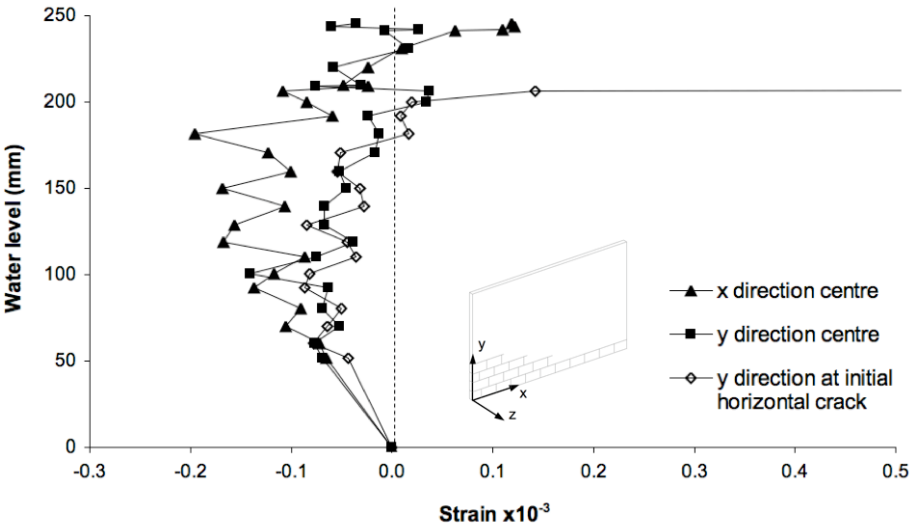


(b)

**Figure 7.7.** Load in-plane x and y direction strains measured during test, (a) specimen H1 AAC block and (b) specimen H3 brick block

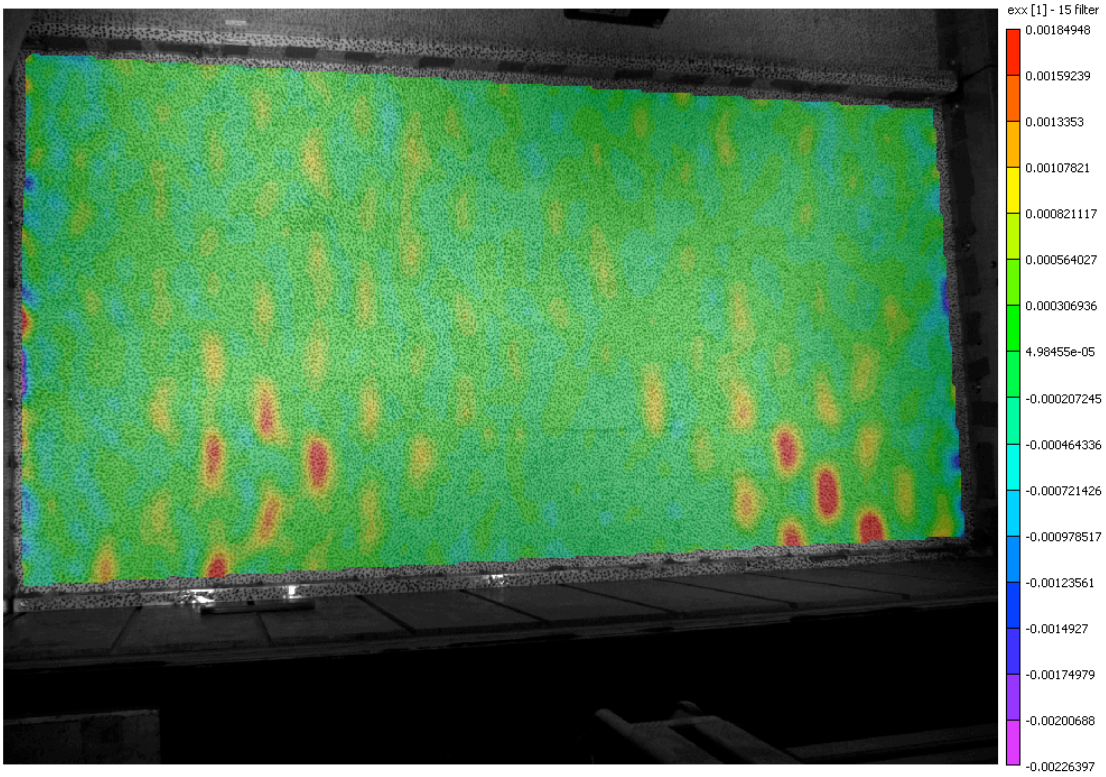


**Figure 7.8.** Contour plot of strain in the x direction for brick block specimen H3 at a water level of 241 mm just prior to failure

## 7.2 Brick specimens

### 7.2.1 Failure mode and load deflection response

#### 7.2.1.1 Effect of mortar strength

The failure modes for the brick wall panels that were constructed with M2 compressive strength mortar, specimens H5 and H6, and M4 compressive strength mortar, specimens H7 and H8, are shown in Figure 7.9. The test conditions (edge supports and imposed vertical axial load) for the specimens were otherwise identical. Cracking was found to initiate horizontally across the wall panels in the lower section and was generally near to the mid point of the ultimate water level. For specimen H5 no cracking was apparent in the specimen prior to failure occurring and horizontal and diagonal cracking occurred simultaneously. The position of the initial crack was also found to be at a height of approximately double the height to the centroid of the hydraulic loading profile at the time of cracking. At the ultimate water level there was generally a combination of diagonal cracking through the mortar joints only and cracking through the units and mortar joints. The crack patterns were similar for M2 and M4 mortar strengths, although it was apparent that some additional cracking occurred in the panels with M4 mortar at failure. Some similarities were observed to the failure modes of the brick block specimens discussed above, however in the brick

block specimens cracking was generally restricted to the mortar joints only. The crack patterns were reasonably similar to those found in the uniform loading tests, as discussed in Section 6.2.2.1, but the pattern was offset towards the base of the specimens in the hydraulic loading tests. As discussed above it was suggested that the loading distribution affected the position of the crack pattern.

As was found with the block specimens failure was rapid and the behaviour between the final crack pattern being evident and collapse was not always captured. Negative deflection at the corners of the panels was however generally observed both immediately prior to and after failure, as shown in Figure 7.10. Negative deflection would be expected at both lower corners and the upper right corner of specimen H7 due to the crack pattern observed, where a pivoting type action would be permitted. At the upper left corner curvature may have accounted for the negative deflection found, as discussed above, however it was evident after failure that this section of the panel was also pivoting about the supports, as shown in Figure 7.10b.

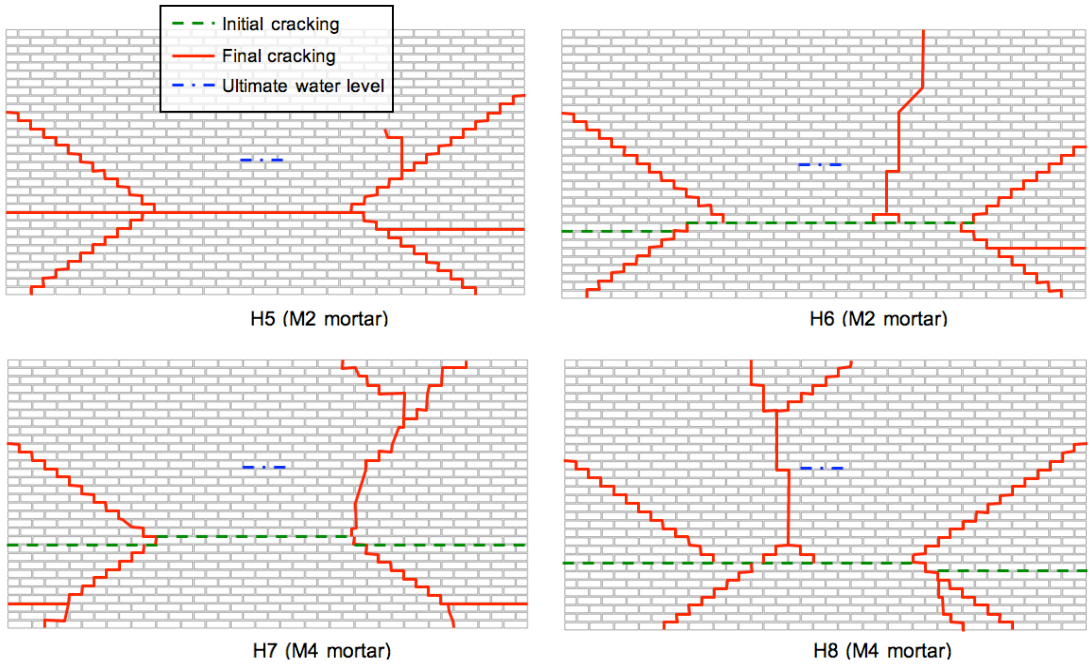


**Figure 7.9.** Failure modes observed for hydraulically loaded brick specimens with different mortar strengths

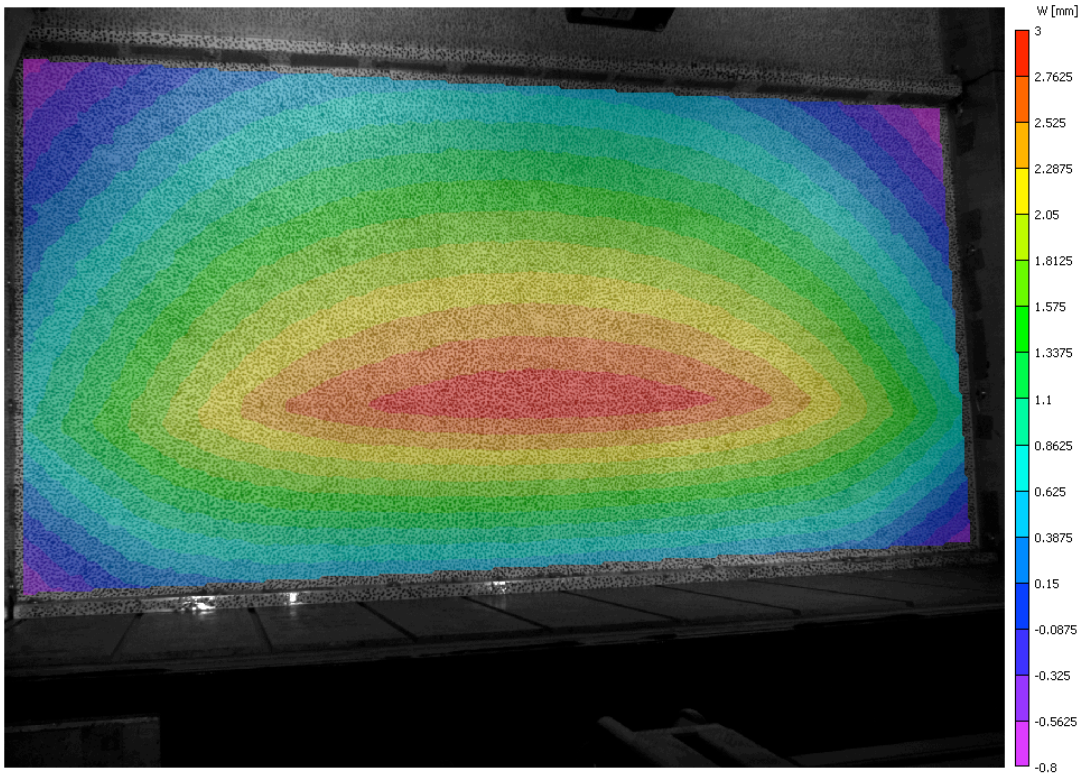


(a)

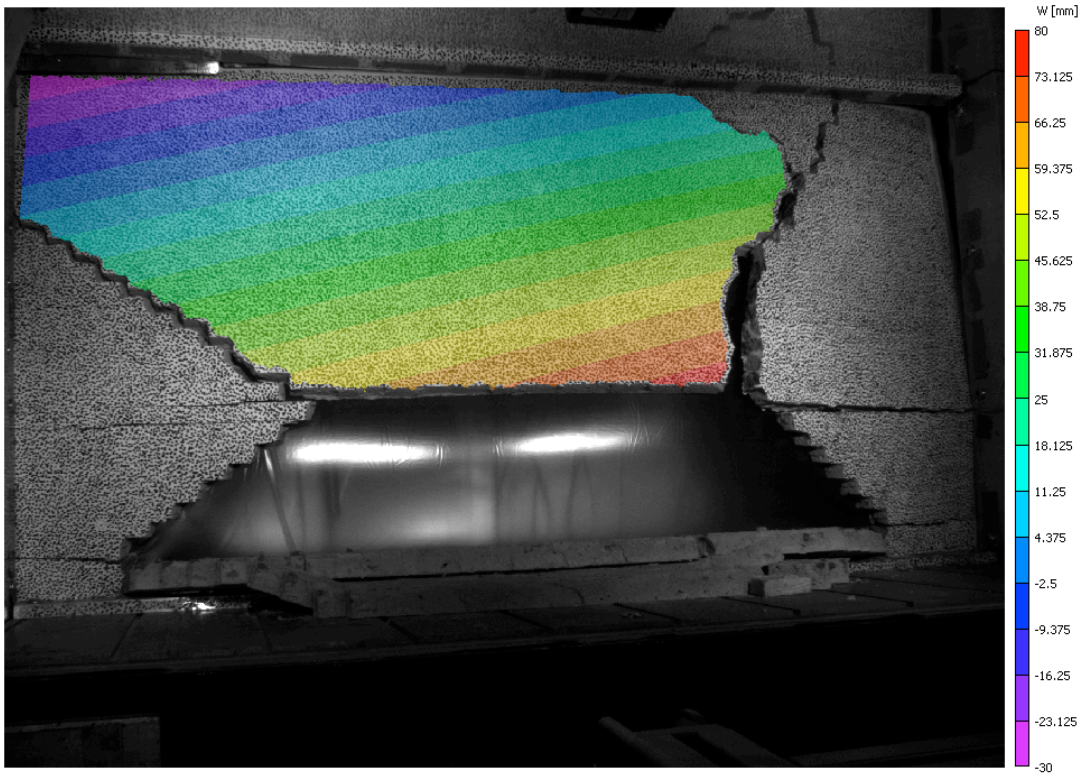


(b)

**Figure 7.10.** Contour plot of z deflections for brick specimen H7 (M4 strength mortar) showing negative deflection at panel corners, (a) immediately prior to failure and (b) following failure

The load z deflection responses for the brick wall panels constructed with M2 and M4 compressive strength mortar are shown in Figure 7.11. The response was initially approximately linear and of similar stiffness for all specimens regardless of mortar strength up until a water level of 100 mm. Following this, the stiffness of the specimens tended to decrease in a non-linear manner until initial cracking was evident. For the wall panels constructed with M2 mortar, specimens H5 and H6, initial cracking and failure was at approximately constant load and no residual strength was apparent. The response for specimens H5 and H6 was very similar despite the slight differences observed in the failure modes.

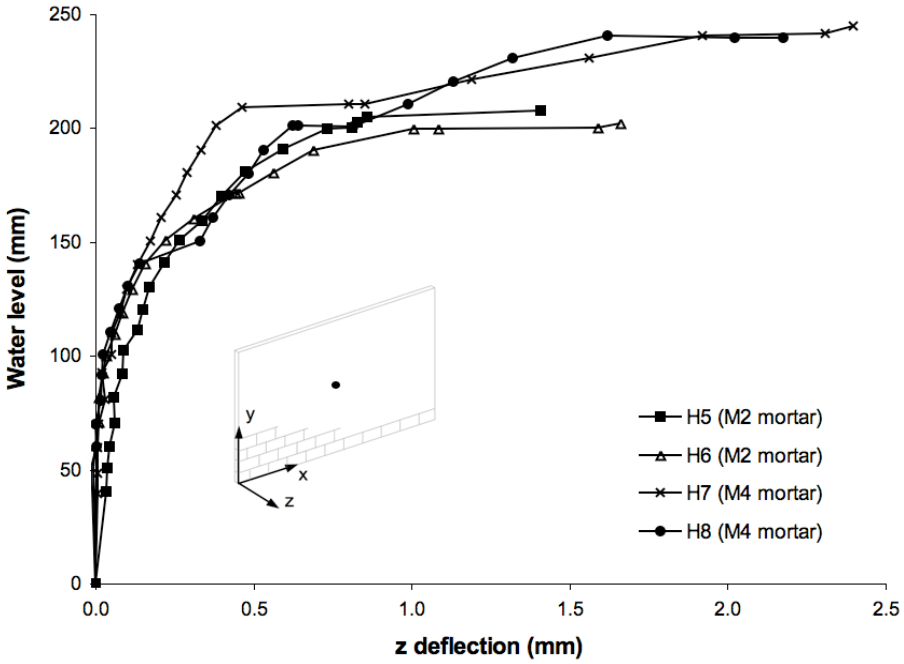


**Figure 7.11.** Load z deflection response for hydraulically loaded brick specimens with different mortar strengths

The pre cracking response of the wall panels constructed with M4 mortar, specimens H7 and H8, was similar until a water level of 140 mm where a step change occurred likely due to bedding in at the upper support. The response that followed was however of comparable stiffness and both specimens showed residual strength capacity following initial cracking. It was found that as the mortar strength was increased, from M2 to M4 compressive strength class, that there was an average 19 % increase in the ultimate water level, although the water level at initial cracking was similar. The ability of the higher mortar strength specimens to sustain further loading was likely due to the increased flexural strength in direction 2, as was found in the tests of wallettes in Chapter 4. The consistency of the results, as given in Table 7.1,

suggests that the improvement in ultimate water level was due to increased mortar strength, rather than being due to natural variation.

When compared to the block specimens it was observed that the response of brick specimens with M2 strength mortar were similar to that of the AAC block, whilst the response of the brick specimens with M4 strength mortar were more comparable to that of the brick block. The uniform loading response showed some similarities to the M2 strength mortar panels, but a lower degree of softening was found prior to initial cracking. Residual strength following cracking was also not apparent in the uniform loading tests of specimens with M2 strength mortar. The response of the uniformly loaded M4 mortar strength specimens prior to cracking differed as the behaviour was linear, although a similar residual strength capacity was found post cracking. A greater difference between the loads at initial cracking was recorded in the uniform loading test, where as in the hydraulic tests they were comparable. The average peak deflections were 64 % of those recorded in the uniform loading tests. It was likely that the reduction was due to differences in the failure mode and speed of the collapse process as was described for the block specimens above.

The ultimate water levels, as given in Table 7.1, correlated well for the repeat specimens, where the ultimate water levels for specimens H5 and H6 were within 3 % of each other, whilst specimens H7 and H8 were within 3 %. The average ultimate water level for specimens H5 and H6 was 205 mm and for specimens H7 and H8 was 244 mm. The variation in the results was similar to that found for the blockwork specimens and for the uniform loading tests discussed in Section 6.2.2.1, proving the repeatability of the experimental procedure. Again, no data was available in the literature with regards to the variability of hydraulically loaded brick specimens. Assessment of the magnitude of the variability for the hydraulic loading tests was therefore only possible by comparison to the values from uniform loading tests. The variability was lower than that reported for uniform loading tests in the literature, where the average difference between the experimental ultimate loads was 39 % (West et al., 1977).

The average ultimate water levels when converted into a total load, using the method described previously, were 0.98 and 1.38 kN for the M2 and M4 mortar strength brick specimens respectively. These values compared well to the total average ultimate loads recorded in the uniform loading tests of 0.92 and 1.51 kN for M2 and M4 mortar strength brick specimens respectively. The total loads for the uniform tests

were calculated from the average experimental uniformly distributed loads of 2.84 and 4.65 kN/m$^2$ for M2 and M4 mortar strength specimens respectively, as detailed in Chapter 6.

Only one other experimental investigation applying hydrostatic loading to brick walls has been identified in the literature, although it was conducted at prototype scale (Pace, 1988). The mortar mixture used in the study was not given, however the average compressive strength of the mortar recorded of 7.58 N/mm$^2$ was similar to that of specimens H7 and H8. Direct comparison to the results from specimens H5 to H8 was not possible for several reasons: additional support was provided to the rear of the walls through a braced timber studwork connected to the masonry by wall ties, the walls were longer at 7.93 m (1321 mm at 1:6 scale), no vertical surcharge was applied to the panel, and the panels were constructed from slightly thinner bricks. However, for the single brickwork specimen tested that had comparable edge support conditions the ultimate water level that was sustained before failure was 1.45 m (241 mm at 1:6 scale). The ultimate water level was very similar to the average results for specimens H7 and H8 despite the differences noted above. In the study (Pace, 1988) it was found that the specimen failed rapidly at the maximum load and prior to this the load-deflection response followed a smooth curve similar to that found for specimens H5 and H6. The crack pattern at failure was not formally recorded, although in the images included in the report it is possible to identify that the panel failed diagonally in the upper section. A full comparison to the patterns observed for specimens H5 to H8 was not possible due to the limited information given. The peak deflections recorded of 0.1 mm (1:6 scale) were significantly lower than those found for specimens H5 to H8. Comparison was made with caution since it was not clear whether measurements were recorded up to a state of collapse. In the uniform loading tests in Chapter 6 it also was noted that the deflections recorded were higher than those from comparable tests in the literature.

#### 7.2.1.2 Effect of different top support conditions and vertical axial load

Two brick specimens were tested to examine the effect of the upper support conditions and vertical axial load when compared to the results from specimens H7 and H8. Specimen H9 was tested with no vertical axial load and the top free, whilst specimen H10 was tested with increased vertical axial load. The specimens were constructed with the same M4 compressive strength class mortar as was used to manufacture panels H7 and H8. The failure modes observed for brick specimens H9 and H10 are shown in Figure 7.12. The failure mode in the lower section of specimen

H9 was similar to that found for H7 and H8, whilst in the upper section of the panel it was considerably different. The differences observed in the upper section were due to the removal of the top support in the test of specimen H9.

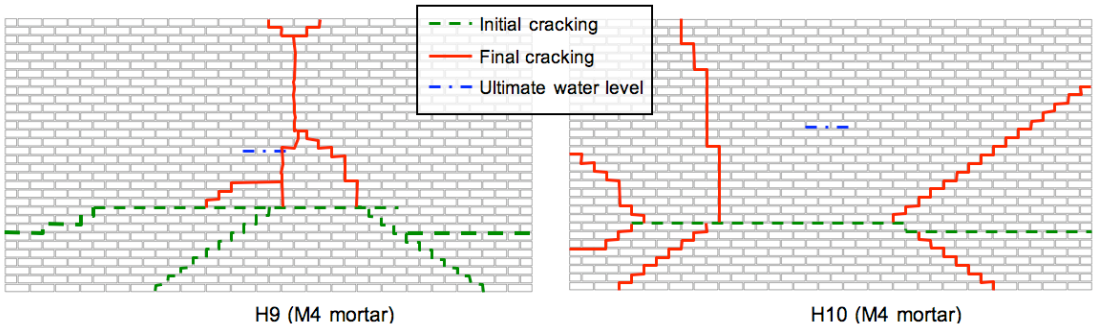


**Figure 7.12.** Failure modes observed for hydraulically loaded brick specimens with varying vertical axial load and the top free (H9) or simply supported (H10)

The crack pattern for H9 was similar to those found for uniformly loaded specimens that were tested with the top free (West et al., 1977). In the previously conducted study of hydraulic loading discussed above a specimen was tested with the top free (Pace, 1988). Again, limited information was given on the failure mode and in the only photograph included in the report it appeared that diagonal cracks had propagated from the base of the panel towards the top, although the lower section of the panel was obscured. It was likely that the length of the panel resulted in the difference in failure mode between specimen H9 and that reported in the previous study (Pace, 1988). The failure mode for specimen H10, as shown in Figure 7.12, was similar to those found for specimens H7 and H8. There appeared to be little effect on the failure mode when the vertical axial load was increased, suggesting that the support conditions were more influential.

The load z deflection responses for specimens H9 and H10, along with the response of specimen H7 for comparative purposes, are presented in Figure 7.13. Specimen H9 was of lower stiffness both before and after initial cracking, when compared to specimen H7. The initial cracking and ultimate water levels were reduced by 10 and 15 % respectively in comparison to specimen H7. It was likely that the omission of the vertical load resulted in the reduced water level at initial cracking, but the reduced stiffness was a combined effect of zero vertical load and lack of support on the top horizontal edge. In addition since a large proportion of the cracks had formed prior to failure it would be expected that the ultimate water level would not be as high as found for specimen H7 where all diagonal cracking occurred simultaneously. The

wall panel tested in the previous study (Pace, 1988) with the top free was not directly comparable for the reasons discussed above, however an ultimate water level of 0.73 m at prototype scale (122 mm at 1:6 scale) was reached before failure. This was considerably lower than the value attained by specimen H9. Previous researchers identified that there was a reduction in the ultimate load of uniformly loaded specimens as the length of the panel increased (West et al., 1977). The significantly shorter panel length and difference in failure mode would likely account for the higher ultimate water level sustained by H9 prior to failure.

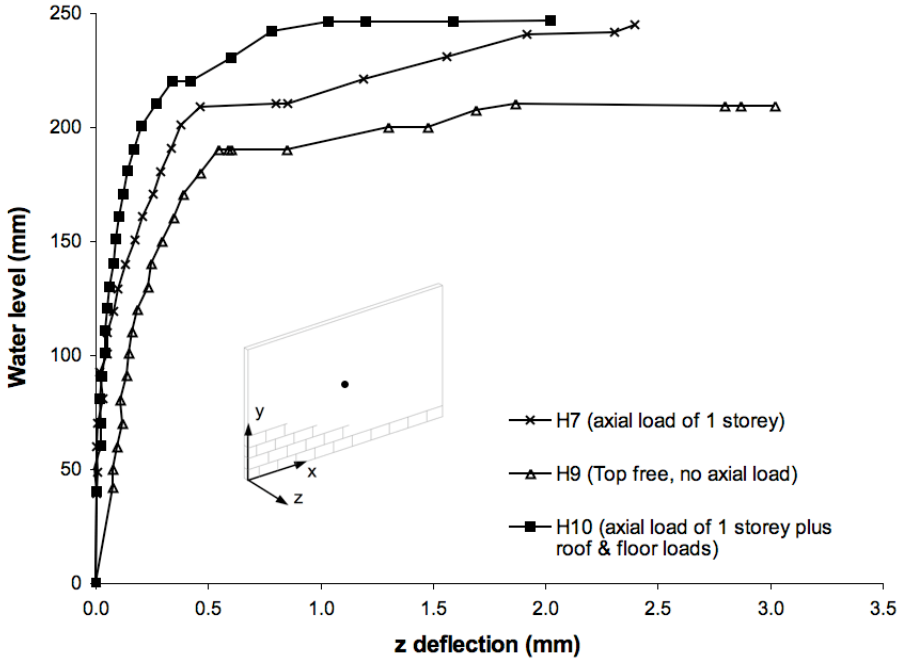


**Figure 7.13.** Load z deflection response for hydraulically loaded brick specimens with varying vertical axial load and the top free or simply supported

The response of specimen H10 both prior to and following initial cracking was stiffer than that of specimen H7, suggesting that the increased vertical axial load affected the behaviour, as shown in Figure 7.13. The vertical axial stress applied to the top of specimen H10 was 0.106 N/mm$^2$, which was more than double that applied to H7 at 0.044 N/mm$^2$. The water level at initial cracking was marginally higher than that of specimen H7 likely as a result of the higher vertical stress in the panel. The ultimate load was however similar and may have been due to the vertical stress having limited effect on the strength of the wall in direction 2. In previous uniform loading tests of wall panels unsupported at the vertical edges it was found that increasing the vertical stress had a positive effect on the ultimate load (West et al., 1971). In the tests the wall panels formed 3 pinned mechanisms and failure only occurred

horizontally along the mortar bed joint. This supports the suggestion that the improvement in the load capacity of specimen H10 up to initial cracking was due to the increased vertical load.

Only one study was identified in the literature that considered the effect of varying the magnitude of precompression on the ultimate load for 2 way spanning wall panels subject to uniform lateral loadings (Hendry et al., 1971). The magnitude of the stress applied to the wall panels tested in the previous study (Hendry et al., 1971) was significantly greater, at 0.48 and 0.54 N/mm$^2$, compared to that applied in this study. It was found in the previous study (Hendry et al., 1971) that there was a 16 % improvement in the ultimate load when the applied stress was increased from 0.48 and 0.54 N/mm$^2$. However the results given (Hendry et al., 1971) should be treated with caution since they were only based on two tests in total (one at each stress level) and no control test was completed with zero applied stress. The typical level of variability between experimental tests, as given above, could also easily account for the 16 % improvement in the ultimate loads previously found (Hendry et al., 1971). It was not possible to consider higher levels of applied stress using the centrifuge test jig designed for this study and such magnitudes of stress would only be possible by incorporating a hydraulic or pneumatic jack arrangement.

#### 7.2.1.3 Effect of openings in wall panels

Two specimens (H11 and H12) were tested with a central opening to assess the effect when compared to the specimens without openings (H7 and H8). The same size opening was used in both specimens and they were constructed with M4 compressive strength class mortar. The failure modes that were observed for the wall panels H11 and H12 with openings are shown in Figure 7.14. Initial cracking occurred horizontally and was generally in line with the base of the opening for specimens H11 and H12. At failure cracks propagated from or near to the corners of the openings towards the supports. It was expected that cracking would generally initiate from the opening since it would introduce a natural weakness into the wall panel. The crack patterns were quite similar in the lower sections of H11 and H12, but different in the upper section.

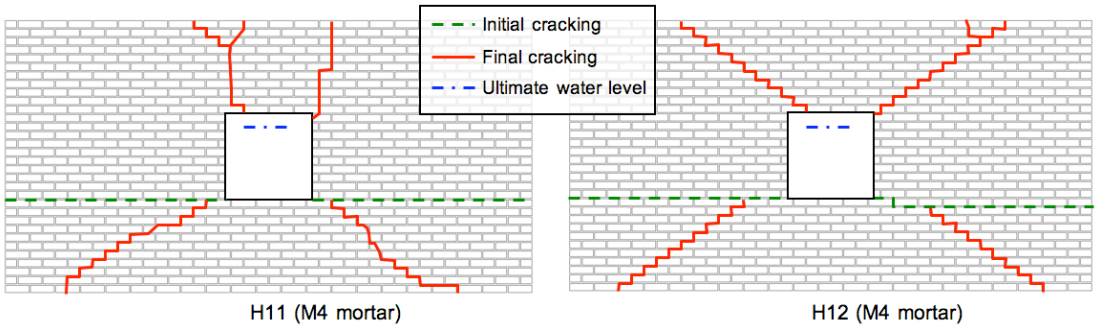


**Figure 7.14.** Failure modes observed for hydraulically loaded brick specimens with openings

There were some similarities to the crack pattern observed in the uniform loading test (specimen W14) as detailed in Chapter 6, where cracks initiated at the corner of the opening. Initial cracking occurred towards the top of the uniformly loaded panel, where as for H11 and H12 it was towards the base, likely due to the loading distribution. This difference in behaviour, between the uniform and hydraulic loading tests, was in agreement with that observed for the panels without openings. At failure there was a significant amount of cracking along the bed joints in the uniformly loaded specimen, where as for H11 and H12 the cracks were generally in the diagonal or vertical direction.

The load z deflection responses for specimens H11 and H12 with openings, and H7 without an opening are presented in Figure 7.15. The load z deflection response of both the panels with openings was observed to be very similar. The initial stiffness was similar to specimen H7 without an opening, but then the stiffness of H11 and H12 started to decrease prior to initial cracking occurring. It was found that there was no deflection at constant load as initial cracking occurred in the specimens with openings and the behaviour was more akin to H5 and H6 where the response followed a smooth curve. The difference in the height of the initial crack on the right hand side of the panels, of one course of bricks, did not appear to affect the response. Following initial cracking the stiffness was comparable for the specimens with and without openings and some residual strength capacity was observed.

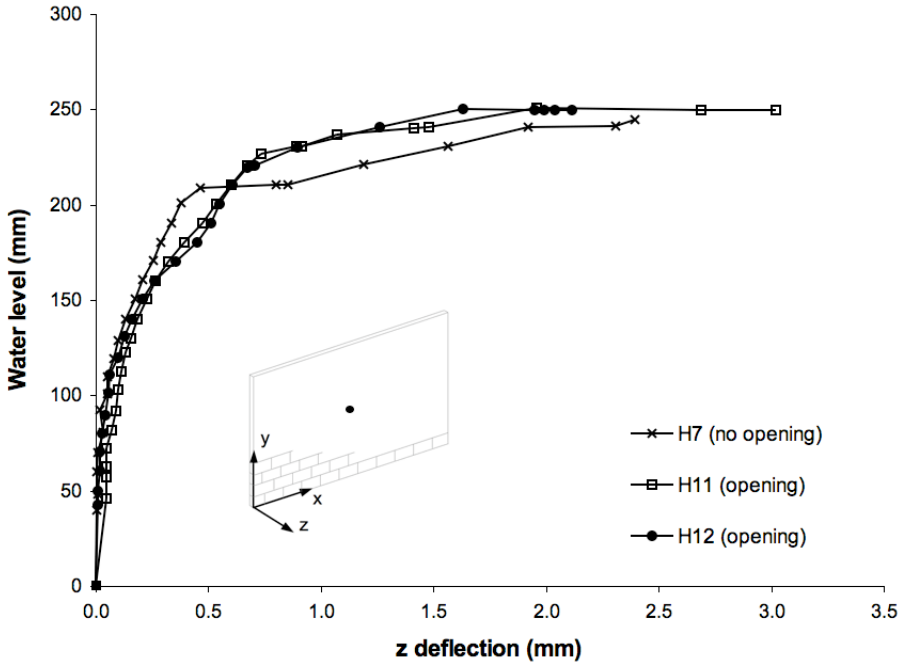


**Figure 7.15.** Load z deflection response for hydraulically loaded M4 mortar strength brick specimens with and without openings (average of deflections to the left and right of opening shown)

In the uniform loading tests, as discussed in Section 6.2.2.1, it was found that the inclusion of an opening similarly had little effect on the load-deflection response and ultimate load. It was suggested that this was due to the small dimensions of the opening relative to those of the panel and the use of a stiff board to cover the opening. The board may have effectively stiffened the wall panel at the location of the opening, where as in removing a section of masonry from the centre of the panel a reduction in stiffness would be expected. The same reasons for the similarity in response and ultimate water level would also apply to the hydraulic tests described here. The equivalent total ultimate load for specimens H11 and H12 was 1.45 kN, calculated using the method above, and was comparable to that recorded in the uniform loading test, of 1.50 kN. The total ultimate load for the uniformly loaded specimen (W14) was calculated from the uniformly distributed ultimate load of 4.62 kN/m$^2$, as given in Chapter 6 Table 6.1.

The ultimate water level of specimens H11 and H12, as given in Table 7.1, compared very well and were within less than 1 % of each other, with an average ultimate water level of 250 mm. This suggests that differences in the crack pattern observed at failure in specimens H11 and H12 had a limited effect on the ultimate capacity of the panel. A wall panel with an opening was subjected to hydraulic load in a previous

study (Pace, 1988), but was tested with the top edge free and was therefore not directly comparable to specimens H11 or H12. However, it was stated (Pace, 1988) that the wall panel failed at a similar load to the specimen tested without an opening. Very limited information was again given on the failure mode and how the opening was covered during test.

### 7.2.2 In-plane response of brick specimens

Figure 7.16 shows the load y deflection response for brick wall panels with and without openings, with differing imposed vertical loads and different support conditions at the top edge. Negligible y deflections were observed in all brick specimens prior to initial cracking occurring. The largest reduction in height prior to initial cracking was in the order of 0.5 mm at prototype scale and would be unlikely to result in any damaging effects to the structure. Post initial cracking the wall panels were found to extend and the general behaviour was similar to that observed for the block specimens discussed in Section 7.1.2. The response was similar to that found for the uniformly loaded brick specimens, where negligible in-plane deflections were recorded prior to cracking and extension occurred post cracking.

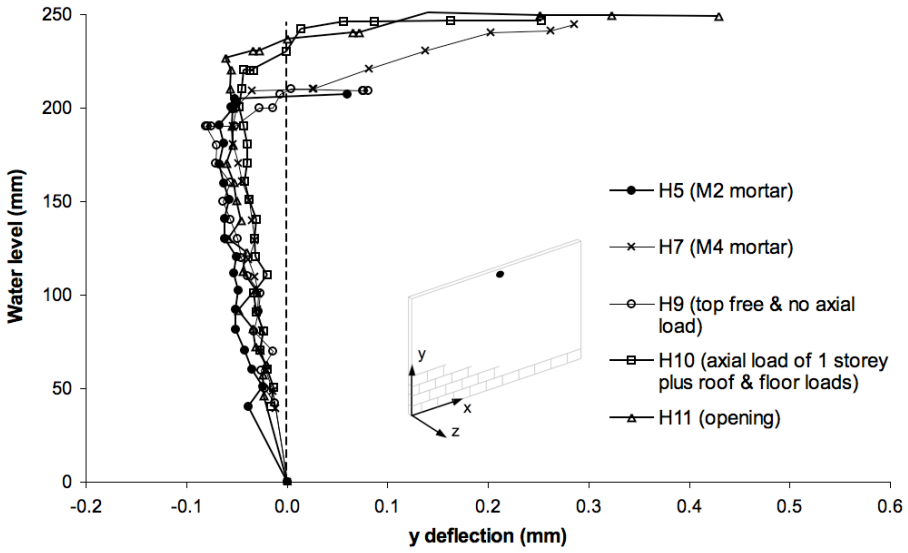


**Figure 7.16.** Load y deflection response measured at top of wall hydraulically loaded brick panels using DIC analysis

The load x deflection responses for brick specimens H5 and H7 without openings are shown in Figure 7.17. The response of the brick specimens with openings and different top edge support conditions were found to be similar and are not presented here. The typical in-plane response of the single leaf brick specimens in the x

direction was found to be similar, being characterised by negligible deflections occurring before initial cracking proceeded by extension after cracking. This behaviour was similar to that found for the block specimens, as detailed in Section 7.1.2. The response was comparable to that observed for the uniformly loaded brick specimens, as detailed in Chapter 6 Section 6.2.2.2. This perhaps confirms that that the panels were initially acting as a composite of the masonry units and mortar and that no cracking was occurring in the perpendicular mortar joints during the initial (pre cracking) stage of loading. The peak x deflections recorded were lower than those in the uniform loading tests, however this may be more related to the ability to capture the rapid failure process rather than values not attaining such high magnitudes.

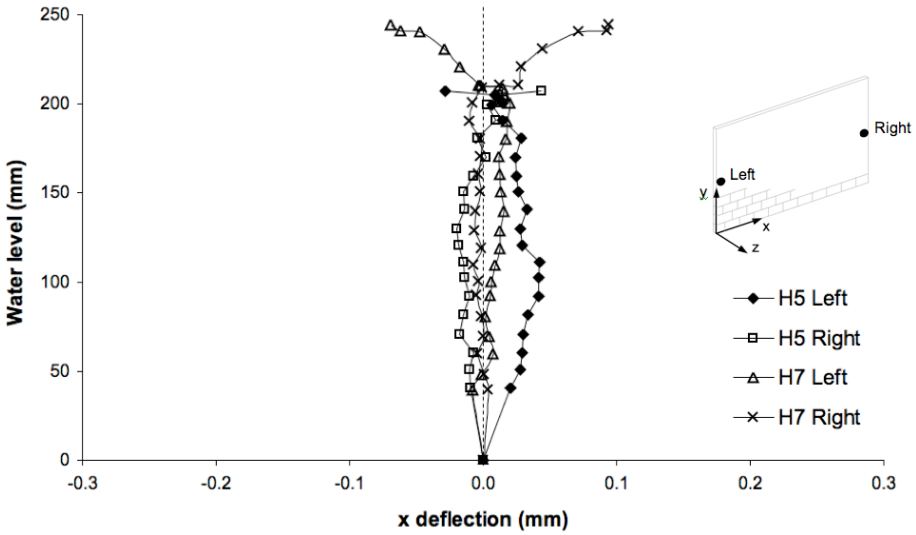


**Figure 7.17.** Load x deflection response measured at mid height at left and right edges of brick wall panel H5 and H7 (M2 and M4 strength mortar respectively)

The extensions in the y direction were 20 % and 75 % greater than those in the x direction at the ultimate water level for specimens H5 and H7 respectively. It would be expected that higher extensions would be found in the y direction in specimen H7, since initial cracking occurred prior to failure allowing for the formation of hinges in the vertical section. The similarity of the x and y deflections found in specimen H5 were likely related to the sudden failure of the panel without any initial pre-failure horizontal cracking, which may have limited the development of deflections in the x direction. There was similarly no clear trend in the peak x and y deflections for the brick specimens constructed with different strength mortars subject to uniform loading, as discussed in Section 6.2.2.2. The differences in the x and y deflections at ultimate load for the uniformly loaded specimens W11 and W12, constructed with M2 and M4 mortar respectively, were however of similar magnitude to those found for H5

and H7. The magnitude of the peak x and y deflections themselves were also found to be very similar for specimens H7 and W12 despite the differences in the loading distribution and failure mode.

A typical load in-plane strain response for a brick specimen is shown in Figure 7.18. Similar responses were found for other brick specimens and these are therefore not presented here. The strains measured in the y direction over a 40 mm gauge length at both the centre of the panel and at the site of the initial horizontal crack were negligible before initial cracking and some scatter was evident. Just prior to initial cracking the strain in the y direction increased, but at a higher rate at the site of the crack than at the centre of the panel. As the initial horizontal crack opened up the strains in the y direction at the centre of the panel remained very small. In the vertical cross section of the wall panel, as shown in Figure 7.19, it was found that the specimen was curved prior to initial cracking, but following this the sections above and below the crack were approximately flat. A similar response in the vertical cross section of z deflections was shown by the block specimens, as shown by Figure 7.4. Following cracking it appeared that any increase in lateral load resulted in displacement of the mechanism in the vertical section, rather than bending of the sections above and below the crack. This can be confirmed by the limited strains in the y direction above and below the initial crack, as shown in Figure 7.20.

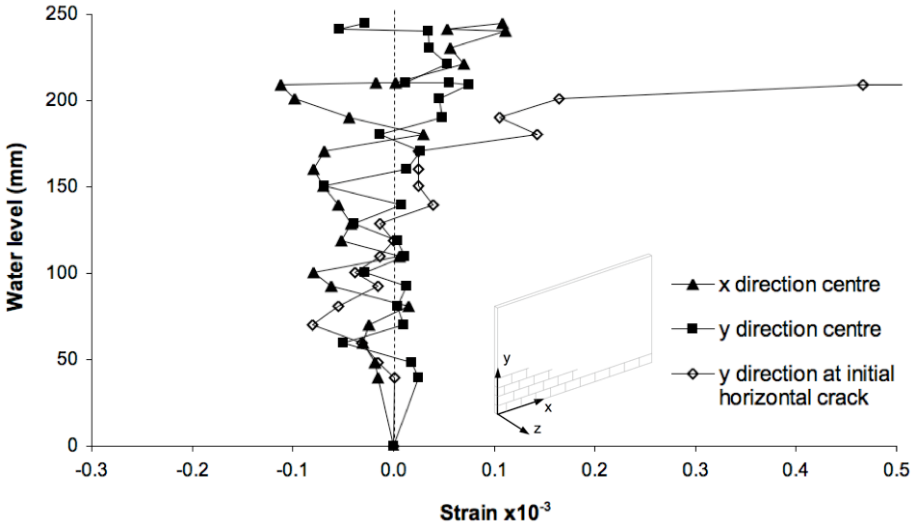


**Figure 7.18.** Load in-plane x and y direction strains measured during test for brick specimen H7 (M4 strength mortar)

The strains in the x direction at the centre of the panel were also negligible and showed a degree of scatter, as shown in Figure 7.18. The strains in the x direction

remained of negligible magnitude throughout the loading process. The highest x direction strains were adjacent to the supports in line with the position of the diagonal cracks, as shown in Figure 7.21. This suggests that the diagonal cracks initiated at the supports and grew towards the central crack as failure proceeded.

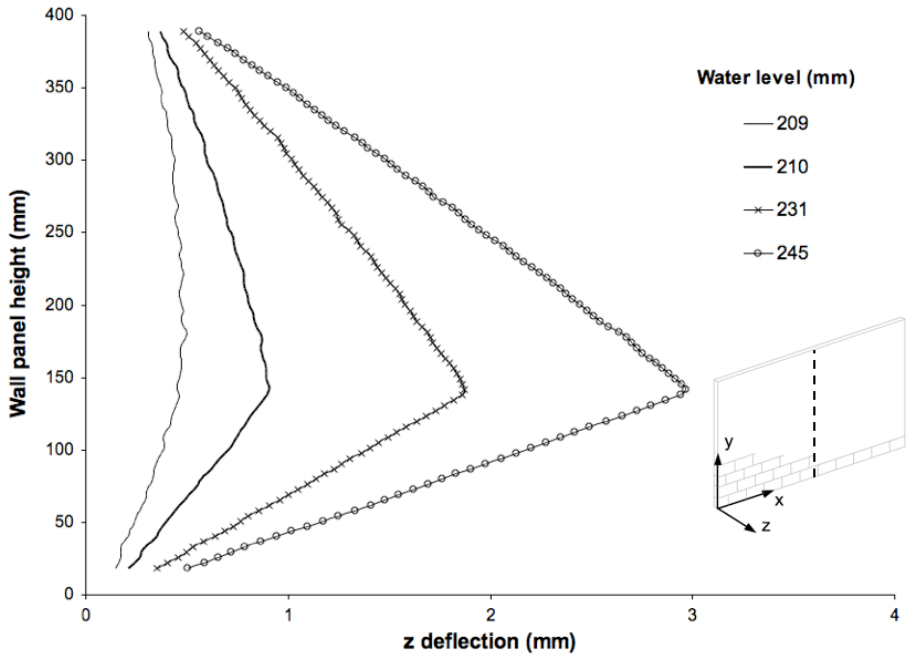


**Figure 7.19.** Wall panel height versus z deflection along vertical centre line for hydraulically loaded brick specimens H7 (M4 strength mortar) at different water levels

The response of the brick specimens in the y direction was similar to that found for the block specimens, as discussed above, where the strains prior to cracking were negligible. Post initial cracking the y direction strains in the block specimens similarly increased at the site of the initial crack, but remained small at the centre of the panel. The behaviour in the x direction was comparable to that found for the block specimens, where negligible strains occurred during the application of the load.

The behaviour differed from that observed in the uniform tests as presented in Chapter 6, where the strains at the centre of the panel generally increased in the y direction during the load application process. In addition the strains in the y direction increased at a similar rate at both the crack and centre of the panel in the uniform loading tests and some residual strain capacity was apparent since the strains remained positive. The strains in the x direction in the uniform loading tests were similarly found to be of low magnitude during the response.

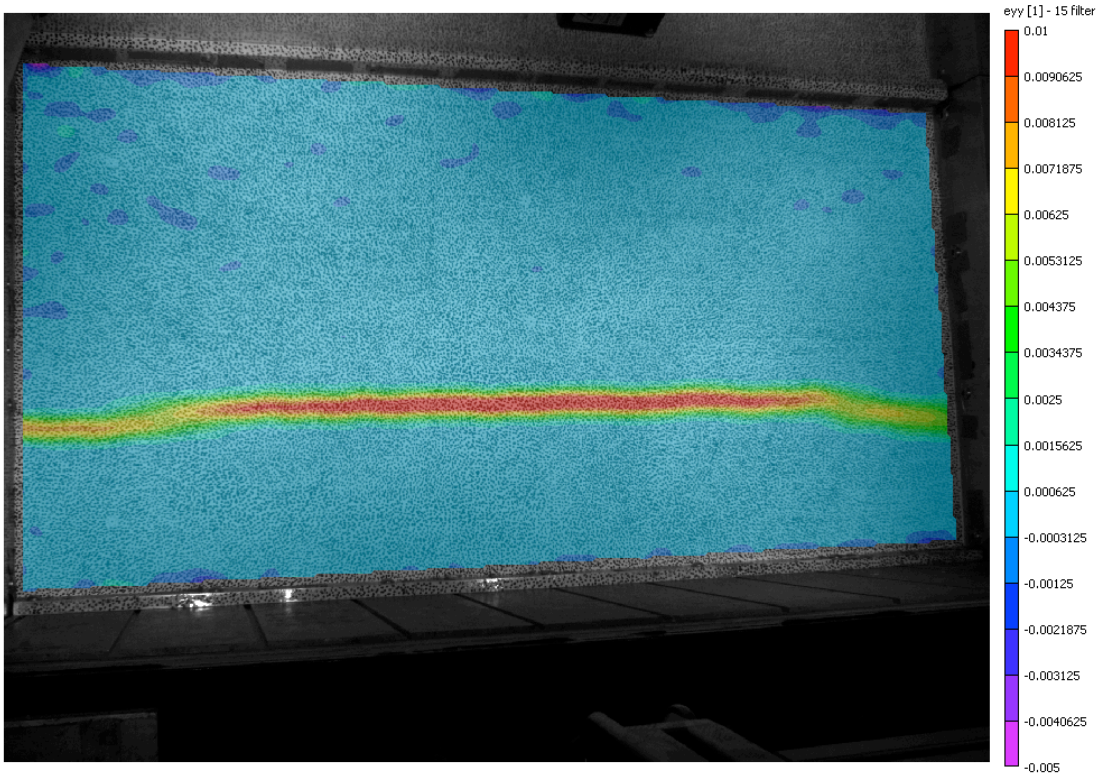


**Figure 7.20.** Contour plot of strain in the y direction for brick specimen H7 at a water level of 221 mm following initial cracking

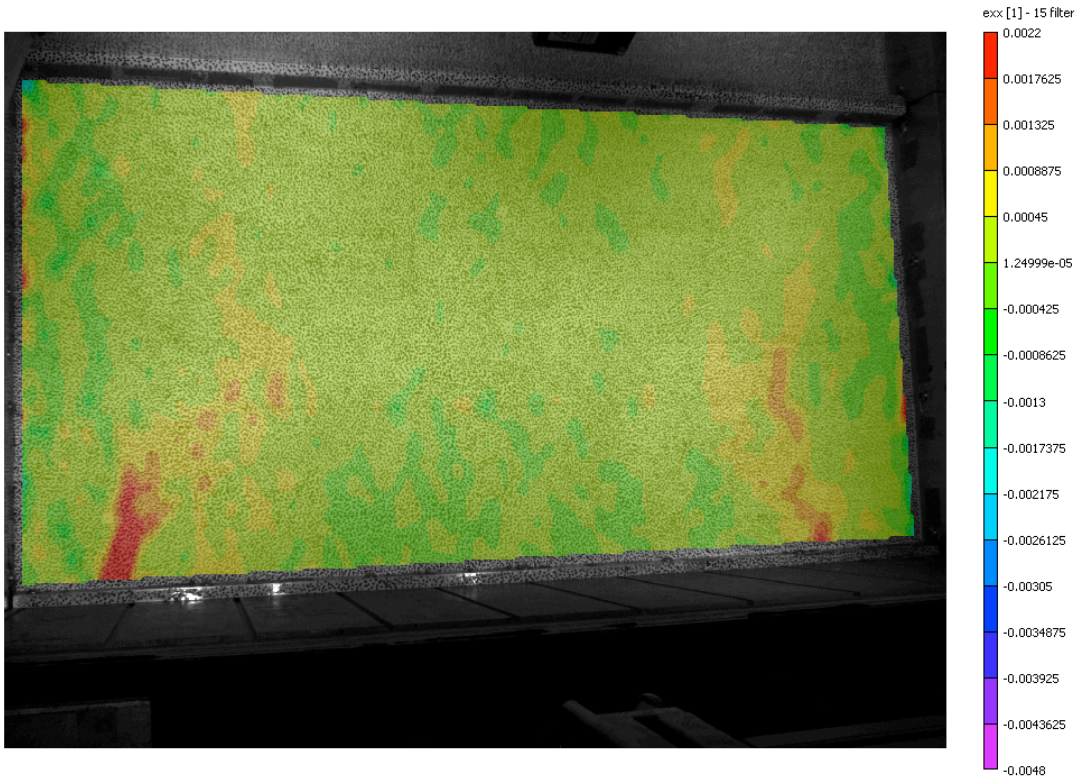


**Figure 7.21.** Contour plot of strain in the x direction for brick specimen H7 at a water level of 245 mm immediately before failure

## 7.3 Cavity wall specimen

### 7.3.1 Failure mode and load deflection response

The failure modes for the inner and outer leaves of the cavity wall specimens H13 to H14 are shown in Figure 7.22. The inner leaves of the cavity wall specimens all initially cracked horizontally near to the base of the panel. The contour plot of the strain in the y direction, as shown in Figure 7.23, revealed that in specimen H13 two horizontal cracks appeared to form simultaneously and similar behaviour was found for specimen H14. For specimen H15, which utilised a brick block inner leaf, only a single initial crack developed. In all specimens the horizontal cracks were typically coincident with the position of the wall ties rather than between them. It would be expected that the cracks would be coincident with the wall ties on the inner leaf, since the position of the wall ties would correspond to the points of the highest applied loads. The cracks at failure in the inner leaves of specimens H13 and H14 were in a combination of directions and some similarities were apparent between the two tests. In comparison to the failure mode observed for the single leaf AAC block specimens (H1 and H2) it was observed that a higher degree of diagonal cracking occurred and vertical cracking was restricted to the right of the H13 and H14. The crack pattern at failure for the inner leaf of specimen H15 was more comparable to those recorded of the single leaf specimens (H3 and H4), although the diagonal cracks were displaced outwards. Some of the cracks at failure were adjacent to the position of the wall ties, however this was not always the case. The wall ties may have resulted in the non-uniform loading distribution applied to the outer leaf being distributed over a larger area when transferred to the inner leaf. For such a scenario it would be expected that the failure mode of the inner leaf would be more similar to those found in the uniformly loaded tests, as detailed in Chapter 6. However, the failure modes observed in the inner leaves of specimens H13 to H15 were offset towards the base of the panels, suggesting that the loading distribution was non-uniform and not more uniformly distributed.

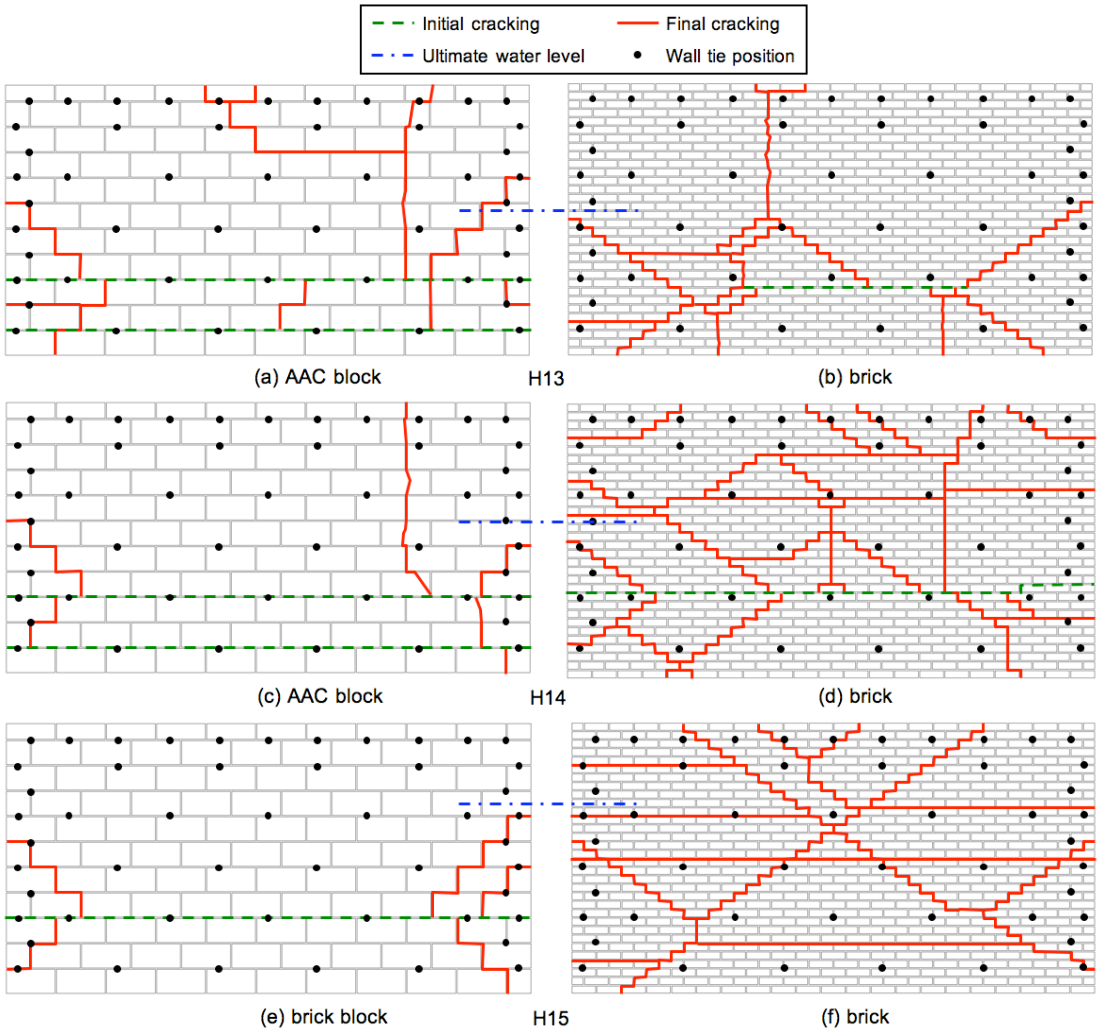


**Figure 7.22.** Failure modes observed for hydraulically loaded cavity wall specimens, where (a), (c) and (e) are the inner leaf and (b), (d) and (f) are the outer leaf (all M2 strength mortar)

Quantifying the failure mode occurring in the outer leaf was more difficult since any viewing opportunities were obscured by the loading arrangement. The outer leaf was removed carefully from the test jig post failure and the positions of any cracks were recorded where possible from the intact sections of the panel. Some assumptions were therefore made with regards to the order in which the cracks occurred and whether the cracks occurred at failure or after collapse. It was found that horizontal cracks occurred in the outer leafs in all specimens, but were not generally in line with those on the inner leaf. The crack patterns at failure were quite different for each specimen and only H13 showed any resemblance to those found for the single leaf specimens (H5 to H8). It was not possible to determine the order of failure of the leaves or if it was simultaneous. No evidence was found of any buckling of the wall ties at the end of the test, although the ties generally became disconnected from one

of the leaves. It was speculated that the disconnection of the ties occurred after collapse and would therefore not influence the failure mode, however this could not be verified during the testing procedure.

A much better correlation was found between the failure modes of the leaves of the uniformly loaded cavity wall assembly and those of the single leaf tests, as detailed in Chapter 6. It was similarly observed that the position of the horizontal cracks were not coincident in both leaves, where cracking was between the rows of wall ties in the outer leaf and along the row of ties in the inner leaf.

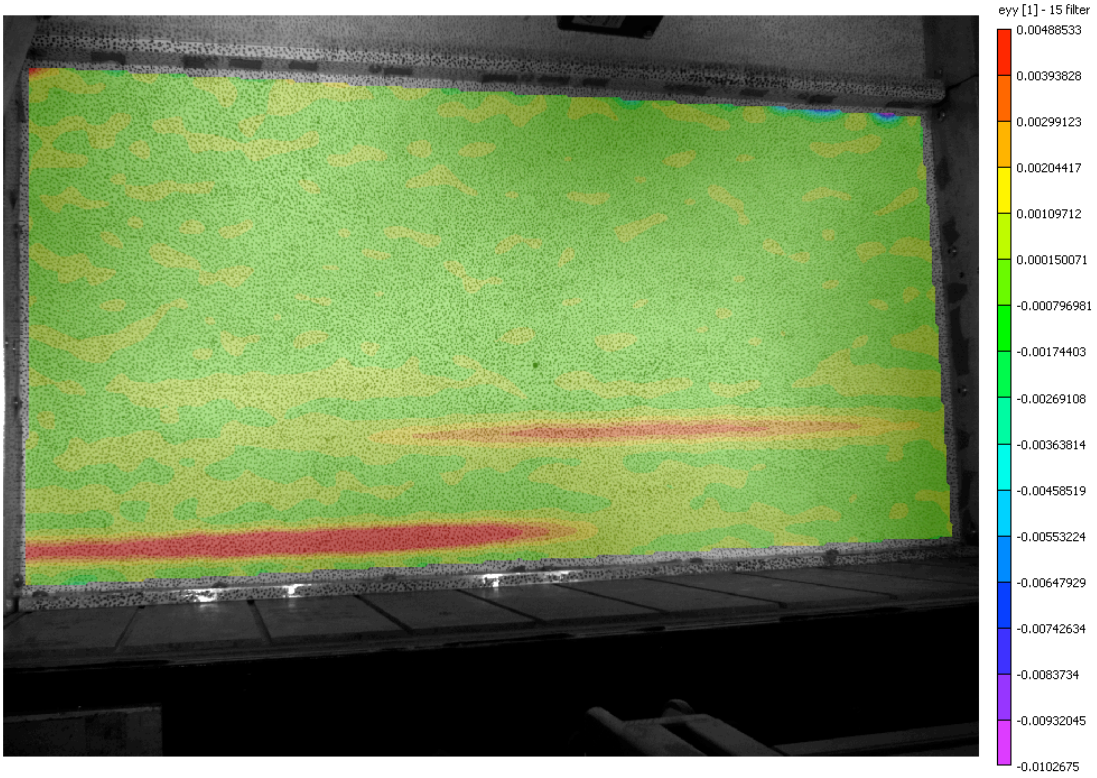


**Figure 7.23.** Contour plot of strain in the y direction for cavity wall specimen H13 (AAC block/brick) at a water level of 180 mm at initial cracking

The load z deflection response for cavity wall specimens H13 to H15 along with the response of the corresponding single leaf tests are presented in Figure 7.24. The load deflection response for specimens H13 and H14 was initially similar, but the stiffness of H13 reduced at a lower water level than H14. The change in stiffness did not correlate to the point of initial cracking in the inner leaves of specimens H13 or H14, as this did not occur until later along the second stage of the response, however it was not possible to verify if this was related to any initial cracking in the outer leaf due to viewing being obscured. There appeared to be no step change in

the response for H13 and H14 following initial cracking in the inner leaves and stiffness remained similar up to final failure. The initial response was comparable to that of the individual leaves constructed from AAC block (H1) and brick (H5), whilst the later part was more similar to that of brick. The peak deflections before failure were similar to those recorded for the uniformly loaded cavity wall specimen, as detailed in Chapter 6.

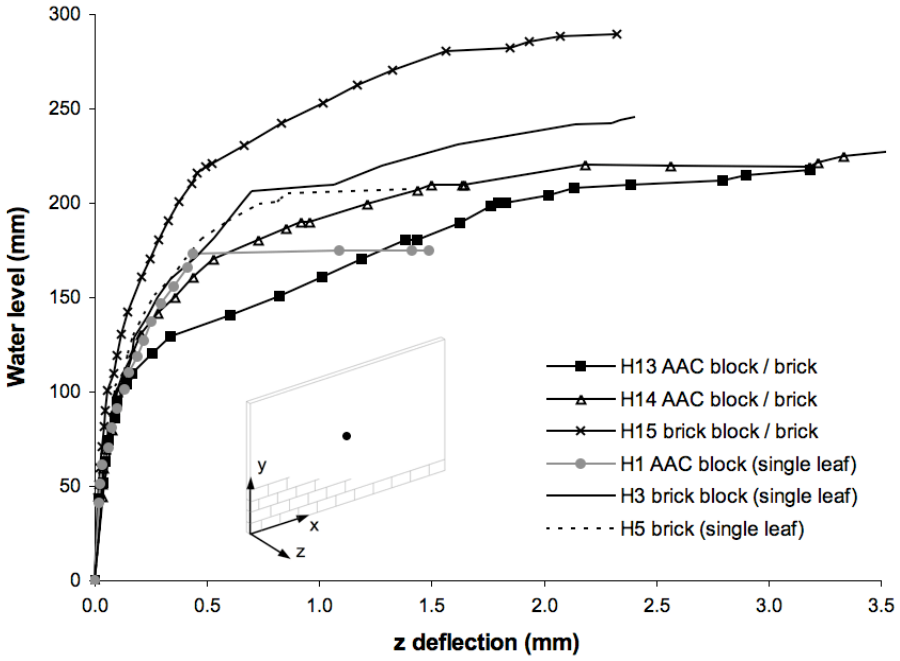


**Figure 7.24.** Load z deflection response for hydraulically loaded cavity wall and single leaf specimens (all M2 strength mortar)

The response of specimen H15 was slightly different to H13 and H14 since the stiffness reduced at a much lower rate and a step change occurred at the point of initial cracking in the inner leaf. Following initial cracking the response was marginally stiffer than those for specimens H13 and H14, but of a similar form. The water levels at both initial cracking and ultimate limit state for specimen H15 were a significantly improvement over specimens H13 or H14. The water level at initial cracking increased by 18 % and the ultimate water level was 29 % greater for specimen H15 when compared to the average of specimens H13 and H14. The response of H15 was similar to that of the brick block specimen (H3), but was of improved stiffness both before and after initial cracking. Specimen H15 did not deflect at constant load following initial cracking as was observed in the brick (H5) or brick block (H3) specimens.

The ultimate water levels reached at failure by specimens H13 and H14, as given in Table 7.1, compared well and were within 5 %, with an average level of 224 mm. The variation in the ultimate water level was in line with the values found for the tests of individual wall panels. The average ultimate water level was improved by 9 % for the cavity wall arrangement when compared to the average of the individual brick leaves (H5 and H6) at 205 mm. The equivalent total experimental ultimate load was calculated as 1.17 kN for specimens H13 and H14 and correlated well to the ultimate load of 1.10 kN for the cavity wall subject to uniform loading. The total ultimate load for the uniformly loaded specimen (W15) was computed from the uniformly distributed ultimate load of 3.41 kN/m$^2$, as given in Chapter 6 Section 6.2.3. Wall panel W15 similarly comprised AAC block inner leaf and brick outer leaf and the position and quantity of wall ties was identical for specimens W15 and H13/14. The ultimate water level, of 289 mm, for H15 was 17 % higher than the average value for the single leaf brick block specimens (H3 and H4) at 248 mm.

The wall ties were assumed to satisfy the requirements in current guidance (BSI, 2005c), as discussed in Chapter 6 Section 6.2.3, such that the ultimate water level of the cavity walls could be considered to be equivalent to the sum of the loading profiles from each individual leaf. To determine the ultimate load for the cavity assemblage from the results of the individual leaf tests it was necessary to calculate total applied load for each panel, sum the values and then compute the height of the equivalent triangular loading profile. The resulting equivalent ultimate level, $D_{Eq}$, for the cavity assemblage from the values for the individual leaves is as given by equation 7.1, where $D_{Inner}$ and $D_{Outer}$ are the ultimate levels for the inner and outer leafs respectively. Using equation 7.1 provided a ultimate level for the cavity assemblage that was 71 % of the direct sum of the individual leaf ultimate levels.

$$D_{Eq} = \sqrt{D_{Inner}^2 + D_{Outer}^2} \qquad 7.1$$

The equivalent ultimate water level when based on the ultimate water levels for the individual leaves and using equation 7.1 was calculated as 273 mm for specimens H13 and H14, which exceeded the average experimental value by 22 %. In the computation $D_{Inner}$ was the average value for specimens H1 and H2, whilst $D_{Outer}$ was the average of specimens H5 and H6. The equivalent ultimate level of 322 mm was similarly calculated for specimen H15 using equation 7.1 and exceeded the experimental value by 11 %. In the calculation $D_{Inner}$ was the average value for

specimens H3 and H4, and $D_{Outer}$ was the average of specimens H5 and H6. The equivalent and experimental values for specimens H13 /H14 and H15 compared well, considering the expected variability in the experimental results. Differences between the equivalent and experimental results may have also been due to the different edge support conditions of the outer brick leaf used in the test and the absence of vertical load on the outer brick leaf in the test. The results indicated that there was a component of composite action of the two leaves that influenced the overall performance of the cavity wall panel assemblies. Full composite action may have been restricted by the edge support conditions utilised for the outer leaf and the design of the wall ties used in the programme.

The experimental data suggests that it would be appropriate to derive an ultimate water level for a cavity wall assembly from the ultimate water levels of the individual leaves using the relationship of equation 7.1. A more detailed experimental study of cavity wall assemblies would however be necessary to ensure that this relationship holds for different edge support conditions for the outer leaf to those considered in this study. The review of the literature revealed that no masonry cavity wall assemblies had previously been tested when subject to hydraulic loading. Masonry panels tested in the only previous study were tied to a timber framework and it would therefore not be appropriate to compare the performance of the cavity walls to these (Pace, 1988).

## 7.4 Conclusions

The failure modes were observed to be comparable between the repeat specimens, although were not generally identical. Such differences were expected due to the inherent variation in the masonry units and the bond between the mortar and unit. The failure modes of the single leaf panels were comparable to those recorded in the uniform loading tests, but were offset towards the base of the specimen due to the non-uniform loading distribution.

Failure of the specimens was generally found to occur rapidly and often without warning. The behaviour differed to that found in the uniform loading tests, where failure was more progressive. Initial cracking and failure were typically coincident for the AAC block and brick specimens constructed with M2 mortar. Residual strength was observed in the brick block, M4 mortar strength brick and cavity wall specimens following the development of initial cracks. Peak deflections were significantly lower in the tests of single leaf specimens, but similar for the cavity wall assemblies when compared to those found in the uniform loading tests. Lower peak deflections in the single leaf specimens were attributed to differences in the failure mode and speed. Negative deflection was generally observed at the corners of the specimens in all the tests and was due to the position of the cracks and the support conditions.

The ultimate water levels were very similar for the repeat specimens for all combinations of materials and mortar proving the repeatability of the manufacturing and testing procedure. The variability in the results was at the lower end of those reported in the literature for similar materials and mortars, although these were subject to uniform lateral load. It was proposed that the ultimate water level could be computed into a total load acting on the wall panel, such that direct comparison could be made to the results of the uniform loading tests. Using this method it was found that the total ultimate loads for the hydraulically loaded specimens correlated well to the corresponding results from the uniform loading tests.

The failure mode of the block specimens was found to be influenced by the strength of the unit rather than the mortar. Cracking was generally limited to the mortar joints in the brick block specimens, but occurred both in the units and mortar joints in the AAC block panels. The initial response and stiffness was similar for all block specimens, but post cracking residual strength was observed in the brick block specimens. The ultimate water level was significantly higher for the brick block wall panels compared to those constructed with AAC block.

Mortar strength had a limited effect on the failure mode and stiffness of the brick specimens, but post cracking residual capacity was observed in the panels constructed with M4 strength mortar. The ultimate water level was improved as mortar strength increased and was likely due to increased flexural strength in direction 2. A similar improvement in ultimate load with mortar strength was recorded in the uniform loading tests.

The failure mode of the brick specimens was affected by the support conditions at the top of the panel, but changing the magnitude of the imposed vertical axial load appeared to have a limited influence. Stiffness was increased with a change in the support conditions at the top of the wall panel and further improved as the vertically imposed load was increased. The ultimate water level was reduced with the omission of the top support, but increasing the vertical load had a limited effect.

The presence of an opening influenced the failure mode, since cracks were observed to form from the base and corners of the opening. The load-deflection response and ultimate water level were similar for panels with and without openings. The small size of the opening and the use of a board to cover it during test were likely the reasons for the similarities recorded. In uniform tests a comparable response and ultimate load was also found for specimen with and without openings.

A limited correlation was observed between the failure modes of the leaves of the cavity walls when compared to those found in the individual wall panel tests. The ultimate water level was significantly improved when the inner leaf was constructed from a material of a higher strength compared to that of the outer leaf. The ultimate water level for the cavity wall specimens was between 89 and 78 % of the equivalent values calculated from the ultimate levels of the individual leaves. The overall performance was therefore due to some combined effect of the two individual leaves, but full composite action was not observed. The support conditions used for the outer leaf may have influenced the overall performance of the cavity wall. The experimental data suggests that the ultimate water level of a cavity wall assembly may be based on the sum of the loading profiles from each individual leaf, however this requires further investigation to corroborate the relationship.

The in-plane behaviour of the block and brick specimens was similar where extension in the x or y directions only occurred following initial cracking. Development of a mechanism in the y direction post cracking accounted for the

extension recorded in the y direction. Extension in the x direction was thought to be due to cracking occurring in the perpendicular mortar joints. The strains measured were found to be negligible prior to initial cracking and some scatter was apparent in the results. The strains post cracking were only observed to increase in magnitude at the site of the initial crack in the y direction, and were due to opening of the crack mouth.

The experimental data established in the hydraulic loading tests was used to validate the theoretical model that was developed, as detailed in Chapter 3. Comparison was additionally completed to the results of the only previous experimental study (Pace, 1988) and a theoretical analysis (Kelman and Spence, 2003a). Alongside the validation process a parametric study was completed to assess the performance of wall panels that were not considered in the experimental programme. The results and discussion of the validation process and parametric study is presented in Chapter 8.

# Chapter 8 Application of the spreadsheet analyses

This Chapter presents the verification of the theoretical analyses to the results from existing analyses and to the experimental results given in Chapters 6 and 7. The theoretical background of the analyses, Spreadsheet Analysis 1 (SA1) and Spreadsheet Analysis 2 (SA2), were detailed and discussed in Chapter 3. This Chapter is split into two Sections: Section 8.1 focuses on the uniform loading analysis, whilst Section 8.2 is concerned with the non-uniform hydraulic loading analysis.

Section 8.1 initially focuses on the verification of SA1 to the method prescribed by Eurocode 6 (BSI, 2005c) for the wall panels considered in this study. Following this, values computed using SA1 were compared to the experimental results from the uniform loading tests from Chapter 6. The methods used to determine the moments of resistance in the analysis, as described in Chapter 3, were also assessed for suitability. The effect of failure mode, vertical imposed load, support conditions, openings and combined action of the leaves of cavity walls were investigated using SA1 and SA2 and compared to the experimental findings where possible. Finally a comparison was made to the results from the analyses to existing experimental and analytical data in the literature.

Section 8.2 presents the verification of SA1 by comparison to the results from an existing theoretical analysis in the literature (Kelman and Spence, 2003a). The results from SA1 were then compared to the experimental values presented in Chapter 6. Analyses SA1 and SA2 were used to investigate the effect of failure mode, vertical imposed load, support conditions, panel length and height, openings and combined action of the leaves of cavity walls. The results from the analyses were compared to findings of an experimental study in the literature. Characteristic water levels were computed using SA1 and the appropriate factors of safety for the wall panels tested in this study and contrasted to guidance in the literature. Finally the resistance of a typical property when subject to hydraulic loading was examined using SA1 and compared to guidance given in the literature.

## 8.1 Wind loading analysis

### 8.1.1 Verfication of analysis SA1 to method given by Eurocode 6

Ultimate loads for the experimental single leaf wall panels were calculated using analysis SA1 and the method prescribed by Eurocode 6 (EC6) (BSI, 2005c). The wall

panels were modelled at prototype scale and were all of identical heights and lengths of 2.452 and 4.755 m respectively, as detailed in Chapter 4 Section 4.1.2. The wall panels were simply supported on all four edges as detailed in Chapter 4 Section 4.1.3. The average experimental flexural strengths ($f_x$) were used in the analysis as given in Table 5.1 in Chapter 5. Other parameters used in the analysis were as given in Table 8.1. The EC6 method was not applicable to the condtions imposed in wall panels W1, W2 and W14 and these were not considered in the verification process. The ultimate loads computed using SA1 and the EC6 method are given in Table 8.2. An example calculation for the EC6 method is given in Appendix 2.

**Table 8.1.** Parameters used in the analysis

| **Masonry material** | **Thickness (m)** | **Density (kg/m$^3$)** | **Vertical load (kN/m)** |
|---|---|---|---|
| AAC Block | 0.100 | 772 | 1.86 |
| AAC Block 2 storey load | 0.100 | 772 | 3.71 |
| Brick Block | 0.100 | 1828 | 4.40 |
| Brick | 0.103 | 1828 | 4.51 |
| Brick 2 storey load | 0.103 | 1828 | 10.82 |

**Table 8.2.** Comparison of analytical uniform ultimate loads from SA1 and EC6 for single leaf panels

| **Specimen reference** | **Masonry / mortar type** | **Analytical ultimate load (kN/m$^2$)** | | **Ratio of SA1/EC6 ultimate loads** |
|---|---|---|---|---|
| | | SA1 | EC6 | |
| W3 & W4 | AAC block / M2 | 2.00 | 1.36 | 1.46 |
| W5[1] | AAC block / M2 | 2.05 | 1.20 | 1.71 |
| W6, W7 & W8 | Brick block / M2 | 2.99 | 3.01 | 0.99 |
| W9, W10 & W11 | Brick / M2 | 2.68 | 2.71 | 0.99 |
| W12 & W13 | Brick / M4 | 3.83 | 3.87 | 0.99 |

[1] 2 storey vertical axial load

The ultimate loads given by the SA1 correlated very well to those calculated using the EC6 method for the brick block and brick specimens (W6 to W13) and were within 1 %, however the values were significantly different for the AAC block panels (W3 to W5). Increasing the vertical axial load, for the case of specimen W5, provided a small increase in the ultimate load in SA1, but this decreased when using the EC6 method. On further investigation it was found that the tabulated values of bending moment coefficients given by EC6 were particularly sensitive for the combination of parameters for the AAC block panels, which included the magnitude of the imposed

vertical axial load. A comparison of the ultimate loads calculated for AAC block using SA1 and the EC6 method for different imposed vertical axial loads is shown in Figure 8.1. When the applied vertical loading was raised in the EC6 method it was found that the ultimate load initially reduced up until a vertical axial load of 5 kN/m, but following this began to increase. It was expected that the ultimate load would increase linearly with the applied vertical load as shown by the results from SA1. Very small changes in other parameters, such as the flexural strength or wall panel dimensions also resulted in unusual values of ultimate loads. This suggested that there could be an anomaly in the EC6 tabulated bending moment coefficients that corresponded to the particular conditions for the AAC block specimens. Analysis SA1 was therefore considered verified for the masonry panels considered in this study when compared to the EC6 method, accepting the possibility that there may be an anomaly in the EC6 tabulated bending moment coefficients for specimens W3 to W5.

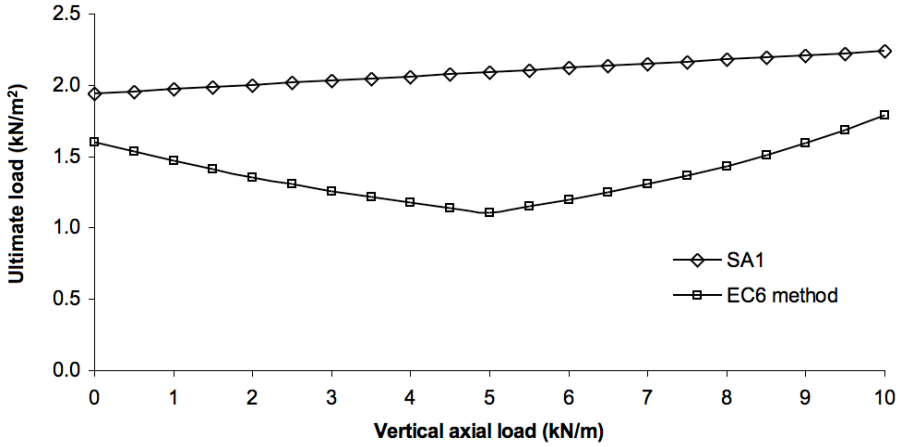


**Figure 8.1.** Variation in analytical ultimate load with applied vertical load for AAC block wall panel using SA1 and the EC6 method

### 8.1.2 Verification of analysis SA1 to experimental results for single leaf panels

The experimental wall panels were modelled at prototype scale using analysis SA1 and the parameters as detailed in Section 8.1.1. Ultimate loads were also computed from the EC6 adjusted (from characteristic to average) flexural strengths, as given in Table 5.2 in Chapter 5. To determine ultimate loads using the friction/overturning resistance methods, as detailed in Chapter 3 Section 3.2.3.1, the parameters given by Table 8.3 were adopted. The calculated and experimental ultimate loads for each uniformly loaded single leaf wall panel are presented in Table 8.4.

**Table 8.3.** Parameters used in the friction/overturning resistance methods (Kelman and Spence, 2003a, Martini, 1998)

| Method | Parameter | Value |
|---|---|---|
| Kelman & Spence | Compression factor, Cf | 0.95 |
| | Coefficient of friction, $\omega$ | 0.30 |
| Martini | Compression factor, Cf | 1.00 |
| | Coefficient of friction, $\omega$ | 1.00 |

**Table 8.4.** Comparison of experimental and analytical uniform ultimate loads for single leaf panels

| Specimen reference | Masonry / mortar type | Experimental ultimte load (kN/m$^2$) | | Analytical ultimate load (kN/m$^2$) | | | |
|---|---|---|---|---|---|---|---|
| | | | | Flexural strength method | | Friction/overturning resistance method | |
| | | Individual test | Average | $f_x$ | $f_x$ EC6 | Kelman & Spence | Martini |
| W1 | AAC block / no mortar | 0.47 | - | - | - | 0.24 | 0.34 |
| W2 | AAC block / sand mortar | 0.24 | - | - | - | 0.24 | 0.34 |
| W3 | AAC block / M2 | 2.09 | 1.84 | 2.00 | 1.59 | 0.24 | 0.34 |
| W4 | AAC block / M2 | 1.59 | | | | | |
| W5[1] | AAC block / M2 | 2.37 | - | 2.05 | 1.65 | 0.40 | 0.57 |
| W6 | Brick block / M2 | 4.87 | 4.82 | 2.99 | 3.29 | 0.56 | 0.80 |
| W7 | Brick block / M2 | 5.12 | | | | | |
| W8 | Brick block / M2 | 4.48 | | | | | |
| W9 | Brick / M2 | 2.72 | 2.84 | 2.68 | 3.46 | 0.59 | 0.78 |
| W10 | Brick / M2 | 2.86 | | | | | |
| W11 | Brick / M2 | 2.94 | | | | | |
| W12 | Brick / M4 | 4.59 | 4.65 | 3.83 | 3.84 | 0.59 | 0.78 |
| W13 | Brick / M4 | 4.70 | | | | | |

[1] 2 storey vertical axial load (all other specimens subject to 1 storey vertical axial load)

Analysis SA1 provided conservative results when the average experimental flexural strengths ($f_x$) were used, with the exception of the AAC block wall panels, specimens W3 and W4, that were overestimated by 9 %. The brick block wall panels, specimens W6 to W8, were particularly poorly modelled and were underestimated by 38 %. The analysis on average underestimated the experimental ultimate loads by 13 %. Average differences between analytical and experimental results calculated using the

yield line method were not given in previous research, however for previously conducted studies (Haseltine et al., 1977, Duarte and Sinha, 1992) average values were calculated as 19 % and 8 % respectively. For the first previous study (Haseltine et al., 1977) the yield line method on average overestimated the experimental strength of the walls, whilst it was under estimated in the second study (Duarte and Sinha, 1992). In both cases the analysis similarly utilised the average flexural strengths determined from wallette tests. The average difference between the results from SA1 and the experimental ultimate loads was in the range reported in the literature, suggesting that such a level of accuracy would perhaps be expected. The ultimate loads that were calculated using the average experimental flexural strengths ($f_x$ test) were therefore considered to compare well to those found in the experimental study.

It was also worth considering the difference in the results from repeat experimental tests reported in Chapter 6 and those reported in the literature to provide an understanding of the typical inherent natural variation that would be expected in masonry. The average difference between the ultimate loads from the repeat experimental tests, as detailed in Chapter 6, was 14 %, whilst the differences in results reported in the literature were 14 % (de Vekey et al., 1986), 18 % (Duarte, 1998) and 39 % (West et al., 1977). The difference in the average results from SA1 were at the lower end of the typical variability expected in experimental tests. The analysis could therefore be used to establish the ultimate loads with a degree of confidence, considering the expected inherent natural variability in masonry and the typical variability expected when applying the yield line method. The accuracy of the analysis could have been influenced by differences between the actual and analytical failure mode, which is examined in further detail in the following section.

Use of the EC6 adjusted to average flexural strength ($f_x$ EC6) in SA1 provided results that underestimated the experimental ultimate loads by an average 23 %, with the exception of the brick specimens constructed with M2 compressive strength mortar (W9 to W11) that were overestimated by 22 %. The ultimate loads determined using the experimental average flexural strengths differed to those calculated from the EC6 adjusted values. The ultimate loads calculated with $f_x$ EC6 were lower than those computed with $f_x$ for the AAC block specimens (W3/W4 and W5) and was expected since the EC6 adjusted flexural strengths were lower those determined experimentally. For the brick block (W6 to W8) and brick M2 compressive strength (W9 to W11) wall panels the ultimate loads calculated with $f_x$ EC6 exceeded the

values computed with $f_x$ and was due to the experimental flexural strengths being lower than the EC6 adjusted strengths. The ultimate loads computed for the brick wall panel constructed with M4 compressive strength mortar were very similar, regardless of the flexural strength used, owing to the similarities in the EC6 adjusted and experimental flexural strengths.

Ultimate loads computed from the EC6 adjusted flexural strengths were also not always conservative compared to the experimental ultimate loads and highlighting the importance of using appropriate values of flexural strength for the masonry panel under analysis. The average differences between the analytical results, using the EC6 adjusted flexural strengths, and the experimental results were, however, within the variation expected as discussed above. Use of the prescribed EC6 characteristic values, which were equal to two thirds of the EC6 adjusted flexural strengths, would provide conservative ultimate loads for all wall panels. The purpose of the characteristic values was to account for variation in the flexural strengths, which would not necessarily be represented by the average. The ultimate loads computed would therefore be safer, but would be lower than those determined using the average flexural strengths. The exception to this would be if the variation between individual wallette results was very low.

The ultimate load computed using Martini's frictional/overturning resistance method (Martini, 1998) gave the best approximation of the experimental value for specimen W1 that was assembled dry without mortar, as given in Table 8.4 and was within 39 % of the experimental ultimate load. In contrast the value calculated using Kelman and Spence's method (Kelman and Spence, 2003a) correlated very well to the experimental load for specimen W2, which was manufactured using sand mortar with no tensile strength. The values differed between the two methods due to the different approach to calculating the lever arm of the friction force and also the different parameters used for the coefficient of friction and compression depth factor. If the values of these parameters were kept the same in both methods then similar ultimate loads were given and it was found that the methods were most sensitive to the level of the coefficient of friction. This suggested that the level of friction differed between the units in specimens W1 and W2, where a higher level occurred in W1 and a lower level in W2. The layer of sand between the units in specimen W2 could have led to a lower coefficient of friction than suggested by the analytical results. The methods however provided very low ultimate loads for all the specimens constructed with cement mortar when compared to the experimental values and those calculated

using the flexural strength method. The methods assumed that the masonry was in an initially cracked state and this was not the case for the specimens constructed with cement mortar. It was clear that applying such a method to uncracked sections would not be appropriate, but could provide good approximation of the ultimate load for panels with zero or very limited flexural strength.

### 8.1.3 Effect of failure mode on the ultimate load

The results given by SA1, as given by Table 8.4, were computed by automatically adjusting the position of the yield lines in order to find the lowest ultimate load, subject to the constraints imposed as detailed in Chapter 3 Section 3.3.5. The position of the yield lines were fixed at the corners of the panels in SA1 and it was often observed that the cracks in the experimental specimens moved away from the corners. In particular a corner lever effect was often observed, where negative deflection, towards the load, occurred at the corners of the specimen at failure. SA2 allowed for the formation of corner levers and was utilised to assess the effect of the failure modes on the ultimate loads calculated. The position of the nodes was adjusted in SA2 such that the position of the yield lines provided an improved approximation of the experimental crack pattern. This process was completed for a number of specimens to assess the impact of the failure mode on the calculated ultimate load. The material parameters used in SA2 were identical to those used to determine the optimised ultimate loads.

The experimental, optimised SA1 and SA2 failure modes for AAC block wall panel W3 are presented in Figure 8.2. The experimental crack pattern was found to be different to that given by SA1 for the AAC block specimen W3, as shown in Figures 8.2a and 8.2b respectively. The ultimate load computed however compared well to the experimental value. Adjusting the position of the nodes in SA2 provided an improved approximation of the experimental crack pattern, as presented in Figure 8.2c. The ultimate load determined from the pattern was 3.39 kN/m$^2$, which vastly exceeded both the experimental and optimised values, given in Table 8.4, by 62 and 70 % respectively. As the corner levers formed then large areas of negative pressure occurred in the corners that equated to a total load of -0.79 kN/m$^2$ and contributed to the higher ultimate load calculated.

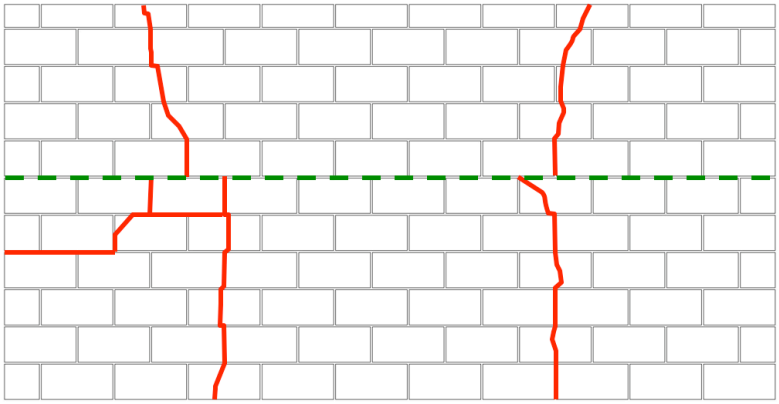

(a)

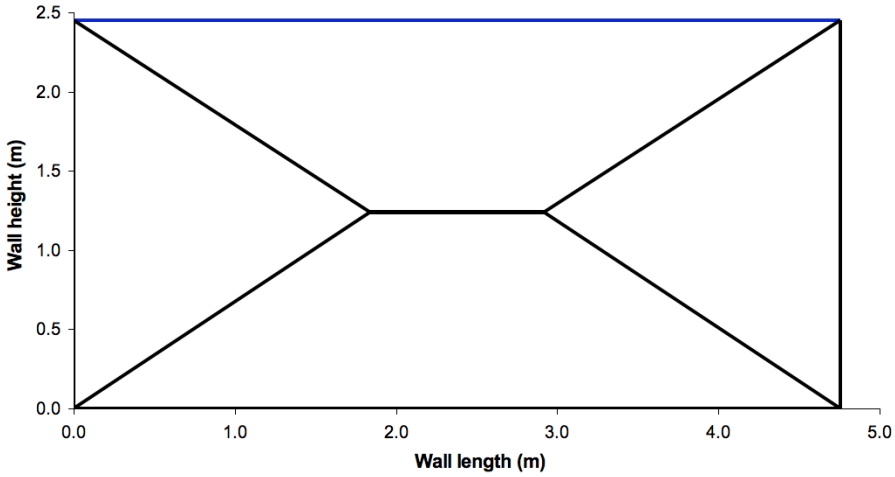


(b)

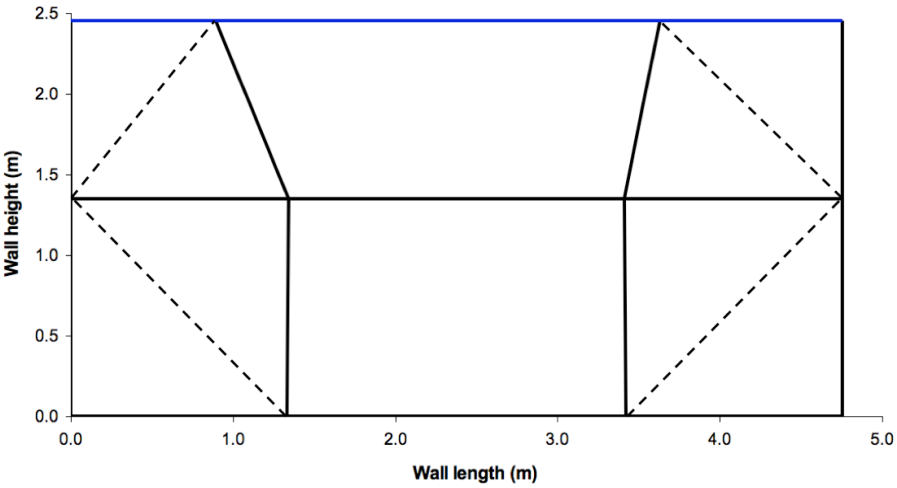


(c)

**Figure 8.2.** Yield line patterns for W3 (a) experimental, (b) optimised using SA1 and (c) using SA2 (dashed lines show position of corner lever pivots)

It was assumed in the yield line method that cracking initiated at the point of highest deflection and propagated towards the supports (Jones, 1962). In the experimental

test it was found that cracking initially occurred horizontally across the specimen and the cracks did not propagate towards the supports until a higher load was attained. The resistance along the initial crack at failure was therefore much lower than that pre-cracking and was limited to a moment resistance due to self-weight and vertically imposed loads. At failure the majority of the work done was therefore expended on forming the cracks that developed towards the supports and may explain why the experimental ultimate load was lower than that from SA2. In the optimised failure mode the majority of the work done was expended along the diagonal cracks (85 %) compared to a smaller amount (15 %) along the central crack and may explain why the ultimate load was comparable to the experimental value. The results illustrated that the failure pattern had a significant effect on the ultimate load, but the value determined by optimisation provided a better representation of the experimental findings.

The failure modes from the experimental test, optimised SA1 analysis and SA2 for brick wall panel W10, constructed with M2 compressive strength mortar, are shown in Figure 8.3. The optimised failure mode for brick specimen W10 was a good approximation of the experimental crack pattern, as shown in Figures 8.3b and 8.3a respectively. The main differences were that the horizontal crack was offset towards the top of the panel and that the diagonal cracks in the lower section formed part way up the side supports rather than at the corners. The position of the initial horizontal crack in the experimental specimen probably resulted in the deviation from the optimised failure mode in the lower section of the panel. The pattern at failure would also be unlikely to form exactly into the corners of the specimen, as was assumed in SA1, even if the cracks were restricted to the mortar joints, due to the format of the masonry units. The position of the yield lines were adjusted to match the experimental pattern, as presented in Figure 8.3c, although it was not possible to model the case where the diagonal cracks formed part way up the side supports. An ultimate load of 2.92 kN/m$^2$ was calculated using SA2 that was 3 % higher than the experimental value and 9 % greater than the optimised value from SA1, as given in Table 8.4. The higher load given by SA2 was due to the small corner levers forming at the upper corners of the panel. Considering the variability reported in the literature and found in the experimental results in Chapter 6, as detailed in Section 8.1.2, then the failure mode was considered to have a limited effect on the ultimate load for this case and SA1 would therefore be an appropriate method to use.

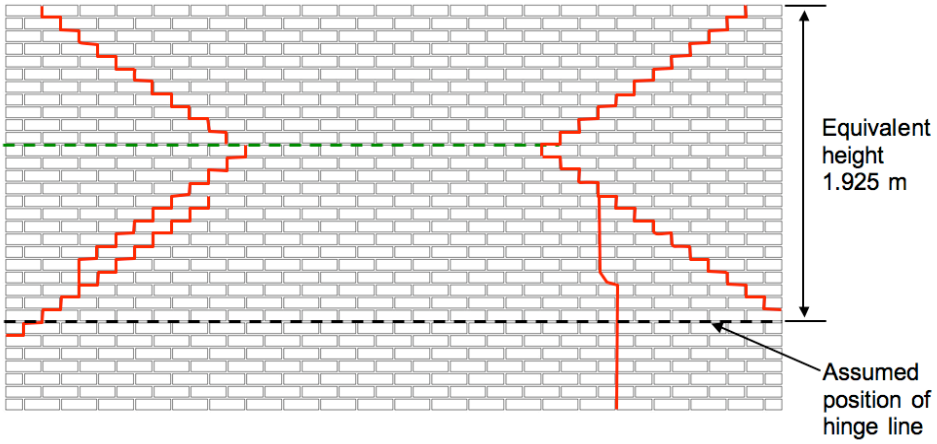


(a)

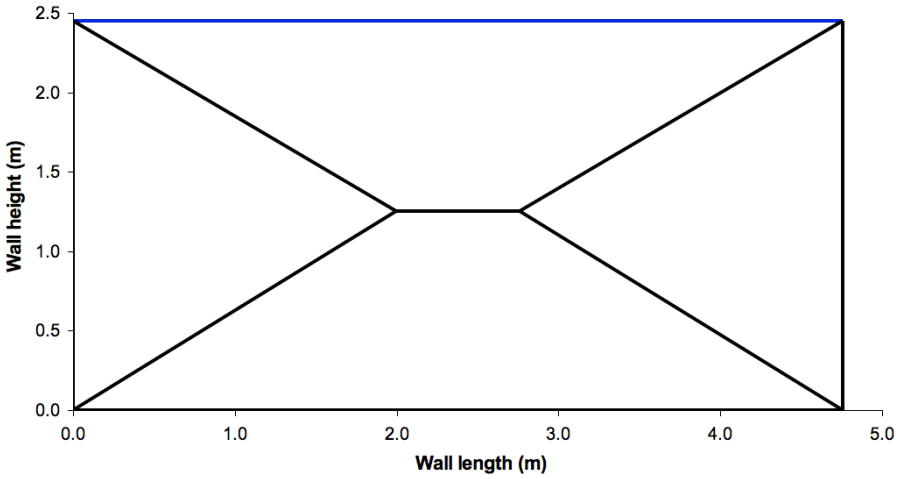


(b)

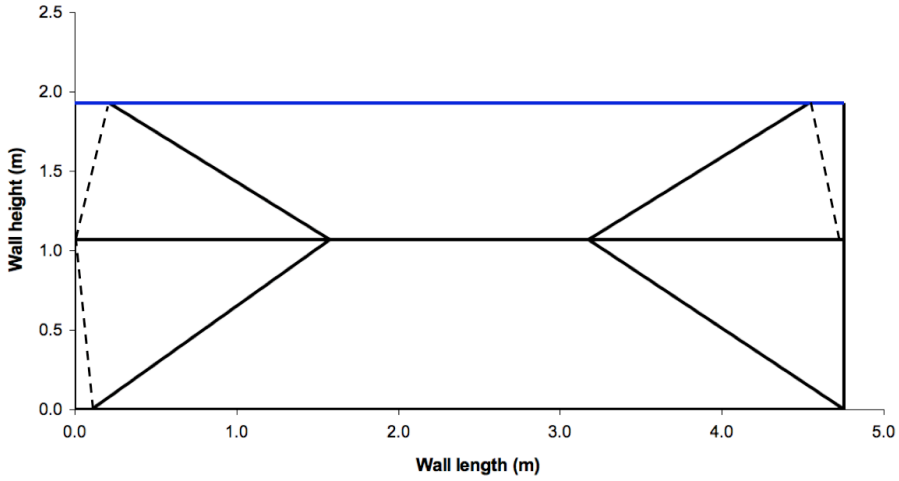


(c)

**Figure 8.3.** Yield line patterns for W10 (a) experimental, (b) optimised using SA1 and (c) using SA2 (dashed lines show position of corner lever pivots)

Specimens W6 and W13 were similarly modelled and ultimate loads were determined using the average experimental flexural strengths ($f_x$). The results were

plotted as a percentage of the experimental values, as presented in Figure 8.4, to enable direct comparison to be made. The optimised failure mode provided a good approximation for specimens W6 (brick block) and W13 (brick with M4 strength mortar) and deviation was again likely associated with the position and earlier formation (pre-failure) of the initial horizontal crack. In all cases the adjusted failure mode, of SA2, resulted in higher ultimate loads than the optimised values from SA1 and these were on average 27 % higher. Specimen W3 was significantly overestimated by SA2, as discussed above, and if this result was omitted the average difference reduced to 11 %. Considering the likely variability, as discussed above, then the failure mode assumed in SA1 provided an acceptable approach to establish the ultimate loads. It would be possible to use additional constraints in the analysis to establish improved failure modes automatically, but this could potentially result in other lower bound results being omitted. Any form of increased restraint at the vertical edges of the panel would also prevent corner levers forming, leading to failure modes that would be similar to the optimised mode.

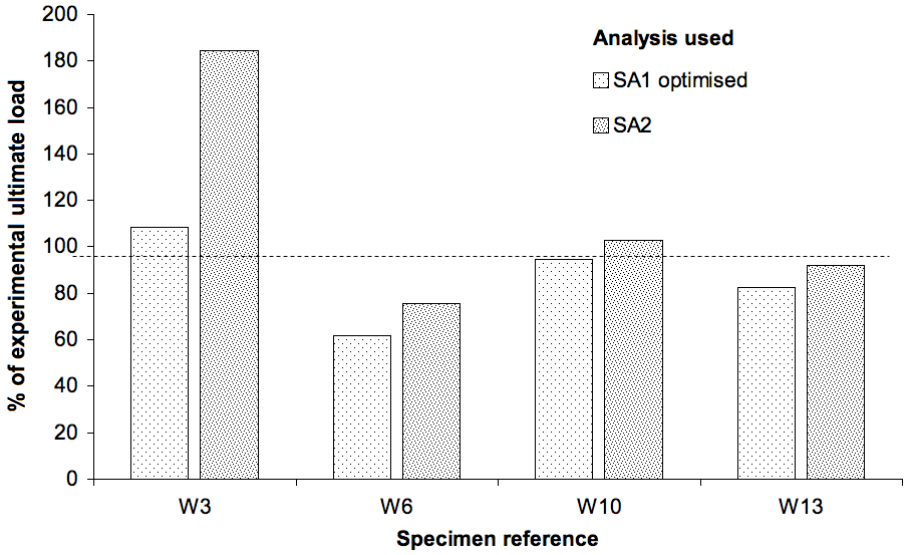


**Figure 8.4.** Comparison of experimental and analytical ultimate loads for the two different analyses

### 8.1.4 Effect of vertical load on ultimate load

It was previously shown in Figure 8.1 that the vertical axial load had a positive effect on the ultimate load for AAC block specimens, due to the inclusion of a moment resistance from self-weight and vertical imposed loads in the analysis. It was only possible to consider imposed loads of up to 10.8 kN/m in the experimental procedure and in the wind loading tests only loads up to 4.5 kN/m were investigated. In a

previous study (Hendry et al., 1971) it was reported that there was a 16 % improvement in the ultimate load when the vertical loading was increased from 48.9 to 55.0 kN/m for brick specimens. However, a control panel was not considered in the study with zero applied vertical load and the results were only based on two tests with no repeats (Hendry et al., 1971). It was therefore of interest to examine if there was a significant effect of vertical loads of higher magnitude than considered in the experimental tests on the ultimate load.

The effect of vertical load on the ultimate load was investigated in SA1 for AAC block, brick with M2 and M4 strength mortar. Applied vertical loads were considered up to 55 kN/m, and a load of 50 kN/m would be typical of a 5 storey property with a habitable loft space. The average flexural strengths from the wallette tests ($f_x$) were used in the analysis. Wall panels of AAC block with M2 compressive strength class mortar, and brick with M2 and M4 compressive strength class mortars were considered in the analysis. The dimensions and support conditions were as for the experimental study, whilst the other parameters used in the analysis were as given by Table 8.1. The effect of increasing the imposed vertical axial load on the ultimate load for the block and brick wall panels is presented in Figure 8.5.

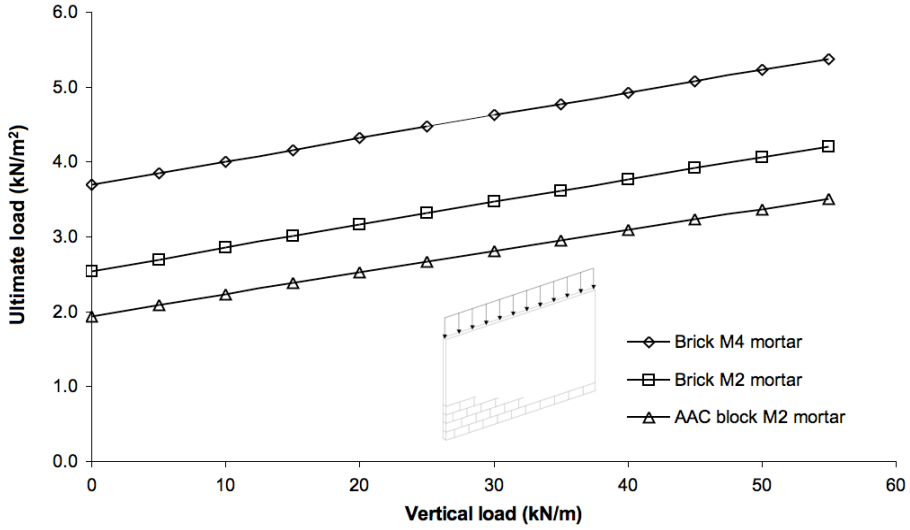


**Figure 8.5.** Variation in ultimate load with imposed vertical load for block and brick wall panels (all edges simply supported)

It was found that increasing the vertical axial load from 0 to 55 kN/m improved the ultimate load by an average of 64 % for all wall panels considered. The linear increase in ultimate load with vertical load was as a result of the inclusion of the moment resistance to vertical loads and self-weight in the analysis in addition to the masonry's flexural strength in direction 1. The dissimilar ultimate loads for each

masonry type at zero applied vertical load were due to the different corresponding flexural strengths. When the vertical loads applied in the previous study (Hendry et al., 1971) were considered in SA1 it was found that the ultimate loads increased by an average of 4 % compared to the value of 16 % given (Hendry et al., 1971). It is suggested that in part the increase in the ultimate load recorded in the previous study (Hendry et al., 1971) may have been attributed to the inherent natural variation in the test specimens. The results illustrated the importance of considering the correct vertical loading for the panel under analysis.

### 8.1.5 Effect of support conditions on the ultimate load

The vertical edge support conditions used in the experimental tests were simple supports rather than fully clamped. The use of such support conditions was discussed and justified in Chapter 4 Section 4.1.3. In a real situation where two walls are bonded at a corner the restraint conditions would likely be somewhere between true simple supports and fully clamped conditions. To assess the effect of vertical supports on the ultimate load SA1 was run with different proportions of the fully clamped conditions, where 0 % corresponded to simply supported and 100 % represented fully clamped conditions. The wall panels considered in the analysis were as detailed in Section 8.1.4. The parameters used in the analysis were otherwise as used for the experimental study. The effect of varying the vertical edge support conditions on the uniformly distributed ultimate load for the block and brick wall panels is presented in Figure 8.6.

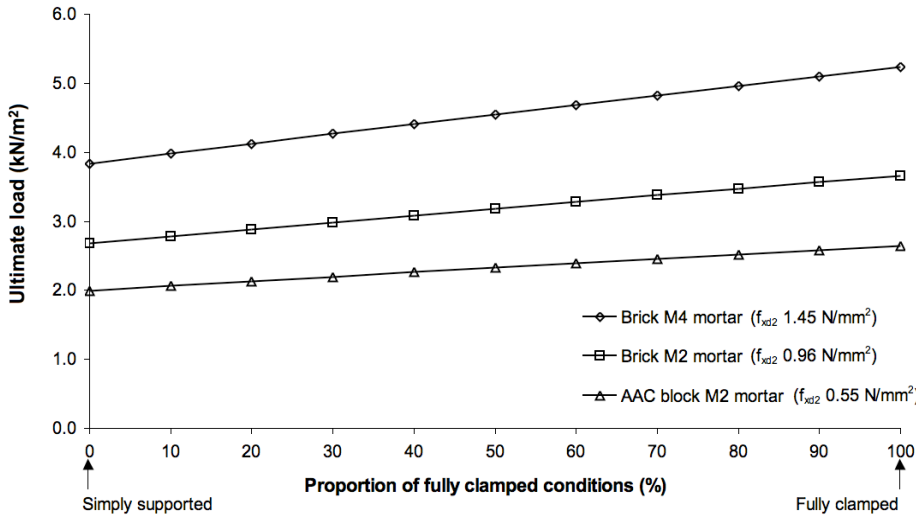


**Figure 8.6.** Variation in ultimate load with different vertical edge support conditions for block and brick wall panels (top and base simply supported)

The ultimate load was found to increase in a linear manner as the vertical support conditions were varied from simply supported to fully clamped for all wall panels considered in the analysis. An average increase of 35 % was found in the ultimate load as the edge support conditions were changed from simple to fully clamped conditions. The response was observed to be more significant for masonry materials that had a higher flexural strength in direction 2 ($f_{xd2}$). For example an improvement of 1.40 kN/m$^2$ in lateral load between simply supported and fully clamped conditions was given for brick with M4 strength mortar with an $f_{xd2}$ or 1.45 N/mm$^2$, compared to an increase of 0.98 kN/m$^2$ for brick with M2 strength mortar with an $f_{xd2}$ or 0.96 N/mm$^2$. It would be expected that the ultimate load would increase as the flexural strength in direction 2 increased since the moments of resistance along the vertical supports were calculated from $f_{xd2}$. Selecting simply supported conditions at the vertical edges would therefore provide conservative results in the absence of the knowing the exact fixity, whereas using fully clamped conditions could overestimate the ultimate load. It was acknowledged in a previous study (Haseltine et al., 1977) that it was difficult to assess the actual restraint at the panel edges, particularly when interconnections to other members were made using ties.

### 8.1.6 Effect of openings on the ultimate load

The ultimate load calculated using the average flexural strength ($f_x$) for the wall panel with an opening (W14), of 3.21 kN/m$^2$, was 31 % lower than found in the experimental study, of 4.62 kN/m$^2$. The difference between the experimental and optimised load was towards the upper end of the expected variability detailed in Section 8.1.2, suggesting that either analysis SA1 was underestimating the ultimate load, or the experimental load was influenced by the test conditions. The experimental load of specimen W14 was possibly overestimated since it was similar to that for the comparable specimens without openings and was likely due to the use of the stiff board to cover the opening. Some difficulties were reported in a previous study (Duarte and Sinha, 1992) with the method used to cover the opening due to the stiffness of the board and the researcher's resorted to transferring the load from the board to the masonry as four point loads. It was also suggested, in Chapter 6, that the similarity in the experimental ultimate loads found for the specimens with and without openings was due to the small area of the opening in relation to the panel area. The difference of 19 % in the analytical results from SA1 for the wall panels with and without openings, however, indicated that there was an effect of the opening in the analysis. It was correctly assumed in the analysis that the loading applied to

the wall panel was distributed uniformly over the wall panel and the board used to cover the opening.

The experimental and optimised SA1 modes of failure for wall panel W14 are presented in Figures 8.7a and 8.7b respectively. The experimental failure pattern was approximated by the optimised mode, but some differences were observed in that the yield lines did not enter the panel's corners and the horizontal yield line that traversed the specimen was not present. The constraints imposed in SA1 prevented the formation a failure mode that would be identical to that observed in the experimental specimen. It was stated in Section 8.1.3 that at failure the majority of the work done was associated with creating the final failure pattern and little was expended along the already formed initial crack. It would therefore be expected that the optimised ultimate load would be similar to the experimental load not lower, which further suggests that the experimental load may have been affected by the test conditions.

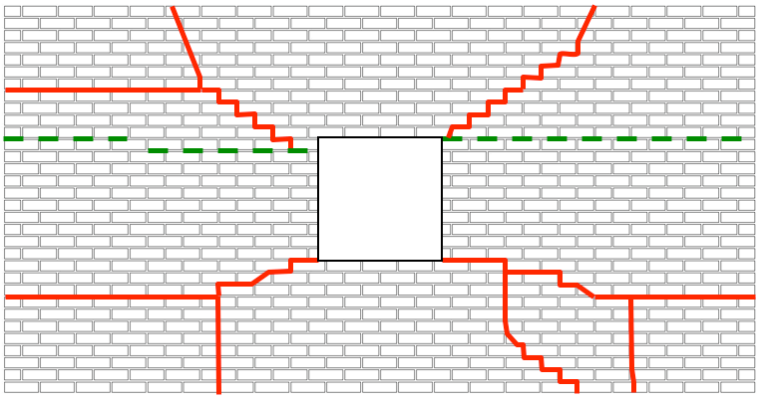

(a) Experimental

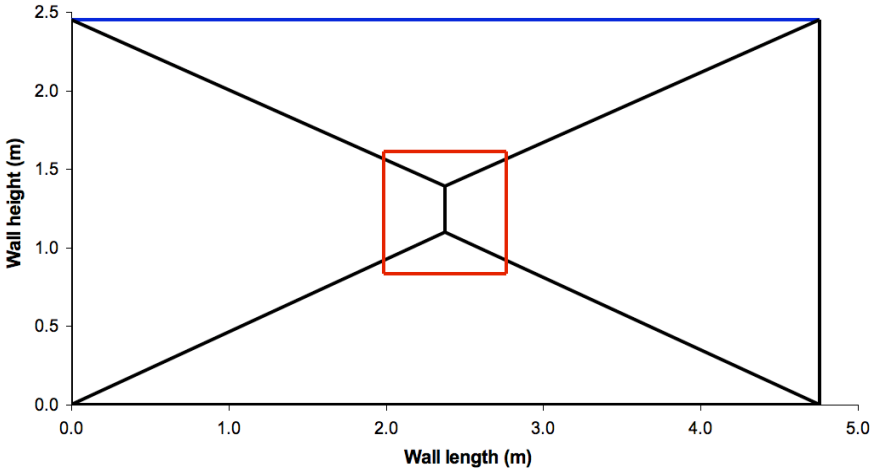


(b) Optimised

**Figure 8.7.** (a) Experimental and (b) optimised analytical failure modes for wall panel W14 with opening

To examine if the failure mode significantly influenced the ultimate load the optimised pattern was compared to two alternative patterns, mode 1 and mode 2. The ultimate loads were calculated using the average experimental flexural strengths and the nodal positions were adjusted manually to achieve the required pattern. The failure patterns for modes 1 and 2 are shown in Figures 8.8a and 8.8b respectively. Mode 1 was very similar to the optimised pattern except the yield lines were positioned to bisect the corners of the opening. The ultimate load given by SA1 with mode 1 of 3.23 kN/m$^2$ was within 1 % of the optimised load and was due to the proximity of the position of the yield lines at the corners of the opening in the optimised and mode 1 solutions. The constraints and optimisation process did not account for the possibility that the corners of the opening would be natural points for cracks to initiate and explains why the optimised pattern did not coincide with the opening's corners.

It was not possible to fully model the experimental pattern using SA2, however it was approximated in mode 2 (Figure 8.8b). The ultimate load for mode 2, of 4.62 kN/m$^2$, significantly exceeded the optimised value by 44 %, but correlated well to the experimental value for specimen W14 of 4.62 kN/m$^2$. This suggests that the failure mode could have resulted in the higher ultimate load found in the experimental study. The optimised or mode 1 failure patterns may not have occurred in the experimental specimens due to the formation of the initial horizontal crack prior to failure. Following initial cracking the wall panel could be assumed to be acting as two separate slabs and, due to the simple support conditions and the curvature of the specimen, negative deflection occurred at the corners of the panel, as apparent in contour plot of z deflections for W15 shown in Figure 8.9. The behaviour observed likely forced the cracks to form towards a location where contact was maintained between the specimen and supports, rather than into the corner where negative deflection was occurring. The results from the analysis suggest that there may be an effect due to the failure mode, but further experimental investigation is required to examine the influence of the stiffness of the board used to cover the opening.

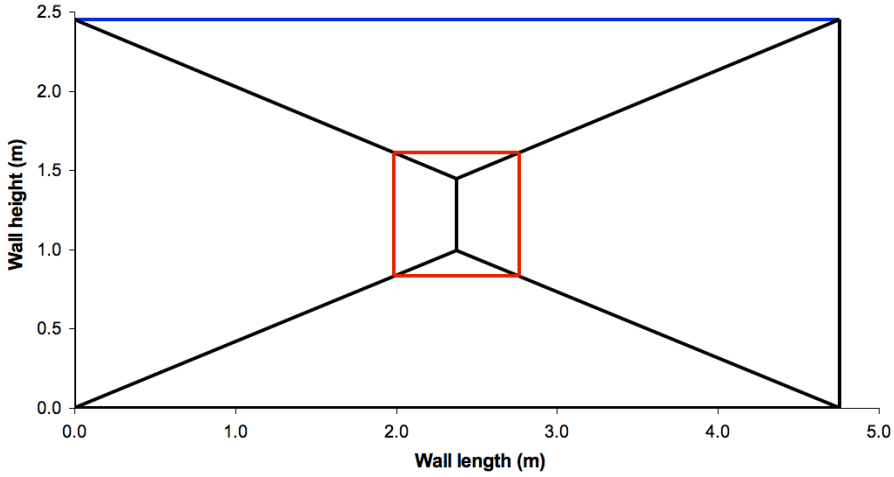


(a) Mode 1 (yield lines cut opening edges)

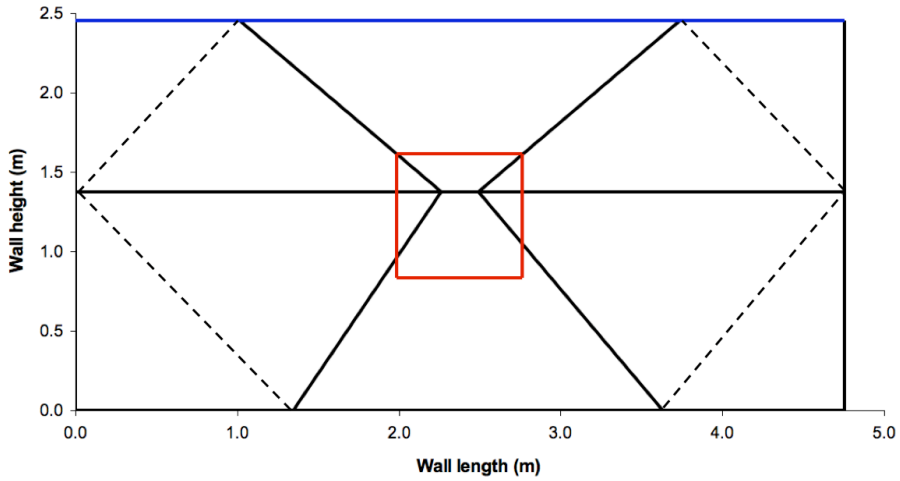


(b) Mode 2 (corner lever failure)

**Figure 8.8.** Alternative failure modes for wall panel W14 with central opening (a) mode 1 and (b) mode 2 (dashed lines show position of corner lever pivots)

Analysis SA1 was utilised to examine the performance of a brick wall panel (M4 strength mortar) with a centrally positioned opening that was varied in both height and length. The dimensions of the wall panels and other parameters were otherwise as for the experimental study. Ultimate loads were computed using the average flexural strengths from the experimental study ($f_x$). The effect of varying the height and length of the centrally positioned opening in the analysis is shown in Figure 8.10. The failure modes for openings of lengths of 0.5 and 2.5 m at different heights are presented in Figures 8.11 and 8.12 respectively. From Figure 8.10 it was observed that the ultimate load decreased as the size of the opening was increased. For openings of lengths up to 0.75 m the ultimate load was approximately equal

regardless of height and was due to a combination of the similar failure modes and proportions of the yield lines within the opening, as apparent in Figure 8.11.

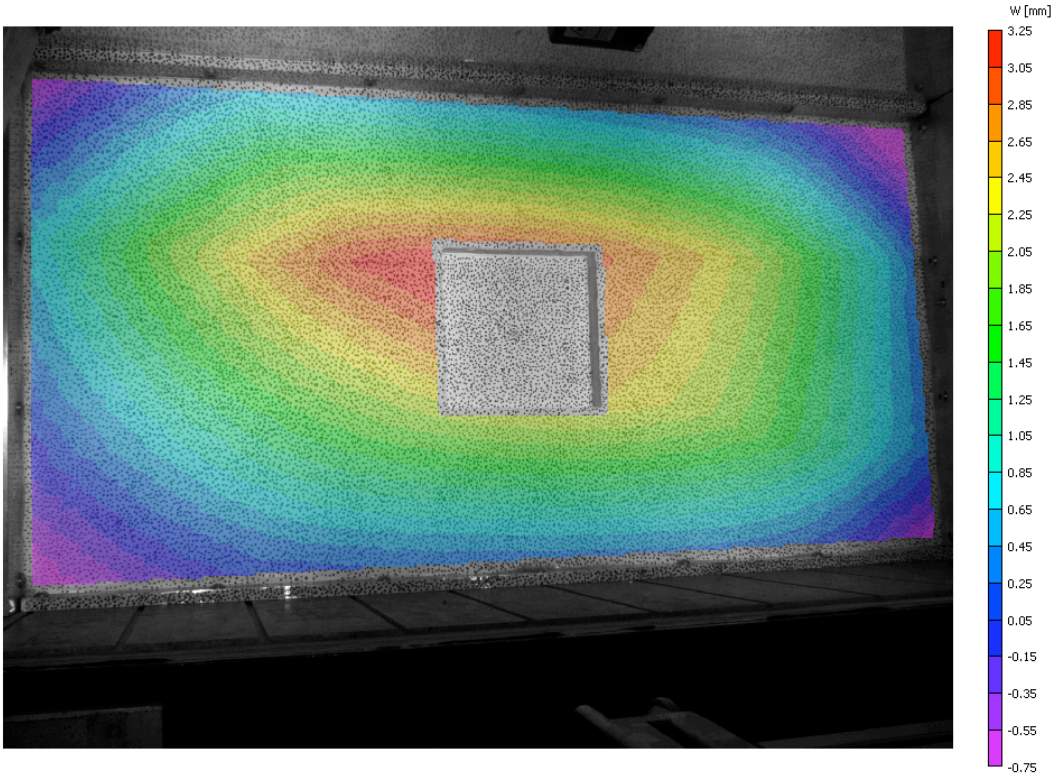


**Figure 8.9.** Contour plot z deflections for specimen W14 illustrating negative deflection at panel corners prior to failure

The ultimate load for openings of height 0.5 m and lengths greater than 0.75 m deviated from the behaviour observed for the other opening sizes and was due to the lower proportion of yield lines being within the opening. A similar effect occurred for the opening of height 1.0 m for lengths greater than 1.75 m. Little difference was found between the ultimate loads for openings of height 1.5 and 2.0 m regardless of length and was again due to the similar failure modes and proportions of yield lines within the opening, as presented in Figure 8.12. Considering the lower value of acceptable error in the analysis of 8 %, as detailed in Section 8.1.2, then results from SA1 illustrated that it would be acceptable to ignore openings of length up to 0.25 m regardless of height. The results therefore indicated that the opening that was utilised in the experimental study should not be ignored in the analysis.

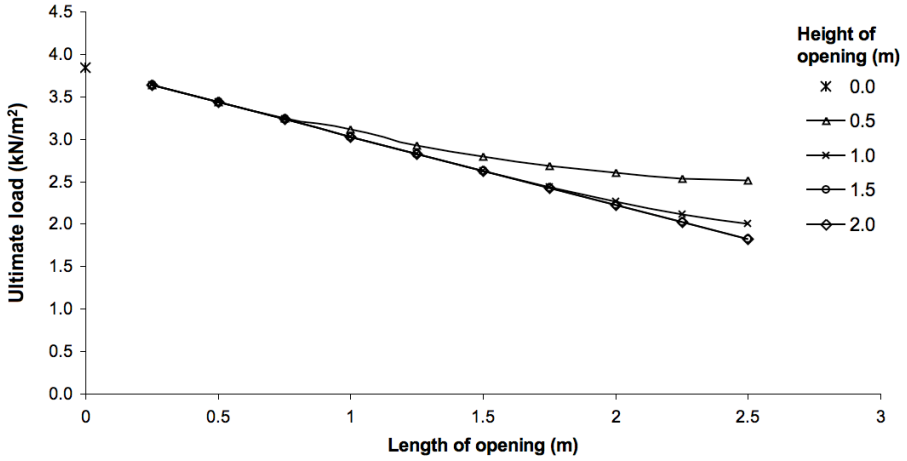


**Figure 8.10.** Variation in ultimate load for openings of different lengths and heights

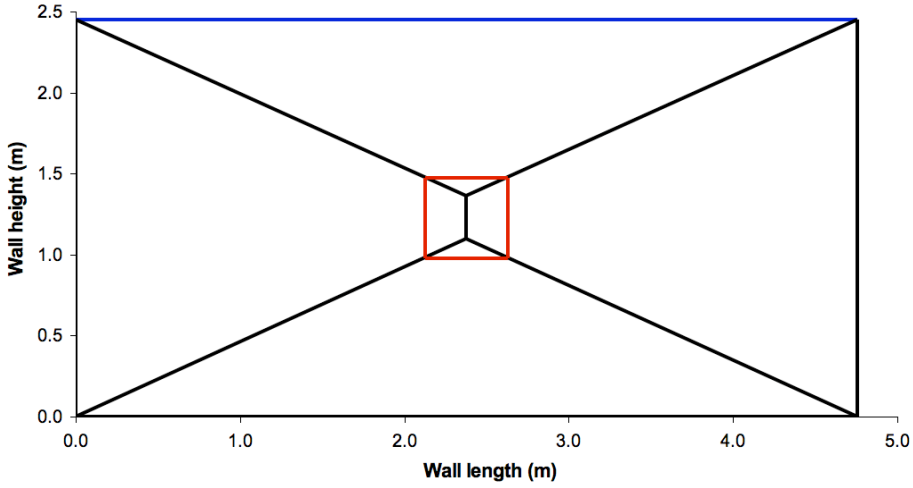


(a) Opening height 0.5 m (14 % of yield lines within opening)

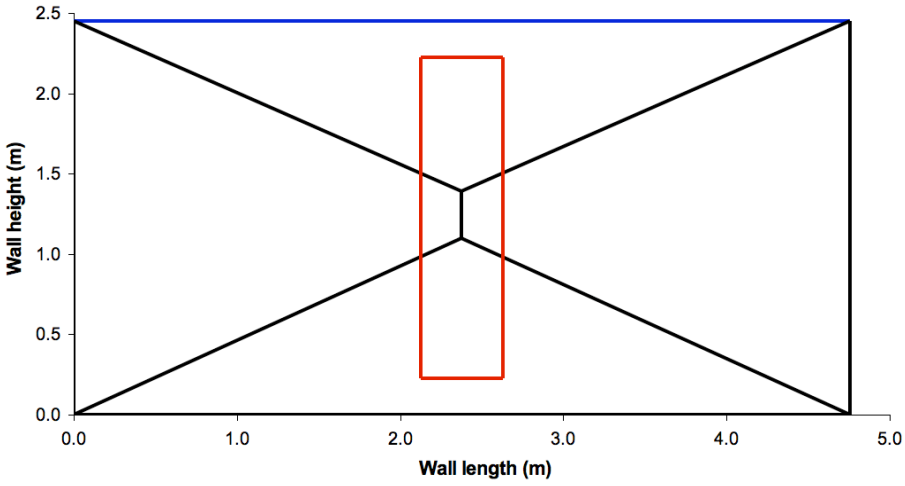


(b) Opening height 2.0 m (14 % of yield lines within opening)

**Figure 8.11.** Failure modes for wall panels with openings of length 0.5 m and height (a) 0.5 m and (b) 2.0 m

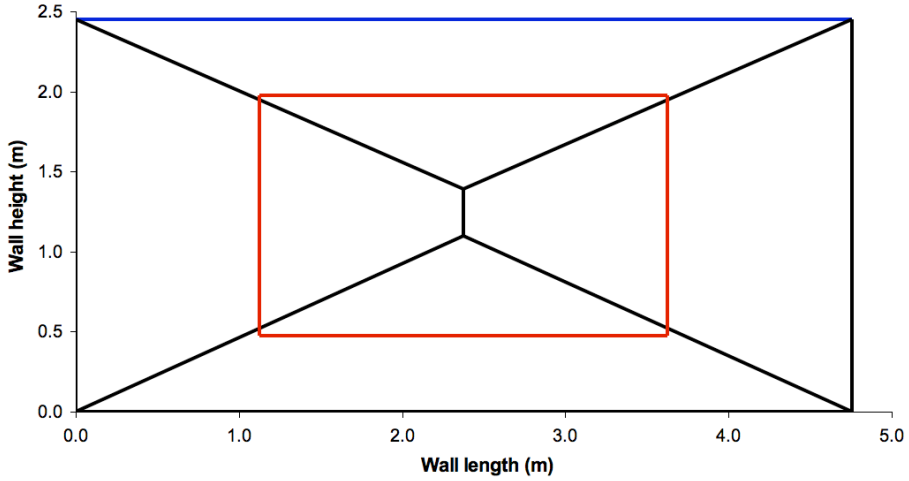


(a) Opening height 1.5 m (54 % of yield lines within opening)

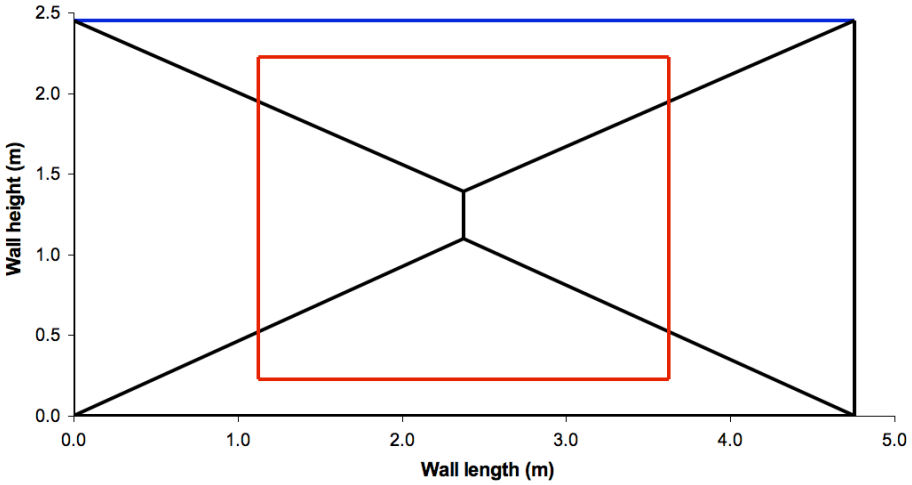


(b) Opening height 2.0 m (54 % of yield lines within opening)

**Figure 8.12.** Failure modes for wall panels with openings of length 2.5 m and height (a) 1.5 m and (b) 2.0 m

Analysis SA1 was further utilised to assess the effect of the position of opening on the ultimate load and this was considered for three opening sizes, as presented in Figure 8.13, whilst other parameters were as for the experimental study. A brick wall panel constructed with M4 compressive strength class mortar was used throughout the analysis, whilst the flexural strengths were the average experimental values. The effect of the horizontal position, for the three opening sizes considered, on the ultimate load is shown in Figure 8.13. The failure modes for the 0.78 x 0.78 m opening at different horizontal positions are presented in Figure 8.14. Failure modes for the openings of length 1.0 m and heights of 1.5 and 2.0 m when positioned 2.0m from the left hand side of the panel are shown in Figure 8.15. It was observed that the ultimate loads were not dependant on the position of the openings when the openings were located between 1.25 and 2.5 m from the edge of the panel. Outside

these limits the behaviour depended on the size of the opening, where higher loads were given by the smaller opening (0.78 x 0.78 m) as it tended towards the edge of the panel. Higher loads were attained for the small opening when positioned near the panel edge due to a lower proportion (10 %) of the yield lines being within the opening compared to when positioned 2.0 m from the edge (20 %), as was apparent in Figure 8.14. The internal energy requirements were therefore lower when the opening was nearer the centre of the panel, which reduced the required external load to cause failure.

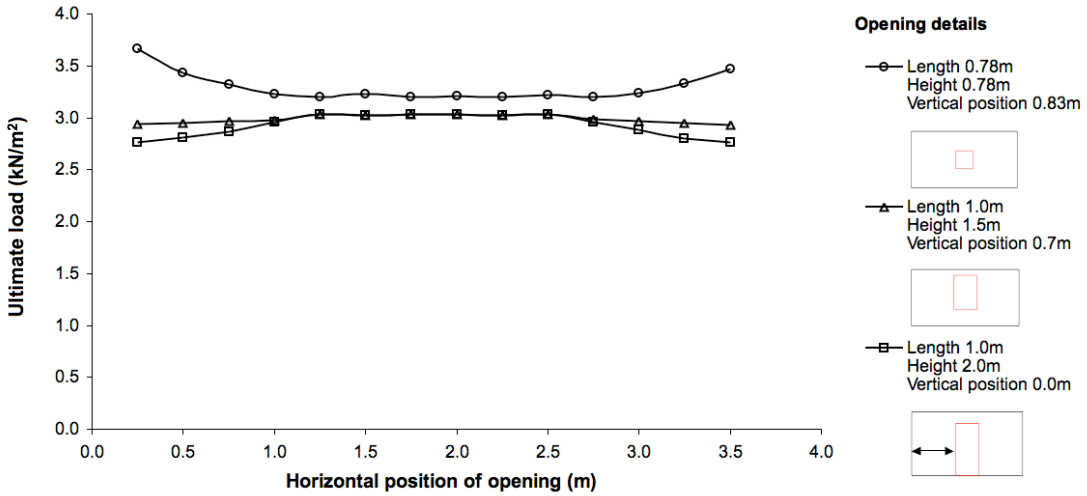


**Figure 8.13.** Variation in ultimate load with horizontal position of opening for openings of three sizes

For larger openings the more critical location was towards the edge of the panel, where the ultimate load reduced by 3 and 9 % for the larger window (1.0 x 1.5 m) and door opening (1.0 x 2.0 m) respectively. For these cases a higher proportion of the yield lines were within the opening when the opening was positioned near the edge compared to when nearer the centre of the panel. A comparable ultimate load was found for both the larger openings when positioned at the centre of the panel and was due to the failure mode and proportion of yield lines cut by the opening being similar, as shown in Figure 8.15.

In summary the results and trends observed indicated that openings positioned in the panel could be modelled with an acceptable degree of accuracy using SA1. The experimental results for wall W14 certainly suggested that there was an impact of the method used to cover the opening during test and this, along with the effect of any framework affixed within the opening, clearly requires further investigation. The

accuracy of SA1 is further examined in Section 8.1.8 by comparison to results in the literature.

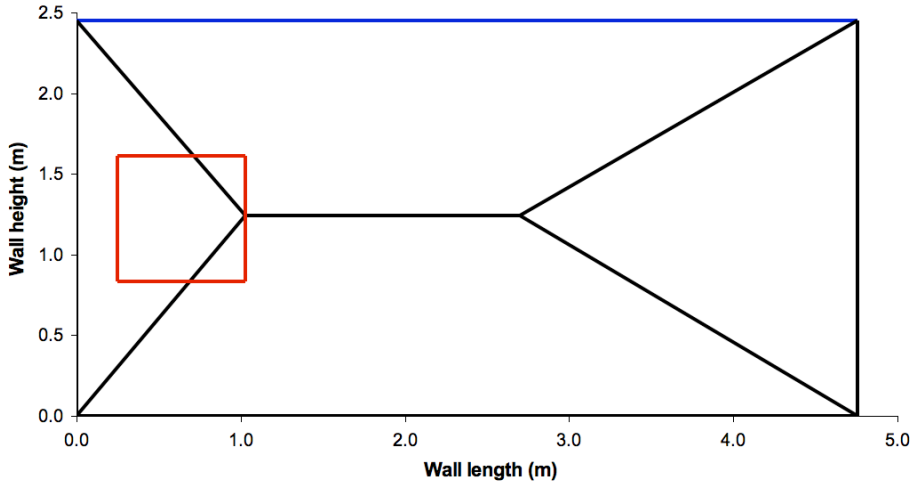


(a) Opening 0.25m from LHS (10 % of yield lines within opening)

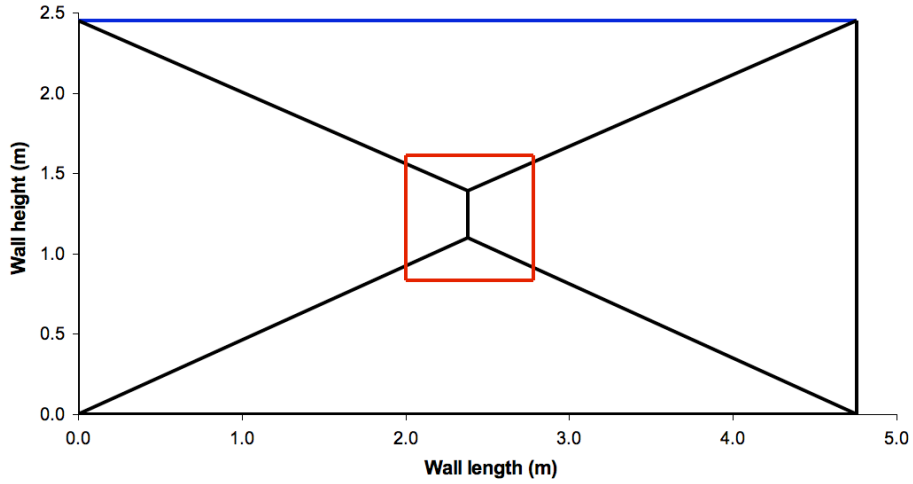


(b) Opening 2.0 m from LHS (20 % of yield lines within opening)

**Figure 8.14.** Failure modes for wall panel with 0.78 x 0.78 m opening when positioned (a) 0.25 m from LHS and (b) 2.0 m from LHS

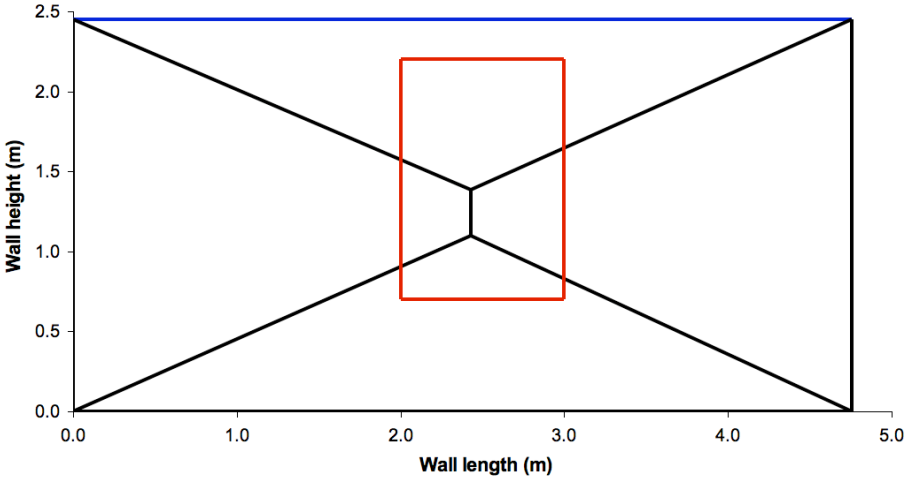


(a) Window opening size 1.0 x 1.5 m (24 % of yield lines within opening)

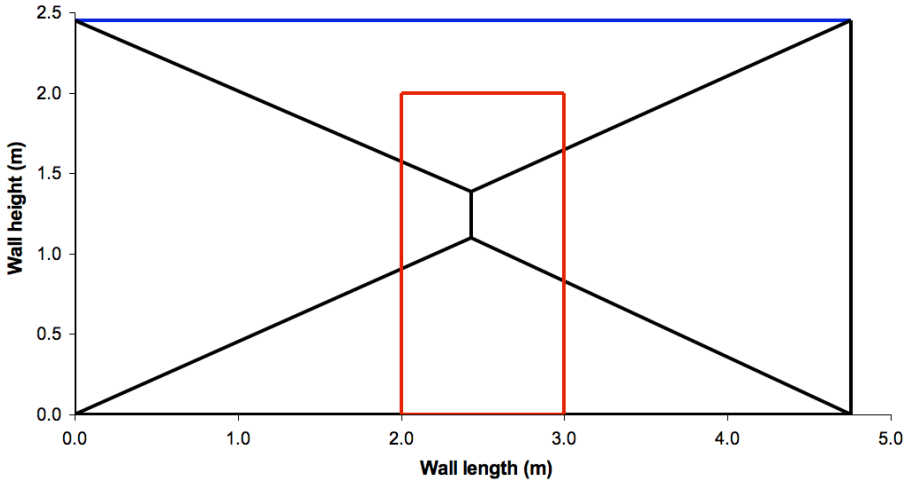


(b) Door opening size 1.0 x 2.0 m (24 % of yield lines within opening)

**Figure 8.15.** Failure modes for wall panel with opening of size (a) 1.0 x 1.5 m and (b) 1.0 x 2.0 m when positioned 2.0 m from LHS

### 8.1.7 Cavity wall assemblies

The cavity wall panel tested in the experimental study comprised of a brick outer leaf and AAC block inner leaf. The brick outer leaf was not subject to any imposed vertical axial loading, whilst the inner AAC block leaf was subject to an imposed vertical loading equivalent to one additional storey. Ultimate loads were determined with SA1 for each leaf of the cavity wall assembly using the average experimental flexural strengths ($f_x$). The overall analytical ultimate load for the cavity wall was assumed equivalent to the sum of the ultimate loads of the individual leafs, as discussed in Chapter 6 Section 6.2.3. The experimental and analytical ultimate loads computed using SA1 for the cavity wall specimen W15 are given in Table 8.5. It was found, as discussed in Chapter 6 Section 6.2.3, that the experimental ultimate load of the cavity wall specimen W15 was 33 % lower the ultimate load determined from the

sum of the individual leaves. Similar to this the ultimate load for the cavity wall, determined from the sum of the analytical ultimate loads from SA1 for the individual leaves using the average flexural strength ($f_x$), overestimated the strength of the experimental panel by 33 %. The experimental ultimate load from the sum of the individual leaves correlated very well to the analytical value, although it was noted that there were differences between the ultimate loads of the individual panels for each case.

It was previously reported (Haseltine et al., 1977) that analytical ultimate loads determined from the sum of the individual leaves both underestimated and overestimate the experimental ultimate loads of cavity walls by up to 44 and 17 % respectively. The difference between the analytical and experimental ultimate loads for specimen W15 was also at the upper end of the variability expected in the results, as discussed in Section 8.1.2. It was likely that the support conditions at the edge of the outer leaf may have reduced the experimental ultimate load of specimen W15 and this requires further investigation. Accepting the typical variation expected in the results, however, suggested that it may be appropriate to derive the strength of the cavity wall from the sum of the analytical ultimate loads for the individual leafs.

**Table 8.5.** Comparison of experimental and analytical ultimate loads for cavity wall panel W15

| **Specimen reference** | **Masonry / mortar type** | **Experimental ultimate load (kN/m$^2$)** | | | **Analytical ultimate load (kN/m$^2$)** (from individual leaves) |
|---|---|---|---|---|---|
| | | Test | Individual leaves | | |
| W15 | Brick outer & AAC block inner / M2 | 3.41 | Inner | 1.84 | 2.00 |
| | | | Outer | 2.70 | 2.54 |
| | | | Sum | 4.54 | 4.54 |

### 8.1.8 Comparison to experimental results in the literature

#### 8.1.8.1 Experimental tests and analysis completed by Chong (1993)

An experimental study previously completed (Chong, 1993) examined the strength of wall panels both with and without openings at prototype scale. This allowed the effect of introducing the opening into the wall panel to be assessed. Both brick and block specimens were tested and were denoted by the prefixes SB and DC respectively. Two cavity walls were also tested, denoted CB01 and 02, that comprised brick leaves connected using flat strip ties. The values determined in the tests were

compared to results from yield line and finite element analysis, although no details were given of the yield line method used. The experimental results detailed provided an opportunity to verify the values computed using SA1 and assess how well the opening was modelled. Analytical values were determined for the wall panels using the parameters given in Table 8.6, whilst the dimensions and support conditions are given in Table 8.7 (Chong, 1993). It was stated that self-weight effects were considered in the analyses and the material density was assumed to be 2000 kg/m$^3$ in the absence of a given value. The ultimate loads given in the previous study (Chong, 1993), from the experimental tests, yield line analysis and FEA, and the analysis completed using SA1 are given in Table 8.7.

**Table 8.6.** Parameters used in the analysis (Chong, 1993)

| **Parameter** | **Value** | | **Units** |
|---|---|---|---|
| | Brick (SB, CB tests)[1] | Block (DC tests)[1] | |
| Equivalent mortar strength class | M4 | M4 | - |
| Flexural strength direction 1, $f_{xd1}$ | 0.74 | 1.37 | N/mm$^2$ |
| Flexural strength direction 2, $f_{xd2}$ | 1.70 | 1.68 | N/mm$^2$ |
| Unit thickness | 0.103 | 0.100 | m |
| Density | 2000 | 2000 | kg/m$^3$ |
| Vertical load | 0.00 | 0.00 | kN/m |

[1]SB brick single leaf, CB cavity brick, DC block single leaf

The inclusion of openings in the wall panels reduced the experimental ultimate load when compared to the control walls without openings, as shown in Table 8.7. It was found in the previous study (Chong, 1993) that the values given by yield line analysis overestimated the ultimate load, whilst those given by finite element analysis generally underestimated the values, as given by Table 8.7. It was stated that the failure mode was generally modelled well using both methods (Chong, 1993). No details were given on how the analytical ultimate load was computed for the cavity walls and the values given were in excess of twice the load established for the corresponding single leaf walls. It was however assumed (Chong, 1993) that the strength of the cavity walls was equal to the sum of the individual leaves for the purpose of analysis. The finite element analysis adopted (Chong, 1993) allowed for the stiffness of the window frame and covering board to be included, but was not clear if there was any attempt to account for this in the yield line method.

**Table 8.7.** Experimental/analytical ultimate loads for a previous study (Chong, 1993) of wall panels with and without openings and analytical ultimate loads determined using SA1

| Test wall | Length x Height (m) | Support conditions[1] | Opening parameters (m) | | Ultimate load (kN/m$^2$) | | | |
|---|---|---|---|---|---|---|---|---|
| | | | Position x, y | Size L x H | Chong (1993) | | | SA1 optimised |
| | | | | | Test | Yield line | FEA | |
| SB01 | 5.615 x 2.475 | A | - | - | 2.8 | 3.16 | 2.46 | 2.38 |
| SB02 | As SB01 | A | 1.68 x 0.90 | 2.26 x 1.13 | 2.4 | 2.59 | 2.16 | 1.90 |
| SB03 | As SB01 | A | 1.34 x 1.50 | 2.94 x 0.53 | 2.3 | 2.44 | 1.91 | 1.95 |
| SB04 | As SB01 | A | 2.35 x 0.00 | 0.91 x 2.03 | 2.2 | 2.57 | 1.94 | 2.14 |
| SB05 | As SB01 | B | - | - | 2.7 | 3.16 | 2.46 | 1.82 |
| SB06 | 2.9 x 2.45 | C | - | - | 7.5 | 8.70 | 6.75 | 8.16 |
| SB07 | As SB06 | C | 1.00 x 0.90 | 0.90 x 0.90 | 5.5 | 6.71 | 5.78 | 5.80 |
| SB09 | As SB01 | D | 3.82 x 0.90 | 0.90 x 0.90 | 2.4 | 3.17 | 2.26 | 3.29 |
| CB01 | As SB01 | A | - | - | 5.8 | 7.08 | 5.05 | 4.76 |
| CB02 | As SB01 | A | As SB02 | As SB02 | 3.8 | 5.81 | 3.46 | 3.79 |
| DC01 | As SB01 | A | - | - | 2.65 | 3.13 | 2.39 | 3.00 |
| DC02 | As SB01 | A | As SB02 | As SB02 | 1.75 | 2.21 | 1.70 | 2.66 |
| DC02B | As SB01 | B | As SB02 | As SB02 | 1.5 | 1.91 | 1.38 | 1.45 |

[1]Type A Base clamped, sides simply supported, top free; Type B Base and sides simply supported, top free; Type C Base clamped, sides and top simply supported; Type D Base and sides clamped, top free

[2]Results given by Chong (1993)

The values computed using SA1 differed to those calculated in the previous study (Chong, 1993) using a yield line method, with varying degrees of under and overestimation in the results. In the absence of details given for the yield line method used it was difficult to make a judgement on why the results differed. The strength of the cavity wall CB01 without an opening was underestimated when based on the sum of the individual leaves, but CB02 with an opening was well modelled. Walls SB05, SB09 and DC02 were particularly poorly modelled in terms of ultimate load, but some explanation of this behaviour could be formed. Wall SB05 was fitted with a

DPC one course of bricks above the base that were subject to fully clamped conditions. The use of a DPC implied simple support conditions, however SB05 performed similarly to SB01 with no DPC and may have been influenced by the proximity of the clamped support and the DPC at the base of the panel. The conditions imposed at the base of wall SB05 in the test were hypothesised to have a higher degree of fixity than the simple support assumed and could be confirmed by the similarity to the experimental ultimate load of SB01. Wall SB09 was built with returns at the vertical edges and the assumption of fully clamped conditions may not have been appropriate. If the support conditions of wall SB09 were assumed to be simply supported then SA1 yields a ultimate load of 2.34 kN/m$^2$, which better reflects the experimental result.

Wall DC02 was significantly overestimated by SA1, but the performance of the panel during testing could account for this. Cracking was noted to occur along the base of the specimen early on in the test and might have resulted in the panel performing as if it were simply supported at the base for the remaining duration of the test. Assuming that wall DCO2 was simply supported at the base provided an ultimate load of 1.45 kN/m$^2$ via SA1, which showed an improved correlation to the experimental result.

The failure modes determined with SA1 by optimisation and those given in the previous study (Chong, 1993) for wall panels SB02 and SB04 are shown in Figures 8.16 and 8.17 respectively. Taking the previous experimental arrangements (Chong, 1993) it was found that the optimised crack patterns developed in SA1 were generally in line with those used in the finite element analysis. It was not stated (Chong, 1993) if the same patterns were used to determine the ultimate loads via the yield line method. It was observed from Figures 8.16 and 8.17 that for wall panels SB02 and SB04 that the optimised modes from SA1 were not completely identical to the experimental/analytical patterns from the previous study (Chong, 1993). Consistency was achieved by manually adjusting the nodal positions in SA1, but this was found to have a limited effect on the ultimate load. For wall panels SB02 and for SB04 an increase of 5 and 2 % was given when compared to the optimised ultimate load respectively. In summary, an average difference of 17 % was found between the experimental values and those from SA1 and was acceptable considering the expected variability as discussed in Section 8.1.2. The comparison that was completed verified that SA1 was capable of producing ultimate loads and modes that

were generally consistent with the experimental results of the previous study (Chong, 1993).

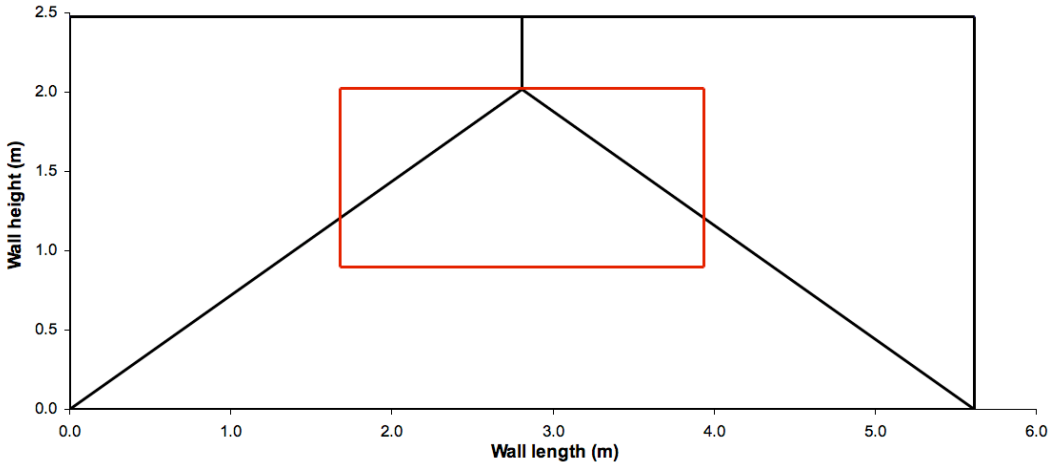


(a)

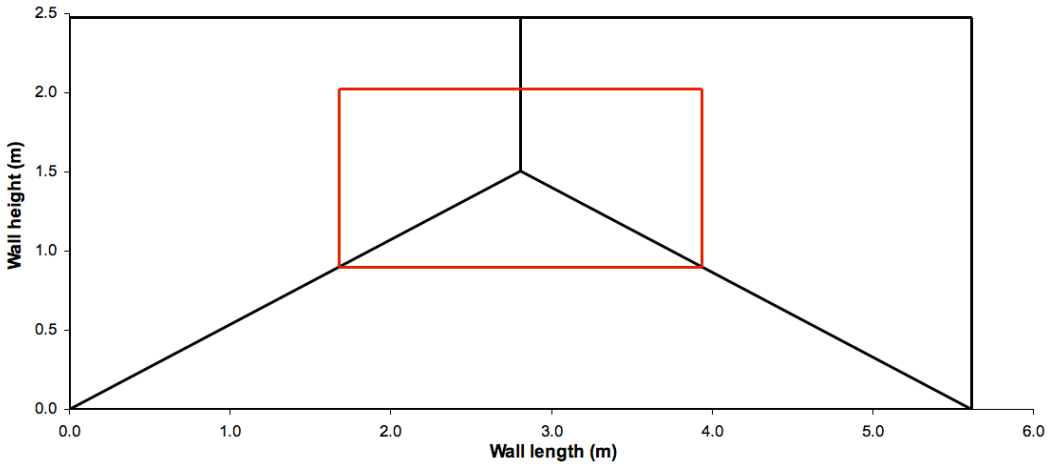


(b)

**Figure 8.16.** Failure modes for panel SB02 (a) SA1 optimised and (b) as experimental / assumed for FEA method (Chong, 1993)

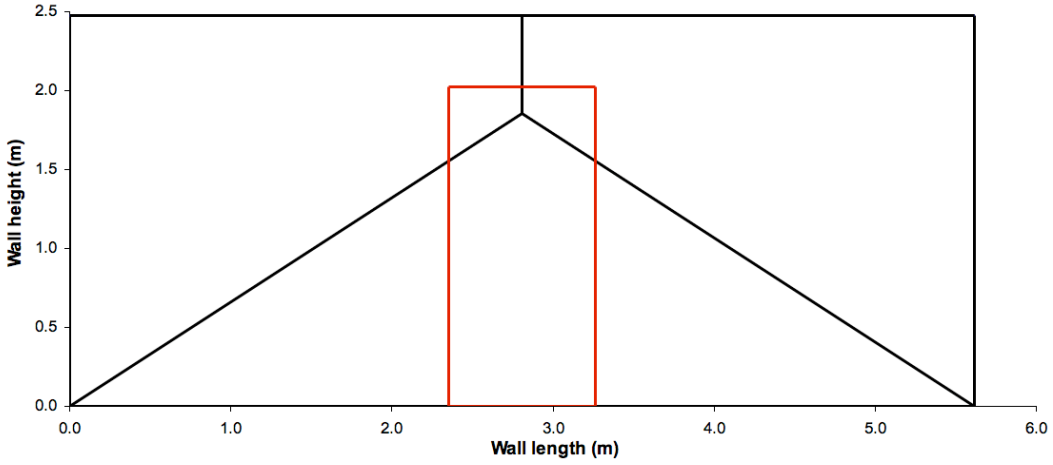


(a)

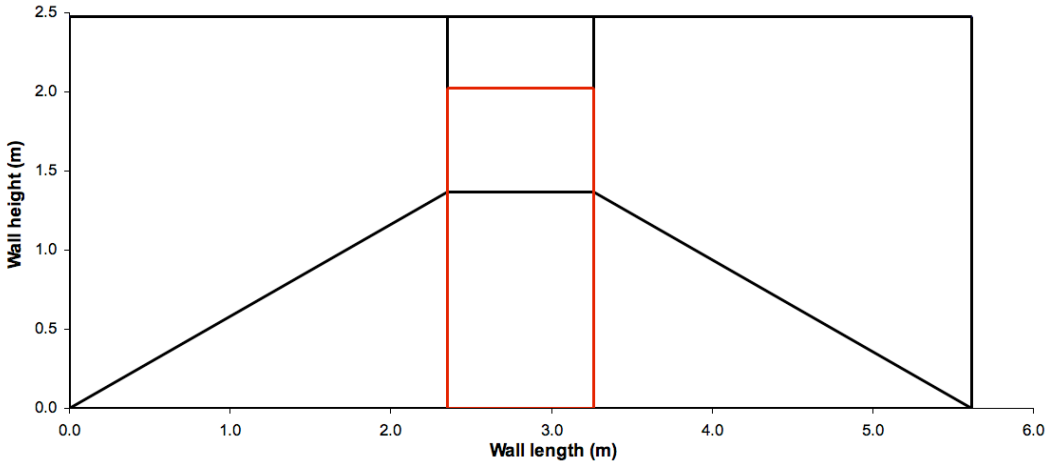


(b)

**Figure 8.17.** Failure modes for panel SB04 (a) SA1 optimised and (b) as experimental / assumed for FEA method (Chong, 1993)

### 8.1.8.2 Experimental tests and analysis completed by Duarte (1998) and Duarte and Sinha (1992)

The results of an experimental study of wall panels with openings that were completed at 1:2 scale have previously been compared to results computed by yield line analysis (Duarte, 1998, Duarte and Sinha, 1992). Sufficient details were provided in the study, as given in Tables 8.8 and 8.9, such that it was possible to analyse the panels to provide some additional verification of SA1. In the study the yield line patterns were fixed and there did not appear to be any attempt to optimise the failure modes. It was acknowledged that the actual modes deviated from the fixed patterns used in the analysis. It was therefore of interest to assess whether the optimised patterns differed to the fixed patterns and how well they correlated to those found in the experimental tests. In all cases it appeared that the effect of self-weight was neglected and to reflect this the density of the material was set to zero to allow

comparison with the results from the previous analysis (Duarte, 1998, Duarte and Sinha 1992). The average experimental and analytical results from the previous study (Duarte, 1998, Duarte and Sinha, 1992) are given in Table 8.9 along with the values computed using SA1. The experimental and analytical failure modes from the previous study (Duarte, 1998, Duarte and Sinha, 1992) and the mode given by optimisation in SA1 for wall panel 8 are shown in Figure 8.18.

**Table 8.8.** Parameters used in the analysis (Duarte, 1998, Duarte and Sinha, 1992)

| **Parameter** | **Value** | **Units** |
|---|---|---|
| Equivalent mortar strength class | M12 | - |
| Flexural strength direction 1, $f_{xd1}$ | 0.84 | $N/mm^2$ |
| Flexural strength direction 2, $f_{xd2}$ | 2.08 | $N/mm^2$ |
| Unit thickness | 0.056 | m |
| Panel height | 1.20 | m |
| Opening length | 0.40 | m |
| Opening height | 0.40 | m |
| Density | 0 | $kg/m^3$ |
| Vertical load | 0.00 | kN/m |

**Table 8.9.** Experimental/analytical ultimate loads for a previous study of wall panels with openings (Duarte, 1998, Duarte and Sinha, 1992) and analytical ultimate loads determined using SA1

| **Test walls** | **Length (m)** | **Support conditions**[1] | **Opening position x, y (m)** | **Ultimate load ($kN/m^2$)** | | | |
|---|---|---|---|---|---|---|---|
| | | | | Duarte, Duarte & Sinha | | | SA1 Optimised |
| | | | | Test | Yield line | SA1[2] | |
| 1&2 | 1.2 | SS | Centre (0.4, 0.4) | 9.1 | 8.7 | 8.66 | 8.33 |
| 3&4 | 1.2 | SS-TF | Centre (0.4, 0.4) | 7.5 | 5.9 | N/A | 5.69 |
| 5&6 | 1.2 | SS-RF | Centre (0.4, 0.4) | 7.1 | 4.5 | N/A | 4.28 |
| 7&8 | 1.8 | SS | Centre (0.7, 0.4) | 5.9 | 5.7 | 5.65 | 5.54 |
| 9&10 | 1.8 | SS-TF | Centre (0.7, 0.4) | 3.5 | 3.4 | N/A | 3.33 |
| 11&12 | 1.8 | SS | Offset (0.9, 0.5) | 6.9 | 6.9 | N/A | 5.90 |
| 13&14 | 1.8 | SS-TF | Top (0.7, 0.8) | 3.7 | 3.3 | N/A | 3.22 |
| 15&16 | 1.8 | SS-RF | Centre (0.7, 0.4) | 2.6 | 3.4 | N/A | 3.29 |

[1]SS all edges simply supported, SS-TF top free else simply supported, and SS-RF right edge free else simply supported

[2]Pattern adjusted manually in SA1 to match that given by Duarte (1998) and Duarte and Sinha (1992)

The yield line patterns that were assumed in the previous study (Duarte, 1998, Duarte and Sinha, 1992) generally provided results that approximated the experimental findings with acceptable accuracy. Walls 5 and 6, which were free on the right hand vertical edge, were however significantly underestimated by the yield line method. It was suggested (Duarte and Sinha, 1992) that there was an anomaly in the experimental results for wall panels 5 and 6, since the strength was similar to walls 3 and 4 despite the differences in support conditions. Where it was possible to match the theoretical yield line pattern given, by manually adjusting the position of the nodes in SA1, good agreement was found and verified the results from the analysis.

The optimised results given by SA1 were consistently lower than those given in the previous study (Duarte, 1998, Duarte and Sinha, 1992), which illustrated that the pattern assumed did not provide the lowest upper bound result. The reason for the differences in the ultimate load determined was due to the assumption the yield lines terminated at the edge of the opening, as shown in Figure 8.18a, which would result in an over estimation of the displacement of the yield lines at the points of coincidence with the opening edge. SA1 allows for the yield lines to be positioned such that they could terminate within the opening, as presented in Figure 8.18b, which was in line with methods presented by others (Islam and Park, 1971, Wagner, 1994). The relationship between the experimental and analytical loads given by SA1 however followed the same pattern as previously found (Duarte, 1998, Duarte and Sinha, 1992), where an acceptable agreement was given to the experimental ultimate loads with the exception of walls 5 and 6. As discussed above the effect of self-weight was ignored in the previous study (Duarte, 1998, Duarte and Sinha, 1992) and when this was included it was found to increase the ultimate load by an average 1 %, which was considered insignificant.

The position of the yield lines assumed in the previous study (Duarte and Sinha, 1992) and in the optimised solution from SA1 differed to those found experimentally, as presented for wall 8 in Figure 8.18. The experimental pattern might have been influenced by the method used to cover the opening, which imposed point loads at the corners of the opening rather than uniform line loads along the perimeter of the opening. SA1 has been verified by comparing the analytical ultimate loads computed to those from experimental tests completed in a previous study (Duarte, 1998, Duarte and Sinha, 1992), however the failure modes were not always accurately modelled.

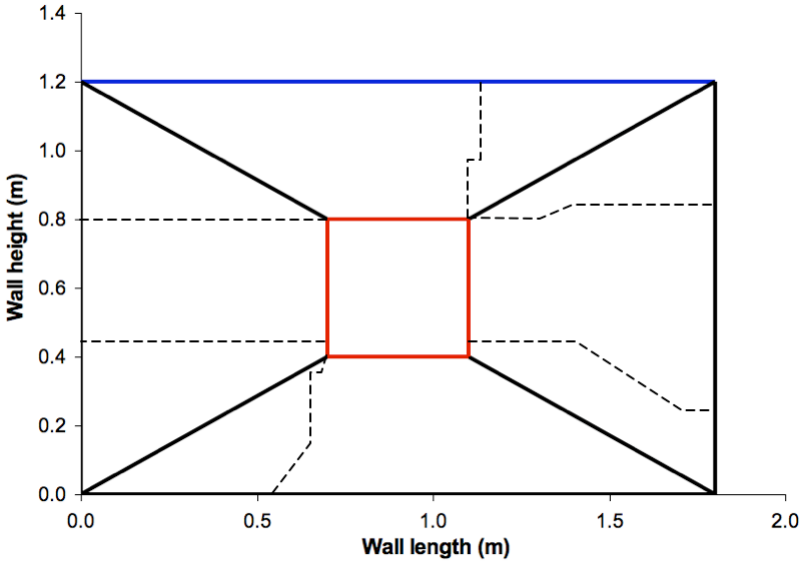


(a)

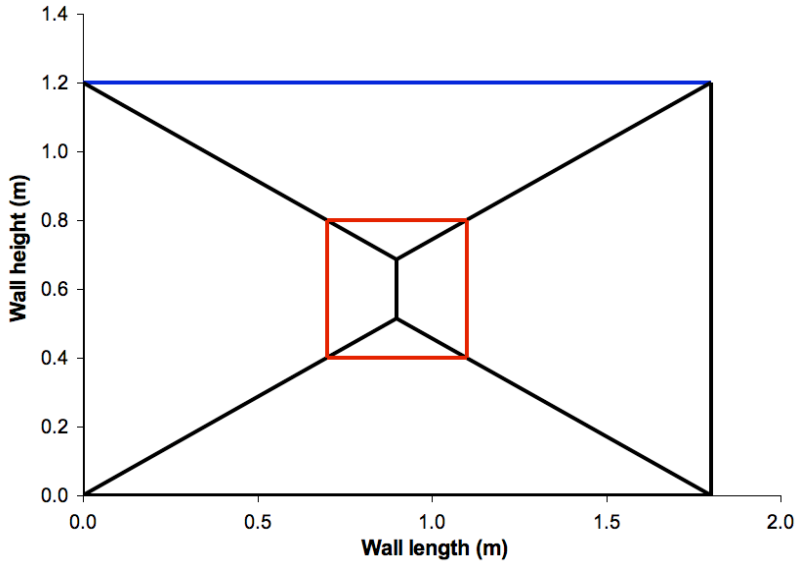


(b)

**Figure 8.18.** Analytical failure modes for wall panel 8 (a) assumed in previous study (Duarte and Sinha, 1992) and (b) optimised using SA1 (dashed lines represent approximate position of cracks in experimental test of wall 8)

## 8.2. Hydraulic loading analysis

### 8.2.1 Verification of analysis SA1 to method given by Kelman and Spence (2003a)

A theoretical analysis has been presented in the literature (Kelman and Spence, 2003a) to determine the ultimate water level that can be retained by masonry wall panels. The analysis was based on a yield line approach and the moments of resistance were developed from frictional and overturning resistance of the sections, rather than utilising flexural strength. The friction/overturning resistance approach was incorporated into SA1, as detailed in Chapter 3 Section 3.2.3.1, and was found to significantly underestimate the ultimate water levels for the specimens tested in this programme. The analysis developed in the previous study (Kelman and Spence, 2003a) was not verified, by either experimental means or by comparison to results in the literature. It was therefore important to firstly verify the results computed using the friction/overturning resistance method in SA1 to those given in the previous study (Kelman and Spence, 2003a), and secondly to compare the results given (Kelman and Spence, 2003a) to values calculated using the flexural strength method in SA1. Comparison with the flexural strength method would further examine whether the approach previously given (Kelman and Spence, 2003a) was appropriate for calculating the ultimate water level of masonry wall panels.

The frictional/overturning resistance method was used in SA1 to determine the ultimate water level with identical parameters as used in the previous study (Kelman and Spence, 2003a), which are given in Table 8.10. The wall panels were clamped at all edges in the analysis in line with the previous study. The length of the wall panel was varied and the proportion of roof and floor load, $\lambda$, was either 0.0 or 0.4. The ultimate water levels from the analysis in the previous study (Kelman and Spence, 2003a) and from SA1 are given in Table 8.11. It was apparent from Table 8.11 that the values from SA1 correlated very well to the values given in the previous study (Kelman and Spence, 2003a). Discrepancies were only observed between values when they were taken from figures, since tabulated values were only given for a limited number of panel lengths. This verified that SA1 produced results that were consistent to those previously found (Kelman and Spence, 2003a) when using the frictional/overturning moment resistance method. The failure modes observed were of the same form as that given in the previous study (Kelman and Spence, 2003a), however modes specific to different wall panel lengths and parameters were not presented. It should be noted that in the study an arbitrary value of 0.2 m was added to the water level to allow for difference in ground level between the inside and

outside of the property for some of the values given. This additional 0.2 m was omitted from all the results in Table 8.11.

**Table 8.10.** Parameters used in analysis (Kelman and Spence, 2003a)

| **Parameter** | **Notation** | **Value** | **Units** |
|---|---|---|---|
| Height | H | 2.40 | m |
| Plan area | A | 55 | $m^2$ |
| Number of floors | j | 2 | No units |
| Proportion of floor/roof load | λ | 0.0 and 0.4 | No units |
| Floor load | – | 50 | $kg/m^2$ |
| Roof load | – | 70 | $kg/m^2$ |
| Compression factor | Cf | 0.95 | No units |
| Coefficient of friction | ω | 0.30 | No units |
| Unit thickness | Tbl | 0.100 | m |
| Unit density | ρ_brick | 1000 | $kg/m^3$ |
| Water density | ρ_water | 1026 | $kg/m^3$ |

**Table 8.11.** Comparison of results given by Kelman and Spence (2003a) and those from SA1 using the friction/overturning resistance method

| Wall panel length, L (m) | Ultimate water level (m) | | | |
|---|---|---|---|---|
| | Proportion of floor/roof load, λ=0 | | Proportion of floor/roof load, λ=0.4 | |
| | Kelman & Spence | SA1 | Kelman & Spence | SA1 |
| 2[1] | 0.83 | 0.83 | 1.51 | 1.51 |
| 3[2] | 0.76 | 0.77 | 1.22 | 1.22 |
| 4[2] | 0.74 | 0.75 | 1.09 | 1.08 |
| 5[1] | 0.73 | 0.73 | 1.00 | 1.00 |
| 6[2] | 0.71 | 0.72 | 0.95 | 0.94 |

[1]Tabulated values given

[2]Values taken from figure

To establish whether the frictional/overturning approach previously presented (Kelman and Spence, 2003a) was appropriate to calculate ultimate water levels for masonry wall panels three cases were examined, as detailed in Table 8.12. Ultimate water levels were determined in SA1 using both the frictional/overturning method and the flexural strength method. Characteristic flexural strengths from the National Annex to EC6 (BSI, 2005d) for block of compressive strength 3.6 $N/mm^2$ and M4 strength class mortar were used in the analysis. The parameters were as detailed in

Table 8.10 unless stated otherwise and wall panels of lengths between 2 and 10 m were modelled. Case 1 utilised the building plan area-based method to determine the vertical load applied to the top of the wall panel as proposed in the previous study (Kelman and Spence, 2003a) and detailed in Chapter 3 Section 3.3.2 and all egdes of the panels were clamped. The concern with basing the vertical load on an area was that the area was kept constant and not varied with the length of the wall. This resulted in the vertical load reducing as wall length was increased. In reality the property plan area would vary due to changes in the length and depth of the building, resulting in a larger area for longer walls and likewise a smaller area for shorter walls. The proportion of the total roof/floor load, $\lambda$, on the outer wall in case 1 was also set at a value of 0.25 that would be a better representation of the situation in a typical property. Case 2 repeated the analysis of case 1 except the vertical load was set to a constant value per metre length of wall and was therefore independent of the plan area. Case 3 was identical to case 2 except the top and bottom of the wall panel were simply supported rather than clamped. The ultimate water levels for each case, calculated using the friction/overturning resistance and flexural strength methods, are shown in Figure 8.19.

**Table 8.12.** Parameters used in comparative analysis completed in SA1

| **Case** | **Friction/overturning resistance method** Kelman and Spence (2003a) | **Flexural strength method**[1] |
|---|---|---|
| 1 | As in Table 8.13 except:<br>$\lambda$ = 0.25 | As in Table 8.13 except:<br>$\lambda$ = 0.25<br>Cf = 0.33<br>$\omega$ = 0.0<br>$f_{xk1}$ = 0.25 N/mm$^2$<br>$f_{xk1}$ = 0.45 N/mm$^2$ |
| 2 | As case 1 above except:<br>$\lambda$ = 0.00<br>Vertical load = 5.59 kN/m | As case 1 above except:<br>$\lambda$ = 0.00<br>Vertical load = 5.59 kN/m |
| 3 | As case 2 above except:<br>Simple supports top and bottom of wall | As case 2 above except:<br>Simple supports top and bottom of wall |

[1]Based on a blockwork of compressive strength 3.6 N/mm$^2$ and M4 strength class mortar from NA to EC6 (BSI, 2005d)

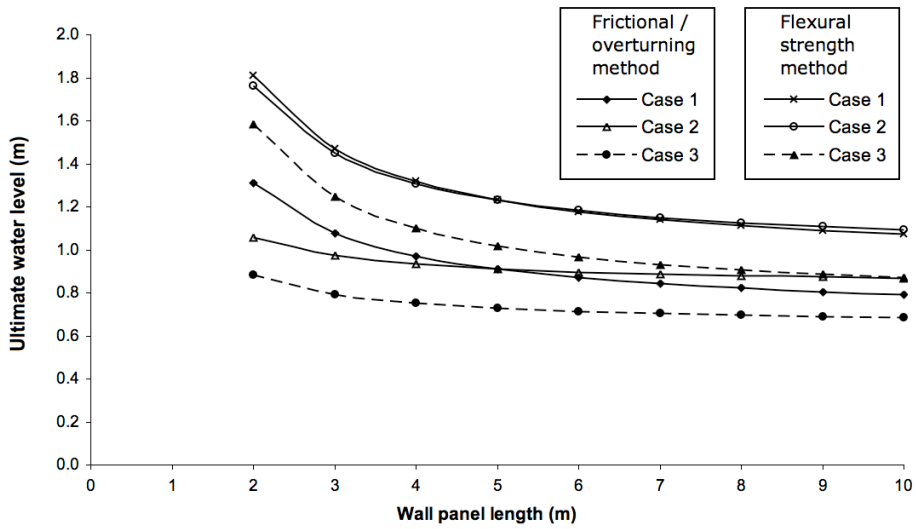


**Figure 8.19.** Variation in ultimate water level for wall panels of different lengths calculated using frictional/overturning resistance and flexural strength methods in SA1 (all panels of height 2.4 m)

It was observed from Figure 8.19 that the frictional/overturning method provided lower ultimate water levels than those calculated using the flexural strength method. Changing the vertical load from a value calculated from the property's plan area (Case 1) to a constant value (Case 2) had a limited influence on water levels computed using flexural strength and was due to the vertical load's moment of resistance in direction 1 being small in relation to the flexural strength in direction 1. A more significant effect was observed when using the friction/overturning method, where the water level varied much less with panel length when the vertical load was constant. The results illustrate that the property plan area should not be kept constant for different panel lengths, but should be proportioned correctly according to the length of the wall panel. The failure modes determined for case 2 using the friction/overturning resistance and flexural strength methods in SA1 are presented in Figures 8.20a and b respectively. It was apparent in Figure 8.20 that the failure modes varied depending on the method used to establish the moment of resistance.

Changing the top and bottom support conditions to simple supports, as in Case 3, reduced the ultimate water level in both methods. Simple supports would be more appropriate at the base of the panel where a damp proof course would be placed and likewise at the top where support would be offered by the floor structure. Clamped conditions at the top of the wall would only be likely when a very stiff reinforced concrete or beam and block type floor was present, which is not particularly common in residential construction. The results of the comparative study further supported the

use of a calculation method based on the flexural strength of the wall panel and not the frictional/overturning resistance.

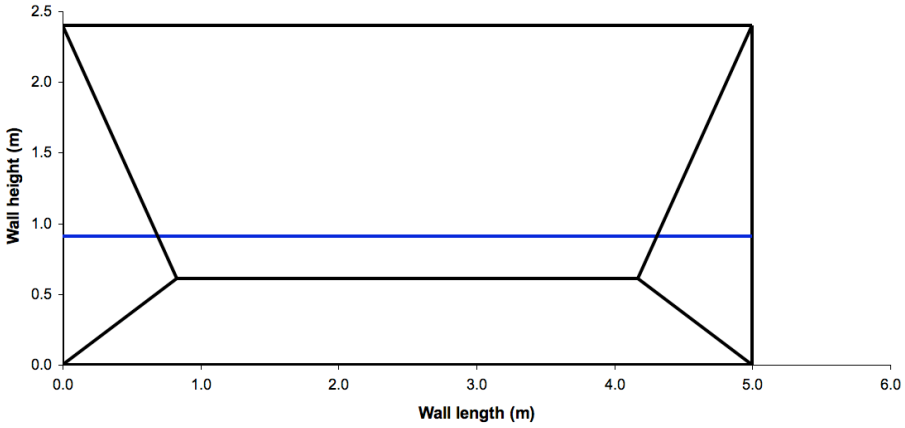


(a)

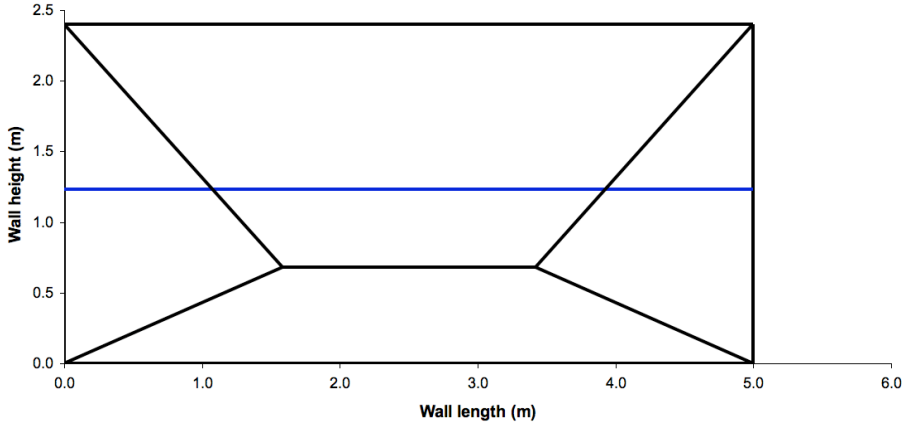


(b)

**Figure 8.20.** Failure modes for a wall panel length of 5m for case 2 (a) friction/overturning and (b) flexural strength methods

In the previous analysis (Kelman and Spence, 2003a) the ultimate water level was based on the strength of the inner leaf of the cavity wall and did not take into account any interaction of the two leaves. It was found in Chapter 7 that the experimentally tested cavity wall panels showed a degree of composite action and their performance was significantly improved when compared to the single leaf walls. If the water were retained outside the property then it would be more appropriate to either consider the strength of the outer leaf or a combined strength of the leaves of the cavity, rather than basing the ultimate water level on the strength of the inner leaf.

It was recommended in the previous study (Kelman and Spence, 2003a) that sealing to heights greater than 1.0 m above ground level should be avoided, however it was

unclear if this included the additional 0.2 m of height between the inner floor and exterior ground level. Factors of safety were, however, not considered in the previous analysis (Kelman and Spence, 2003a) and the water levels calculated were ultimate levels and not characteristic levels. Based on the results presented in Figure 8.19, for case 2 using the frictional/overturning method, then it was apparent that only a wall of 2 m in length could withstand a water level marginally higher than 1.0 m prior to failure and longer walls would fail before 1.0m was achieved. If the support conditions were different to those assumed (Kelman and Spence, 2003a), for example simple supports at the top and bottom of the panel, then this situation would be worsened and failure would occur between 0.9 and 0.7 m dependant on panel length. The results were also dependant on vertical loading (by definition of the method) and any reduction in this would have a significant impact on the ultimate water level. The values determined using the flexural strength method were improved, but wall panels of lengths over 4m in case 3 were still close to the recommended level of 1.0m. Clearly it would not be appropriate to recommend sealing to such a level as proposed (Kelman and Spence, 2003a) when failure could occur with the range specified. A more suitable approach would be to make an assessment of the actual building using the analysis, including any combined effects of cavity walls, and apply the appropriate factors of safety to determine a characteristic water level that can be safely retained, rather than an ultimate level.

### 8.2.2 Verification of analysis SA1 with experimental results for single leaf panels

The analytical ultimate water levels were calculated for the wall panels considered in the experimental study using analysis SA1 and the parameters as detailed in Section 8.1.1 and Table 8.1. The modelling procedure was completed at prototype scale and the experimental ultimate levels from Chapter 7 were scaled by the scaling factor of 6. The ultimate levels were calculated using the average flexural strengths from the wallette tests ($f_x$) as given in Chapter 5 Table 5.1, and the EC6 adjusted flexural strengths ($f_x$ EC6) as given in Table 5.2. The ultimate water levels computed for the wall panels with SA1 are given in Table 8.13.

It was observed from Table 8.13 that the ultimate water levels that were determined using the average flexural strengths from the wallette tests ($f_x$) compared well to the experimental values, with the exception of the brick block specimens H3 and H4 that was underestimated by 14 % in the analysis. The results provided by the analysis were either equal to or lower than the experimental ultimate water levels, with the

exception of specimen H9 that was marginally overestimated by SA1. The analysis was found to underestimate the ultimate water level of all the experimental specimens in Table 8.9 by 3 % on average. Converting the ultimate levels into total ultimate loads, as detailed in Chapter 7 Section 7.1.1, and subsequent evaluation of the variation between the experimental and analytical loads, permitted comparison to the variation reported in previous uniform loading analyses, as discussed in Section 8.1.2. It was found that, on completing this process, the analysis on average underestimated total experimental ultimate loads applied to the wall panels by 6 %. Considering the typical variation expected in the analysis, as discussed in Section 8.1.2, then the analytical results were a very good representation of the experimentally derived ultimate water levels.

**Table 8.13.** Comparison of experimental and analytical ultimate water levels for single leaf panels computed using the flexural strength method in SA1

| **Specimen reference** | **Masonry / mortar type** | **Experimental ultimate water level at prototype scale (m)** | | **Analytical ultimate water level (m)** | |
|---|---|---|---|---|---|
| | | Individual test | Average | $f_x$ | $f_x$ EC6 |
| H1 | AAC block / M2 | 1.05 | 1.09 | 1.09 | 0.99 |
| H2 | | 1.12 | | | |
| H3 | Brick block / M2 | 1.47 | 1.46 | 1.29 | 1.34 |
| H4 | | 1.50 | | | |
| H5 | Brick / M2 | 1.25 | 1.23 | 1.23 | 1.37 |
| H6 | | 1.21 | | | |
| H7 | Brick / M4 | 1.48 | 1.46 | 1.43 | 1.43 |
| H8 | | 1.44 | | | |
| H9 | Brick / M4 | 1.25 | - | 1.28 | 1.28 |
| H10 | Brick / M4 | 1.48 | - | 1.46 | 1.46 |

The analytical ultimate water levels determined from the EC6 adjusted ($f_x$ EC6) flexural strengths, similarly, compared well to the experimental ultimate levels. The analysis again underestimated the ultimate level of the brick block specimens (H3 and H4), but by a lower proportion (11 %) compared to when the average test flexural strengths were utilised. The improved value given for specimens H3 and H4 was due to the EC6 adjusted flexural strengths exceeding those found in the wallette tests. The average experimental ultimate level for the brick wall panels constructed with M2 mortar (H5 and H6) was overestimated by 11 % when the EC6 adjusted flexural strengths were used in the analysis. The variation in the results for

specimens H5 and H6 was similarly related to differences between the experimental and EC6 adjusted flexural strengths. The analysis was found to on average underestimate the experimental ultimate levels by 6 % when the EC6 adjusted flexural strengths were utilised. When computed into total loads, as detailed above, the analysis underestimated the strength of the experimental specimens by 12 %, which was within the expected variation, as discussed in Section 8.1.2. The results obtained from SA1 with the EC6 adjusted flexural strengths were not always conservative with respect to the experimental ultimate water levels, and this again highlighted the importance of utilising the appropriate flexural strengths for the wall panel in consideration where possible.

The results were not presented for either frictional/overturning resistance method as they were previously found, in Section 8.1.2, to be unsuitable for application to uncracked masonry panels. In summary, the results from SA1 illustrated that the ultimate water levels could be established with a good degree of accuracy. The position of the yield lines in the analysis was generally considered to be an acceptable representation of the experimental failure modes, considering the constraints utilised in the analysis. The main differences in the failure modes that were observed in the optimised and experimental cases was that corner levers were observed to form in the specimens due to the position of the yield lines. Possible effects of differences between the failures modes of the optimised analytical solutions and as observed in the experimental tests are examined in the following section.

### 8.2.3 Effect of failure mode on the ultimate water level

The analytical values presented in Table 8.13 were the lower of the upper bound solutions determined by optimisation in SA1. To assess the impact of the position of the yield lines SA2 was utilised in which the formation of corner levers could be considered and the results were compared to the optimised values. Where possible the position of the yield lines were adjusted to provide a better representation of those observed in the experimental tests. Parameters used in the investigation were otherwise identical to those used in the optimised solutions formed with the average flexural strengths ($f_x$). The effect of failure mode on the ultimate water level of wall panel H1 that was constructed with AAC block and M2 compressive strength mortar was examined and the experimental, SA1 optimised and SA2 failure modes are shown in Figures 8.21a, b and c respectively.

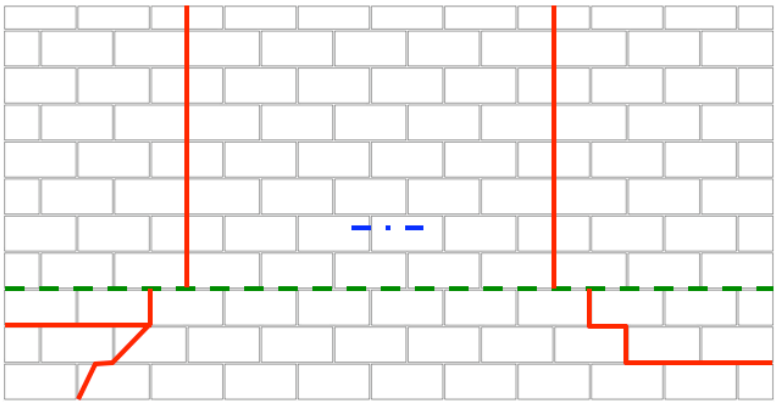

(a)

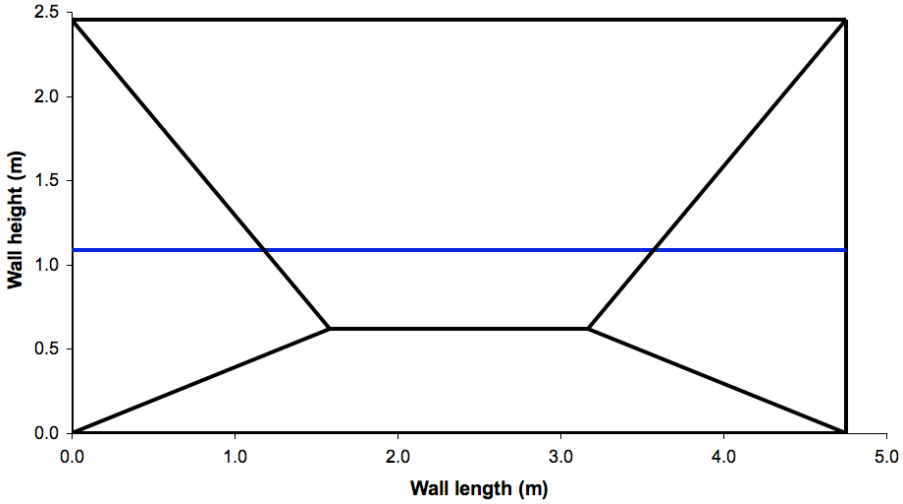


(b)

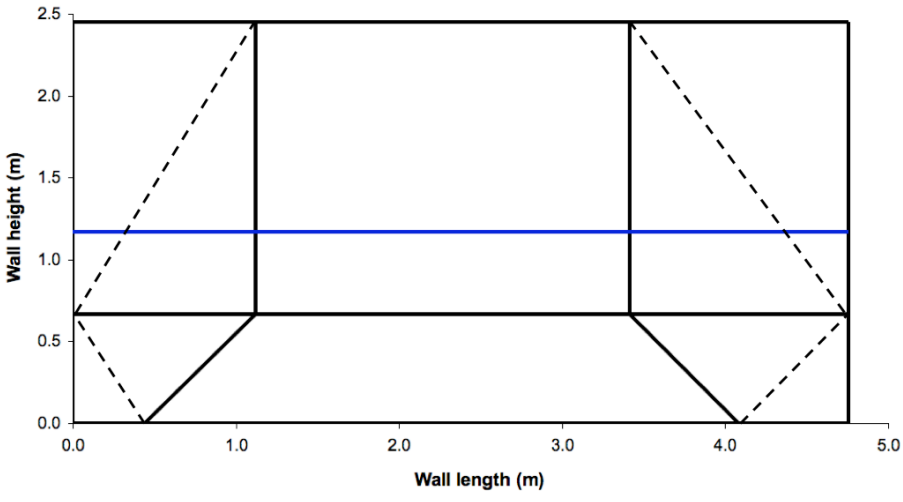


(c)

**Figure 8.21.** Yield line patterns for AAC block specimen H1 (a) experimental, (b) optimised using SA1 and (c) using SA2 (dashed lines show position of corner lever pivots)

For specimen H1 it was observed, from Figures 8.21a and b, that the optimised pattern was comparable to the experimental pattern in the bottom section of the panel and the position of the horizontal crack was similar. The horizontal crack could not traverse the length of the panel in the optimised SA1 solution due to the yield line pattern selected. In the upper section of the panel the optimised pattern differed as the yield lines were constrained to the corners in SA1. Repositioning the yield lines in SA2 provided a significantly improved approximation of the experimental crack pattern, as shown in Figure 8.21c. The ultimate water level was determined as 1.17 m and was 7 % higher than the optimised value. The value obtained from SA2 however further overestimated the experimental water level by an additional 11 %. The optimised failure mode was likely not observed in the upper section of the experimental specimen due to the formation of the initial horizontal crack that traversed the specimen. The deflected shape of the upper section of the panels resulted in negative deflection in the corners and, as described in Section 8.1.6, may have resulted in the cracks forming towards a location away from the corners of the specimen.

The process was repeated for brick specimen H5 that was constructed with M2 compressive strength mortar and the experimental, SA1 optimised and SA2 failure modes are presented in Figures 8.22a, b and c respectively. It was found that the pattern determined by optimisation for brick specimen H5, as shown in Figure 8.22b, provided a reasonable approximation of the experimental pattern, as presented in Figure 8.22a, but the most significant differences were again observed in the top section of the panel. In the upper section of experimental specimen H5 the yield lines tended to the side supports such that the slab created at failure would rotate about a line formed between the two upper cracks. It would therefore be appropriate to model the panels with a total height equivalent to the position of the upper crack, particularly since the applied lateral load was below this level. For specimen H5 the equivalent panel height was set as 1.68 m to be in line with the diagonal crack in the upper left hand section of experimental pattern. The resulting pattern provided a better approximation to that observed in the experimental test, as shown in Figure 8.22c. The ultimate water level was calculated at 1.29 m and exceeded the optimised and experimental values by 5 and 3 % respectively. The optimised solution may have not been observed in the experimental specimen due a combination of the load being offset towards the base of the wall and the panel being able to pivot away from the upper support at failure as a result of the simple support conditions imposed.

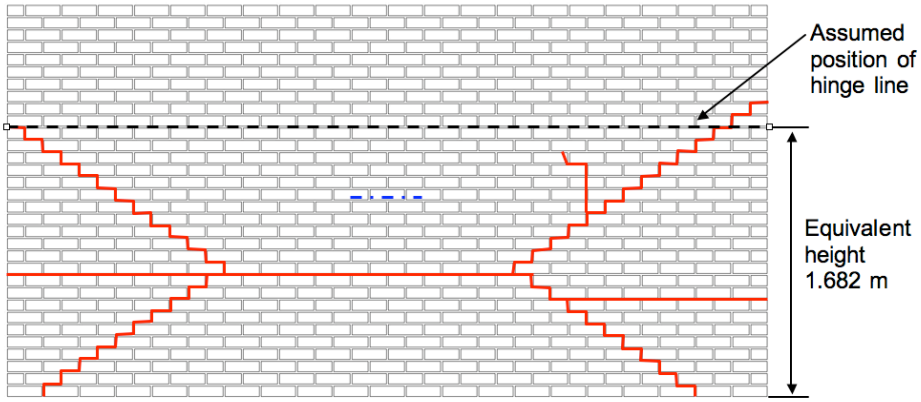


(a)

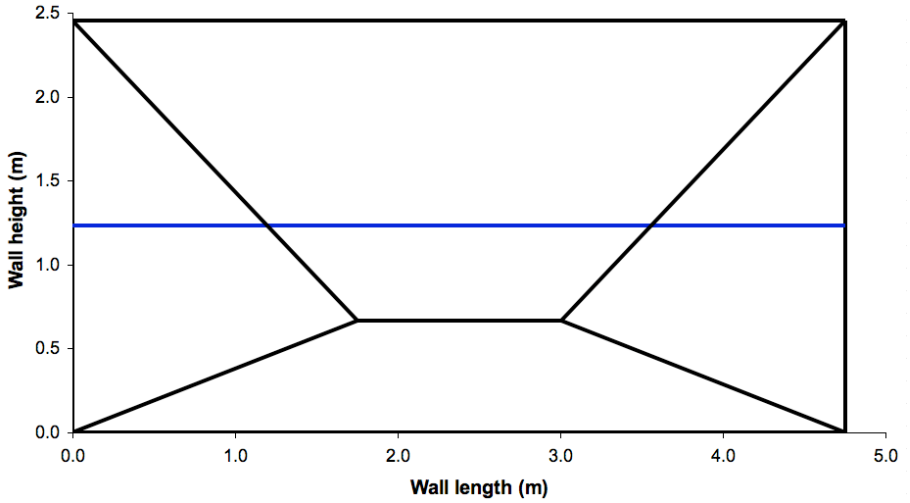


(b)

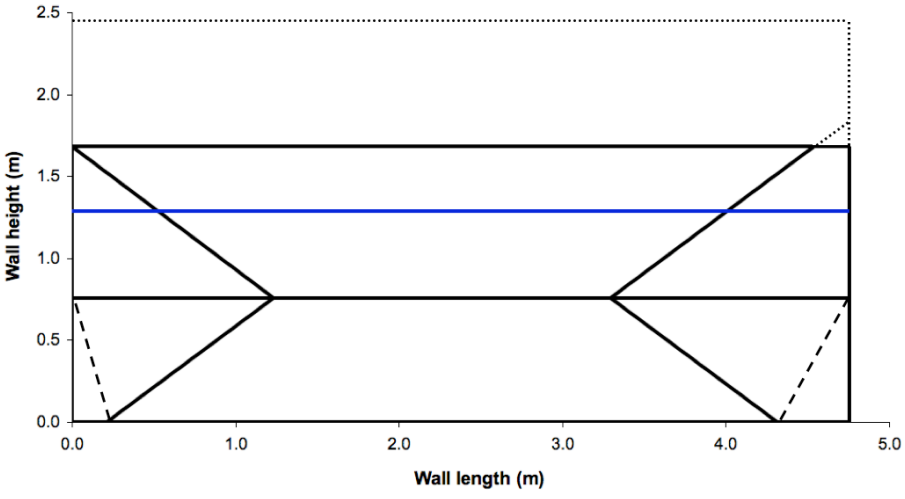


(c)

**Figure 8.22.** Yield line patterns for H5 (a) experimental, (b) optimised using SA1 and (c) using SA2 with reduced wall panel height (dotted line represents actual panel size, dashed lines show position of corner levers pivots)

Values were also similarly determined for specimens H3 and H7 using SA2. To evaluate the overall difference between the experimental findings, the analytical results were plotted as a percentage of the experimental ultimate water levels, as shown in Figure 8.23. It was found that the average difference between the optimised results and those from SA2 was 7 % (for specimens H1, H3, H5 and H7). This suggests that in general the use of an optimised failure pattern which approximated that observed in experimental tests would be appropriate. It should be noted that the results derived from SA2 required the position of the yield lines to be manually adjusted and to obtain such values automatically would necessitate the use of additional constraints. This could actually result in other correct lower upper bound solutions being missed leading to overestimation of the ultimate levels.

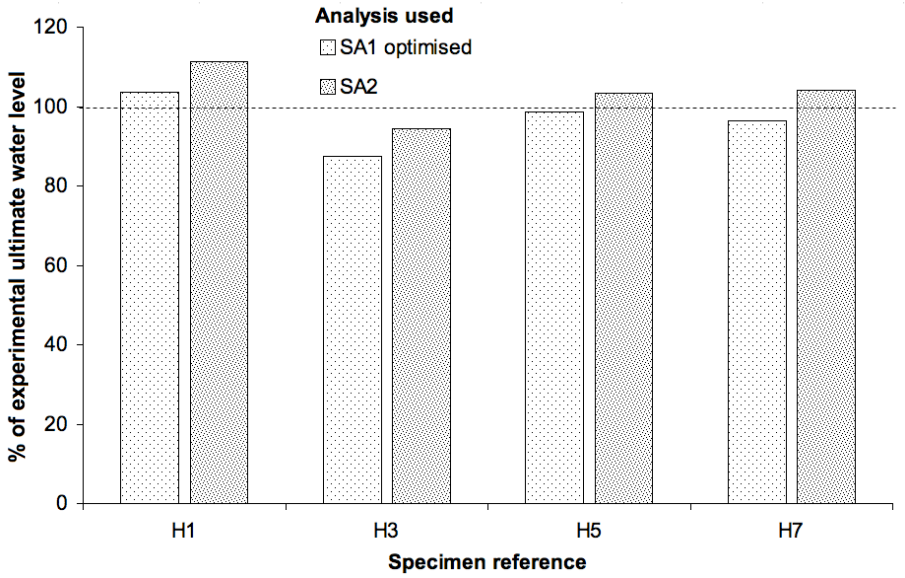


**Figure 8.23.** Comparison of experimental and analytical ultimate water levels for the two different analyses

### 8.2.4 Effect of vertical load on the ultimate water level

The effect of varying the vertically applied load between 4.5 kN/m (walls H7 and H8) and 10.8 kN/m (wall H10) was investigated in the experimental programme and found to have little effect on the ultimate water level. An insignificant increase of 2 % was found in the corresponding results from SA1, as detailed in Table 8.9. As discussed in Section 8.1.4, a significant effect of the imposed vertical load on the ultimate load of uniformly loaded specimens was reported in a previous study (Hendry et al., 1971). It was therefore important to assess the effect of vertically applied loads above those applied in the experimental study. Vertical loads of up to 55 kN/m were similarly modelled as for the uniform analysis presented in Section

8.1.4. The wall panel dimensions were as in the experimental study and simple support conditions were assumed at all edges. The procedure was completed for brick with M2 and M4 compressive strength class mortar and AAC block with M2 compressive strength class mortar. The average experimental flexural strengths ($f_x$) were used in SA1 to determine the ultimate water levels, whilst other parameters were as given in Table 8.1. The effect of varying the vertical imposed load on the ultimate water level for the block and brick wall panels analysed is shown in Figure 8.24.

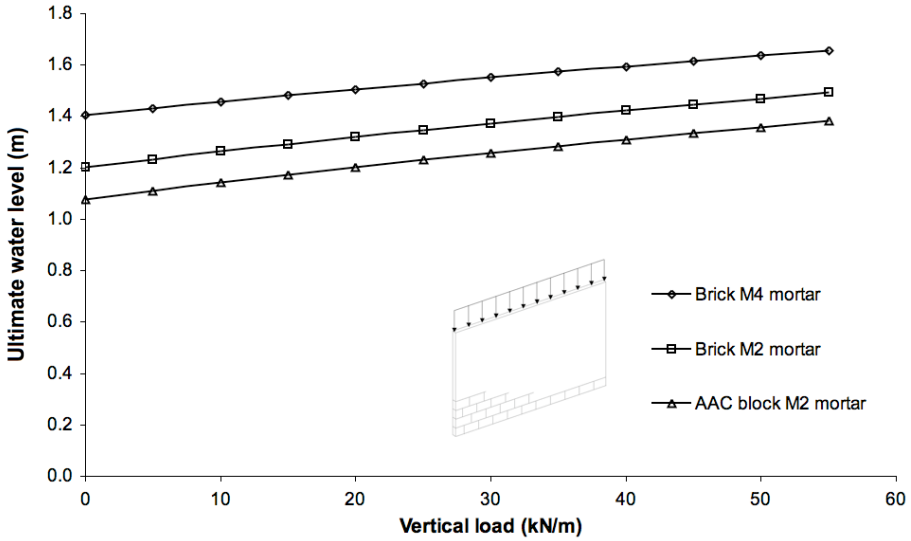


**Figure 8.24.** Variation in ultimate water level with imposed vertical load for block and brick wall panels (all edges simply supported)

It was observed from Figure 8.24 that increasing the vertical load provided a significant increase in the ultimate water level. An average 22 % increase in the ultimate water level arose between the minimum and maximum applied vertical load. As discussed in Section 8.1.4, the linear response was due to the incorporation of a moment resistance to vertical loads and self-weight in the analysis. An average 4 % increase in the total ultimate load, computed from the ultimate water levels, was found when considering the vertical loads applied in the previous study (Hendry et al., 1971) of 48.9 and 55.0 kN/m. The favourable increase was in line with that found in the uniform analysis (4 %), but was considerably lower than the 16 % reported in the previous study (Hendry et al., 1971). It was suggested in Section 8.1.4 that the larger differences reported in the previous study (Hendry et al., 1971) could in part be related to the inherent natural variability in the specimens, since no repeat tests were completed.

To allow comparison of the results to the uniform loading analysis the ultimate water levels were converted into total lateral loads. It was found that the total lateral load applied to the wall panels increased by an average 53 % as the imposed vertical load was increased from 0 to 55 kN/m. The effect of increasing the imposed vertical load in the uniform analysis was found to be of higher magnitude at 64 %, as detailed in Section 8.1.4, and was related to the difference in the failure mode. Figure 8.25 shows the hydraulic failure modes for the brick wall panel constructed with M4 compressive strength mortar at imposed vertical loads of 0 and 55 kN/m. For the uniform loading the failure mode remained approximately symmetric about a horizontal line regardless of the applied vertical load, whilst for the hydraulically loaded case it was found that the position of the yield lines varied according to the load. The effect of the increased moment, due to the vertical load (and self-weight), was therefore offset slightly in the hydraulic loading analysis as a result of the variation in the failure mode.

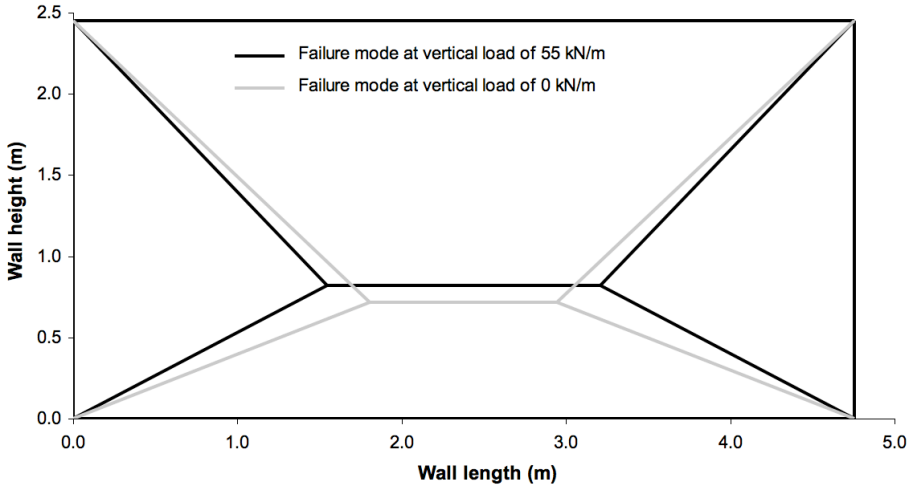


**Figure 8.25.** Failure modes for hydraulically loaded wall panel at vertical loads of 0 and 55.0 kN/m

At vertical loads of approximately 11.0 kN/m, that would be typical of a 2 storey building, the improvement in the water level was small and could easily be overshadowed by other effects in the failure process. It is also important to consider the typical arrangement in a cavity wall construction, where the outer leaf would primarily be subject to self-weight and the inner leaf would sustain the floor and roof loads. For the case of brick outer and AAC block inner leaves at an applied vertical load of 11.0 kN/m, the results suggest that the outer leaf would be the stronger of the two, despite the higher vertical load applied to the inner. This somewhat verifies that

the loading arrangement used in the experimental cavity wall tests, where only the inner leaf was vertically loaded, would have little influence on the results.

### 8.2.5 Effect of panel length and height on the ultimate water level

To investigate the effect of varying the length and height of the panel SA1 was run with walls of different proportions. The unit and mortar combinations for the wall panels considered in the analysis were as detailed in Section 8.2.4. In all cases the average experimental flexural strengths ($f_x$) were used to compute the ultimate levels and no vertical load was applied to the top of the wall. The effect of panel length and height on the ultimate water level for the three wall panels investigated in SA1 is presented in Figure 8.26.

As expected, it was found for all materials and mortar combinations that as the length of the wall reduced that the ultimate water level increased, as shown in Figure 8.26. As the panels became longer a larger proportion of the total length of the yield lines were in the weaker direction 1 rather than the stronger direction 2. The internal energy requirements to cause failure, therefore, became comparatively lower as the panel length increased and resulted in the lower ultimate water levels observed.

The variation between the results for panels of different heights became less significant at lengths over 6 and 5 m for the brick and AAC block walls respectively. For short panels the effect of height was more pronounced due to a higher proportion of the yield lines being in the stronger direction 2 than the weaker direction 1. The internal energy required for failure therefore increased with height for the short panels and resulted in the behaviour apparent in Figures 8.26a, b and c. For longer panels, the effect of the increased proportion of the yield lines in direction 2 diminished and the ultimate water level became more dependant on the strength in direction 1. The total length of the yield lines in direction 1 was proportional to panel length and explains why the ultimate water levels were found to be almost independent of height at longer panel lengths. As expected a more significant effect on the ultimate level, particularly at shorter panel lengths, was also observed as the flexural strength increased.

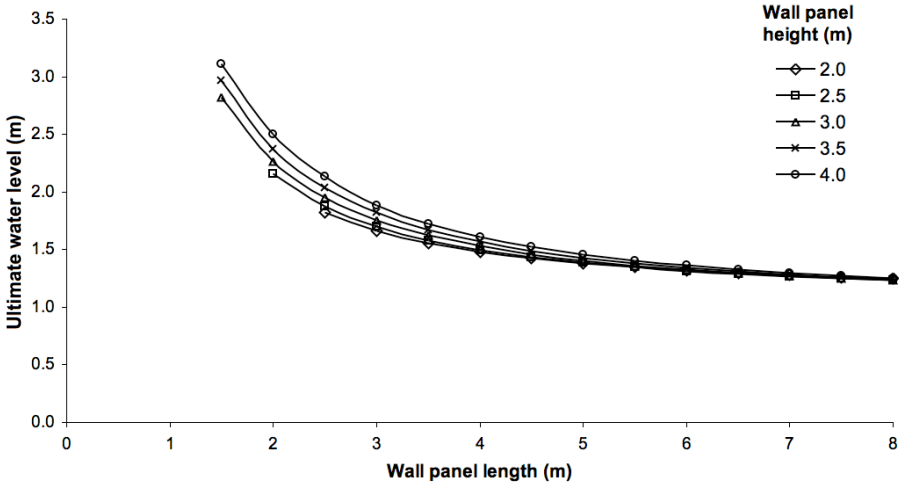


(a) Brick M4 strength mortar

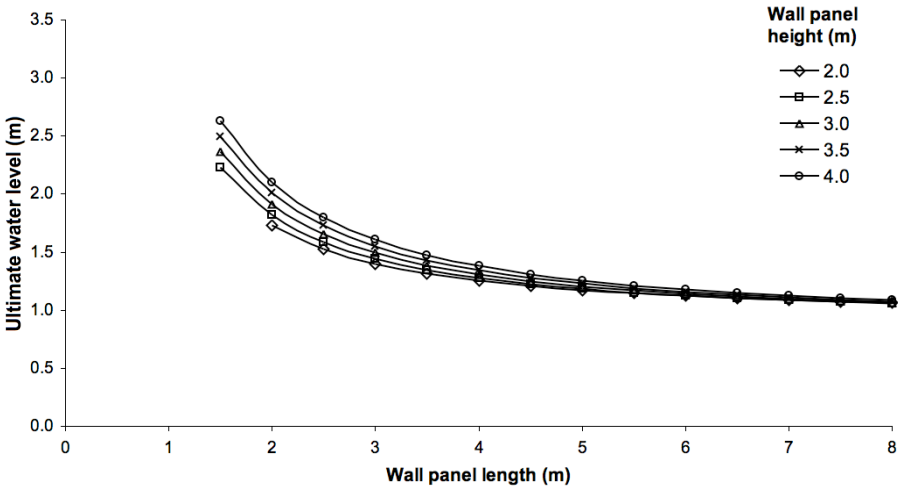


(b) Brick M2 strength mortar

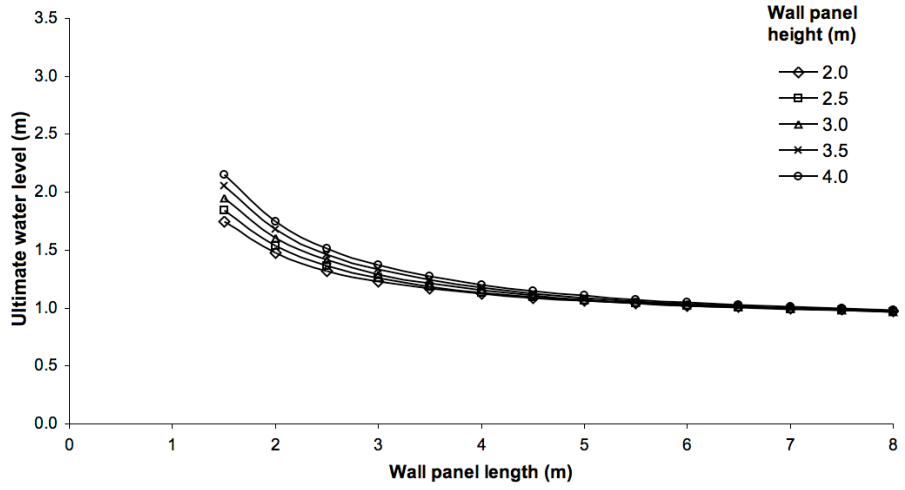


(c) AAC block M2 strength mortar

**Figure 8.26.** Variation in ultimate water level with panel length and height for wall panels of (a) brick M4 strength mortar, (b) brick M2 strength mortar and (c) AAC block M2 strength mortar

### 8.2.6 Effect of support conditions on the ultimate water level

As discussed in Section 8.1.5 the vertical support conditions in the experimental tests were simply supported, but it was likely that partial support conditions would occur at the intersection of two walls in a real property. To assess the effect of this on the ultimate water level the vertical support conditions were varied within analysis SA1. The masonry and mortar combinations considered were as given in Section 8.2.4 and the wall panels were modelled with the top edge simply supported and free. The conditions were otherwise as in the experimental study and the average flexural strength ($f_x$) was used in the analysis. The effect of varying the vertical edge support conditions on the ultimate water level for wall panels with the top edge simply supported and free are shown in Figures 8.27a and b respectively.

It was observed in Figures 8.27a and b that the ultimate water level increased in a linear manner as the vertical edge support conditions tended towards fully clamped. The trend was similar for panels with both the top simply supported and the top free, as apparent in Figures 8.27a and 8.27b respectively. A slightly increased response was recorded as the flexural strength increased in direction 2 ($f_{xd2}$), as was found in the uniform analysis discussed in Section 8.1.5. An increase of 0.20 m in the ultimate water level was given for brick with M4 strength mortar ($f_{xd2}$=1.45 N/mm$^2$) compared to 0.16 m for brick with M2 strength mortar ($f_{xd2}$=0.96 N/mm$^2$) when the support conditions were changed from simply supported to fully clamped. The behaviour was again expected since the moments of resistance along the yield lines formed at the vertical supports were established from the flexural strength in direction 2. Basing the calculations on simple support conditions for a real situation may provide conservative results, but without knowing the exact fixity at the supports this may be a more suitable approach.

The self-weight of the panel and the vertical applied loads would result in a moment resistance to overturning at the base of the wall when a simple support condition was utilised. When this was included in the calculations it was found to marginally improve the performance of the wall panels compared to those excluding the moment resistance, as shown in Figure 8.27a. Since the moment resistance was dependant on self-weight and vertical load then it would be particularly important when considering materials of high density or when large vertical surcharges were applied.

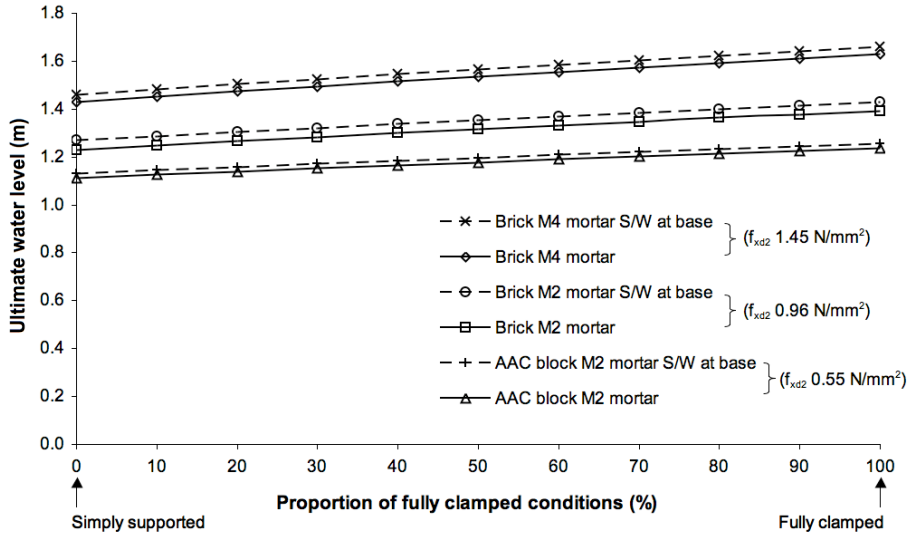


(a) Top and base simply supported

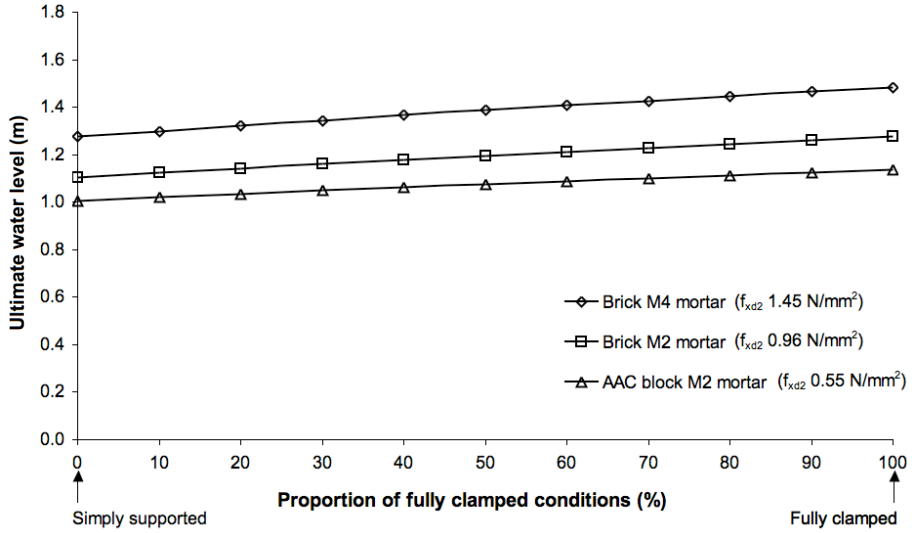


(b) Top free and base simply supported

**Figure 8.27.** Variation in ultimate water level with different vertical edge support conditions for block and brick wall panels (a) top and base simply supported and (b) top free and base simply supported

### 8.2.7 Effect of openings on the ultimate water level

The ultimate water level calculated using the average flexural strength ($f_x$) for the wall panel with an opening (specimens H11 and H12), of 1.36 m, was 9 % lower than the average experimental value of 1.50 m. When computed into total loads, to permit comparison to uniform loading conditions, the variation between the experimental and analytical loads was found to be 17 % and this was an acceptable tolerance considering the expected variability in the analysis and experimental results, as discussed in Section 8.1.2. The average experimental ultimate water level was

similar to that found for the wall panels without openings (H7 and H8) of 1.46 m and further indicated that there may have been some effect due to the method used to cover the opening as was discussed for the uniform loading analysis in Section 8.1.6. The parametric study completed for uniform loading conditions, as detailed in Section 8.1.6, however illustrated that the opening should not be ignored in the analysis.

Figure 8.28 presents the experimental and SA1 optimised failure modes for wall panels H11 and H12. It was observed from Figure 8.28 that the optimised failure mode was a good approximation of the experimental patterns recorded for specimens H11 and H12, considering the constraints imposed in the analysis. The main difference in the optimised and experimental patterns was in the upper section of the panels where the cracks typically propagated from the top corners of the opening and not from part way up the sides. As was suggested in the uniform analysis in Section 8.1.6, it was likely that the initial horizontal crack, in addition to the stiffness of the board used to cover the opening, resulted in the experimental failure modes observed. The contour plot of z deflections for wall panel H11 immediately prior to failure is shown in Figure 8.29. It was observed in Figure 8.29 that similar negative deflection was apparent at the corners of the specimens prior to failure as was found for the uniformly loaded specimen (W14).

To assess if there was any impact of the failure mode on the ultimate water level the optimised results from SA1 were compared to two alternative patterns, mode 1 and mode 2. The alternative failure modes were obtained by manually adjusting the position of the yield lines and the water level was adjusted to balance the work equation using the ‘Goal Seek’ tool in the spreadsheet. The failure patterns for modes 1 and modes 2 are presented in Figures 8.30a and 30b respectively. Mode 1, as presented in Figure 8.30a, was observed to be an improved representation of the experimental pattern observed in wall H12, but the ultimate water level was only found to increase by 2 % when compared to the optimised value. Mode 2, as shown in Figure 8.30b, was obtained using SA2 and provided an improved representation of the experimental pattern observed in wall H11, but only increased the ultimate water level by 4 % when compared to the optimised value. The differences to the experimental, when converted to total ultimate loads, for mode 1 and mode 2 were computed as 14 and 10 % respectively. The increase in the total ultimate load for both modes 1 and 2 was considered insignificant when compared to the expected variability likely in the experimental and analytical results, as discussed in Section 8.1.2.

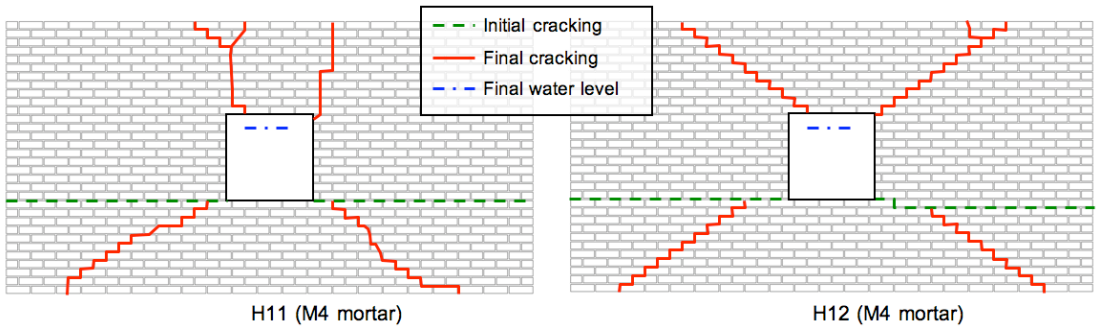


(a) Experimental

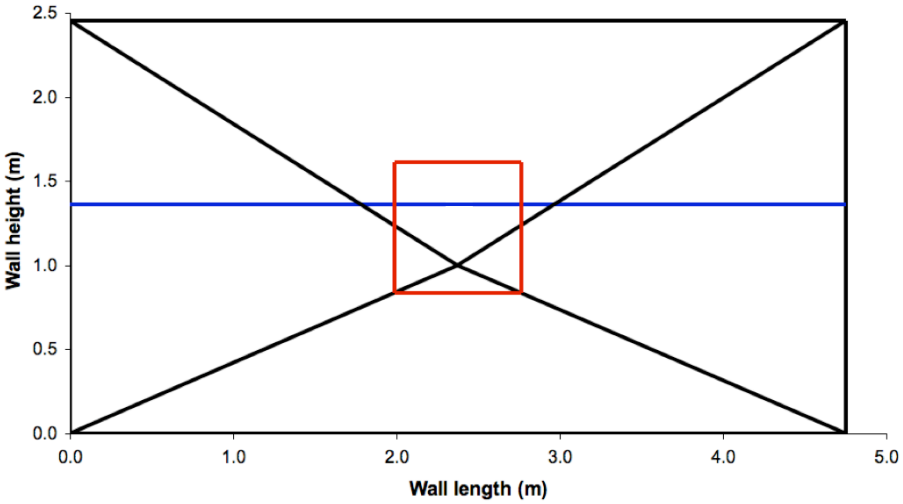


(b) Optimised

**Figure 8.28.** (a) Experimental and (b) optimised analytical failure modes for wall panel with opening

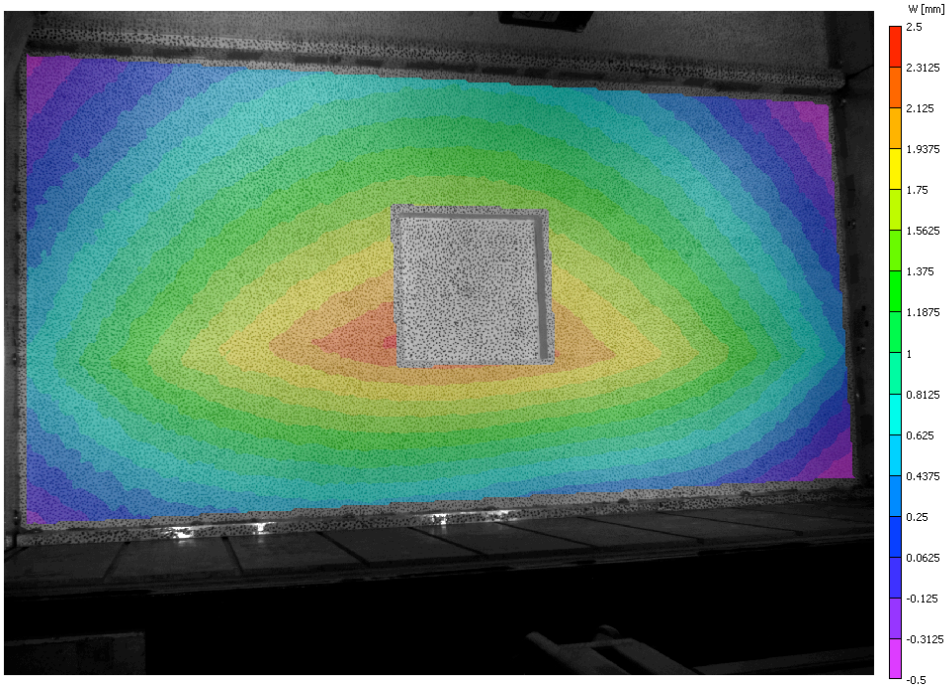

**Figure 8.29.** Contour plot z deflections for specimen H11 illustrating negative deflection at panel corners prior to failure

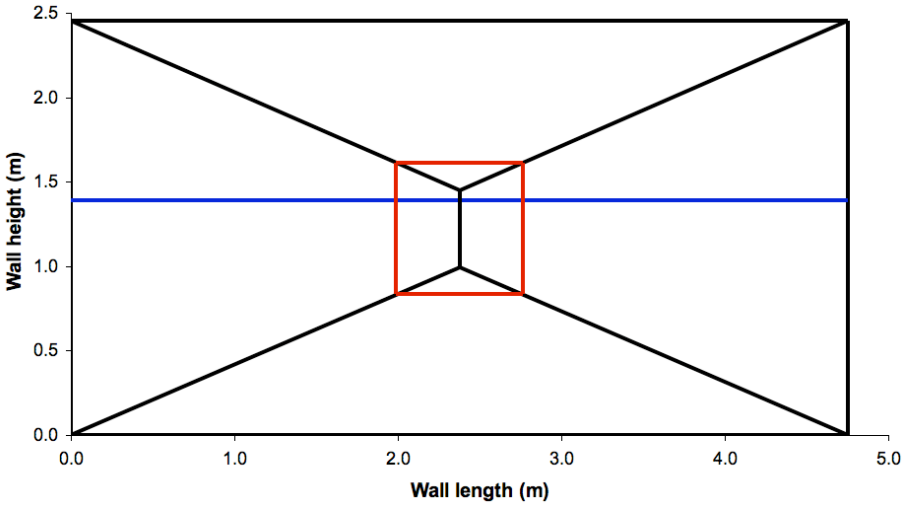


(a) Mode 1

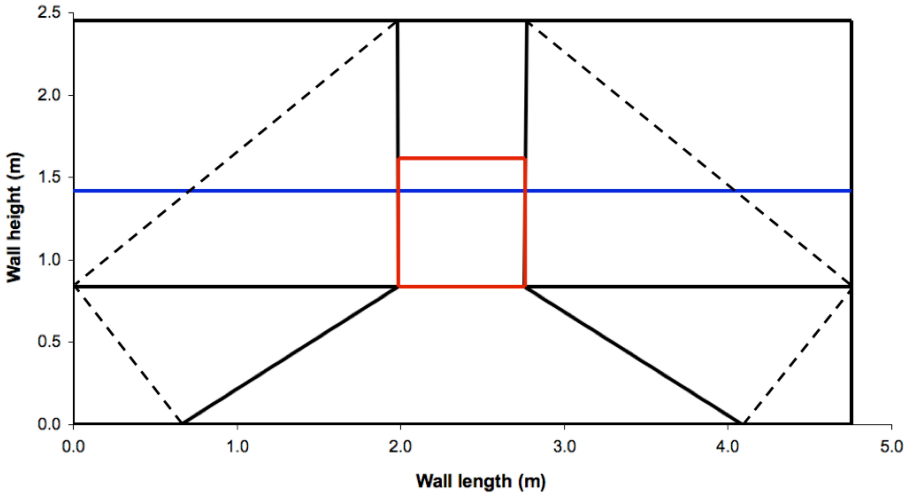


(b) Mode 2

**Figure 8.30.** Alternative failure modes for wall panel with central opening (a) mode 1 and (b) mode 2 (dashed lines show position of corner lever pivots)

The corners of the opening would be natural points for cracks to initiate and propagate from and it would be possible to include constraints to force yield lines to be positioned at the corners of the opening. It was, however, likely that the failure mode observed in the experimental specimens was influenced by the stiffness of the board used to cover the opening. The board may have stiffened the vertical edges of the opening and effectively prevented cracks from initiating in a position similar to that found in the optimised mode. Constraining the analysis to attain patterns that were different may therefore provide unrealistic failure modes and could result in valid lower ultimate loads being missed. Therefore, it was considered that the

optimised solution obtained from SA1 provided the most appropriate calculation method for a wall panel with an opening.

Only one size of opening was considered in the experimental study and it was found to have a limited effect on the ultimate water level attained, which may have been partly due to the small size of the opening in relation to the dimensions of the wall panel. To assess the impact of larger openings analysis SA1 was run with apertures of different proportions. The performance of a brick wall panel constructed with M4 compressive strength mortar was examined, with the same dimensions as for the experimental study. The average experimental flexural strengths ($f_x$) were used in the analysis and the opening was maintained at a central position. The ultimate water levels calculated for the wall panel with openings of different lengths and heights are shown in Figure 8.31. The failure modes given in the analysis for openings of 1 and 2.5 m in length are presented in Figures 8.32 and 8.33 respectively.

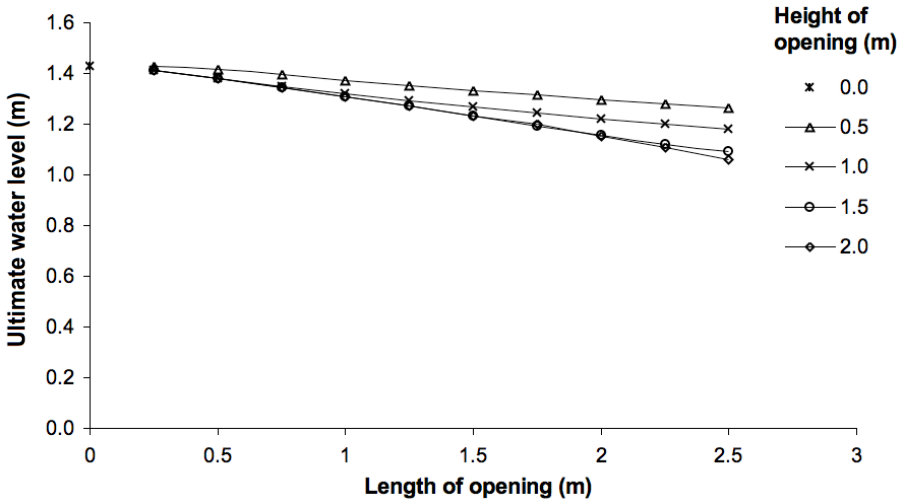


**Figure 8.31.** Variation in ultimate water level for openings of different lengths and heights

It was apparent in Figure 8.31 that as the length and height of a centrally positioned opening increased, the ultimate water level decreased. Similar ultimate water levels were given for openings of heights of 1.0 m or greater and for lengths up to 1.0 m, due to the similar failure modes and proportions of the yield lines with the opening, as apparent in Figure 8.32. The smallest height opening (0.5 m) provided the largest ultimate water level and was due to the small proportion of yield lines being cut by the opening as presented in Figure 8.33.

In the uniform loading tests it was suggested that openings of length 0.25 m could be neglected, regardless of height, and would result in an acceptable error of 8 % in the ultimate load. Neglecting similar sized openings for the case of hydraulic loading would result in a much lower error of 2 % (considered as total loads). Adopting a similar error of 8 % would allow openings of length 0.5 m to be neglected, regardless of height, but would not be recommended in the absence of experimental data.

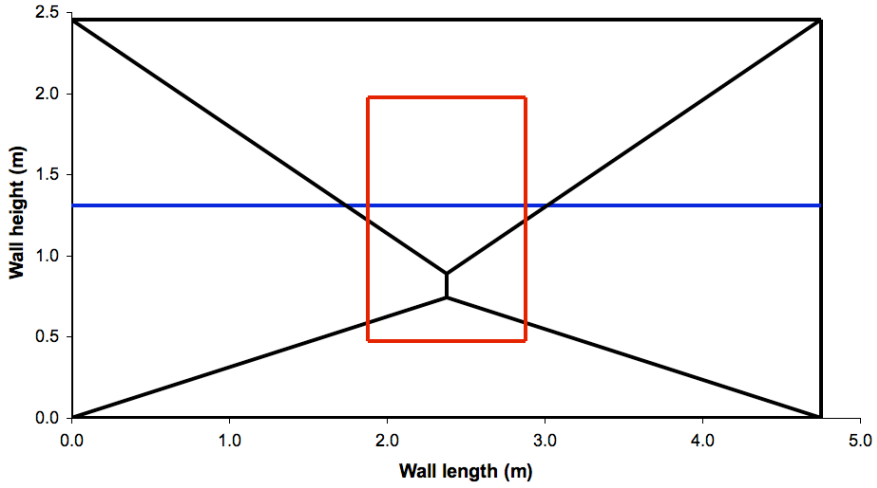


(a) Opening height 1.5 m (23 % of yield lines within opening)

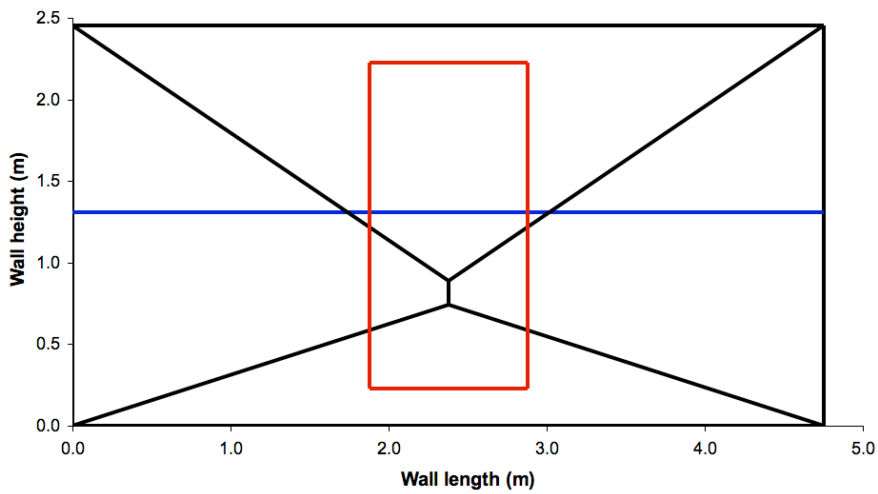


(b) Opening height 2.0 m (23 % of yield lines within opening)

**Figure 8.32.** Optimised failure modes for panels with openings of 1m in length and (a) 1.5 m and (b) 2.0 m in height

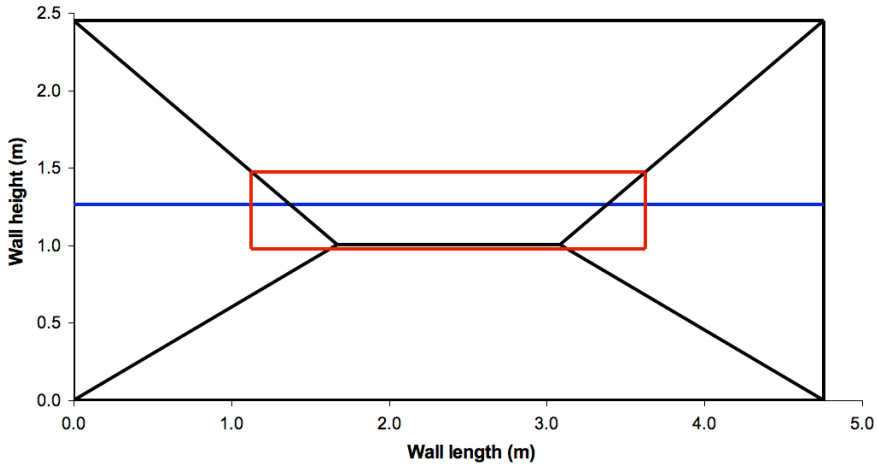


(a) Opening height of 0.5 m (35 % of yield lines within opening)

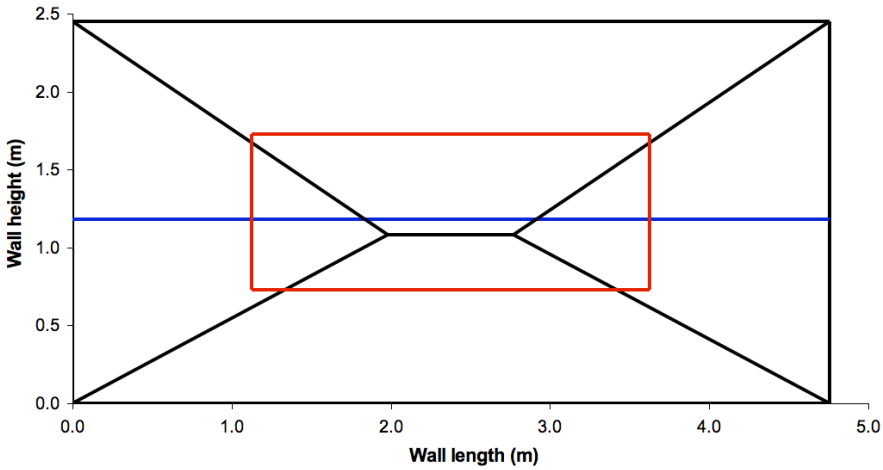


(b) Opening height of 1.0 m (45 % of yield lines within opening)

**Figure 8.33.** Optimised failure modes for panels with openings of 2.5 m in length and (a) 0.5 m and (b) 1.0 m in height

The effect of the horizontal position, measured from the left hand edge of the wall panel, for three different sized openings was investigated with analysis SA1. The brick wall panel considered in the analysis utilised M4 compressive strength mortar and was of the same dimensions as considered in the experimental study. The dimensions of the openings investigated are shown in Figure 8.34, whilst other parameters were as given in Table 8.1. The ultimate water levels calculated for the three openings at different horizontal positions are shown in Figure 8.34. Failure modes for the window sized (1.0 x 1.5 m) and door sized (1.0 x 2.0 m) openings at different horizontal positions are presented in Figures 8.35 and 8.36 respectively.

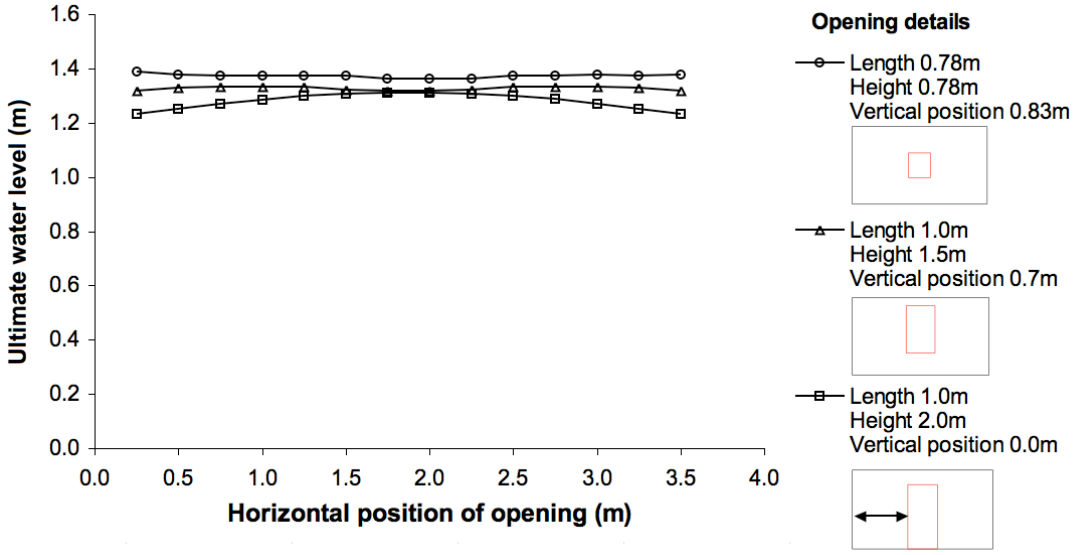


**Figure 8.34.** Variation in ultimate water level with horizontal position of opening for openings of three sizes

It was observed in Figure 8.34 that the horizontal position of the window-sized openings (0.78 x 0.78 and 1.0 x 1.5 m) had an insignificant effect on the ultimate water level, where the average variation between the maximum and minimum levels was 2 %. The failure modes differed depending on the position of the opening, as shown in Figure 8.35, but the comparable ultimate water levels were due to the proportions of yield lines within the openings being similar. A different behaviour was found for the small opening (0.78 x 0.78 m) in the uniform analysis, as detailed in Section 8.1.6, which was due to the yield line pattern being symmetric about a horizontal centre line rather than offset towards the base as in the hydraulic loading analysis. The increased ultimate load, as the opening tended to the panel edge, in the uniformly loaded analysis was due to a lower proportion of the yield lines being encompassed in the opening.

For the door sized opening (1.0 x 2.0 m) the variation in the ultimate water level with horizontal position was of higher magnitude (6 %), but could still be considered insignificant compared to the acceptable variation in the analysis. The ultimate water level decreased as the horizontal position became closer to the panel edge for the door sized opening. The proportion of yield lines within the opening was found to be similar when the door sized opening was positioned at 0.25 and 2.0 m from the left hand edge, as shown in Figure 8.36. A higher proportion of the yield lines cut were in direction 2 as the door sized opening approached the edge of the specimen and, since the strength was higher in direction 2, this had a more significant reduction on

the internal energy requirements at failure. The position of openings of large heights was therefore more critical when determining the ultimate level.

As was found in the uniform analysis, SA1 was capable of delivering results in terms of both failure modes and ultimate water levels for wall panels with an acceptable degree of accuracy. The trends observed in parametric study of size and position was explained by the relationship between the yield lines inside and outside the opening. The experimental results from specimens H11 and H12 again suggested that there was some effect due to the stiffness of the board, and this requires further experimental investigation.

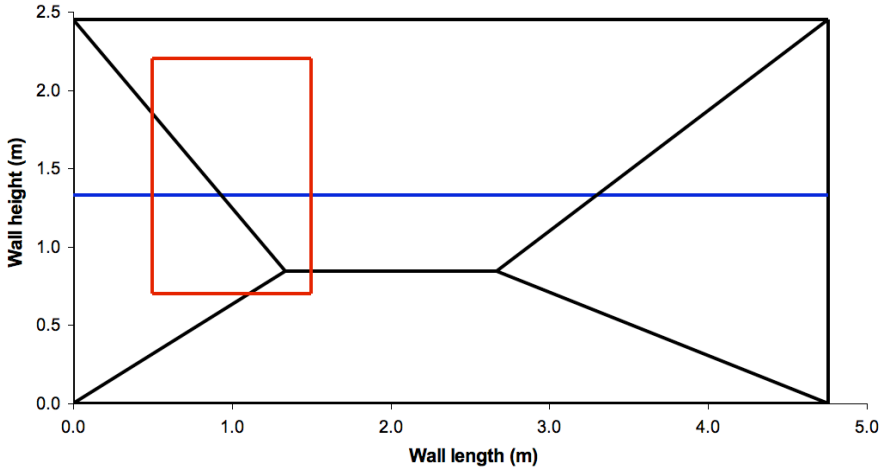


(a) Opening 0.5 m from LHS (18 % of yield lines within opening)

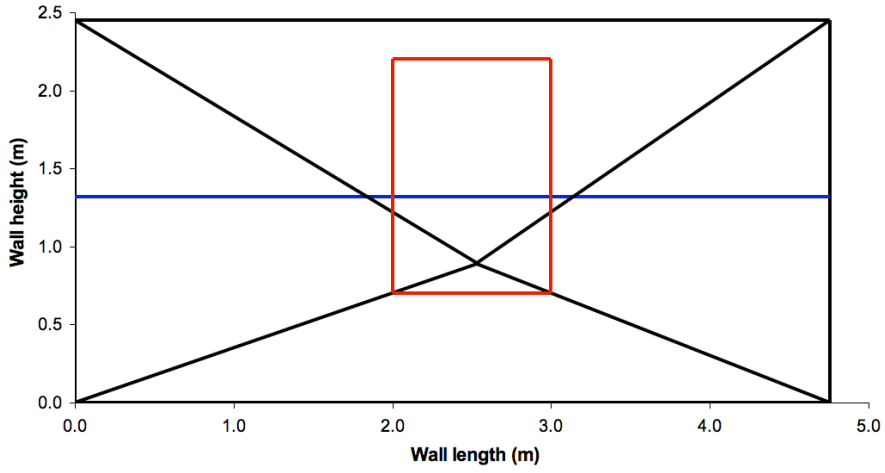


(b) Opening 2.0 m from LHS (21 % of yield lines within opening)

**Figure 8.35.** Failure modes for wall panel with 1.0 x 1.5 m opening when positioned (a) 0.5 m from LHS and (b) 2.0 m from LHS

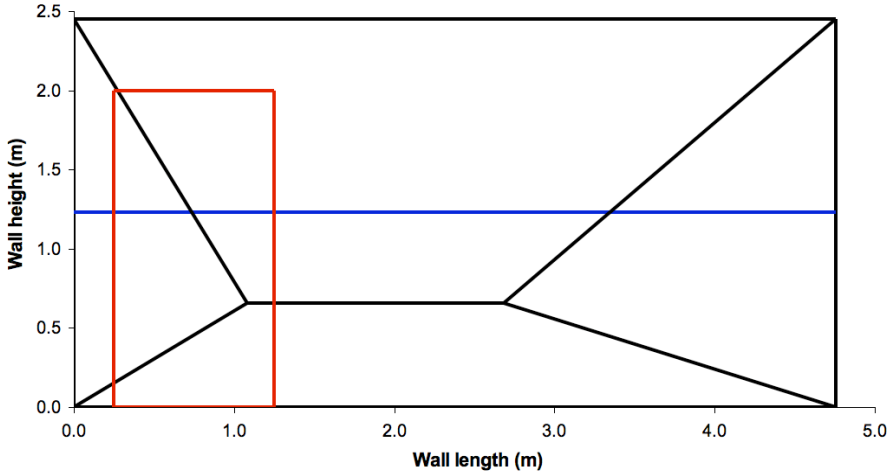


(a) Opening 0.25 m from LHS (26 % of yield lines within opening, 38 % in direction 2)

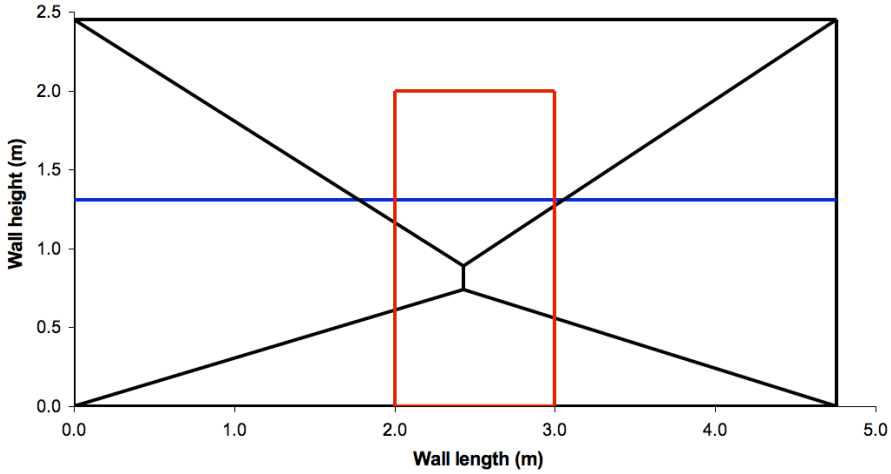


(b) Opening 2.0 m from LHS (23 % of yield lines within opening, 25 % in direction 2)

**Figure 8.36.** Failure modes for wall panel with 1.0 x 2.0 m door opening when positioned (a) 0.25 m from LHS and (b) 2.0 m from LHS

### 8.2.8 Cavity wall assemblies

Three cavity wall panels were tested in the experimental study: H13 and H14, which each comprised brick outer and AAC block inner leaves, and H15 that was constructed from a brick outer leaf and brick block inner leaf. The vertical loading conditions for the inner and outer leaves were as described in Section 8.1.7. Analysis SA1 was utilised to calculate ultimate water levels for each leaf of the cavity wall assembly. The average experimental flexural strengths ($f_x$) were used in the analysis and other parameters were as given in Table 8.1. The equivalent analytical ultimate water levels ($D_{Eq}$) were determined from the values for the corresponding inner ($D_{Inner}$) and outer ($D_{Outer}$) leaves using equation 7.1 given in Chapter 7. The

experimental and analytical ultimate water levels for the cavity wall assemblies are given in Table 8.14.

**Table 8.14.** Comparison of experimental and analytical ultimate water levels for cavity wall panels

| **Specimen reference** | **Masonry / mortar type** | **Experimental ultimate water level (m)** | | | | **Analytical ultimate water level (m)** (from individual leaves) |
|---|---|---|---|---|---|---|
| | | Individual test | Average | Leaf | Individual leaves | |
| H13 | Brick outer & AAC block inner / M2 | 1.31 | 1.34 | $D_{Inner}$ | 1.09 | 1.09 |
| H14 | | 1.37 | | $D_{Outer}$ | 1.23 | 1.20[1] |
| | | | | $D_{Eq}$ | 1.64 | 1.62 |
| H15 | Brick outer & brick block inner / M2 | 1.73 | - | $D_{Inner}$ | 1.49 | 1.29 |
| | | | | $D_{Outer}$ | 1.23 | 1.20[1] |
| | | | | $D_{Eq}$ | 1.93 | 1.76 |

[1]No vertical load applied to outer leaf

The equivalent analytical ultimate water level for cavity wall panels H13 and H14, calculated from the analytical ultimate levels for the individual leaves, exceeded the average experimental ultimate level by 21 %. In the experimental study it was found that the equivalent experimental ultimate level exceeded the average experimental by a similar proportion (22 %), as detailed in Chapter 7 Section 7.3.1. The variation between the experimental and analytical results for H13 and H14 was 46 % when considered as total loads applied to the wall panels. The difference between the analytical and experimental total loads exceeded that found in the analysis of the uniformly loaded wall panel and was at the upper end of the expected range of deviation reported in the literature, as discussed in Section 8.1.7.

In the analysis each leaf was assumed to be simply supported at all edges, whilst in the experimental test the outer leaf was supported via wall ties at the edges. It was difficult to make a judgement of the impact of the different support conditions for the outer leaf between the experiment and analysis, but providing simple supports to the outer leaf, as assumed in the analysis, may increase the ultimate water level. A lower proportion of the load would have to be sustained by the inner leaf if simple supports were utilised at the edges of the outer leaf in the experimental procedure, since some of the load would be transferred to the supports rather than through the wall ties. The results further suggested that there was a level of composite action

occurring in cavity wall H13 and H14, but the support conditions utilised for the outer leaf may have influenced the overall performance of the experimental specimens

The equivalent analytical ultimate level for specimen H15 correlated very well to the experimental value recorded in the test and was within 1%. When considered as a total applied load the difference between the equivalent analytical and experimental total loads was 3 % and was well within the range reported in the literature. The experimental and analytical equivalent ultimate levels were, however, dissimilar and varied by 10 %, which was predominantly due to the difference in the ultimate levels for the inner brick block leaf (Table 8.14). It was apparent from the results that there was a greater degree of composite action occurring in specimen H15 than found for specimens H13 and H14. The results suggested that the overall performance of a cavity wall panel may be influenced by the strength of the weaker leaf, and that complete composite action may not occur when dissimilar strength leafs are utilised. In summary, the analytical results illustrated that it would be appropriate to determine the equivalent ultimate level for a cavity wall from the ultimate levels for the individual leaves when the wall ties are capable of adequately transferring the required loads. The effect of the support conditions to the outer leaf on the performance of the cavity wall panel, however, requires further investigation.

### 8.2.9 Comparison to experimental results in the literature

The only experimental study found in the literature of masonry panels subject to hydraulic loadings was completed on prototype scale brick and block walls that were 2.438 m in height and 7.925 m in length (Pace, 1988, Pace and Campbell, 1978). The masonry unit types, dimensions and mortar compressive strengths assumed for analysis purposes are given in Table 8.15. Three brick wall panels were tested that were connected to a timber frame structure via wall ties at an approximate density of 3.6 ties per $m^2$. One blockwork wall was tested to failure, but it was not clear whether the panel was tied back to the timber structure or not and no failure pattern was given. The support conditions for all the panels were equivalent to a simple support at the base and fully clamped conditions at the vertical edges, whilst differing support conditions were investigated at the top of the panel, as detailed in Table 8.16. Brick wall 2 also had a door opening positioned centrally of width 1.079 m and height 2.032 m. Results were also presented (Pace, 1988) from the test of an entire property, although it was not possible to accurately model any sections of the property as the details of the test were extremely limited. The ultimate water levels

found in the previous experimental programme (Pace, 1988, Pace and Campbell, 1978) for each wall panel are given by Table 8.16.

**Table 8.15.** Parameters assumed in the analysis (Pace, 1988, Pace and Campbell, 1978)

| Unit | Unit thickness (m)[1] | Density of masonry (kg/m$^3$) | Mortar compressive strength class | Flexural strength (N/mm$^2$)[2] | |
|---|---|---|---|---|---|
| | | | | $f_{xk1}$ | $f_{xk2}$ |
| Brick | 0.089 | 2000 | M4 | 0.40 | 1.10 |
| Block | 0.102 | 2000 | M4 | 0.25 | 0.45 |

[1]Assummed values

[2]From National Annex to Eurocode 6 (BSI, 2005d)

**Table 8.16.** Experimental and analytical ultimate water levels for USACE study (Pace, 1988, Pace and Campbell, 1978)

| Test details | Water level (m) | | | |
|---|---|---|---|---|
| | Experimental ultimate | Analytical | | |
| | | Optimised ultimate | As experimental pattern ultimate | Characteristic - optimised pattern[5] |
| Block wall 1 - top free | 1.10[1] | 0.83 | N/A[3] | 0.53 |
| Brick wall 1 - top free | 0.77[1] | 0.93 | 1.06 | 0.59 |
| Brick wall 2 - opening top free | 0.87[1] | 0.86 | 1.05 | 0.54 |
| Brick wall 3 - top SS | 1.45[2] | 1.01 | 1.12[4] | 0.62 |

[1]Peak value from load-deflection response

[2]Peak value given

[3]No experimental failure mode given for block wall 1

[4]Determined using SA2

[5]Factors of safety $\gamma_f$=1.5 and $\gamma_M$=2.3

The experimental ultimate water level for brick wall 2 with the opening exceeded that of brick wall 1. Although no discussion of this was made, it was possible that the method used to cover the opening that comprised of a timber frame and board stiffened the panel in this area. The addition of the support at the top of brick wall 3 almost doubled the ultimate water level when compared to brick wall 1. Limited information was recorded with regards to the crack pattern at failure, but figures included provided some details for the brick walls. The analyses developed in this programme were used to establish analytical results for each experimental arrangement given in the previous study (Pace, 1988, Pace and Campbell, 1978).

Flexural strengths were not provided for the masonry so values prescribed in EC6 (BSI, 2005d) were assumed as detailed in Table 8.15. The ultimate water levels calculated for the wall panels using SA1 are given by Table 8.16.

The It was apparent from Table 8.16 that the optimised analytical results calculated using SA1 underestimated the strength of block wall 1 and brick wall 3 by 33 and 44 % respectively, whilst overestimated the strength of brick wall 1 by 21 %. The ultimate water level from SA1 for brick wall 2 was within 1 % of the experimental result. The deviation found may have been related to the differences between the experimental and optimised SA1 failure modes and this is investigated in the following section. An experimental failure mode was not provided for block wall 1 so this is not examined further. It should also be noted that the failure modes for the brick walls were obtained from photographs and some assumptions were made with regards to the positions of the cracks where they were obscured by the test set up. Figures 8.37 and 8.38 show the optimised and as experimental failure modes for brick walls 1 and 2 respectively.

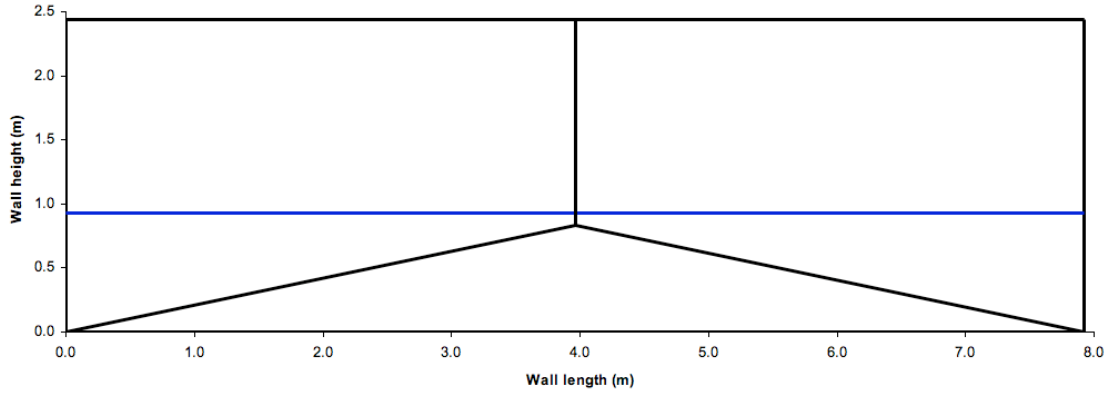


(a)

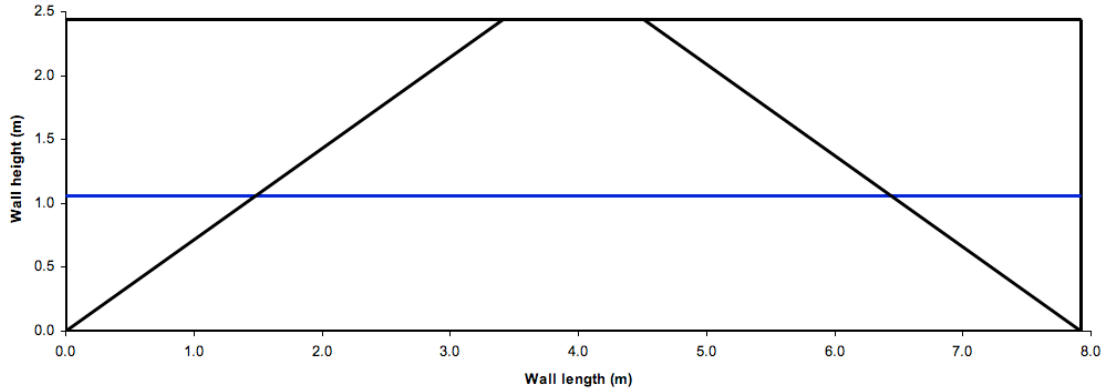


(b)

**Figure 8.37.** (a) Optimised and (b) as experimental failure modes for brick wall 1 (Pace, 1988)

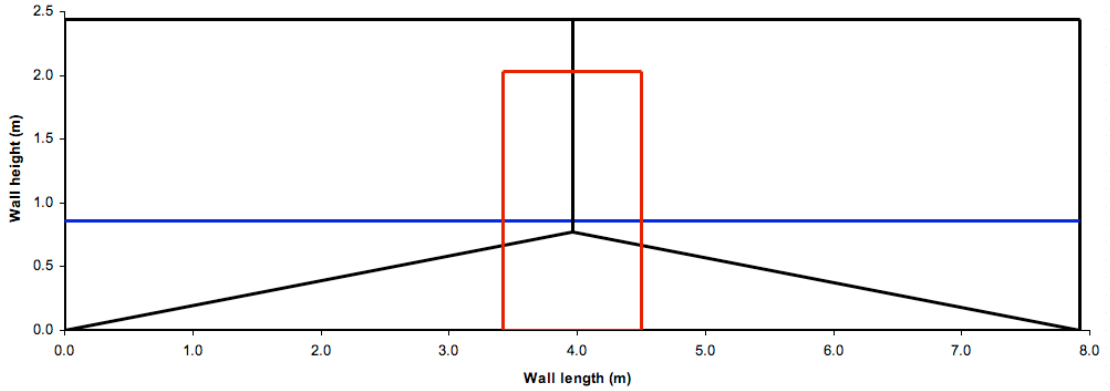


(a)

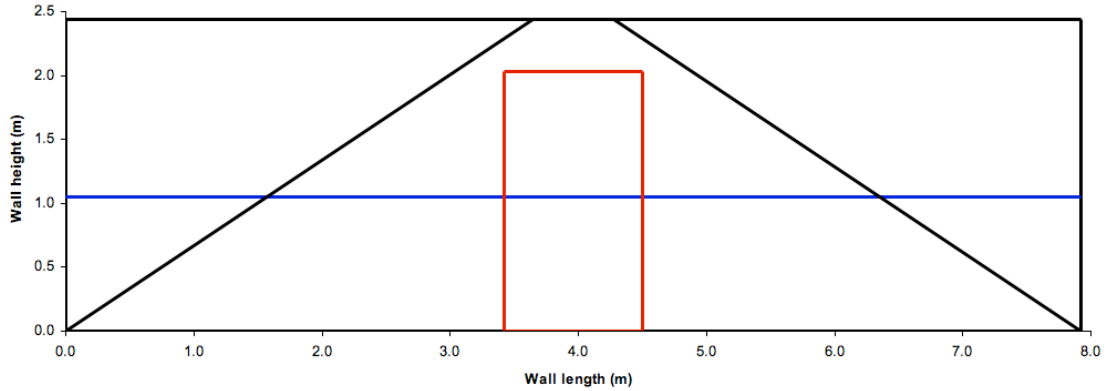


(b)

**Figure 8.38.** (a) Optimised and (b) as experimental failure modes for brick wall 2 (Pace, 1988)

It was observed from Figures 8.37 and 8.38 that the optimised failure modes were dissimilar to the experimental patterns recorded for brick walls 1 and 2. On adjusting the analysis to obtain the experimental patterns for brick walls 1 and 2, the experimental ultimate water level was further overestimated by 37 and 20 % respectively. The optimised solution therefore provided a better approximation of the ultimate water level, but the exact failure mode was not attained. The difference in the optimised and experimental failure modes for wall panels 1 and 2 may have been affected by the interaction of the timber frame and the masonry panel that was not included in the analysis. Difficulties were also acknowledged in the previous study (Pace, 1988) in modelling the interaction of the timber frame and it was also ignored in the limited amount of finite element analysis that was completed. The method used to cover the opening in brick wall 2 may have also stiffened the wall panel and affected the failure mode. Verification of the effect of the timber frame and cover applied to the opening on the failure mode would necessitate further experimental investigation that was outside the scope of this study.

Figure 8.39 presents the optimised and as experimental failure modes form brick wall 3. It was observed from Figure 8.39 that the optimised failure mode for brick wall 3 was similar to the experimental failure mode except the cracks in the upper section of the panel were offset from the corners in the experimental specimen. SA2 was used to establish the a failure mode that was similar to the experimental, however it was not possible to verify if the horizontal crack that traversed the length of the wall was present in the experimental specimen. The ultimate water level from the SA2 solution was higher than that given by optimisation and was within 29 % of the experimental load. The experimentally observed failure mode may have deviated from the upper corners of the specimen due to the stiffness of the junction between the upper simple support and the vertical masonry returns. The difference between the ultimate levels computed for the experimental pattern and from the optimised solution were within 11 %. Underestimation of the experimental ultimate water level was likely due to the interaction of the timber frame and the masonry wall.

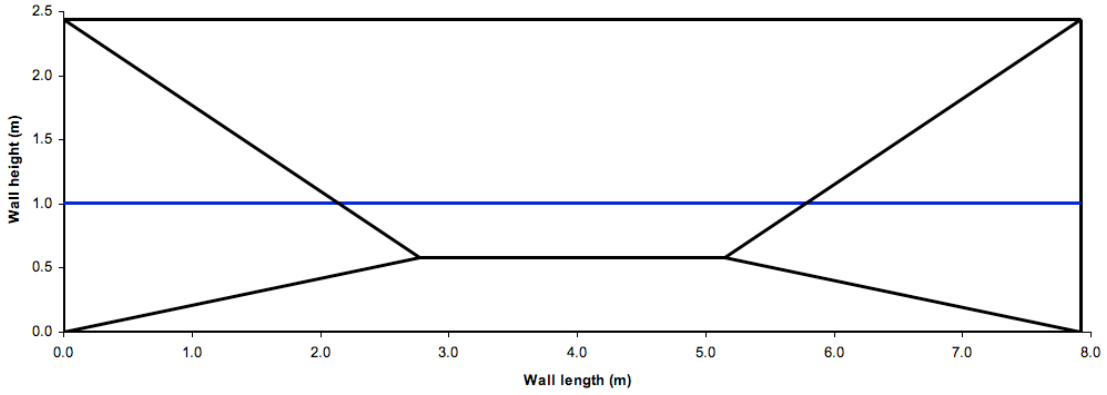


(a)

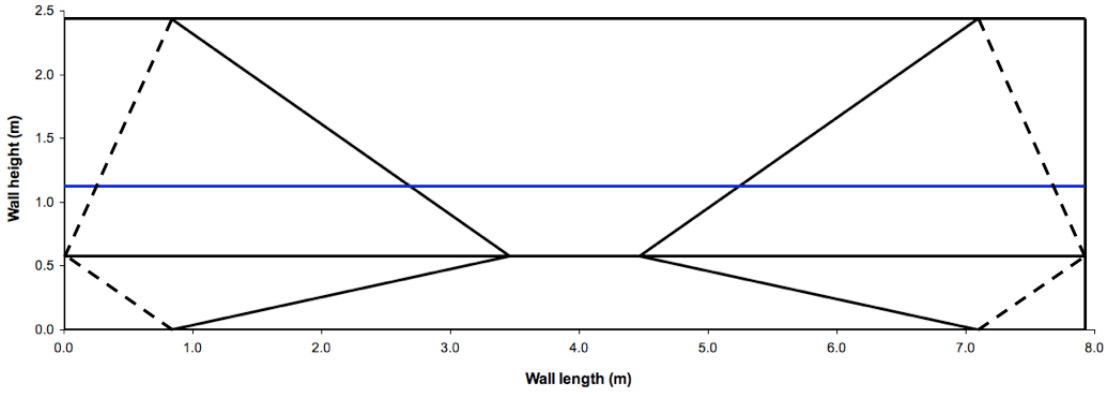


(b)

**Figure 8.39.** (a) Optimised and (b) as experimental failure modes for brick wall panel 3 (Pace, 1988) (dashed lines show position of corner lever pivots)

The optimised SA1 and experimentally determined ultimate water levels were converted to total ultimate loads to permit comparison to the reported variation in uniform loading tests and analysis, as discussed in Section 8.1.2. The experimental ultimate loads were underestimated by 76, 2 and 107 % for block wall 1, brick wall 2 and brick wall 3 respectively, and overestimated by 47 % for brick wall 1, when compared to those calculated with SA1. The variation found suggested that the optimised results were not a good representation of the experimental findings for the wall panels without openings, considering the expected variation discussed in Section 8.1.2. The lower variation associated with brick wall 2 with an opening should be treated with caution, due to the differences in the SA1 optimised and experimental failure modes, as discussed above. The differences found were likely due to the assumptions made regarding the materials (unit size, density and flexural strength) and the interaction of the timber frame and the wall panels.

It was concluded in the previous study (Pace, 1988) that the upper bound of the water level should be based on an arbitrarily selected limit of deflection of 0.25 mm, but without any real justification. From this limiting factor it was established (Pace, 1988) that all panels could sustain 0.640 m of water and that safety factors should be applied to this, rather than the actual ultimate load. As was discussed in the literature review, the characteristic water level was later increased (Pace, 1988), without justification, to 0.9 m, which was arbitrarily selected from tests on an entire property. The characteristic water levels that were computed using the optimised solution in SA1 with $\gamma_f$ of 1.5 and $\gamma_M$ of 2.3 were all found to be lower than 0.640 m, as given in Table 8.16, but in differing proportions dependant on the panel configuration. Following the approach to determine the characteristic levels given in the previous study (Pace, 1988) and outlined above would not be straightforward and would require factors of safety that depended on the panel configuration. It should also be noted that only brick wall 3 attained the lower characteristic level of 0.6 m given in the literature (Communities & local government, 2007) and all specimens fell short of 0.9 m as given by others (FEMA, 2008a, ODPM, 2003, Pace, 1988). This further highlighted that the characteristic water level of 0.9m was inappropriate and 0.6 m was not always safe for all conditions. The results illustrated that a much more suitable approach would be to follow the limit state approach of SA1 using consistent factors of safety to determine the actual characteristic water level for the panel under consideration.

### 8.2.10 Establishing characteristic water levels

The results computed so far have not included any factors of safety, such that they could be compared directly to the experimental ultimate loads where possible. The limit state design utilised in the analysis however requires the application of factors of safety to establish the characteristic water level that can be retained from the ultimate level determined for the wall panel. It was apparent in the literature that characteristic levels quoted were often based on arbitrarily selected limits, or no regard was given to applying suitable safety factors (Kelman and Spence, 2003a, Pace, 1988, Pace and Campbell, 1978). In addition the guidance, with regards to a suitable characteristic level, that is given in the literature is contradictory, where some sources quote that 0.9 m as a characteristic water level (FEMA, 2008a, ODPM, 2003, Pace, 1988), whilst others quote 0.6m (Communities & local government, 2007). It was therefore important to establish the characteristic levels for the experimentally tested wall panels to allow comparison to both values given in the literature to evaluate if the guidance was appropriate.

The global factor of safety comprised a factor of safety for the loads and a factor of safety for the materials (strictly quality of workmanship), as was detailed in Chapter 3 Section 3.3.5. The factor of safety on the load ($\gamma_f$) was prescribed as 1.5 in the Eurocode – Basis of structural design (BSI, 2005e), whilst the factor of safety for the materials ($\gamma_M$) could take a value of either 2.3 or 2.7 depending on the quality of the construction of the masonry according to the National Annex to Eurocode 6 (BSI, 2005d). A good degree of quality control was utilised in the wall panel manufacture technique, such that a factor of safety on the materials of 2.3 would be appropriate, however a value of 2.7 would represent the worst case scenario. The characteristic water levels were computed using the EC6 prescribed (BSI, 2005d) characteristic flexural strengths ($f_{xk}$ EC6) in SA1. The characteristic flexural strengths were used rather than the experimental values to ensure the approach was in line with the calculation method given in EC6 for uniform loading conditions. Other parameters used in the analysis were as given in Table 8.1 and the equivalent characteristic levels were computed for the cavity walls from the characteristic levels for the corresponding individual leaves. The characteristic water levels calculated for the hydraulically loaded specimens are shown in Figure 8.40.

It was apparent in Figure 8.40 that only specimen H15 (Brick block/brick cavity wall) attain a characteristic water level of 0.9 m, which was specified as the upper characteristic water level in the literature. All other specimen configurations failed to

attain a characteristic level of 0.9 m, regardless of the level of quality control imposed during construction. All specimens attained a characteristic level of 0.6 m or more, with the exception of the AAC block specimen (H1 & H2), for which characteristic levels of 0.53 and 0.49 m were computed for a factor of safety of 2.3 and 2.7 on the materials respectively. The results clearly illustrated that for the particular conditions imposed in the experimental tests that a characteristic level of 0.9 m quoted in the literature (FEMA, 2008a, ODPM, 2003, Pace, 1988) would generally be inappropriate, whilst the characteristic level of 0.6 m was not suitable for every case. It is recommended that a limit state deign using SA1 would offer a much more suitable approach than specifying a universal characteristic level that had no regard for the particular conditions for the wall in question.

In the parametric study it was found that the ultimate water level reduced as the length of the wall panel increased and was affected by the size of the opening in the wall. To assess the impact of such conditions outside the scope of the experimental study, the walls of a typical property were analysed using SA1 and the results of this process are presented in Section 8.2.11.

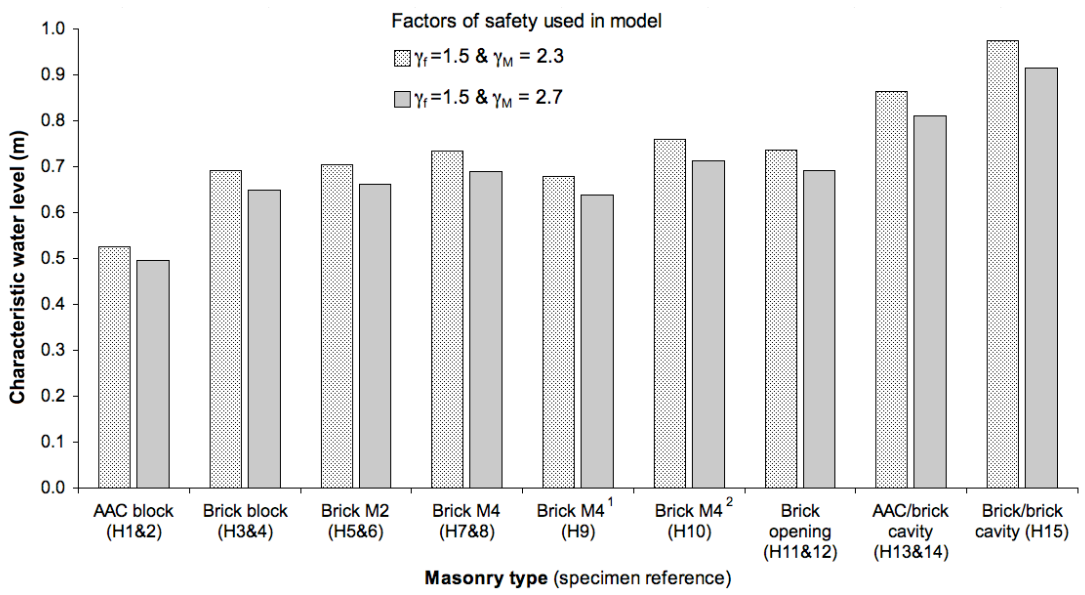


**Figure 8.40.** Characteristic water levels for experimentally tested panels

[1]Specimen H9 tested with the top free and zero applied vertical load

[2]Specimen H10 subject to vertical loads from roof, floor and 1 storey of masonry

### 8.2.11 Application of the analysis to a typical property

The modelling process so far has been based on the application of the analysis to discrete wall panels and in a typical property the dimensions, vertical loading and number and size of openings would vary. To assess the performance of a typical property, sections of the walls were considered as discrete wall panels with the appropriate edge support and vertical loadings applied. In a previous study (Edgell and de Vekey, 1986b) a layout was given that was most frequently used for the construction of new properties. A similar layout has been adopted for this analysis, as shown in Figure 8.41, although doors were positioned on the front and rear walls instead of window openings and the thickness of the wall was increased to 303 mm as required by current Regulations (ODPM, 2004).

The front and rear ground floor walls were analysed along with a section of the side wall from the front (or rear) of the property to the central load bearing wall using SA1. The support conditions at the base and top of the panels were assumed to be simply supported, whilst the edges were modelled with both simple and fully clamped supports. Moment resistance was also assumed to occur at the base of the panel due to the self-weight of the masonry and the vertical imposed load. The property was constructed with brick outer leaf and an AAC block inner leaf (3.6 $N/mm^2$ compressive strength grade). Characteristic flexural strengths given by the National Annex to EC6 (BSI, 2005d) for a M4 mortar strength class were used in the analysis. The height of the wall panels was 2.91 m, whilst the lengths and vertical loadings used in the analysis were as given by Table 8.17. It was not possible to vary the vertical loadings along the length of the wall in the analysis so average values were used. In reality the loading along the wall would vary slightly due to the presence of openings and the triangular section of masonry in the side (gable) wall. A factor of safety of 1.5 was applied to the loadings (BSI, 2005e), whilst a value of 2.3 was used for the materials (control of execution) (BSI, 2005d). The equivalent characteristic water level for the cavity wall panels was calculated from the characteristic levels for the individual leaves using equation 7.1, as given in Chapter 7 Section 7.3.1. The optimised characteristic water levels for the panels analysed are given in Table 8.18.

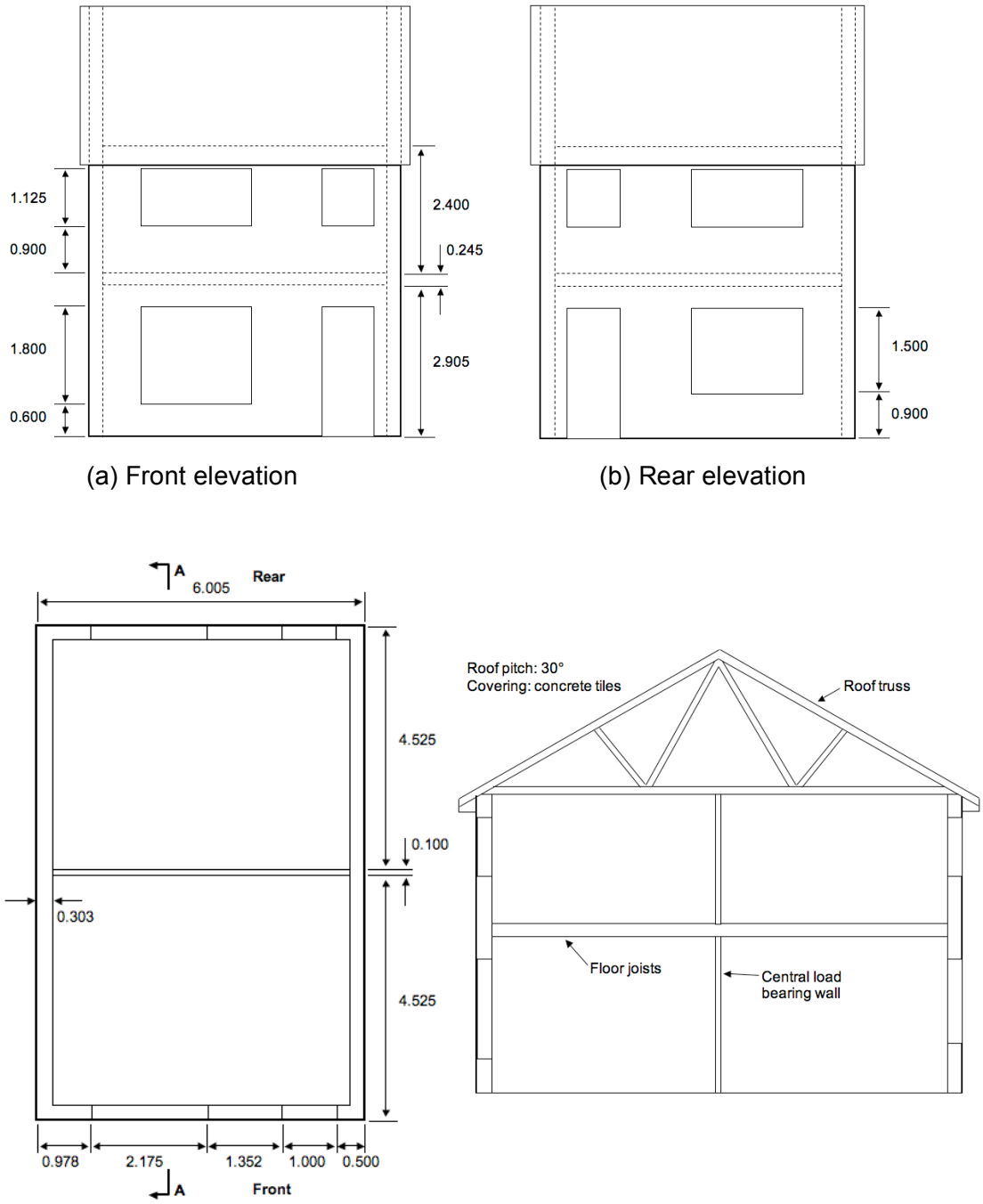


(a) Front elevation (b) Rear elevation

(c) Plan of ground floor (d) section A-A

**Figure 8.41.** Layout of the typical property adapted from Edgell and de Vekey (1986b) Note: larger opening in ground floor of front of property compared to rear

**Table 8.17.** Parameters used in the analysis of a typical property

| **Parameter** | **Front/rear wall** | | **Side wall** | |
|---|---|---|---|---|
| | Outer leaf | Inner leaf | Outer leaf | Inner leaf |
| Panel length (m) | 6.01 | 5.40 | 4.53 | 4.22 |
| Roof load (kN/m) | 0 | 3.88 | 0 | 0 |
| Floor load (kN/m) | 0 | 4.44 | 0 | 0 |
| Masonry load (kN/m) | 3.32 | 1.32 | 6.81 | 2.81 |
| Total vertical load (kN/m) | 3.32 | 9.63 | 6.81 | 2.81 |

**Table 8.18.** Characteristic water levels for wall panels of typical property

| **Leaf** | **Characteristic water level (m)** | | | | | |
|---|---|---|---|---|---|---|
| | Front wall | | Rear wall | | Side wall | |
| | Vertical edges SS | Vertical edges C | Vertical edges SS | Vertical edges C | Vertical edges SS | Vertical edges C |
| $D_{Outer}$ | 0.60 | 0.71 | 0.65 | 0.73 | 0.80 | 0.91 |
| $D_{Inner}$ | 0.58 | 0.60 | 0.58 | 0.63 | 0.61 | 0.68 |
| $D_{Eq}$ | 0.83 | 0.93 | 0.87 | 0.96 | 1.01 | 1.13 |

It was apparent, from Table 8.18, that the side walls were stronger than the front or rear walls and was as a direct result of the shorter panel length and absence of openings. The front cavity wall sustained the lowest equivalent characteristic water level out of the three wall panels modelled and was due to the large window opening. To determine a characteristic level for the entire property the most suitable approach would be to base it on that of the weakest wall, which in this case was the front wall. Using this value would suggest that a maximum characteristic water level of 0.83 or 0.93 m could be retained by the property depending on whether the vertical edges were assumed to be simply supported or clamped respectively. As discussed in Section 8.2.10 above, contradictory guidance was given with regards to characteristic levels in the literature, where some quoted 0.6 and others 0.9 m as safe. The values determined for the front wall of the property exceeded 0.6m, but were lower than 0.9 m when simple supports were assumed at the vertical edges of the panel. This somewhat supports the statement made above that one value would not be suitable for all cases and that a more suitable approach would be to determine property specific characteristic levels with the analysis.

If no combined action of the leaves of the cavity wall was assumed and only the outer leaf was subject to the pressure of the water then the characteristic levels

would be reduced further. Considering the case for simple supports at the vertical edges then the characteristic level for the outer leaf of the front wall was identical to the lower value in the guidance. This could be further reduced if a lightweight block was used instead of the brick or a lower strength mortar was utilised. In such a situation retaining the upper value quoted in the literature could at a minimum lead to minor cracking in the wall and in the worst case could result in failure. Clearly some further verification of the analysis is required for conditions not covered in the experimental tests, but it would however offer a more appropriate solution than currently given in the guidance.

## 8.3 Conclusions

### 8.3.1 Conclusions – Wind loading analysis

The results given by SA1, for the wall panels considered in this study, were generally consistent with the values given by the existing EC6 calculation method for uniformly loaded wall panels (BSI, 2005c). The exception to this was the AAC block wall panels that were not consistent between the analyses, however, it was found that there were some anomalies in the tabulated bending moment coefficients in the EC6 analysis for this particular case.

Generally SA1 provided conservative ultimate loads when using the mean flexural strength when compared to the experimental values. The ultimate loads given by SA1 were however considered to be acceptable considering the expected variation, which was at the lower end of those typical of the literature. The exception to this was the cavity wall, which was overestimated, but could be explained by the support conditions utilised in the experimental test.

Use of the EC6 adjusted (to average) flexural strengths in the analysis resulted in ultimate loads that were not always conservative when compared to the experimental loads. The friction/overturning resistance methods given in previous studies (Kelman and Spence, 2003a, Martini, 1998) could approximate the ultimate load of the panels with zero tensile strength, but were not appropriate for calculating the strength of uncracked sections.

Failure modes were found to influence the ultimate load calculated by the analyses, particularly due to the formation of corner levers. It would be difficult to incorporate these in an analysis effectively without omitting possible correct lower ultimate loads and different support conditions would likely eliminate the formation of corner levers.

The non-corner lever optimised approach using SA1 is therefore recommended. Increasing the vertical load and increasing the level of restraint at the vertical edges of the panel was found to have a favourable effect on the ultimate load.

The analytical ultimate load was found to decrease as the size of an opening was increased, but it would be feasible to ignore openings of length up to 0.25 m regardless of height. The influence of the position of an opening on the ultimate load depended on its size, where for small openings the critical location was towards the centre and for larger openings was towards the edges of the panel. The behaviour found was due to the proportion of yield lines being cut by the opening varying with the opening position and size.

SA1 provided ultimate loads of an acceptable correlation to the results of previous experimental studies, including wall panels with openings. It is therefore recommended that SA1 would be suitable to calculate the ultimate loads of wall panels subject to wind loading according to EC6 including those with openings.

### 8.3.2 Conclusions - Hydraulic loading analysis

SA1 produced identical results to those given in a previous theoretical study (Kelman and Spence, 2003a). The method used to determine the vertical loadings and the support conditions employed at the top and bottom of the wall panels were however questioned. Varying the vertical loadings and support conditions were found to have a significant influence on the performance of the wall panels. The ultimate water levels computed using the friction/overturning resistance methods were lower than those determined from the flexural strengths. This further suggests that the friction/overturning resistance methods were not appropriate for calculating the strength of uncracked sections.

A good correlation was found when the experimental ultimate water level of the single leaf walls without openings was compared to the analytical results from SA1 using the average experimental flexural strengths. The panels with openings were underestimated, likely due to the stiff board being used to cover the opening in the experimental tests. The strength of the AAC block/brick cavity walls (H13 and H14) were overestimated by the analysis, whilst the brick block/brick cavity wall (H15) was modelled well. As was concluded for the uniform loading tests, it was likely that the support conditions used for the outer leaf affected the experimental results and this requires further investigation. The ultimate water levels were converted to total loads

to permit comparison to uniform loading conditions, and it was found that the results given by SA1 were within the reported variation.

The results given by SA1, similarly, correlated well to the experimental ultimate water levels when the EC6 adjusted (to average values) flexural strengths were utilised. The strength of the brick M2 compressive strength mortar wall panels (H5 and H6) were overestimated due to the EC6 adjusted flexural strengths exceeding those found in the experimental tests. It was concluded that where possible the correct flexural strengths should be adopted for the wall panel under analysis, however, utilising the EC6 characteristic flexural strengths would allow for such deviation.

The effect of adjusting the crack pattern from that established using the optimised solution had a limited effect on the results for the panels with and without openings. Attempting to force the analysis to produce similar failure modes to those experimentally observed could result in other lower upper bound results being missed and should be avoided. Using the optimiser to establish the lowest upper bound results would be most suitable method to determine the analytical strength of a panel.

Vertical load was found to have a favourable effect on the computed ultimate water level and highlighted that it should be included in the analysis. Increasing the length of the wall resulted in a reduction of the ultimate water level for all material and mortar combinations, due to decreasing effect of the moment resistance in direction 2 with panel length. The ultimate level increased as the height of the wall panel became greater, but as for longer panels this effect was reduced. The effect of length and height was more significant for masonry of higher flexural strength.

Altering the fixity at the vertical edges from simply supported to fully clamped resulted in a linear increase in the ultimate water level. The exact fixity at the corner where the two masonry panels joined was assumed to be simply supported, however this could be a proportion of the fully clamped condition in reality. This assumption could lead to marginally conservative results. Correctly allowing for the self-weight moment resistance at the base of the panel provided a small increase in panel strength, but would be more significant for vertical surcharges of higher magnitude.

Increasing the height and length of the opening in the analysis was found to reduce the ultimate level and was due to a larger proportion of the yield lines being cut by

the opening, however for heights above 1.5 m similar values were given. Varying the position of the opening along the length of the panel was more critical for larger apertures such as doors.

Including factors of safety in the calculation reduced the ultimate levels as would be expected. The upper characteristic level of 0.9 m given in guidance was only attained by specimen H15, a cavity wall panel constructed with brick and brick block leaves, when factors of safety were applied, whilst the lower characteristic level of 0.6 m was not suitable for all cases. A similar conclusion was drawn when SA1 was applied to the walls of a typical property, where the characteristic level for the weakest wall was lower than the upper limit in the literature. For the worst case, for example where weaker materials were utilised or no composite action occurred in the cavity wall, then the lower characteristic level given in the literature might not be attained. It is suggested that providing such fixed characteristic levels in the literature should be avoided and that following the limit state calculation procedure in SA1 would be more appropriate.

Some difficulties were experienced in comparing the results from the analysis to the only previous experimental study due to the lack of information given. The variation between the results given by the analysis and the experimental values were found to exceed that reported in the literature and was suggested to be due to the interaction of the timber frame, which was not modelled, and the assumptions made regarding the materials.

In summary it is recommended that SA1 should be adopted to determine the hydraulic capacity of masonry wall panels using the flexural strength method. The results given demonstrate that this would be a more appropriate approach than providing one characteristic level to fit all situations as currently specified in guidance. Further experimental investigation of panels with the different parameters detailed above would aid in verification of the results from the analysis in these areas. This should include effect of support conditions, different sized panels and openings and further investigation of cavity specimens.

# 9 Conclusions and recommendations for further work

## 9.1 Conclusions

The literature review revealed that a number of researchers had completed experimental studies and modelling of masonry wall panels subject to uniform (wind) lateral loading. The yield line method was shown to provide a suitable approach to determine the uniform ultimate load of masonry wall panels and is incorporated in the current Eurocode 6 (EC6) for the design of masonry structures (BSI, 2005c). Finite element analysis was also found to have been successfully employed to analyse masonry and a number of different material interaction models have been proposed. It was identified that only one previous experimental study had been completed to determine the strength of masonry when subject to non-uniform (hydraulic) lateral loads. Later to this, a purely analytical study, using the yield line method, was completed, but was not verified by any experimental tests. No clear method to determine the characteristic load of masonry subject to hydraulic loads was identified in the literature.

It was also apparent from the literature review that masonry can be modelled successfully at a reduced scale and this can be advantageous in terms of cost and productivity. Masonry assemblages, wall panels, buildings and arch bridges have been tested at reduced scale and the ultimate loads and failure modes have been shown to compare well to the prototype. In some cases the stiffness of the model was found to be lower than the prototype. Self-weight effects were found to have been generally correctly considered, by employing methods to pre-stress the masonry or completing testing within a centrifuge.

An experimental method has been developed to construct model (1:6) scale wall panel and wallette specimens from brick or block units. Masonry units used in the specimens were successfully cut from prototype materials, whilst the mortar manufactured was correctly scaled. The method allowed openings to be easily added into the wall panels during the construction process. Wallette specimens were tested according to BS EN 1052-2 (BSI, 1999b) to establish mechanical properties for the modelling process. It was found that the brick specimens showed an improvement in strength as the mortar strength was increased. The failure modes were consistent for all the brick specimens, where a failure occurred along the bed joints in direction 1 and through the units/mortar joints in direction 2. Block specimens tested in direction

1 showed a comparable strength and identical failure mode to the brick specimens constructed using the same mortar.

The brick block and AAC block specimens tested in direction 2 were found to be stronger and weaker than the brick equivalents respectively. A size effect with respect to internal flaws could have influenced the strength of the brick block specimens, particularly since a different failure mode was observed. The lower strength of the AAC block specimens was due to the lower unit strength. The average flexural strengths determined from the test values were not always consistent with the adjusted to average EC6 values that were calculated from the characteristic flexural strengths prescribed by the National Annex to EC6 (BSI, 2005d).

The stiffness of the wallettes was found to increase as mortar strength increased. Initially the specimens responded linearly, but at higher loads non-linear behaviour occurred and was attributed to initiation and propagation of cracking. Some difficulties were found in capturing post peak behaviour, but softening was on occasion observed.

A testing jig was manufactured to allow wall panels to be tested using the centrifuge, such that self-weight effects were correctly considered. Either uniform wind loads or non-uniform hydraulic loads could be applied to the wall panel during the test and a vertical surcharge could be added to the top of the specimen. The testing procedure was remotely monitored and recorded using video equipment, a datalogger and a 3D digital image correlation system. Fifteen wall panels were tested with a uniformly applied lateral load to simulate wind loads, and those constructed with mortar exhibited a yield line type failure mode. Initial cracking tended to occur horizontally across the specimens, followed by further cracking that was generally diagonal in direction. Diagonal cracking was typically through the units and joints for the AAC block specimens, and along the mortar joints for the brick and brick block specimens. Some cracking also occurred through the units for the higher strength M4 mortar brick wall panels, suggesting that the strength of the mortar and units were similar. The failure modes of repeat specimens were generally consistent. Uplift was observed to occur at the corners of the specimens, due to simple supports being utilised at the panel edges and the cracks not entering into the corners of the specimen.

The ultimate loads of the AAC block specimens were considerably lower than the brick block specimens and the load-deflection response given was also of lower stiffness. This suggested that the unit strength and stiffness had a considerable influence on the ultimate load and response. The ultimate load increased as mortar strength increased from M2 to M4 for the brick wall panels. Variations between the ultimate load for repeat specimens was low and in line with those reported in the literature. Little effect on the ultimate load was shown when an opening was positioned at the centre of the panel and this was attributed to the method used to cover the opening and its small size relative to the overall size of the wall panel. A similar initial load-deflection response was shown by all brick specimens, but the wall panels constructed with M4 mortar were able to sustain further loading post initial cracking. The in-plane response found was generally of extension in both the x and y directions following initial cracking. The strain data obtained prior to and during test supports the use of scale specimens and proved that self-weight was correctly modelled during the centrifuge tests.

In addition, a small study of wall ties was completed to examine the feasibility of bonding wall ties between two wall panels to manufacture a cavity wall specimen. The bonded on wall ties were found to perform well in compression, but had limited strength in tension, and were therefore deemed suitable for the lateral loading tests where only compressive forces would be likely. A cavity wall panel was successfully constructed using the bonded on wall ties, but when the specimen was tested with a uniformly applied load it failed at a load equivalent to 75% of the sum of the individual leaves. The ultimate load was likely lower than that expected due to the support conditions of the outer leaf.

Fifteen wall panels were manufactured and tested with non-uniformly applied lateral load in order to simulate hydraulic loading conditions. The failure modes that were generally observed were similar to those found in the uniformly loaded tests, but were offset towards the base of the panels. Rapid failure generally occurred in the specimens and post initial cracking residual strength was only shown in the brick block, brick M4 mortar and cavity specimens. The peak deflections in the single leaf wall specimens were lower than those recorded in the uniform loading tests and were attributed to the failure speed. Repeat specimens exhibited very similar failure modes and ultimate water levels, proving the viability of the experimental procedure. As was found in the uniform loading tests, the strength of the brick block walls exceeded that

of the AAC block specimens, whilst for the brick wall panels the load capacity increased as mortar strength increased.

The ultimate water level was found to decrease when both the top support and vertical load was removed, for the case of brick with M4 compressive strength mortar. However, no significant effect was shown on the ultimate water level when increasing the vertical load with support at the top edge of the wall panel, for specimens similarly constructed with brick and M4 compressive strength mortar. The failure mode differed for the wall panel with the top edge free, but was in line with yield line patterns proposed for such support conditions. Generally it was observed that extension occurred in the wall panels in the x and y directions following initial cracking. The strain measurements acquired from the DIC analysis showed some scatter and were negligible before initial cracking occurred. Post initial cracking the strain in the y direction was only found to increase at the site of the initial crack.

Similarly to the behaviour shown in the uniformly loaded tests, the introduction of an opening in two panels had little effect on the strength when compared to the corresponding walls tested without openings. The failure mode however differed, since cracks propagated from the corners of the openings. The cavity walls tested showed a limited correlation to the failure modes of the corresponding single leaf tests and the ultimate water levels were up to 22 % lower than the equivalent depths calculated from the ultimate levels of the individual leaves. Similarly to the conclusion drawn for the uniform loading tests, it was possible that the support conditions used for the outer leaf may have contributed to the performance of the cavity walls.

Spreadsheet software has been utilised to develop two analyses that can determine the ultimate or characteristic load of uniformly and/or hydraulically laterally loaded masonry wall panels. The yield line method was adopted and optimisation was completed using an inbuilt numerical solver. In spreadsheet analysis 1 (SA1) the position of the yield lines were fixed at the corners, whilst in spreadsheet analysis 2 (SA2) the yield lines did not have to coincide with the corners such that corner levers could form. The analyses allowed for openings in the wall panels, different edge support conditions, wall ties and a vertical surcharge. A flexural strength or frictional/overturning moment resistance may be considered in the analyses.

SA1 was verified by completing a comparison to the ultimate loads computed using the EC6 (BSI, 2005c) method. The ultimate loads determined using SA1 were

generally in line with those from the EC6 method. Verification of SA1 was completed using the results from the uniform loading tests and generally provided a good representation of the experimental loads when the average flexural strengths from wallette tests were used. The analysis underestimated the strength of the panel with an opening, but the experimental value was likely influenced by the method used to cover the opening. The strength of the cavity was overestimated, but was due to the calculation being based on the sum of the individual leaves. Deviations between the analysis and the experimental values were found to be at the lower end of values reported in the literature, where yield line analysis had been adopted. Further verification was completed by comparing the results from SA1 to values from previous experimental studies. SA1 gave a poor representation of the ultimate loads of the wall panels constructed with cement mortar when the frictional/overturning methods proposed by Kelman and Spence (2003a) and Martini (1998) were utilised. These methods were found to be more appropriate for wall panels constructed dry or with very weak mortar.

Verification of SA1 for non-uniform hydraulic loading was initially completed by comparing the results given by SA1 to those of a previous theoretical study (Kelman & Spence, 2003a). Identical results were given by SA1, but it was found that the method given (Kelman and Spence, 2003a) to determine the vertical loads was questionable and the upper and lower boundary conditions used (Kelman and Spence, 2003a) were perhaps not fully justified. The results given by either of the frictional/overturning resistance methods further suggested that such approaches were not suitable for establishing the strength of a wall panels constructed using cement mortar. The results from the non-uniform hydraulic loading tests were used to verify SA1 and generally a good correlation was given in terms of the ultimate water level when the average flexural strengths were utilised. Similarly to that found in the verification of the uniform loading type the walls with openings were underestimated by the analysis. The ultimate water levels computed for the AAC block / brick cavity walls (H13 and H14) were overestimated by the analysis, but the value found for the brick block / brick cavity wall (H15) correlated well. The deviation in the results for the wall panels with openings and the cavity walls was more likely due to the particular conditions in the experimental tests, as discussed above, rather than poor prediction by the analysis.

The ultimate water levels calculated using the EC6 adjusted (to average) flexural strengths correlated well to the experimental test results, however the strength of the

brick M2 compressive strength mortar wall panels (H5 and H6) were overestimated. It was suggested that where possible the appropriate flexural strengths should be utilised in analysis, although the EC6 characteristic values may be used that allow for greater degree of variability in the flexural strengths. Further verification of SA1 was completed using a previous experimental study conducted by Pace (1988) and the variation in the results given by the analysis were found to exceed those reported in the literature. It was likely that the assumptions made with regards to the materials and the interaction of the timber frame affected the results given by SA1.

SA1 did not always predict the correct failure mode, particularly where corner levers were found to form. SA2 allowed the failure mode to be correctly modelled and resulted in an increased ultimate load for the case of uniform loading when compared to the results from SA1. A less significant effect was found when SA2 was utilised to determine the ultimate water levels for the case of hydraulic loading, when compared to those obtained from SA1. It was difficult to optimise the failure mode in SA2 to achieve that of the experimental case and the results given by SA2 were obtained by manually adjusting the yield line patterns. A situation could arise when a valid lower collapse load could be missed by trying to force the failure pattern to a certain position and would not be advised. It would be recommended that SA1 would be the most suitable approach to determining the ultimate loads and would likely result in slightly conservative ultimate loads or water levels.

The parametric study completed for uniform lateral loading considered different vertical axial loads, edge support conditions, opening sizes and opening positions. The ultimate load increased when either the vertical load or level of support at the panel edges were increased. The ultimate load decreased with an increase in opening size, but was also dependant on the opening position. The critical location for small openings was as the centre of the wall panel, but for larger openings it was near the edge of the panel.

A parametric study was completed for hydraulic loading that considered different vertical loads, panel lengths and heights, edge support conditions, and opening sizes and positions. Similarly to that found with the uniform loading analysis, the ultimate water level increased when the vertical imposed load was increased or the support conditions at the panel edges were changed from simply supported to fully clamped. This illustrated the importance of correctly modelling the vertical load and edge support conditions for the wall panel under consideration. Wall panels that were short

and tall were found to have the highest resistance to hydraulic loads and a more significant effect was shown when the length was varied as opposed to the height. The overall strength of the masonry also affected the relationship between the ultimate water level and the panel length and height. The ultimate water level was reduced when openings of larger dimensions were positioned in the wall panel, whilst the effect of the opening position was more significant for larger openings.

When factors of safety were incorporated into SA1 only the brick block/brick cavity wall panel (H15) could meet the requirements of the upper limit (0.9 m) specified in the published guidance, whilst the single leaf AAC block walls (H1 and H2) failed to meet the lower value given (0.6 m). This supported the need for a suitable approach for the calculation of characteristic water levels rather than the use of values given by guidance. SA1 was applied to the structure of a typical domestic building and the characteristic water level of the weakest wall exceeded the recommended lower characteristic level (0.6 m) given in published guidance by 38 %. However, if combined action of the cavity leaves did not occur or weaker materials were utilised, then the characteristic water level might not reach the lower value given in guidance. This demonstrated that correct calculation should be completed rather than assuming a “one size fits all” approach.

In summary the main objectives of the research programme that were set out in the introduction have been met. It is recommended that SA1 would provide the most suitable approach for determining the strength of masonry wall panels subject to either uniform or non-uniform lateral loadings. For wall panels constructed with cement mortar then flexural strength should be used in the analysis rather than a friction/overturning resistance. There is certainly scope to further validate the analysis for different conditions, which is discussed in the following section.

## 9.2 Recommendations for further work

### 9.2.1 Continuation of the model scale hydraulic test programme

It would be possible to extend the test programme to examine the effect on the ultimate water level of different sized panels, different sized openings, higher vertical loads and different constraint conditions at the vertical edges of the panel. It would also be of interest to consider different methods to cover the opening during the tests, for example insert a frame and board inside the opening rather then employ the technique used in this study. Considering a number of different sized openings, as well as multiple openings, would allow an assessment of the influence of the

stress concentrations at the corners of the openings on the failure mode. Testing of such parameters would be readily accomplishable using the existing experimental set up and panel manufacture technique employed.

In addition construction methods that employ different techniques could be explored via an experimental investigation. Current construction methods often use a timber frame construction to which an outer cladding of brick or block is applied. Cavity type assemblies that comprise brick or block outer skins and timber inner frames could readily be constructed and tested at small scale using the procedures developed. Other construction techniques such as precast concrete or structurally insulated panelised systems could also be investigated in a similar manner.

Consideration could also be given to the effect of cyclic loading on the performance of the masonry wall panel. For example the water level could be raised to the characteristic level for a number of cycles to asses if any long term damage would be likely. This would be particularly relevant to properties that would be subject to regular flooding. The procedure could be completed using the existing test set up, with only minor modifications being required to allow the water level to be raised and lowered.

### 9.2.2 Design guidance

It has been shown that the results from SA1 developed in this study correlated well to those obtained from the experimental tests. In the absence of a suitable design guide or calculation method it is proposed that the method utilised in SA1 could be adopted to allow the calculation of characteristic water levels for hydraulically loaded masonry structures. The current method given in EC6 (BSI, 2005) for uniformly loaded panels uses tabulated bending moment coefficients that are based on height to length and orthogonal strength ratios. Similar tables of bending moment coefficients could be developed for the case of hydraulically loaded panels to allow calculation to be completed (or checked) without utilising the spreadsheet analysis directly. The advantage of utilising the spreadsheet analysis would be that openings in the panels and vertical loadings could be accounted for in a much simpler manner than through using the tabulated values of bending moment coefficients. Ideally, before introducing the analysis into design guidance, further experimental tests should be completed to examine parameters outside of this study, with particular focus on different sized panels, openings and cavity wall assemblies. It was found in Chapter 8 that the failure modes predicted by the analysis for panels with openings did not

always coincide with the opening corners and it would be of importance to examine the experimental behaviour of wall panels with openings of the dimensions that were theoretically investigated.

### 9.2.3 Hydrodynamic effects

The programme of work presented in this thesis has only considered the hydrostatic forces that result from floodwaters, however properties, particularly those near to rivers or in costal locations, could be subject to both hydrostatic and hydrodynamic forces upon their external walls. Hydrodynamic forces would result from the action of waves, flow of river water where overtopping has occurred, or the flow of excess surface water. The application of a combined hydrodynamic and hydrostatic force could have a significant effect on the performance of a masonry structure and failure would likely occur at lower water levels than those found in this study. The action of the hydrodynamic forces could be both parallel and perpendicular to the wall panel depending on the aspect of the property in relation to the moving floodwater. To consider such combined loadings would require modification of the experimental set up, and could be achieved by incorporating a pump or wave generator to exert the necessary hydrodynamic force. The analysis that has been developed in this study allows for a hydrodynamic effect to be considered and completing an experimental investigation would further allow this to be validated.

### 9.2.4 Testing of flood protection systems

The experimental method developed could be utilised to test a range of flood protection systems at model scale. Testing at reduced scale could offer significant savings in terms of time and cost, as well as reduce health and safety concerns when compared to completing such a programme at full scale. Products such as door barriers, property waterproofing systems and air vent covers would be relatively straightforward to scale. In addition strengthening procedures, including the application of a fibre-reinforced layer to the exterior of the masonry or post tensioning, could be assessed to ascertain if the performance of a hydraulically loaded panel could be improved. Techniques that utilise fibre-reinforced polymers have already proved successful in strengthening masonry subject to dynamic forces arising from earthquakes (Hamed and Rabinovitch, 2010, Lunn and Rizkalla, 2011).

# References

ANDERSON, C. (1976) Lateral loading tests on concrete block walls. *The Structural Engineer,* 54**,** 239-257.

ANDERSON, C. (1984) Arching action in transverse laterally loaded masonry wall panels. *Structural Engineer, Part B: R&D Quarterly,* 62 B**,** 12-23.

ANDERSON, C. & HELD, L. C. (1986) The effect of sand grading on mortar properties and the tensile bond of brickwork specimens. *Masonry (1) Proc. British Masonry Society.* London, Mellor-Green Laboratory.

BAKER, L. R. (1972) Manufacture and testing of model brickwork wind panels. *Structural models conference.* Sydney, Australia, Cement and Concrete Association of Australia.

BAKER, L. R. (1981) The flexural action of masonry structures under lateral load. PhD Thesis, Deakin University.

BEAN POPEHN, J. R., SCHULTZ, A. E., LU, M., STOLARSKI, H. K. & OJARD, N. J. (2008) Influence of transverse loading on the stability of slender unreinforced masonry walls. *Engineering Structures,* 30**,** 2830-2839.

BRINCKER, R. (1984) Yieldline theory and material properties of laterally loaded masonry walls. *Masonry International,* 1.

BSI (1970) Structural recommendations for load-bearing walls. CP111. London, BSI.

BSI (1978) BS 5628:Part 1:1978 Code of practice for use of masonry. *Part 1. Structural use of unreinforced masonry.* London, BSI.

BSI (1986) DD 140-1:1986 Wall ties. *Part 1: Methods of test for mortar joint and timber frame connections.* London, BSI.

BSI (1987) DD 140-2:1987 Wall ties. *Part 2: Recommendations for design of wall ties.* London, BSI.

BSI (1999a) BS EN 1015-11:1999 Methods of test for mortar for masonry. *Part 11: Determination of flexural and compressive strength of hardened mortar.* London, BSI.

BSI (1999b) BS EN 1052-2:1999 Methods of test for masonry. *Part 2: Determination of flexural strength.* London, BSI.

BSI (2000a) BS EN 846-5:2000 Methods of test for ancillary components for masonry. *Part 5: Determination of tensile and compressive load capacity and load displacement characteristics of wall ties (couplet test).* London, BSI.

BSI (2000b) BS EN 846-6:2000 Methods of test for ancillary components for masonry. *Part 6: Determination of tensile and compressive load capacity and load and load displacement characteristics of wall ties (single end test).* London, BSI.

BSI (2000c) BS EN 197-1:2000 Cement. *Part 1: Composition, specifications and conformity criteria for common cements.* London, BSI.

BSI (2000d) BS EN 846-5:2000 Methods of test for ancillary components for masonry. *Part 5: Determination of tensile and compressive load capacity and load displacement characteristics of wall ties (couplet test).* London, BSI.

BSI (2001a) BS 8000-3:2001 Workmanship on building sites *Part 3: Code of practice for masonry.* London, BSI.

BSI (2001b) BS EN 459-1:2001 Building lime. *Part 1: Definitions, specifications and conformity criteria.* London, BSI.

BSI (2002) BS EN 13139:2002 Aggregates for mortar. London, BSI.

BSI (2003a) BS EN 771-1:2003 Specification for masonry units. *Part 1: Clay masonry units.* London, BSI.

BSI (2003b) BS EN 771-4:2003 Specification for masonry units. *Part 4: Autoclaved aerated concrete masonry units.* London, BSI.

BSI (2005a) BS 5628-1:2005 Code of practice for the use of masonry. *Part 1: structural use of unreinforced masonry.* London, BSI.

BSI (2005b) BS 5628-3:2005 Code of practice for the use of masonry. *Part 3: materials and components, design and workmanship*. London, BSI

BSI (2005c) BS EN 1996-1-1:2005 Eurocode 6 - Design of masonry structures. *Part 1-1 General rules for reinforced and unreinforced masonry structures.* London, BSI.

BSI (2005d) NA to BS EN 1996-1-1:2005 UK national annex to Eurocode 6: Design of masonry structures. *Part 1-1 General rules for reinforced and unreinforced masonry structures.* London, BSI.

BSI (2005e) BS EN 1990: 2002+A1:2005 Eurocode - basis of structural design. London, BSI.

BSI (2006) BS EN 1996-3:2006 Eurocode 6 - Design of masonry structures. *Part 3: Simplified calculation methods for unreinforced masonry structures.* London, BSI.

BSI (2009a) PAS 1188-1:2009 Flood protection products - specification. *Part 1: Building aperture products.* London, BSI.

BSI (2009b) PAS 1188-2:2009 Flood protection products - specification. *Part 2: Temporary products.* London, BSI.

BSI (2009c) PAS 1188-3:2009 Flood protection products - specification. *Part 3: Building skirt systems.* London, BSI.

BSI (2011) BS EN 772-21:2011 Methods of test for masonry units. *Part 21: Determination of water absorption of clay and calcium silicate masonry units by cold water absorption.* London, BSI.

CASAPULLA, C. (2008) Lower and upper bounds in closed form for out-of-plane strength of masonry structures with frictional resistances. *Structural Analysis of Historic Construction: Preserving Safety and Significance - Proceedings of the 6th International Conference on Structural Analysis of Historic Construction, SAHC08.* Bath.

CHONG, V. L. (1993) The behaviour of laterally loaded masonry panels with openings. PhD Thesis, Plymouth University.

CHONG, V. L., MAY, I. M. & MA, S. Y. A. (1991) An investigation of the behaviour of laterally loaded masonry panels using non-linear finite element program. *Computer methods in structural masonry (1).* Swansea, G.N. books and journals Ltd.

CHONG, V. L., SOUTHCOMBE, C. & MAY, I. M. (1992) The behaviour of laterally loaded masonry panels with openings. *3rd International masonry conference.* London, The British Masonry Society.

COMMUNITIES & LOCAL GOVERNMENT (2007) Improving the flood performance of new buildings - flood resilient construction. London, Dept. communities & local goverment.

COMMUNITIES & LOCAL GOVERNMENT (2010) Planning policy statement 25: development and flood risk. London, Dept. Communities & Local Government.

CORREA, M. R. S. (2012) Masonry engineering in Brazil past development, current overview, future improvements. *15th International brick and block masonry conference.* Florianopolis, Brazil.

CURTIN, W. G. (1986) The influence of horizontal shear strength on the orthogonal ratio of masonry. *Proc 1st International masonry conference.* London, Mellor-Green Laboratory.

DAVEY, N. & THOMAS, F. G. (1950) The structural uses of brickwork. *The Institution of Civil Engineers, Structural and Building Engineeering division,* 8**,** 1-54.

DAVIES, M. C. R., HUGHES, T. G. & TAUNTON, P. R. (1998) Centrifuge testing of model masonry arch bridges. *Proc. Institution of Civil Engineers Geotechnical Engineering* 131**,** 141-145.

DE VEKEY, R. C. & WEST, H. W. H. (1980) FLEXURAL STRENGTH OF CONCRETE BLOCKWORK. *Magazine of Concrete Research,* 32**,** 206-218.

DE VEKEY, R. C. (1986) Towards a UK performance standard for wall ties. *Proc 1st International masonry conference.* London, Mellor-Green Laboratory.

DE VEKEY, R. C., BRIGHT, N. J., LUCKIN, K. R. & ARORA, S. K. (1986) Research results on autoclaved aerated concrete blockwork. *The Structural Engineer,* 64A**,** 332-340.

DE VEKEY, R. C. & REED, W. J. (1986) The structural performance of cavity wall ties. *Masonry (1) Proc. Britich Masonry Society.* London, Mellor-Green Laboratory.

DUARTE, R. B. (1993) A study of the lateral strength of brickwork panels with openings. PhD Thesis, University of Edinburgh.

DUARTE, R. B. (1998) The design of unreinforced brickwork panels with openings under lateral pressure. *Masonry International,* 11**,** 97-101.

DUARTE, R. B. & SINHA, B. P. (1992) Lateral strength of brickwork panels with openings. *Proceedings of the Institution of Civil Engineers, Structures and Buildings,* 94**,** 397-402.

EDGELL, G. J. (2005) Masonry. *Structural Engineer,* 83**,** 27-31.

EDGELL, G. J. & DE VEKEY, R. C. (1986a) Robust house: implications for building regulations. *Proc 1st International masonry conference.* London, Mellor-Green Laboratory.

EDGELL, G. J. & DE VEKEY, R. C. (1986b) Robustness tests on a domestic house: compressive loading tests on walls. IN WEST, H. W. H. (Ed.) *Masonry (1) Proc. British Masonry Society.* London, British Masonry Society.

EDGELL, G. J. & KJAER, E. (2000) Lateral loading behaviour of walls with openings. *12th International brick and block masonry conference.* Madrid Spain.

EGERMANN, R., COOK, D. A. & ANZANI, A. (1991) An investigation into the behaviour of scale model brick walls. *Proc. 9th International brick and block conference* Berlin.

ENVIRONMENT AGENCY (2009) Flooding in England: A national assessment of flood risk. Bristol, Environment Agency.

ENVIRONMENT AGENCY WALES (2009) Flooding in Wales: A national assessment of flood risk. Cardiff, Environment Agency Wales.

FEATHERSTON, C. A., EATON, M. J. & HOLFORD, K. M. (2011) Modelling the Effects of Geometric Imperfections on the Buckling and Initial Post-buckling Behaviour of Flat Plates Under Compression Using Measured Data. *Strain*.

FEMA (2005) Enclosures and breakaway walls. *Home builder's guide to costal construction.* Washington, FEMA - US Dept. Homeland Security.

FEMA (2008a) Dry floodproof your building. Washington, FEMA - US Dept. Homeland Security.

FEMA (2008b) Openings in foundation walls and wall of enclosures. Washington, FEMA - US Dept. Homeland Security.

FEMA (2009) Homeowner's guide to retrofitting - six ways to protect your home from flooding. Washington, FEMA - US Dept. Homeland Security.

FITCHEN, J. (1981) *The construction of gothic cathedrals: A study of medieval vault erection,* Chicago, University of Chicago Press.

FORDHAM, A. A. (1938) The history of the theory of structures. *The Structural Engineer,* 16**,** 154-163.

FRIED, A., ANDERSON, C. & GAIRNS, D. A. (1986) A comparative study of experimental techniques for determining the flexural resistance of masonry. *Proc 1st International masonry conference.* London, Mellor-Green Laboratory.

FRIED, A. N., MARROCCHINO, E., BRADSELL, C. & ROBERTS, J. J. (2005) Unreinforced solid dense concrete block walls constructed using thin joint technology. *Structural Engineer,* 83**,** 33-37.

GAIRNS, D. A. & SCRIVENER, J. C. (1988) The effect of masonry unit characteristics on panel lateral capacity. *8th International brick and block masonry conference.* Dublin.

GOLDING, J. M. (1991) Practical design of laterally loaded masonry panels. *Structural engineer London,* 69**,** 55-65.

GUTTERIDGE, H. (1931) Portland cement. *The Structural Engineer,* 9**,** 358-367.

HAMED, E. & RABINOVITCH, O. (2010) Lateral out-of-plane strengthening of masonry walls with composite materials. *Journal of Composites for Construction,* 14**,** 376-387.

HAMILTON, S. B. (1939) Masonry construction. *The Structural Engineer,* 17**,** 42-60.

HASELTINE, B. A. & TUTT, J. N. (1986) Implications of research on design recommendations. *Structural Engineer,* 64 A**,** 341-350.

HASELTINE, B. A., WEST, H. W. H. & TUTT, J. N. (1977) Design of walls to resist lateral loads: Part 2. *The Structural Engineer,* 55**,** 422-430.

HENDRY, A. W. (1973) The lateral strength of unreinforced brickwork. *The Structural Engineer,* 51**,** 43-50.

HENDRY, A. W. & MURTHY, C. K. (1965) Comparative tests on 1/3 and 1/6 scale model brickwork piers and walls. *Proc British Ceramic Society - Load bearing brickwork.* London, British Ceramic Society.

HENDRY, A. W., SINHA, B. P. & MAURENBRECHER, A. H. P. (1971) Full scale tests on the lateral strength of brick cavity walls with precompression. *Proc British Ceramic Society - Load bearing brickwork (4).* London, British Ceramic Society.

HENDRY, A. W. (1990) *Structural masonry,* London, Macmillan.

HERBERT, D. M. (2009) Modelling cathedral buttresses. MSc Thesis, Cardiff University.

HEYMAN, J. (1966) The stone skeleton. *International Journal of Solids and Structures,* 2**,** 249-279.

HEYMAN, J. (1992) How to design a cathedral: some fragments of the history of structural engineering. *Proceedings of the Institution of Civil Engineers, Civil Engineering,* 92**,** 24-29.

HORNE, M. R. (1979) *Plastic Theory of Structures,* Oxford, Pergamon Press.

HUERTA, S. (2006) Geometry and equilibrium: the gothic theory of structural design. *The Structural Engineer,* 84**,** 23-28.

HUGHES, T. G., DAVIES, M. C. R., TAUNTON, P. R. & BURROUGHS, P. O. (2002) Centrifuge testing of small scale masonry. *Masonry International,* 15**,** 80-86.

HUGHES, T. G. & KITCHING, N. (2000) Small scale testing of masonry. *Proc. 12th International brick and block masonry confrerence.* Madrid.

ISLAM, S. & PARK, R. (1971) Yield-line analysis of two way reinforced concrete slabs with openings. *The Structural Engineer,* 49**,** 8.

JENKINS, G. J., MURPHY, J. M., SEXTON, D. M. H., LOWE, J. A., JONES, P. & KILSBY, C. G. (2009) UK Climate Projections: Briefing report. Exeter, UK.

JOHANSEN, K. (1972) *Yield-line formulae for slabs,* London, Cement and Concrete Association.

JONES, L. L. (1962) *Ultimate load analysis of reinforced and prestressed concrete structures,* London, Chatto and Windus.

KELMAN, I. & SPENCE, R. (2003a) A limit analysis of unreinforced masonry failing under flood water pressures. *Masonry International,* 16**,** 51-61.

KELMAN, I. & SPENCE, R. (2003b) A flood failure flowchart for buildings. *Proceedings of the Institution of Civil Engineers: Municipal Engineer,* 156**,** 207-214.

KRAWINKLER, H. (1988) State-of-the art report scale effects in static and dynamic model testing of structures. *Proc. 9th world conference on earthquake engineering.* Tokyo-Kyoto, Japan.

LEAKE, J. (2007) Labour plans flood defence cuts as Britian flounders in the deluge. *The Sunday Times.* London, News International.

LOURENCO, P. B. (2000) Anisotropic Softening Model for Masonry Plates and Shells. *Journal of Structural Engineering,* 126**,** 1008-1016.

LOVEGROVE, R. (1988) A discussion of 'yieldlines' in unreinforced masonry. *The Structural Engineer,* 66**,** 5.

LUNN, D. S. & RIZKALLA, S. H. (2011) Strengthening of infill masonry walls with FRP materials. *Journal of Composites for Construction,* 15**,** 206-214.

LYNCH, G. (2007) *The History of Gauged Brickwork: Conservation, Repair and Modern Application*, Elsevier/Butterworth-Heinemann.

MARK, R. (1984) *Experiments in gothic structure,* Massachusetts, The MIT Press.

MARTINI, K. (1998) Finite element studies in the two-way out-of-plane failure of unreinforced masonry. *Proc. 6th national conference on Earthquake Engineering.* Seattle, Washington, Earthquake engineering research institute.

MAY, I. M. & MA, S. Y. A. (1986) Design of masonry panels under lateral load. *Proc 1st International masonry conference.* London, Mellor-Green Laboratory.

MAY, I. M. & TELLETT, J. (1986) Non-linear finite element analysis of reinforced and unreinforced brickwork. *Proc. British Masonry Society,* 1.

MCDONALD, L. (2000) Hydraulic lime mortar for the house of the future. *The Structural Engineer,* 78**,** 12-16.

MOHAMMED, A. (2006) Experimental comparison of brickwork behaviour at prototype and model scales. PhD Thesis, Cardiff University.

MOHAMMED, A. & HUGHES, T. G. (2011) Prototype and model masonry behaviour under different loading conditions. *Materials and Structures,* 44**,** 53-65.

MOHAMMED, A., HUGHES, T. G. & MUSTAPHA, A. (2011) The effect of scale on the structural behaviour of masonry under compression. *Construction and Building Materials,* 25**,** 303-307.

MOORE, J. F. A. (1986) The resistance of masonry to lateral loading. *The Structural Engineer,* 64A**,** 319-320.

MORTON, J. (1986) The design of laterally loaded walls. The brick development association.

MORTON, J. & HENDRY, A. W. (1971) A theoretical investigation of the lateral strength of brick walls with precompression. *Proc British Ceramic Society - Load bearing brickwork (4).* London, British Ceramic Society.

MURTHY, C. K. & HENDRY, A. W. (1966) Model experiments in load bearing brickwork. *Building Science,* 1**,** 289-298.

NG, C. L. (1996) Experimental and theoretical investigation of the behaviour of brickwork cladding panel subjected to lateral loading. PhD Thesis, University of Edinburgh.

ODPM (2003) Preparing for floods: interim guidance for improving the flood resistance of domestic and small business properties. London.

ODPM (2004) The building regulations 2000. *Part A - Structure.* London, NBS.

ORDUNA, A. & LOURENCO, P. B. (2005a) Three-dimensional limit analysis of rigid blocks assemblages. Part I: Torsion failure on frictional interfaces and limit analysis formulation. *International Journal of Solids and Structures,* 42**,** 5140-5160.

ORDUNA, A. & LOURENCO, P. B. (2005b) Three-dimensional limit analysis of rigid blocks assemblages. Part II: Load-path following solution procedure and validation. *International Journal of Solids and Structures,* 42**,** 5161-5180.

PACE, C. E. & CAMPBELL, R. L. (1978) Structural integrity of brick-veneer buildings. Vicksburg, USA, USACE.

PACE, C. E. (1988) Flood proofing tests - Tests of materials and systems for flood proofing structures. Washington D.C., USA, USACE.

PITT, M. (2008) The Pitt review - Learning lessons from the 2007 floods. London, UK Government.

RAFIQ, M. Y., ZHOU, G. C. & EASTERBROOK, D. J. (2003) Analysis of brickwork panels subjected to lateral loading using correctors. *Masonry International,* 16**,** 75-82.

RILEM (1991a) LUMA6 Compressive strength of mortar. *Part 7 Structures and masonry.* London, E & FN Spon.

RILEM (1991b) LUMB2 Flexural strength of small wall specimens. *Part 7 Structures and masonry.* London, E & FN Spon.

RILEM (1991c) LUMC2 Full-scale wall out-of-plane flexural test. *Part 7 Structures and masonry.* London, E & FN Spon.

ROYLES, R. & HENDRY, A. W. (1991) Model tests on masonry arches. *Proceedings of the Institution of Civil Engineers, Structural and Building Board,* 91**,** 299-321.

SEPA (2011) The national flood risk assessment. Stirling, SEPA.

SINHA, B. P. (1978) A simplified ultimate load analysis of laterally loaded model orthotropic brickwork panels of low tensile strength. *The Structural Engineer,* 56B**,** 81-84.

SINHA, B. P. & HENDRY, A. W. (1968) Further tests on model brick walls and piers. *Proc British Ceramic Society - Load bearing brickwork (3).* London, British Ceramic Society.

SINHA, B. P., LOFTUS, M. D. & TEMPLE, R. (1979) Lateral strength of model brickwork panels. *Proc. Institution of Civil Engineers,* 67**,** 191-197.

STERN, N. (2007) The economics of climate change - the Stern review. Cambridge, UK Government.

SUI, C. & RAFIQ, M. Y. (2009) Laterally loaded masonry wall panels: a review of numerical methods. *Masonry International,* 22**,** 47-52.

SWEENEY, S. C., HORNEY, M. A. & ORTON, S. L. (2005) Seismic Response of a Half-Scale Masonry Building with Flexible Diaphragms. Champaign, IL, U.S. Army Engineer Research and Development Center.

TAUNTON, P. R. (1997) Centrifuge modelling of soil/masonry structure interaction. PhD Thesis, University of Wales, Cardiff.

TEMPLETON, W., EDGELL, G. J. & DE VEKEY, R. C. (1986) The robustness of the domestic house part 3: positive wind pressure test on gable wall. *Proc 1st International masonry conference.* London, Mellor-Green Laboratory.

THE SCOTTISH GOVERNMENT (2011) Building (Scotland) regulations 2004. Edinburgh, The Scottish Government.

THOMAS, K. (1968) The strength, function and other properties of wall ties. *Proc British Ceramic Society - Load bearing brickwork (3).* London, British Ceramic Society.

THORP PRECAST (2005) Case study: MediSense UK - brick faced cladding panels. *Available from: http://thorpprecast.co.uk/Medisense%20Oxon.pdf.* [Accessed: 29th May 2012]

TIMOSHENKO, S. & WOINOWSKY-KRIEGER, S. (1959) *Theory of plates and shells*, McGraw-Hill.

TOMAZEVIC, M. & KLEMENC, I. (1997) Verification of seismic resistance of confined masonry buildings. *Earthquake Engineering and Structural Dynamics,* 26**,** 1073-1088.

TOMAZEVIC, M., LUTMAN, M. & WEISS, P. (1996) Seismic upgrading of old brick-masonry urban houses: Tying of walls with steel ties. *Earthquake Spectra,* 12**,** 599-622.

TOMAZEVIC, M. & VELECHOVSKY, T. (1992) Some aspects of testing small-scale masonry building models on simple earthquake simulators. *Earthquake Engineering & Structural Dynamics,* 21**,** 945-963.

TUTT, J. N. (1988) Replacement ties in cavity walls. London, CIRIA.

WAGNER, P. (1994) Yield line analysis of slabs with covered openings. *26th DoD Explosives Safety Seminar.* Miami, Florida, US Navy.

WEST, H. W. H., HODGKINSON, H. R. & HASELTINE, B. A. (1977) The resistance of brickwork to lateral loading: Part 1 - Experimental methods and results of tests on small specimens and full sized walls. *The Structural Engineer,* 55**,** 411-421.

WEST, H. W. H., HODGKINSON, H. R., HASELTINE, B. A. & DE VEKEY, R. C. (1986) Research results on brickwork and aggregate blockwork since 1977 *The Structural Engineer,* 64A**,** 320-331.

WEST, H. W. H., HODGKINSON, H. R. & WEBB, W. F. (1971) The resistance of brick walls to lateral loading. *Proc British Ceramic Society - Load bearing brickwork (4).* London, British Ceramic Society.

WHEATER, H. S. (2006) Flood hazard and management: a UK perspective. *Philosophical transactions of The Royal Society,* 364**,** 2135-2145.

WIENERBERGER (2009) *The brick book*, Wienerberger Ltd.

WILLIAMS, G. P. (1978) Flood proofing of buildings. *Canadian building digests,* 198.

ZHOU, G., RAFIQ, M., BUGMANN, G. & EASTERBROOK, D. (2006) Cellular Automata Model for Predicting the Failure Pattern of Laterally Loaded Masonry Wall Panels. *Journal of Computing in Civil Engineering,* 20**,** 400-409.

# Appendix 1 Integration of pressure functions

The following appendix details the expansion of the integrals given by equations 3.21 to 3.26 in chapter 3 that determine the forces at the centres of pressures and moments on the triangular sub elements of the slabs.

Expansion of equation 3.17 to determine force at centre of pressure for left hand triangular sub element:

$$F_{LHS} = \int_{x_1}^{x_2} \int_{y=A_1x+B_1}^{y=A_2x+B_2} \left(a_p + b_p x + c_p y\right) dy dx$$

$$F_{LHS} = \int_{x_1}^{x_2} \left| a_p y + b_p xy + \frac{c_p y^2}{2} \right|_{y=A_1x+B_1}^{y=A_2x+B_2} dx$$

$$F_{LHS} = \int_{x_1}^{x_2} \left[ a_p\left(A_2x + B_2 - A_1x - B_1\right) + b_p x\left(A_2x + B_2 - A_1x - B_1\right) + \frac{c_p}{2}\left(\left(A_2x + B_2\right)^2 - \left(A_1x + B_1\right)^2\right) \right] dx$$

$$F_{LHS} = \int_{x_1}^{x_2} \left[ a_p\left(B_2 - B_1\right) + x\left(a_pA_2 - a_pA_1 + b_pB_2 - b_pB_1\right) + b_pA_2x^2 - b_pA_1x^2 + \frac{c_p}{2}\left(\left(A_2x + B_2\right)^2 - \left(A_1x + B_1\right)^2\right) \right] dx$$

$$F_{LHS} = \left| a_p\left(B_2 - B_1\right)x + \frac{x^2}{2}\left(a_pA_2 - a_pA_1 + b_pB_2 - b_pB_1\right) + b_p\left(\frac{A_2x^3}{3} - \frac{A_1x^3}{3}\right) + \frac{c_p}{2}\left(\frac{\left(A_2x + B_2\right)^3}{3A_2} - \frac{\left(A_1x + B_1\right)^3}{3A_1}\right) \right|_{x_1}^{x_2}$$

$$F_{LHS} = \left| a_p\left(B_2 - B_1\right)x + \left(a_p\left(A_2 - A_1\right) + b_p\left(B_2 - B_1\right)\right)\frac{x^2}{2} + b_p\left(A_2 - A_1\right)\frac{x^3}{3} + \frac{c_p}{2}\left(\frac{\left(A_2x + B_2\right)^3}{3A_2} - \frac{\left(A_1x + B_1\right)^3}{3A_1}\right) \right|_{x_1}^{x_2}$$

$$F_{LHS} = \left[ \begin{array}{l} a_p\left(B_2 - B_1\right)\left(x_2 - x_1\right) + \left(a_p\left(A_2 - A_1\right) + b_p\left(B_2 - B_1\right)\right)\left(\frac{x_2^2 - x_1^2}{2}\right) + b_p\left(A_2 - A_1\right)\left(\frac{x_2^3 - x_1^3}{3}\right) \\ + \frac{c_p}{6}\left(\frac{\left(A_2x_2 + B_2\right)^3}{A_2} - \frac{\left(A_1x_2 + B_1\right)^3}{A_1} - \frac{\left(A_2x_1 + B_2\right)^3}{A_2} + \frac{\left(A_1x_1 + B_1\right)^3}{A_1}\right) \end{array} \right]$$

Expansion of equation 3.18 to determine force at centre of pressure for right hand triangular sub element:

$$F_{RHS} = \int_{x_2}^{x_3}\int_{y=A_1x+B_1}^{y=A_3x+B_3}\left(a_p + b_p x + c_p y\right)dydx$$

$$F_{RHS} = \int_{x_2}^{x_3}\left| a_p y + b_p xy + \frac{c_p y^2}{2}\right|_{y=A_1x+B_1}^{y=A_3x+B_3} dx$$

$$F_{RHS} = \int_{x_2}^{x_3}\left[ a_p\left(A_3x + B_3 - A_1x - B_1\right) + b_p x\left(A_3x + B_3 - A_1x - B_1\right) + \frac{c_p}{2}\left(\left(A_3x + B_3\right)^2 - \left(A_1x + B_1\right)^2\right)\right]dx$$

$$F_{RHS} = \int_{x_2}^{x_3}\left[ a_p\left(B_3 - B_1\right) + x\left(a_pA_3 - a_pA_1 + b_pB_3 - b_pB_1\right) + b_pA_3x^2 - b_pA_1x^2 + \frac{c_p}{2}\left(\left(A_3x + B_3\right)^2 - \left(A_1x + B_1\right)^2\right)\right]dx$$

$$F_{RHS} = \left| a_p\left(B_3 - B_1\right)x + \frac{x^2}{2}\left(a_pA_3 - a_pA_1 + b_pB_3 - b_pB_1\right) + b_p\left(\frac{A_3x^3}{3} - \frac{A_1x^3}{3}\right) + \frac{c_p}{2}\left(\frac{\left(A_3x + B_3\right)^3}{3A_3} - \frac{\left(A_1x + B_1\right)^3}{3A_1}\right)\right|_{x_2}^{x_3}$$

$$F_{RHS} = \left| a_p\left(B_3 - B_1\right)x + \left(a_p\left(A_3 - A_1\right) + b_p\left(B_3 - B_1\right)\right)\frac{x^2}{2} + b_p\left(A_3 - A_1\right)\frac{x^3}{3} + \frac{c_p}{2}\left(\frac{\left(A_3x + B_3\right)^3}{3A_3} - \frac{\left(A_1x + B_1\right)^3}{3A_1}\right)\right|_{x_2}^{x_3}$$

$$F_{RHS} = \left[\begin{array}{l} a_p\left(B_3 - B_1\right)\left(x_3 - x_2\right) + \left(a_p\left(A_3 - A_1\right) + b_p\left(B_3 - B_1\right)\right)\left(\frac{x_3^2 - x_2^2}{2}\right) + b_p\left(A_3 - A_1\right)\left(\frac{x_3^3 - x_2^3}{3}\right) \\ + \frac{c_p}{6}\left(\frac{\left(A_3x_3 + B_3\right)^3}{A_3} - \frac{\left(A_1x_3 + B_1\right)^3}{A_1} - \frac{\left(A_3x_2 + B_3\right)^3}{A_3} + \frac{\left(A_1x_2 + B_1\right)^3}{A_1}\right) \end{array}\right]$$

Expansion of equation 3.19 to determine moment in x direction for left hand triangular sub element:

$$Mx_{LHS} = \int_{x_1}^{x_2} \int_{y=A_1x+B_1}^{y=A_2x+B_2} \left(a_p + b_p x + c_p y\right) x dy dx$$

$$Mx_{LHS} = \int_{x_1}^{x_2} \left| a_p xy + b_p x^2 y + \frac{c_p xy^2}{2} \right|_{y=A_1x+B_1}^{y=A_2x+B_2} dx$$

$$Mx_{LHS} = \int_{x_1}^{x_2} \left[ a_p x\left(\left(A_2x+B_2\right)-\left(A_1x+B_1\right)\right) + b_p x^2\left(\left(A_2x+B_2\right)-\left(A_1x+B_1\right)\right) + \frac{c_p}{2}\left(x\left(A_2x+B_2\right)^2 - x\left(A_1x+B_1\right)^2\right)\right] dx$$

$$Mx_{LHS} = \int_{x_1}^{x_2} \left[ \begin{array}{l} a_p\left(\left(A_2-A_1\right)x^2+\left(B_2-B_1\right)x\right) + b_p\left(\left(A_2-A_1\right)x^3+\left(B_2-B_1\right)x^2\right) \\ + \frac{c_p}{2}\left(A_2^2x^3 + 2A_2B_2x^2 + B_2^2x - A_1^2x^3 - 2A_1B_1x^2 - B_1^2x\right) \end{array} \right] dx$$

$$Mx_{LHS} = \left| \begin{array}{l} a_p\left(\left(A_2-A_1\right)\frac{x^3}{3}+\left(B_2-B_1\right)\frac{x^2}{2}\right) + b_p\left(\left(A_2-A_1\right)\frac{x^4}{4}+\left(B_2-B_1\right)\frac{x^3}{3}\right) \\ + \frac{c_p}{2}\left(\frac{A_2^2x^4}{4} + \frac{2A_2B_2x^3}{3} + \frac{B_2^2x^2}{2} - \frac{A_1^2x^4}{4} - \frac{2A_1B_1x^3}{3} - \frac{B_1^2x^2}{2}\right) \end{array} \right|_{x_1}^{x_2}$$

$$Mx_{LHS} = \left| \begin{array}{l} a_p\left(\left(A_2-A_1\right)\frac{x^3}{3}+\left(B_2-B_1\right)\frac{x^2}{2}\right) + b_p\left(\left(A_2-A_1\right)\frac{x^4}{4}+\left(B_2-B_1\right)\frac{x^3}{3}\right) \\ + \frac{c_p}{2}\left(\frac{x^4}{4}\left(A_2^2-A_1^2\right) + \frac{2x^3}{3}\left(A_2B_2-A_1B_1\right) + \frac{x^2}{2}\left(B_2^2-B_1^2\right)\right) \end{array} \right|_{x_1}^{x_2}$$

$$Mx_{LHS} = \left[ \begin{array}{l} a_p\left(\frac{\left(A_2-A_1\right)}{3}\left(x_2^3-x_1^3\right) + \frac{\left(B_2-B_1\right)}{2}\left(x_2^2-x_1^2\right)\right) \\ + b_p\left(\frac{\left(A_2-A_1\right)}{4}\left(x_2^4-x_1^4\right) + \frac{\left(B_2-B_1\right)}{3}\left(x_2^3-x_1^3\right)\right) \\ + \frac{c_p}{2}\left(\frac{\left(x_2^4-x_1^4\right)}{4}\left(A_2^2-A_1^2\right) + \frac{2\left(x_2^3-x_1^3\right)}{3}\left(A_2B_2-A_1B_1\right) + \frac{\left(x_2^2-x_1^2\right)}{2}\left(B_2^2-B_1^2\right)\right) \end{array} \right]$$

Expansion of equation 3.20 to determine moment in y direction for left hand triangular sub element:

$$My_{LHS} = \int_{x_1}^{x_2} \int_{y=A_1x+B_1}^{y=A_2x+B_2} \left(a_p + b_p x + c_p y\right) y dy dx$$

$$My_{LHS} = \int_{x_1}^{x_2} \left[ \frac{a_p y^2}{2} + \frac{b_p x y^2}{2} + \frac{c_p y^3}{3} \right]_{y=A_1x+B_1}^{y=A_2x+B_2} dx$$

$$My_{LHS} = \int_{x_1}^{x_2} \left[ \frac{a_p}{2}\left(\left(A_2x+B_2\right)^2 - \left(A_1x+B_1\right)^2\right) + \frac{b_p x}{2}\left(\left(A_2x+B_2\right)^2 - \left(A_1x+B_1\right)^2\right) + \frac{c_p}{3}\left(\left(A_2x+B_2\right)^3 - \left(A_1x+B_1\right)^3\right) \right] dx$$

$$My_{LHS} = \int_{x_1}^{x_2} \left[ \begin{array}{l} \frac{a_p}{2}\left(\left(A_2x+B_2\right)^2 - \left(A_1x+B_1\right)^2\right) + \frac{b_p}{2}\left(A_2^2x^3 + 2A_2B_2x^2 + B_2^2x - A_1^2x^3 - 2A_1B_1x^2 - B_1^2x\right) \\ + \frac{c_p}{3}\left(\left(A_2x+B_2\right)^3 - \left(A_1x+B_1\right)^3\right) \end{array} \right] dx$$

$$My_{LHS} = \left| \begin{array}{l} \frac{a_p}{2}\left(\frac{\left(A_2x+B_2\right)^3}{3A_2} - \frac{\left(A_1x+B_1\right)^3}{3A_1}\right) + \frac{b_p}{2}\left(\frac{A_2^2x^4}{4} + \frac{2A_2B_2x^3}{3} + \frac{B_2^2x^2}{2} - \frac{A_1^2x^4}{4} - \frac{2A_1B_1x^3}{3} - \frac{B_1^2x^2}{2}\right) \\ + \frac{c_p}{3}\left(\frac{\left(A_2x+B_2\right)^4}{4A_2} - \frac{\left(A_1x+B_1\right)^4}{4A_1}\right) \end{array} \right|_{x_1}^{x_2}$$

$$My_{LHS} = \left| \begin{array}{l} \frac{a_p}{2}\left(\frac{\left(A_2x+B_2\right)^3}{3A_2} - \frac{\left(A_1x+B_1\right)^3}{3A_1}\right) + \frac{b_p}{2}\left(\frac{x^4}{4}\left(A_2^2 - A_1^2\right) + \frac{2x^3}{3}\left(A_2B_2 - A_1B_1\right) + \frac{x^2}{2}\left(B_2^2 - B_1^2\right)\right) \\ + \frac{c_p}{3}\left(\frac{\left(A_2x+B_2\right)^4}{4A_2} - \frac{\left(A_1x+B_1\right)^4}{4A_1}\right) \end{array} \right|_{x_1}^{x_2}$$

$$My_{LHS} = \left[ \begin{array}{l} \frac{a_p}{2}\left(\frac{\left(A_2x_2+B_2\right)^3}{3A_2} - \frac{\left(A_1x_2+B_1\right)^3}{3A_1} - \frac{\left(A_2x_1+B_2\right)^3}{3A_2} + \frac{\left(A_1x_1+B_1\right)^3}{3A_1}\right) \\ + \frac{b_p}{2}\left(\left(\frac{x_2^4 - x_1^4}{4}\right)\left(A_2^2 - A_1^2\right) + \frac{2}{3}\left(x_2^3 - x_1^3\right)\left(A_2B_2 - A_1B_1\right) + \left(\frac{x_2^2 - x_1^2}{2}\right)\left(B_2^2 - B_1^2\right)\right) \\ + \frac{c_p}{3}\left(\frac{\left(A_2x_2+B_2\right)^4}{4A_2} - \frac{\left(A_1x_2+B_1\right)^4}{4A_1}\frac{\left(A_2x_1+B_2\right)^4}{4A_2} + \frac{\left(A_1x_1+B_1\right)^4}{4A_1}\right) \end{array} \right]$$

Expansion of equation 3.21 to determine moment in x direction for right hand triangular sub element:

$$Mx_{RHS} = \int_{x_2}^{x_3}\int_{y=A_1x+B_1}^{y=A_3x+B_3}\left(a_p + b_p x + c_p y\right)x\,dy\,dx$$

$$Mx_{RHS} = \int_{x_2}^{x_3}\left|a_p xy + b_p x^2 y + \frac{c_p xy^2}{2}\right|_{y=A_1x+B_1}^{y=A_3x+B_3} dx$$

$$Mx_{RHS} = \int_{x_2}^{x_3}\left[a_p x\left(\left(A_3x+B_3\right)-\left(A_1x+B_1\right)\right) + b_p x^2\left(\left(A_3x+B_3\right)-\left(A_1x+B_1\right)\right) + \frac{c_p}{2}\left(x\left(A_3x+B_3\right)^2 - x\left(A_1x+B_1\right)^2\right)\right]dx$$

$$Mx_{RHS} = \int_{x_2}^{x_3}\left[\begin{array}{l} a_p\left(\left(A_3-A_1\right)x^2+\left(B_3-B_1\right)x\right) + b_p\left(\left(A_3-A_1\right)x^3+\left(B_3-B_1\right)x^2\right) \\ +\frac{c_p}{2}\left(A_3^2x^3+2A_3B_3x^2+B_3^2x-A_1^2x^3-2A_1B_1x^2-B_1^2x\right)\end{array}\right]dx$$

$$Mx_{RHS} = \left|\begin{array}{l} a_p\left(\left(A_3-A_1\right)\frac{x^3}{3}+\left(B_3-B_1\right)\frac{x^2}{2}\right) + b_p\left(\left(A_3-A_1\right)\frac{x^4}{4}+\left(B_3-B_1\right)\frac{x^3}{3}\right) \\ +\frac{c_p}{2}\left(\frac{A_3^2x^4}{4}+\frac{2A_3B_3x^3}{3}+\frac{B_3^2x^2}{2}-\frac{A_1^2x^4}{4}-\frac{2A_1B_1x^3}{3}-\frac{B_1^2x^2}{2}\right)\end{array}\right|_{x_1}^{x_2}$$

$$Mx_{RHS} = \left|\begin{array}{l} a_p\left(\left(A_2-A_1\right)\frac{x^3}{3}+\left(B_2-B_1\right)\frac{x^2}{2}\right) + b_p\left(\left(A_2-A_1\right)\frac{x^4}{4}+\left(B_2-B_1\right)\frac{x^3}{3}\right) \\ +\frac{c_p}{2}\left(\frac{x^4}{4}\left(A_2^2-A_1^2\right)+\frac{2x^3}{3}\left(A_2B_2-A_1B_1\right)+\frac{x^2}{2}\left(B_2^2-B_1^2\right)\right)\end{array}\right|_{x_2}^{x_3}$$

$$Mx_{RHS} = \left[\begin{array}{l} a_p\left(\frac{\left(A_3-A_1\right)}{3}\left(x_3^3-x_2^3\right)+\frac{\left(B_3-B_1\right)}{2}\left(x_3^2-x_2^2\right)\right) \\ +b_p\left(\frac{\left(A_3-A_1\right)}{4}\left(x_3^4-x_2^4\right)+\frac{\left(B_3-B_1\right)}{3}\left(x_3^3-x_2^3\right)\right) \\ +\frac{c_p}{2}\left(\frac{\left(x_3^4-x_2^4\right)}{4}\left(A_3^2-A_1^2\right)+\frac{2\left(x_3^3-x_2^3\right)}{3}\left(A_3B_3-A_1B_1\right)+\frac{\left(x_3^2-x_2^2\right)}{2}\left(B_3^2-B_1^2\right)\right)\end{array}\right]$$

Expansion of equation 3.22 to determine moment in y direction for right hand triangular sub element:

$$My_{RHS} = \int_{x_2}^{x_3}\int_{y=A_1x+B_1}^{y=A_3x+B_3}\left(a_p + b_p x + c_p y\right) y\,dy\,dx$$

$$My_{RHS} = \int_{x_2}^{x_3}\left[\frac{a_p y^2}{2} + \frac{b_p x y^2}{2} + \frac{c_p y^3}{3}\right]_{y=A_1x+B_1}^{y=A_3x+B_3} dx$$

$$My_{RHS} = \int_{x_2}^{x_3}\left[\frac{a_p}{2}\left(\left(A_3x+B_3\right)^2 - \left(A_1x+B_1\right)^2\right) + \frac{b_p x}{2}\left(\left(A_3x+B_3\right)^2 - \left(A_1x+B_1\right)^2\right) + \frac{c_p}{3}\left(\left(A_3x+B_3\right)^3 - \left(A_1x+B_1\right)^3\right)\right] dx$$

$$My_{RHS} = \int_{x_2}^{x_3}\left[\begin{array}{l}\frac{a_p}{2}\left(\left(A_3x+B_3\right)^2 - \left(A_1x+B_1\right)^2\right) + \frac{b_p}{2}\left(A_3^2x^3 + 2A_3B_3x^2 + B_3^2x - A_1^2x^3 - 2A_1B_1x^2 - B_1^2x\right) \\ + \frac{c_p}{3}\left(\left(A_3x+B_3\right)^3 - \left(A_1x+B_1\right)^3\right)\end{array}\right] dx$$

$$My_{RHS} = \left|\begin{array}{l}\frac{a_p}{2}\left(\frac{\left(A_3x+B_3\right)^3}{3A_3} - \frac{\left(A_1x+B_1\right)^3}{3A_1}\right) + \frac{b_p}{2}\left(\frac{A_3^2x^4}{4} + \frac{2A_3B_3x^3}{3} + \frac{B_3^2x^2}{2} - \frac{A_1^2x^4}{4} - \frac{2A_1B_1x^3}{3} - \frac{B_1^2x^2}{2}\right) \\ + \frac{c_p}{3}\left(\frac{\left(A_3x+B_3\right)^4}{4A_3} - \frac{\left(A_1x+B_1\right)^4}{4A_1}\right)\end{array}\right|_{x_1}^{x_2}$$

$$My_{RHS} = \left|\begin{array}{l}\frac{a_p}{2}\left(\frac{\left(A_3x+B_3\right)^3}{3A_3} - \frac{\left(A_1x+B_1\right)^3}{3A_1}\right) + \frac{b_p}{2}\left(\frac{x^4}{4}\left(A_3^2 - A_1^2\right) + \frac{2x^3}{3}\left(A_3B_3 - A_1B_1\right) + \frac{x^2}{2}\left(B_3^2 - B_1^2\right)\right) \\ + \frac{c_p}{3}\left(\frac{\left(A_3x+B_3\right)^4}{4A_3} - \frac{\left(A_1x+B_1\right)^4}{4A_1}\right)\end{array}\right|_{x_2}^{x_3}$$

$$My_{RHS} = \left[\begin{array}{l}\frac{a_p}{2}\left(\frac{\left(A_3x_3+B_3\right)^3}{3A_3} - \frac{\left(A_1x_3+B_1\right)^3}{3A_1} - \frac{\left(A_3x_2+B_3\right)^3}{3A_3} + \frac{\left(A_1x_2+B_1\right)^3}{3A_1}\right) \\ + \frac{b_p}{2}\left(\left(\frac{x_3^4 - x_2^4}{4}\right)\left(A_3^2 - A_1^2\right) + \frac{2}{3}\left(x_3^3 - x_2^3\right)\left(A_3B_3 - A_1B_1\right) + \left(\frac{x_3^2 - x_2^2}{2}\right)\left(B_3^2 - B_1^2\right)\right) \\ + \frac{c_p}{3}\left(\frac{\left(A_3x_3+B_3\right)^4}{4A_3} - \frac{\left(A_1x_3+B_1\right)^4}{4A_1} - \frac{\left(A_3x_2+B_3\right)^4}{4A_3} + \frac{\left(A_1x_2+B_1\right)^4}{4A_1}\right)\end{array}\right]$$

# Appendix 2 Example EC6 wind loading calculation

The following appendix details an example of the Eurocode 6 (BSI, 2005c) method to calculate the uniform lateral load capacity of a masonry wall panel. The calculation was completed for the brick wall panel constructed with M2 compressive strength mortar (panel reference W9, W10 & W11) as detailed in Chapter 8 Section 8.1.1. The wall panel was simply supported along all edges (EC6 wall support condition E) and subject to a vertical axial load. The parameters used in the analysis are detailed in Table A2.1. The average experimental flexural strengths ($f_x$) as given in Table 5.1 in Chapter 5 are used in the calculation and for completeness are given in Table A2-1.

**Table A2-1. Parameters used in the EC6 analysis**

| Parameter | Value | Units |
|---|---|---|
| Length (l) | 4.755 | m |
| Height (h) | 2.452 | m |
| Ratio of height to length (h/l) | 0.52 | No units |
| Thickness ($T_{bl}$) | 0.1025 | m |
| Vertical axial load ($V_{udl}$) | 1828 | kN/m |
| Density of masonry ($\rho_{brick}$) | 4.51 | kg/m$^3$ |
| Flexural strength direction 1 ($f_{xd1}$) | 0.44 | N/mm$^2$ |
| Flexural strength direction 2 ($f_{xd2}$) | 1.02 | N/mm$^2$ |

To determine the moment of resistance it is firstly necessary to calculate the section modulus, Z, per unit length or height as given by equation 1.

$$Z = \frac{1000 \times \left(T_{bl} \times 1000\right)^2}{6}$$
$$Z = \frac{1000 \times \left(0.1025 \times 1000\right)^2}{6} \qquad (1)$$
$$Z = 1751042 mm^3$$

The applied design vertical compressive stress, $\sigma_d$, due to self-weight and the imposed vertical axial load provides a positive beneficial effect on the moment resistance in direction 1 and is assumed to be acting at mid height of the wall panel as given by equation 2.

$$\sigma_d = \frac{V_{udl} \times 1000 + \rho_{brick} g \frac{h}{2} T_{bl} \times 1}{Tbl \times 1000 \times 1000}$$

$$\sigma_d = \frac{4.51 \times 1000 + 1828 \times 9.81 \times \frac{2.452}{2} \times 0.1025 \times 1}{0.1025 \times 1000 \times 1000} \quad (2)$$

$$\sigma_d = 0.066 N / mm^2$$

It follows that the design moments of resistance in direction 1, $M_{Rd1}$, per unit length and direction 2, $M_{Rd2}$, per unit height are given by equations 3 and 4 respectively (EC6 clause 6.3.1) (BSI, 2005c).

$$M_{Rd1} = \left(f_{xd1} + \sigma_d\right) Z$$

$$M_{Rd1} = \left(0.44 + 0.066\right) \times 1751042 \quad (3)$$

$$M_{Rd1} = 886 Nm / m$$

$$M_{Rd2} = f_{xd2} Z$$

$$M_{Rd2} = 1.02 \times 1751042 \quad (4)$$

$$M_{Rd2} = 1786 Nm / m$$

The design value for the applied moments for a plane of failure parallel (direction 1) to the bed joints, $M_{Ed1}$, per unit length and a plane of failure perpendicular (direction 2) to the bed joints, $M_{Ed2}$, per unit height are given by equations 5 and 6 respectively (EC6 clause 5.5.5) (BSI, 2005c).

$$M_{Ed1} = \alpha_1 W_{Ed} l^2 \quad (5)$$

$$M_{Ed2} = \alpha_2 W_{Ed} l^2 \quad (6)$$

Where $\alpha_1$, $\alpha_2$ are bending moment coefficients that depend on the support conditions, l is the panel length and $W_{Ed}$ is the applied lateral load. Bending moment coefficients are tabulated in EC6 (as $\alpha_2$ values only) according to the height to length ratio and the orthogonal ratio. The orthogonal ratio, $\mu$, of the flexural strengths is given by equation 7.

$$\mu = \frac{f_{xd1} + \sigma_d}{f_{xd2}}$$
$$\mu = \frac{0.44 + 0.066}{1.02} \quad (7)$$
$$\mu = 0.50$$

The value of $\alpha_2$ is obtained from the tabulated values in EC6 - Annex E - wall support condition E (BSI, 2005c) by interpolation and was equal to 0.029. The value of $\alpha_1$ was determined from $\alpha_2$ using equation 8.

$$\alpha_1 = \mu\alpha_2$$
$$\alpha_1 = 0.50 \times 0.029 \quad (8)$$
$$\alpha_1 = 0.0145$$

The EC6 method assumes that at ultimate limit state that the applied design moment, $M_{Ed}$ is equal to the design value of the moment of resistance, $M_{Rd}$ (EC6 clause 6.3.1) (BSI, 2005c). In this case it is required to establish the ultimate uniformly applied lateral load, $W_{Ed}$, and this is given by either rearranging equations 3 and 5 or equations 4 and 6.

From equations 3 and 5:

$$W_{Ed} = \frac{M_{Rd1}}{\alpha_1 l^2}$$
$$W_{Ed} = \frac{886}{0.0145 \times 4.755^2} \quad (9)$$
$$W_{Ed} = 2.71 kN/m^2$$

From equations 4 and 6:

$$W_{Ed} = \frac{M_{Rd2}}{\alpha_2 l^2}$$
$$W_{Ed} = \frac{1786}{0.029 \times 4.755^2} \quad (10)$$
$$W_{Ed} = 2.71 kN/m^2$$

# Appendix 3 Publications

HERBERT, D. M., GARDNER, D. R., HARBOTTLE, M. & HUGHES, T. G. (2013) Uniform lateral load capacity of small-scale masonry wall panels. *Materials and Structures*.

HERBERT, D. M., GARDNER, D. R., HARBOTTLE, M. & HUGHES, T. G. (2012) The strength of masonry walls when subject to flood loading. IN ROMAN, H. R. & PARSEKIAN, G. A. (Eds.) *15th International brick and block masonry conference.* Florianopolis, Brazil.

HERBERT, D. M., GARDNER, D. R., HARBOTTLE, M., THOMAS, J. & HUGHES, T. G. (2011) The development of a new method for testing the lateral load capacity of small-scale masonry walls using a centrifuge and digital image correlation. *Construction and Building Materials,* 25**,** 4465-4476.